A STUDY OF THE BEHAVIOUR OF PRESSURIZED PIPING ELBOWS

PhD Thesis submitted to The University of Strathclyde

ASNAWI LUBIS

DEPARTMENT OF MECHANICAL ENGINEERING
THE UNIVERSITY OF STRATHCLYDE
GLASGOW
2003

ACKNOWLEDGEMENTS

I am pleased to acknowledge all those individuals who gave me support and advice during my candidature. First of all, I would like to express my sincere gratitude to my supervisor, Professor James T Boyle, for his time, expert advice, support, and encouragement. I would like further to express my sincere appreciation to Dr Donald Mackenzie for his advice in finite element modelling and Dr James Wood for his discussion on path-dependency in a non-linear analysis and his guidance on obtaining the stress-intensification factor from finite element generated data. My sincere gratitude is also due Dr David Nash, Dr Tugrul Comlekci and Dr Robert Hamilton, from whom I got valuable experiences on finite element analysis.

My personal thanks are due, in particular, to the Department of Mechanical Engineering, The University of Strathclyde for the facilities enabling me to complete the work of this thesis, especially the use of ANSYS through an educational software license. I should also express my sincere gratitude to my institution in Indonesia, The University of Lampung, for providing 42 month scholarship under an Engineering Education Development Project (EEDP) of the Higher Education Directorate General. Special thanks are finally, but not least, due to my wife, Linda, and my daughter, Lulu, for their patience being neglected during the preparation of this thesis, and my parents in Indonesia for their endless praying for my success

Glasgow, August 2003

Asnawi Lubis

CONTENTS

LIST OF FIGURES

NOTATIONS

The following symbols are used in this thesis and are defined where they first appear in the text. Some symbols have been assigned more than one meaning, but it will be clear from the context.

A, ΔA	area of pipe cross-section, change of area of pipe cross-section, mm^2
D	shell bending stiffness, N.mm
D	outside diameter, mm
E	Young's modulus, N/mm^2
I	Second moment are of cross-section, mm^4
$L = R\alpha$	Equivalent length of a straight pipe, mm
L	length of straight tangent pipe, mm
M	bending stress resultants, N.mm
M, M_t	applied bending moment, applied torsion moment, N.mm
M_i, M_o	in-plane bending, out-of-plane bending, N.mm
N	stretching stress resultants, N/mm
R	pipe bend radius, mm
U	strain energy due to deformation of pipe cross-section
X_ξ, X_k, X_i	pressure reduction on ovalisation, flexibility, and stress-intensification
a	a coefficient represents the dependence of k and γ on radius ratio
b	a coefficient represents the dependence of k and γ on radius ratio
c	distance from central axis of a pipe cross-section, mm
d	inside diameter
i, i_p	Stress-int factor without internal pressure, with internal pressure
i_i, i_o	in-plane, out-of-plane, stress-intensification factor
k, k_p	Flexibility factor without internal pressure, with internal pressure
k_i, k_o	in-plane flexibility factor, out-of-plane flexibility factor

r	pipe cross-section radius, mm
t	thickness of pipe, mm
u	axial displacement
v	tangential displacement
w	radial displacement
$\alpha, \Delta\alpha$	bend angle, changes of bend angle, deg
$\Delta\alpha_c$	rotation of end section of a curved pipe (pipe bend)
$\Delta\alpha_s$	rotation of end section of a straight pipe
Δy	vertical bulging (contraction of in-plane diameter), mm
δ_H	horizontal flattening of the pipe cross-section, mm
ε	mid-surface stretching strain
γ	stress-intensification factor
γ_i, γ_o	in-plane stress-intensification, out-of-plane stress-intensification
φ	rotation of end-section of a pipe bend
φ_1	rotation of section connection a pipe bend with loaded tangent
φ_2	rotation of section connection a pipe bend with fixed tangent
$\lambda = tR/r^2$	pipe bend paramater, pipe factor
ϕ	circumferential (hoop) direction for a toroidal coordinate system
θ	longitudinal (axial) direction for a toroidal coordinate system
$\theta_x, \theta_y, \theta_z$	rotation of the end section of a loaded tangent about X, Y, and Z-axis
$\rho = R/r$	radius ratio
σ, σ_{max}	stress, maximum stress, N/mm^2
σ_n	nominal bending stress in a straight pipe, N/mm^2
σ_x, σ_r	axial stress, radial stress, N/mm^2
$\sigma_\phi, \sigma_\theta$	hoop stress, longitudinal stress, N/mm^2
τ	Shear stress, N/mm^2
ν	Poisson's ratio
χ	Curvature of the mid-surface
ξ, ξ_n	ovalisation factor, nominal ovalisation
ξ_p	ovalisation factor with internal pressure
$\psi = pR^2/Ert$	Pressure parameter

ABSTRACT

The behaviour of piping elbows under bending and internal pressure is more complicated than expected. The main problem is that the coupling of bending and internal pressure is non-linear; stress and displacement cannot be added according to the principle of superposition. In addition, internal pressure tends to act against the effect caused by the bending moment. If bending moment ovalises the elbow cross-section, with internal pressure acting against this deformation, then the deformed cross-section tries to deform back to the original circular shape. It is then introduced the term "pressure reduction effect". Current design piping code treats the pressure reduction effect equally for in-plane (closing and opening) moment and out-of-plane moment.

In this thesis, the pressure reduction effect is reassessed for in-plane closing moment through parametric study by performing detailed large deformation finite element analysis. The study is then extended to assess the pressure reduction effect for in-plane opening moment and out-of-plane moment. Approximate formulae for ovalisation, flexibility, and stress-intensification factor are developed through a systematic analysis of the finite element generated data. Comparison of results presented in this thesis and the current ASME piping code for the pressure reduction effect under in-plane closing bending confirms that the ASME code formulae underestimates the pressure reduction for flexibility and stress-intensification. If the ASME formulae are applied for in-plane opening bending and out-of-plane bending, it overestimates the pressure reduction for the flexibility factor. If the ASME formulae for the pressure effect on stress-intensification factor is applied, it underestimates the pressure reduction for closing bending and out-of-plane bending, but overestimates for opening bending. It is therefore proposed that different formula for different direction of bending load should be used and the results presented in this thesis should be useful for this purpose.

CHAPTER 1

INTRODUCTION

This chapter introduces the concepts of flexibility and stress-intensification factors for a smooth curved pipe that are discussed in subsequent chapters. The background to the pressure reduction effect is also described.

1.1 Background

Piping systems are an indispensable feature of the petrochemical industry and power plant technology among many others. In such systems, straight tubes are dominant, but problems of plant layout, etc., obviously make it necessary for pipe runs to change direction. One way of getting the line of the pipe to change direction is by using piping elbows or bends. However, elbows are also introduced to absorb thermal expansion because of its greater flexibility compared to an equivalent straight pipe.

The behaviour of a smooth piping elbow under simple mechanical loads such as bending and pressure is rather curious. Engineer's theory of beam bending for a straight pipe with circular cross section and the familiar equations for a pressurised thin pipe are perfectly satisfactory, very simple and describe the resulting stress systems accurately. Similarly the stress system in a solid curved beam under in-plane bending is a classical solution, familiar to all engineers, and again straightforward. So it comes as some surprise to most professional engineers that the behaviour of a curved beam with a thin-walled section (a pipe bend) under in-plane bending is not straightforward and further, that simple closed-form solutions are difficult. It is perhaps even more of a surprise when it is realised that the combination of bending and internal pressure is very complex – indeed requiring a non-linear solution!

However it was also well known in the first half of the last century that internal pressure was a complicating factor. The stresses from in-plane bending and internal pressure did not appear to be additive and the flexibility could be reduced in a non-proportional manner. It was realised by several authors in the 1950's: Kafka and Dunn [29][1], Crandall and Dahl [27], Rodabaugh and George [30] and Reissner [33] – that the source of the problem was a non-linear interaction between bending and pressure. Essentially the deformation and stress from combined bending and pressure could not be added. A simple explanation [67] can be based on the 'Haigh effect' [11], which in itself is not very well known by professional engineers working with pressurised equipment. In fact, it is documented in the Engineering Science Data Unit [39]. Any pipe, straight or curved, subject to internal pressure departs significantly from simple engineer's theory if the pipe cross section is not circular (say induced by manufacture). The magnitude of this effect depends upon the geometry of the pipe bend and loading acting on it. The problem is that the deformation of the pipe cross-section can no longer be assumed to be small, and subsequently the analysis is much more complex and non-linear (although of course still amenable to finite element analysis). There is in fact a large rotation of the shell wall. In a pipe bend, even if the cross section is initially circular, any applied bending will ovalise the cross section, and if pressure is present the Haigh effect will be important. The main result is that the coupling of bending and pressure in a pipe bend is non-linear. While the applied moment tends to flatten the cross section of the bend, the internal pressure tries to work against this - it tries to open up the bend (the Bourdon Effect). Modified flexibility and stress factors – known as the 'pressure reduction effect' - from the Rodabaugh and George analysis [30] in 1957 have been incorporated into the ASME B31.3 Process Piping code [120] and again are used to this day, virtually unchanged. The ASME B31.1 Power Piping code [114] does not specify the Rodabaugh & George modifications, but does allow modified flexibility and stress factors to be used.

[1]References are ordered chronologically; for a publication year, alphabetically.

Simple flexibility and stress factors derived from simplified analyses in the 1950's, together with the approximate pressure reduction effect, continue to be used in routine piping system flexibility analysis. These factors were derived for the specific load case of pure in-plane closing moment and internal pressure and are used, usually without modification, for in-plane opening moments and out-of-plane loading. Apart from a detailed study by Boyle & Spence [57] on the nature of the non-linear effect and by Spence & Thomson [81, 85] on the influence of end effects (that is pure bending is not assumed, for example attached straight pipes and rigid flanges), which was previously developed by Thomson [73], very little has been reported on the pressure correction apart from ad hoc finite element analyses of specific piping elbow configurations. This is quite surprising when it is realised that a non-linear finite element analysis of a piping elbow under any bending mode and internal pressure can be carried out easily with modern commercial FEA software.

1.2 Flexibility and Stress-Intensification Factors

A piping elbow is introduced into a piping system to absorb thermal expansion, because it has greater flexibility under bending compared to a straight pipe. Straight pipe, in general, can be adequately represented by simple beams with circular cross-section. However, the pipe bend is much more difficult to analyse, because in addition to undergoing the usual beam deformation, the cross-section of the pipe bend becomes oval in shape due to bending. Typical ovalisation of a circular cross-section pipe bend under in-plane (closing and opening) and out-of-plane moment are shown in Fig.1.1.

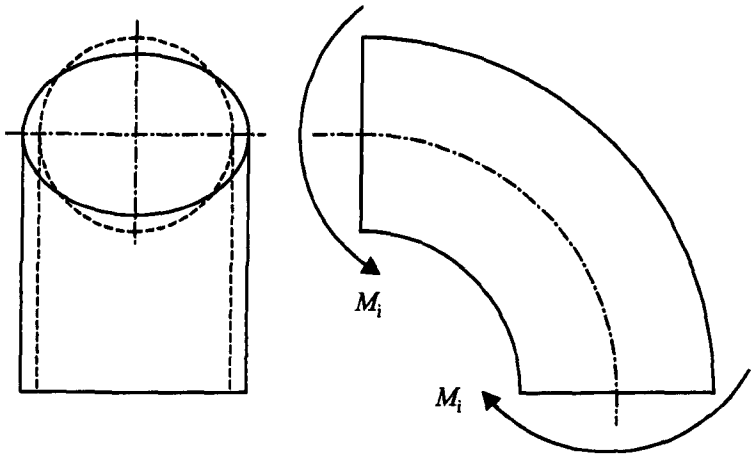

(a) in-plane closing bending

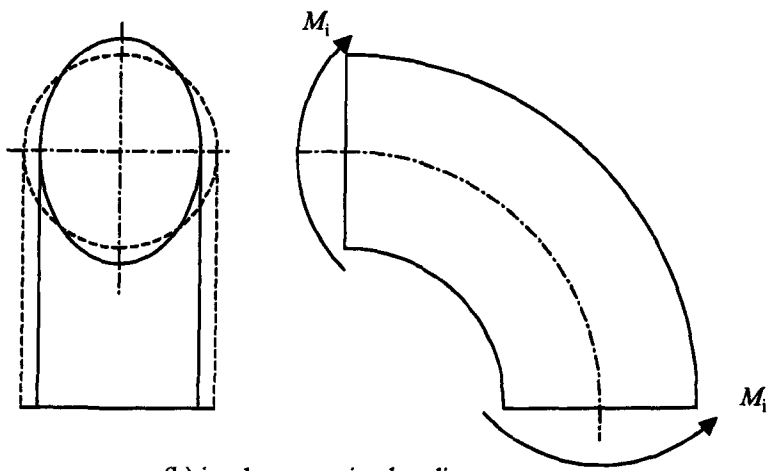

(b) in-plane opening bending

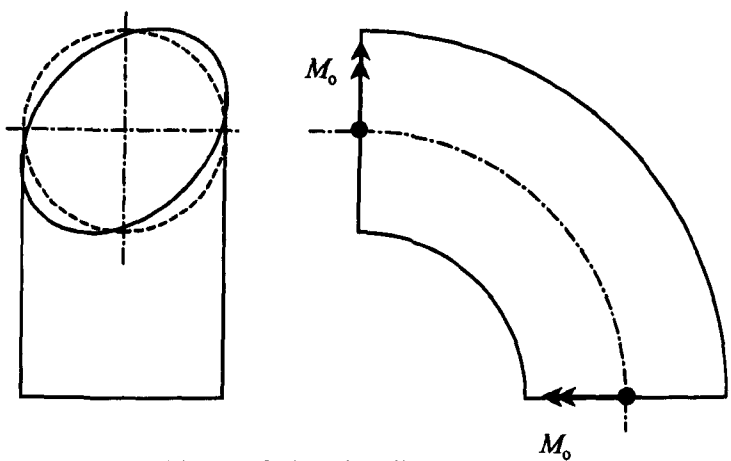

(c) out-of-plane bending

Fig.1.1 Cross-sectional ovalisation of a pipe bend due to bending (a) in-plane closing bending, (b) in-plane opening bending, (c) out-of-plane bending

The dashed line in these figures (circular shape) is undeformed cross-section and the solid line (elliptical shape) is the deformed cross-section. Figure 1.1(a) shows that cross-sectional ovalisation due to in-plane closing moment (decrease the radius of curvature) has a major axis perpendicular to plane of the bend. Under in-plane opening moment (increase the radius of curvature), the major axis of the deformed oval cross-section lies in the plane of the bend as shown in Fig.1.1(b). Figure 1.1(c) shows that a pipe bend under an out-of-plane moment deforms into oval shape with major axis inclined by about 45-deg from the plane of the bend. It seems that the direction (but not the magnitude) of cross-section ovalisation of a pipe bend under an out-of-plane moment is a different condition of in-plane closing and opening [13].

Due to cross-sectional ovalisation, the relation between bending and change in subtended angle for the in-plane bending of curved tube (Fig.1.2(a)), can be calculated as follows [Kitching, 45]:

$$\frac{M(1-\nu^2)}{EI} = \frac{1}{k}\frac{1}{R}\frac{\Delta\alpha}{\alpha} \qquad (1\text{-}1)$$

where M = applied bending moment, N.mm

ν = Poisson's ratio

E = Young's modulus, N/mm^2

I = Moment inertia of the cross-section, mm^4

R = Pipe bend radius, mm

α, $\Delta\alpha$ = subtended angle, change of subtended angle, deg.

k = flexibility factor

It is well known that the relation between applied bending moment and resulting angle of rotation of the end section of a straight pipe having '*the equivalent*' length $L = R\alpha$ (Fig.1.2(b)) is:

$$\frac{M(1-\nu^2)}{EI} = \frac{\Delta\alpha}{L} = \frac{1}{R}\frac{\Delta\alpha}{\alpha} \qquad (1\text{-}2)$$

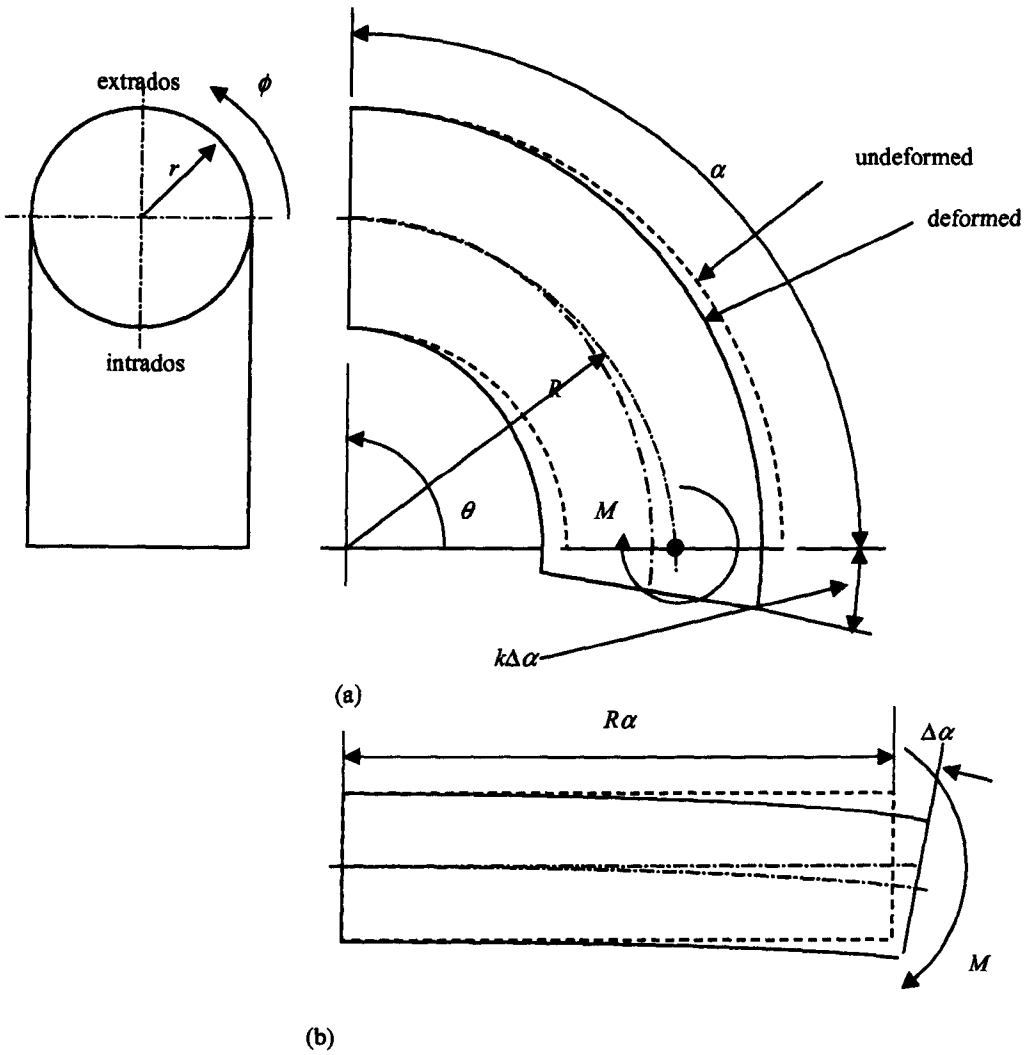

Fig.1.2 Pipe subjected to in-plane moment, (a) pipe bend, (b) equivalent straight pipe

A measure of the additional flexibility of a curved pipe over equivalent straight pipe can be found by dividing the change in subtended angle of a curved pipe to the rotation of end section of an equivalent straight pipe due to the same bending moment. Hence, the *'flexibility factor'* can be defined as:

$$k = \frac{\Delta\alpha_c}{\Delta\alpha_s} > 1 \qquad (1\text{-}3)$$

where $\Delta\alpha_c$ = the rotation of the end section of a curved pipe (pipe bend)

$\Delta\alpha_s$ = the rotation of the end section of a straight pipe

The cross-sectional ovalisation also causes the stress distribution to be different from that computed by curved beam theory [32, 116]. The stress distribution in a curved pipe is also different from that computed by straight beam bending theory ($\sigma = My/I$). In this sense, the maximum local stresses in curved pipe are larger than the maximum stresses in a corresponding straight pipe under equal bending moment. The maximum bending stress in a curved pipe could then be written as:

$$\sigma_{max} = \gamma \frac{Mr}{I} \tag{1-4}$$

where γ = '*stress-intensification factor*' ($\gamma > 1$)

M = Applied bending moment, N.mm

r = pipe cross-section radius, mm

I = Moment inertia of the cross-section

Explanation to this phenomenon was first given mathematically by von Karman [2] in 1911 who introduced flexibility and stress-intensification factors using a simple analysis based on an energy method for in-plane bending. Based on some simplifying assumptions and taking only the first term of the trigonometric series for the radial displacement w, (Fig.1.3), von Karman proposed the pioneering expression for flexibility factor as follows:

$$k = \frac{12\lambda^2 + 10}{12\lambda^2 + 1} \tag{1-5}$$

where λ = Pipe bend parameter or pipe factor, defined as

$$\lambda = \frac{tR}{r^2} \tag{1-6}$$

where t = Pipe wall thickness, mm

R = Pipe bend radius, mm

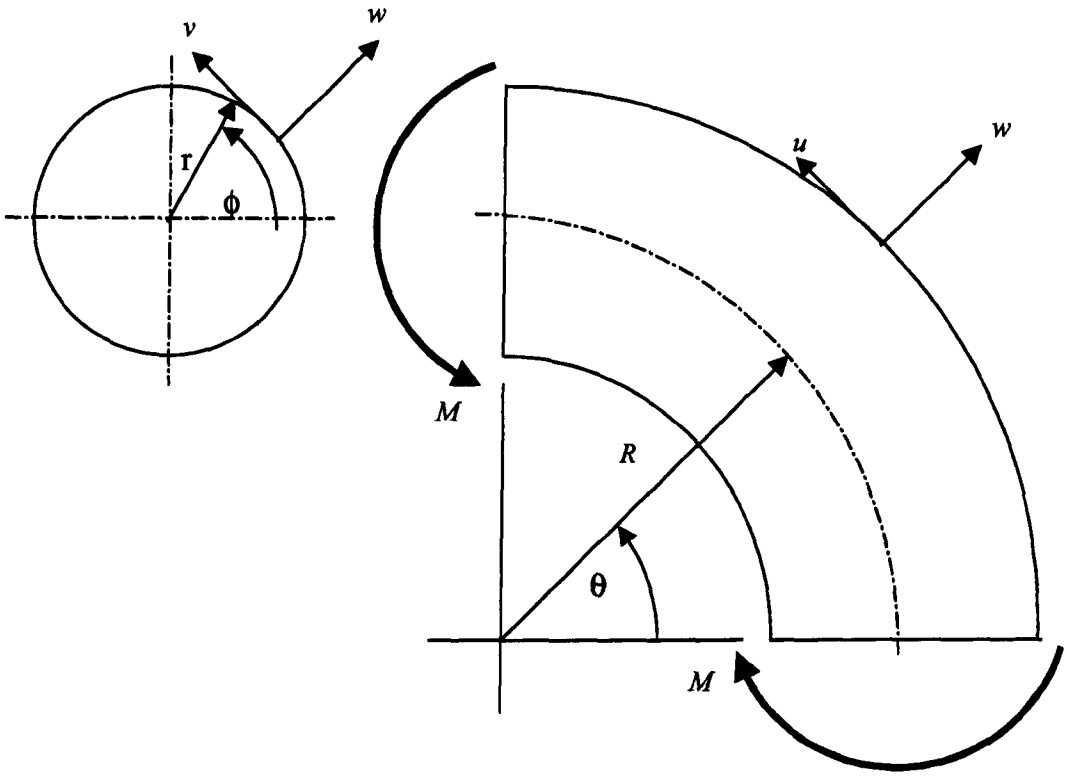

Fig.1.3 Displacement in a pipe bend; longitudinal u, tangential v, and radial w

It was found later by Clark and Reissner [20] in 1951 that the simple von Karman formula, eqn (1-5), predicted the flexibility factor quite well for pipe bends having pipe factors of 0.5 and greater. For pipe bends of low pipe factors ($\lambda < 0.5$), it was necessary to take more than one term of the trigonometric series of the radial displacement. As a result, the analysis becomes more complicated. Clark and Reissner [20] then proposed an asymptotic solution to solve the differential equation of this problem and obtained the following simplified formula for flexibility and stress-intensification factors:

$$k = \frac{1.65}{\lambda} \tag{1-7}$$

$$\gamma = \frac{1.89}{\lambda^{2/3}} \tag{1-8}$$

Equations (1-7) and (1-8) have been obtained for Poisson's ratio $\nu = 0.3$.

The Clark and Reissner's flexibility factor, eqn (1-7) remains in the current design piping code, ASME B31.1 power piping code [114] and ASME B31.3 process piping code [120]. In these piping codes, the maximum stress in a pipe bend is calculated as:

$$\sigma_{max} = i\frac{Mr}{I}$$

where i is stress-intensification factor adopted from the fatigue test of Markl [23] in 1952, that is:

$$i = \frac{0.9}{\lambda^{2/3}} \tag{1-9}$$

Equations (1-7) and (1-9) are applicable for pipe bend under moment loading only. The effect of internal pressure was not considered. In the presence of internal pressure, flexibility and stress-intensification factors would be reduced and the *term "pressure reduction"* was introduced.

1.3 Pressure Reduction Effect

In 1957, Rodabaugh and George [30] used a simple potential energy approach similar to that of von-Karman to analyse the effect of internal pressure for the case of pure in-plane bending under a closing moment. In this, the work done by the pressure is assumed to be a 'second-order' effect in changing the cross sectional area of the pipe. With the assumption of a *'long radius bend'* they showed that the flexibility and stress factors not only depend on a *pipe bend parameter* $\lambda = Rt/r^2$, where R is the radius of the bend, r the mean cross sectional radius of the pipe (assuming a thin section) and t the thickness, but also on a *pressure parameter* ψ, where

$$\psi = \frac{pR^2}{Ert} \tag{1-10}$$

where p is internal pressure. They further formulated the pressure reduction effect on the flexibility and stress-intensification factors as follows:

$$k_p = \frac{k}{1+6\left(\frac{p}{E}\right)\left(\frac{r}{t}\right)^{7/3}\left(\frac{R}{r}\right)^{5/2}} \tag{1-11}$$

$$i_p = \frac{i}{1+3.25\left(\frac{p}{E}\right)\left(\frac{r}{t}\right)^{5/2}\left(\frac{R}{r}\right)^{2/3}} \tag{1-12}$$

where p is the internal pressure and E the elastic modulus. In the above, k and i are flexibility and stress-intensification factor respectively in the absence of internal pressure, adopted from the asymptotic solution of Clark and Reissner [20] for flexibility factor and fatigue test of Markl [23] for stress-intensification factor. The equations (1-11) and (1-12) appear in the ASME B31.3 process piping code [120] as the pressure reduction effect on flexibility and stress, (but, interestingly, not in the ASME B31.1 [114]). Figure 1.4 and 1.5 show flexibility and stress-intensification factors for typical pipe bend geometry according to equation (1-11) and (1-12) respectively.

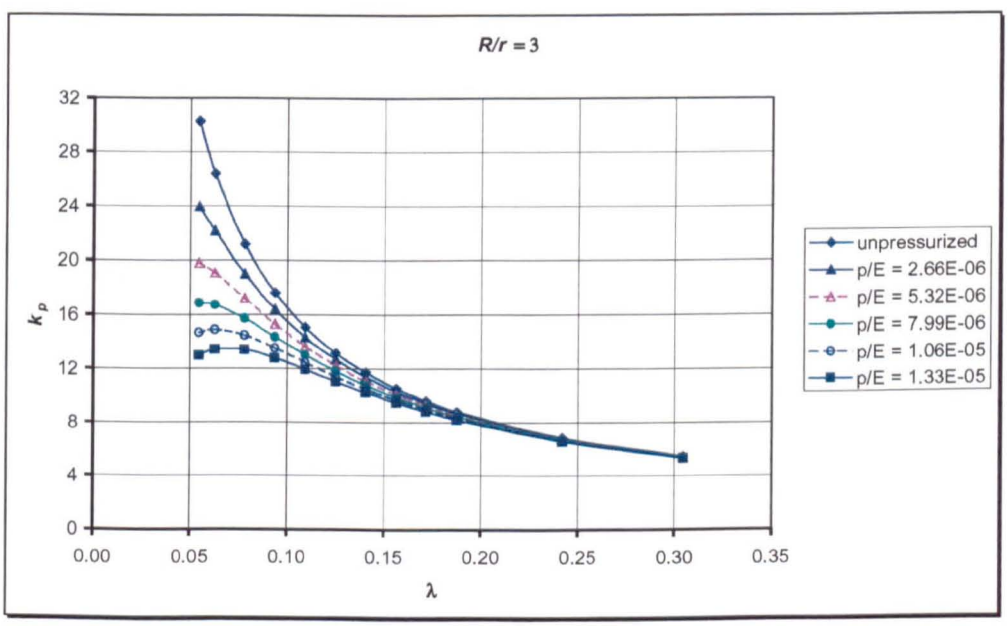

Fig.1.4 Flexibility factor from Rodabaugh & George [30], eqn (1-11)

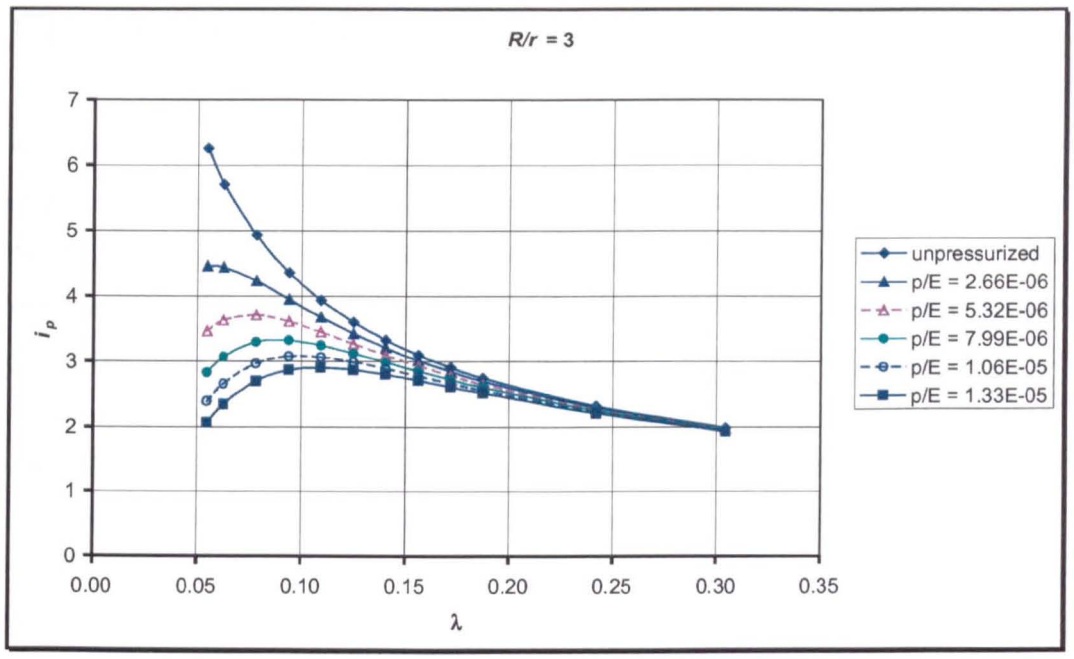

Fig.1.5 Stress-intensification factor from Rodabaugh & George [30], eqn (1-12)

The non-linear nature of the effect is apparent – this derives from the so-called '*second-order*' term in the work done by the pressure to change the cross sectional area of the pipe. In terms of deformation this is equivalent to including 'first-order' large deformation effects. The implication is that moderately large deformation in the form of a *finite rotation* of the shell wall has a significant effect on the flexibility of a pipe bend and therefore must be included to correctly represent the behaviour under combined load for this component [27, 33]. Again the Haigh effect gives a simple mechanical explanation.

Clearly the pressure reduces the flexibility and stress factor – making the bend less flexible, but also reducing the 'high' stress levels resulting from applied bending, usually associated with flexible pipe bends. Internal pressure essentially has the effect of strengthening (indeed reinforcing) the bend, but renders it less flexible.

1.4 Aim of the Thesis

As mentioned in the foregoing, simple formula to include the pressure reduction effect on flexibility and stress factors which were derived from simplified analyses in the 1950's, continue to be used in routine piping system flexibility design and analysis today. These factors were derived for the specific load case of pure in-plane closing moment and internal pressure and are used, usually without modification, for in-plane opening moments and out-of-plane loading. In addition, the effect of internal pressure on elbows other than 90-deg subtended angle has not been considered. A better understanding of this non-linear behaviour and quantification of the effect of internal pressure on elbows of various bend angles could facilitate a better and safer design.

The purpose of this thesis is to re-assess the pressure reduction equations using finite element analysis. Extensive study on the non-linear behaviour of piping elbows of various geometric configurations subject to in-plane (closing and opening) and out-of-plane bending and internal pressure is presented in this thesis. Specifically the standard Rodabaugh & George non-linear pressure reduction equations for in-plane closing moment are checked in a systematic study.

1.5 Structure of the Thesis

The remaining of this thesis is organised as follows: A literature review of the behaviour of pipe bends under different types of loading is presented in Chapter 2. This begins with a summary of stress induced in a straight pipe under various types of loading. It is then followed by a short review on the membrane behaviour of pipe bends under internal pressure. The concepts of flexibility and stress-intensification factors are then reviewed with special attention to the available useful formulae. The final section to this Chapter is a review on the pressure reduction effects.

Chapter 3 presents a literature review of the behaviour of piping elbows. In this Chapter, the effect of end constraint and bend angle is reviewed, focusing on the numerical and finite element modelling for piping elbows analysis. Finite element modelling aspects include geometry modelling, selecting element type, boundary conditions, applying loads, and interpretation of results are discussed.

In Chapter 4, detailed finite element modelling and analysis of piping elbows using ANSYS shell elements is presented. A detailed finite element convergence study to find the optimum number of elements is presented. In this chapter, path dependency of the structures is investigated to find the correct way for applying bending and pressure loading.

Chapter 5 presents new results for *in-plane closing bending* load. Approximate formulae are presented for ovalisation, flexibility, and stress-intensification factors under both unpressurised and pressurised conditions. Approximate formulae for unpressurised condition follow the form of equation proposed by Fujimoto and Soh [133], while the derivation of approximate formula for pressurised condition follows the outlines of the work of Rodabaugh and George [37]. Chapter 6 presents similar results for *in-plane opening bending*. In the discussion to Chapter 6, flexibility and stress-intensification factor for *S-shaped back-to-back 90-deg pipe elbows* are presented in order to verify the accuracy of the approximate formula developed previously.

Results of analysis for *out-of-plane bending* are presented in Chapter 7. Approximate formulae for flexibility and stress-intensification factors are given. The results for ovalisation factor are excluded, since there is some ambiguity as to the location of its maximum value, being strongly dependent on the geometry, especially on bend angle. Chapter 8 closes the thesis with a summary and concluding remarks along with some recommendations for future work.

CHAPTER 2

BEHAVIOUR OF PIPE BENDS: FLEXIBILITY AND STRESS-INTENSIFICATION FACTORS

Many investigators have carried out structural analysis of pipe bends theoretically and experimentally as well as numerically since the original work of von Karman. This chapter is intended to give a review or summary of the available theoretical and experimental work to date of the behaviour of piping elbow. Factors affecting the flexibility and stress-intensification are discussed. Of course, special attention is focused on the pressure reduction effect. However, to begin with an overview of the mechanical behaviour of pipework is presented.

2.1 Stresses Induced in Straight Pipe

During operation, piping systems experience a variety of loads. Boyle [115] classified the loads according to their effect as follows:

(1) Internal (and external) pressure

(2) Dead weigh effect of piping together with insulation and contained fluid

(3) Thermal expansion and possibly through wall thermal gradient

(4) Dynamic loading due to wind, earth quake or blast loading

All these loads can induce stress in piping systems. In what follows, some basic features of the stresses induced by different types of loading on straight pipe are summarised:

2.1.1 Pressure Stress

It is well known from elementary strength of materials that the pressure stresses in long thin walled straight pipe (Fig.2.1) under internal pressure are given by:

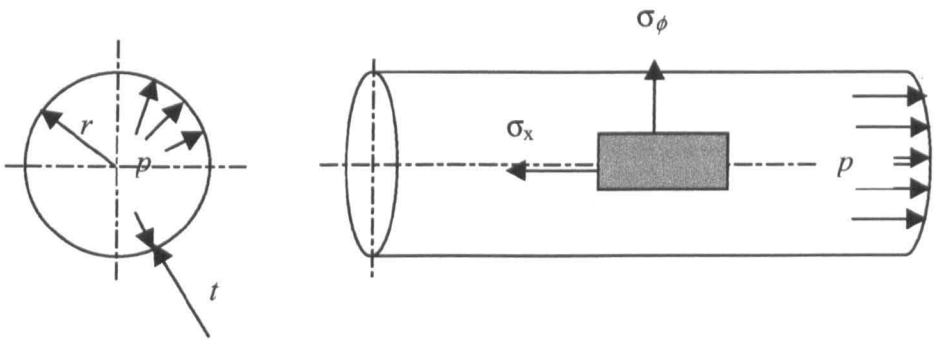

Fig.2.1 Pressure stress in a long thin-walled cylinder

$$\sigma_x = \frac{pr}{2t} \qquad \text{Axial stress} \qquad (2-1)$$

$$\sigma_\phi = \frac{pr}{t} \qquad \text{Hoop stress} \qquad (2-2)$$

If the pipe is thick-walled (Fig.2.2), the longitudinal (axial) and hoop (circumferential) stresses are given by Lame's equation:

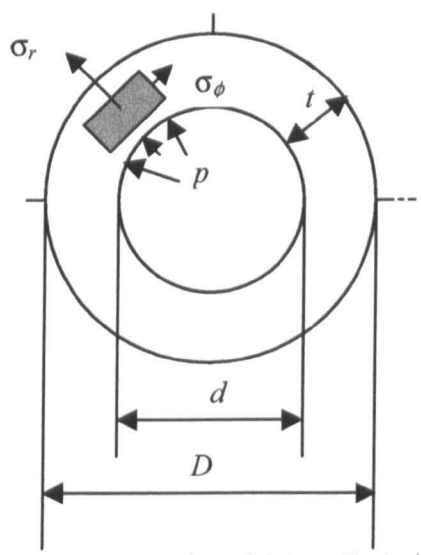

Fig.2.2 Pressure stress in a thick walled pipe

$$\sigma_x = \frac{pd^2}{4t(d+t)} \qquad \text{average} \qquad (2-3)$$

$$\sigma_\phi\big|_d = \frac{p(D^2+d^2)}{D^2-d^2} \qquad \text{inner surface} \qquad (2-4a)$$

$$\sigma_\phi\big|_D = \frac{2pd^2}{D^2-d^2} \qquad \text{outer surface} \qquad (2-4b)$$

where D and d is outside and inside diameter of the cross-section respectively. The radial stress σ_r is $-p$ at the inner surface and ($r = d/2$) and zero at the outer surface ($r = D/2$).

2.1.2 Torsion Stress

A thick walled pipe loaded by torsion M_t (Fig.2.3) will induce a shear stress τ:

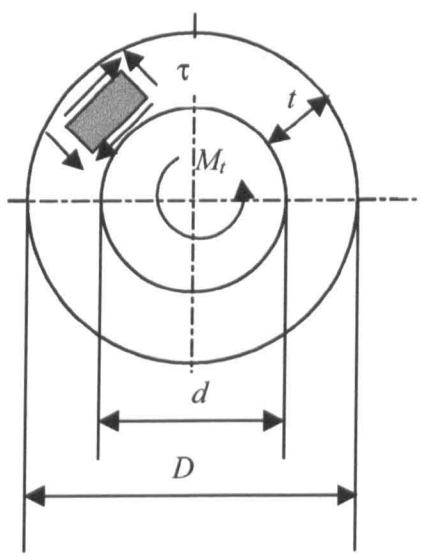

Fig.2.3 Torsion stress in long thick walled pipe

$$\tau = \frac{M_t(d+2t)}{4I} \qquad \text{at the outermost fiber} \qquad (2-5)$$

where I is second moment of area of the pipe cross-section.

$$I = \frac{\pi}{64}\left(D^4 - d^4\right) \tag{2-6}$$

For thin-walled tubes, the shear stress due to torsion can be further simplified to the following:

$$\tau = \frac{M_t}{2At} \tag{2-7}$$

where $A = \pi r^2 t$ is the enclosed area of the pipe centre line

2.1.3 Bending Stress

Euler's theory of bending makes two simplifying assumptions, which captures the essential behaviour of long slender straight or solid curved beam under bending:

- Plane cross-sections remain plane during bending
- The cross-section of the beam does not deform during bending

With these assumptions, only longitudinal (axial) stress and strain are induced due to bending. For a long straight pipe under a bending moment M (Fig.2.4) the longitudinal stress σ_x for a thin pipe ($d \approx D$) is:

$$\sigma_x = \frac{Mr}{I} \tag{2-8}$$

For a thick-walled straight pipe, the bending stress at the outside surface is given as:

$$\sigma_x\big|_D = \frac{M(d+2t)}{2I} \tag{2-9}$$

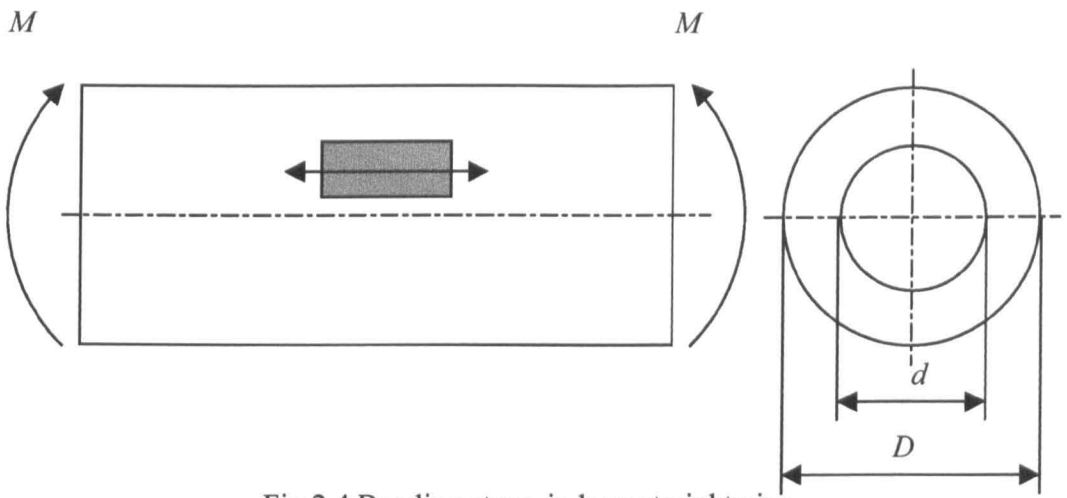

Fig.2.4 Bending stress in long straight pipe

where I is moment of inertia of the cross-section; for thin and thick-walled pipes, I is given in equations (2-10) and (2-11) respectively:

$$I = \pi r^3 t \tag{2-10}$$

$$I = \frac{\pi}{64}\left(\mathrm{D}^4 - d^4\right) \tag{2-11}$$

For a straight pipe under orthogonal bending (combined bending in plane of the paper M_i and bending out-of-plane of the paper M_o (Fig.2.5)), the maximum stress at the outside surface of a thick-walled pipe having inside diameter d and outside diameter D is:

$$\sigma_x\big|_D = \frac{D}{2I}\sqrt{M_i^{\,2} + M_o^{\,2}} \tag{2-12}$$

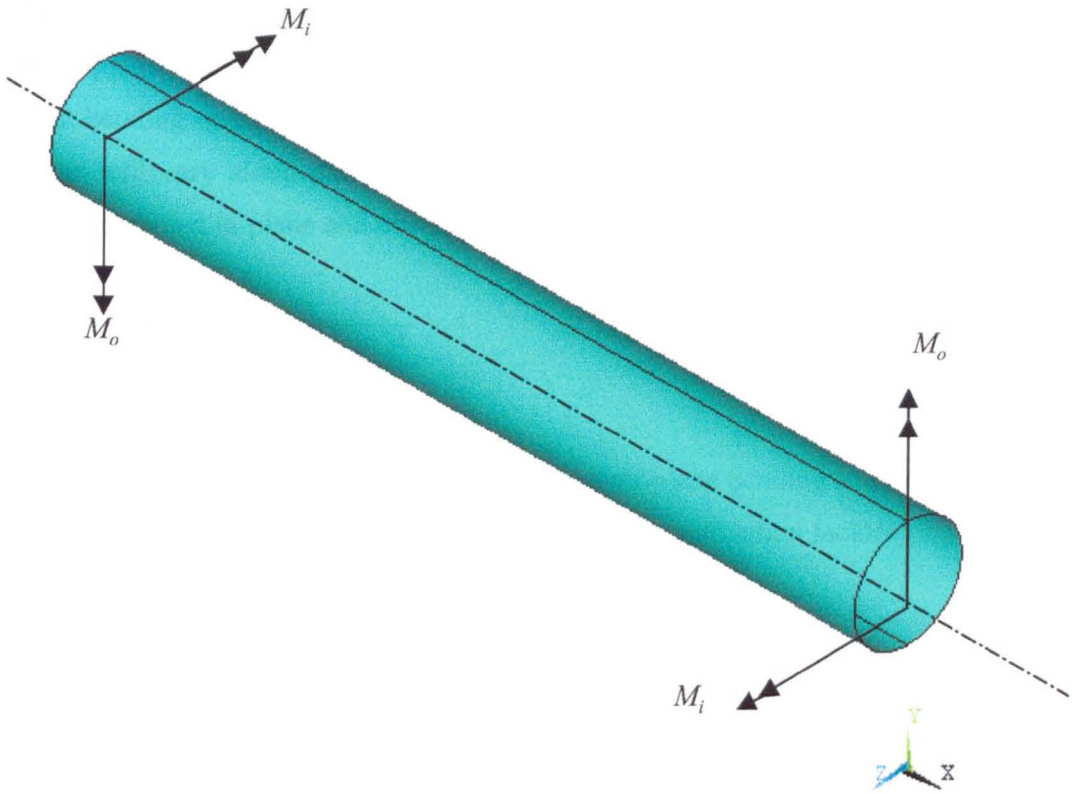

Fig.2.5 Straight pipe under orthogonal bending

2.2 Bending Load on a Pipe Bend

Some important piping components can not be directly modelled using simple bending theory as in the above. In particular a "*pipe bend*" (Fig.2.6) is more flexible than an equivalent straight pipe or solid curved beam since its cross-section becomes oval under bending moment. For a closing bending, the ovalisation of the cross-section leads to increased flexibility and induces higher, and more complex, longitudinal and hoop stress distribution than those given above. This additional flexibility of the curved pipe is of course taken into account in the piping design codes using a *flexibility factor*. In addition, the stress level must also be modified using the concept of *stress-intensification factor*.

The bending load on a pipe bend can include three modes of bending: in-plane, Mi, out-of-plane, M_o, and torque, M_t as shown in Fig.2.6. It should be noted that while in-plane bending can be constant along the bend axis, both out-of-plane bending and torque will vary along the axis. The maximum longitudinal stress in curved pipe under combined in-plane and out-of-plane moment is then calculated from eqn (2-12)

$$\sigma_x|_D = \frac{D}{2I}\sqrt{(i_i M_i)^2 + (i_o M_o)^2} \tag{2-13}$$

where M_i and M_o is the applied in-plane and out-of-plane bending respectively

i_i and i_o is in-plane and out-of-plane stress-intensification factors

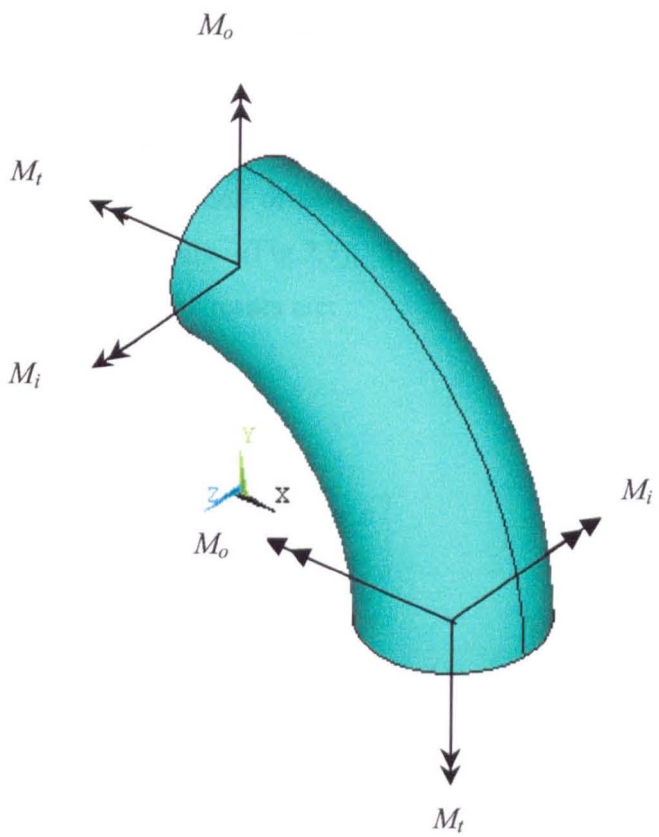

Fig.2.6 Moment component in a pipe bend

The stress-intensification factor i and flexibility factor k of a pipe bend under bending will be considered more detail in the third section of this chapter. In the section what follows, the behaviour of pipe bend under internal pressure is summarised.

2.3 Pipe Bends Subjected to Internal Pressure: Membrane Behaviour

The behaviour of a pipe bend of perfectly circular cross-section and uniform wall thickness under internal pressure alone can be approximated well by the membrane action (the flexure of the surface being ignored), which could result from the same loading on a toroidal shell of the same cross-section.

A curved tube with a constant radius of curvature can be considered as a sector of a closed toroidal shell of revolution. For a circular cross-section toroidal shell under internal pressure (Fig.2.7), Flugge [50] showed that the longitudinal and circumferential stresses are:

$$\sigma_\theta = \frac{pr}{2t} \tag{2-14}$$

$$\sigma_\phi = \frac{pr}{2t}\left[\frac{2\rho + \cos\phi}{\rho + \cos\phi}\right] \tag{2-15}$$

where $\rho = R/r$ is radius ratio, and ϕ is circumferential angle measured from extrados toward intrados position (Fig.2.7). However, these equations are not completely satisfactory in that when the displacement are evaluated via the stress-strain relation, they give rise to singularities in displacement. Some progress for the determination of displacement was made by Dean [12] in 1939 using a method of successive approximation. He suggested that any acceptable stress solution would have to involve bending stress (plus the corresponding shear stress across the shell

thickness). A further analysis was carried out by Jordan [34] in 1962 who employed the ideal membrane theory but omitted some assumptions in the linear theory.

The above equations are suitable for most purpose. Equation (2-14) indicates that the longitudinal stress in a pipe bend due to internal pressure is independent of the radius ratio ρ and circumferential position ϕ. This expression is exactly the same as for a pressurised straight pipe with closed ends, see eqn (2-1). In contrast, hoop stress due to internal pressure depends on both radius ratio ρ and circumferential position ϕ as given by equation (2-15). Membrane hoop stress on a pipe bend under an internal pressure p (p/E = 1.33E-05) is plotted in Fig.2.8 for typical pipe bend geometry (t/r = 0.03).

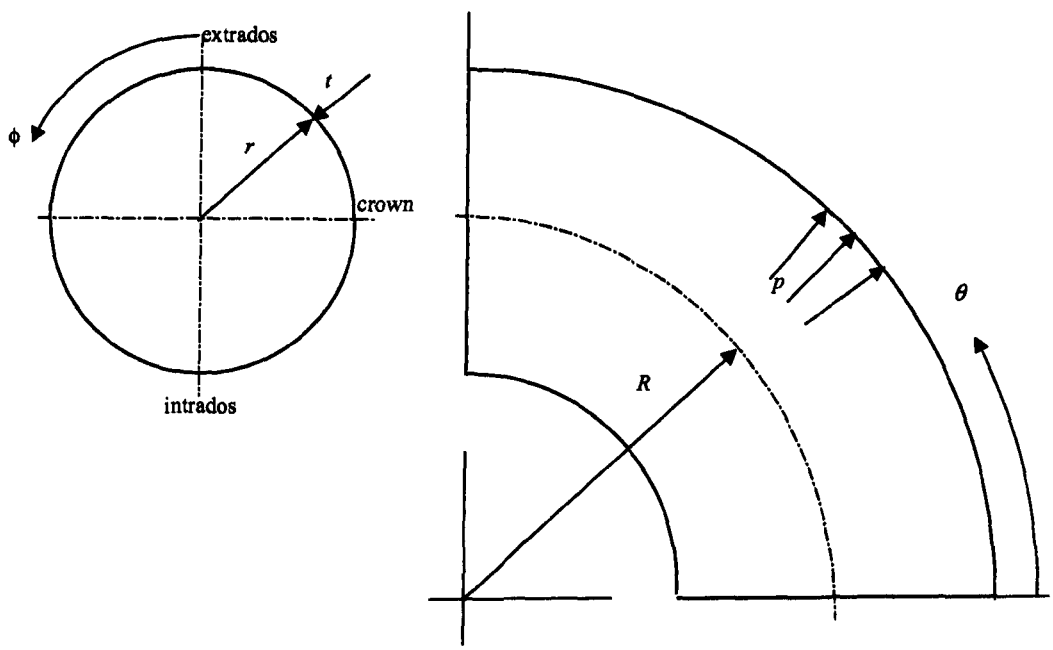

Fig.2.7 Sector of toroidal shell loaded by internal pressure

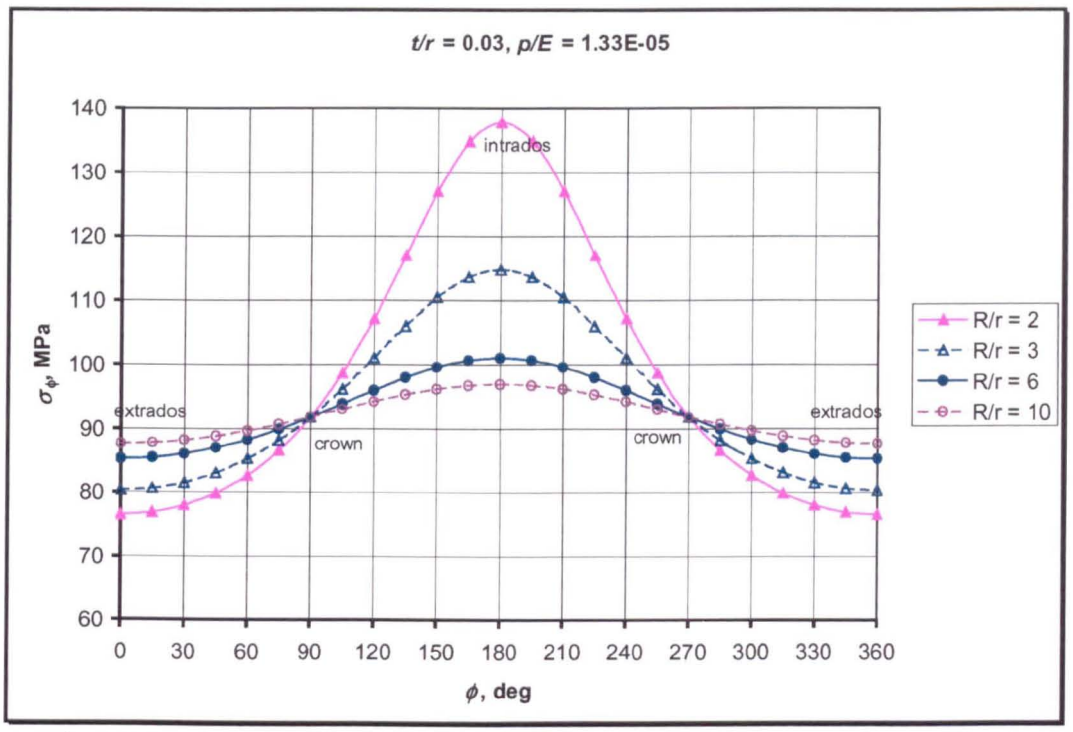

Fig.2.8 Hoop stress distribution in a toroidal shell under internal pressure load

It can be seen from Fig.2.8 that the maximum hoop stresses occurs at the intrados and the minimum at the extrados. The longitudinal and hoop stresses are differentiated by the term in the square bracket in eqn (2-15) as a function of radius ratio and circumferential position. Table 2.1 summarises this term for the extrados, crown and intrados position according to the following equation:

$$\sigma_\phi = \frac{pr}{2t} F(\rho), \qquad F(\rho) = \begin{cases} \dfrac{2\rho+1}{\rho+1} & \text{for extrados} \\ 2 & \text{for crown} \\ \dfrac{2\rho-1}{\rho-1} & \text{for intrados} \end{cases} \tag{2-16}$$

Table 2.1 $F(\rho)$ for extrados, crown, and intrados

R/r	Extrados ($\phi = 0$)	Crown ($\phi = 90$)	Intrados ($\phi = 180$)
2	1.667	2.0	3.000
3	1.750	2.0	2.500
4	1.800	2.0	2.333
5	1.833	2.0	2.250
6	1.857	2.0	2.200
7	1.875	2.0	2.167
8	1.889	2.0	2.143
9	1.900	2.0	2.125
10	1.909	2.0	2.111

It will be shown later how this membrane behaviour is modified for (nonlinear) bending behaviour.

2.4 Pipe Bends Subjected to Bending: Flexibility and Stress-Intensification Factors

A curved pipe (pipe bend) is known from the von Karman [2] analysis in 1911 to be more flexible in bending than an equivalent straight pipe of the same cross-section. Moreover, a thin walled curved pipe may be much more flexible than what is predicted by simple curved beam theory. According to von Karman, the increase in flexibility of a curved pipe under bending results from the ovalisation of the cross-section. The effect of this ovalisation further produces a circumferential bending stress much larger than in an equivalent straight pipe, and also an increase in longitudinal stress in proportion to added flexibility. This section is intended to give a review or summary of the behaviour of pipe bends under bending moment.

2.4.1 In-Plane Bending of Pipe Bend

According to Wahl [7], it was first demonstrated experimentally by Bantlin [1] in 1910, that a curved pipe behaves differently under load from that predicted by ordinary beam theory. He made a series of tests on large pipe bends having thin walls made of seamless steel tubing, and found that the actual deflection was much greater than that calculated using the ordinary beam theory.

The first mathematical explanation of this behaviour was developed by von Karman [2] in 1911. He analysed a pipe bend with circular cross-section and uniform wall thickness under in-plane bending. In developing his theory, the following assumptions were incorporated:

(1) A plane section before bending remains so after bending (as in simple theory of beam bending)

(2) The deformation would be small

(3) The degree of ovalisation is uniform over entire length of the pipe (the '*pure bending*' assumption)

(4) The circumferential mid-surface is inextensible (in simple term, the cross-section deforms into an oval with constant perimeter). Based on this assumption, the maximum hoop stress at the inner surface would be equal in magnitude and opposite in sign to the maximum hoop stress at the outer surface. In addition, the hoop stress at the middle surface would be zero at the crown.

(5) The bend radius is much larger than the pipe cross-section radius (the long radius assumption)

The deformation of cross-section can be described mathematically using radial displacement, w and tangential displacement, v, (Fig.2.9). Von Karman expressed the radial displacement w as a trigonometric series, taking acount of the symmetry of deformation:

$$w = a_2 \cos 2\phi + a_4 \cos 4\phi + a_6 \cos 6\phi + \ldots + a_{2n} \cos 2n\phi, \qquad n = 1,2,3,\ldots \qquad (2\text{-}17)$$

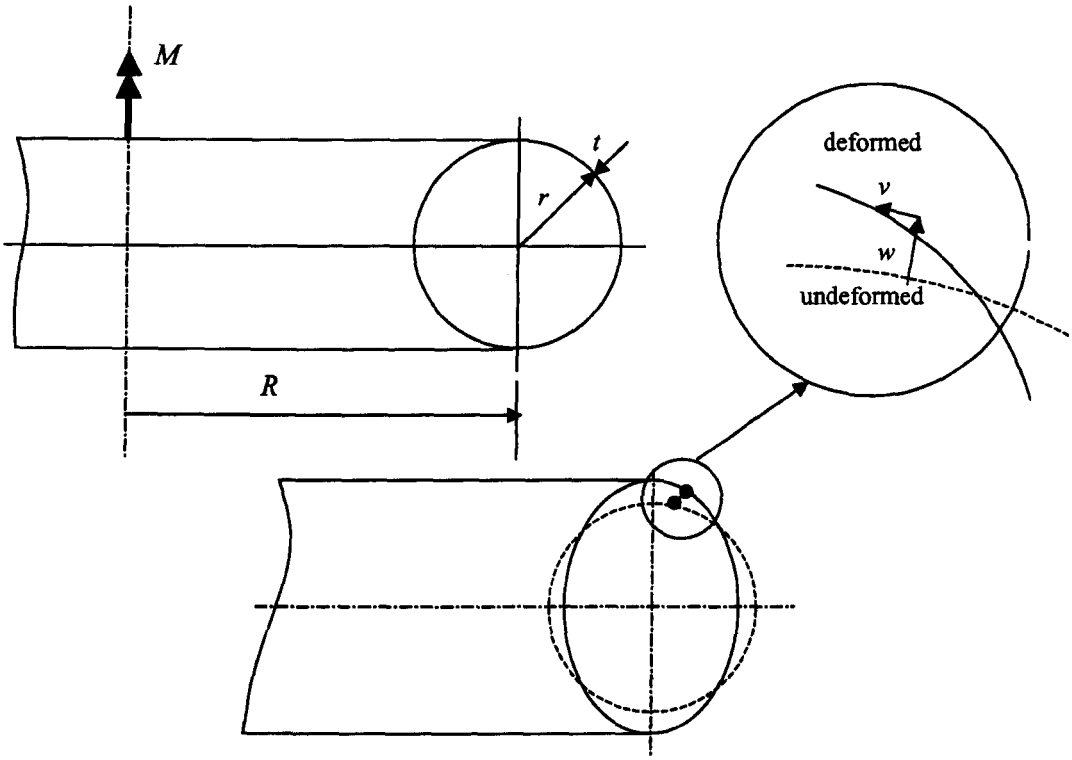

Fig.2.9 Deformation of pipe bend due to pure bending

Based on assumption (4), the tangential and radial displacement is further related in simple form as follows:

$$w = \frac{dv}{d\phi} \tag{2-18}$$

Von Karman used the theorem of minimum potential energy to determine the unknown coefficients of the equation (2-17). The total potential energy to be minimised is the strain energy due to deformation of the cross-section, U, and the work done by the applied bending moment, M, in changing the curvature of the centre line as represented by the change in subtended angle of the end section $\Delta\alpha$:

$$\Pi = U - M\Delta\alpha \tag{2-19}$$

von Karman defined the end rotation of smooth pipe bend under an in-plane moment loading as:

$$\frac{d\alpha}{\alpha} = k\left(1-\nu^2\right)\frac{MR}{EI} \qquad (2-20)$$

However from the ordinary theory of beam bending, the end rotation of a straight pipe of length $L = R\alpha$ under in-plane bending is:

$$\frac{d\alpha}{\alpha} = \left(1-\nu^2\right)\frac{MR}{EI} \qquad (2-21)$$

By dividing the equation (2-20) with equation (2-21), the flexibility factor k can be obtained using the following definition:

$$k = \frac{\text{the end rotation of a pipe bend under a given moment load}}{\text{the end rotation of an equivalent length of straight pipe under the same load}}$$

For a pipe bend of long radius (assumption 5), sufficient accuracy was obtained by taking only the first term of the trigonometric series of the radial displacement ($w = a_2 \cos 2\phi$). For this approximation, von Karman obtained the flexibility factor as follows:

$$k = \frac{12\lambda^2 + 10}{12\lambda^2 + 1} \qquad (2-22)$$

where λ is a flexibility characteristic of the bend called '*pipe bend parameter*', or '*pipe factor*', defined as:

$$\lambda = \frac{tR}{r^2} \qquad (2-23)$$

The variation of flexibility factor with pipe bend parameter according to equation (2-22) is shown in Fig.2.10.

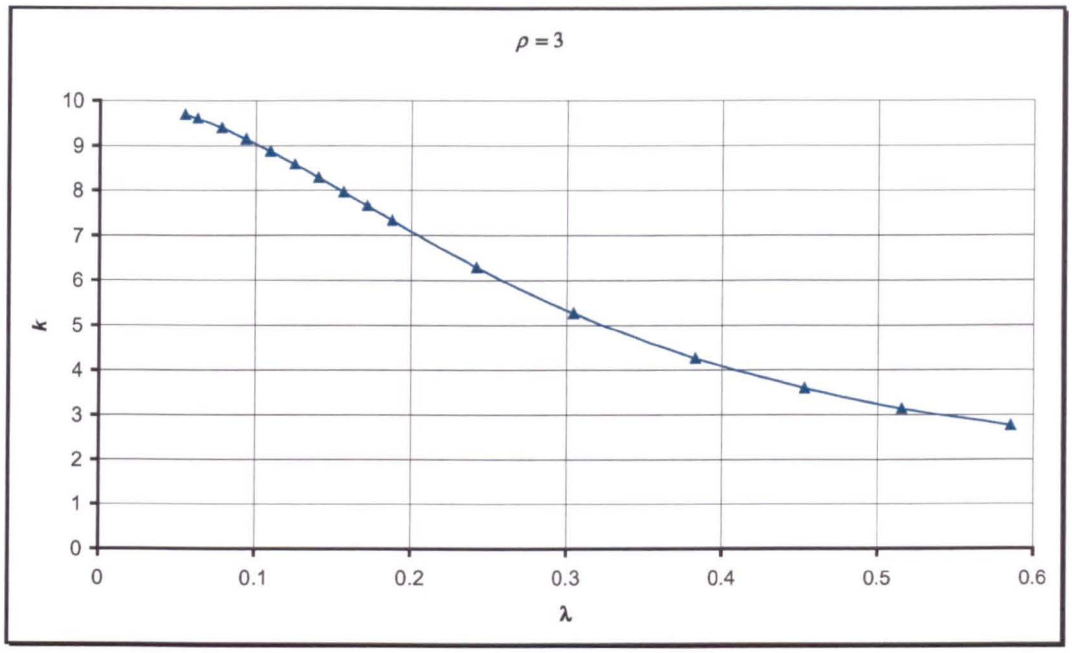

Fig.2.10 Von Karman's first approximation for flexibility factor

The longitudinal and circumferential (hoop) stress factors (Fig.2.11) are also calculated:

$$\frac{\sigma_\theta}{\sigma_n} = \left[k\cos\phi - k_s\cos^3\phi\right] \pm \frac{3}{2} v k_s \lambda \cos 2\phi \qquad (2-24)$$

$$\frac{\sigma_\phi}{\sigma_n} = v\left[k\cos\phi - k_s\cos^3\phi\right] \pm \frac{3}{2} k_s \lambda \cos 2\phi \qquad (2-25)$$

where v is Poisson's ration and σ_n is the nominal bending stress in a straight pipe:

$$\sigma_n = \frac{Mr}{I} = \frac{M}{\pi r^2 t} \qquad (2-26)$$

and

$$k_s = \frac{12}{12\lambda^2 + 1} \qquad (2-27)$$

There is no significant meaning of equation (2-27). It was introduced solely for the simplification of equations (2-24) and (2-25).

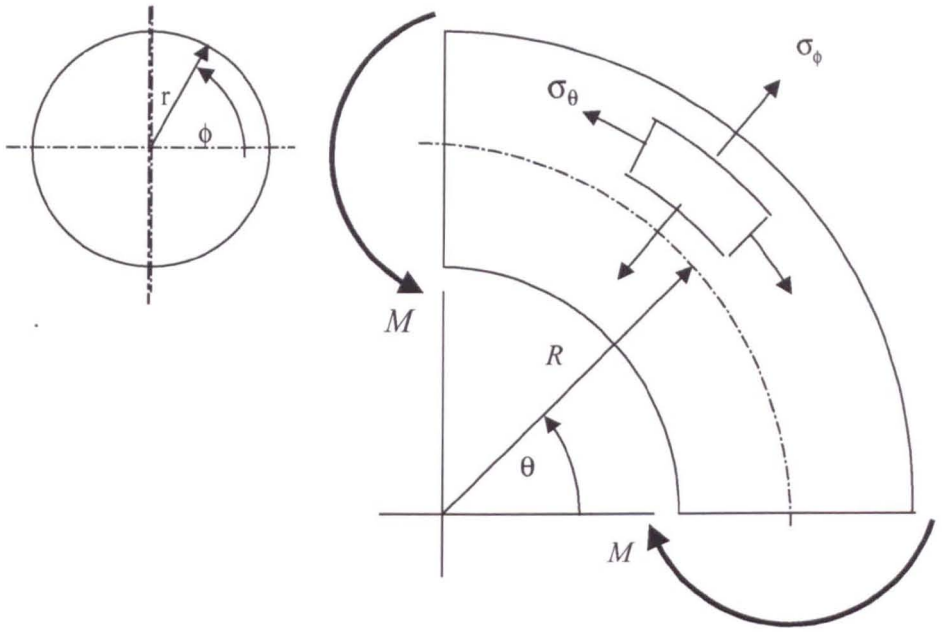

Fig.2.11 Longitudinal and hoop stresses in a pipe bend due to bending

Typical longitudinal and hoop (circumferential) stress distributions are shown in Fig.2.12 and 2.13 respectively.

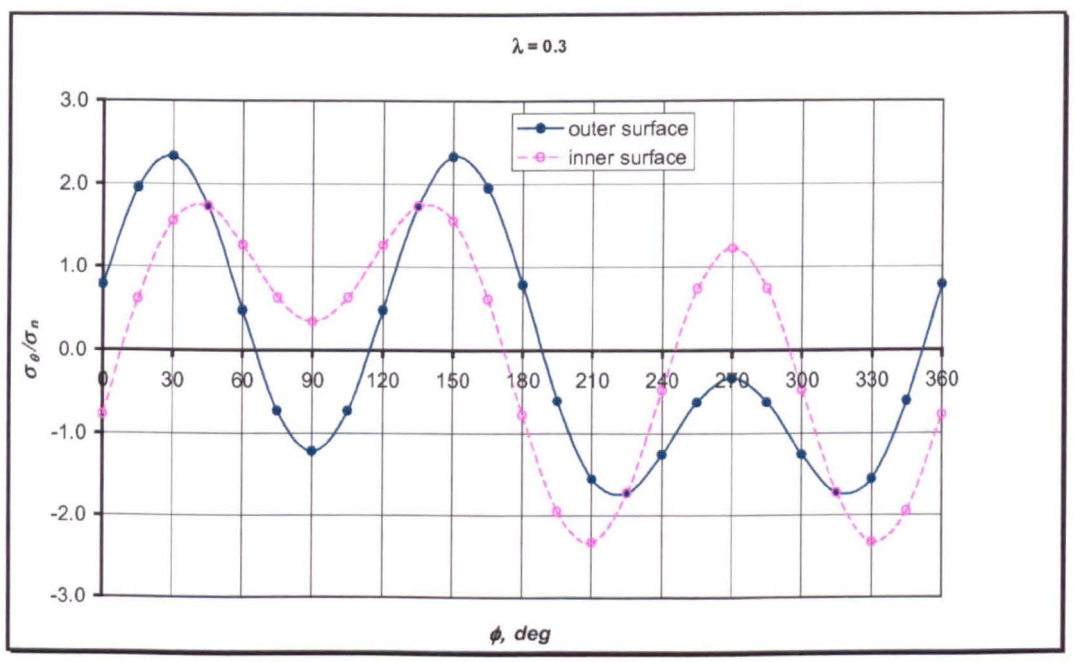

Fig.2.12 von Karman's first approximation – longitudinal stress distribution

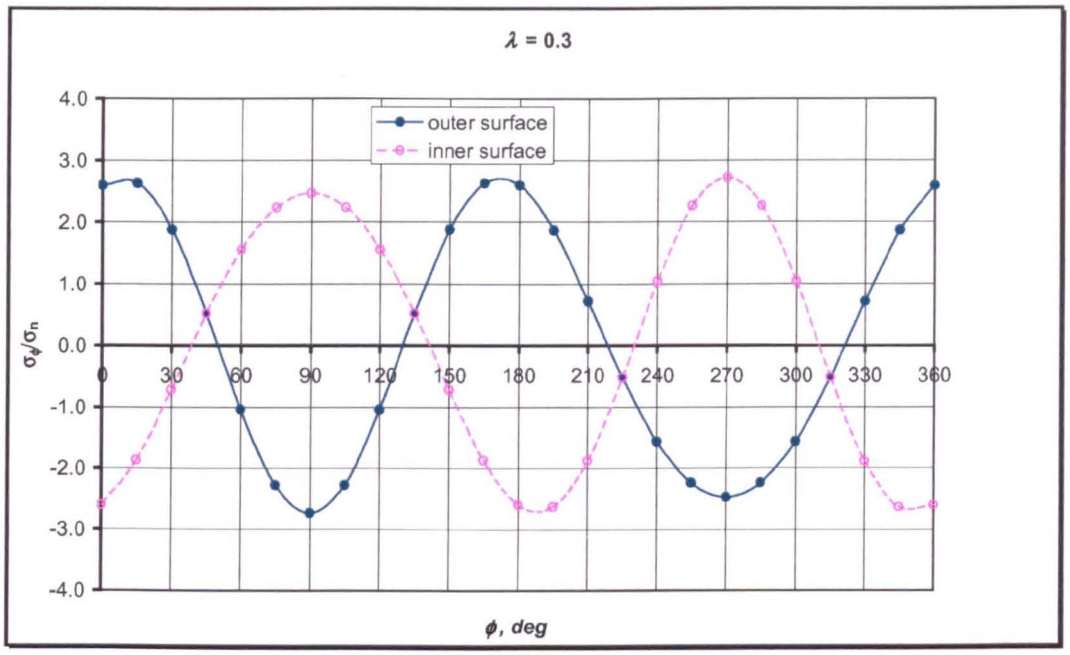

Fig.2.13 von Karman's first approximation – hoop stress distribution

In 1922, Crocker and Sanford [3] investigated the problem of bending of curved tubes using the formula for bending of curved beam as well as carried out experiment of various types of pipe bends. The results of their investigation showed a good agreement between curved beam formula and experiment for some cases, but the bends was found to be more flexible than the formula indicated in other cases. These irregularities was believed to be caused by the distortion of the cross-section, which was not taken into account in their analysis.

In a series of paper, Hovgaard [4, 5, 6] developed another solution for the bending of a pipe bend. By incorporating the same basic assumptions of von Karman but using a structural mechanics approach (rather than a strain energy approach), Hovgaard then reproduced the von Karman first approximation for the flexibility factor. In addition, Hovgaard gave more detail on the degree of ovalisation of the cross-section, in which the amount of vertical bulging (contraction of the in-plane diameter connecting extrados and intrados) of deformed pipe cross-section under in-plane bending, Δy (Fig.2.14) was given by the following:

$$\frac{\Delta y}{r} = \frac{kMR}{EI}\left(\frac{120}{120\lambda^2 + 101}\right) \qquad (2-28)$$

where r is pipe cross-section radius, mm

k = von Karman flexibility factor (eqn (2-22))

M = applied bending moment, N.mm

R = pipe bend radius, mm

E = Young's modulus, N/mm^2

I = moment of inertia of the cross-section

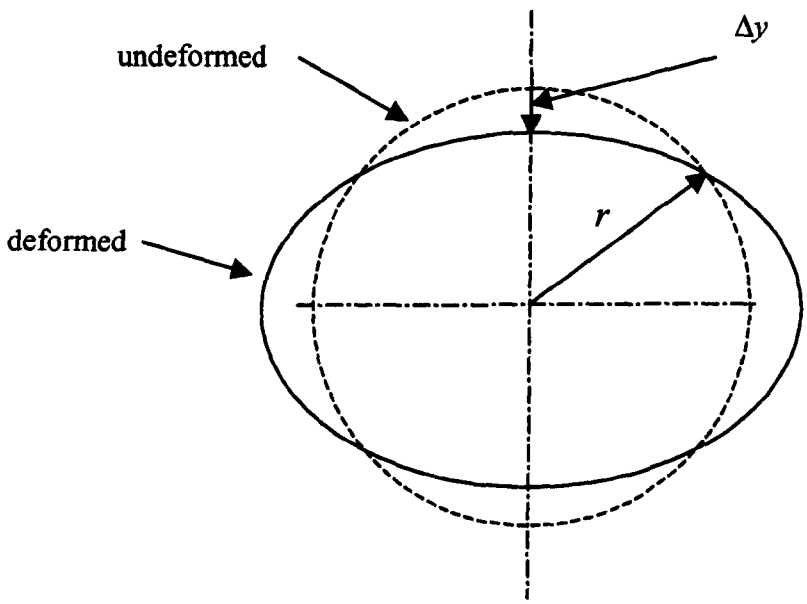

Fig.2.14 Ovalisation of pipe bend cross-section showing vertical bulging Δy

Using the assumption (5) of section 2.3.1, Wahl [7] in 1927 also determined the vertical bulging and arrived at a slightly different formula:

$$\frac{\Delta y}{r} = \frac{kMR}{EI}\left(\frac{12}{12\lambda^2 + 10}\right) \qquad (2-29)$$

In 1929, Shipman [8] used the '*Lorenz*' formula for flexibility factor instead of Karman's formula for calculating reaction force and moment in pipeline due to expansion and internal pressure. In the discussion to Shipman's paper [8] Jenks

extended the von Karman analysis to include curved pipes of low pipe bend parameter ($\lambda \leq 0.05$). For all values of pipe bend parameter, the von Karman's flexibility factors could then be written as:

$$k = \frac{12\lambda^2 + 10 - j}{12\lambda^2 + 1 - j} \tag{2-30}$$

where j is a complicated function of λ varying from unity for $\lambda = 0$ to zero for $\lambda =$ infinity, as tabulated below:

λ	j
0.00	1.00000
0.05	0.76250
0.10	0.56840
0.20	0.30740
0.30	0.17640
0.40	0.11070
0.50	0.07488
0.75	0.03526
1.00	0.02026

Figure 2.15 shows a comparison of the flexibility factors due to von Karman [2] and Jenks for typical pipe bend geometry. It can be seen that flexibility factor from the first approximation of von Karman is in good agreement with Jenks formula for pipe bend parameters greater than about 0.5. in which the stress factor could be represented by the following (see Fig.2.11):

- Longitudinal stress at outer surface

$$\frac{\sigma_\theta}{\sigma_n} = k\left[\sin\phi + \frac{4k-4}{k}\left(\frac{\nu\lambda}{2}\cos 2\phi - \frac{1}{3}\sin^3\phi\right)\right] \tag{2-31}$$

- Hoop stress at outer surface

$$\frac{\sigma_\phi}{\sigma_n} = k\left[\nu\sin\phi + \frac{4k-4}{k}\left(\frac{\lambda}{2}\cos 2\phi - \frac{1}{3}\nu\sin^3\phi\right)\right] \tag{2-32}$$

➢ Longitudinal stress at middle surface

$$\frac{\sigma_\theta}{\sigma_n} = k \sin\phi \left[1 - \frac{4k-4}{3k} \sin^2 \phi \right] \qquad (2-33)$$

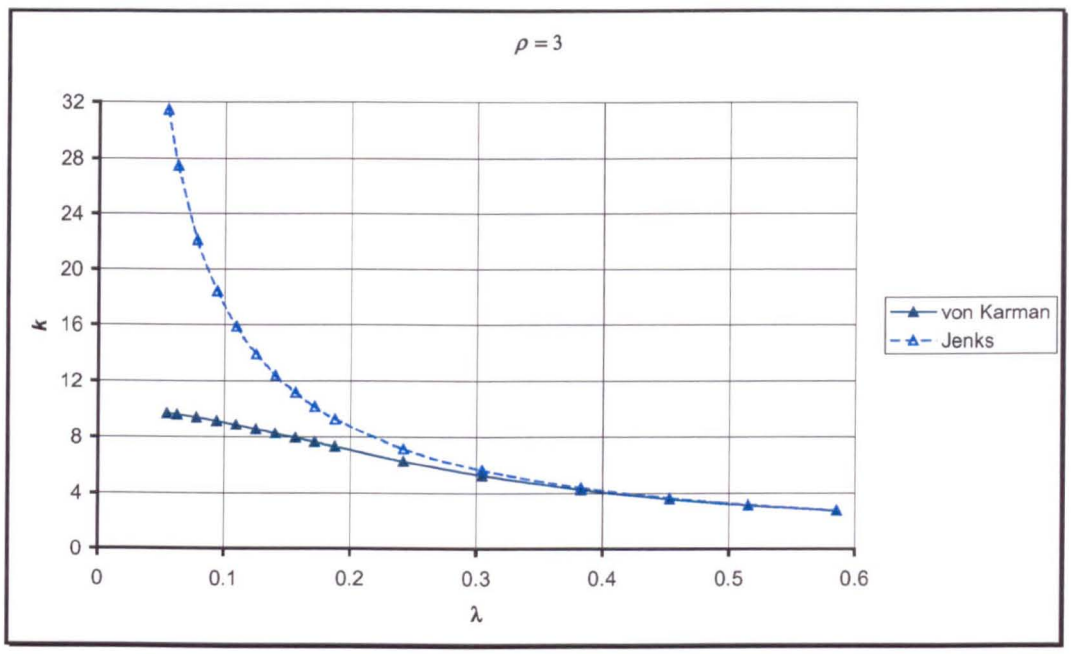

Fig.2.15 Flexibility factors under in-plane bending due to Karman [2] and Jenks [8]

In 1948, Huber [18] presented a solution for bending of curved pipes of elliptical cross-section. The von Karman assumptions were used and the theory of minimum potential energy was also used. For the special case of circular cross-section, the flexibility factor was shown to be in the form:

$$k = \frac{12\lambda^2 + 5.45}{12\lambda^2 + 0.58} \qquad (2-34)$$

Until the 1950's, the Karman expression for flexibility factor was generally used in the design and analysis of piping systems. Wahl [7] in 1927 for example, used this formula to present formulas, tables, and diagrams for determining forces and couples

produced at the fixed ends of pipe bends of various standard forms when subjected to thermal expansion. Cope and Wert [9] in 1932 used the von Karman flexibility factor to calculate the end displacement of the free tangent of an L-shaped pipe elbow arrangement based on the so-called '*graph-analytical method*' which uses an area-moment diagram and the principle of superposition. The von Karman flexibility factor was also used by Hovgaard [10] in 1935 to analyse stress in three dimensional pipe bends.

In 1949, Reissner [19] reconsidered the Karman problem from the point of view of the theory of symmetric thin elastic shells. Based on small deformation theory and the pure bending assumption, two simultaneous differential equations, which were used extensively by Reissner to analyse a variety of shell geometries, were developed. Reissner also derived a method of solving these equations using an '*asymptotic*' series method for various geometric parameters but did not present a solution for the pipe bend.

In 1951, Clark and Reissner [20] did present solutions to Reissner's shell theory by treating pipe bends essentially as part of a toroidal shell. They obtained solution to the von Karman problem in terms of two independent shell variables; the rotation of tangent to the shell wall, β (Fig.2.16) and a stress function, ψ, resulting in two differential equations. The ovalisation of an initially circular cross-section bend was assumed to be symmetrical about the tube diameter normal to its plane of curvature. They made a closed form mathematical analysis of the problem and obtained general trigonometric and asymptotic solutions for the stress and flexibility factors. These are summarised below:

Using a trigonometric series solution, the flexibility and stress factors were obtained as given in the following equations:

$$k = \frac{12\lambda^2 + 10\left(1-\nu^2\right)}{12\lambda^2 + \left(1-\nu^2\right)} \qquad (2\text{-}35)$$

$$\frac{\sigma_\theta}{\sigma_n} = \sin\phi + \frac{3(1-\nu^2)}{12\lambda^2 + (1-\nu^2)}\sin 3\phi \qquad (2-36)$$

$$\frac{\sigma_\phi}{\sigma_n} = \frac{18\lambda}{12\lambda^2 + (1-\nu^2)} \qquad (2-37)$$

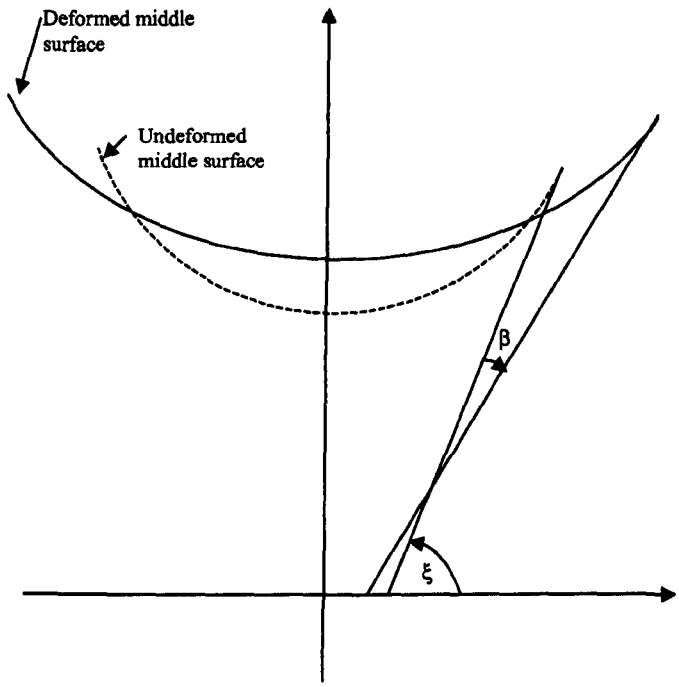

Fig.2.16 Deformation of the middle surface of cross-section under bending

Using an asymptotic solution, the following very much simpler formulae were obtained:

$$k = \frac{\sqrt{3(1-\nu^2)}}{\lambda} \qquad (2-38)$$

$$\left.\frac{\sigma_\theta}{\sigma_n}\right|_{\max} = 0.683\frac{(1-\nu^2)^{1/3}}{\lambda^{2/3}} \qquad (2-39)$$

$$\left.\frac{\sigma_\phi}{\sigma_n}\right|_{\max} = \frac{-1.861}{(1-\nu^2)^{1/6}\lambda^{2/3}} \qquad (2-40)$$

Equations (2-39) and (2-40) indicated that the maximum stress factor (stress-intensification factor) occurs in the hoop direction as a compressive stress. For ν = 0.3, the flexibility and stress-intensification factors can be further written as:

$$k = \frac{1.65}{\lambda} \tag{2-41}$$

$$i = \frac{1.89}{\lambda^{2/3}} \tag{2-42}$$

Note that the notation 'i' has been used for stress-intensification factor and 'the minus sign' has been omitted for simplicity.

Using the asymptotic solution, Clark and Reissner also produced a formula for the amount of flattening in the horizontal direction (Fig.2.17):

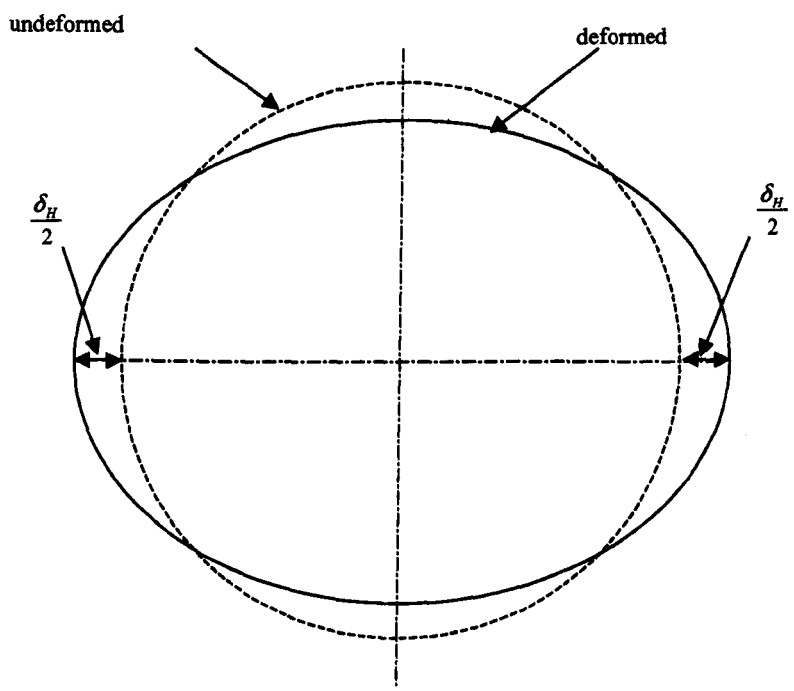

Fig.2.17 Amount of horizontal flattening under an in-plane moment

$$\frac{\delta_H}{t} = \sqrt{12(1-\nu^2)}\left(\frac{r}{t}\right)^2\left(\frac{\sigma_n}{E}\right) \qquad (2-43)$$

where ν = Poisson's ratio

r = pipe cross-section radius, mm

t = wall thickness, mm

E = Young's modulus, mm

σ_n = Nominal bending stress in a straight pipe, eqn (2-26)

It can be seen from equation (2-43) that the amount of horizontal flattening (ovalisation) is independent on the pipe bend radius, R.

In 1952, Markl [23] performed an extensive series of fatigue tests on piping elbows following his previous similar test on piping elbows, which was compared to double-mitred pipe bends [17]. From his experimental results, a flexibility factor identical to the equation (2-41) could be derived. In addition, the following stress-intensification factor for a pipe bend under in-plane bending was proposed:

$$\gamma_i = \frac{0.90}{\lambda^{2/3}} \qquad (2-44)$$

It can be seen that the stress-intensification factors proposed by Markl [23] based on fatigue tests is almost exactly half of the asymptotic solution of Clark and Reissner [20].

The Clark & Reissner [20] and Markl [23] formulae for flexibility and stress-intensification factors, given by equations (2-41) and (2-44), formed the basis for the ANSI (American National Standards Institute) code for piping design and flexibility analysis. These remain in the code to this day! (ASME B31.1 power piping code [114] and ASME B31.3 process piping code [120]).

Nevertheless, various studies aimed at improving these formulae for the simple '*pure bending*' problem have been published. Views which have resulted in useable formulae are described below:

In 1977, Ohtsubo and Watanabe [59] used a novel finite element 'ring' method to investigate the flexibility and stresses of pipe bends. In 1978, Ohtsubo and Watanabe [61] further employ the ring element for some typical example pipe bends, but did not produce a useful formula for flexibility and stresses. Summary of graphs were produced in their 1977 paper [59] from which they obtained the following formula for in-plane flexibility factor:

$$k = 1 + 9.324\frac{1}{\rho}\left(1 - 1.347\frac{1}{\rho}\right) + \frac{1.537\left(1 - 0.1355\frac{1}{\rho}\right)}{\lambda} \qquad (2\text{-}45)$$

It can be seen this formula includes the radius ratio $\rho = R/r$

In 1988, Calladine [91] used a novel complementary energy method based on a 'new' simple formulation of shell theory to derive a simple formula for flexibility and stress-intensification factors for pipe bend subject to in-plane bending:

$$k = 1 + \frac{3}{4\lambda^2} \qquad (2\text{-}46)$$

$$\left.\frac{\sigma_\theta}{\sigma_n}\right|_{max} = \frac{0.685}{\lambda^{2/3}} \qquad (2\text{-}47)$$

$$\left.\frac{\sigma_\phi}{\sigma_n}\right|_{max} = \frac{1.8}{\lambda^{2/3}} \qquad (2\text{-}48)$$

It can in fact be seen that the hoop stress factor is close to the asymptotic solution of Clark and Reissner [20], while the flexibility factor is substantially different in form.

In 1988, Fujimoto and Soh [92] carried out a very detailed finite element analyses (using the MSC/NASTRAN finite element program) to study the flexibility of thin-walled, large diameter ($r/t \geq 50$), piping elbows under in-plane bending. A Parametric survey was performed with pipe bend parameters in the range of $0.01 \leq \lambda \leq 0.2$ and with radius ratio R/r equal 2 and 3. From their study, empirical formulae for the in-plane flexibility factor were proposed:

$$k_i = \frac{1.65}{\lambda}\left[0.876 - \frac{1.89E-07}{\lambda^{2.93}}\right] \qquad \text{for} \frac{R}{r} = 2 \qquad (2\text{-}49)$$

$$k_i = \frac{1.65}{\lambda}\left[0.908 - \frac{2.63E-07}{\lambda^{1.46}}\right] \qquad \text{for} \frac{R}{r} = 3 \qquad (2\text{-}50)$$

It can be seen that this reduces almost to the classic Clark and Reissner [20] solution if the second term in the bracket is negligible.

Apart from these studies, most other attempts to establish more realistic flexibility and stress-intensification factors have related to removing the assumption of pure bending. This requires including 'end effect' – tangent pipes and flanges – and possibly varying the bend angle. Such studies usually result in charts and tables from numerical (finite element) analysis rather than simple formulae. These will be reviewed in Chapter 3.

2.4.2 Out-of-Plane Bending of a Pipe Bend

In 1943, Vigness [13] presented an extensive analysis of three-dimensional pipe systems by considering the problem of out-of-plane bending on pipe bends. He used the same assumptions as those in von Karman analysis but represented the tangential displacement in cosine trigonometric series:

$$v = c_1 \cos 2\phi + c_2 \cos 4\phi + c_3 \cos 6\phi + \ldots + c_n \cos 2n\phi, \qquad n = 1,2,3,\ldots \qquad (2\text{-}51)$$

Equations (2-51) indicates that the tangential displacement is zero at the angle of 45-deg from the neutral axis, which is the position of the major and minor axis of deformed cross-section under an out-of-plane bending. He considered only the first term of the series ($v = c_1 \cos 2\phi$), and on condition of the inextensibility of the middle surface of the cross-section, the radial displacement is accordingly written as:

$$w = -2c_1 \sin 2\phi \tag{2-52}$$

He further followed the procedure of von Karman analysis using the theory of minimum potential energy and arrived at the same expression for flexibility factor. He therefore concluded that the flexibility factor for pipe bend is the same under an in-plane and out-of-plane bending. It should be noted however that he considered only a small section of the cross-section $d\alpha$ in order to apply pure bending assumption. This assumption produces small error in results for in-plane bending of pipe bends, but might produce great error for out-of-plane bending as there is a torsional component at every cross-section of the bend (section 2.2 & Fig.2.6). The torsional component however does not produce significant deformation to the cross-section and that the flexibility increase only due to bending component.

Vigness [13] further expressed the radial displacement, eqn (2-52) in the following form:

$$\frac{w}{r} = \left(\frac{12}{12\lambda^2 + 1}\right)\frac{MR}{EI}\sin 2\phi \tag{2-53}$$

where w = radial displacement, mm

r = cross-section radius, mm

M = applied bending load, N.mm

R = pipe bend radius, mm

E = Young's modulus, N/mm^2

I = cross-section moment of inertia, mm^4

λ = pipe bend parameter

The radial displacement of the cross-section due to out-of-plane bending produces longitudinal and circumferential stresses as given by the following equation:

$$\frac{\sigma_\theta}{\sigma_n} = \frac{(12\lambda^2 - 8)\cos\phi + 12\cos^3\phi}{12\lambda^2 + 1} \tag{2-54}$$

$$\frac{\sigma_\phi}{\sigma_n} = \frac{18\lambda}{12\lambda^2 + 1}\sin 2\phi \tag{2-55}$$

where ϕ is circumferential position along the cross-section measured from central axis of the bend toward extrados (Fig.2.11)

Maximum longitudinal and circumferential stress (longitudinal and circumferential stress-intensification factor) can be obtained from equations (2-54) and (2-55) and are given in the following equations:

$$\left.\frac{\sigma_\theta}{\sigma_n}\right|_{\phi=0} = \frac{12\lambda^2 + 4}{12\lambda^2 + 1} \tag{2-56}$$

$$\left.\frac{\sigma_\phi}{\sigma_n}\right|_{\phi=45} = \frac{18}{12\lambda^2 + 1} \tag{2-57}$$

From Markl's 1952 [23] fatigue test on piping elbows discussed above, the stress-intensification factor for out-of-plane bending was found to be:

$$\gamma_o = \frac{0.75}{\lambda^{2/3}} \tag{2-58}$$

while the flexibility factor remained the same.

In 1970, Kitching [42] presented more detailed longitudinal and circumferential stress factors for pipe bends under out-of-plane bending as follows:

$$\frac{\sigma_\theta}{\sigma_n} = \frac{k}{1-\nu^2}\left[\pm 3\nu\lambda a_1 \sin 2\phi + \left(1+\frac{3a_1}{2}\right)\sin\phi + \frac{a_1}{2}\sin 3\phi\right] \tag{2-59}$$

$$\frac{\sigma_\phi}{\sigma_n} = \frac{k}{1-\nu^2}\left[\pm 3\lambda a_1 \sin 2\phi + \nu\left\{\left(1+\frac{3a_1}{2}\right)\sin\phi + \frac{a_1}{2}\sin 3\phi\right\}\right] \tag{2-60}$$

where

$$a_1 = \frac{-3}{5+6\lambda^2} \tag{2-61}$$

In fact these simple results described above are almost all that are available for the problem of out-of-plane bending. However as described both Ohtsubo & Watanabe [59] and Fujimoto and Soh [92] derived useful formulae for out-of-plane bending form finite element analysis:

From Ohtsubo and Watanabe [59] a flexibility factor for out-of-plane bending can be obtained as:

$$k = -\frac{2}{\nu} + 32.89\frac{r}{R}\left(1-1.255\frac{r}{R}\right) + \frac{1.565\left(1-0.667\frac{r}{R}\right)}{\lambda} \tag{2-62}$$

From Fujimoto and Soh [92] empirical formula for out-of-plane flexibility factors can be obtained as:

$$k_o = \frac{1.65}{\lambda}\left[0.911 - \frac{5.55\times 10^{-5}}{\lambda^{2.21}}\right] \qquad \text{for } \frac{R}{r} = 2 \tag{2-63}$$

$$k_o = \frac{1.65}{\lambda}\left[0.931 - \frac{6.40\times 10^{-4}}{\lambda^{1.28}}\right] \qquad \text{for } \frac{R}{r} = 3 \tag{2-64}$$

2.5 Effect of Radius Ratio

The classical linear theory for bending of a curved pipe developed by von Karman [2] was based on the long-radius assumption. On this assumption, the neutral axis was considered to be coinciding with the centreline. Based on this assumption, the radial displacement can be represented by only the first term of the trigonometric series solution, (see equation (2-17)). This assumption leads to a poor approximation if applied to pipe bend of short radius. An additional geometric parameter is required: this seems out to be the '*radius ratio*'.

Refinement of long radius theory has been carried out by Beskin [14] in 1945. Von Karman's method of solution was adopted but additional Fourier terms for the radial displacement were used to make the method of solution applicable to pipe bends of short radius. In the third section of his paper, a study was made of the significance of omitting the term containing radius ratio ρ. He concluded that for the case of short-radius bend, the flexibility factor remains fairly accurate but stress-intensification factor will not be correct, when the term $1/\rho$ ($= r/R$) is omitted in the analysis. For pipe bends of low pipe factor, Beskin's flexibility factor closely follows the asymptotic solution of Clark and Reissner [20]. In the discussion to Beskin's paper [14], Symonds and Vigness [15] suggested keeping more than one term of the trigonometric series when the pipe bend parameter λ is less than about 0.5.

In 1952, Gross [24] and Gross and Ford [25] made static loading tests on smooth pipe bends of short radius having cross-section diameter ranging from 3 to 12-in. In these tests, measurement of stresses on both the inner and outer surface of the tube wall was made, together with measurement of flexibility and cross-section flattening. This experiment confirmed that the hoop tensile stress was larger than the longitudinal tensile stress on the outside surface. Gross established for the first time by experiment that the largest stress in pipe bends under bending occur on the inside surface in the hoop direction in the vicinity of crotch.

From measurement, Gross [24] found that for a pipe bend under in-plane bending the maximum hoop stress on the inside surface is considerably greater than the maximum hoop stress on the outer surface. Also, if the distribution of hoop stress is assumed linear, there is a compressive hoop stress at the middle surface at the crown. This indicated that the von Karman assumption on extensibility of the circumferential mid-surface is not justified. A simple method for calculating the hoop compressive stress was proposed to be used as correction by adding the value to the compressive hoop stress at the inside surface and subtracting it from tensile hoop stress at the outside surface. It was concluded that the stress and flexibility of a short-radius pipe bend (low pipe bend parameters) could be predicted with high accuracy if:

(1) The von Karman analysis is extended to the third approximation for the trigonometric series solution of radial displacement.

(2) The assumption of inextensibility of circumferential mid-surface is omitted by considering the effect of hoop compressive stress.

Extension of the von Karman analysis to the second and third approximation for the trigonometric series of the radial displacement has also been done by Gross [24], where the flexibility factors is given in the following:

$$k_2 = \frac{105 + 4136\lambda^2 + 4800\lambda^4}{3 + 536\lambda^2 + 4800\lambda^4} \tag{2-65}$$

$$k_3 = \frac{252 + 73912\lambda^2 + 2446176\lambda^4 + 2822400\lambda^6}{3 + 3280\lambda^2 + 329376\lambda^4 + 282400\lambda^6} \tag{2-66}$$

Spence [43] called these approximations "*lower bound*" flexibility factors.

Figure 2.18 shows the flexibility factors of pipe bends under in-plane bending for the first, second, and third approximation of the von Karman's solution. It can be seen from Fig.2.18 that the flexibility factor obtained from the first approximation of von Karman's solution is sufficient for a pipe bend having pipe bend parameter of 0.5 and greater.

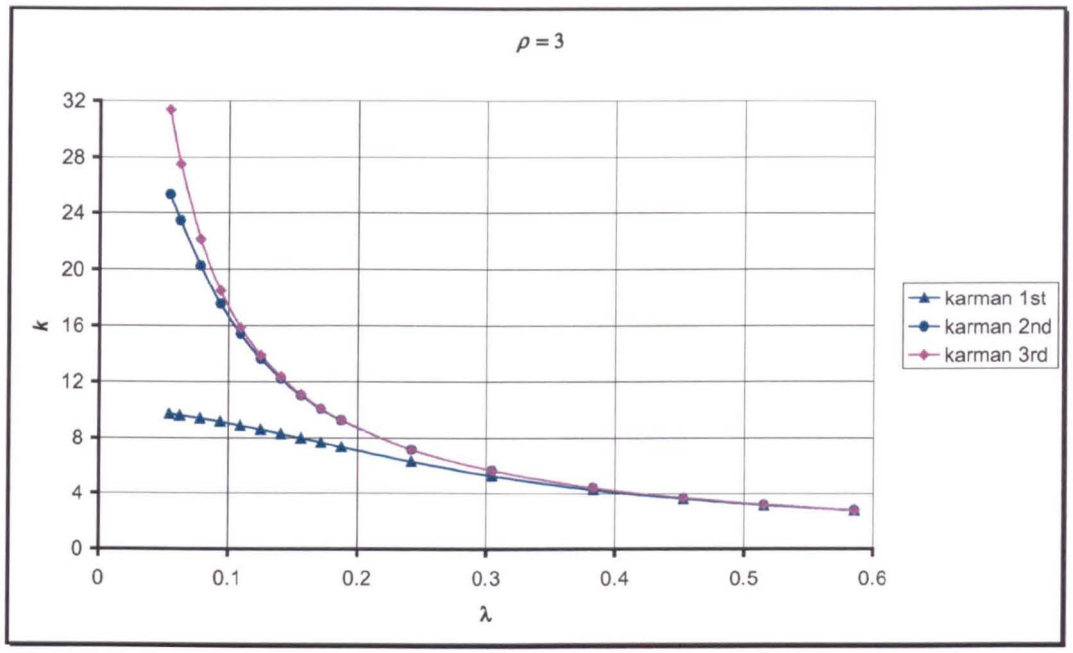

Fig.2.18 Flexibility factors of pipe bends obtained from the von Karman's solution

In 1955, Vissat and Buono [26] reported strain gage investigations for in-plane bending of short-radius bends having radius ratio ρ equal to 3 for 180-deg return and equal to 2 for 90-deg bend. The λ-values ranging from 0.0714 to 0.7404. However, they adopted an unusual definition for the flexibility factor, which included the flexibility of connected tangent pipes as given in the following follows:

$$k = \frac{\Delta}{\frac{2\pi R^2}{EI}\left(\frac{\pi R}{4} + L\right)} \qquad \text{for 180 - deg elbows} \qquad (2-67)$$

$$k = \frac{\Delta}{\frac{\pi R^2}{EI}\left(\frac{\pi R}{4} + L\right)} \qquad \text{for 90 - deg elbows} \qquad (2-68)$$

where Δ is the measured deflection of the end of loaded tangent.

From their experimental result, they pointed out that the theory of long radius bends ($\rho \geq 10$) might be used to compute the value of k with a good agreement. For short radius elbows, the empirical expression below has been suggested for computing the flexibility factor:

$$k = \frac{1.40}{\lambda} \tag{2-69}$$

For calculating stress-intensification factor, they pointed out that the theory of long radius bends could not be used for short-radius bends. Instead, they suggested using the empirical formulation below for calculating the longitudinal and circumferential stress-intensification factor for short-radius bend:

$$\left.\frac{\sigma_\theta}{\sigma_n}\right|_{\max} = \frac{1.20}{\lambda^{0.67}} \tag{2-70}$$

$$\left.\frac{\sigma_\phi}{\sigma_n}\right|_{\max} = \frac{1.07}{\lambda^{0.78}} \tag{2-71}$$

In general, the experimental results reported by Vissat and Buono validated Beskin's conclusion that (a) flexibility factor derived using long-radius theory should apply almost equally as well as to short-radius bend, and (b) stress-intensification factor calculated using the long-radius theory are not applicable to short-radius bend and elbows.

In 1957, Turner and Ford [31] gave a fairly extensive review of the various analytical methods for pipe bends and provided a detailed numerical analysis using shell theory. The so-called long-radius assumption was eliminated in their numerical analysis. In 1966, Findlay and Spence [35] made an experimental analysis for in-plane bending of a 90-deg pipe bend and found that the theory by Turner and Ford [31] gave the best comparison with the experimental results. However, it was impractical to solve for stresses without the aid of a computer.

In 1967, Jones [36] presented a theoretical analysis on in-plane bending of short radius pipe bend as a generalisation of the von Karman theory of pipe bend [2]. The theory of von Karman has been established on the basis of long radius bend in which the shifting of neutral axis toward the centre of curvature has been neglected. The theory developed by Jones for short radius elbow shows that there is a shifting of the neutral axis toward the centre of curvature.

In 1967, Smith [37] followed the approach of Turner and Ford [31] to develop a numerical analysis for out-of-plane bending case. The basic assumptions were similar to those made by Turner and Ford [31], applying small deformation theory and omit the long radius assumption. The analysis by Turner and Ford [31] for in-plane bending and by Smith [37] for out-of-plane bending formed the basis for BS806 [98] design curve for pipe bends.

In 1968, Cheng and Thailer [40] presented a general solution of a curved tube under in-plane end-moment using thin shell theory. They derived the identical equilibrium and compatibility equation to those derived by Clark and Reissner [20]. By minimizing the complementary energy using the Rayleigh-Ritz method, they further show that their solution is valid for any value of radius ratio r/R.

The most complete 'closed form' solution to this problem was developed by Cheng and Thailer [41] in 1970. Their solution was based on the two differential equations for equilibrium and compatibility due to Clark and Reissner [20], but without their simplifying assumption that the radius ratio $1/\rho$ would be small. The results from their modified solution for flexibility factor was in a very good agreement with the asymptotic solution derived by Clark and Reissner. For stress-intensification factor however, they pointed out that the asymptotic solution of Clark and Reissner [20] is theoretically valid only for radius ratio equal to zero. For $1/\rho$ different from zero, they suggested using the modified asymptotic solution given below:

$$\gamma = 1.986\frac{\left(1-\nu^2\right)}{\lambda^{2/3}}\left[0.495\frac{1}{\rho}\frac{\lambda^{1/3}}{\left(1-\nu^2\right)^{1/6}}+1\right] \qquad (2-72)$$

For $\nu = 0.3$, equation (2-71) can be approximately reduced to:

$$\gamma = \frac{0.9}{\lambda^{2/3}}\left[\frac{1}{\rho}\lambda^{1/3} + 2\right] \qquad (2-73)$$

If the term in the square bracket is neglected, the eqn (2-72) reduced to the fatigue test result of Markl [23]. If only the radius ratio ρ is neglected, en (2-72) approached the asymptotic solution of Clark and Reissner [20].

The effect of radius ratio on flexibility and stress-intensification factors is more significant when bend angle and end constraints are also included. These effects will be reviewed in Chapter 3.

2.6 Pressure Reduction Effect

In section 2.4, it was mentioned that if a pipe bend is loaded by in-plane bending, this action tends to close the bend (decrease the radius of curvature) and its circular cross-section deforms into an approximately elliptical shape without appreciable change in 'perimeter'. Due to this mode of distortion of the cross-section, there will be a small change in the enclosed cross-section. It follows that if the pipe bend in this state of deformation is subjected to further internal pressure, the overall flexibility of the pipe must be expected to be somewhat smaller than in the absence of internal pressure, because the internal pressure tends to open the bend.

A detailed 'closed form' analytical solution for combined bending and pressure load is very difficult unless it is carried out through numerical analysis. The reason for this is the so-called "Haigh effect" [11]. The stresses in a pipe under internal pressure are essentially membrane, but any pipe, straight or curved, subjected to internal pressure departs significantly from simple bending theory, if the pipe cross-section is

not circular and secondary bending stresses occur in the region of geometric imperfection [115]. This large bending stress, induced by the tendency to become circular in cross-section, can be considered as being produced by incompatibility of deformation of membrane analysis [46]. The main reason is that the coupling of bending and pressure in the pipe bend is non-linear; while the applied moment tends to flatten the cross-section, the internal pressure works against this, trying to reduce the ovalisation and open up the bend, known as the Bourdon effect [16, 28]. The effect of internal pressure in an elastic curved pipe deforming due to in-plane closing bending is therefore to reduce its inherent flexibility. This effect is small for rather heavy pipe. For very thin pipe however, the effect of internal pressure can become pronounced, and cannot be neglected in flexibility and stress-intensification factors. The purpose of this section is to review the fundamental work to date on a pipe bend under combined bending and pressure.

In 1927, Wahl [7] addressed a question whether the steam internal pressure would reduce the cross-sectional flattening of a pipe bend resulting from bending load. A simple formula was derived by minimisation of the total potential energy based on a small deformation assumption. The symmetry condition was taken into account by considering only a quadrant of the ring. Due to internal pressure p, the vertical bulging Δy of the deformed oval cross-section would be reduced by the amount, $\in$ (Fig.2.19) and can be calculated as follows:

$$\frac{\in}{\Delta y} = \left(\frac{1}{1-\nu^2}\right)\frac{pr^3}{3D} \qquad (2-74)$$

where ν = Poisson's ratio

D = shell bending stiffness, as can be found in standard texts of shell theory:

$$D = \frac{Et^3}{12(1-\nu^2)} \qquad (2-75)$$

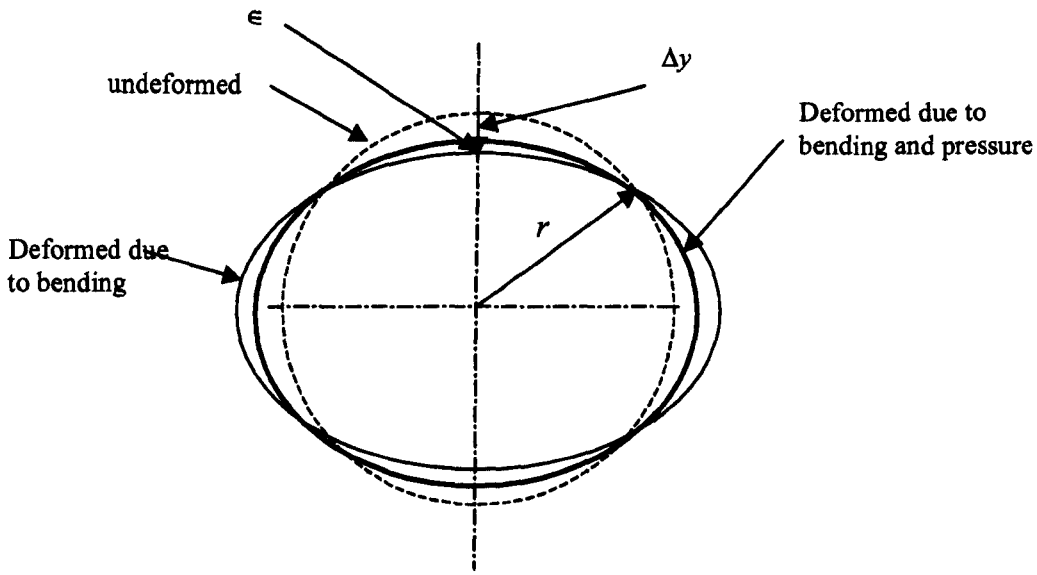

Fig.2.19 Effect of internal pressure on cross-sectional ovalisation

Equation (2-74) indicated that the pressure reduction effect on cross-sectional ovalisation is independent on the pipe bend radius *R*. Wahl [7] did not produce a closed form solution for the pressure reduction effect on flexibility and stress-intensification factors, only on the degree of ovalisation, ϵ.

The first theoretical approach to account for the effect of internal pressure on flexibility and stress factors was made by Kafka and Dunn [29] in 1956. The von Karman analysis for in-plane bending was extended to take the effect of internal pressure into account. In addition to the von Karman assumption, the following assumptions were incorporated in their theoretical development:

(1) The tube centerline is the neutral axis. For in-plane bending, therefore, the deformed cross-section is considered symmetrical in the plane of the bend and perpendicular to the plane of the bend, from which it follows that the tangential displacement of nodes at crown, intrados, and extrados are zero.

(2) The circumferential middle surface is inextensible, and a filament in this direction is distorted by pure bending only

(3) The longitudinal middle surface is extensible, and a filament in this direction is distorted by normal force only.

As in von Karman's analysis, Kafka and Dunn used the principle of minimum potential energy. The total strain energy in the tube wall per unit length when an element of a pipe bend of the angle $d\alpha$ is increased to $d\alpha + \Delta d\alpha$ (Fig.2.20) was approximately given as follows:

$$U = \frac{1}{2}\int_0^{2\pi} rN_\theta \varepsilon_\theta + \frac{1}{2}\int_0^{2\pi} rM_\phi \chi_\phi \qquad (2\text{-}76)$$

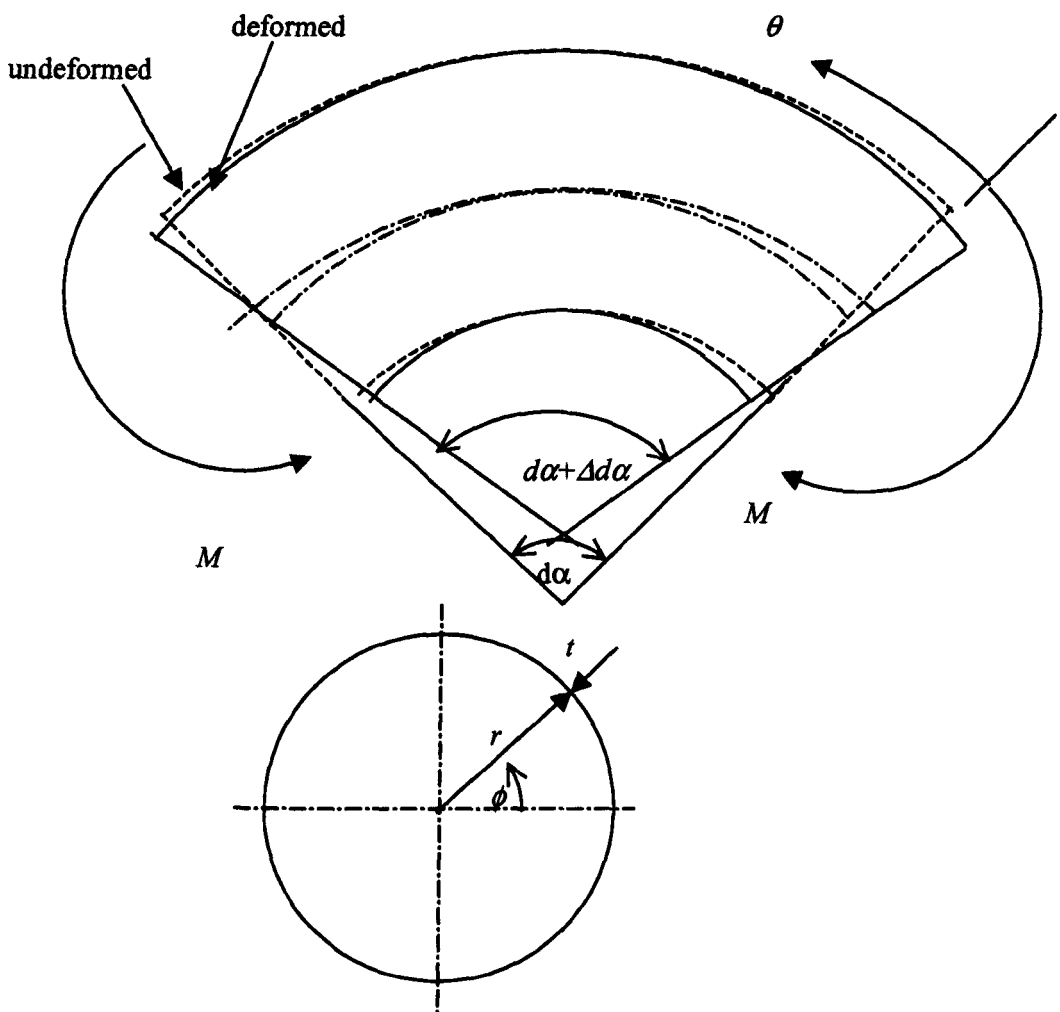

Fig.2.20 Element of a pipe bend subjected to in-plane bending

The first and second term in the right hand side of equation (2-76) is the strain energy due to normal force in the longitudinal direction and due to bending in the

circumferential direction respectively. The terms under the integral are the membrane force and bending moment in a shell of revolution, which are related to the strains of the middle surface and changes in curvature respectively in the following well-known relations:

$$\left.\begin{aligned} N_\phi &= \frac{Et}{1-\nu^2}\left[\varepsilon_\phi + \nu\varepsilon_\theta\right] \\ N_\theta &= \frac{Et}{1-\nu^2}\left[\varepsilon_\theta + \nu\varepsilon_\phi\right] \end{aligned}\right\} \qquad (2\text{-}77)$$

$$\left.\begin{aligned} M_\phi &= -D\left[\chi_\phi + \nu\chi_\theta\right] \\ M_\theta &= -D\left[\chi_\theta + \nu\chi_\phi\right] \end{aligned}\right\} \qquad (2\text{-}78)$$

where N = stretching stress resultants, N/mm

M = bending stress resultants, N.mm

E = Young's modulus, N/mm^2

t = wall thickness, mm

ν = Poisson's ratio

D = shell bending stiffness, eqn (2-75)

χ = shell curvature

If a pipe bend is considered as part of a toroidal shell, the mid-surface stretching strains, ε_θ, ε_ϕ, and curvatures, χ_θ χ_ϕ in the equations (2-77) and (2-78) can be related to the tangential displacement, v, and radial displacement, w as follows:

$$\varepsilon_\phi = \frac{1}{r}\left(\frac{dv}{d\phi} - w\right) \qquad (2\text{-}79a)$$

$$\varepsilon_\theta = \frac{\sin\phi}{R}(v\cot\phi - w) + \rho(\theta) \qquad (2\text{-}79b)$$

$$\chi_\phi = \frac{1}{r^2}\frac{d}{d\phi}\left(v + \frac{dw}{d\phi}\right) \qquad (2\text{-}80a)$$

$$\chi_\theta = \frac{\cos\phi}{rR}\left(v + \frac{dw}{d\phi}\right) + \psi(\theta) \qquad (2\text{-}80b)$$

The terms $\rho(\theta)$ in eqn (2-79b) and $\psi(\theta)$ in eqn (2-80b) represent additional longitudinal strain and additional change in curvature respectively due to bending. On the assumption that the pipe centreline is the neutral axis, Kafka and Dunn gave the functions of $\rho(\theta)$ and $\psi(\theta)$ as follows:

$$\rho(\theta) = \frac{r \sin\phi}{R} \frac{\Delta d\theta}{d\theta} \tag{2-81}$$

$$\psi(\theta) = \frac{\sin\phi}{R} \frac{\Delta d\theta}{d\theta} \tag{2-82}$$

The energy stored in the system, which must be minimised, is then:

$$U' = U - p.\Delta A \tag{2-83}$$

where $p.\Delta A$ is the elastic work done on the tube wall by the internal pressure during deformation of the cross-section, acting against the deformed condition caused by bending and ΔA is the changes in pipe bore area (the area of quadrilateral ABB'A' in Fig.2.21).

Based on assumption (1) of the above, Kafka and Dunn further expressed the tangential displacement in the form of a trigonometric sine series:

$$v = \sum_{1}^{\infty} C_k \sin 2K\phi \tag{2-84}$$

And from assumption (2), the radial displacement is obtained from eqn (2-79a):

$$w = \frac{dv}{d\phi} \tag{2-85}$$

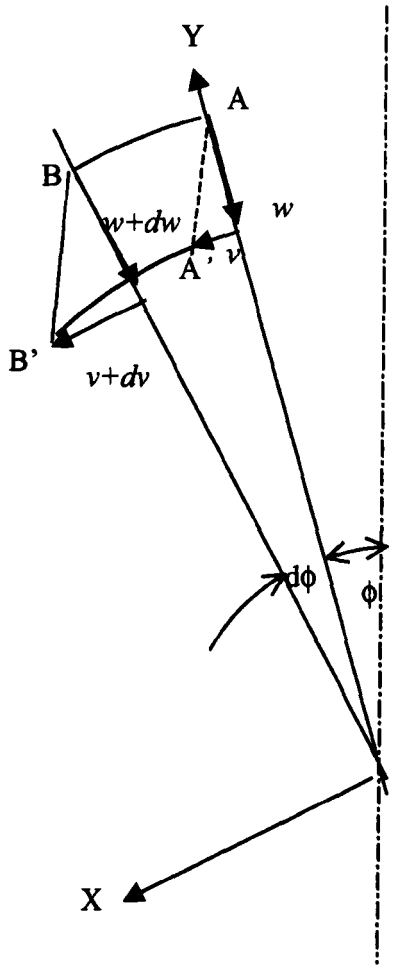

Fig.2.21 Distortion of an element of pipe cross-section

They further expressed the changes of pipe bore area ΔA as a function of the coefficients of the series of the tangential displacement, C_K, as follows:

$$\Delta A = -2\pi \sum_{k=1}^{\infty} \left(4K^4 - K^2\right) C_K{}^2 \qquad (2\text{-}86)$$

Using eqns (2-76) through (2-86), the total strain energy in eqn (2-83) then reduced to an equation as a function of the coefficients, C_K's. These coefficients are then determined by the minimisation of the total energy U':

$$\frac{\partial U'}{\partial C_K} = 0, \qquad K = 1,2,3,... \qquad (2\text{-}87)$$

Upon obtaining the C_K's, the total strain energy U' can be then set to be equal to the work done by applied end moment (Fig.2.20) from the principle of virtual work (external work equals internal energy):

$$U' = \frac{1}{2}\frac{M\Delta d\alpha}{Rd\alpha} \tag{2-88}$$

From eqn (2-88), the term $(\Delta d\alpha)/(d\alpha)$ can be found as a function of applied moment M. This term can be further divided by similar term for a straight pipe to find the flexibility factor.

For the first and second approximation to the trigonometric series of the tangential displacement, Kafka and Dunn obtained the following formula for flexibility factors:

$$k_1 = \frac{1}{1 - \dfrac{R^2 B^2 \left(1-\nu^2\right)}{EAtr^3}} \tag{2-89a}$$

$$k_2 = \frac{1}{1 + \dfrac{R^2\left(1-\nu^2\right)}{\pi Etr^3}\left[a_{11}\rho_1^2 + a_{22}\rho_2^2 - 2a_{12}\rho_1\rho_2 - 2b_1\rho_1 - 2b_2\rho_2\right]} \tag{2-89b}$$

In the above, A, B, and the term in the square bracket of equation (2-89b) are functions of geometry of the pipe bend and internal pressure, p. These functions are given in Appendix C2

A stress-intensification factor, based on stress in the longitudinal direction, was also presented. For the first and second approximation to the series, the longitudinal stress-intensification factor was as follows:

$$\left.\begin{aligned} \beta_1 &= k_1\left(1 - \frac{2B}{rA}\right) && \text{for } \frac{6B}{A} < r \\ \beta_1 &= \frac{2}{3}k_1\sqrt{\frac{rA}{6B}} && \text{for } \frac{6B}{A} > r \end{aligned}\right\} \tag{2-90a}$$

$$\left.\begin{aligned} \beta_2 &= 1+\frac{4\rho_2-2\rho_1}{r} && \text{for } 60\rho_2+r>6\rho_1 \\ \beta_2 &= k_2\sqrt{z}\left[1-\frac{2z\rho_1}{r}-\frac{\rho_2}{r}\left(20z-24z^2\right)\right], && \text{for } 60\rho_2+r<6\rho_1 \end{aligned}\right\} \qquad (2\text{-}90b)$$

where

$$z=\frac{3\rho_1+30\rho_2-\sqrt{(3\rho_1+30\rho_2)^2-120r\rho_2}}{120\rho_2} \qquad (2\text{-}91)$$

Kafka and Dunn did not produce the circumferential stress-intensification factor, but indicated that this stress-intensification factor might be derived from:

$$\sigma_\phi=\frac{N_\phi}{t}\pm\frac{6M_\phi}{t^2} \qquad (2\text{-}92)$$

In 1957, Rodabaugh and George [30] revisited the work of Kafka and Dunn [29], also using a potential energy approach. A theoretical analysis for flexibility and stress-intensification factor for a pipe bend under pure in-plane and out-of-plane bending combined with internal pressure was developed. The effect of internal pressure was considered by simply extending the energy method used by von Karman [2] for in-plane bending and the energy method used by Vigness [13] for out-of-plane bending. The pressure effect was included in the solution as in Kafka and Dunn [29]: an extra potential energy term due to pressure acting on the change of area of the cross-section resulting from ovalisation due to bending. The equations were based on second-order approximation to thin shell theory and assumed the bend cross-section initially circular and that the end effects are negligible. It was shown that the flexibility factor not only depends on pipe bend parameter λ, but also depends on internal pressure parameter ψ, where:

$$\psi=\frac{pR^2}{Ert} \qquad (2\text{-}93)$$

The flexibility factors for a pressurised pipe bend was then finally expressed in the form:

$$k_p = \frac{k}{1+6\left(\frac{p}{E}\right)\left(\frac{r}{t}\right)^{7/3}\left(\frac{R}{r}\right)^{1/3}} \tag{2-94}$$

where, k is flexibility factor in the absence of internal pressure taken from the asymptotic solution of Clark and Reissner [20]. The second term of the denominator in equation (2-94) is the *pressure reduction effect* on the flexibility factor (pressure stiffening effect). This term is a function of non-dimensional pressure p/E, cross-section to thickness ratio r/t, and radius ratio R/r.

For a pipe bend under in-plane bending with internal pressure, the longitudinal and circumferential stress factor were then expressed in the following form:

$$\frac{\sigma_\theta}{\sigma_n} = \frac{k_p}{1-\nu^2}\left\{\mp 3d_1\nu\lambda\cos 2\phi + \left(1+\frac{3d_1}{2}\right)\sin\phi - \frac{d_1}{2}\sin 3\phi\right\} \tag{2-95a}$$

$$\frac{\sigma_\phi}{\sigma_n} = \frac{k_p}{1-\nu^2}\left\{\mp 3d_1\lambda\cos 2\phi + \nu\left[\left(1+\frac{3d_1}{2}\right)\sin\phi - \frac{d_1}{2}\sin 3\phi\right]\right\} \tag{2-95b}$$

where d_1 is defined as:

$$d_1 = \frac{3}{5+6\lambda^2+24\psi} \tag{2-96}$$

For a pipe bend subjected to out-of-plane bending and internal pressure the longitudinal and circumferential stress factors were given in the form:

$$\frac{\sigma_\theta}{\sigma_n}=\frac{k_p}{1-\nu^2}\left\{\pm 3d_1\nu\lambda\sin 2\phi+\left(1+\frac{3d_1}{2}\right)\cos\phi-\frac{d_1}{2}\cos 3\phi\right\} \quad (2\text{-}97a)$$

$$\frac{\sigma_\phi}{\sigma_n}=\frac{k_p}{1-\nu^2}\left\{\pm 3d_1\lambda\sin 2\phi+\nu\left[\left(1+\frac{3d_1}{2}\right)\cos\phi-\frac{d_1}{2}\cos 3\phi\right]\right\} \quad (2\text{-}97b)$$

Stress-intensification factors may be derived from equation (2-95) and (2-97), by differentiating with respect to circumferential angle ϕ. These equations indicated that the maximum stress is obtained for in-plane bending and that it occurs in the hoop direction at the inner surface as compression stress for in-plane closing moment and tensile stress for in-plane closing moment. In a similar form to equation (2-94), the stress-intensification factors for combined loading of bending and internal pressure were given in the following form:

$$\gamma_p=\frac{\gamma}{1+3.25\left(\frac{p}{E}\right)\left(\frac{r}{t}\right)^{5/2}\left(\frac{R}{r}\right)^{2/3}} \quad (2\text{-}98)$$

Equation (2-94) for flexibility factor and equation (2-98) for stress-intensification factor are adopted in the ASME code for power piping [114] and ASME code for process piping [120] to account for the pressure reduction effect. These equations are applied equally to account for the pressure reduction effect for both in-plane (closing and opening) and out-of-plane bending regardless the total angle of the bend, (it will be shown in this study using non-linear finite element analysis that the pressure reduction effect is not the same in magnitude for in-plane and out-of-plane bending. In addition, it will be shown that the pressure reduction effect for in-plane bending is different markedly for the closing and opening case).

In 1956, Crandall and Dahl [27] presented an alternative approach to account for the pressure reduction effect by following the general outline of Clark and Reissner [20] for the problem of in-plane bending load by using the differential equations for large deflection of thin shell, but did not really present any useful results. Calladine [91]

inspected some of the asymptotic calculations done by Crandall and Dall [27] and arrived at the following expression for flexibility factor:

$$k_p = \frac{k}{1+4.6\left(\frac{p}{E}\right)\left(\frac{r}{t}\right)^3 \lambda^{2/3}} \tag{2-99}$$

In 1959, Reissner [33] proposed a differential equation for the non-linear correction to originally curved tubes and introducing the effect of internal pressure on the bending of slightly curved tubes. The solution to this correction was given in the form of a trigonometric series:

$$\beta_m = \sum A_{mn} \sin 2n\phi \tag{2-100}$$

where β is a thin shell deformation variable being the rotation of the tangent to meridian of the cross-section. (Fig.2.16).

For the first and second approximation to this series, eqn (2-100), the flexibility factor can be expressed in the following form:

$$k_p = \frac{1+\frac{pr^3}{3D}+\frac{10\left(1-\nu^2\right)}{12\lambda^2}}{1+\frac{pr^3}{3D}+\frac{\left(1-\nu^2\right)}{12\lambda^2}} \tag{2-101a}$$

$$k_p = \frac{1+\frac{pr^3}{3D}+\frac{10\left(1-\nu^2\right)}{12\lambda^2}-f}{1+\frac{pr^3}{3D}+\frac{\left(1-\nu^2\right)}{12\lambda^2}-f} \tag{2-101b}$$

being the first (a) and second (b) approximation, where:

$$f = \frac{\frac{5(1-\nu^2)^2}{12\lambda^4}}{240 + 16\frac{pr^3}{D} + \frac{34(1-\nu^2)}{5\lambda^2}} \qquad (2\text{-}102)$$

When internal pressure $p = 0$, equation (2-101a) reduces to the formula given by von Karman.

In 1972, Blomfield and Turner [47] updated the numerical analysis of Turner and Ford [31] to solve the problem of in-plane bending of a pipe bends combined with internal pressure. Design curves for pipe bend under bending and pressure were derived from Blomfield and Turner [47] and well documented in the ESDU No.74043 [52]. In these curve, flexibility factor was plotted against pipe bend parameter, λ, for various values of internal pressure parameter, pR^2/Ert.

In 1972, Dodge and Moore [48] developed stress indices and flexibility factors of a pipe bend by modifying the minimum potential energy solution of Rodabaugh and George [30] to provide a more accurate approximation for the circumferential membrane stress and used it as a basis for a detailed stress index development. They used the experimental data obtained by Rodabaugh and George [30] for the case of in-plane bending as one problem and showed that the overall agreement for experimental stress is good for the inside and outside surface and especially good for maximum values. They concluded that the modified minimum potential energy solution to Rodabaugh and George [30] made by a correction on circumferential membrane stress was the most suitable analytical method for developing stress indices and flexibility factor for elbow and curved pipe.

The modified solution was solved by numerical analysis (and a FORTRAN computer code was released into the public domain). A parameter survey using pipe bend parameter λ, pressure parameter ψ, and radius ratio ρ, was carried out. Numerical values of $k_p(\lambda, \psi)$ were obtained from the equation below:

$$k_p = \frac{1}{1+\frac{3}{2}d_1} \tag{2-103}$$

where d_1 is given in equation (2-96).

Figure 2.22 shows the flexibility factor obtained by Dodge and Moore as a function of the pipe bend parameter λ and internal pressure parameter ψ.

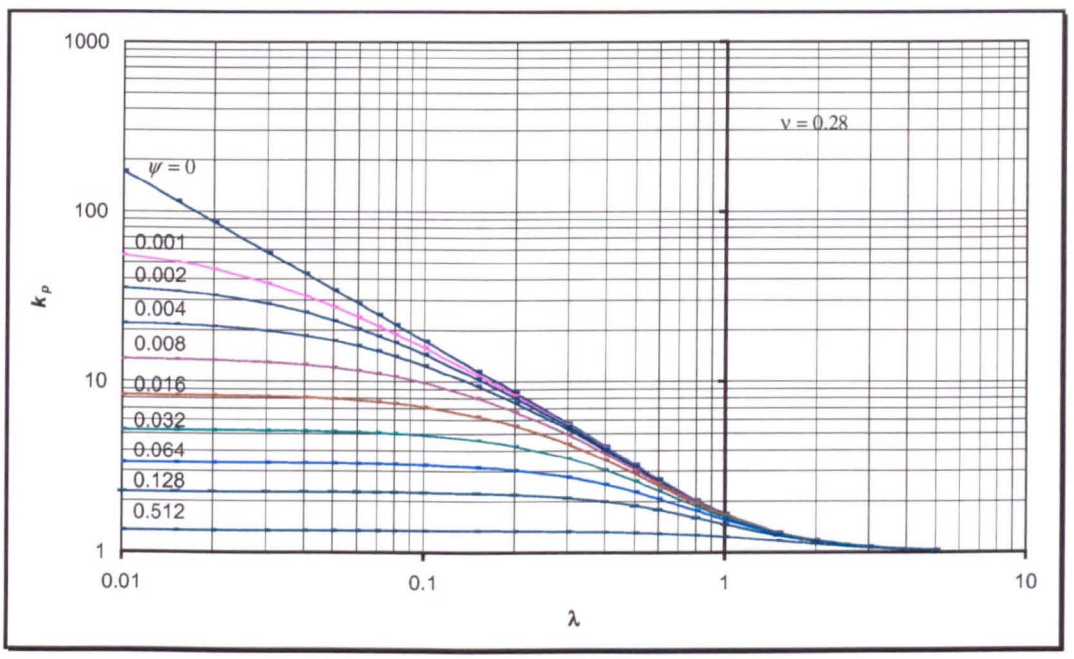

Fig.2.22 Flexibility factor for pipe bends under bending and pressure

From figure 2.22, Dodge and Moore further gave a closed form solution for flexibility factor of pressurised pipe bends:

$$k_p = \frac{1.66\lambda^{-1}}{1+1.75\lambda^{-4/3}\exp\left(-1.15\psi^{-1/4}\right)} \tag{2-104}$$

Using this modified solution, Dodge and Moore further suggested using the following equations for circumferential stress factors of piping elbows under in-plane and out-of-plane bending respectively in place of equation (2-95b) and (2-97b) of Rodabaugh and George [30] formula:

For in-plane bending:

$$\frac{\sigma_\phi}{\sigma_n}=\frac{k_p}{1-\nu^2}\left\{\mp 3d_1\lambda\cos 2\phi-\frac{1}{\gamma}\left[\left(1+\frac{3d_1}{2}\right)\cos\phi-\frac{d_1}{6}\cos 3\phi\right]\cos\phi\right\} \qquad (2\text{-}105)$$

For out-of-plane bending:

$$\frac{\sigma_\phi}{\sigma_n}=\frac{k_p}{1-\nu^2}\left\{\mp 3d_1\lambda\sin 2\phi+\frac{1}{\gamma}\left[\left(1+\frac{3d_1}{2}\right)\sin\phi-\frac{d_1}{6}\sin 3\phi\right]\sin\phi\right\} \qquad (2\text{-}106)$$

In 1980, Boyle and Spence [67] developed a simple elastic analysis for the behaviour of an oval cross-section pipe bend under in-plane bending and internal pressure as part of a study of out-of-round and variable thickness pipes. The problem was solved using the theorem of minimum potential energy of a ring section of unit length. For the special case of circular cross-section pipe bend under bending and internal pressure, a simplified flexibility factor was obtained as follows:

$$k=\left(1-\nu^2\right)\frac{1+\dfrac{5}{6\lambda^2}+\dfrac{pr^3}{3D}}{1+\dfrac{1}{12\lambda^2}+\dfrac{pr^3}{3D}} \qquad (2\text{-}107)$$

Finally, Orinyak [102] in 1997 developed a formula for determining the amount of 'restoration' toward its original circular shape of an oval shape deformed cross-section pipe bend due to in-plane bending. Referring to Fig.2.19, the formula proposed was as follows:

$$\frac{\epsilon}{\Delta y} = \frac{3D}{3D + PR^3 t} \tag{2-108}$$

where Δy is the vertical bulging of pipe bend cross-section due to in-plane bending as given by the following:

$$\Delta y = \left(1 - \nu^2\right)\frac{4MR^2}{Et^3} \tag{2-109}$$

Unlike the formula shown by Wahl [7], eqn (2-74), the formula presented by Orinyak for the effect of internal pressure on cross-sectional ovalisation show a dependency on pipe bend radius R.

The analytical solutions of Kafka and Dunn [29], Rodabaugh and George [30], Reissner [33], and finally Dodge and Moore [48] remarkably remain the few studies which aim to produce a simple explanation and analysis of the pressure reduction effect on the mechanics of pipe bend behaviour. As will be seen in the next chapter, the problem has not even been re-examined in much detail in the more recent literature.

2.6 Summary

A comprehensive review of the theoretical development of the flexibility and stress-intensification factors of pipe bend has been presented. It should be noted that the main feature of the theories is that they involve some assumptions in order to simplify the problem. The 'long radius assumption' is probably the most difficult assumption to be omitted. With this assumption, the problem of the bending of a pipe bend become so simple and a closed form solution for the flexibility and stress-intensification factor become possible to be developed. The 'inextensibility' assumption of the mid-surface in the circumferential direction is also hardly omitted in the theoretical analysis of the bending of pipe bend. All the theoretical analysis

reviewed above ignore 'end effects' (and make the pure bending assumption). The pressure reduction effect on the flexibility and stress-intensification factors have been equally applied to both in-plane (closing and opening) and out-of-plane bending, regardless of the total angle of the bend. It is however expected that the pressure reduction effect should be different for these three directions of moment, as the stiffness of a pipe bend is different for in-plane closing and opening moment as well as out-of-plane moment. In addition, a pipe bend would tend to behave as a straight pipe as the total angle of the bend approaches hypothetically zero. Some investigators have tried to develop a theoretical analysis, taking the effect of bend angle into account, however, the analysis was not clear from the assumptions. Finite element analysis could be an alternative to carry out parametric studies in order to obtain closed form solution for the flexibility and stress-intensification factors of pipe bends. In the next chapter, an extensive review on finite element modelling and analysis of piping elbows is presented. Using finite element methods, the 'end effects' can be taken into account.

Appendix C2

Equations in this appendix are taken from Kafka and Dunn [35] for calculation of flexibility and stress-intensification factor corresponding to Equations (2-89) through (2-91):

$$A = \frac{5}{2}\frac{Etr}{R^2\left(1-\nu^2\right)} + \frac{36D}{r^2}\left(\frac{1}{r} + \frac{4\nu}{15\pi R}\right) + 12P \qquad \text{(A2-1)}$$

$$\mathrm{B} = \frac{3}{2}\frac{Etr^2}{R^2\left(1-\nu^2\right)} + \frac{4D\nu}{\pi Rr} \qquad \text{(A2-2)}$$

$$\mathrm{D} = \frac{\mathrm{Et}^3}{12\left(1-\nu^2\right)} \qquad \text{(A2-3)}$$

$$\mathrm{a}_{11} = \frac{5}{2}\frac{\mathrm{E}\pi\mathrm{tr}}{\mathrm{R}^2\left(1-\nu^2\right)} + \frac{36\pi\mathrm{D}}{\mathrm{r}^3} + \frac{144\nu D}{15Rr^2} + 12\pi P \qquad \text{(A2-4)}$$

$$\mathrm{a}_{12} = \frac{5}{4}\frac{E\pi tr}{R^2\left(1-\nu^2\right)} + \frac{96}{7}\frac{\nu D}{Rr^2} \qquad \text{(A2-5)}$$

$$\mathrm{a}_{22} = \frac{17}{2}\frac{E\pi tr}{R^2\left(1-\nu^2\right)} + 3600\frac{\pi D}{r^3} + \frac{1600}{7}\frac{\nu D}{Rr^2} + 240\pi P \qquad \text{(A2-6)}$$

$$\mathrm{b}_1 = \frac{3}{2}\frac{E\pi tr^2}{R^2\left(1-\nu^2\right)} + \frac{4\nu D}{Rr} \qquad \text{(A2-7)}$$

$$\mathrm{b}_2 = \frac{8\nu D}{Rr} \qquad \text{(A2-8)}$$

$$\rho_1 = \frac{a_{12}b_2 + a_{22}b_1}{a_{11}a_{22} - a_{12}^2} \qquad \text{(A2-9)}$$

$$\rho_2 = \frac{a_{12}b_1 + a_{11}b_2}{a_{11}a_{22} - a_{12}^2} \qquad \text{(A2-10)}$$

CHAPTER 3

BEHAVIOUR OF PIPING ELBOWS: NUMERICAL AND FINITE ELEMENT ANALYSIS

A comprehensive literature review on the theoretical development of the behavior of pipe bends has been presented in Chapter 2. The aim there was to focus on the development of useful simple design formulae. The main feature therefore was that these analyses involve simplifying assumptions in order to make the problem solveable in closed form. Therefore so-called 'end effect', and the 'bend angle' are usually ignored in the theoretical analysis especially for 'long radius bend'. Accordingly, the stress values at any cross-section can be assumed proportional to the moment acting at that cross-section and not a function of length of the bend (pure bending assumption). An alternative approach in which the assumptions are more fundamental but less restrictive is provided by the use of numerical analysis and in particular finite element method. As computer technology advances, more and more powerful finite element analysis (FEA) software becomes available with innovative finite element technology. Application of the finite element method for the solution of the piping elbow has grown intensively. The flexibility of a pipe bend can be easily determined using a modern nonlinear finite element analysis. The versatility and cost-effectiveness of the finite element analysis in practical use allows detailed parametric study on the nonlinear behavior of a pipe elbow. The purpose of this chapter is now to present a review or summary of the work to date on numerical and finite element analysis of the behavior of piping elbows. The review will be focused on the application of available finite element program software for analyzing the behavior of piping elbows. This should provide a clear idea for modeling piping elbows, using ANSYS, as will be given in the next chapter. The review is not intended to go in detail on the formulation of the finite element itself, but it is rather intended to review finite element analysis of piping elbows.

3.1 Pipe Bends with End Constraints

In a real piping system, pipe bend may be connected to adjacent straight pipe by smooth welded joints as shown schematically in Fig.3.1(a), or alternatively it may be connected by flanged joints, as shown in Fig.3.1(b). For this case, the von Karman assumption of constant deformation and stresses along the length of the bend and independent of the subtended angle of the bend is no longer appropriate. When a bend is part of the real piping system, the ovalisation is constrained by the connection. This affects the flexibility and stresses to a greater or lesser extent depending on the types of end constraint. The effect of end constraint is much influenced by the radius ratio as well as the total bend angle.

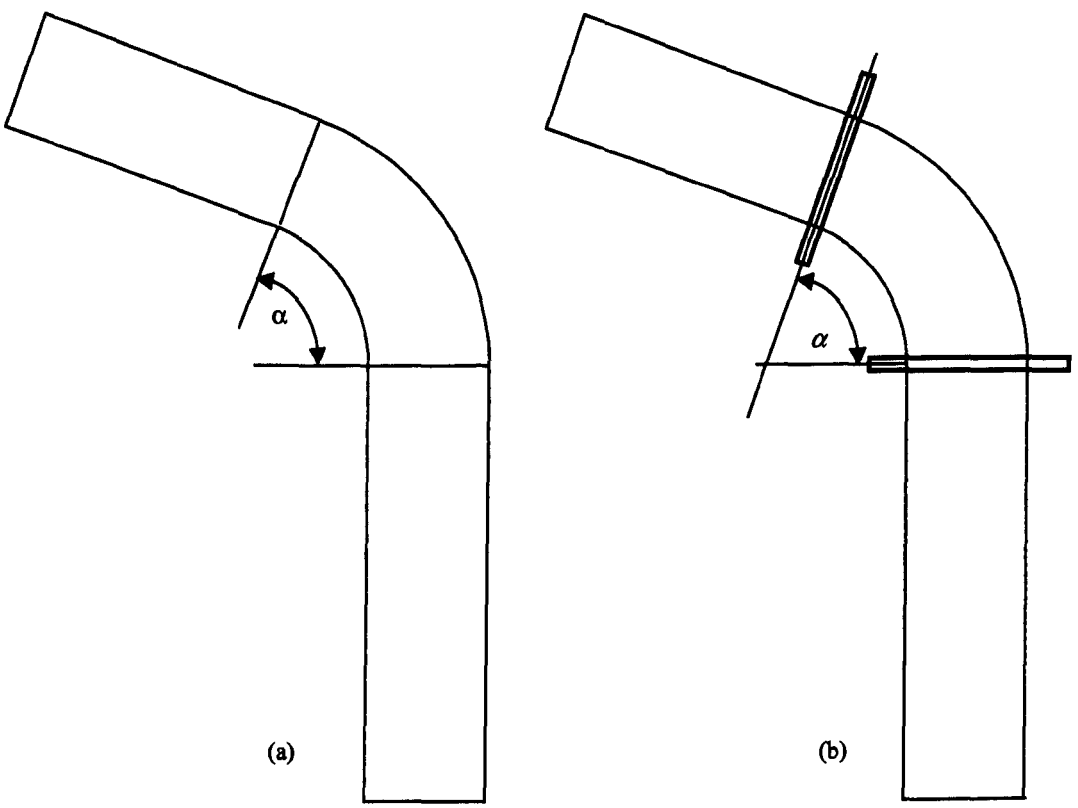

Fig.3.1 (a) Pipe bend jointed smoothly (tangent) to straight pipes, (b) Pipe bend joined to straight pipes by flanges

In 1946, Symonds and Vigness [15] presented some experimental results, which demonstrated the importance of end effects. Both flanged and tangent pipe constraints were considered and they showed that the most severe form of end constraint is flanged. The general conclusion from these studies was that the dependence of flexibility on radius ratio ρ can be neglected, but the stress distribution was affected significantly by radius ratio ρ.

In 1951, Pardue and Vigness [21] carried out experimental investigations on 90 and 180-deg return bends, thin-walled and short-radius, to study the effect of end restraints. They tested a series of tube bends having radius ratio (ρ) equal three and thickness to cross-section radius ratio (t/r) ranging from 0.015 to 0.044. They considered two main types of end constraint: (1) the tube bends were joined to straight tube at both ends of equal length greater than 5 times pipe diameter, typically as shown in Fig.3.1(a), and (2) the tube bend was terminated by flanges, typically as shown in Fig.3.1(b). It was found that elbows having radius ratio about two or three, were greatly affected by the length of the bends (total bend angle). As the angle of the bends decreased, the point of maximum stresses shifted toward the intrados, producing an increasing discrepancy between theory and experiment.

In a study of end effects, Gross and Ford [25] in 1952 experimentally determined the variation of ovalisation along the bend with flanged tangents and demonstrated the progressive decrease away from the mid-section of the bend. In the discussion to this paper, Pardue and Vigness published further experimental results and pointed out that the maximum hoop stress factor shifted from its normal position on the crown toward the intrados as the bend length decreased and end-constraint became more rigid.

In 1975, Natarajan and Blomfield [55] carried out finite element analysis to study the effect of end constraints on flexibility and stress factors of short-radius pipe bends under in-plane moment. For this analysis a doubly-curved thin shell element was formulated and used. The effect of flanges as well as straight tangents were considered. It was concluded that a flange does not have any effect on flexibility and

stresses of a pipe bend if it is located far from the bend-straight pipe junction. It was also found that the flexibility factors of a pipe bend with both ends of the tangent pipe terminated by flanges were lower than with one end flanged. For a short radius pipe bend with both ends terminated by a tangent, it was found that the maximum stress occurred on the inside surface of the mid-section at around 95-deg from the extrados in the hoop direction.

With regard to the arc length of the bends, the finite element analysis carried out by Natarajan and Blomfield [55] demonstrated that the relationship between flexibility factor and the bend angle could not be approximated as a linear relation. From a study of maximum stresses in pipe bends of different angles, but of same pipe bend parameters, it was found that the maximum stress occurred at the mid-section of the bend on the inside surface in the hoop direction for a 180-deg pipe bend and moved toward the intrados at 105-deg from the extrados for a 30-deg pipe bend. If the bend angle was further reduced, the maximum stress moved to the intrados at the outside surface along the longitudinal direction, thus behaving like a straight pipe.

In 1979, Findlay and Spence [63] presented a theoretical solution for the flexibility and of a pipe bend with end effects subjected to in-plane bending as an extension of the von-Karman analysis. The end restraint was rigid flanges at both ends of the bend as schematically shown in Fig3.2. The analysis was based on an energy method by representing the radial displacement, w, in the form of a Fourier series:

$$w = \sum_m \sum_n C_{mn} \cos 2n\phi \cos^2\left(\frac{m\pi}{\alpha}\right)\theta \qquad (3\text{-}1)$$

where $m = 1, 3, 5, \ldots$, and $n = 1, 2, 3, \ldots$

Eqn (3-1) indicated that some degree of ovalisation of the cross-section would be expected in the mid-section of the bend but the effect of the rigid flanges would be to retain the initial circularity at the ends. On the assumption of inextensibility of the

cross-section centerline on any longitudinal position, the corresponding tangential displacement becomes:

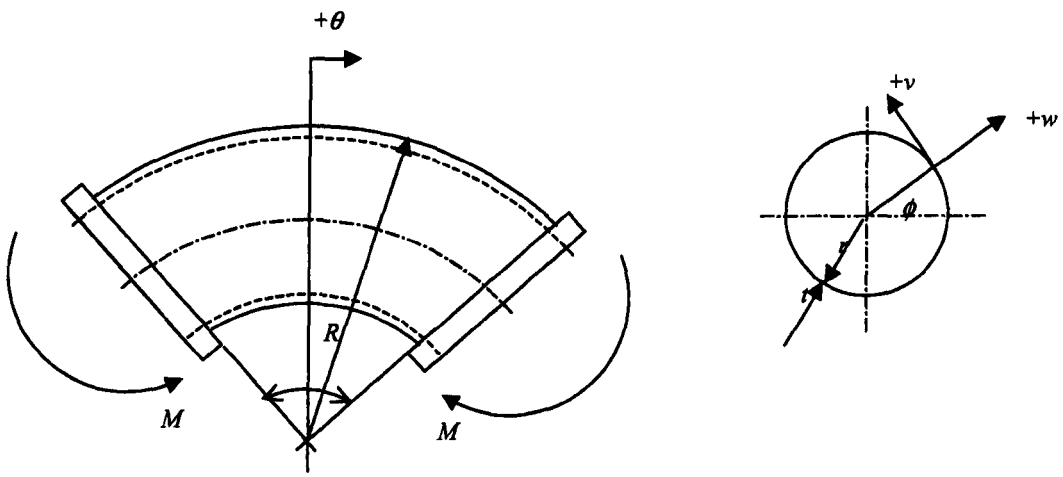

Fig.3.2 Pipe bend investigated by Findlay and Spence [63]

$$v = -\sum_m \sum_n C_{mn} \left(\frac{1}{2n}\right) \sin 2n\phi \cos^2\left(\frac{m\phi}{\alpha}\right)\theta \qquad (3-2)$$

With the assumption of a 'long-radius bend', and that the wall thickness is sufficiently 'thin', minimization of the total potential energy leads to the following equation for the overall flexibility factor:

$$k_\alpha = \frac{(\delta\alpha)EI}{MR\alpha} = \frac{1-\nu^2}{U_{\min}} \qquad (3-3)$$

Several useful graphs were produced, which showed that the flexibility of a pipe bend was greatly influenced by a rigid flange, being varied with pipe bend parameter, λ, and the total angle of the bend, α. Findlay and Spence [64] later presented a detailed experimental analysis together with a theoretical development for the stresses of the same problem. It was shown that the maximum stresses were greatly influenced by the flange constraints but the maximum stress for a 180-deg bend was not much different from the unconstrained Karman theory.

In 1979, Whatham and Thomson [66] presented an analysis of pipe bends with flanged tangents using the Novozhilov thin shell theory. Flexibility factors for 90 and 180-deg pipe bends with various lengths of flange tangent, L, (Fig.3.3) under separated loading of in-plane bending and pressure loading were presented. They concluded that flanged tangents do not affect the flexibility or stresses in a smooth pipe bend if the tangents are more than one-pipe circumference in length.

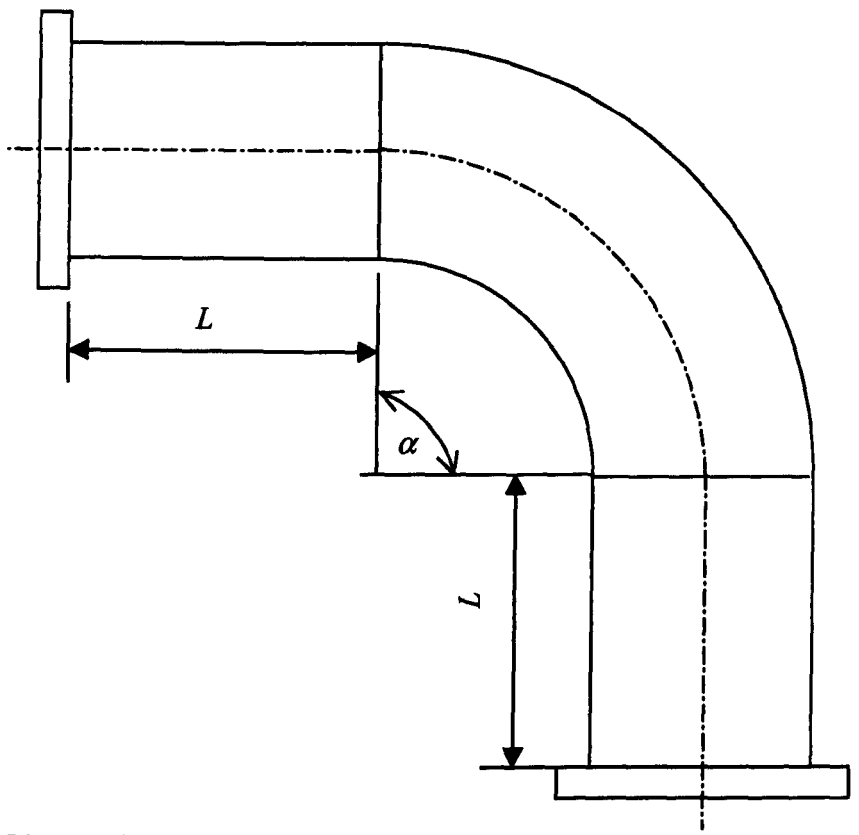

Fig.3.3 Pipe elbow with end flanged investigated by Whatham and Thomson [66]

In 1983, Spence and Thompson [83] presented an elastic analytical solution to obtain the maximum stress and flexibility factor of the flanged tangent smooth pipe bend under in-plane bending as investigated by Whatham and Thompson (Fig.3.2). The displacements were expressed in a trigonometric series and the displacement series coefficients were obtained by minimizing the total energy with respect to all of the unknown coefficients. It was shown that the flexibility of a pipe bend increased rapidly with increasing length of tangent until the tangent pipe length was approximately equal to the pipe circumference. The flexibility of bends connected to

tangent pipe was lower than predicted by theories ignoring end effects, particularly for pipe bends having angle less than 90-deg. It was noted that the difference in flexibility factor of bends with $\lambda = 3$ and $\lambda = 2$ was less than 6 percent for bend angles greater than 90-deg, but increased to 13 percent for 45-deg bends. The reduction of flexibility factor with bend angle was greater for a constant radius ratio, ρ.

The variation of flexibility factor with pipe bend parameter was found to be approximately linear in log-log plots for all bend angles and radius ratio. Based on this finding, Spence and Thomson proposed a formula for flexibility factor as follows:

$$\left.\begin{aligned} k &= \mu\frac{1.54}{\lambda} && \text{for } \rho = 10 \\ k &= \mu\frac{1.48}{\lambda} && \text{for } \rho = 3 \\ k &= \mu\frac{1.45}{\lambda} && \text{for } \rho = 2 \end{aligned}\right\} \qquad (3\text{-}4)$$

where μ is a correction factor whose values depend on radius ratio, ρ, and bend angle, α, as tabulated below:

ρ \ α	90-deg	45-deg	20-deg
10	0.96	0.88	0.66
3	0.92	0.75	0.47
2	0.89	0.68	0.41

With regard to the maximum stress, it was found that maximum hoop stress factor occurs approximately at $\phi = 95$-deg from extrados. This angle increases with lower bend angle and smaller radius ratio.

In 1986, Hubner [88] used a semi-membrane theory and adopted the long radius assumption to study the effect of end flanges on flexibility, cross-sectional distortion, and stress distribution of a pipe bend under in-plane bending. The stresses in the longitudinal direction were assumed as membrane states, while in the circumferential direction were assumed to be bending stress states. The theory developed was based on the thin shell assumption, small displacements, and the long radius assumption. However, Hubner did not produce any useful graphs or closed form solutions for cross-sectional ovalisation, flexibility, and stress-intensification factors.

In 2002, Orynyak [124] presented a theoretical study of the effect of end constraints on cross-sectional ovalisation of a pipe bend. Three special cases of end effect of 90-deg pipe bends were considered: (1) rigid fixation at both ends as shown in Fig.3.4(a), (2) Fixation at both ends by thin rigid plate as shown in Fig.3.4(b), and (3) both ends are connected to straight pipe tangent to the bend as shown in Fig.3.4(c). The results were presented in the form of charts only for the circumferential displacement at the mid-section of the bends.

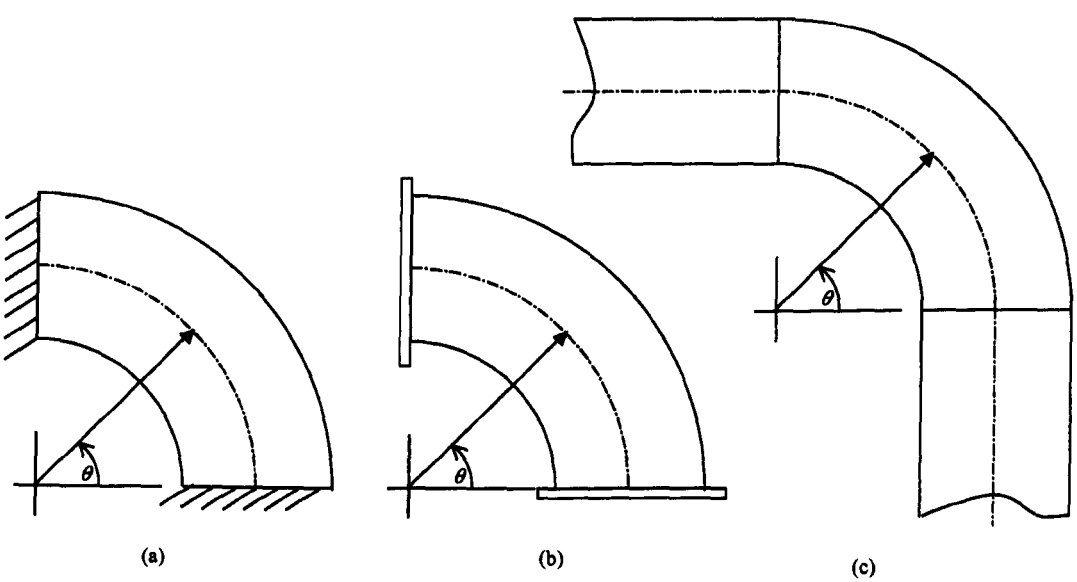

Fig.3.4 Types of end effects considered in Orinyak' analysis [124]

3.2 S-Shaped Back-to-Back Pipe Bends

Natarajan and Blomfield [55] further extended their finite element analysis of end effects on flexibility and stress factors of pipe bends under in-plane moment to study the behaviour of 90-deg S-shaped back-to-back bends as shown in Fig.3.5. For this kind of bend connection under an in-plane moment as shown, the lower bend (bend A) is subjected to closing moment and the upper bend (bend B) is subjected to opening moment. It was found that the flexibility and stresses were reduced from the corresponding values of a single 90-deg bend. If they are connected to form an 180-deg bend, these factors are increased.

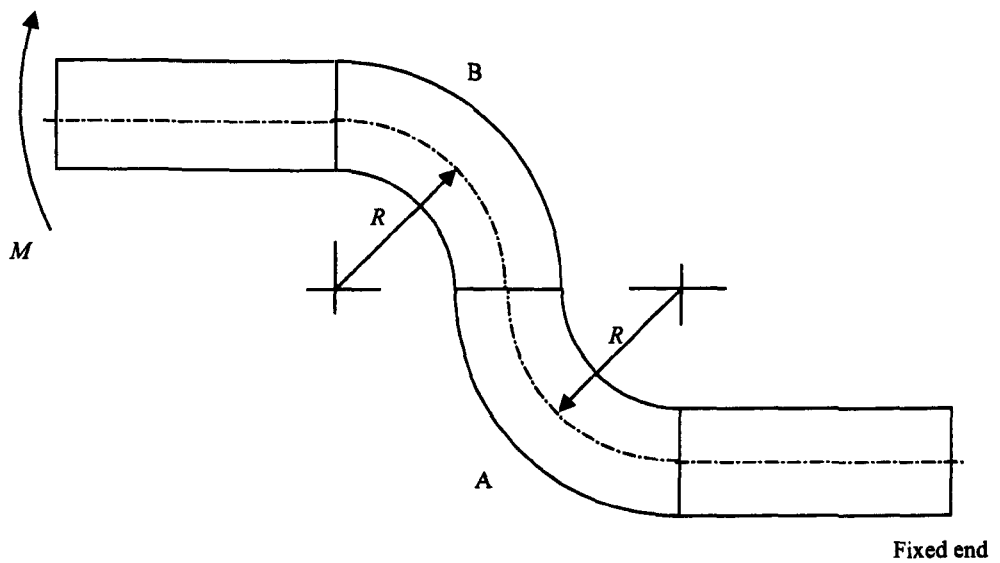

Fig.3.5 S-shaped back-to-back 90-deg pipe bends

In 1989, Glickstein and Schmitz [93] performed a further finite element study of the flexibility factor of S-shape back-to-back 90-deg pipe elbows with equal tangent as shown in Fig.3.5 as investigated by Natarajan and Blomfield [55]. The configuration of S-shaped elbow arrangement was further extended to include intermediate tangents. In their studies, the length of tangent was varied, and the bend angle consisted of 45 or/and 90-deg as shown in Fig.3.6. All the elbows analyzed had cross-section to thickness ratio of r/t = 32.5 and radius ratio ρ = 3.05. The thickness was 0.245-in and the maximum length of tangent was four times the cross-section radius. The pipe bend parameter λ was 0.0904.

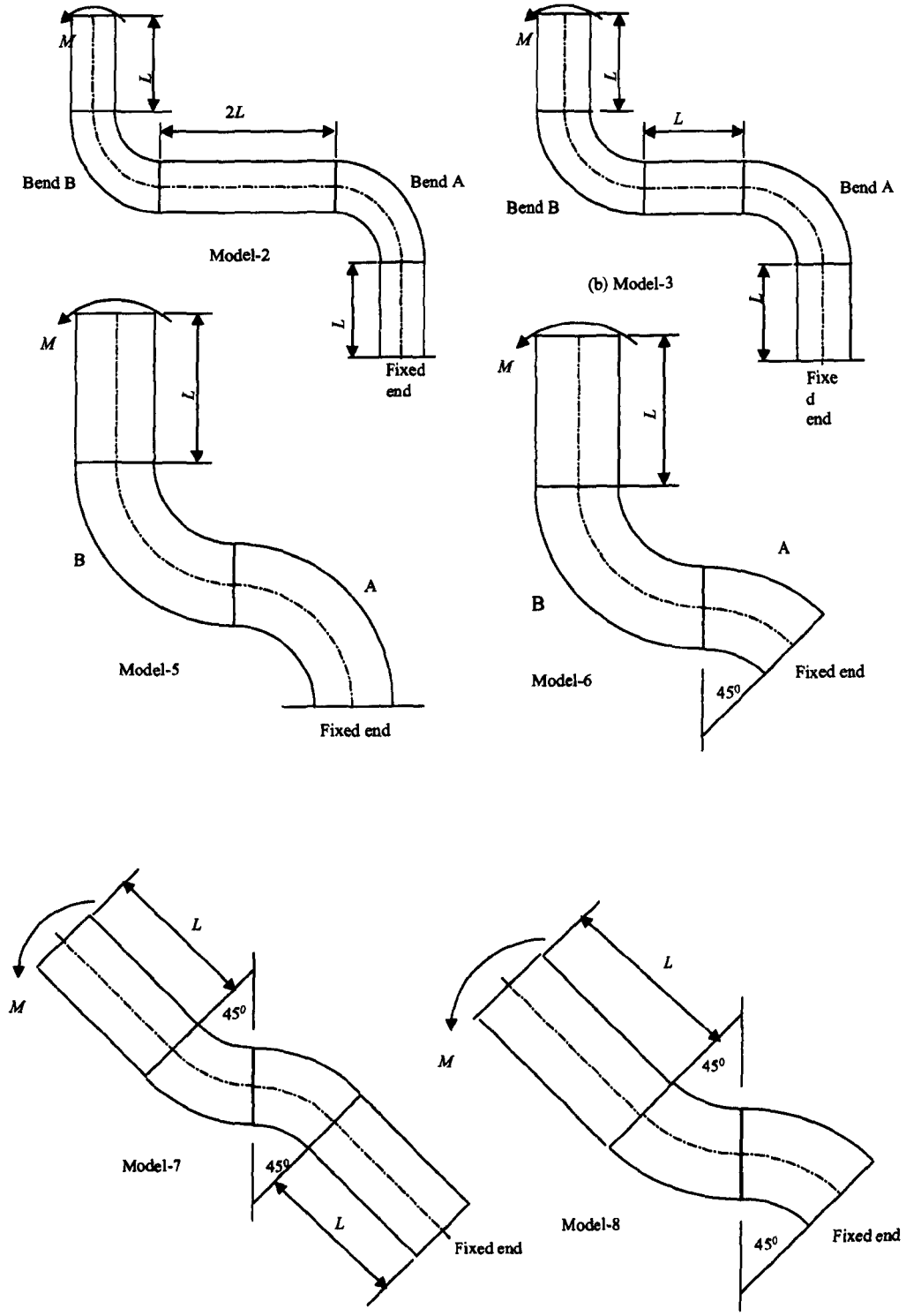

Fig.3.6 S-shaped model of pipe bends investigated by Glickstein & Schmitz [93]

The bend arrangement of Fig.3.5 as investigated by Natarajan and Blomfield [55] was model 4 in the analysis of Glickstein and Schmitz [93]. For this elbow arrangement, they found that the flexibility factor was 25 percent lower than the asymptotic formula of Clark and Reissner [20] for a single 90-deg bend. The flexibility of the fixed bend in model 5 was 154% lower than corresponding bend in model 4. It is surprising that the results presented by Glickstein & Schmitz show elbows under closing moment stiffer than under opening moment. This might not be expected, however, it should be noted that the analysis of Glickstein and Schmitz does not take the large deformation effect into account.

In 1991, Glickstein and Schmitz [96] presented a further analysis for this problem in regard of the maximum stresses. The main conclusion from their studies was that the restraining effect of back-to-back elbows causes a significant reduction in the stress-intensification factor.

3.3 FE Modeling for Pipe Elbow Analysis

This section is intended to present a brief review of finite element modeling in the analysis of piping elbows. This should provide a clear idea on the modeling aspects of piping elbow analysis for the studies carried out in the next chapter.

3.3.1 Piping Elbow Subjected to Bending

In 1974, Mello and Griffin [53] performed a series of inelastic (elastic-plastic) finite element analyses to determine the plastic collapse loads of 304 stainless steel, large diameter, long radius pipe elbows under in-plane closing moment. The analyses were based on nominal piping dimensions: the configurations of elbow consisted of straight tangent – quarter bend – straight tangent as shown in Fig.3.7. The specially developed constant bending, three-node, elbow element of the MARC Finite Element

Analysis program was used. In this special element, the end restraint of the straight pipe at the elbow intersection is neglected, assuming constant ovalisation of cross-section over the entire length of the bend (the pure bending assumption). Beam elements were used for the straight tangent. The analysis accommodated material strain hardening, stress redistribution, and ovalisation of the elbow cross-section. They pointed out that more integration points around the pipe circumference would give better results. This is expected, as more integration points are needed to reduce gross discontinuities in stresses around the circumference of the elbow.

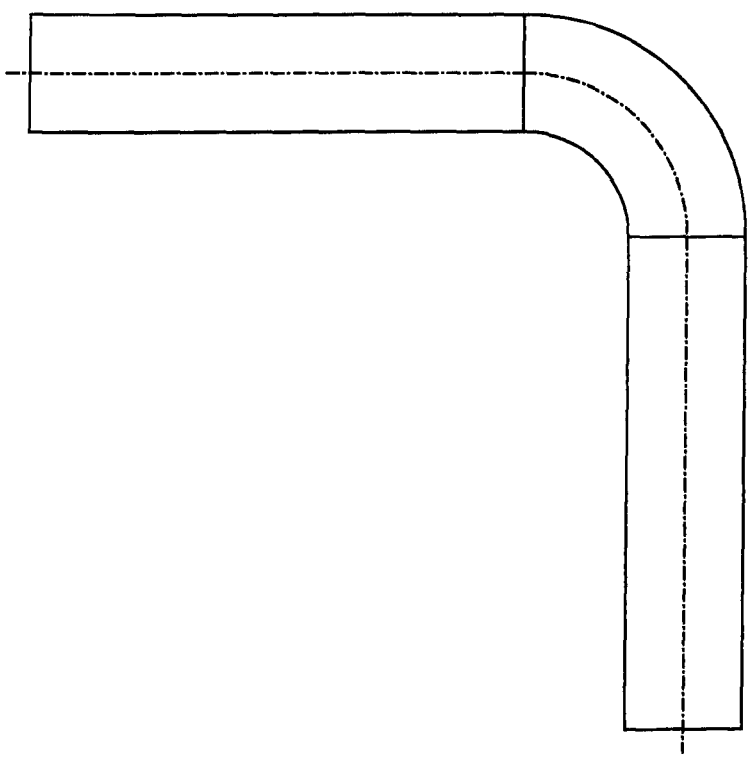

Fig.3.7 Piping elbow consists of straight tangent – quarter bend – straight tangent

In 1977, Kano et al [58] performed a three-dimensional finite element elastic analysis of a pipe elbow (Fig.3.7) under in-plane and out-of-plane moment. The elbow analyzed was thin-walled, large diameter and long radius, having 823.9 mm *OD*, 1219.2 mm bend radius (*R*), and 11.1 mm thickness (*t*), corresponds to 0.08 pipe bend parameter (λ). One end of the tangent was fixed and the other end subjected to in-plane and out-of-plane moment. The following three different models of element were used:

(1) Quadrilateral thin-shell element in the ANSYS program (SHELL43). Using this element, the elbow part was divided into 32 element in the circumferential direction and 20 element in longitudinal direction. Straight tangent was divided into 12 element in the axial direction.

(2) Quadrilateral high-order solid element in the ASKA program (HEXEC-27). Using this element, the number of element in the circumferential and longitudinal direction of the elbow was 16 and 10 respectively. The straight tangent was divided into 6 element in the axial direction. Only one element through the thickness of the elbow and straight tangent.

(3) Combination of elbow and beam element in the MARC program (ELEMENT 17 for the elbow and ELEMENT 14 for the straight tangent). The elbow part consisted of 32 integration points and 8 elements in the circumferential and longitudinal direction respectively.

With respect to stress distribution, fairly good agreement was obtained between the shell element of the ANSYS and solid element of the ASKA. Computed stress by the elbow and beam element of the MARC program were relatively large compared with those obtained by the other two models. They pointed out that this difference is due to the fact that the elbow elements are joined with the adjacent element only via the central position of the section and the individual elbow element can ovalise independently, thereby causing a rather high degree of ovalisation. In contrast to the shell element, it was connected with one another and the ovalisation thus becomes continuous in the axial direction due to the restraint by all adjacent elements.

In 1977, Sobel [60] used another special MARC pipe bend element (library element 17) to investigate the in-plane bending behavior of piping elbow. This element is an axisymmetric isoparametric shell element that has been modified through the addition of 'beam-type' deformation mode. The element assumes that each elbow element deforms uniformly over the entire length of the bend with the amount of the deformation being dependent on the magnitude of the applied bending moment. It does not account for the stiffening effect (end effect) provided by straight portions of the piping structures.

The elbow configuration consists of an elbow with straight tangent attached at both ends as typically shown in Fig.3.7. The end of one tangent was fixed and the end of the other tangent subjected to in-plane closing moment. A finite element convergence study was performed to find the optimum number of elements. Because the MARC 17 element cannot account for non-uniform ovalisation of the elbow cross-section due to end effects, only the number of integration points in the hoop direction was refined during finite element convergence analysis. The finite element convergence study was based on the hoop and axial stresses. The optimum (upper bound) number of integration points in the hoop direction was proposed as follows:

$$n_{opt} = \frac{17}{\lambda^{1/3}} \qquad (\lambda < 3.5) \qquad (3\text{-}5)$$

It was concluded that the maximum stress in a 90-deg elbow under in-plane bending is the hoop stress located very close to the crown at the inside surface, and shifted in a very small distance toward intrados as the radius ratio ρ, and pipe bend parameter λ, are decreased. This might also be true for a 180-deg pipe bend, but not for a pipe bend whose bend angle is smaller than 90-deg.

In 1979, Kano et al [65] performed a detailed finite element analysis to study the behavior of L-shaped and U-shaped pipe elbow assemblies loaded by in-plane and out-of-plane moments. The analysis was carried out using a doubly curved quadrilateral thin-shell element (ELBOW6) of the FINAS computer program. The elbow analyzed was 316 stainless steel, thin-walled, large diameter and long radius, having 812.8 mm *OD*, 1219.2 mm bend radius (*R*), and 11.1 mm thickness (*t*), corresponds to 0.0842 pipe bend parameter (λ). The elbow configurations investigated were as follows (Fig.3.8):

(1) L-shaped model: consists of straight pipe – quarter bend – straight pipe.
(2) U-shaped model-1: consists of straight pipe – 180 bend – straight pipe.
(3) U-shaped model-2: consists of straight pipe – quarter bend – straight pipe – quarter bend – straight pipe.

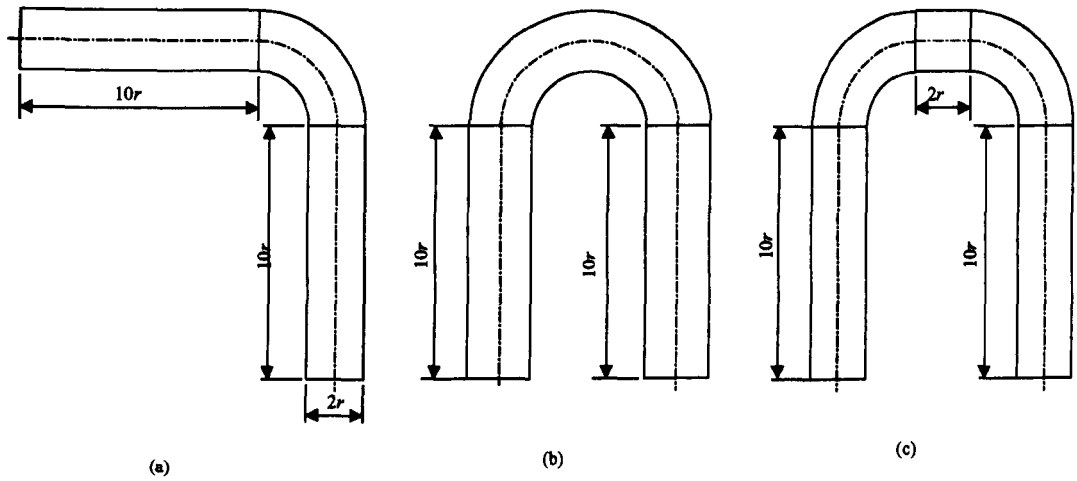

Fig.3.8 Piping elbow configuration considered by Kano et al [65]

The length of all straight tangents was 10 times the cross-section radius, except the intermediate tangent in U-shaped model 2 was 2 times the radius of the cross-section. One end of the assemblies was fixed and the other end subjected to in-plane and out-of-plane lateral load.

Comparing the U-shaped model of Fig.3.8(a) and (b), they noticed that there was a significant reduction of the maximum stresses at the center section of the assembly (50%) if an intermediate short tangent is inserted between the two 90-deg bend, particularly for in-plane bending. In general, the flexibility factor and stresses obtained using the detailed finite element analysis were lower than those obtained using the ASME Code Section III. The difference was even bigger for out-of-plane moment, especially for U-shaped bend where torsional moment is dominant at the mid-section of the bend.

In 1980, Dhalla [68] presented guidelines for selection of element size for a nonlinear finite element analysis of thin-walled piping elbows. The doubly curved rectangular isoparametric shell element of the MARC computer program was used. The length of straight tangent was eight times the cross-section radius. One end of the straight tangent was fully fixed and the other end subjected to an in-plane

moment. The moment loading was applied at a beam node located at the center of the end of the free tangent, schematically shown in Fig.3.9.

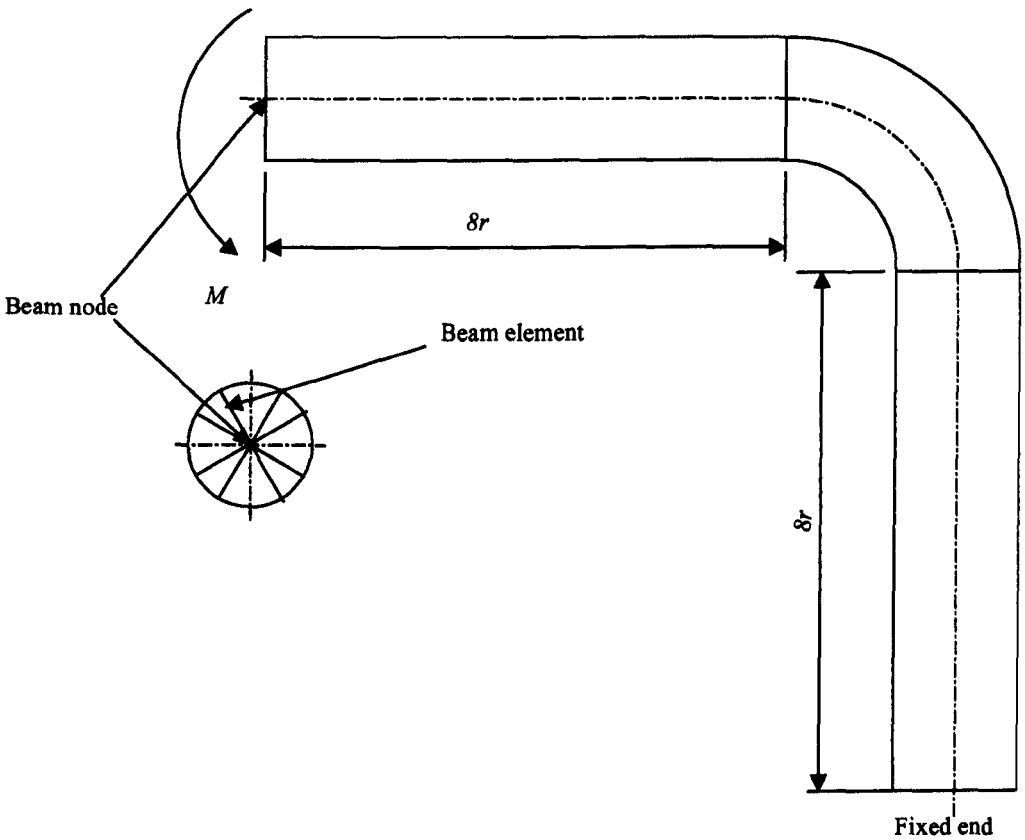

Fig.3.9 Pipe elbow considered by Dhalla [68] in a finite element study

A finite element convergence study was performed for elastic analysis under in-plane moment loading to take advantage of the symmetry in geometry and deformation, and accordingly, only one-quarter of the model was analyzed. The element size in both hoop (circumferential) and longitudinal direction was refined independently based on the observed hoop and longitudinal stress distribution around the mid-elbow cross-section. It was found that the longitudinal mesh refinement does not significantly influence either the overall deformation behavior or the maximum stresses (at the mid-section of the elbow).

In the study for the elastic-plastic collapse analysis, Dhalla further employed odd number of elements around the semi-circumference so that the center of one of the elements would be at the crown of the elbow where the maximum hoop stress is expected to be located at this position for a 90-deg pipe elbow. Large deformation effects were included in the analysis. Mesh refinement in the hoop direction was also performed in the plastic collapse analysis. It was concluded that the numerical accuracy of the plastic collapse load can be improved primarily by mesh refinement as well as load-step refinement, and not by the inclusion of large deformation effect.

In 1980, Sobel and Newman [70] performed a simplified nonlinear finite element analysis for the plastic bending of 304 strainless steel, 16-in piping elbow loaded by in-plane moment, again using the library element 17 of the MARC finite element analysis program. The main aim was to find the correlation of in-plane collapse load between finite element analysis and experimental results. The elbow configuration consisted of straight tangent–quarter bend–straight tangent (Fig.3.10). Each straight portion was modeled using a beam element (library element 14). The elbow part consisted of one element in the longitudinal direction and 34 integration points in the circumferential direction. One end of the tangents was fixed and the other end was subjected to an in-plane closing moment modeled as rotation controlled. Geometric nonlinear effects (large deformation) were included in the analysis. The deformation variable considered was rotation of the loaded end section, vertical displacement of the loaded end and the hoop strain at the mid-section of the bend. It was found that the maximum strain in an elbow was a hoop strain at the mid-section of the elbow located between 90 and 100-deg from extrados. The position of the maximum hoop strain was closer to ϕ =100-deg at the first load level and it progressively moved toward, and eventually became closer to, the crown with increasing load. This might be true also for elbow of 180-deg, but not for elbow whose bend angle is smaller than 90-deg, as it tends to behave like a straight pipe when the bend angle hypothetically approaches zero.

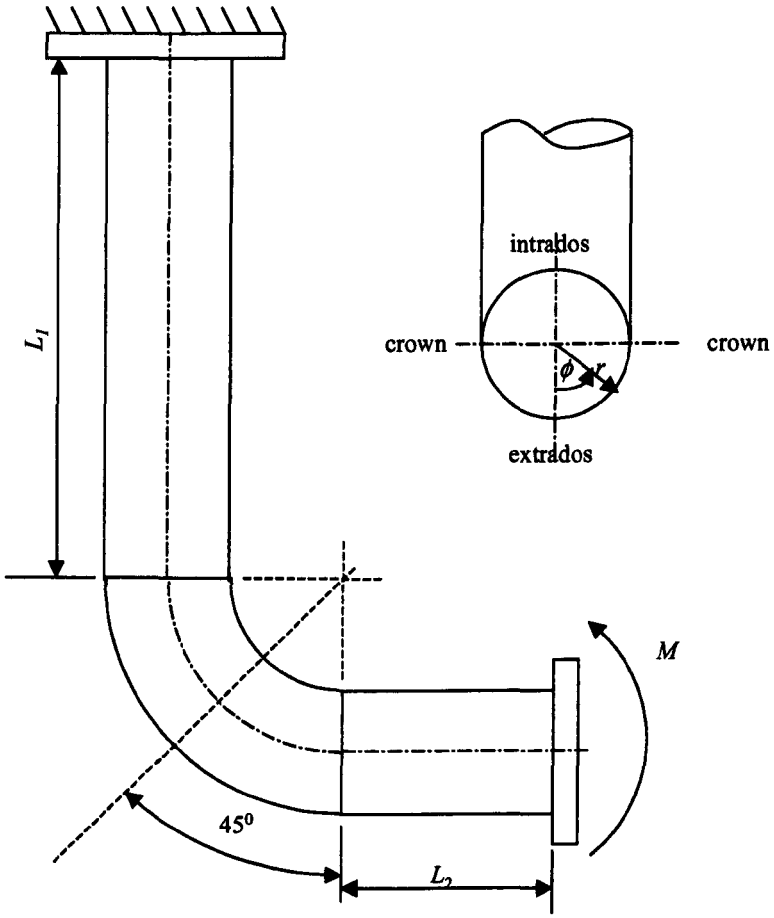

Fig.3.10 Pipe Elbow investigated by Sobel and Newman [70]

In 1982, Rodabaugh and Moore [77] presented the results of a finite element parametric study for short-radius elbows with long tangents under in-plane and out-of-plane moments. The parameters of interest were $\rho = 2$ and 3, bend angle (α) = 45. 90, and 180-deg. Pipe bend parameters (λ) were in the range of $0.05 \leq \lambda \leq 1.5$. Twenty-four models were analyzed for in-plane moment, M_i, and out-of-plane moment, M_o, using a finite element computer program EPACA and thick shell element. The model consisted of a bend with straight tangents attached at both ends (Fig.3.11). The boundary condition was fully fixed at one end of the tangent with the other tangent subjected to in-plane or out-of-plane moment.

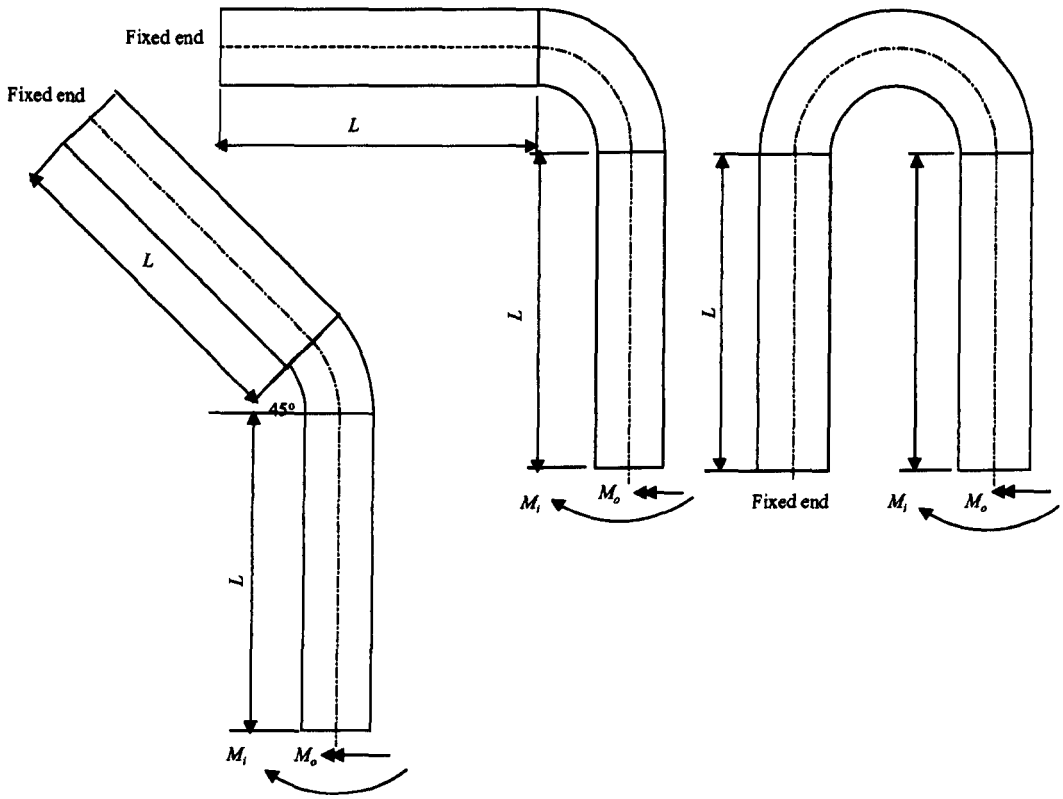

Fig.3.11 Pipe elbow configuration investigated by Rodabaugh and Moore [77]

It was found that the maximum stress in most of the elbows considered for the in-plane bending case occurred in the hoop direction on the inside surface located at the crown of the mid-section of the elbow. For some dimensions considered, the finite element results indicated inconsistency of the location of the maximum stress. The fundamental finding from their finite element study was that the maximum stresses for 90 and 180-deg elbows are not significantly affected by the straight long tangent. For 45-deg elbows, a significant reduction in maximum stress was apparent. They did not include elbows of bend angle less than 45-deg in their analysis, but recommended a simple formula for the stress index with the assumption that the stress index would be equal 1 for bend angle approaching zero. For out-of-plane moment, the maximum stress was found to be less than those for in-plane bending as expected, approximately by the ratio of $0.88\lambda^{2/3}$.

The finite element results also indicated that the flexibility factors of 180-deg elbows are about the same as for 90-deg elbows in the case of in-plane bending. With the judgment that the flexibility factors for 180-deg bends should be the same as given by the assumption of pure bending the following equations were recommended for the in-plane flexibility factors:

$$\left.\begin{aligned} k_i &= \frac{1.65}{\lambda}, && \text{for } \alpha \geq 180\text{-deg} \\ k_i &= \frac{1.30}{\lambda}, && \text{for } \alpha = 90\text{-deg} \\ k_i &= \frac{1.10}{\lambda} && \text{for } \alpha = 45\text{-deg} \\ k_i &= 1.00 && \text{for } \alpha = 0 \end{aligned}\right\} \qquad (3\text{-}6)$$

For out-of-plane bending, the equation below was proposed for flexibility factor valid for all values of bend angles:

$$k_o = \frac{1.25}{\lambda} \qquad (3\text{-}7)$$

Also in 1982, Thomas [78] applied the STAGSC finite difference thin shell computer program to analyze flexibility factor and stress indices of 90-deg pipe elbows under in-plane and out-of-plane bending. The symmetry condition in geometry and deformation for in-plane bending case was taken into account using only half of the circumference. The 'element size' of the elbow part in the circumferential and longitudinal direction was 15-deg and 7.5 deg respectively. The length of straight tangent was chosen to be 6 times the nominal radius. Two elbow geometries were analyzed, both having wall thickness (t) of 12.7 mm and radius ratio (R/r) of 3. The outside diameter was 610 mm and 914 mm which corresponds to pipe factors of 0.1304 and 0.0857 respectively. One end of the tangent was fully fixed and the other and subjected to bending moment applied as a line loading varying linearly across the pipe diameter as shown in Fig.3.12.

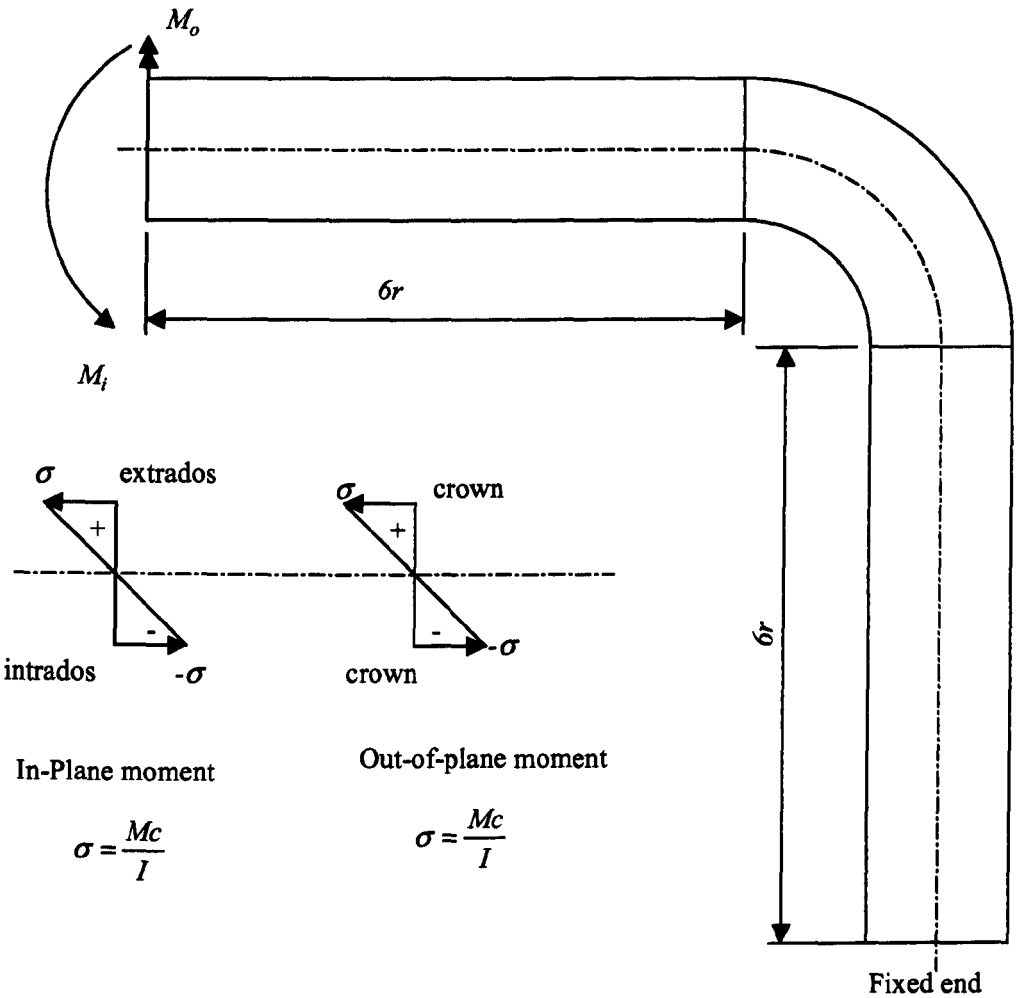

Fig.3.12 Pipe Elbow investigated by Thomas [78]

The flexibility factor was computed by linearisation of the axial displacement of the nodes at the bend-straight pipe junction to obtain the angular end rotation as the slope of the straight line. Thomas found that a tangent length of six times the cross-section radius was adequate to eliminate the end effect on ovalisation of the elbow cross-section. The elbow would be twice as stiff as an isolated elbow if a rigid flange was present at one end and a tangent pipe at the other end. The presence of a rigid flange near one end of the elbow shifted the maximum ovalisation from the mid-section of the elbow towards the other end. It was shown that in-plane and out-of-plane flexibility factors become nearly compararable if rigid flanges were attached at both ends of the elbow.

In 1986, Sobel and Newman [89] carried out simplified and detailed finite element analysis of piping elbows under in-plane closing moment. The elbow configuration considered and finite element procedure were similar to their earlier work in [70]. One end of the tangent was fixed and the other end subjected to an in-plane closing moment applied on the beam-node at the center of free end cross-section. In the simplified analysis, the special pipe bend element (MARC element 17) was again used to model the elbow part and the MARC beam element 14 was used to model the straight pipe portion. Consequently, the end effect provided by the straight pipe portion was neglected in this analysis. In the detailed analysis, an iso-parameteric, doubly-curved, quatrilateral shell element 4 was used for the entire component (elbow and straight tangent portion) which accounts for stress stiffening effect. The number of elements of the elbow part was 7 elements in the axial direction and 34 elements in the hoop direction. The total number of elements and nodes was 133 and 178 respectively. The deformation variables considered were the rotation of loaded end section, the vertical displacement of the center of this section, and the hoop strain at the crown for the outer surface. It was found that the moment-deformation curve predicted using the element 4 was in close agreement with the experimental moment-deformation curve. It was also shown that the element 17 analysis overestimated the experimental deformation, especially in the plastic region of the moment-deformation curve.

In 1987, Dhalla [90] performed a detailed nonlinear finite element analysis of two experimentally tested 16-in elbows loaded by in-plane moment. The elbow configuration and boundary conditions were similar to the analysis of Sobel and Newman [89]. Average dimensions were used which came from the pretest report. The study used the MARC fully compatible doubly curved isoparametric thin shell (library element 4) taking account of both geometric and material nonlinearity. The stiffening effect of the straight tangent welded to the ends of the bend was included in the analysis. The element size was based on the finite element convergence study performed by Dhalla [68] leading to the number of elements and nodes of 140 and 186 respectively. The analysis showed that the shell analysis predictions [90] were in

better agreement with the experimental results than the corresponding simplified pipe bend analysis since the latter neglects the end stiffening effect and elbow ovalisation.

In 1988, Fujimoto and Soh [92] carried out finite element analysis of thin-walled piping elbows under in-plane and out-of-plane moments. The elbow configuration analyzed consisted of a 90-deg bend connected with straight tangents at both ends (Fig.3.12). The length of each tangent was $7r$, where r is the cross-section radius. One end of the tangent was fixed and the other end was subjected to moment loading applied as shear loading. A parametric survey of pipe factors was performed in the region of $0.01 \leq \lambda \leq 0.2$. The radius ratio ρ was set to be 2 or 3. The 4-node isoparametric shell element of the MSC/NASTRAN finite element program was used for modeling. A flexibility factor under in-plane bending k_i was derived from the rotation θ_x, of the end section of the loaded tangent (Fig.3.13). Accordingly, the flexibility factor was calculated as follows:

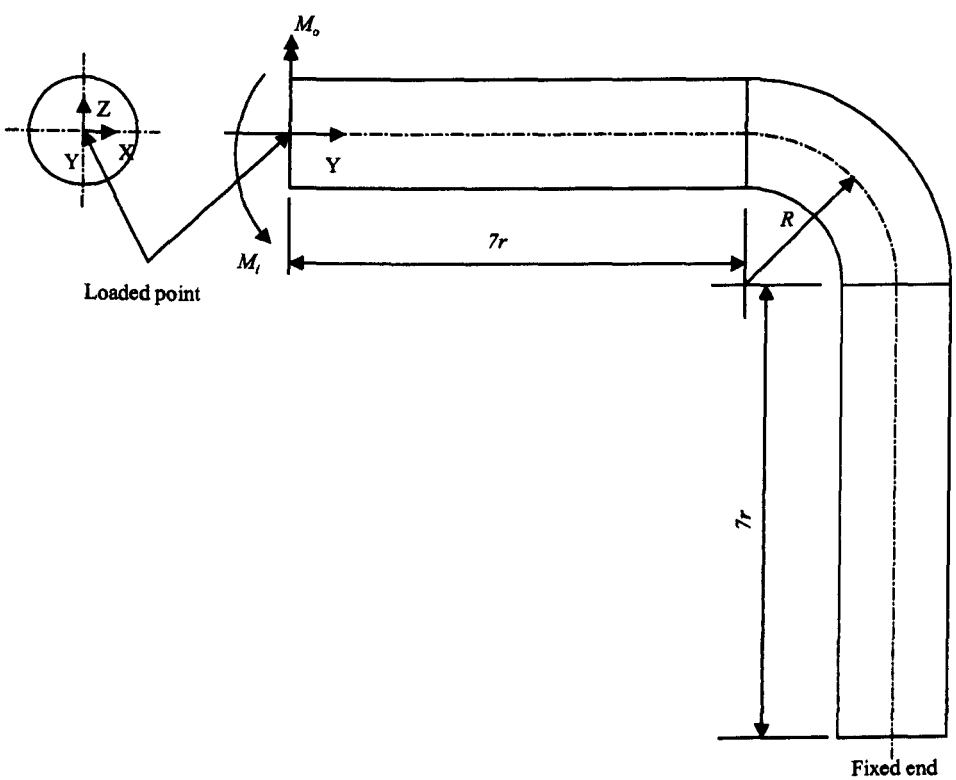

Fig.3.13 Pipe elbow investigated by Fujimoto and Soh [92]

$$k_i = \frac{\frac{EI\theta_x}{M_i} - 2L}{1.571R} \tag{3-8}$$

where E = Young's modulus, N/mm^2

I = second moment of area, mm^4

θ_x = in-plane rotation of the end section of the loaded tangent, rad

M_i = applied in-plane moment, N.mm

L = length of loaded tangent, mm

R = pipe bend radius, mm

A flexibility factor under out-of-plane bending k_o was derived from the rotation θ_y and θ_z of the end section of the loaded tangent. Accordingly, the flexibility factor was calculated as follows:

$$k_o = \frac{1}{2}\left(k_{oy} + k_{oz}\right) \tag{3-9}$$

where k_{oy} and k_{oz} are the flexibility factors under an out-of-plane moment M_y and M_z respectively, calculated using the following formulae:

$$k_{oy} = \frac{\frac{EI\theta_y}{M_o} + 0.65R}{0.5R} \tag{3-10a}$$

$$k_{oz} = \frac{\frac{EI\theta_z}{M_o} - 2.3L - 1.021R}{0.7854R} \tag{3-10b}$$

where θ_y = the rotation about Y-axis of the end section of the loaded tangent, rad

θ_z = the rotation about Z-axis of the end section of the loaded tangent, rad

M_o = applied out-of-plane moment, N.mm

It should be noted from the above formula that the flexibility of the straight tangents was included in the calculation of the flexibility factor for the pipe bend. Based on the above procedure, empirical formula for in-plane and out-of-plane flexibility factors was produced for radius ration $\rho = 2$ and 3 in the following form:

$$k = \frac{1.65}{\lambda}\left[a - \frac{b}{\lambda^c}\right] \tag{3-11}$$

where a, b, and c are constants whose values depend on the radius ratio ρ. It was observed that the formula proposed by Fujimoto and Soh, only the first term in the square bracket is important, while the second term could be neglected without significant loss in accuracy. It should be noted that large deformation effects were not included in their analysis. This form of formula, as well as similar forms for stress-intensification factors, will be examined in the Chapter 5 and the remaider of the thesis.

In 1989, Suzuki and Nasu [94] performed a nonlinear finite element analysis of 12-in and 24-in outside diameter but-welded elbows subjected to in-plane bending. The elbow configuration consisted of a 90-deg bend having radius ratio ρ equal 3 connected to straight tangents at both ends. The bends and straight pipes were modeled using the four-node flat shell element of the ADINA finite element analysis program having five degree-of-freedom per node. The main aim was to verify the accuracy of this element in comparison with the experimental data. The number of elements in the longitudinal direction of the elbow part was 20. The number of elements in the circumferential direction was 24 elements around the semi-circumference. The element size in the hoop direction was finer around the crown (30-deg toward intrados and extrados), being 5-deg per element. The element size of the remaining 12 segments was 10-deg per element. Both geometric and material non-linearity were included in the analysis. It was found in general that the finite element results were in good agreement with the experimental load-displacement curve, cross-sectional ovalisation, and strain distribution. However, the element size

used in the circumferential direction was too fine which could be reduced using a non-flat (curve) shell element.

In 1993, Hose and Kitching [99] presented a series of finite element analyses using ABAQUS of pipe bends of laminated composite loaded by in-plane and out-of-plane moment. The main aim was to assess the effect of straight tangent on flexibility and stress-intensification factor. The nominal cross-section radius (r), radius ratio (R/r), and pipe bend parameter (λ) were 128.5 mm, 1.94 and 0.144 respectively. The pipe bend was connected to straight pipe at both ends (Fig.3.14) having length of over 10 times the cross-section radius. The S8R shell element with quadratic displacement was used. Symmetry condition in geometry and deformation under in-plane bending was taken into consideration by modeling only one-fourth of the structure. The element size of the elbow part in circumference and longitudinal direction was 11.25 and 7.5-deg respectively. The number of elements in the axial direction of the attached tangent was 13.

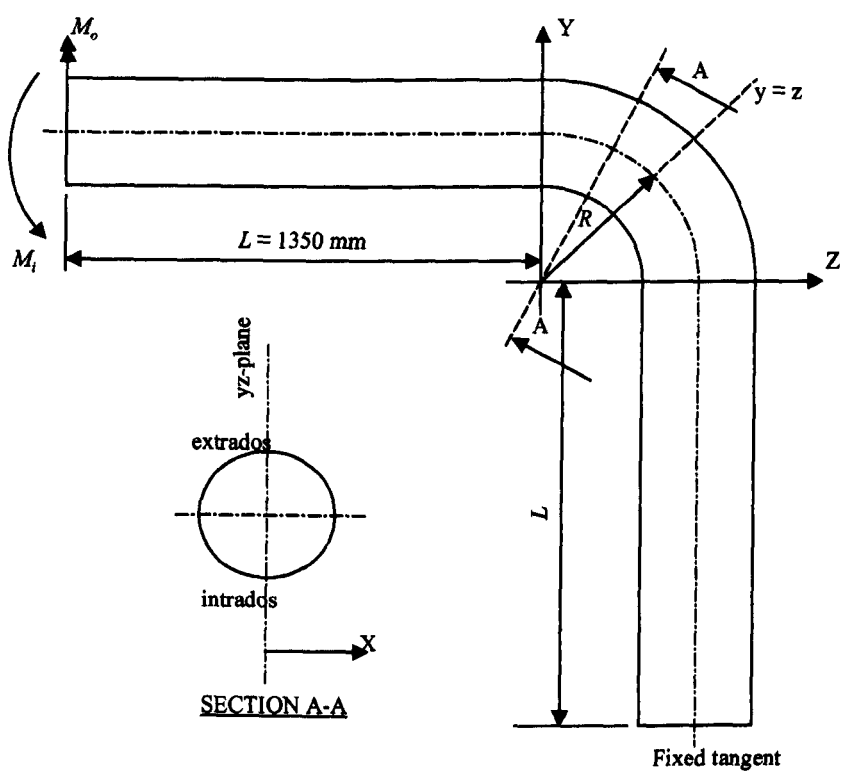

Fig.3.14 Geometry of the pipe elbow investigated by Hose and Kitching [99]

For in-plane bending load, symmetry conditions were imposed on the model boundary plane: z = 0 and y = x, where XY-plane is the plane of the bend in which a 90-deg elbow divided into two of 45-deg elbow by the line y = x (as shown in Fig.3.14). For out-of-plane bending, symmetry was imposed on the plane y = x, but antisymmetry on the plane z = 0. The end flange of the straight tangent was modeled as a rigid body using a multi-point constraint (not shown in Fig.3.14). This was done by connecting each of the nodes on the perimeter of the flange to the node at the tangent pipe axis to which in-plane moment of 2.119 kN.mm was applied. The flexibility factor under in-plane bending was calculated from the rotation of end flange (φ) using the following formula:

$$k_i = \frac{2\left(\frac{EI\varphi}{M_i} - L\right)}{R\alpha} \qquad (3\text{-}12)$$

where E = Young's modulus, N/mm^2

I = second moment of area of the pipe cross-section, mm^4

φ = rotation of the end section of the loaded tangent about X-axis, rad

M_i = applied in-plane moment, N.mm

L = length of the loaded tangent, mm

R = pipe bend radius, mm

α = total bend angle, rad

Elbows of bend angle 60 and 180-deg were also investigated for in-plane bending. It was shown that the maximum stress (hoop stress) was located at the crown for the 180-deg bend, and moved progressively toward the intrados for the smaller bend angle. This trend was also reported by Pardue and Vigness in their discussion to the paper by Gross and Ford [25]. It was reported that the reduction in flexibility factor for 90 and 60-deg elbows compared to 180-deg elbow was 8% and 17% respectively.

The flexibility factor for a 90-deg pipe elbow under an out-of-plane moment, M_o, was calculated using the following equation:

$$k_0 = \frac{\frac{EI\varphi}{M_0} - \frac{L}{2}(2+\nu) - \frac{R}{4}(1-\nu)\left(\frac{\pi}{2}-1\right)}{\frac{R}{4}\left(\frac{\pi}{2}+1\right)} \qquad (3\text{-}13)$$

where φ is the out-of-plane rotation of the end section of the loaded tangent (about the Y-axis) due to an out-of-plane moment M_o (=M_y). It can be seen that the length of the tangent was included in the calculation of the flexibility factor. It was reported that the out-of-plane flexibility factor was 11% lower than those computed under the pure bending assumption (ignoring end effects).

In 1998, Matzen and Yu [104] performed a set of nonlinear finite element analyses to determine the ASME Code B_2 stress indices for 304 stainless steel, seamless, pipe elbows under in-plane and out-of-plane bending. The nominal radius (r), thickness (t), and radius ratio (ρ) were 1.1105 in, 0.154 in, and 3 respectively. The corresponding pipe bend parameter (λ) is then 0.375. The elbow was connected to straight pipes at both ends having ten times the radius of the cross-section in length. Symmetry conditions in geometry and deformation under in-plane bending were taken into account by modeling only one-quarter of the structure. The SHELL43 element of the ANSYS v5.1 finite element analysis program was used. This is a four-noded flat shell element with six degrees of freedom at each node: translations in the nodal x, y, and z directions and rotations about the nodal x, y, and z axes. The element size of the elbow section in the longitudinal and circumferential direction was 11.25-deg and 22.5-deg respectively; the number of elements in the axial direction of the straight tangent was 10 elements. For in-plane bending loading, one end of the model was pinned and the in-plane moment was applied as a prescribed displacement along the line connecting the two ends as shown in Fig.3.15. For out-of-plane moment loading, one end of the model was fixed and the other end was subjected to bending applied as a transverse displacement at the free end. Geometric nonlinearity was included in the analysis.

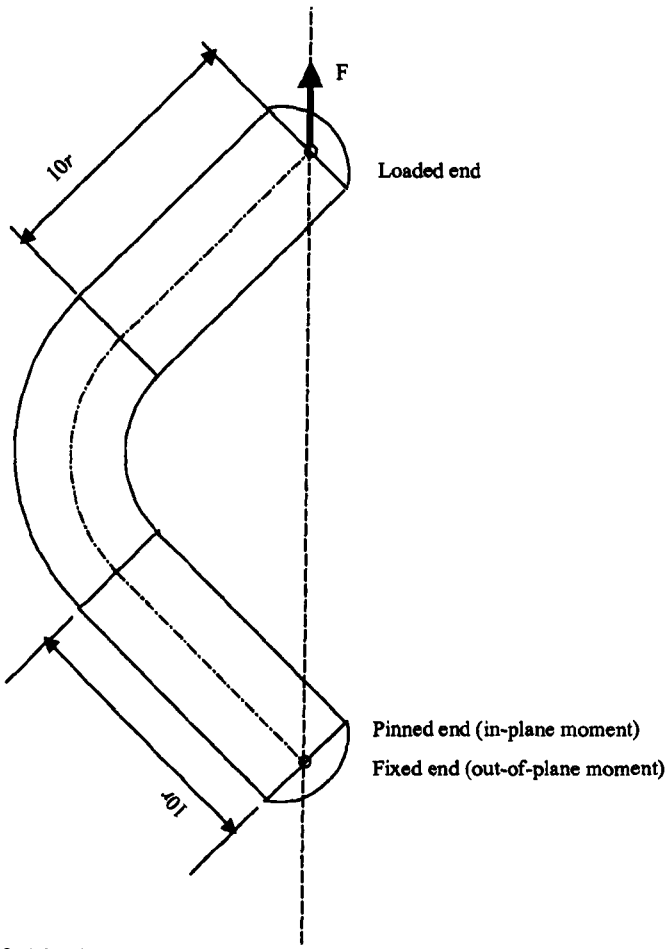

Fig.3.15 Pipe Elbow investigated by Matzen and Yu [104]

Matzen and Yu [104] found that in general that the stress indices obtained from the finite element analysis were about 50% smaller than those obtained using the ASME Code. They did not mention the source of this difference, but they were confident about the analytical procedure they used. It is observed that the B_2 stress index values they produced indicated that the indices under out-of-plane bending was greater than those under in-plane opening moment, but smaller than those under in-plane closing moment; this might not be expected. It could be that the element size they used was too coarse, especially since they used a flat shell element.

In 1998, Shalaby and Younan [105] performed nonlinear finite element analysis of a 90-deg, 16-in nominal diameter pipe elbow under in plane bending. The radius ratio (ρ) and wall thickness (t) of the elbow were 3 and 0.41 in respectively,

corresponding to a pipe bend parameter (λ) of 0.1615. The special pipe bend element ELBOW31B of the ABAQUS finite element computer program was used in the analysis. The element was based on a model which assumes that the ovalisation of the cross-section is constant over the axial length of the element with the amount of ovalisation being dependent on the magnitude of applied moment. The number of elements was 12 elements in the longitudinal direction with the number of integration point around the pipe cross-section and across the thickness of 20 and 7 respectively (Fig.3.16b) The elbow analyzed was neither connected to straight tangent pipe nor terminated by flanges (Fig.3.16a). One end of the elbow was fixed but the radial displacement was allowed to eliminate end stiffening on cross-sectional ovalisation. The other end was subjected to an in-plane moment applied as rotation controlled. Geometric nonlinearity was included in the analysis.

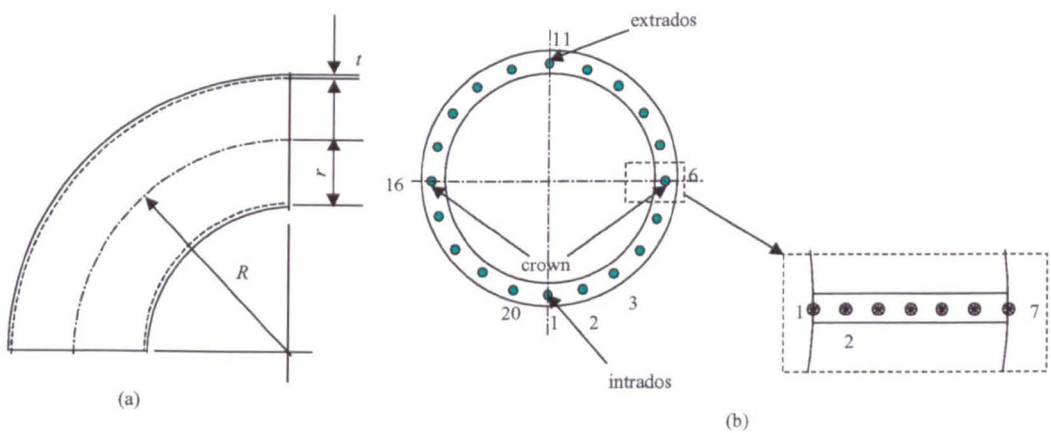

Fig.3.16 Typical ABAQUS ELBOW element used by Shalaby and Younan [105]

Shalaby and Younan found that the maximum equivalent stress under in-plane closing moment was located at the crown. The stress and strain distribution in the elastic range was found to be the same between in-plane closing and opening moment but with opposite signs. In the plastic range, it was found that, as expected, the elbow under opening moment was stiffer than under closing moment.

In 1999, Liu et al [107] carried out a detailed linear elastic finite element analysis to determine the ASME Code B_2 and C_2 stress indices for feeder type pipe bends. The

8-node SOLID45 element of the ANSYS v5.3 was used. The feeder bends were connected to straight tangents having a length of 10 times the cross-section radius. The element size in the circumferential and longitudinal direction of the elbow part was 10-deg and 11.25-deg respectively. The number of elements across the thickness was 3 elements. At the end of each straight tangent pipe, 36 beam elements (BEAM4) were used to connect the node at center of the cross-section to the nodes at the circumference of the loaded end section, as typically shown in Fig.3.9 [Dhalla, 68]. They found that in general the B_2 and C_2 stress indices were lower than those calculated using the ASME Boiler & PV Code. It was also found for in-plane bending that only the closing mode exhibits an actual collapse load, while the opening mode shows the stiffening trend. They argue for this difference that the cross-sectional ovalisation in the bend region reduces the stiffness for the closing bending and increase the stiffness for opening bending.

In 1999, Yu and Matzen [109] extended their previous analysis of B_2 stress indices of 2-in nominal diameter of pipe elbows [104] to include elbows having 4, 6, and 8-in nominal diameters and various wall thicknesses loaded by an in-plane moment. Finite element modeling and analysis was carried out again using the SHELL43 element of the ANSYS finite element analysis program. The effect of tangent length was studied under three modes of moment loading: in-plane closing, in-plane opening and out-of-plane moment. The study of length of tangent was performed by including geometric nonlinearity, leading to a final value of length of tangent of ten times the cross-section radius. The results showed that elbows under in-plane opening moment exhibit structural hardening behaviour, while elbows under in-plane closing moment exhibit structural softening behaviour. The effect of flange location from the elbow-straight tangent junction on the B_2 stress index was also studied. It was found that the B_2 stress indices were slightly reduced as the flange is placed closer to the junction.

In 2000, Ohtaki [112] investigated the elastic stresses of 90-deg pipe bends under out-of-plane bending using finite element analysis. The analysis was based on the displacement method using a special 4-node toroidal shell element. A parametric

study for two values of radius ratio (ρ) and five values of pipe factor (λ) was carried out. The pipe bend was discretisized into toroidal shell elements. The number of elements in the longitudinal and circumferential directions were 6 and 16 respectively. The total number of degree of freedom was 1344. One end of the elbow was clamped and the other end was subjected to out-of-plane moment applied as rotation controlled. Geometric nonlinearity was included in the analysis. The unknown displacement was obtained by minimizing the total potential energy. Stresses distributions for the mid-section of the bend were produced which showed that the maximum stress occurred in the hoop direction at the inside surface and has the opposite sign to the maximum stress at the outside surface. For the same pipe factor, λ, with different radius ratio, ρ, the results show that a pipe bend of long radius produces greater maximum stress.

In 2001, Kumar and Saleem [117] used ANSYS v5.3 to investigate the effect of bend angle (α) on the B_2 and C_2 stress indices. The parameter of bend angle was 15, 30, 45, 60, 75, and 90-deg. The other parameters of interest were as follows: nominal radius (r) in the range of 2.5 to 20 in, thickness (t) in the range of 0.203 to 1.031 in, radius ratio (ρ) in the range of 2.6 to 3.0, and pipe bend parameter (λ) in the range of 0.18 to 0.62. The finite element model was generated using the SHELL63 element of ANSYS v5.3. This is a flat shell element having both bending and membrane capabilities with six degrees of freedom at each node: translations in the nodal x, y, and z directions and rotations about the nodal x, y, and z-axes. The element size in the longitudinal and circumferential direction was 3 and 10-deg respectively. The number of elements in the axial direction of the tangent was 15. The elbows were connected to straight pipes of $10r$ in length at both ends (as shown in Fig.3.17). One end of the tangent was fully fixed and the other end subjected to applied moment. A moment load of 1000 lb-in was applied at the central node of the end section of the loaded tangent. This node was connected to all nodes around the circumference of the end section of loaded tangent, following Dhalla [68], as schematically shown in Fig.3.9. The results show that the values of B_2 and C_2 increase as the bend angle increases with the rate of increase reducing as the bend angle increases. They found that in general the B_2 and C_2 stress indices produced by their analysis were much

lower than those calculated using the ASME Code. For bend angles 90-deg and lower, the dependence of the B_2 and C_2 on the bend angle was found to be of the form:

$$B_2 = 1.0 + \left(\frac{1.30}{\lambda^{2/3}} - 1.0\right)\sin\theta \geq 1.0 \qquad (3\text{-}14a)$$

$$C_2 = 1.5 + \left(\frac{1.95}{\lambda^{2/3}} - 1.5\right)\sin\theta \geq 1.5 \qquad (3\text{-}14b)$$

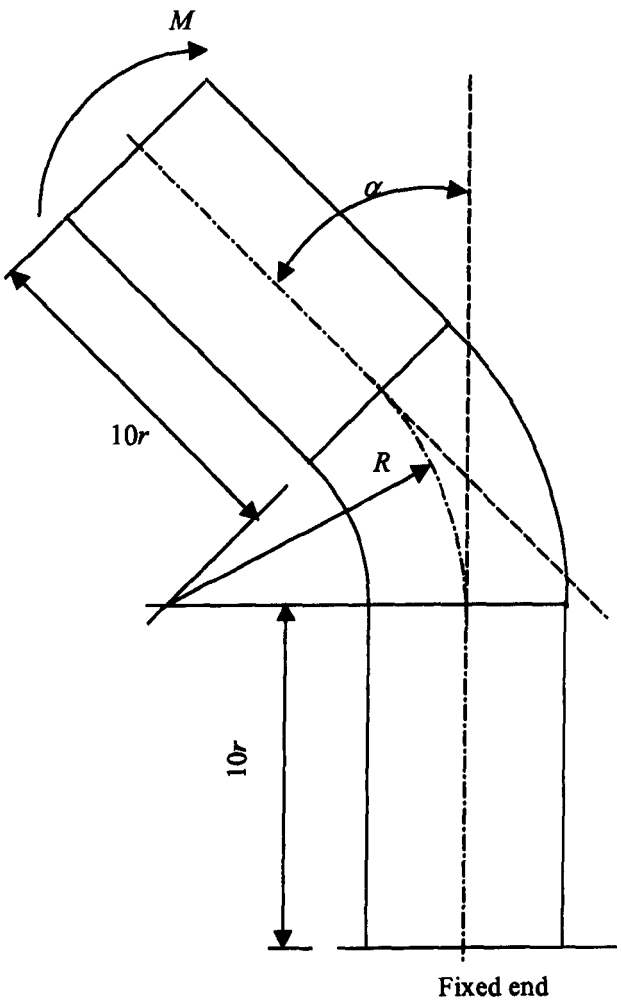

Fig.3.17 Pipe elbows investigated by Kumar and Saleem [117]

In 2002, Kumar and Saleem [122] later extended their previous analysis [117] to elbows with large-angle bend. The bend angles considered were 90, 105, 120, 135, 150, 165, and 180-deg. It was found for all directions of moment loading that the B_2

and C_2 stress indices produced in their analyses were much lower than those calculated using the ASME Code. For bend angles in the range of 90 and 180-deg, the dependence of the B_2 and C_2 on the bend angle was found to be of the form:

$$B_2 = \frac{1.1 + 0.2\sin(\alpha - 90)}{\lambda^{2/3}} \geq 1.0 \qquad (3\text{-}15a)$$

$$B_2 = \frac{1.95}{\lambda^{2/3}} \geq 1.5 \qquad (3\text{-}15b)$$

It should be noted that large deformation effects were not included in their analysis, and also that the results were found to be conservative. The reason for not including large deformation effects in their analysis is not clear, but might be because they used the SHELL63 element. In the preliminary study by the author of this thesis, it was found that the SHELL63 element was not suitable for modeling curved members when the large deformation effect included, because the element would be much distorted in the curved region. For small deformation analysis, SHELL63 element of the ANSYS would be acceptable to model curved members.

In 2002, Tan and Matzen [125] simulated an in-plane bending test of an L-shape pipe bend using the SHELL181 element of the ANSYS finite element program. This element is a four-node flat (non-curved) shell element with six degrees of freedom at each node: translations in the x, y, and z directions, and rotations about the x, y, and z-axes. The length of the straight tangent was approximately ten times the cross-section radius. A quarter model was used with doubly-symmetric boundaries. Average measured thickness was used in both the elbow portion and straight tangent portion. The elbow portion consisted of 8 and 16 elements along the longitudinal and circumferential directions respectively. To simulate the end fixture of the experiment, a stiff thick plate was used; the in-plane moment was applied as displacement control at the node located at the center of the rigid flat. Rigid body motion was prevented by constraining the intrados nodes (this should not be necessary if a half model was used, rather than a quarter model). Large deformation and active stress stiffening was included in the solution control. It was found that the

FEA results for the cross-sectional ovalisation and strains were not in good agreement with the test results. They did not address the reason for this poor agreement, but it could be due to the element size. It should be noted that the element size in the longitudinal direction was 11.25-deg and the element size in the hoop direction (responsible for the ovalisation) was 22.5-deg. This element size might be too coarse together with the fact that a flat (non-curve) shell element was used, resulting in a large amount of discretization error associated with the lack of coupling between membrane and bending actions within individual elements. Cook [113] suggested that the element size of a flat shell element should be no more than roughly 10-deg in the hoop direction.

In 2002, Tan et al [126] simulated an out-of-plane bending test for the elbow configuration investigated by Tan and Matzen [125]. In this simulation, the SHELL43 and SHELL181 of the ANSYS 5.6 were used. The shell element S8R5 and the elbow element ELBOW31 of the ABAQUS finite element package were also used to simulate the test. In all cases, large deformation and stress stiffening were included in the analysis. They discovered that there was a lack of convergence with the shell analysis they used. In regard to the load-strain curve, it was found that the agreement between FEA and experimental results was poor. Again, they did not address the source of this problem. In fact, they used the same element size as used by Tan and Matzen [125] and it was mentioned previously that the element size they used was simply too coarse for a flat shell element.

3.3.2 Piping Elbows Subjected to Bending and Pressure

In this sub-section, finite element modeling of piping elbows under bending and internal pressure is reviewed. In the remainder of the thesis, the term 'pressure' will be simply used for 'internal pressure'

In 1983, Natarajan and Mirza [80] used a doubly curved quadrilateral shell element to study the effect of internal pressure on the stress-intensification factor of short-

radius pipe elbows with end constraints and various bend angles loaded by in-plane bending. One end of the tangents was fixed and the other end subjected to consistent nodal force corresponding to an in-plane moment. The value of moment M and internal pressure p was taken to be 197663 N.m and 0.184 MPa respectively. In their finite element analysis, internal pressure along with in-plane moment were applied at the same time and stress-distribution and maximum stress at the mid-section of the bend is calculated. It was found that the moment load predominated: the pressure load does not change the pattern of the stress distribution and the location of maximum stress at the mid-section of the elbow from those distributions obtained under an in-plane moment loading. This trend might be changed if the level of internal pressure increased beyond a certain level [Boyle & Spence, 57]. For 90-deg pipe elbows, it was shown that the pressure reduction effect on the stress-intensification factor was greater for elbows of low pipe factor. The relation between stress-intensification factor and the bend angle was found to be non-linear for combined bending and pressure load.

In their study of the B_2 stress indices using a finite element analysis, Yu and Matzen [109] investigated the effect of internal pressure on the B_2 stress indices of pipe elbows under in-plane moment. An internal pressure of 100 psi and a displacement controlled load associated with in-plane closing or opening moment were applied. Incremental internal pressure was applied as a first load step and incremantal in-plane moment was applied as the second load step. From the load versus end-deformation curve, it was found that internal pressure tends to make the elbow stiffer, with the stiffening changes under closing moment greater than those under opening moment.

In 1998, Shalaby and Younan [106] performed nonlinear analysis to investigate the effect of internal pressure on the limit moment of pipe elbows under in-plane closing moment. The radius ratio and nominal diameter of the elbow was similar to their previous paper [105], but with various thickness parameter (pipe schedule). Ten values of wall thickness (t) ranging from 0.165 to 1.031 in., corresponding to pipe bend parameters (λ) between 0.0632 and 0.4417 were used. The number of elements

and integration points was similar to the previous paper [105]. Also as in their previous paper [105] one end of the elbow was fully fixed and the other end subjected to an in-plane closing moment. Internal pressure load was applied as the first load-step in one step, and an in-plane moment as the second load step was incremented in several sub-steps. The closed end condition was simulated by applying edge pressure of the intensity of $pr/2t$ at the free end of the elbows. In-plane bending was applied in a similar manner to the previous paper [105]. Both geometric and material nonlinearity were included in the analysis. It was shown using a moment-end rotation curve that internal pressure increased the limit moment. They addressed this trend as a result of increasing the elbow cross-section stiffness due to internal pressure. The stiffening effect of the internal pressure was shown to be dependent on the cross-section to thickness ratio (r/t), being more pronounced for a higher value of (r/t). It was concluded that the stiffening effect of internal pressure was directly associated with the geometric nonlinearities by showing that neglecting the large displacements in the analysis results in a decrease to the limit moment.

In 1999, Shalaby and Younan [108] used the same finite element modeling procedure as in their previous analysis [106] to carry out a similar analysis to study the effect of internal pressure on in-plane opening limit moment. As in their previous paper, only 90-deg elbows were included in the study. From the moment-end rotation curve, it was shown for zero internal pressure that limit moments were higher in the case of an opening moment as compared to the case of a closing moment, but the overall behaviour in the elastic regime was the same under both closing and opening bending. When internal pressure was included, it was shown that internal pressure increased the limit moments for closing case, but decreased them for opening case. It was shown also that the effect of internal pressure on the in-plane limit moment depends on the value of pipe bend parameter, λ; it was more pronounced at low value of λ and high value of (r/t).

In 2000, Chattopadhyay et al [111] used a general-purpose finite element program NISA to investigate the collapse moment of pressurised pipe elbows. The elbow configuration consisted of 90-deg bend connected with straight tangents at both ends

having 6 times the cross-section radius in length. The radius ratio ρ was 3 with cross-section radius to thickness r/t in the range of 5 to 12.5, corresponding to pipe bend parameters λ in the range of 0.24 to 0.6. A twenty-node solid element was used to model the structures. Symmetry in geometry and deformation was taken into account by modeling only one-fourth of the structures. The total number of elements and nodes were 195 and 1508 respectively, consisting of 15 elements in the circumferential direction, 13 elements in the longitudinal direction, and one element across the thickness. One end of the tangent was fully fixed and the end of the other tangent was subjected to in-plane moment and edge pressure to simulate the closed end condition (Fig.3.18a). A multi point constraint was used at the end of loaded tangent.

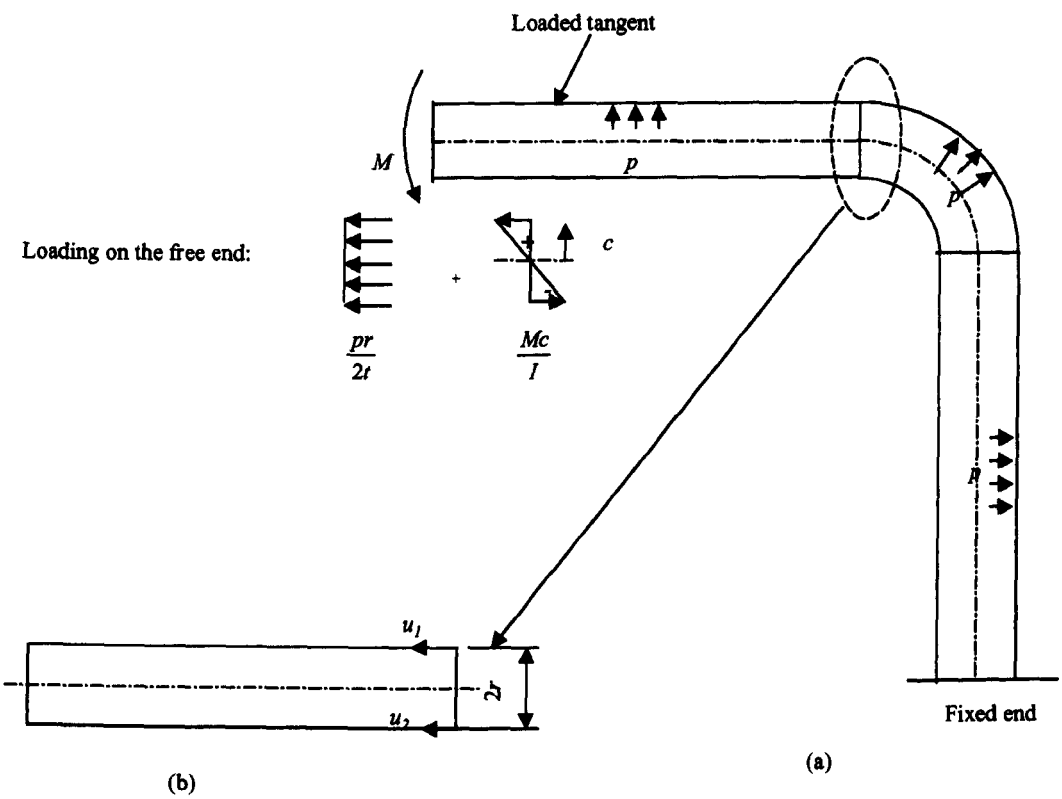

Fig.3.18 Pipe elbow loaded by in-plane moment and internal pressure

A constant internal pressure was applied as first load step and incremental in-plane bending as the second load step. The minimum and maximum load step for in-plane

moment was 10.2 and 102 kN.mm respectively. The closed end condition for the internal pressure load was simulated by applying axial edge pressure of intensity *pr/2t* at the end of the loaded tangent. The bending moment was simulated as a triangularly varying edge pressure with a value obtained from:

$$\sigma = \frac{Mc}{I} \tag{3-16}$$

where M is applied moment, c is distance from the neutral axis $(-r \leq c \leq r)$, and I is the second moment of area of the cross-section.

Both geometric and material nonlinearity was included in the analysis. The end rotation was derived from the finite element generated data using the following formula:

$$\varphi = \tan^{-1}\left(\frac{u_1 - u_2}{2r}\right) \tag{3-17}$$

where u_1 and u_2 are the axial displacements of nodes at the extrados and intrados positions respectively of the section connecting elbow with the loaded tangent (Fig.3.18b). It should be noted that equation (3-18) assumes zero of vertical bulging at the bend-straight pipe junction. In fact, there will be a small vertical bulging Δy at this section, and if this effect were taken into account, equation (3-17) would become:

$$\varphi = \tan^{-1}\left(\frac{u_1 - u_2}{2r + \Delta y}\right) \tag{3-18}$$

From the moment-end rotation curve, they showed that for zero internal pressure the elastic response of the pipe elbows were almost the same for in-plane closing and opening moment. Based on this elastic trend, they concluded that geometric non-linearity was not significant in the elastic response, but could be significant in the

plastic response. It was shown for in-plane closing bending load that internal pressure stiffens the elbow in the direction of applied moment, being more significant for thinner elbows (higher value of (r/t)). A simple expression for the effect of internal pressure on the limit moment was proposed:

$$M_L = \frac{1.122}{\lambda^{2/3}} + \frac{0.175p}{\lambda} - 0.508p^2 \qquad \text{for in - plane closing bending} \qquad (3\text{-}19)$$

$$M_L = \frac{1.047}{\lambda^{1/3}} + \frac{0.124p}{\lambda^{1/2}} - 0.568p^2 \qquad \text{for in - plane opening bending} \qquad (3\text{-}20)$$

where p is a dimensionless pressure: $p = \frac{P}{\sigma_Y}\frac{r}{t}$

and σ_Y is the yield stress, MPa.

Equations (3-19) and (3-20) were found to be applicable for the value of pipe bend parameter λ in the range of 0.24 to 0.6, and the value of non-dimensional pressure, p in the range of 0.0 to 1.0. By examining these equations, it can be shown that internal pressure has a stiffening effect for $\lambda < 0.344$ and a weakening effect for $\lambda > 0.344$ for the case of a closing moment. For the opening bending case, internal pressure has a stiffening effect for $\lambda < 0.281$, and a weakening effect for $\lambda > 0.281$.

In 2001, Mourad and Younan [118] performed non-linear analyses of pressurized 304 stainless steel 90-deg pipe elbows subjected to out-of-plane bending, mainly to determine the out-of-plane limit moment. The bends were of short- radius having radius ratio equal to three, where the cross-section radius was 8 in. All the geometry considered was similar to those studied in [105]. The special elbow element ELBOW32 of the ABAQUS finite element analysis program was used. This element allows continuous displacement across element boundaries, uses Fourier interpolation in the circumferential direction and quadratic polynomial interpolation in the circumferential direction. The number of longitudinal elements was taken as 12 with the number of integration point in the circumferential direction and across the thickness being 20 and 7 respectively, see Fig.3.15. One end of the elbow was

fixed and the other end subjected to an out-of-plane moment loading applied as rotation controlled. Internal pressure was incremented as the first load step and out-of-plane moment as the second load step. Both internal pressure and moment loading were ramped to their maximum value taking both geometric and material nonlinearity into account. The closed end condition was simulated by applying edge axial pressure with an intensity of $pr/2t$ at the free end. It was found that internal pressure tends to reduce the ovalisation of the cross-section. It was found also that the critical cross-section was found to be located at the loaded end of the elbow. This might be expected if the applied out-of-plane moment produced pure bending at the loaded end and pure torsion at the fixed end (for a 90-deg bend). The maximum ovalisation was also expected to occur in this section.

In 2002, Mourad and Younan [123] extended their previous analysis [118] to cover pipe bends with different pipe bend parameters. The radius ratio, ρ, was similar to the previous paper [118] but the wall thickness, t, varied from 0.165-in to 1.031-in, corresponding to pipe bend parameters in the range of 0.0632 to 0.4417. The material model, element type, and element size, was similar to the previous paper [118]. One end of the elbow was fully fixed, but the cross-section at this section was allowed to deform, to eliminate end effects. The pressure and bending load were applied in a similar manner to their previous study [118]. They found that internal pressure increased the limit moment and that the limit moment was higher for pipe bends of high pipe bend parameters, but the effect of internal pressure were found to be more pronounced with elbows of low pipe bend parameters (smaller wall thickness). Comparing the results to the case of in-plane bending, they also found that the difference in limit moment was very small between in-plane and out-of-plane closing moment, being larger in the case of out-of-plane moment. They concluded that internal pressure tends to maintain the roundness of the cross-section, thereby increasing the stiffness and strength of the bend as a whole in both in-plane and out-of-plane bending.

3.4 Summary

Application of the finite element method to study the behavior of piping elbows began some thirty years ago. Solid elements, shell elements, and specially developed pipe bend elements have been used. Some researchers have shown that the finite element results are in close agreement for models using solid and shell elements. The results obtained using specially developed pipe bend elements are usually slightly higher. The reason for this difference is that the ovalisation is continuous across the element boundary for shell and solid elements, while in the case of pipe bend element, the ovalisation is not continuous because the element is connected only at the element 'centre'. Current pipe bend elements have accounted for the continuity of displacement across the element boundary, however the usual assumptions are still adopted in the element formulation. The shell element is believed to be the best choice to model pipe elbow structures with almost no assumptions involved other than the 'thin-shell' assumptions. However, as will be seen in the rest of the thesis, care must be taken in deriving the flexibility factor from the nodal displacement: this issue should not be a problem if a computer with high performance is available. Apart from ad hoc finite element analysis of specific elbow configurations to find the pressure reduction effect on the limit moment, it is apparent from the foregoing review that the 'pressure reduction effect' on flexibility and stress-intensification factors has never been completely examined in the available modern commercial finite element analysis software and computer technology. The remainder of this thesis aims to reassess the pressure reduction effects on the elastic flexibility and stress-intensification factors by performing a non-linear finite element analysis using ANSYS. Finite element modeling and analysis procedures will be fully described in the next Chapter.

CHAPTER 4

FE MODELING OF PIPING ELBOWS USING ANSYS

A fairly comprehensive review on finite element modeling in elbow analysis using various finite element software packages has been presented in Chapter 3. Some researchers have used special pipe bend elements with certain limitations in accuracy. Other researchers have used solid elements suitable for thick-walled pipe, and shell element for thin-walled pipe. In this chapter, finite element modeling and analysis using ANSYS shell elements is presented. In the preliminary studies of this thesis, ANSYS v5.6 [110] was used. Most of the data used in the derivation of the empirical formula has been generated using ANSYS v5.7 [113] and later using ANSYS v6.1 [119]. In what follows, all the ANSYS versions used in this study will be simply quoted as ANSYS. Throughout, the APDL (ANSYS Parametric Design Language) based on FORTRAN code has been extensively used to develop parametric models and to carry out a series of analyses automatically: all required data (geometric value, and stresses) are written into files during each analysis and generated graphically and numerically immediately afterwards. However these will only be reported in the Appendices.

4.1 Geometry

The piping elbow configuration used in this study is of a typical straight tangent pipe–bend–straight tangent pipe as typically shown in Fig.4.1. The length of each of the tangent pipes was taken as fifteen times the radius of the pipe cross-section. This length of tangent was so chosen that it is proportional to the length of elbow for

radius a ratio equal to 10, the maximum radius ratio used in this study. This length of tangent might look disproportional for a short radius elbow, but overall, conforms to the minimum length of tangent suggested recently by Matzen and Yu [104] of ten times the cross-section radius, r, in order for the elbow to be unaffected by the end condition. The ESDU Item No.75014 [54] suggested that the length of straight tangent should be greater than $6r$. The effect of using adjacent straight tangent less than $6r$ will be to reduce both flexibility and maximum stress. Throughout a convergence analysis using finite element method, Dhalla [68] also suggested that the length of tangent pipe of $6r$ might be adequate to eliminate the end effect on cross-sectional ovalisation.

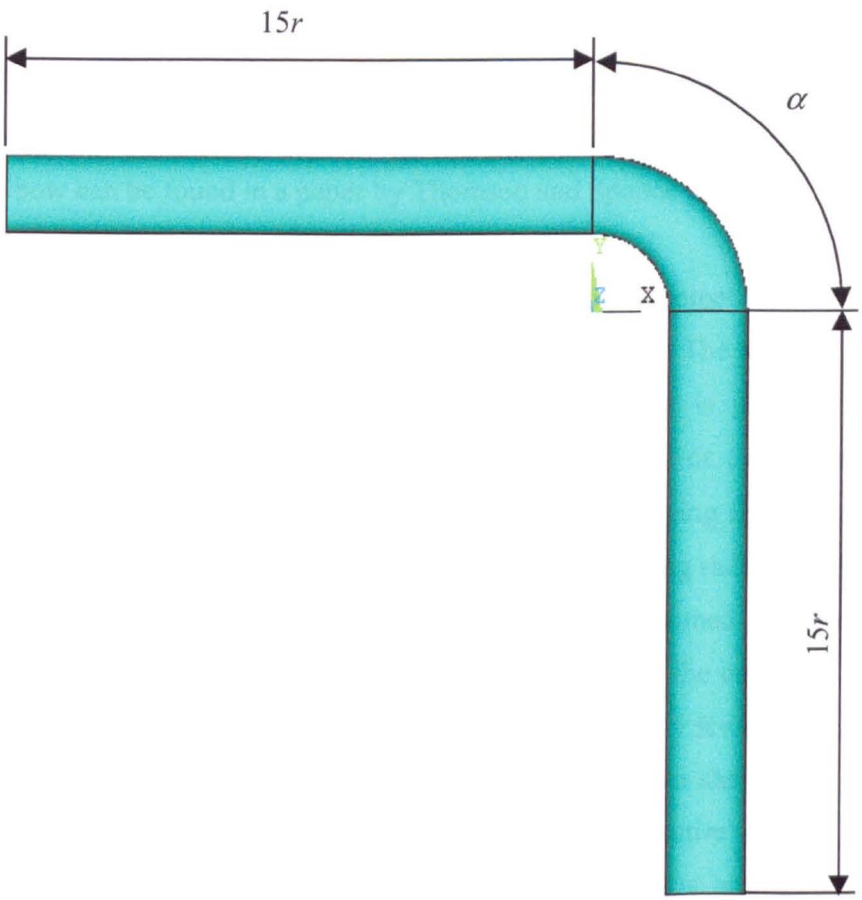

Fig.4.1 Typical elbow configuration considered shown with attached equal tangent

In the present study, the ends of the straight tangents are not terminated by flanged. The introduction of flanges closer than $6r$ will reduce the flexibility and maximum stress [54]. The effect of flanges becomes marked as the bend angle becomes smaller. General solution for the effect of flange on a 180-deg pipe bend under an in-plane bending can be found in a paper by Thailer and Cheng [44] which was developed using the principle of minimum potential energy. Other general solution for the effect of flange on in-plane bending behaviour of pipe bend can be found in [49, 76, 79, 82]. Finite element code was used by Natarajan and Mrza [75] to study the effect of flange on out-of-plane behaviour of pipe bends. The finite element code was further used by Natarajan and Mirza [87] to carry out a similar study to that conducted by Thomson [73] and to study the effect of flange on behaviour of 90-deg pipe elbow [95]. The ESDU No.81041 [74] provide useful graphs for flexibility and stresses for flanged pipe bend with various bend angle under in-plane bending which was derived from Thomson [73] based on small deformation elastic thin shell theory using the minimum total potential energy. An excellent survey on the end effect in piping elbow can be found in a paper by Thomson and Spence [86].

Parameter survey has been based on a range of typical pipe geometies:
The bend angles considered were 30, 45, 60, 90, and 180-deg. The nominal radius (r) is 6-in. It is assumed that the cross-section of the pipe is perfectly circular. Theoretical analysis for pipe bend of non-circular (elliptical or oval) cross-section can be found in [22, 45, 46]. The radius ratio ($\rho = R/r$) ranging from short to long radius. Recall that Rodabaugh and George [30] assumed a long radius bend, where R is very much bigger than r. The curvature of the bend is assumed constant over the entire length of the bend. For analysis of pipe bend in which the curvature along the length of the bend is not uniform can be found in a paper by Kwee [69]. The pipe schedule (wall thickness, t) was chosen in the range for a thin shell ($t/r < 0.1$). It is further assumed that the thickness is uniform over the entire of the structures although it is usually expected that thickening at the intrados and thinning at the extrados could result from bending process during manufacturing of a pipe bend. For studies of the effect of variation in wall thickness on flexibility and stresses in a pipe bend can be found in many published paper. Spence and Findlay [71], Kitching and

Hose [97], and recently Cherniy [127] developed a theoretical analysis of in-plane bending of pipe bend with variable thickness under in-plane bending. The effect of variation in wall thickness on flexibility and stresses in a pipe bend was also analyzed by Thomas [72] using STAGS finite element program and by Natarajan and Mirza [84] using a specially developed doubly-curved shell element. Most of the analyses represent the variation in wall thickness in trigonometric form such that produces thickening at the intrados and thinning at the extrados, while thickness remain unchanged at the crown.

Eight values of wall thickness (t) were used which ranged from 3.9624 mm to 14.2748 mm, representing pipe schedule, from sch.5s to sch.60. Corresponding pipe bend parameters λ are given in Table 4.1.

Table 4.1 Geometry of pipe elbows to be considered, r = 152.4 mm (6-in)

t, mm	$\rho = R/r$				
	2	3	5*	6	10
3.9624	0.0520	0.0780	0.1300	0.1560	0.2600
4.5720	0.0600	0.0900	0.1500	0.1800	0.3000
6.3500	0.0833	0.1250	0.2083	0.2500	0.4167
8.3820	0.1100	0.1650	0.2750	0.3300	0.5500
9.5250	0.1250	0.1875	0.3125	0.3750	0.6250
10.3125	0.1353	0.2030	0.3383	0.4060	0.6767
12.7000	0.1667	0.2500	0.4167	0.5000	0.8333
14.2748	0.1873	0.2810	0.4683	0.5620	0.9367

For in-plane closing moment and bend angle (α) of 30, 45, and 60-deg, the analysis was performed for radius ratios (ρ) equal to 2, 3, 5, and 10. For other moments, the analysis was performed for ρ = 2, 3, 6, and 10. Table 4.2 summarizes the matrix of bend angle (α) and radius ratio (ρ) considered in this study for in-plane (closing and opening) moment, and out-of-plane moment. For every direction of bending, the number of analyses were 160 (=5 values for bend angle (α) x 4 values for radius ratio (ρ) x 8 values for thickness (t)). To follow closely the form of the pressure reduction effect proposed by Rodabaugh and George [30] as given in equations (2-94) and (2-

98), the parameters of interest were radius ratio (R/r) and pipe cross-section to thickness ratio (r/t). The results for the same value of pipe factor λ were not therefore presented.

Table 4.2 Parameter of bend angle, α, radius ratio, ρ, and direction of moment

Bend angle	$\rho = R/r$				
	2	3	5	6	10
30-deg	Closing Opening Out	Closing Opening Out	Closing	 Opening Out	Closing Opening Out
45-deg	Closing Opening Out	Closing Opening Out	Closing	 Opening Out	Closing Opening Out
60-deg	Closing Opening Out	Closing Opening Out	Closing	 Opening Out	Closing Opening Out
90-deg	Closing Opening Out	Closing Opening Out		Closing Opening Out	Closing Opening Out
180-deg	Closing Opening Out	Closing Opening Out		Closing Opening Out	Closing Opening Out

Referring to Table 4.2, there is no specific reason why some cases were not investigated. In the early parametric study for closing bending, R/r = 2, 3, 5, and 10 were investigated. However, it seems that there is a big gap from R/r = 5 to 10 compared to the gap from 2 to 3, and then to 5. And then for 90 and 180-deg bend, R/r = 6 were investigated rather than R/r = 5. For the rest of parametric study for opening bending and out-of-plane bending, R/r = 5 has been replaced by R/r = 6. For similarity, it was planned to go back investigating R/r = 6 for closing bending for bend angle of 30, 45, and 60-deg. But because of limitation of time, this analysis was abandoned. However the derived formula might not be significantly affected.

Since only elastic analyses will be carried out in this study, the only material properties required in this study are Young's modulus E, and Poisson's ratio ν. The nominal values for E and ν were taken to be 207000 N/mm^2 and 0.3 respectively.

4.2 Element Type and Meshing

The element type used to represent the elbow section and tangent pipe is the 8-node high-order SHELL93 elastic element. This is a curve (non-flat) shell element with six degrees of freedom at each node: translations in the nodal x, y, and z directions and rotations about the nodal x, y, and z-axes. The deformation shapes are quadratic in both in-plane directions. The curve shell element was chosen instead of a flat shell element, mainly to avoid large discretization error, and thus, to make the results of analysis more reliable, compared to an analysis using the same element size of a flat shell element. Solid elements may also be used, but as shown by Matzen and Yu [104] for typical elbow geometries, using solid elements did not improve the detail of the result. This is probably caused by ill-conditioned finite element equations when the wall thickness becomes very small compared with the other dimensions. Another reason for not using solid elements is that the model will consist of an excessive number of elements should the number of elements across the thickness be more than one. As reported in the previous chapter, the ANSYS solid element, however, has been used by Liu et al [107] to determine the B_2 and C_2 stress indices for feeder type bends. ANSYS solid element was also used by Weiβ et al [101] to study carrying capacity of a pipe bend under pressure cycling.

The bend part was modeled in a toroidal co-ordinate system and the straight tangent pipes were modeled in cylindrical co-ordinate systems. Two different geometry models were created, one for in-plane bending, in which a-half model was used due to symmetrical nature of deformation, and a complete model for the out-of-plane bending case. As reported in the previous Chapter, some investigators have modeled the elbow configuration by only one-quarter of the model, taking the doubly

symmetric condition into consideration, see for example, Dhalla [68], Hose and Kitching [99], Matzen and Yu [104], and Tan and Matzen [125]. However, it was noticed that rigid body motion has to be prevented by constraining the intrados node [Tan and Matzen, 125], resulting in a high stress concentration. For this reason, the elbow configuration was modeled as a half, with the plane of the bend being the plane of symmetry.

The element size in the longitudinal direction of the elbow part was chosen as 3^0 for each element; the number of elements in the axial direction of each tangent pipe was then taken to be 15 elements. The element size in the tangent pipe had no significant influence on the general behavior of the model, provided that the transition is sufficiently smooth and the maximum aspect ratio is maintained. To achieve this, the element size in each tangent was generated in such a way that a smooth transition of the element size is maintained in the elbow-straight pipe junction. The element size in the hoop direction was chosen after performing finite element convergence analysis. Details of the finite element convergence study are described in the following:

4.3 Finite Element Convergence Study

It is usually necessary to perform a finite element convergence study to find the optimum number of elements. As shown by Sobel [60], a finer mesh does not always give an accurate result. He showed that with a certain number of elements, the stresses converge to some value and as the number of elements increase, the stresses become divergent. In short, the solution could become inaccurate if the element size is too fine. In what follows, a finite element convergence study is performed to establish the optimum number of elements.

In this study, the element size in the axial direction (3^0 for each element) was maintained constant while the element size in the hoop direction was refined. The finite element convergence analysis was performed under in-plane closing bending

for a typical geometry of elbow configuration: $\alpha = 90^0$, $\rho = 3$, and $t/r = 0.03$. The cut end of the vertical tangent is fully fixed and bending load is applied at the cut end of the horizontal tangent. The vertical and horizontal tangents are further quoted as "*fixed tangent*" and "*loaded tangent*" respectively for the remainder of the thesis. The convergence analysis was based on the amount of flattening and the stresses at the crown of mid section of the elbows, the amount of rotation of the section connecting the bend and straight tangent, and the displacements of the loaded end section.

Figure 4.2 shows the amount of horizontal flattening of the crown node at the mid-section of the elbow plotted against the number of shell element along the semi-circumference of the bend. It can be seen that as the number of elements increases beyond 18 along the semi-circumference, the amount of horizontal flattening does not increase significantly. It might be concluded, based on the flattening of the cross-section that the optimum element size in the circumferential direction is 10-deg.

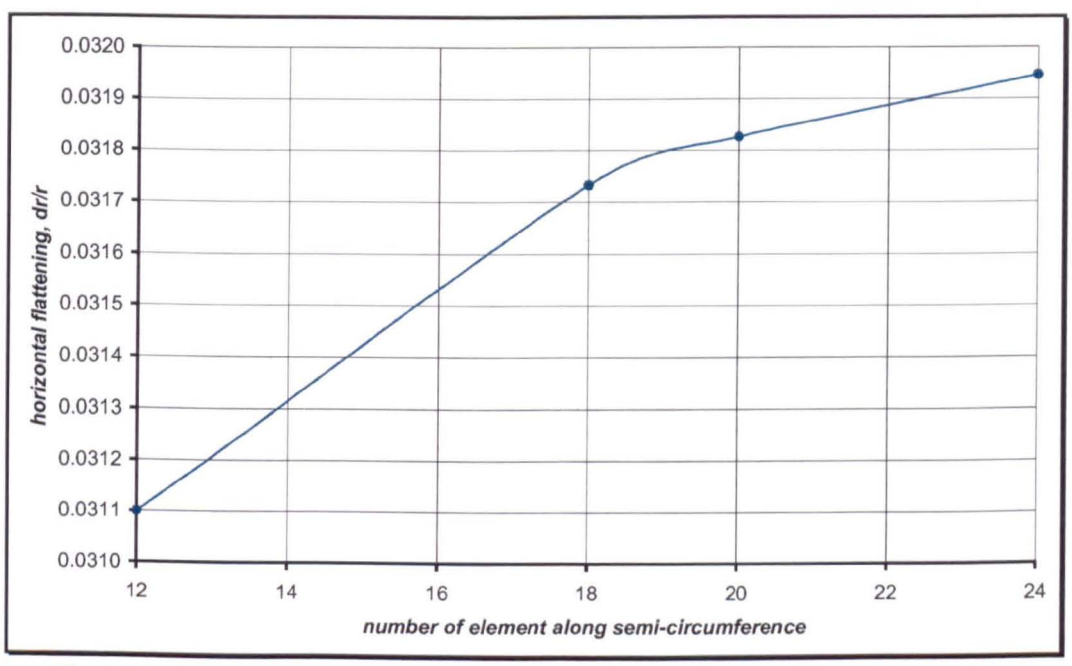

Fig.4.2 FE convergence analysis based on the amount of horizontal flattening

Figure 4.3 and 4.4 show the longitudinal and hoop stress factor respectively at the crown of the mid-section of the bend plotted against the number of elements along the semi circumference. Stress factor is defined as the stress obtained from finite element result normalized by the nominal bending stress (eqn 2-26)). Again, it can be seen that the accuracy does not increase significantly as the number of elements increases beyond 18 element along the semi circumference.

Figure 4.5 shows the rotation of the pipe section at the connection between the elbow and the loaded tangent (end rotation of the elbow). It can be seen that the end rotation of the elbow again does not increase significantly as the number of elements along the semi circumference increases beyond 18 elements.

Figure 4.6 and 4.7 show the amount of x-displacement and downward y-displacement respectively of the loaded end section. Again, it can be seen that the accuracy does not increase significantly as the number of elements increases beyond 18 element along the semi circumference.

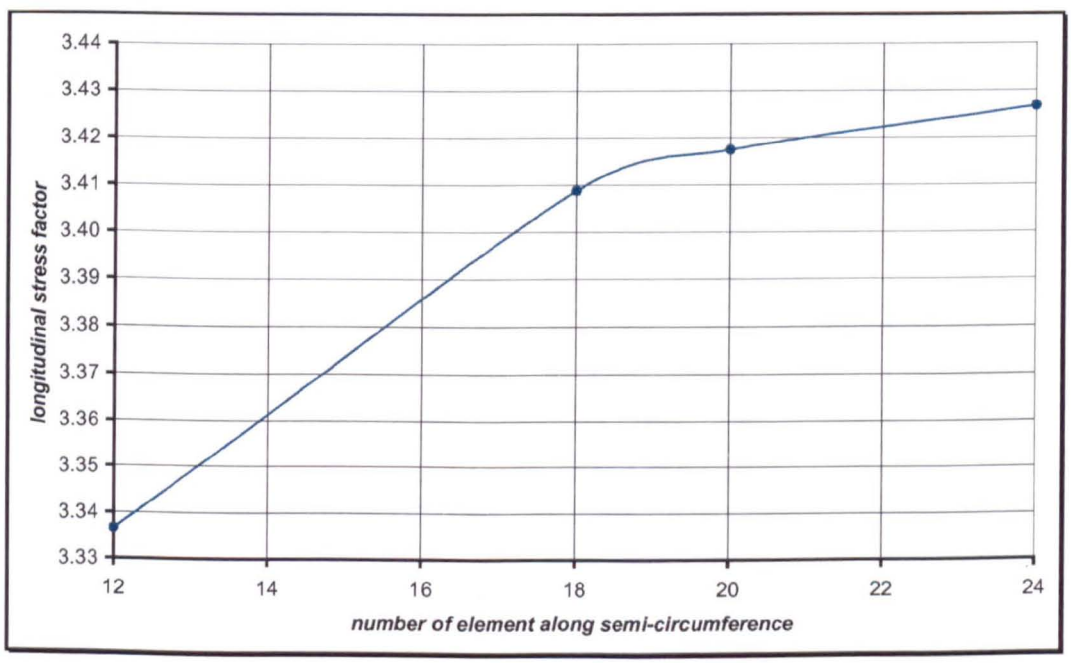

Fig.4.3 FE convergence analysis based on longitudinal stress factor

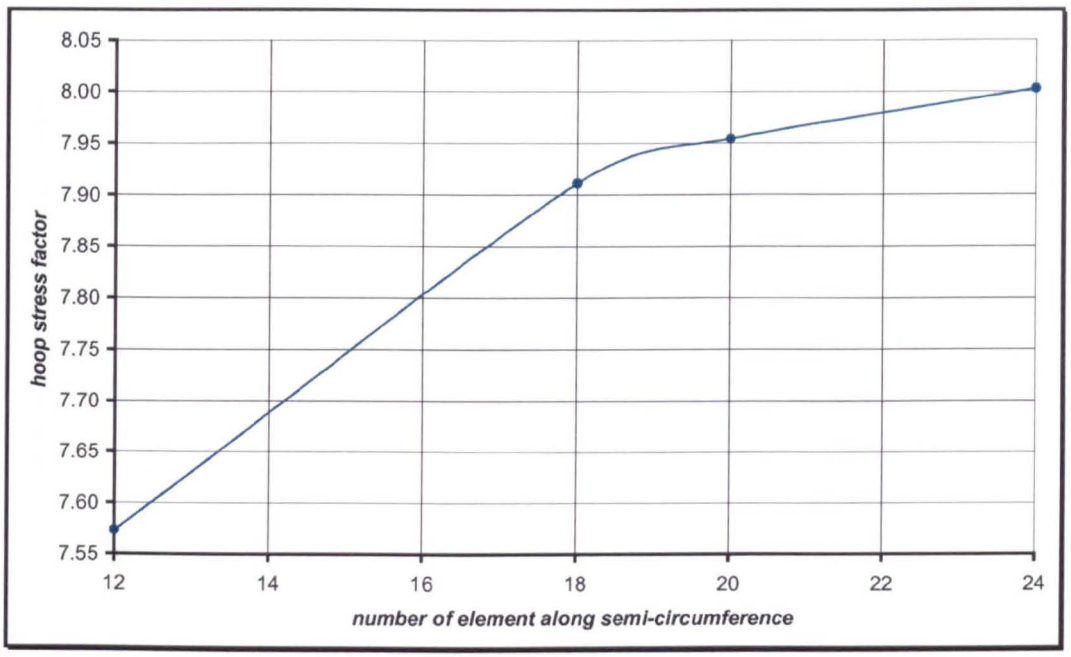

Fig.4.4 FE convergence analysis based on hoop stress factors

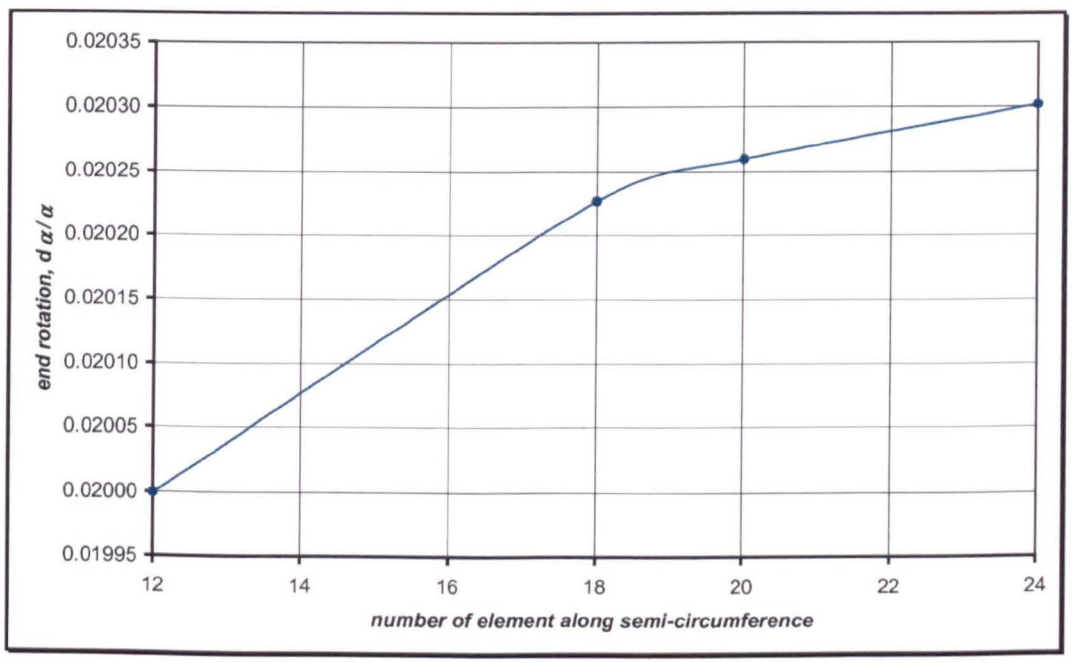

Fig.4.5 FE Convergence analysis based on the end rotation of the elbow

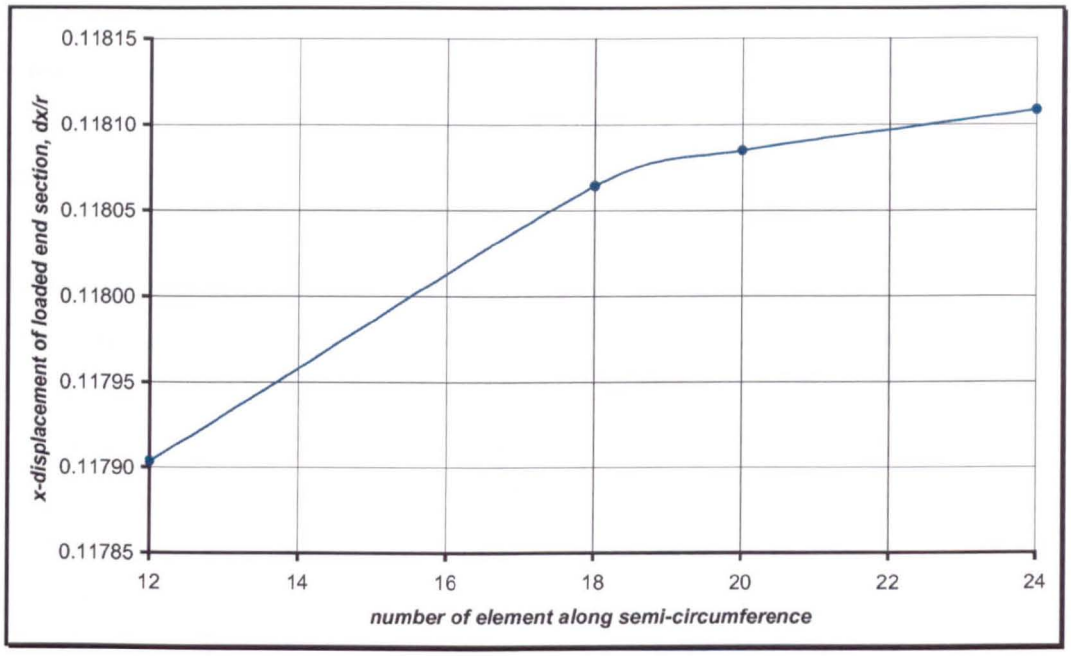

Fig.4.6 FE convergence analysis based on the x-displacement of loaded end section

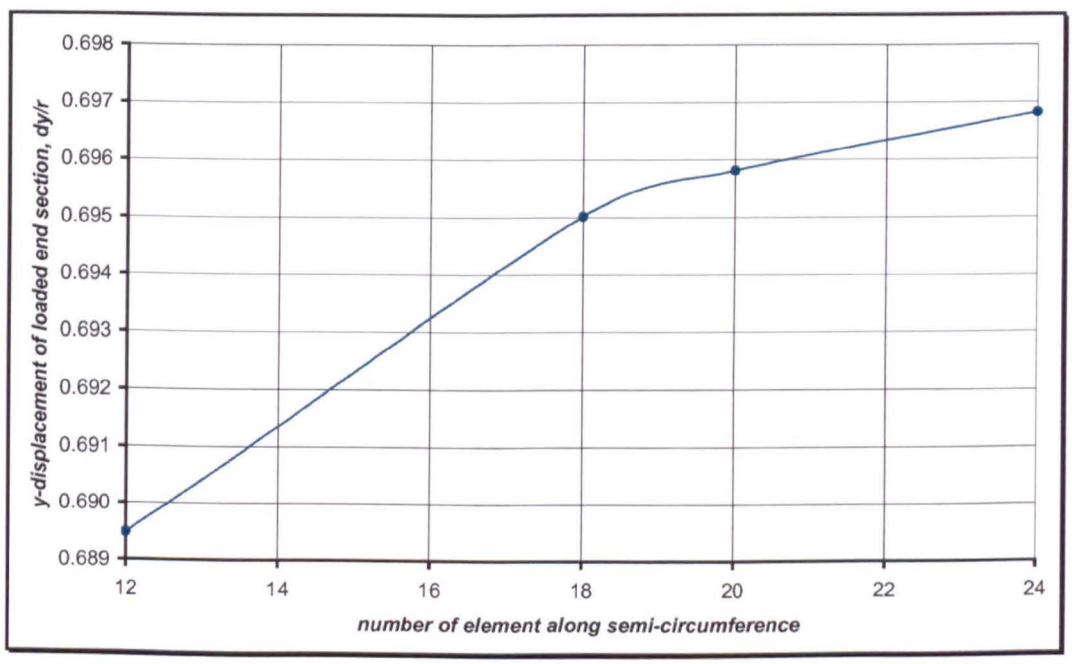

Fig.4.7 FE convergence analysis based on the y-displacement of loaded end section

So, from the finite element convergence analysis as shown in these figures, the element size in the hoop direction was chosen to be 10-deg. The total number of shell elements and associated nodes are given in Table 4.3. Typical finite element mesh is shown in Fig.4.8.

Table 4.3 Total number of shell elements and nodes

Bend angle	Number of shell elements		Number of associated nodes	
	In-plane	Out-of-Plane	In-Plane	Out-of-Plane
30-deg	720	1440	2277	4392
45-deg	810	1620	2557	4932
60-deg	900	1800	2837	5472
90-deg	1080	2160	3397	6552
135-deg	1350	2700	4237	8172
180-deg	1620	3240	5077	9792

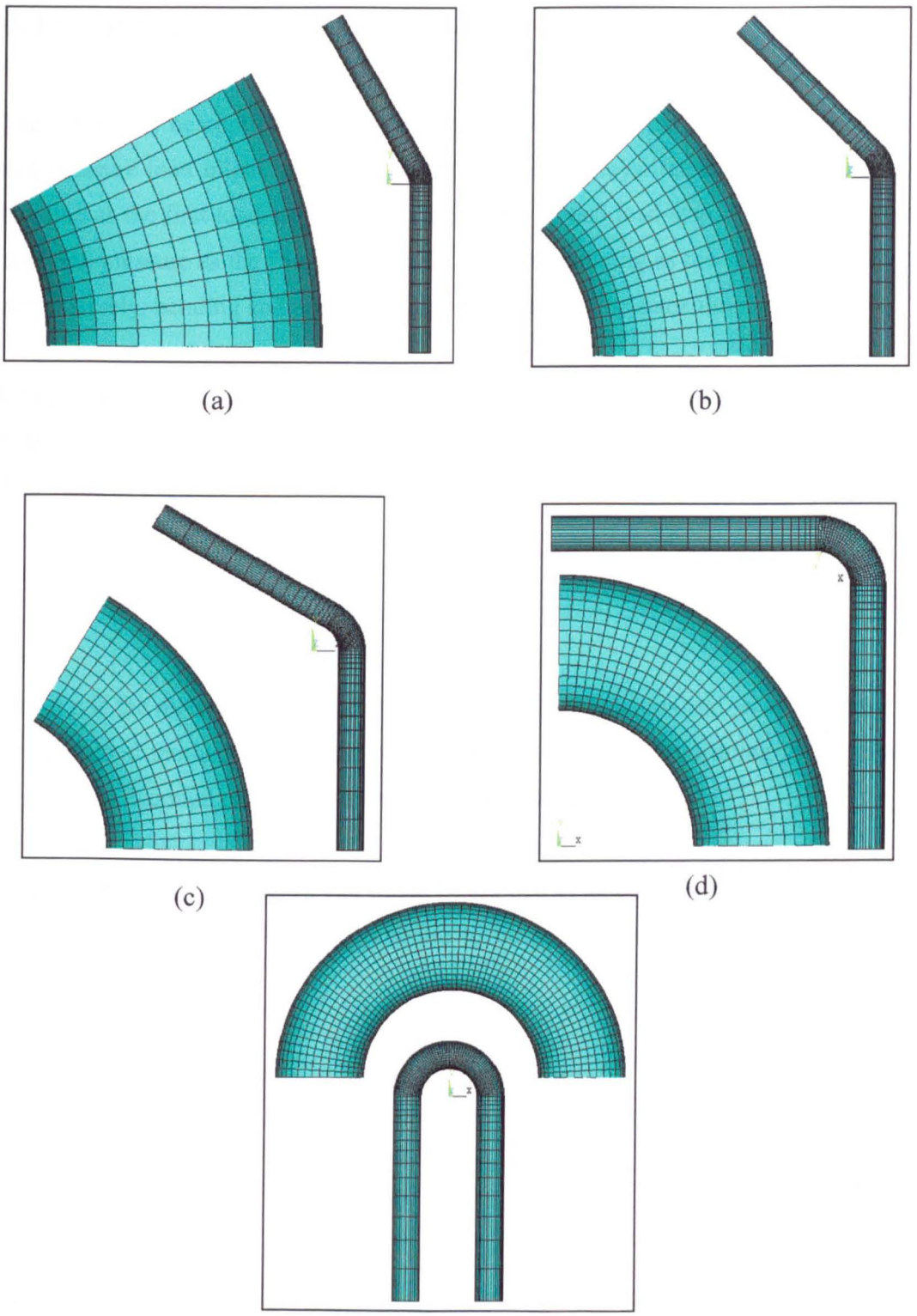

Fig.4.8 Typical finite element mesh for piping elbows subjected to bending: (a) in-plane bending, (b) out-of-plane bending

4.4 Loading – Path Dependency

The loading to be applied is bending moment, M, and internal pressure, p. Bending and pressure load might be applied in three different ways: the first is by applying bending as the first load-step and pressure as the second load-step. The second is by applying pressure as the first load-step followed by bending as the second load-step. Alternatively, bending and pressure might be applied at the same time.

Bending moment might be simulated as triangularly varying gradient edge pressure at the free end, see for example, Chattopadhyay et al [111] and Chattopadhyay [121]. The value of the edge pressure can be obtained from simple beam theory as:

$$\sigma_b = \frac{Mc}{I} \tag{4-1}$$

where c is the distance from central axis (equal to r at extrados and $-r$ at intrados), I is the second moment area of the cross-section. (ANSYS allows doing so by using the SFGRAD command before the edge pressure is applied).

Internal pressure at the closed end might be applied as an edge pressure acting on the lines of the free end. The edge pressure to be applied can be obtained from the following equation:

$$\sigma_p . 2\pi r t = P . \pi r^2$$

or

$$\sigma_p = \frac{pr}{2t} \tag{4-2}$$

The edge pressure (eqn (4-2)) should be applied as 'follower load'. Fortunately, the ANSYS program always treats the pressure as a follower load. Pressure load is considered as a surface load, and in ANSYS, surface load always act normal to the deflected element surface. See section 8.1.2.3 of the ANSYS on-line help [119].

If internal pressure with a closed end condition is applied as the first load step and bending moment as the second, the bending moment may be simulated as triangularly varying edge pressure, as explained by Chattopadhyay et al [111]. If bending and edge pressure loads are applied at the same time in proportional way, the bending can also be simulated as varying edge pressure with the magnitude of the algebraic sum of the bending and edge pressure as shown in Fig.4.9. (The ANSYS SFGRAD command, however, cannot be used if the bending moment is applied as the first load step and internal pressure with closed end condition as the second, because all subsequent edge pressure after the SFGRAD command would follow this gradient).

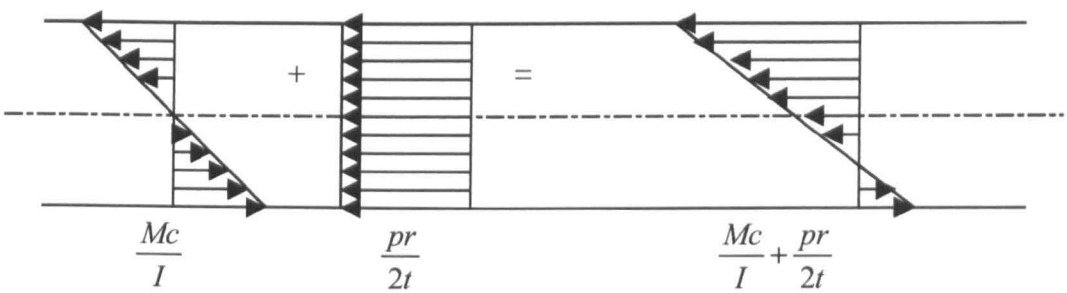

Fig.4.9 Bending and closed end pressure are applied as single edge pressure

To avoid this problem if any order of loading is required the bending load should be applied on a node at the centre of the free end. This node was connected to all nodes at the circumference of the free end using beam element having the same material properties as the shell element but with relatively higher stiffness than the shell element. For this purpose, the ANSYS BEAM4 element having six degrees of freedom, the same number degree of freedom as the SHELL93 element, is used, as shown in Fig.4.10. Another advantage of using the beam element to simulate the rigid link at one end of the tangent is the possibility of obtaining the end reaction force and moment should the piping bend configuration be subjected to thermal loading. Using the ANSYS BEAM4 element to simulate the rigid link at the loaded end section was also implemented by Liu et al [107]. However, how many times the BEAM4 element was made stiffer than the shell element was not mentioned in their paper.

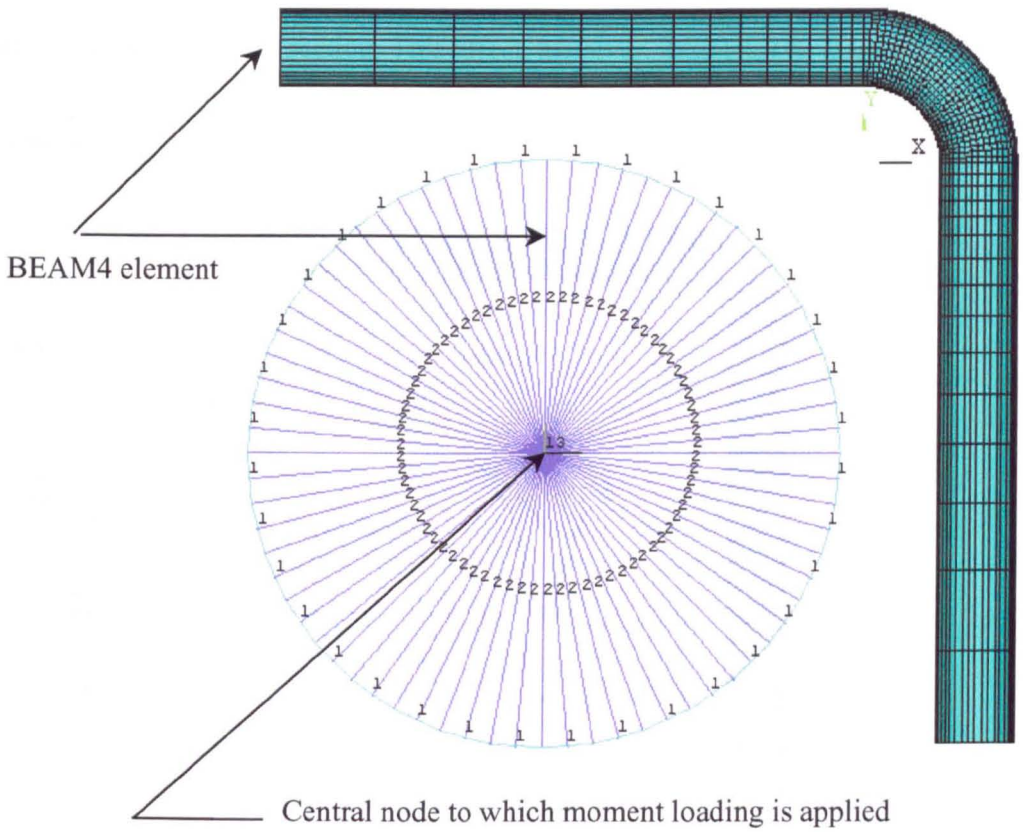

Fig.4.10 BEAM4 element is used at the free end of loaded tangent

Square beam element having dimension of 12mm x 12mm has been chosen and its Young's modulus was determined through a convergence analysis:

The convergence analysis for determining the stiffness of the beam element in these figures has been performed for 90-deg elbows having radius ratio (ρ) = 3 and thickness to cross-section radius ratio (t/r) = 0.03 loaded by in-plane closing bending. The convergence analysis was checked for stresses and horizontal flattening at crown of the mid-section of the elbow (section A-A), rotation of section at elbow-loaded tangent junction (section B-B), and displacements and rotation of the central node of loaded end section (section C-C) as shown in Fig.4.11. The effect of (E_{beam}/E_{shell}) for an out-of-plane bending were not investigated. It probably would make a difference

since there would be some coupling bending and axial stiffness due to the deformation of the end section. This effect, however, might not be large.

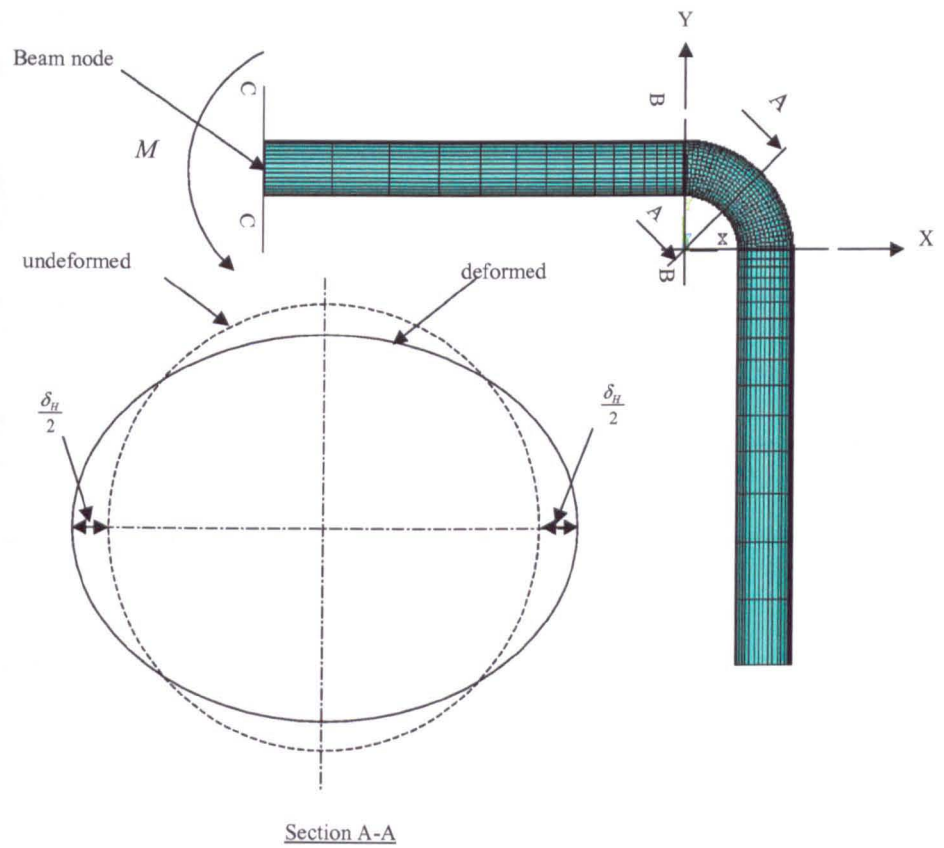

Fig.4.11 Sections of a pipe elbow used for stiffness convergence analysis

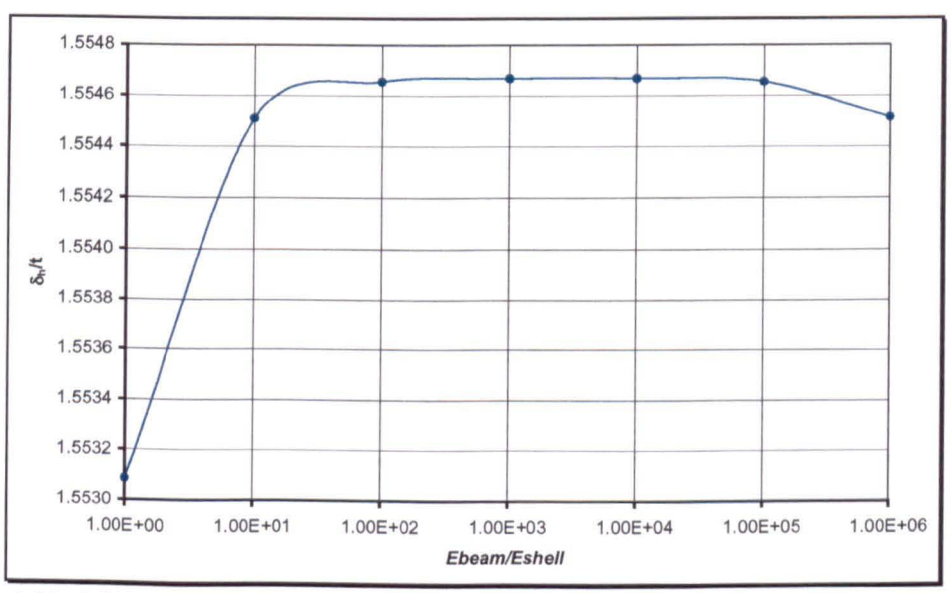

Fig.4.12 Stiffness convergence analysis for BEAM4 element based on horizontal flattening

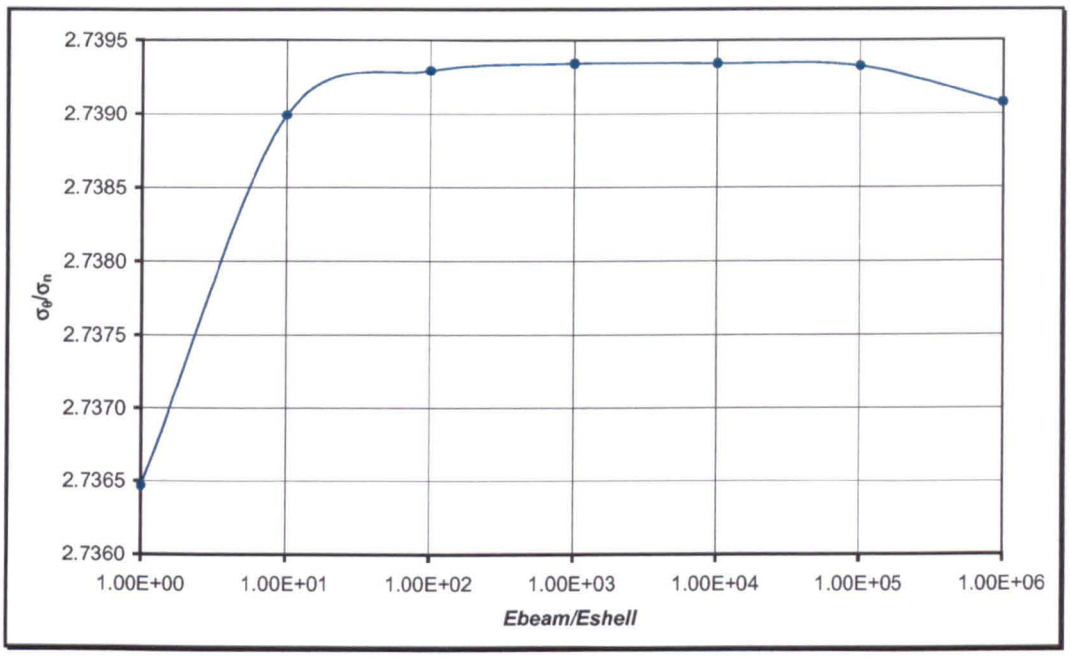

(a)

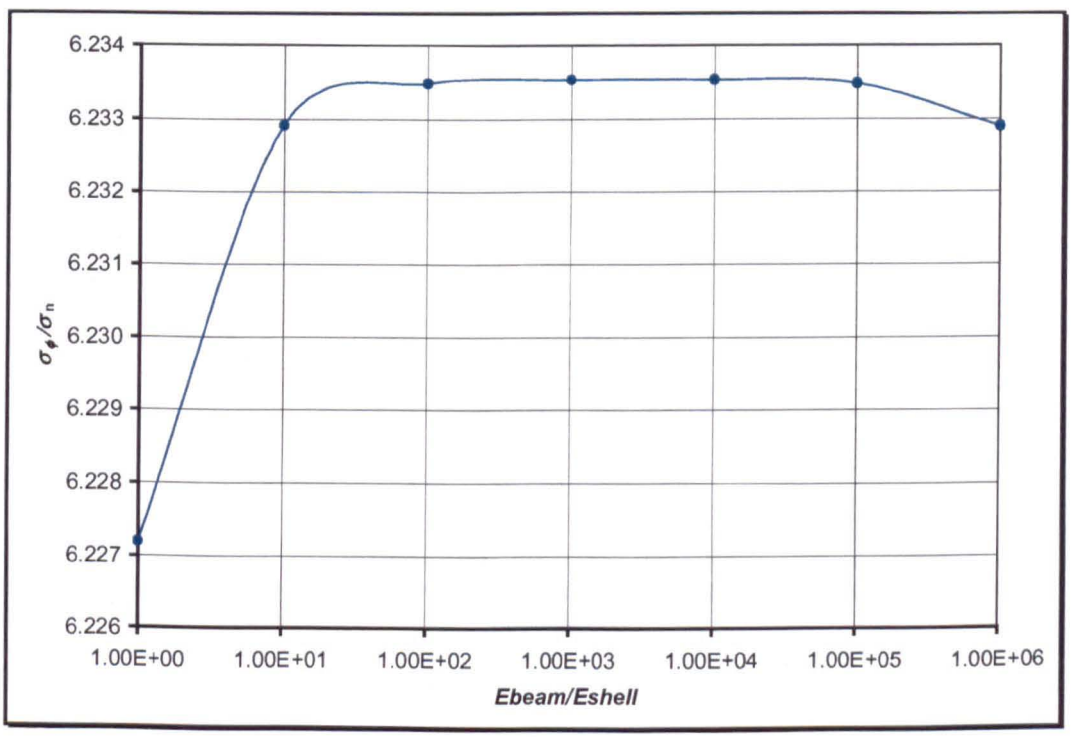

(b)

Fig.4.13 Stiffness convergence analysis for BEAM4 element based on stress factors (a) longitudinal stress, (b) hoop stress

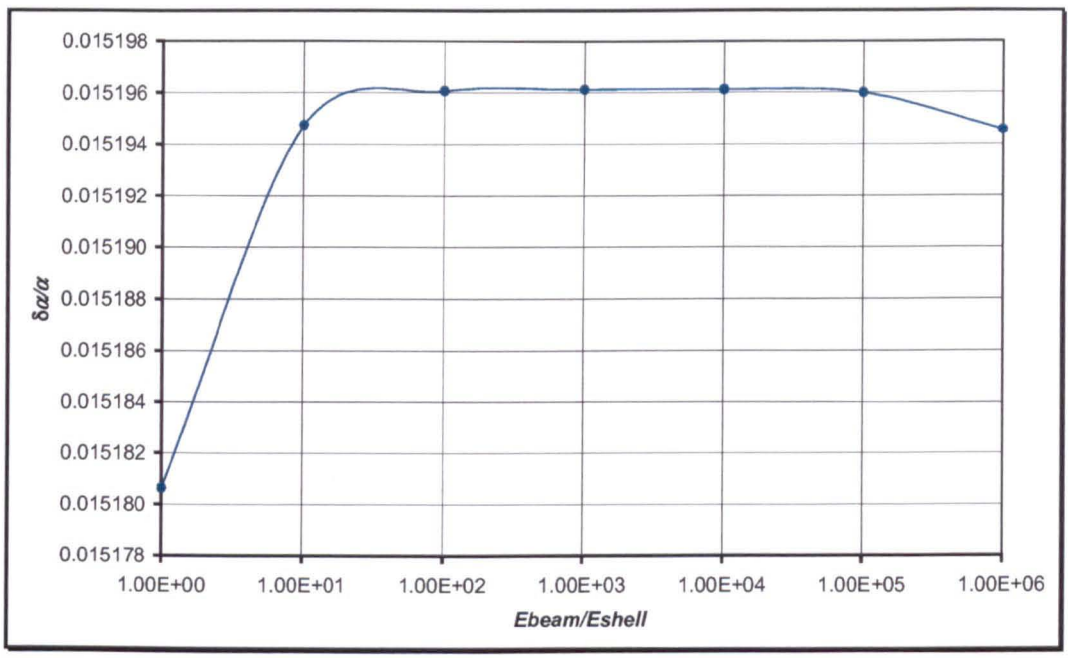

Fig.4.14 Stiffness convergence analysis for BEAM4 element based on end rotation

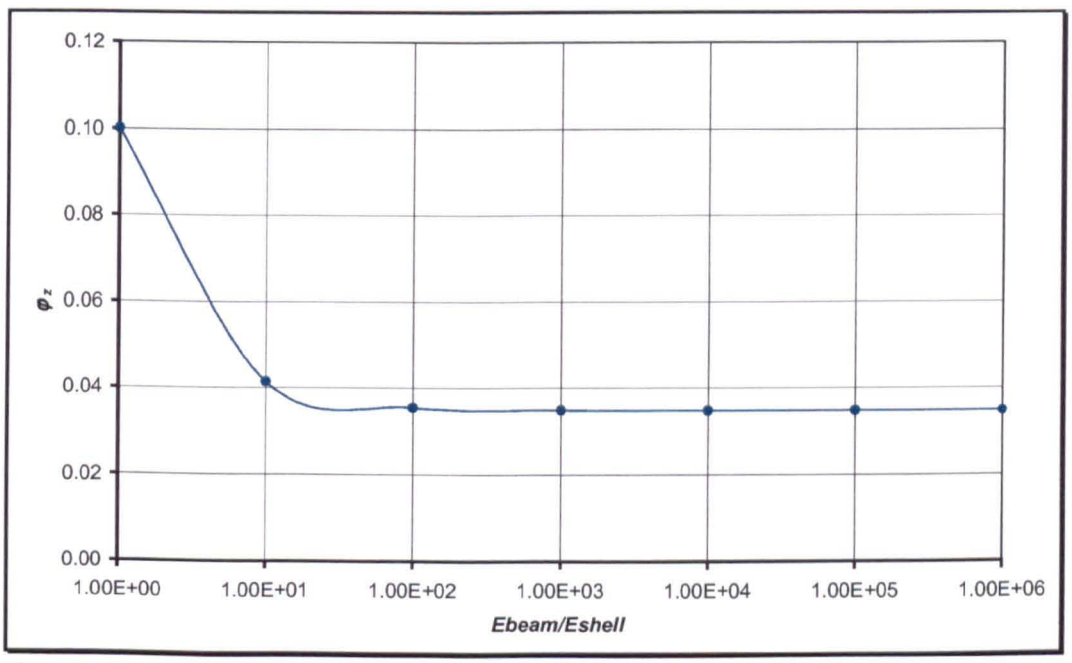

Fig.4.15 Stiffness convergence analysis for BEAM4 element based on z-rotation of the beam node

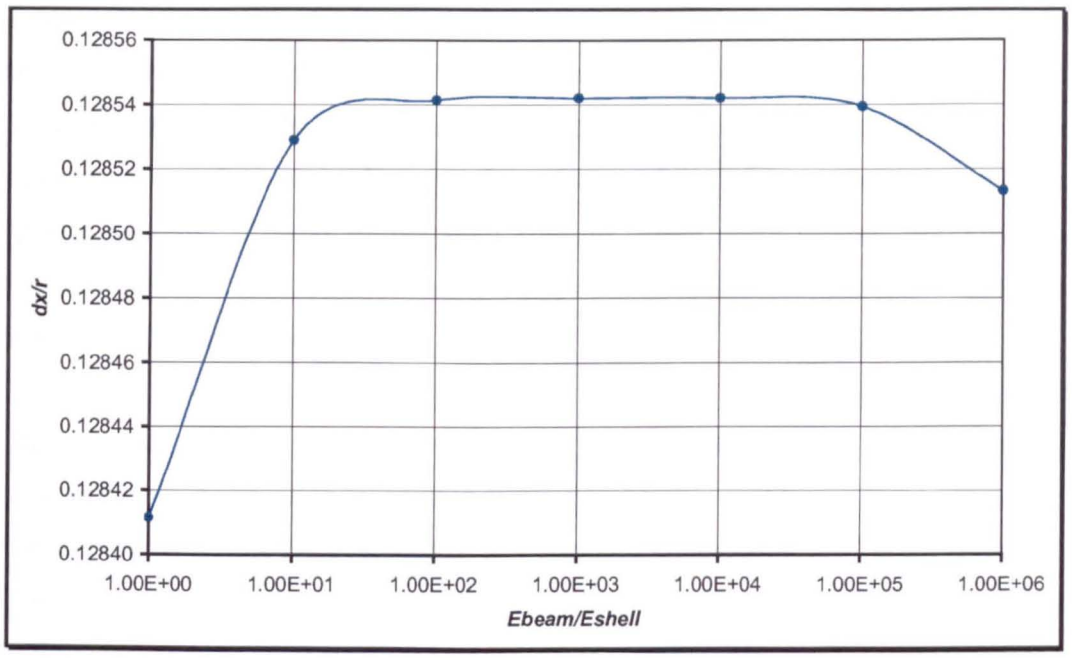

(a)

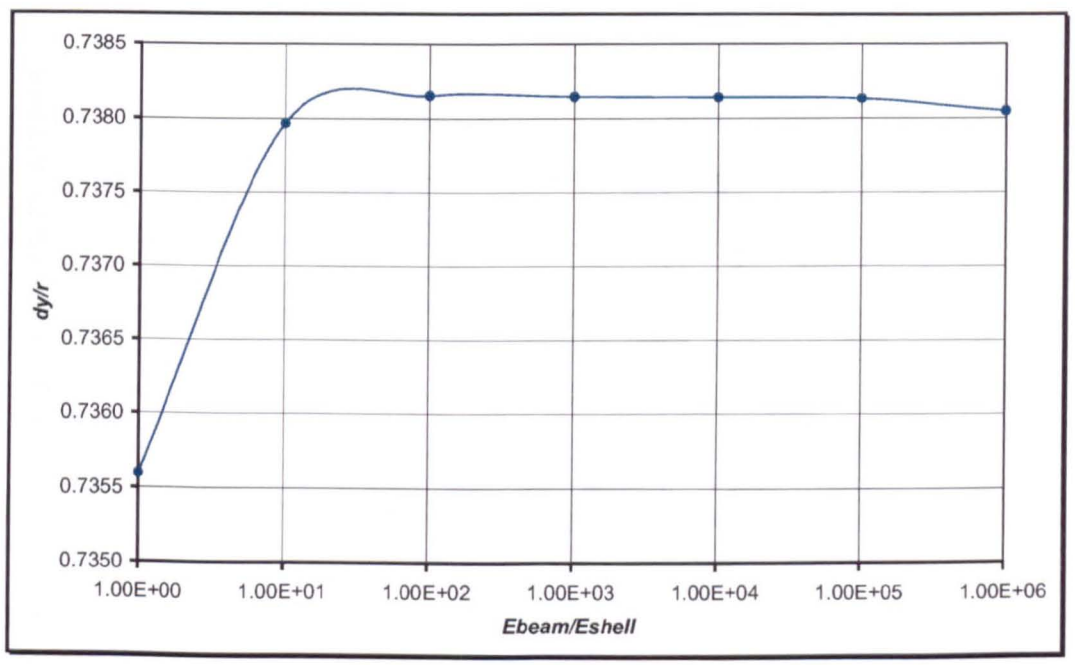

(b)

Fig.4.16 Stiffness convergence analysis for BEAM4 element based on the displacements of the beam node: (a) x-displacement, (b) y-displacement

From numerical point of view, it probably would not produce a significant error if the elasticity of the beam element has the same value as the elasticity of the shell element. However, from the trends of these graphs al always concerning in a convergence analysis, it is clear that the stiffness of the BEAM4 element should be greater than the stiffness of the shell element. From these figures, the Young's modulus of the beam element has been chosen as 1.00E+03 times the Young's modulus of the shell element.

The accuracy of using the beam element as a rigid link and applying the bending moment at the beam node was tested for a straight pipe cantilever (Fig.4.17) where the theoretical results are available in any standard engineering mechanics textbook. The results are given in Table 4.4 for the nodal downward displacement of the loaded end section and the axial stress at half-length of the pipe. The results were compared with the results produced if the bending is applied as gradient edge pressure.

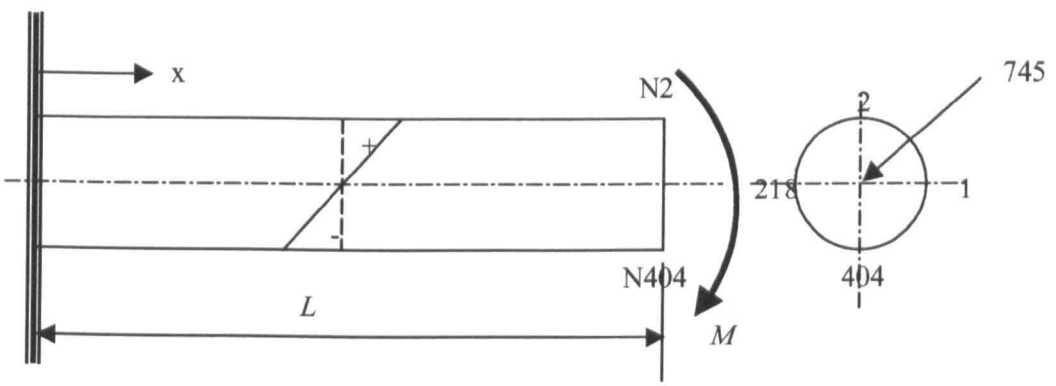

Fig.4.17 Straight pipe cantilever under bending moment

Table 4.4 Straight pipe cantilever under bending load

	End displacement, mm					σ_x (MPa)
	N745	N1	N218	N2	N404	
Theory	1.5393	---	---	---	---	10.791
FE (BEAM4)	1.5586	1.5586	1.5586	1.5586	1.5586	10.783
FE (SFGRAD)	---	1.6449	1.6449	1.5977	1.5977	11.281

Table 4.4 has been obtained using a bending moment of 3.6 x 10^6 N.mm for straight cantilever pipe having dimensions and Young's modulus as follows:

L = 3000 mm

r = 152.4 mm

t = 4.572 mm (sch.10s)

E = 207000 MPa

The maximum axial stress in Table 4.4 is calculated according to Equation (4-1) and maximum displacement is calculated by the following small deformation formula:

$$y_{max} = \frac{M}{EI}\left(\frac{x^2}{2}\right)_{max} = \frac{ML^2}{2EI} \qquad (4-3)$$

It can be seen from Table 4.4 that there is a small cross-section distortion if the bending load is applied as a gradient edge pressure. This is indicated by inequality of downward displacement between nodes at the neutral axis and nodes at most distance from the neutral axis at the loaded end. The cross-section distortion, in turn, rises the maximum axial stress. Conversely, it is clearly seen that there is no cross-sectional distortion, if beam element is used as rigid constraint and bending is acted on beam node at the centre of loaded end. It should be noted that the results in Table 4.4 were obtained under small deformation analysis. Under this condition, it is usually expected that the finite element results (marked as BEAM4 and SFGRAD in Table 4.4) produce the same maximum stresses and deflection. The difference in Table 4.4 probably caused by the edge pressure, in which ANSYS always treats the pressure load as follower load even in a small deformation. It is therefore suggested to activate the large deformation effect if pressure load included in an analysis. In what follows, the moment will be applied at the beam node and the beam elements are used to simulate rigid link at the loaded end.

The loading consists of bending moment, M, and internal pressure, p. There is no specific guidance for determining the level of loading. In this analysis, the level of bending moment, M, and internal pressure, p, were establish based on a large

deformation analysis of a 90-deg thin-wall pipe bend of short radius. Referring to Table 4.1, the dimension used for establishing the load are:

Bend angle (α) = 90-deg
Radius ratio ($\rho = R/r$) = 3
Thickness to cross-section radius ratio (t/r) = 0.026

If non-linear solution in a large deformation analysis convergence to the bending moment M for (t/r) = 0.026, it should also converge to the same moment M for (t/r) > 0.026.

The procedure to establish the level of loads is as follows: A high level of in-plane bending is applied. The load for the final converged solution is recorded and the maximum von-Mises stress at the mid-section of the bend is recorded. And then internal pressure alone is applied and the maximum stress at every load step is recorded. Internal pressure that gives the same maximum von-Mises stress at the mid-section of the bend is then chosen for the rest of the analysis. This procedure leads to the following loads:

M = 2.0E+07 N.mm
p = 2.756 M.Pa (400 psi).

Referring to Table 4.1, the nominal bending and pressure stresses corresponds to the loads applied are given in Table 4.5. The nominal bending and pressure stress is given by equation (2-26) and (2-14) respectively.

Now that the bending and internal pressure loading can be applied in any order without any difficulty, it needs to be checked how the order of loading influences the behaviour. In what follows, the system under consideration is checked for typical geometry before performing a parametric study whether the system is conservative or non-conservative. An analysis of a conservative system is *path-independent*: load can usually be applied in any order and in any number of increments without affecting

the end result. Conversely, an analysis of a non-conservative system is *path-dependent*: the actual load-response history of the system must be followed closely to obtain accurate results. Path dependent problems usually require the loads to be applied slowly, by dividing the load steps into many load sub-steps.

Table 4.5 Nominal bending and pressure stresses

t, mm	I, mm^4	Nominal stresses, N/mm^2	
		Bending	Pressure
3.9624	44061887	69.17543	53
4.5720	50840638	59.95204	45.93333
6.3500	70611998	43.16547	33.072
8.3820	93207837	32.70111	25.05455
9.5250	1.06E+08	28.77698	22.048
10.3125	1.15E+08	26.57946	20.36433
12.7000	1.41E+08	21.58273	16.536
14.2748	1.59E+08	19.20172	14.71174

4.5 Non-linear Solution

In a non-linear problem, the relation between applied load and resulting displacement ceases to be linear. The fundamental characteristic of non-linear structure behaviour is a changing structural stiffness. Large displacement and rotation (i.e., not negligible compared with initial dimensions) is a source of non-linearity. This type of non-linearity is called "*geometric non-linearity*". Another type of non-linearity is "material non-linearity" arising from non-linear stress-strain relation. Only the former type of non-linearity is considered in this study.

Geometric non-linearity arises when deformations are large enough to significantly alter the way load is applied or the way load is resisted by structures. Large rotation also causes pressure loads to change in direction, and also to change in magnitude if there is a significant change in the area to which the pressure load applied. This is expected for the case of bending of a pressurised pipe bend.

There has been some debate on the order of bending and pressure loading in a real piping system. Some suggested that internal pressure should be applied in an initial step and subsequently held constant. The rationale behind keeping pressure constant is that internal pressure generally does not increase during service, whereas bending moment may increase significantly in an accidental condition [111]. Some suggested that bending moment could be an initial loading and internal pressure is the subsequent loading. Some suggested that bending and internal pressure could rise at the same time. To end this debate, preliminary studies are carried out on typical geometry of pipe bend:

An elbow of 90-deg bend angle, radius ratio (ρ) = 3, and thickness to cross-section radius ratio (t/r) = 0.03 is investigated. Large deformation effect of course is included in the analysis.

The non-linear problem which results is solved in a sequence of linear steps. ANSYS solves the non-linear problem using the Newton-Raphson method by dividing the load into several sub-steps in a series of load increments. (A full description of this method and the modified Newton-Raphson method can be found in a standard text-book by Cook [100]). By default the convergence criteria in ANSYS was based on force and moment. Because internal pressure produced tensile membrane and tensile membrane stress increases the bending stiffness for pipes of sufficiently thin, non-linear option "stress stiffening" was included in the analysis. Other non-linear options included in ANSYS are "*predicted corrector*" method and "*bisection*" method.

For confirmation of the path-dependency, the graph of the rotation of the pipe section connecting the elbow and the loaded tangent is developed in Fig.4.18. The graph of horizontal flattening plotted as radial displacement of node at the crown of the mid-section of the bend is shown in Fig.4.19. Figure 4.20 shows the hoop stress factor plotted for node at the crown of the mid-section. It can be seen from these figures that the final results are not affected by the order of loading applied. In short, the system under consideration is a conservative system (path-independent).

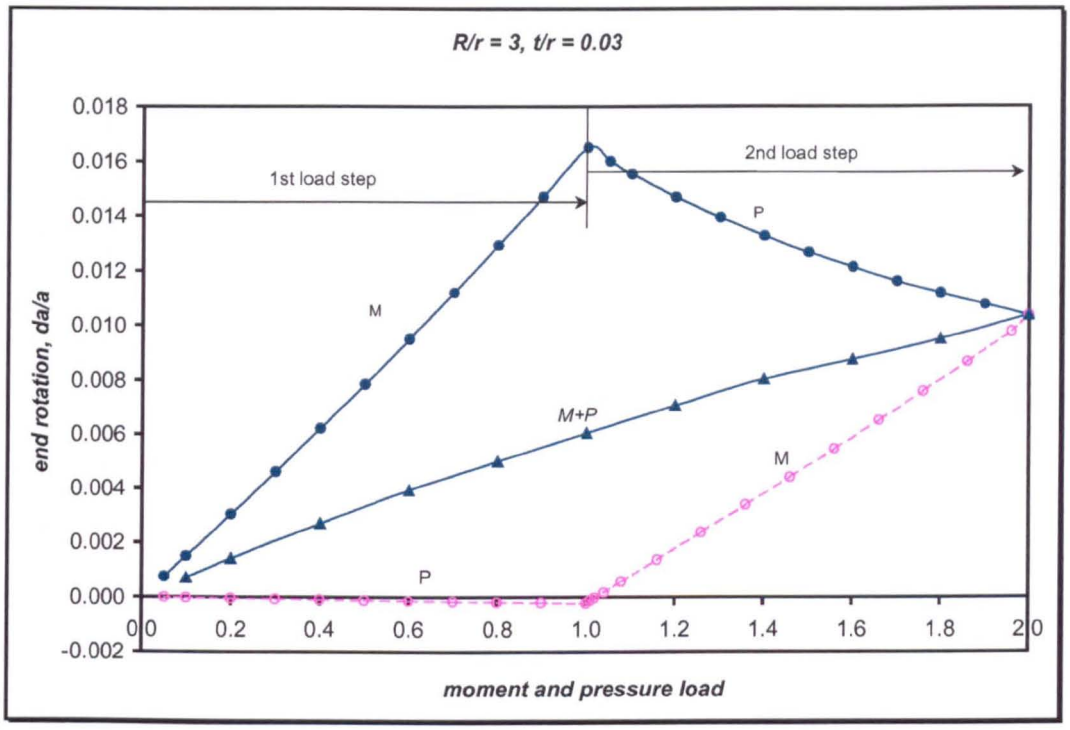

Fig.4.18 End rotation plotted against loading shows path-dependency

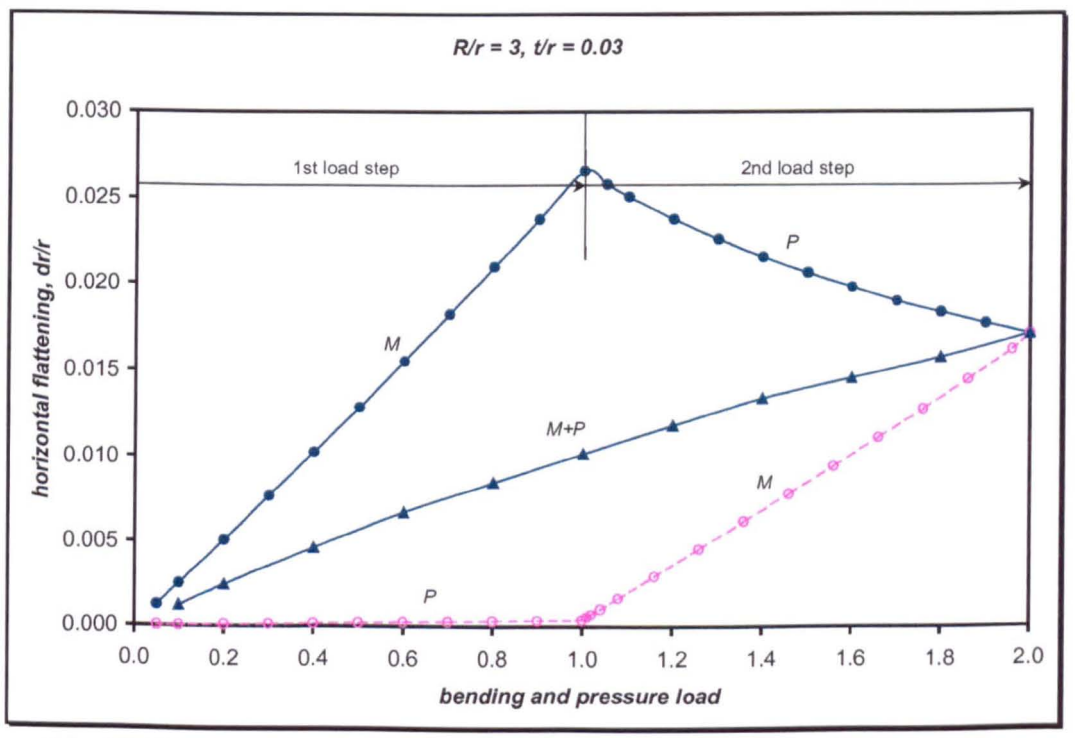

Fig.4.19 Horizontal flattening plotted against loading shows path-dependency

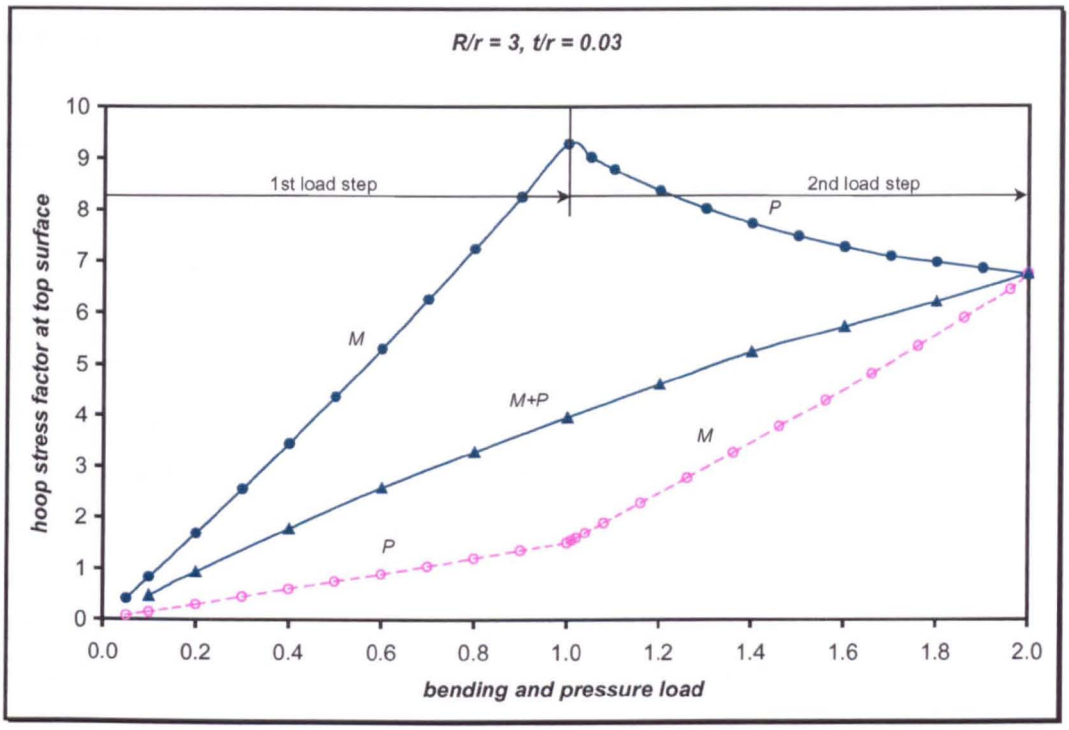

Fig.4.20 Hoop stress factor plotted against loading shows path-dependency

The value of the abscissa in these figures should be easy to read. For example, if bending load, M, followed by internal pressure, p, the value of 0.5 means M = 0.5 x 2.0E+07 N.mm, and the value of 1.5 means p = (1.5-1) x 2.756 M.Pa. If internal pressure, p, followed by bending load, M, the value of 0.5 means p = 0.5 x 2.756 M.Pa, and the value of 1.5 means M = (1.5-1) x 2.0E+07 N.mm. If bending and internal pressure rise at the same time, the value of 1.2 means M = 0.6 x 2.0E+07 MPa and p = 0.6 x 2.756 M.Pa.

It is interesting to note that if internal pressure is applied subsequent to bending load, the structural response in the second load step shows a non-linear trend. The reason for this could be explained by the "Haigh effect" The non-linearity could also be seen if bending and internal pressure load arises at the same time in a proportional manner. The non-linearity can hardly be seen when internal pressure is the first load step and internal pressure is the subsequent loading.

4.6 Summary

The details of the finite element modelling procedure to be used in this study have been described, this includes a finite element convergence analysis and a path-dependency study in line with the non-linear problem. It has been found that the system under consideration is a path-independent structure. Accordingly, the bending and internal pressure can be applied in any order without affecting the final results. Since an objective of this thesis is to find the pressure reduction effect, it is intended to apply bending moment as a first load step followed by internal pressure as a second load step. By doing so the effect of internal pressure on reducing flexibility and stresses can be evaluated for every sub-step of the analysis. This is beneficial, because solution time is reduced as compared to the case where the pressure is a first load step and bending is the subsequent loading.

The main results which will be presented in this work are cross-sectional ovalisation, flexibility factors, and stress-intensification factors for in-plane bending load. However for out-of-plane bending load, the results which will be presented are flexibility and stress-intensification factors. The reason for this difference is that the location of maximum radial displacement changes for every bend angle and radius ratio, and sometimes its location also change for different values of wall thickness. The ANSYS general post-processor (the /POST1) and the ANSYS time-history post-processor (the /POST26) are used to obtain the stresses and displacement. Results for in-plane closing and opening moment will be presented in Chapter 5 and Chapter 6 respectively. The result of analysis for out-of-plane bending will be presented in Chapter 7.

CHAPTER 5

IN-PLANE CLOSING BENDING

A distinct feature of piping elbow deformation is the ovalisation of its cross-section under the action of external bending moment. The ovalisation makes the elbow more flexible than an equivalent length and cross-section of straight pipe. The presence of internal pressure further reduces the ovalisation and stiffens the elbows in the direction of applied bending. The purpose of this chapter is to evaluate the pressure reduction effect on cross-sectional ovalisation, end-rotation (flexibility factors) and stress-intensification factors resulting from the action of in-plane closing bending.

The results from the action of bending alone will be first established and formulae for ovalisation, flexibility, and stress-intensification factors are derived. The pressure reduction effect is then evaluated and formulae developed. The effect of bend angle on results from both the action of bending alone and the internal pressure is also studied.

5.1 Ovalisation Factor

Under in-plane closing moment, the cross-section deforms into an oval shape with its major axis perpendicular to the plane of the bend. This type of deformation is here called "*positive flattening*". Positive flattening is evaluated as diameter expansion from crown to crown at the mid-section of the bend.

Typical positive flattening for a 90-deg bend is shown in Fig.5.1. This figure is plotted for radius ratio $\rho = 3$, and thickness to cross-section radius $t/r = 0.026$ under an in-plane closing moment $M = 2.0E+07$ N.mm.

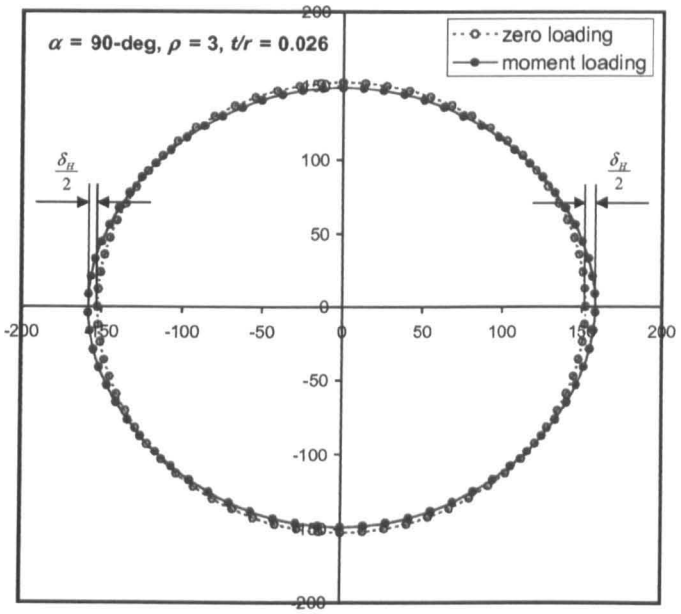

Fig.5.1 Typical cross-sectional ovalisation under in-plane closing bending

Recall the asymptotic solution of Clark and Reissner [24], the amount of flattening in the horizontal direction (here defined as 'positive flattening') was proposed in a non-dimensional form in eqn (2-43):

$$\frac{\delta_H}{t} = \sqrt{12(1-\nu^2)}\left(\frac{r}{t}\right)^2 \frac{\sigma_n}{E} \tag{5-1}$$

It can be noticed that the positive flattening proposed by Clark and Reissner is independent of the pipe bend radius, R, and was related to the nominal bending stress in a straight pipe, σ_n. Equation (5-1) might be used for calculation of the amount of flattening in a straight pipe under bending. Because it was related to the nominal bending stress in a straight pipe, eqn (5-1) will be further defined as 'nominal ovalisation'.

In this section, an ovalisation factor for piping elbows under in-plane closing moment and internal pressure will be developed, and formula for design purpose will be proposed. Ovalisation factor, ξ, is defined as positive flattening obtained from finite element analysis (typically shown in Fig.5.1) divided by the nominal ovalisation (eqn.4-1):

$$\xi = \frac{(\delta_H / t)_{FE}}{\xi_n} \tag{5-2}$$

where ξ_n is nominal ovalisation, as given in eqn (5-1).

Figure 5.2 shows a typical moment vs. positive flattening curve plotted for a 90^0 elbow under in-plane closing moment. The ordinate in Figure 5.2 is non-dimensional moment $m = M/D$, where M is applied bending moment and D is the shell bending stiffness as given in equation (2-75). It can be seen from Fig.5.2 that a pipe elbow under in-plane closing bending exhibits a structural softening behaviour, but the magnitude of non-linearity is essentially small.

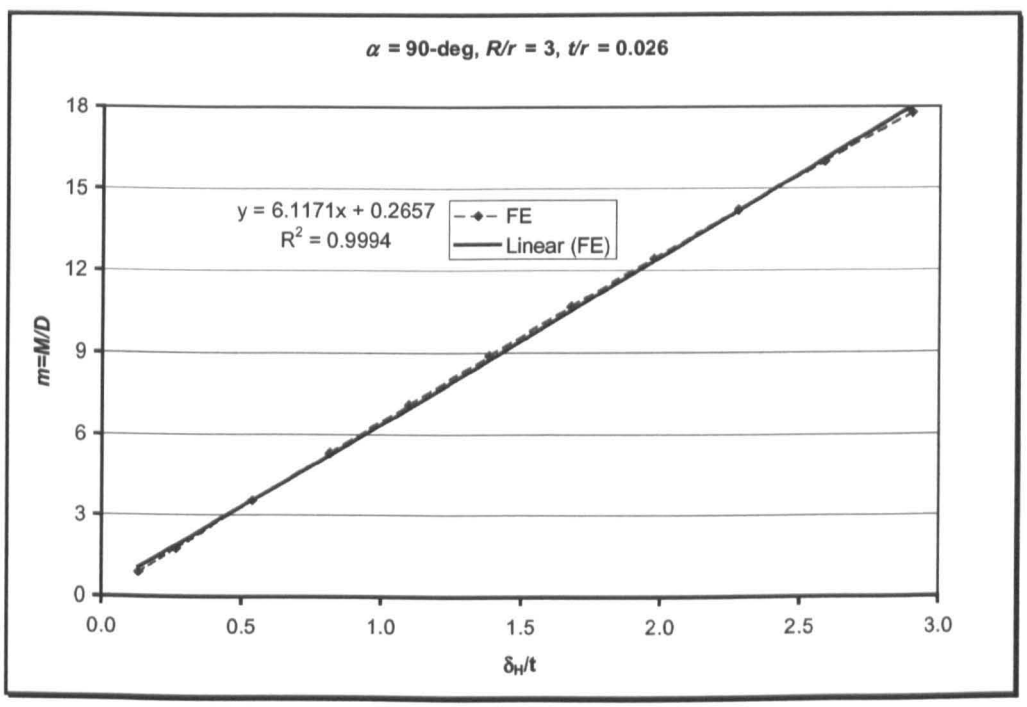

Fig.5.2 Typical moment versus positive flattening under in-plane closing bending

Figure 5.3 shows the ovalisation factor of 90-deg pipe elbows plotted against pipe bend parameter, λ, for various radius ratio, ρ. It can be clearly seen that the ovalisation factor very much depends on pipe bend parameter λ and radius ratio ρ. As shown in Fig.5.3, the relation of ovalisation factor, ξ, and pipe bend parameter, λ, is essentially linear in a log-log plot, especially for elbows of short radius bend. Accordingly, the relation can be expressed in the following form:

$$\xi = \frac{p}{\lambda^q} \tag{5-3}$$

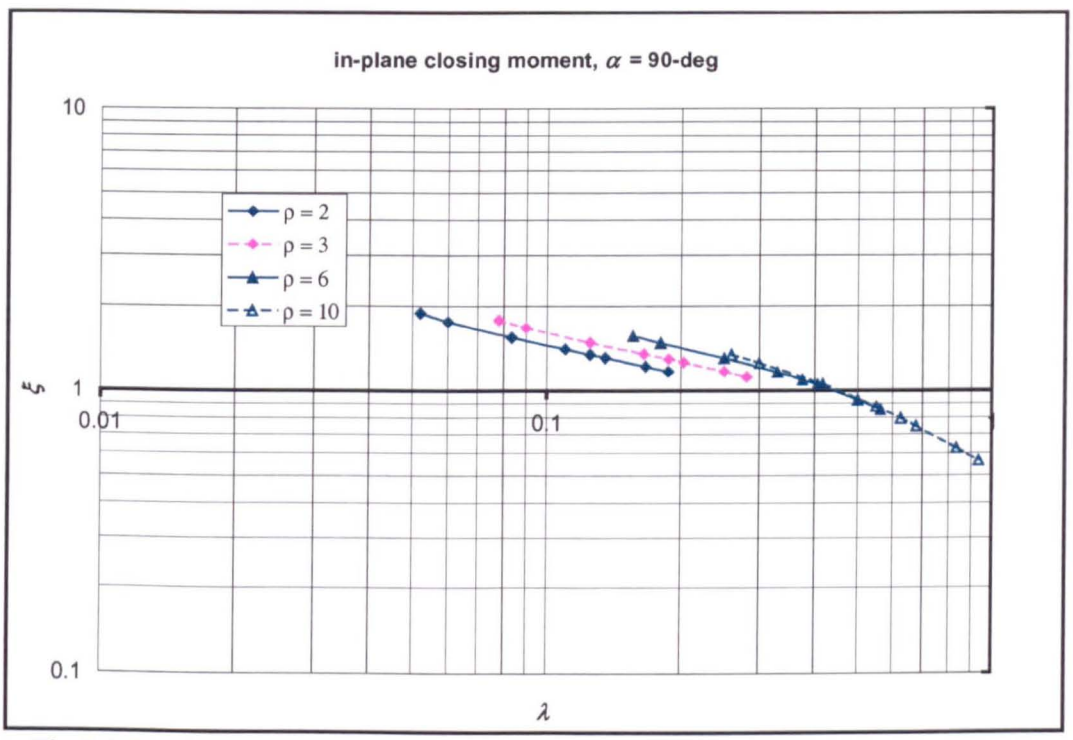

Fig.5.3 Ovalisation factor under in-plane closing bending for 90-deg pipe elbows

By the method of curve fitting, formulae for the ovalisation factor can be derived from these figures. Taking the effect of radius ratio into account, the ovalisation factors for 90-deg pipe elbows are given in the following equations:

$$\xi = \frac{0.6324}{\lambda^{0.3642}} \qquad \text{for} \frac{R}{r} = 2 \qquad (5-4)$$

$$\xi = \frac{0.714}{\lambda^{0.354}} \qquad \text{for} \frac{R}{r} = 3 \qquad (5-5)$$

$$\xi = \frac{0.6823}{\lambda^{0.4563}} \qquad \text{for} \frac{R}{r} = 6 \qquad (5-6)$$

$$\xi = \frac{0.5648}{\lambda^{0.6715}} \qquad \text{for} \frac{R}{r} = 10 \qquad (5-7)$$

In can be seen from equations (5-4) through (5-7) that the ovalisation factor is not only function of pipe bend parameter, λ, but also function of radius ratio *R/r*. These equation are not in suitable form for design purposes. However these equation can be expressed in the following form:

$$\xi = \frac{0.565}{\lambda^{2/3}}[f(\lambda)] \qquad (5-8)$$

where $f(\lambda)$ represents the dependence of ovalisation factor on radius ratio, (*R/r*). This results in $f(\lambda)$ be different for every radius ratio. It should be noted that eqn (5-8) was expressed based on the ovalisation factor for a long radius bend, (*R/r*) = 10.

Following the procedure of Fujimoto and Soh [92], equations (5-4) through (5-7) can be written in the following form

$$\xi = \frac{0.565}{\lambda^{2/3}}[0.9501 + 0.1682\ln(\lambda)] \qquad \text{for} \frac{R}{r} = 2 \qquad (5-9)$$

$$\xi = \frac{0.565}{\lambda^{2/3}}[1.1179 + 0.2177\ln(\lambda)] \qquad \text{for} \frac{R}{r} = 3 \qquad (5-10)$$

$$\xi = \frac{0.565}{\lambda^{2/3}}[1.1781 + 0.1966\ln(\lambda)] \qquad \text{for} \frac{R}{r} = 6 \qquad (5-11)$$

$$\xi = \frac{0.565}{\lambda^{2/3}}[0.9996 + 0.0001\ln(\lambda)] \qquad \text{for} \frac{R}{r} = 10 \qquad (5-12)$$

In the above formulae, the effect of radius ratio was taken into account with a reference to the ovalisation factor for pipe elbows of radius ratio equal 10 (long radius bend). In equation (5-12) therefore, the term in the square bracket could be neglected without any significant loss in accuracy. Figure 5.4 shows the ovalisation factor obtained from finite element (FE), equations (5-4) through (5-7), and equations (5-9) through (5-11). It can be seen that the proposed equations fit well the results from finite element.

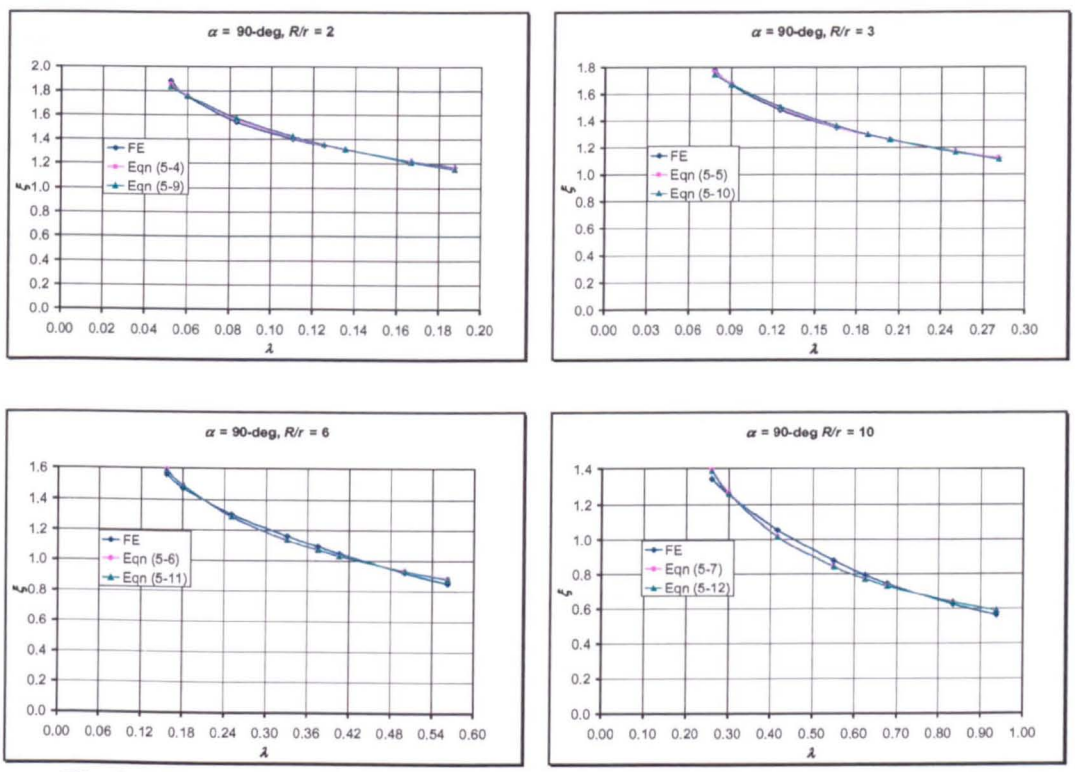

Fig.5.4 Comparison for ovalisation between derived formula and FE results

The form of formulae proposed by Fujimoto and Soh [92] for flexibility factor was followed here for ovalisation factor. It can be seen that the dependence of ovalisation factors on radius ratio is represented by logarithmic functions of pipe bend parameter, λ. Whereas Fujimoto and Soh [92] found that the dependence of flexibility factor on radius ratio represented by a power function of λ, see equation (2-49) and (2-50). This difference will be considered more detail in Section 5.2 (Flexibility Factors)

5.1.1 Effect of Bend Angle on Ovalisation Factor

To account for the effect of bend angle on ovalisation factor other than 90-deg, pipe elbows having bend angle of 30, 45, 60, and 180-deg has been studied. Figure 5.5 through 5.8 show graphs for ovalisation factor plotted against pipe bend parameter. It can be seen from these graphs that the relation between ovalisation factor and pipe bend parameter is essentially linear in log-log graph for all bend angles considered, especially for elbows of short-radius bend. For long radius elbows, the graph is not exactly linear, especially for large angle bend (90-deg and greater), but this deviation is not significant from the practical point of view for the purpose of development a simple formula.

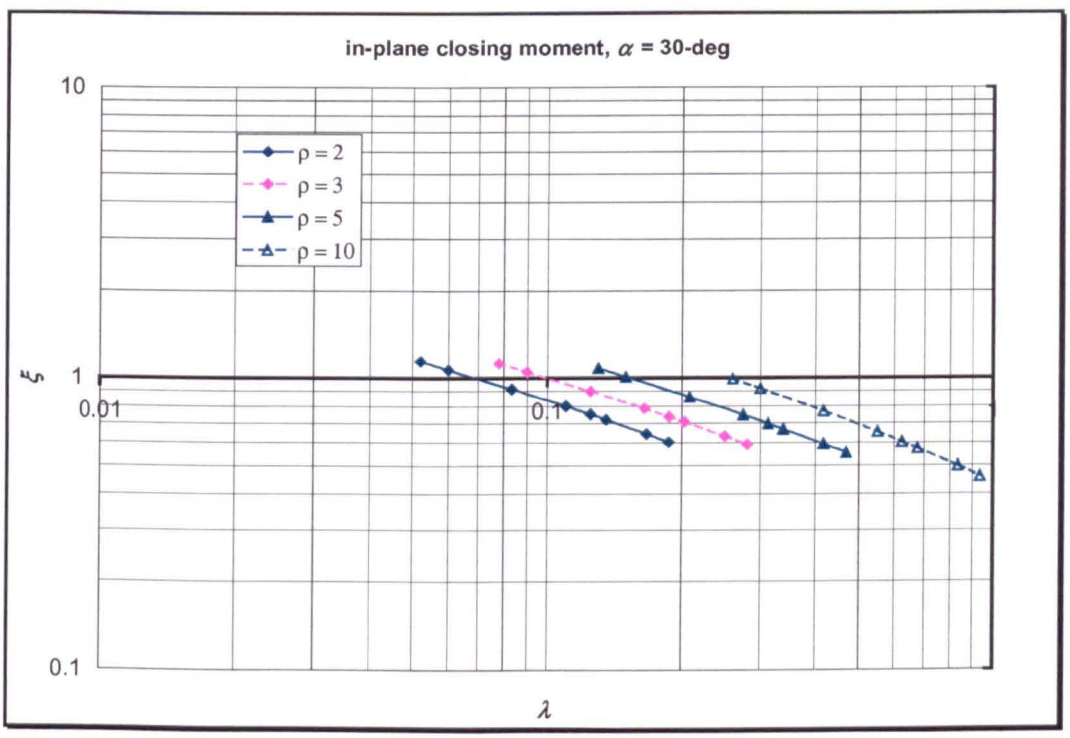

Fig.5.5 Ovalisation factor under in-plane closing bending for 30-deg pipe elbows

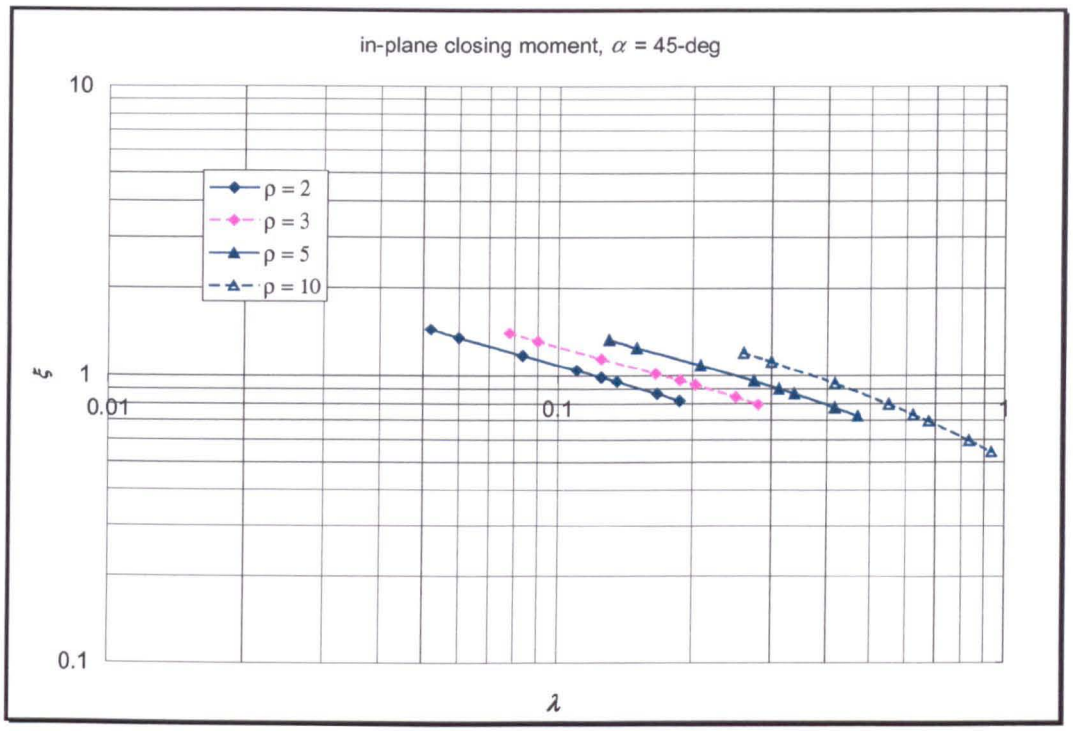

Fig.5.6 Ovalisation factor under in-plane closing bending for 45-deg pipe elbows

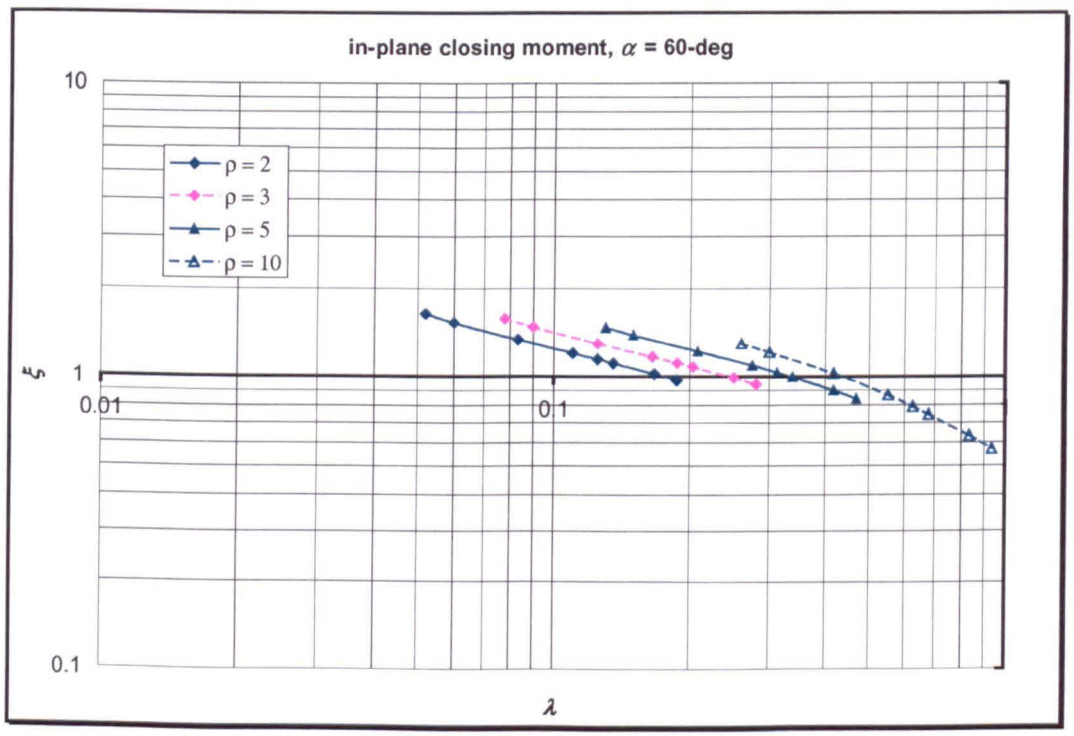

Fig.5.7 Ovalisation factor under in-plane closing bending for 60-deg pipe elbows

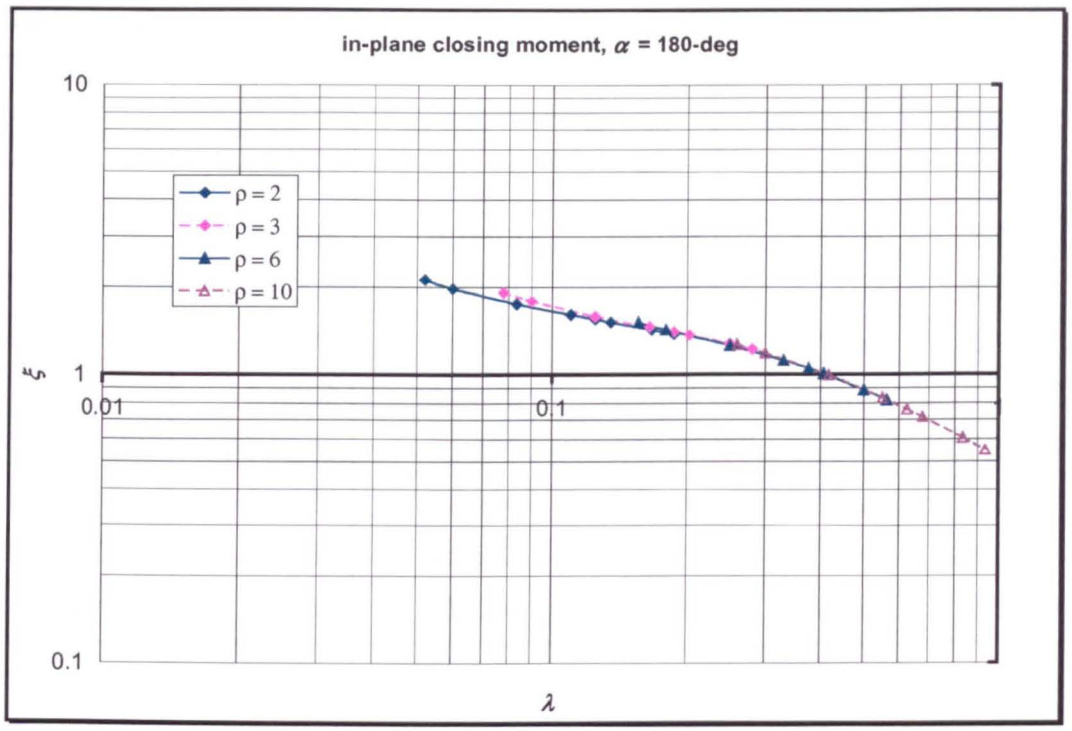

Fig.5.8 Ovalisation factor under in-plane closing bending for 180-deg pipe elbows

Using the procedure described above, the ovalisation factor of pipe elbows for the bend angles considered, can be expressed by the following approximate formula:

$$\xi = \frac{0.565}{\lambda^{2/3}}[a + b\ln(\lambda)] \qquad (5\text{-}13)$$

where a, and b are functions of radius ratio ρ, as given in Table.5.1 and Table.5.2 respectively.

Table 5.1 The value of coeffecient "*a*" in equation (5-12) for various bend angles

ρ	Bend angle				
	30-deg	45-deg	60-deg	90-deg	180-deg
2	0.4434	0.6346	0.7722	0.9501	1.1437
3	0.5395	0.7603	0.9193	1.1179	1.2303
4	0.6006	0.8293	0.9936	1.1430	1.2145
5	0.6577	0.8922	1.0509	1.1651	1.1801
6	0.6897	0.9050	1.1024	1.1781	1.1247
7	0.7235	0.9279	1.1187	1.1907	1.0705
8	0.7528	0.9454	1.1096	1.1542	1.0362
9	0.7787	0.9593	1.0751	1.0915	1.0074
10	0.7968	0.9554	1.0115	0.9996	0.9669

Table 5.2 The value of coefficient "*b*" in equation (5-12) for various bend angles

ρ	Bend angle				
	30-deg	45-deg	60-deg	90-deg	180-deg
2	0.0543	0.0954	0.1266	0.1682	0.2156
3	0.0686	0.1219	0.1635	0.2177	0.2463
4	0.0756	0.1356	0.1802	0.2251	0.2352
5	0.0800	0.1414	0.1866	0.2161	0.2182
6	0.0816	0.1418	0.1812	0.1966	0.1806
7	0.0792	0.1326	0.1625	0.1705	0.1599
8	0.0732	0.1152	0.1310	0.1261	0.1196
9	0.0636	0.0896	0.0867	0.0673	0.0703
10	0.0526	0.0539	0.0324	0.0001	0.0151

It can be seen from these Figures and Tables that the ovalisation factor is also very much affected by bend angle. Tables 5.1 and 5.2 indicated that the ovalisation factor is directly proportional to the bend angle for elbows of short radius. As shown in Fig.5.9, the curves are parallel for short-radius bends. Figure 5.10 shows that the ovalisation factor for elbows of long radius is directly proportional to the bend angle

for elbows of 90-deg and smaller. Figure 5.10 shows that the ovalisation factor for 180-deg elbows can be considered less than those for 90-deg elbows but greater than those for 45-deg elbows.

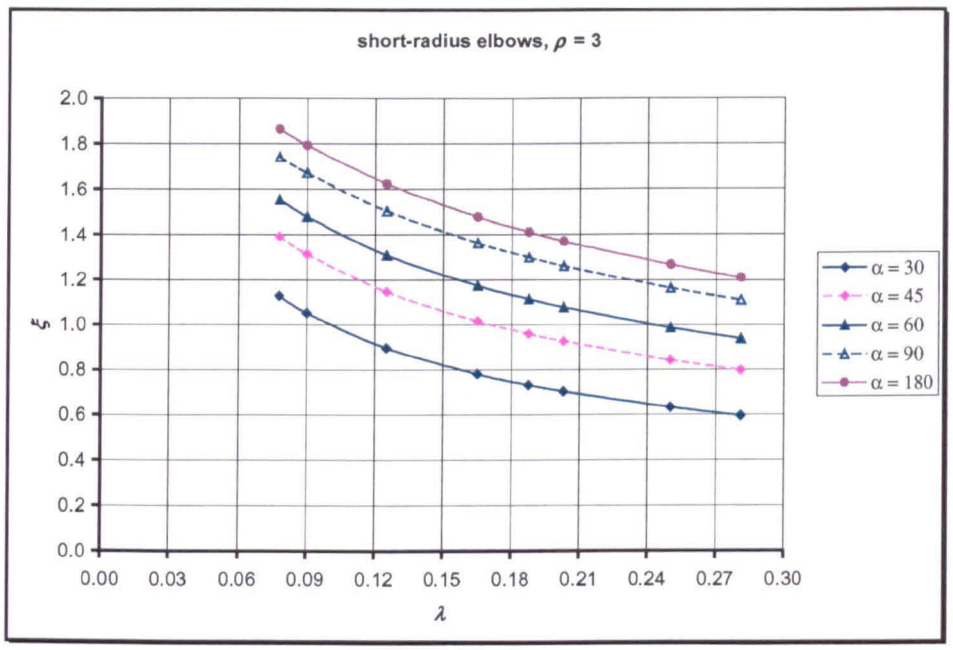

Fig.5.9 Ovalisation factor for short-radius pipe elbows with various bend angles

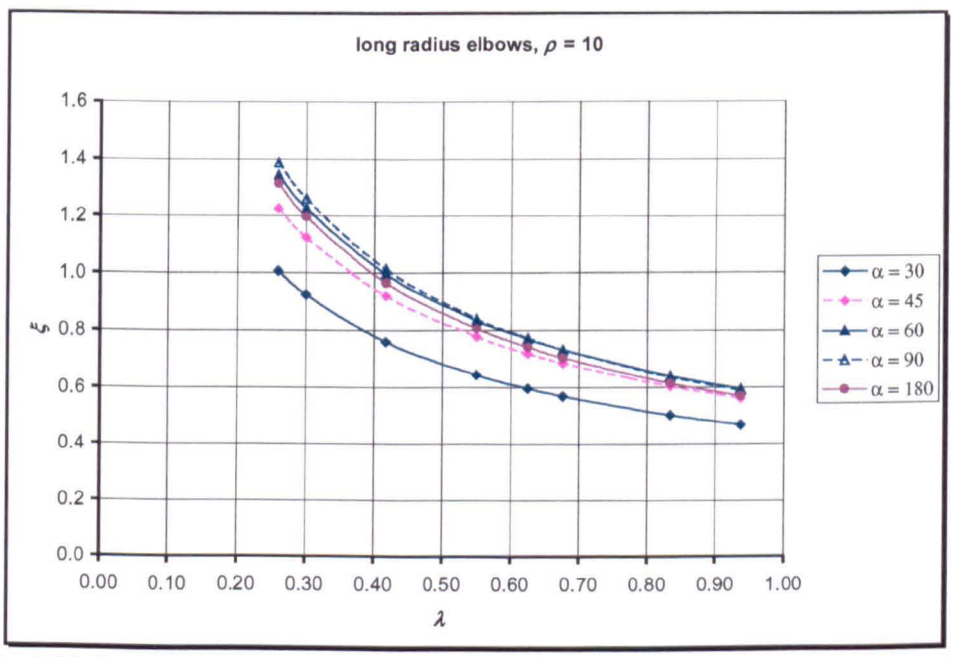

Fig.5.10 Ovalisation factor for long-radius pipe elbows with various bend angles

5.1.2 Pressure Reduction Effect

When internal pressure is applied to the ovalised elbows resulting from in-plane bending load, it tries to push the deformed cross-section back to its original circular shape. This phenomenon is typically shown in Fig.5.11.

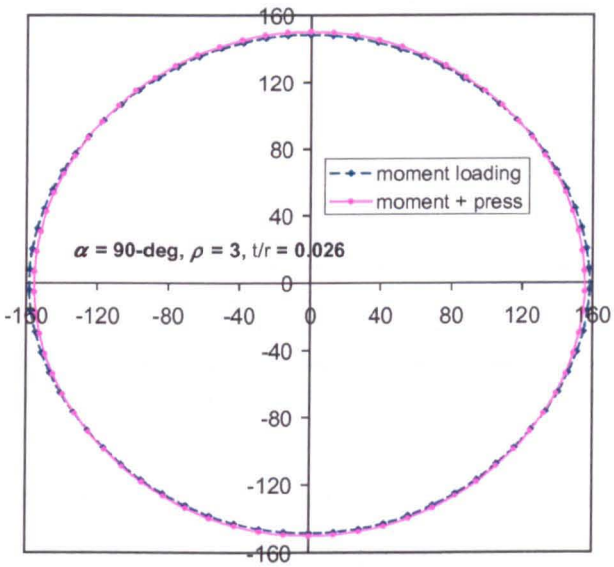

Fig.5.11 Typical pressure reduction effect on cross-sectional ovalisation

To assess the pressure reduction effect on the ovalisation factor, attention has been focused on the radial displacement of the crown node at the mid-section of the bend, where the maximum value is expected to be located. Fig.5.12 shows a typical pressure – ovalisation factor curve plotted for a 90-deg bend under in-plane closing moment.

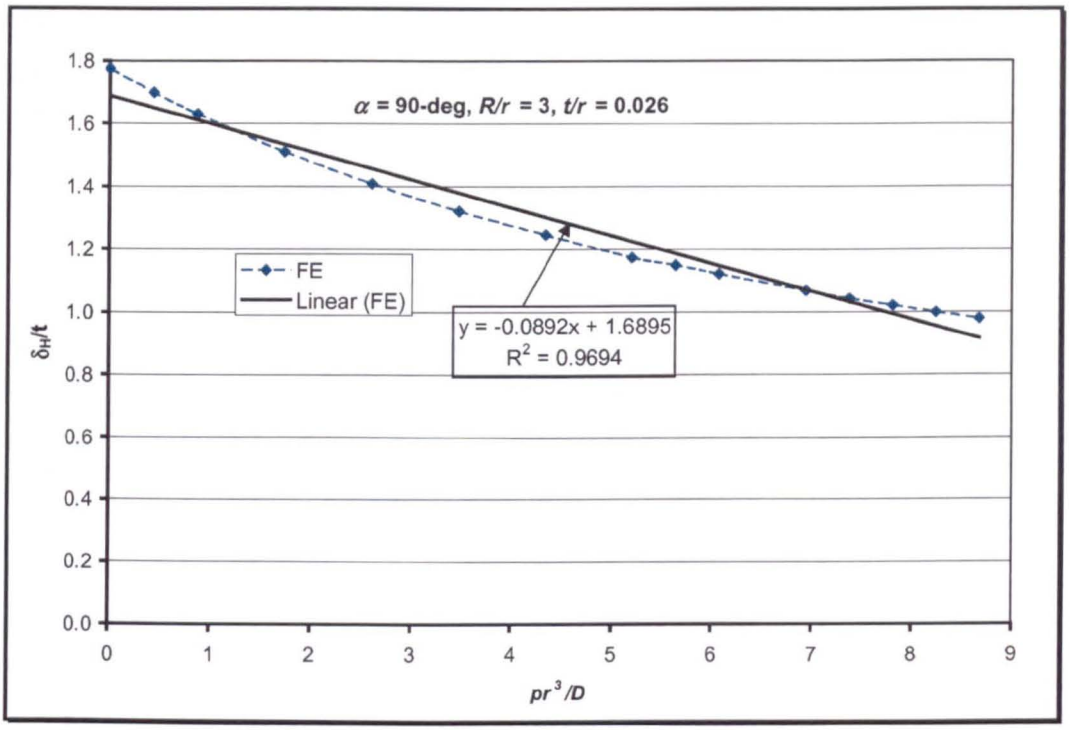

Fig.5.12 Pressure – ovalisation factor curve under an in-plane closing bending

In Fig 5.12, the abscissa value of 0.0 represents the final load step of the moment loading, and the start of subsequent internal pressure loading. It can be clearly seen that the relation between internal pressure loading and positive flattening is non-linear. This figure shows the "*Haigh effect*" [12] where non-linearity is present whenever internal pressure acts on a pipe of non-circular cross-section. In this study, the internal pressure load was applied to elbows of oval cross-section resulting from an in-plane closing moment.

Fig.5.13 through 5.16 show the ovalisation factor of 90-deg pipe elbows plotted against pipe bend parameter, λ, for various radius ratio, ρ. These figures show clearly that the presence of internal pressure reduces the ovalisation factor resulting from in-plane closing moment loading. The pressure reduction is more pronounced for thin walled piping elbows (low pipe bend parameter). It is interesting to note from these figures that internal pressure does not always reduce the ovalisation factor, but it can also increase the ovalisation factor, depending on the thickness to cross-section radius ratio. In this section, the pressure reduction effect on the ovalisation factor is

evaluated and empirical formulae are developed and proposed. The procedure of Rodabaugh and George [30] is followed.

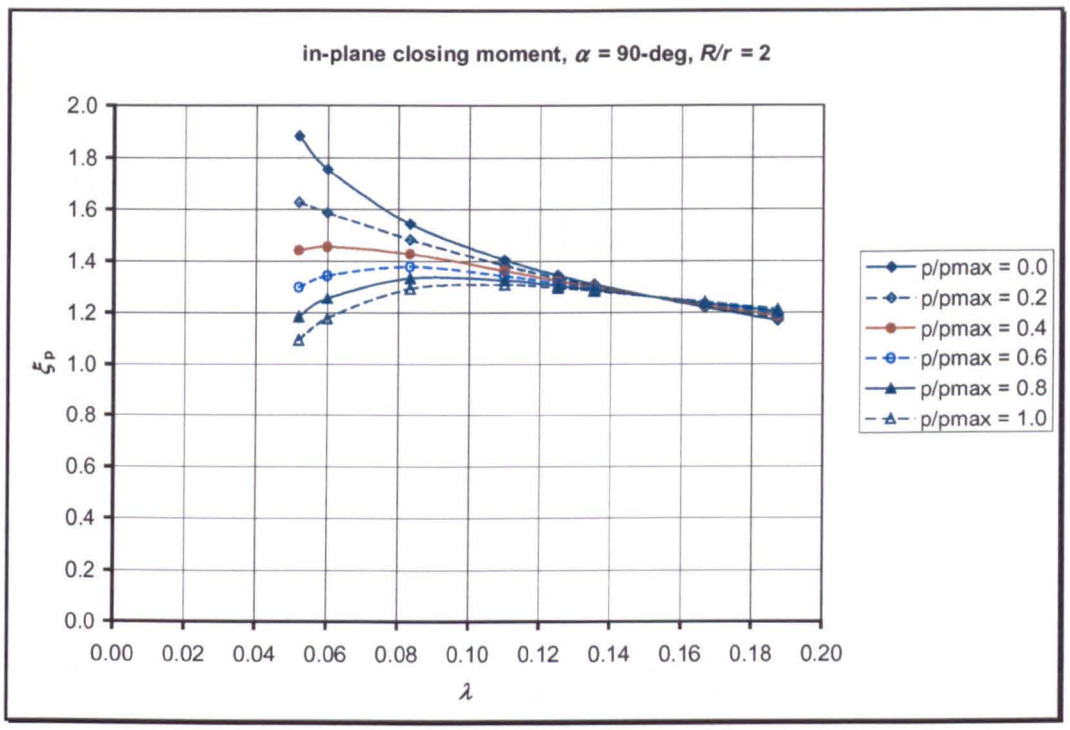

Fig.5.13 Pressure reduction on ovalisation factor for 90-deg elbows: $R/r = 2$

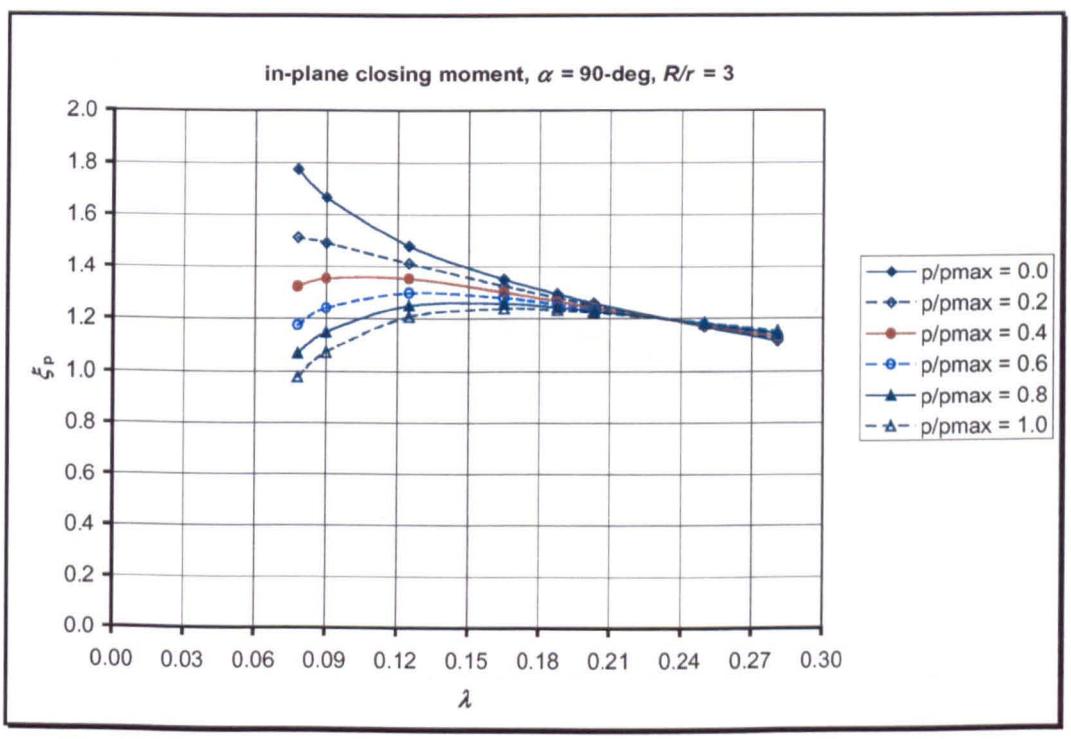

Fig.5.14 Pressure reduction on ovalisation factor for 90-deg elbows: $R/r = 3$

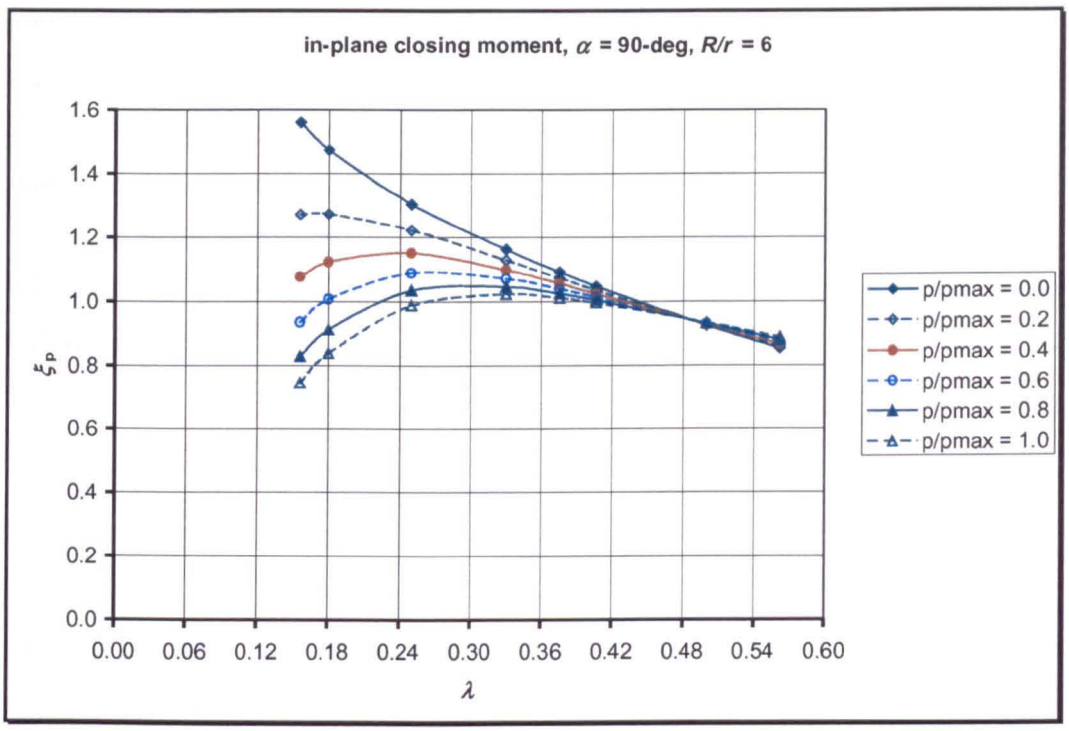

Fig.5.15 Pressure reduction on ovalisation factor for 90-deg elbows: $R/r = 6$

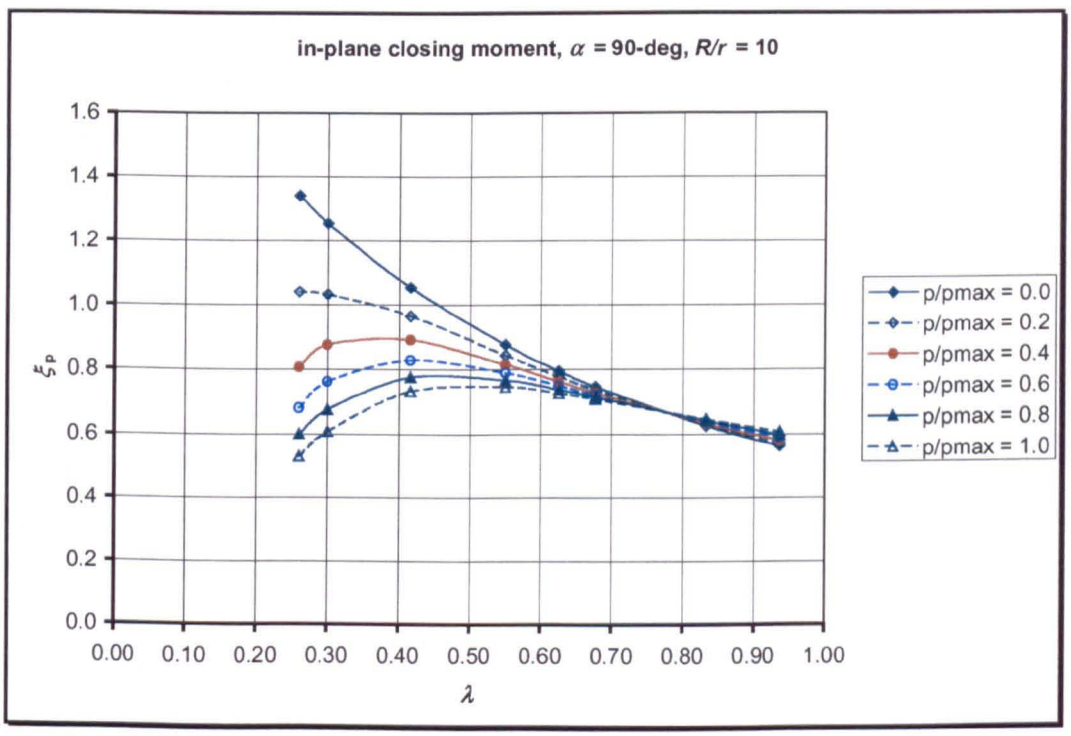

Fig.5.16 Pressure reduction on ovalisation factor for 90-deg elbows: $R/r = 10$

In the above figures, pmax is the maximum internal pressure applied in this study (pmax = p = 2.756 M.Pa) and p is the portion of pressure load. If internal pressure load is divided into ten sub-steps, the graphs in the above figures represent the 2nd, 4th, 6th, 8th, and 10th sub-step. The terms p and pmax are only used in graphs, but it should be understood from the context.

When internal pressure is included, the ovalisation factor can be expressed in the following form:

$$\xi_p = \frac{\xi}{1 + X_w\left(\frac{p}{E}, \frac{r}{t}, \frac{R}{r}\right)} \tag{5-14}$$

where ξ represent the ovalisation factor in the absence of internal pressure as given in equation (5-3). The second term in the denominator represents the pressure reduction effect: it is a function of non-dimensional pressure *p/E*, non-dimensional thickness *r/t*, and radius ratio *R/r*.

To develop an expression for the pressure reduction effect, equation (5-14) is further written in the following form:

$$\frac{\xi}{\xi_p} - 1 = X_\xi\left(\frac{p}{E}, \frac{r}{t}, \frac{R}{r}\right) \tag{5-15}$$

The left-hand side of equation (5-15) for 90-deg elbows is obtained from finite element generated data as shown in Fig.5.13 through 5.16. This quantity is plotted against *p/E* and *r/t* for constant radius ratio *R/r*, and against *p/E* and *R/r* for constant non-dimensional thickness *r/t*. The procedure is described as follows:

From figure 5.14 for *R/r* = 3, the pressure reduction as given by equation (5-15) can be plotted against *p/E* and *r/t* as shown in figure 5.17(a) and (b).

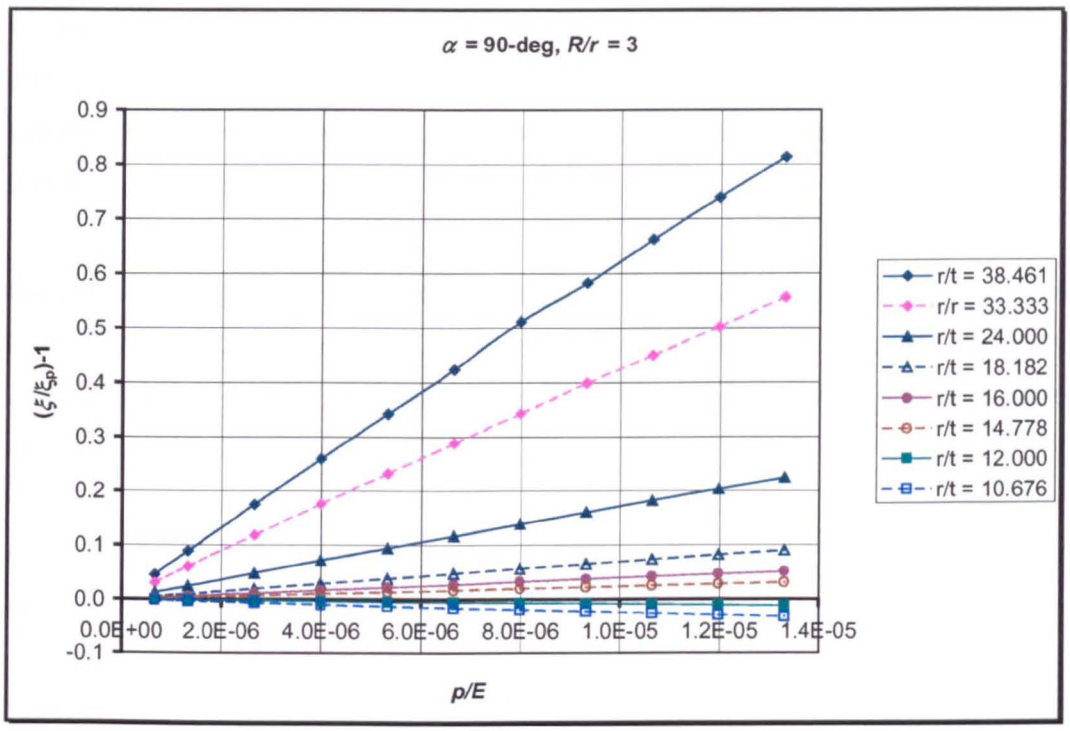

(a)

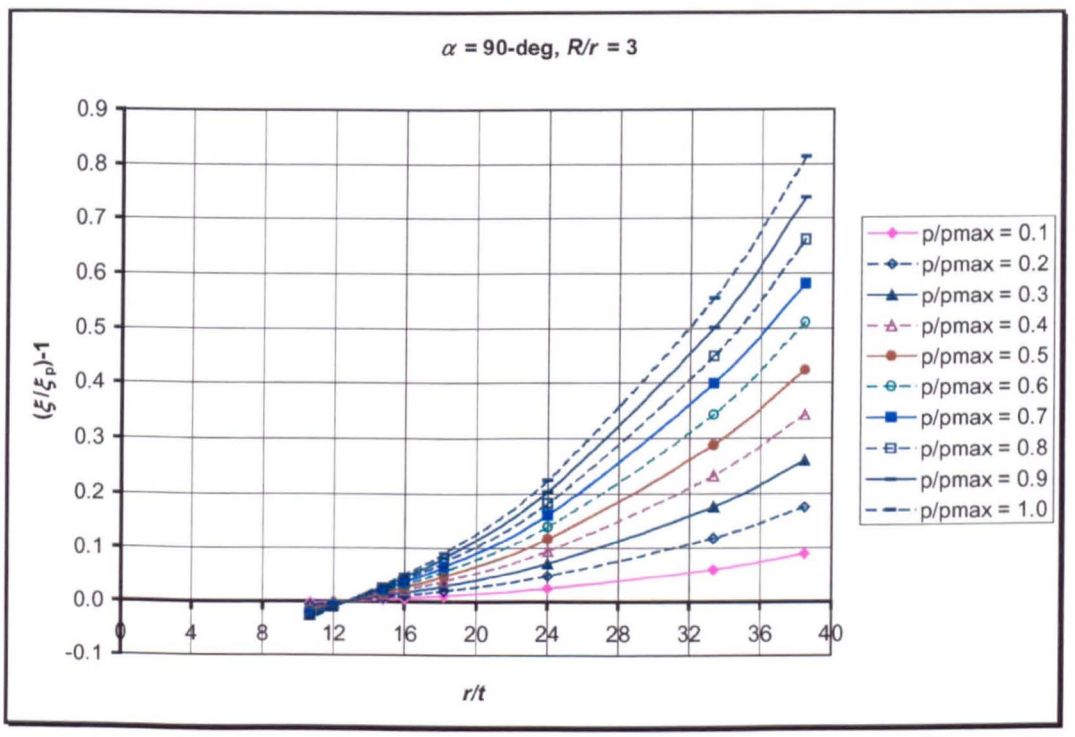

(b)

Fig.5.17 Pressure reduction plotted for $R/r = 3$ against (a) p/E, (b) r/t.

Figure 5.17(a) reveals that internal pressure reduces the ovalisation factor for r/t greater than certain value, but increases the ovalisation for r/t smaller than this value. Figure 5.17(b) reveals that internal pressure reduce the ovalisation for $r/t > 13.33$, but increases the ovalisation for $r/t < 13.33$.

By plotting the pressure reduction as given by equation (5-15), similar trend was found for R/r = 2, 6, and 10. Surprisingly, the point where the reduction effect of internal pressure become increasing effect is identical for all radius ratio, at a value of r/t about 13.33.

Figure 5.18 and 5.19 shows the pressure reduction effect plotted against p/E and R/r respectively for $t/r = 0.03$.

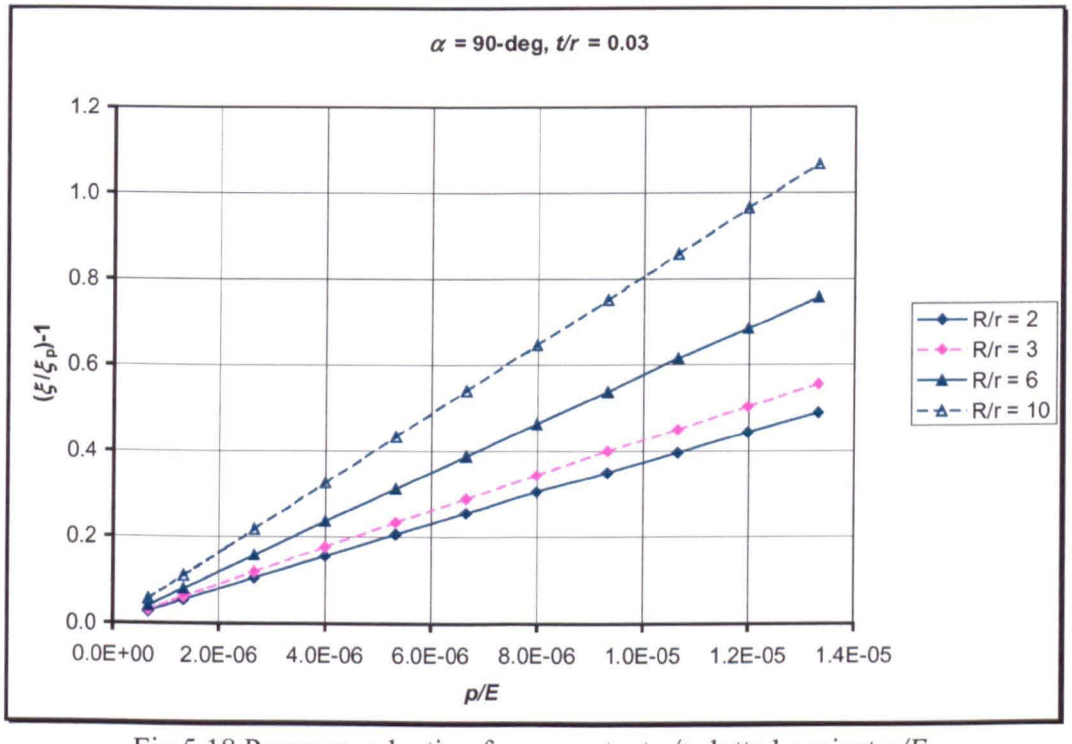

Fig.5.18 Pressure reduction for a constant r/t plotted against p/E

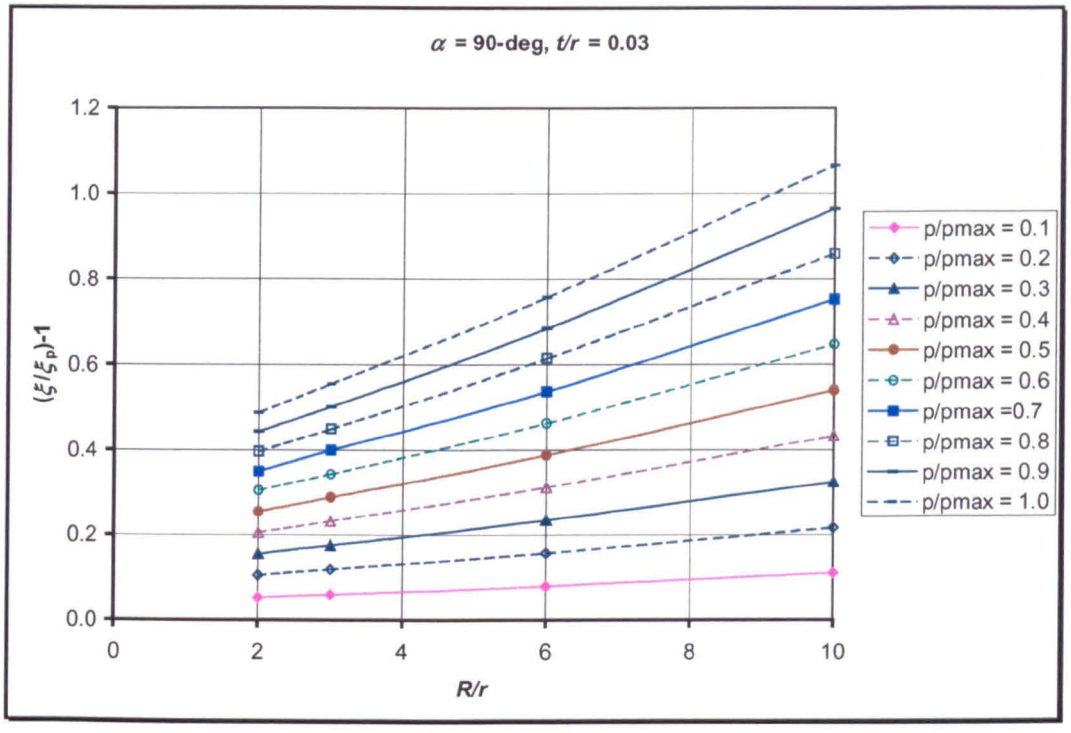

Fig.5.19 Pressure reduction for a constant *r/t* plotted against *R/r*

To follow the procedure of Rodabaugh and George [30], it is necessary to plot the pressure reduction in a log-log plot. Figure 5.20 shows a log-log plot corresponding to Fig.5.17 for a constant radius ratio. Pressure reduction in a log-log for a constant thickness corresponding to Fig.5.18 and 5.19 is shown in Fig.5.21.

It should be noted that negative values could not be plotted in log-log graph. Referring to Table 4.1, the values of thickness of 12.7 and 14.2748 are therefore not plotted in Fig.5.20.

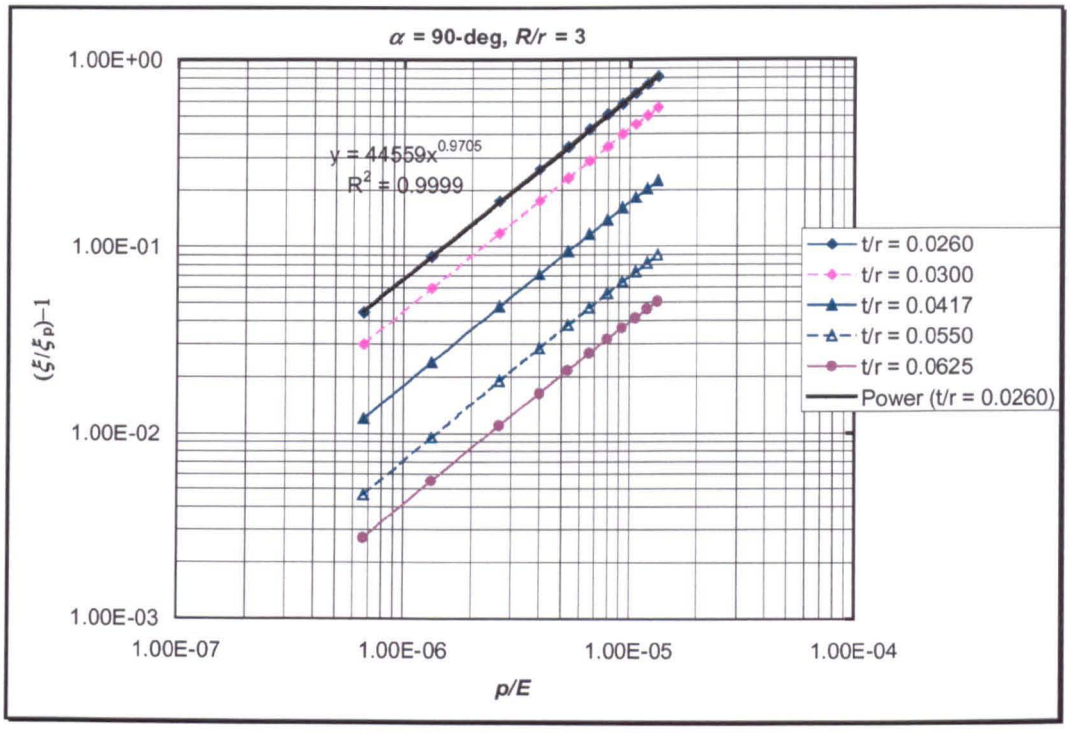

(a)

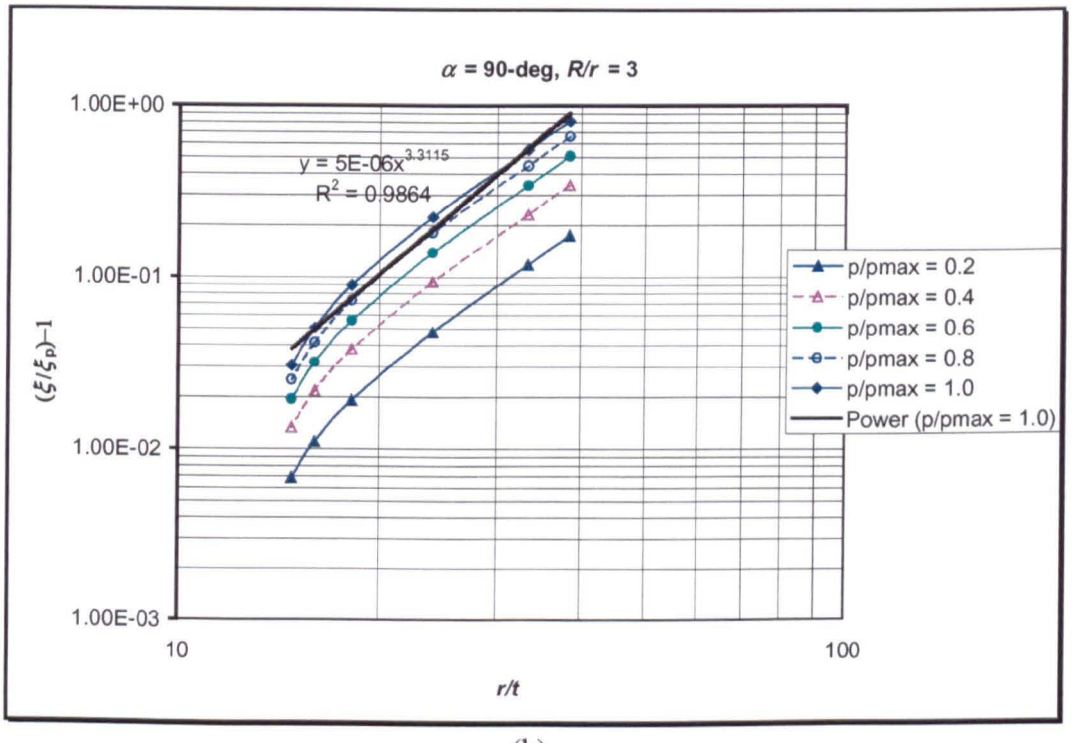

(b)

Fig.5.20 Pressure reduction for constant radius ratio plotted against (a) *p/E*, (b) *r/t*

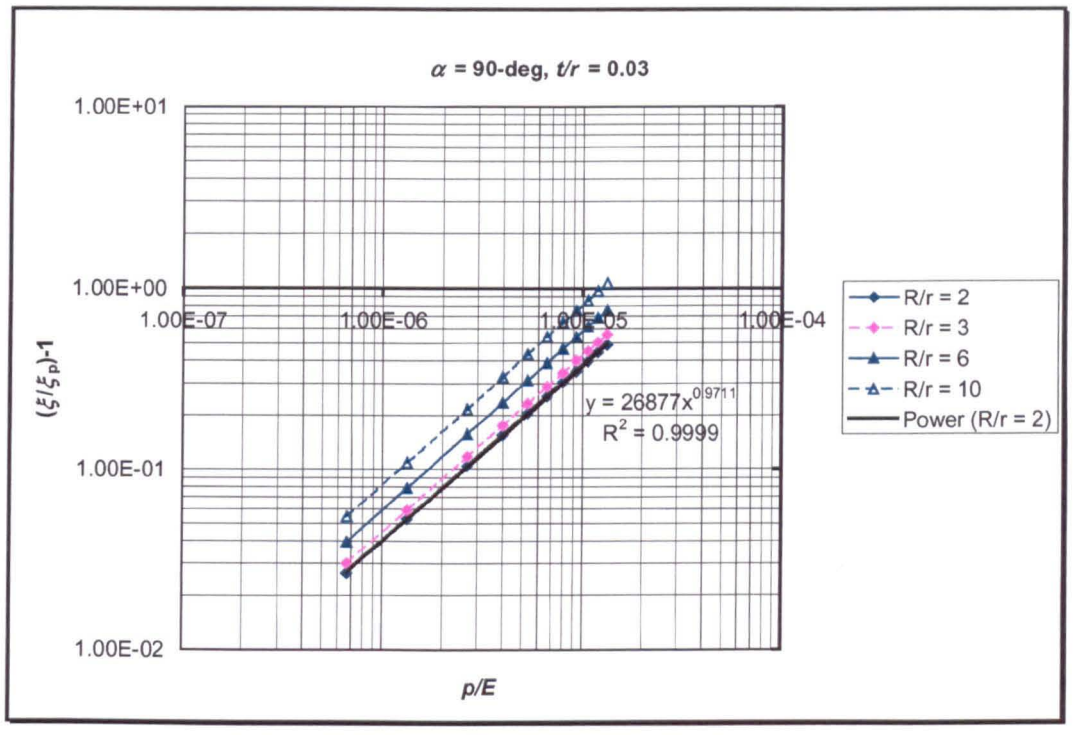

(a)

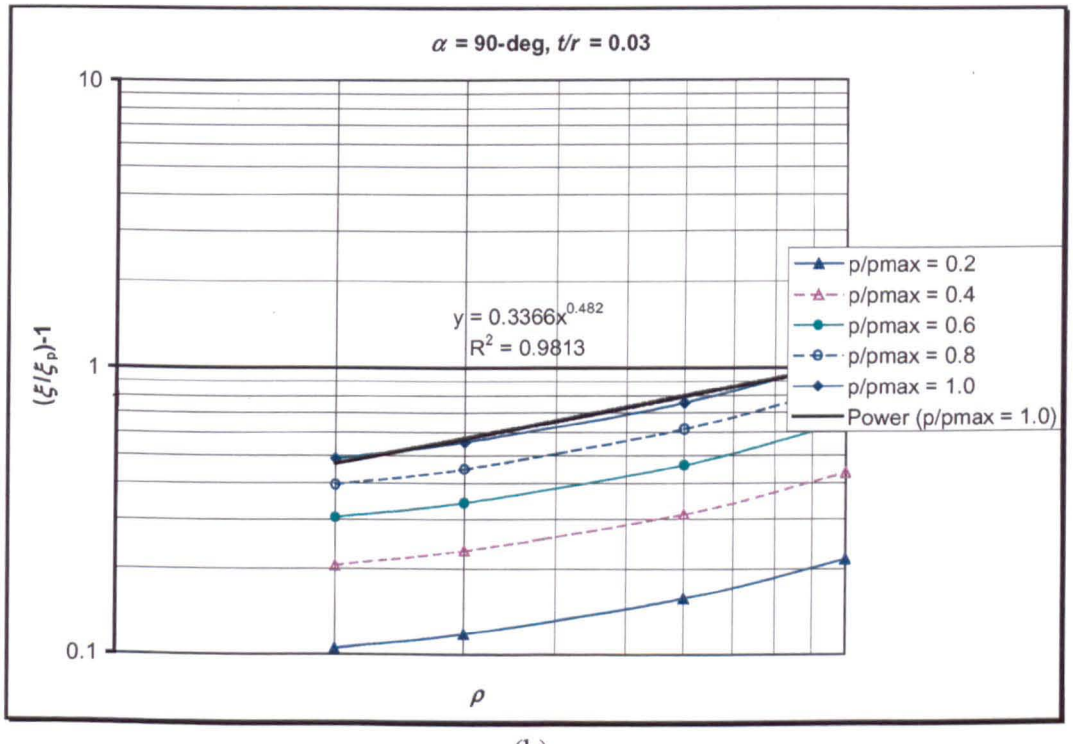

(b)

Fig.5.21 Pressure reduction at constant thickness plotted against (a) *p/E*, (b) *R/r*

Similar log-log plots for the pressure reduction (eqn (5-15)) to Fig.5.20 and 5.21 were plotted for all values of *R/t* and *r/t*. For brevity, those plots are not shown in this thesis, but can be easily derived (plotted) from Fig.A5.4 of Appendix AC5 ($\alpha = 90^0$).

From Fig.5.20 and 5.21, it can be seen that linear relationships are obtained. There is a slight deviation from linearity if the pressure reduction plotted against *r/t* and ρ, but this deviation is small. For all plots for different values of *R/r* and *r/t*, it has been found that the trends of all curves are similar. From all graphs, it has been found that the indices of *p/E*, *r/t*, and *R/r* are approximately 1, 3.33, and 0.464. Careful study of Fig.5.20 and 5.21 along with Fig.5.13 through 5.19 leads to the following equation for ovalisation factor of 90-deg elbows:

$$\xi_p = \frac{\xi}{1 + 0.205\left(\frac{p}{E}\right)\left(\frac{r}{t}\right)^{10/3}\left(\frac{R}{r}\right)^{0.464}}; \qquad \text{for} \frac{r}{t} > 13.333 \tag{5-16}$$

The value of the coefficient 0.205 was obtained based on *R/r* = 10, p/pmax = 1.0, and *r/t* = 38.461. The condition where equation is valid (for *r/t* > 13.33) were established based on Fig.5.13 through 5.17 and similar plots for all radius ratio (not shown).

5.1.3 Effect of Bend Angle on Pressure Reduction

Equation (5-16) is valid for assessing the pressure reduction effect for elbows having 90-deg bend angle. In this section, the effect of bend angle on pressure reduction is studied and simple formulae proposed.

The Ovalisation factor for in-plane closing moment for various bend angles is shown in Fig.A5.1 through A5.5 in Appendix AC5. By constructing similar graphs to Fig. 5.20 and 5.21 for various bend angles, approximately straight lines have again been obtained to develop an expression for pressure reduction in term of non-dimensional pressure *p/E*, non-dimensional thickness *r/t*, and radius ratio *R/r*. A formula for

ovalisation factor is then derived based on the procedures described above for 90-deg elbows and the results are summarised in the following equations:

$$\xi_p = \frac{\xi}{1+0.405\left(\frac{p}{E}\right)\left(\frac{r}{t}\right)^{10/3}\left(\frac{R}{r}\right)^{0.165}}; \quad \text{for} \begin{cases} \alpha = 30\text{-deg} \\ \frac{r}{t} > 14.485 \end{cases} \tag{5-17}$$

$$\xi_p = \frac{\xi}{1+0.305\left(\frac{p}{E}\right)\left(\frac{r}{t}\right)^{10/3}\left(\frac{R}{r}\right)^{0.275}}; \quad \text{for} \begin{cases} \alpha = 45\text{-deg} \\ \frac{r}{t} > 13.75 \end{cases} \tag{5-18}$$

$$\xi_p = \frac{\xi}{1+0.255\left(\frac{p}{E}\right)\left(\frac{r}{t}\right)^{10/3}\left(\frac{R}{r}\right)^{0.355}}; \quad \text{for} \begin{cases} \alpha = 60\text{-deg} \\ \frac{r}{t} > 13.447 \end{cases} \tag{5-19}$$

$$\xi_p = \frac{\xi}{1+0.155\left(\frac{p}{E}\right)\left(\frac{r}{t}\right)^{10/3}\left(\frac{R}{r}\right)^{0.590}}; \quad \text{for} \begin{cases} \alpha = 180\text{-deg} \\ \frac{r}{t} > 13.333 \end{cases} \tag{5-20}$$

The conditions of validity of the above equations were based on Fig.A5.1 through A5.5 of Appendix AC5. For a bend angle, α, it is interesting to note that the value of *r/t* where equations are valid does not depend on radius ratio, *R/r*, (consequently, also not depend on pipe bend parameter, λ). From these figures, it can be noticed for all radius ratios, that the pressure reduction (eqn (5-15)) becomes negative at the same value of pipe bend parameter.

Equations (5-16) through (5-20) can be expressed in an alternative form by noting that:

$$\left(\frac{r}{t}\right)^{10/3} = \left(\frac{r}{t}\right)^{3}\left(\frac{1}{\lambda}\right)^{1/3}\left(\frac{R}{r}\right)^{1/3}$$

Using this relation, the following expressions for ovalisation factor are also obtained with the above limitation for the values of *r/t*:

$$\xi_p = \frac{\xi}{1+0.110\left(\frac{pr^3}{3D}\right)\left(\frac{1}{\lambda}\right)^{1/3}\left(\frac{R}{r}\right)^{0.530}} \qquad \text{for } \alpha = 30\text{-deg} \qquad (5\text{-}21)$$

$$\xi_p = \frac{\xi}{1+0.085\left(\frac{pr^3}{3D}\right)\left(\frac{1}{\lambda}\right)^{1/3}\left(\frac{R}{r}\right)^{0.670}} \qquad \text{for } \alpha = 45\text{-deg} \qquad (5\text{-}22)$$

$$\xi_p = \frac{\xi}{1+0.070\left(\frac{pr^3}{3D}\right)\left(\frac{1}{\lambda}\right)^{1/3}\left(\frac{R}{r}\right)^{0.765}} \qquad \text{for } \alpha = 60\text{-deg} \qquad (5\text{-}23)$$

$$\xi_p = \frac{\xi}{1+0.055\left(\frac{pr^3}{3D}\right)\left(\frac{1}{\lambda}\right)^{1/3}\left(\frac{R}{r}\right)^{0.860}} \qquad \text{for } \alpha = 90\text{-deg} \qquad (5\text{-}24)$$

$$\xi_p = \frac{\xi}{1+0.045\left(\frac{pr^3}{3D}\right)\left(\frac{1}{\lambda}\right)^{1/3}\left(\frac{R}{r}\right)^{0.970}} \qquad \text{for } \alpha = 180\text{-deg} \qquad (5\text{-}25)$$

where D is the shell bending stiffness that can be found in any textbook of shell theory as given in equation (2-75).

5.2 Flexibility Factors

The flexibility factor is defined as the ratio of end rotation of a pipe bend to the end rotation of an equivalent length, and cross-section, of a straight pipe under the same moment loading. There is consequently a need to calculate the end rotation of the pipe bend end section. In what follows, the procedure to do so is described.

5.2.1 End Rotation

Under in plane bending load, the end of a bend at the junction with the loaded tangent will rotate through an angle φ_1, and the end of a bend at the junction with the fixed tangent will rotate through an angle φ_2, where $\varphi_1 > \varphi_2$. The relative end rotation is obtained as the difference in rotation of these ends. The deflection of a piping elbow showing these end rotations under in-plane closing moment is shown in Fig.5.22.

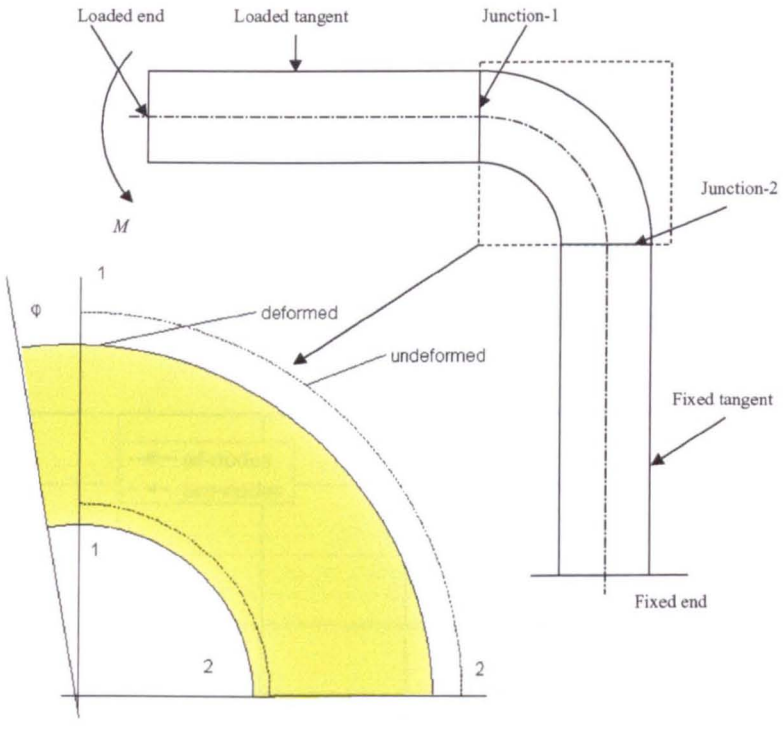

Fig.5.22 deflection of a pipe elbow under in-plane closing bending

The rotation of both ends can be obtained in the finite element analysis from the axial displacement of the nodes at each end of the bend-straight pipe junction. The nodal co-ordinate system of nodes at the junction has to be in a cylindrical co-ordinate system associated with the co-ordinate system of each tangent. This method of finding the end rotation was implemented by Thomas [78].

Axial displacement of nodes at junction-1 in Fig. 5.22 is plotted in Fig.5.23 for a typical case (α = 90-deg, R/r = 3, t/r = 0.03). The displacement is plotted as the abscissa and the position from the central axis is plotted as the ordinate. It can be seen that the variation of axial displacement across the section is essentially linear. A very small amount of warping (plane sections do not remain plane) can be seen, but it is clear that the end sections rotate in an approximately planar manner. The linear relationship between the axial displacement of nodes at the junction of the bend with the loaded tangent written as:

$$y_1 = m_1 x + c_1 \tag{5-26}$$

where y is position from central axis, x is nodal axial displacement, and m_1 and c_1 are constant coefficients.

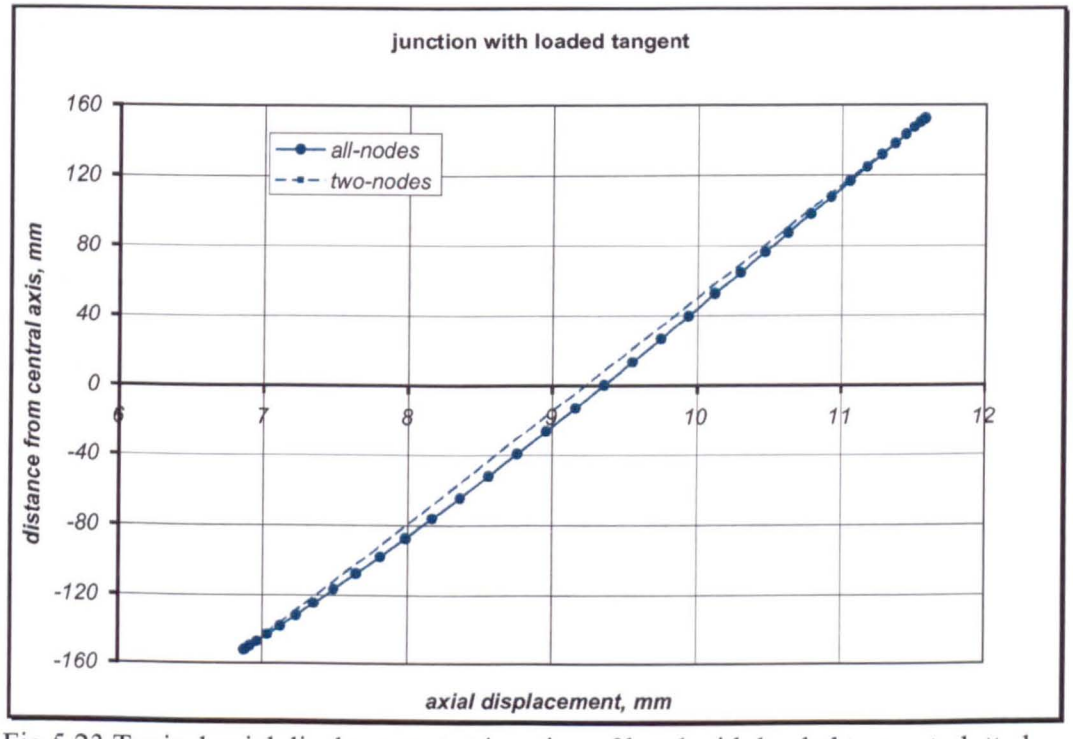

Fig.5.23 Typical axial displacement at junction of bend with loaded tangent plotted for α = 90-deg, R/r = 3, and t/r = 0.03.

The axial displacement of the nodes at junction–2 in Fig.5.22 is plotted in Fig.5.24. A similar linear equation to equation (5-26) which represents the axial displacement of nodes at the junction of the bend with the fixed tangent is:

$$y_2 = m_2 x + c_2 \tag{5-27}$$

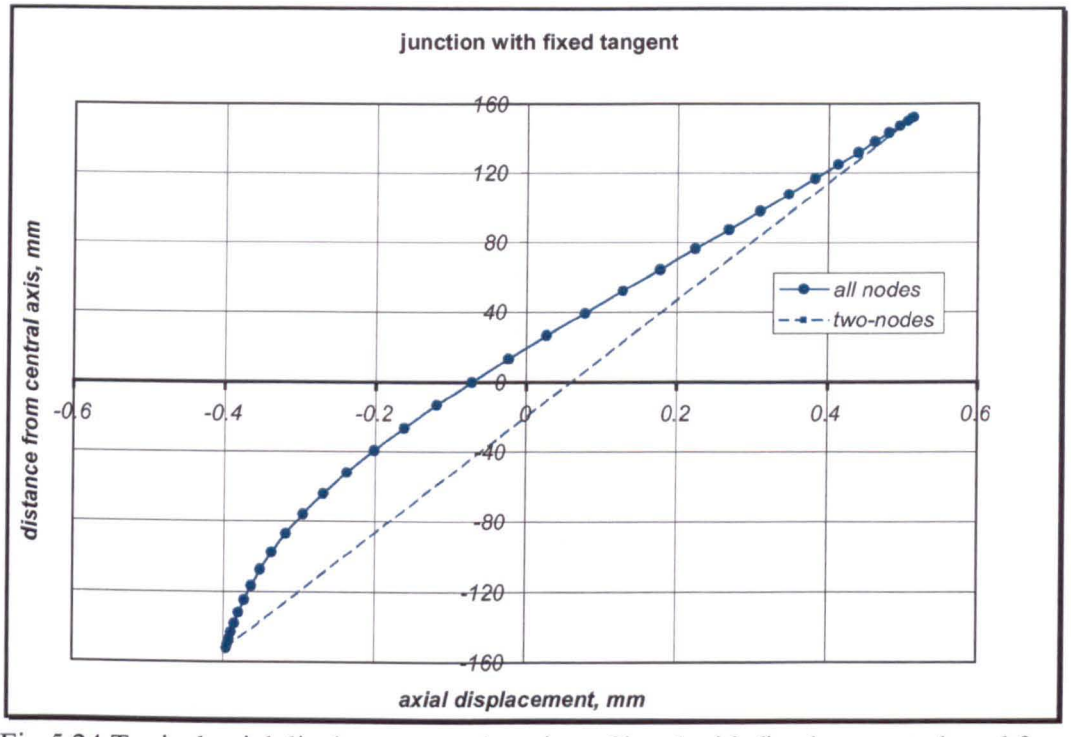

Fig.5.24 Typical axial displacement at junction of bend with fixed tangent plotted for $\alpha = 90$-deg, $R/r = 3$, and $t/r = 0.03$.

The relative end rotation can then be finally obtained from the trigonometric tangent formula as follows:

$$\tan(\varphi_1 - \varphi_2) = \frac{\frac{1}{m_1} - \frac{1}{m_2}}{1 + \frac{1}{m_1 m_2}} \tag{5-28}$$

The foregoing procedure for obtaining the end rotations was implemented by Thomas [78]. This procedure, however, might be expensive in a non-linear finite

element analysis, because the linear equations of the axial nodal displacement, eqns (5-26) and (5-27), must be constructed for every load step to find the gradient: get the axial displacement using the ANSYS general processor (the /POST1), put the data into EXCEL spreadsheet, graph the data, fit the data into a linear equation, and finally find the end rotation from the gradient of this equation.

The dashed line in Fig.5.23 and 5.24 is a straight line connecting two opposite nodes along an in-plane diameter at the bend junction with the loaded tangent and the fixed tangent respectively. It can be seen that the equation for this line has nearly the same gradient as the gradient of the straight line obtained from linearisation of axial displacement of all nodes, especially for nodes at the junction with the loaded tangent. There is slightly greater difference in gradient (more warping) at the junction-2, however the rotation at this end is very small compared with the other end of the elbow (the scale is different in both Fig.5.23 and 5.24). Examination of Fig.5.23 and 5.24 reveals that by considering only the axial displacement of two opposite extrados and intrados nodes, produced only very small difference in relative rotation compared to the relative rotation obtained by considering the axial displacement of all nodes at the junction. For the sake of simplicity, it is therefore concluded that it is sufficient to obtain the equivalent rotation from the axial displacement of only two opposite nodes along the in-plane diameter. In this sense, the end rotation of the loaded and the fixed tangent is obtained from:

$$\varphi_1 = \tan^{-1}\left(\frac{dz_1}{2r + \Delta y_1}\right) \qquad (5\text{-}29a)$$

$$\varphi_2 = \tan^{-1}\left(\frac{dz_2}{2r + \Delta y_2}\right) \qquad (5\text{-}29b)$$

where, dz is the difference in axial displacement of extrados and intrados nodes

Δy is diameter contraction from extrados to intrados nodes.

The relative end rotation is then obtained by subtraction of equation (5-29b) from equation (5-29a). In the following, the end rotation will be calculated by means of equation (5-29).

The latter procedure to obtain the end rotation as described above was implemented by Chattopadhyay [111], but did not include the diameter contraction from extrados to intrados: the second term of the denominator in the equation (5-29) was neglected as shown in eqn (3-17).

A typical moment-end rotation curve is shown in Fig.5.25. This is plotted for a bend angle (α) of 90-deg, radius ratio (R/r) equal to 3, and thickness to pipe cross-section radius ratio (t/r) equal to 0.026. It can be seen from the moment-end rotation curve that elbows under in-plane closing moment exhibit a structural softening behaviour but the non-linearity is essentially small.

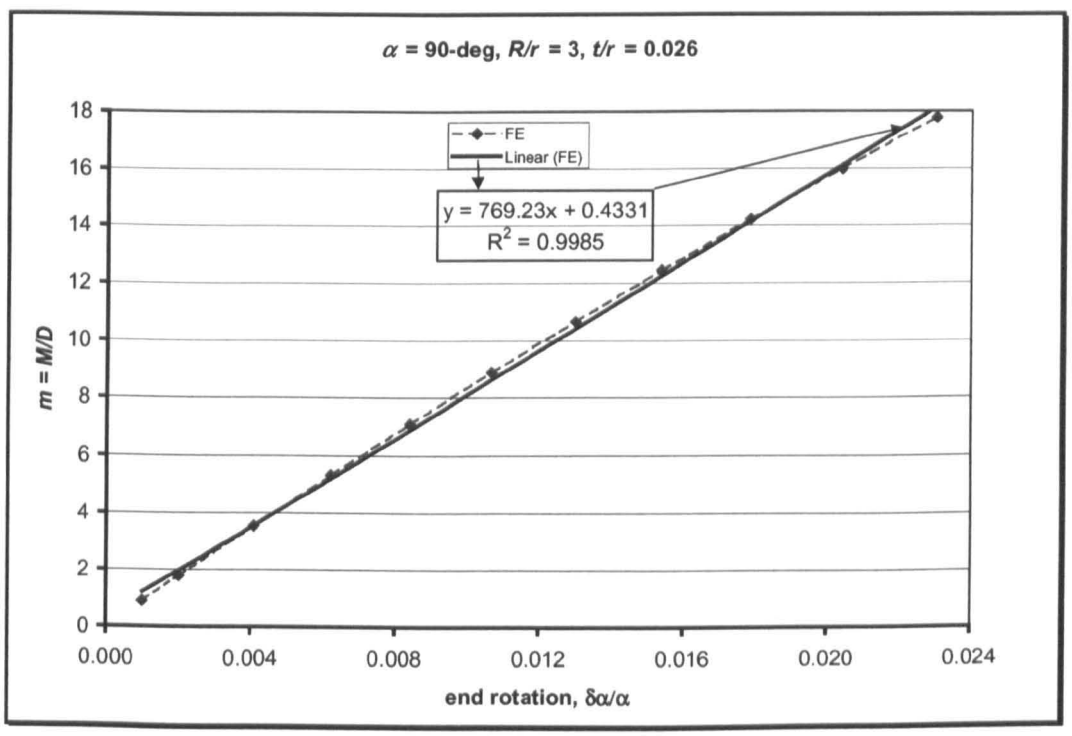

Fig.5.25 Typical moment – end rotation curve under in-plane closing bending

The end rotation $\Delta\alpha$ of a straight pipe is calculated from the modified bending formula [43]:

$$\Delta\alpha = \frac{ML(1-\nu^2)}{EI} \tag{5-30}$$

where M is the applied moment, L is the length of pipe, and $I = \pi r^3 t$

For a solid curved beam with circular cross-section and bend angle α ($L = R\alpha$), the end rotation can be written as:

$$\frac{\Delta\alpha}{\alpha} = \frac{M(1-\nu^2)}{E\pi r^2}\left(\frac{R}{r}\frac{1}{t}\right) \tag{5-31}$$

Because of the cross-sectional ovalisation, the end rotation of a pipe bend is then:

$$\frac{\Delta\alpha}{\alpha} = \frac{kM(1-\nu^2)}{E\pi r^2}\left(\frac{R}{r}\frac{1}{t}\right) \tag{5-32}$$

where k is the required flexibility factor. The flexibility factor is therefore obtained from equation (5-32) using the end rotation of the bend, $\Delta\alpha/\alpha$, obtained from finite element analysis using the linearisation procedure described in the above. All other variables in equation (5-32) are known.

Figure 5.26 shows the flexibility factor of 90-deg pipe elbows plotted against pipe bend parameter, λ, for various values of radius ratio, ρ. It can be clearly seen that the flexibility factor is dependent on pipe bend parameter, λ, and radius ratio, ρ, but its dependency on the radius ratio seems to be not significant. As shown in Fig.5.26, the relation between flexibility factor, k, and pipe bend parameter, λ, is approximately linear in a log-log graph. Accordingly, the relation can be expressed in the following approximation form:

$$k = \frac{p}{\lambda^q} \tag{5-33}$$

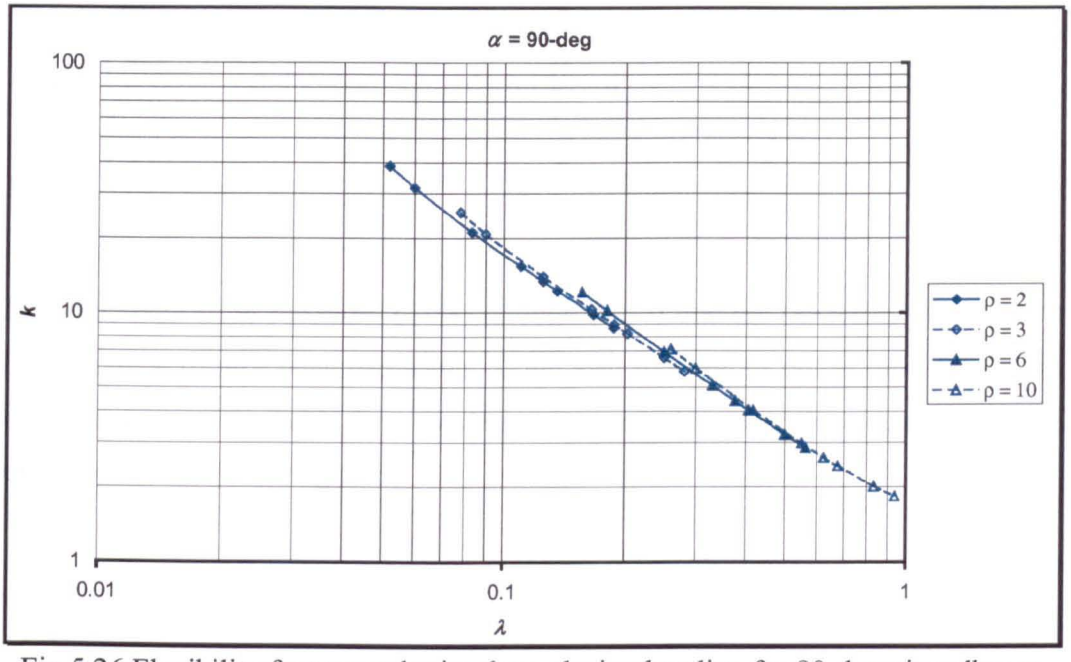

Fig.5.26 Flexibility factors under in-plane closing bending for 90-deg pipe elbows

Figure 5.26 shows that the flexibility factor for 90-deg pipe elbows can almost be represented by a single curve for various radius ratios, ρ, indicating that the flexibility factor can be expressed as a function of a single parameter, λ, with little dependency on radius ratio, ρ.

In this thesis an attempt is made to obtain empirical formulae for flexibility factors from finite element generated data. As usual, flexibility factors depend on pipe bend parameter, λ: high flexibility factor is obtained for smaller pipe bend parameters. By curved fitting and taking the effect of radius ratio into account, expressions for the flexibility factor for 90-deg pipe elbows under in-plane closing moment can be obtained:

$$k = \frac{1.213}{\lambda^{1.160}} \qquad \text{for} \frac{R}{r} = 2 \qquad (5-34)$$

$$k = \frac{1.342}{\lambda^{1.139}} \qquad \text{for} \frac{R}{r} = 3 \qquad (5-35)$$

$$k = \frac{1.466}{\lambda^{1.131}} \qquad \text{for} \frac{R}{r} = 6 \qquad (5-36)$$

$$k = \frac{1.632}{\lambda^{1.074}} \qquad \text{for} \frac{R}{r} = 10 \qquad (5-37)$$

In can be seen from equations (5-34) through (5-37) that the flexibility factor is not only function of pipe bend parameter, λ, but also function of radius ratio *R/r*. These equation are not in suitable form for design purposes. However these equation can be expressed in the following form:

$$k = \frac{1.65}{\lambda}[f(\lambda)] \qquad (5-38)$$

where $f(\lambda)$ represents the dependence of flexibility factor on radius ratio, (*R/r*). This results in $f(\lambda)$ be different for every radius ratio. It should be noted that eqn (5-38) was expressed based on the asymtotic solution of Clark and Reissner [20], see equation (2-41).

Following the procedure of Fujimoto and Soh [92], equations (5-34) through (5-37) can be written in the following form:

$$k = \frac{1.65}{\lambda}[0.6715 - 0.1716\ln(\lambda)] \qquad \text{for } \rho = 2 \qquad (5-39)$$

$$k = \frac{1.65}{\lambda}[0.7800 - 0.1485\ln(\lambda)] \qquad \text{for } \rho = 3 \qquad (5-40)$$

$$k = \frac{1.65}{\lambda}[0.8775 - 0.1364\ln(\lambda)] \qquad \text{for } \rho = 6 \qquad (5-41)$$

$$k = \frac{1.65}{\lambda}[0.988 - 0.0774\ln(\lambda)] \qquad \text{for } \rho = 10 \qquad (5-42)$$

In the above equations, the term outside of the square bracket is the asymptotic solution of Clark and Reissner [20] as adopted in the current design piping code [114, 120]. It can be seen that for pipe elbows of long radius, as indicated in equation (5-42), the term in the square bracket might be neglected without any significant loss in accuracy. The above form of equation for in-plane flexibility factor of 90-deg pipe elbows was first proposed by Fujimoto and Soh [92], but the results were only presented for $\rho = 2$ and 3, as given in equations (2-49) and (2-50). In the formulae proposed by Fujimoto and Soh, the second term in the square bracket was expressed in 'power equation form' (not in 'logarithm form'), and seems that this term might be totally omitted. It should be noted, however, that the large deformation effects were not included in their analysis.

Figure 5.27 shows the flexibility factor obtained from finite element (FE), in comparison to those calculated using equations (5-34) through (5-37), and equations (5-39) through (5-42). It can be seen that the proposed equations fit well the results from finite element.

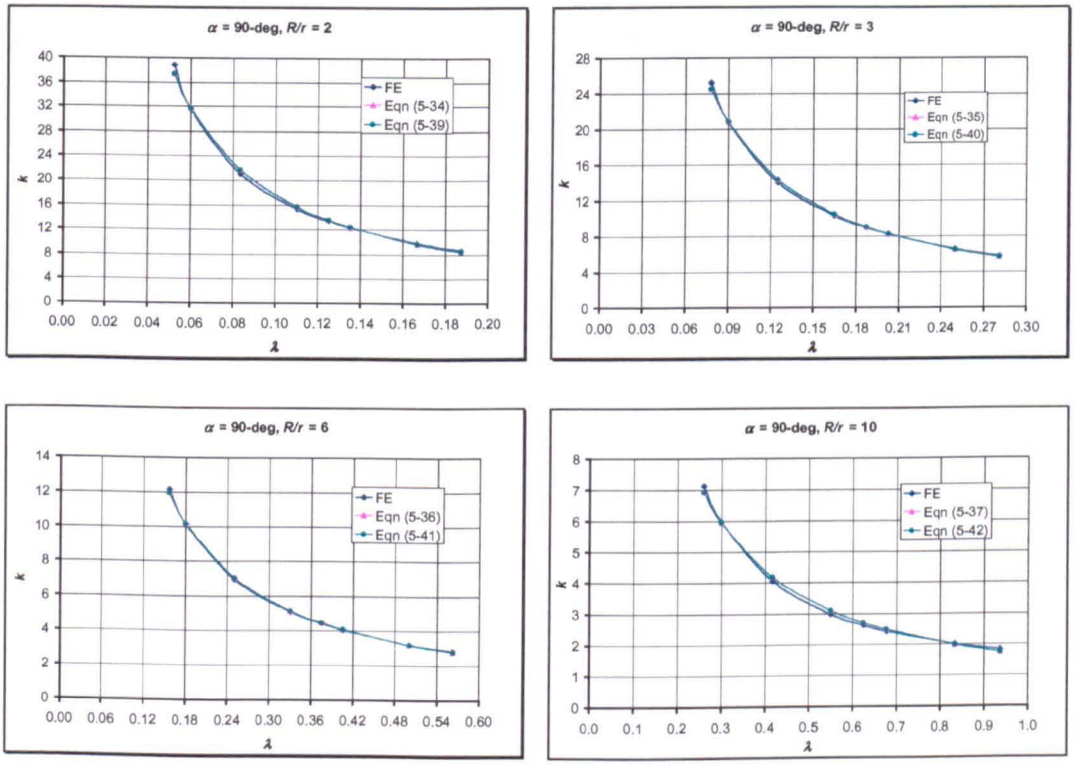

Fig.5.27 Comparison for flexibility factor between derived formula and FE results

5.2.2 Effect of Bend Angle on Flexibility Factor

It can be visualised that as the bend angle of pipe elbows approaches 'hypotheticals' zero, it tends to behave as a straight pipe. To account for the effect of bend angle on flexibility factor other than 90-deg, pipe elbows having bend angle of 30, 45, 60, and 180-deg have been studied. Figure 5.28 through 5.31 show graphs for flexibility factor plotted against pipe bend parameter. It can be seen from these graphs that the relation between flexibility factor and pipe bend parameter is again essentially linear in log-log plot for all bend angles considered.

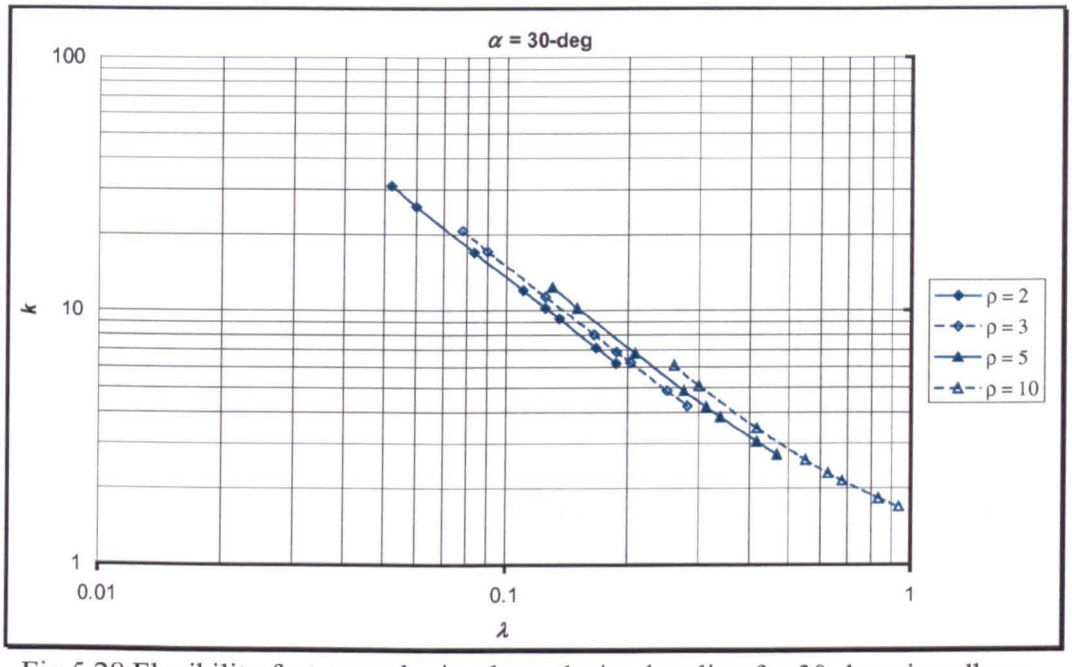

Fig.5.28 Flexibility factors under in-plane closing bending for 30-deg pipe elbows

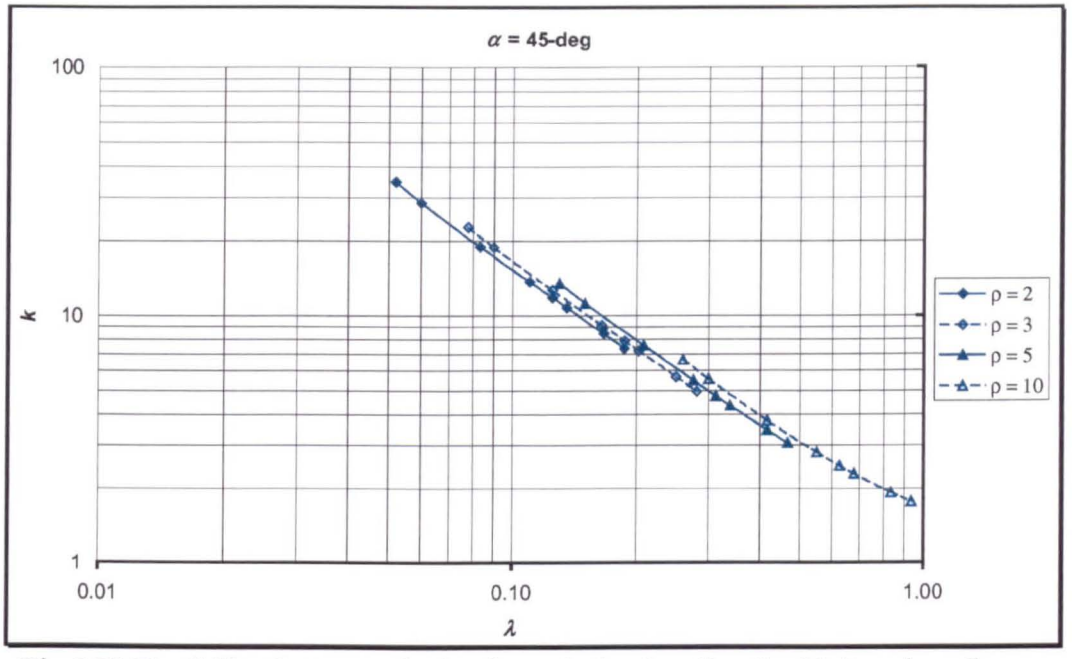

Fig.5.29 Flexibility factors under in-plane closing bending for 45-deg pipe elbows

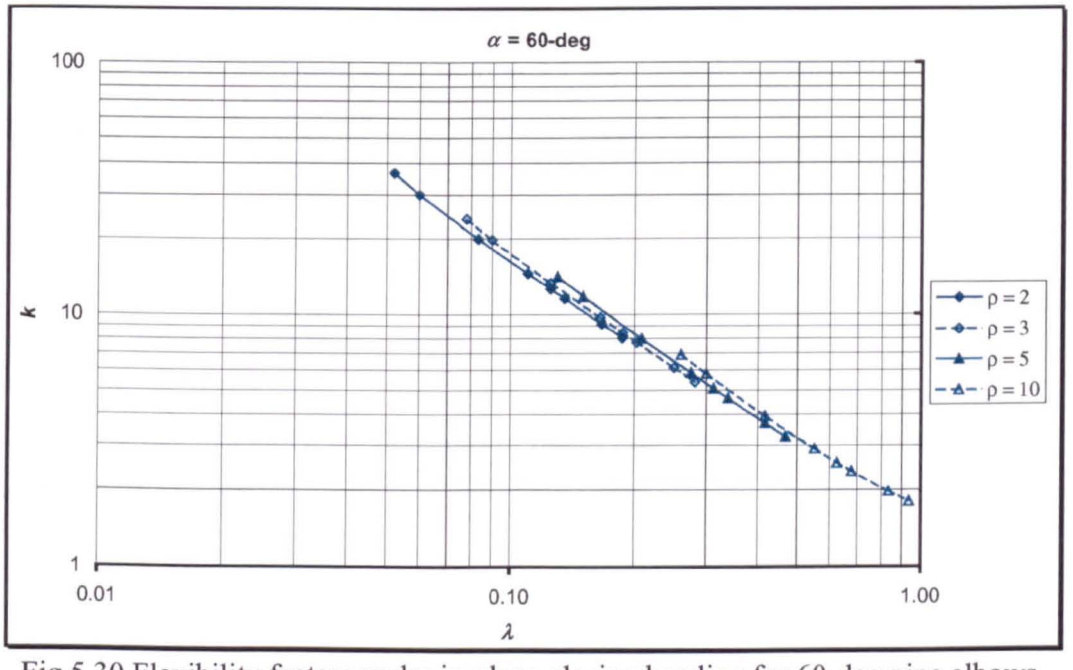

Fig.5.30 Flexibility factors under in-plane closing bending for 60-deg pipe elbows

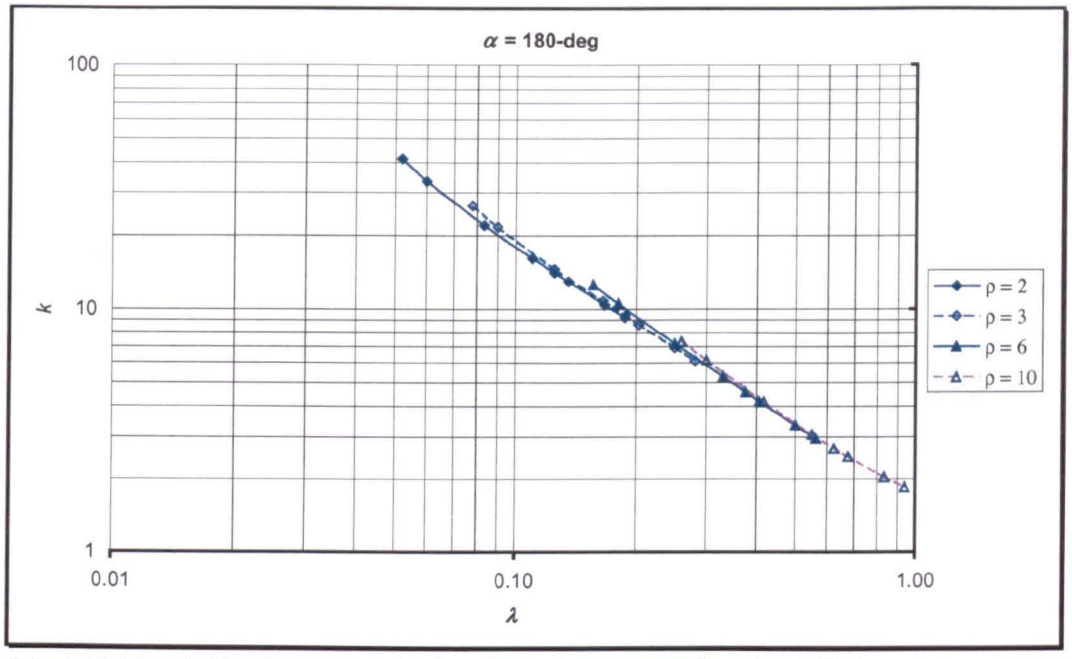

Fig.5.31 Flexibility Factors under in-plane closing bending for 180-deg pipe elbows

Using the procedure described in section 5.1 for determining ovalisation factor, the flexibility factor for pipe elbows can be expressed by the following approximate formulae:

$$k = \frac{1.65}{\lambda}[a - b\ln(\lambda)] \qquad (5-43)$$

where coefficient a and b are functions of radius ratio, ρ, as summarised in Table 5.3 and 5.4 respectively.

Table 5.3 Values for coefficient 'a' in equations (5-43) for various bend angles

ρ	α				
	30-deg	45-deg	60-deg	90-deg	180-deg
2	0.3340	0.5120	0.5237	0.6715	0.7090
3	0.4545	0.6110	0.6990	0.7800	0.8290
4	0.5659	0.6734	0.7659	0.8133	0.8692
5	0.6280	0.7380	0.8010	0.8551	0.8950
6	0.7097	0.7853	0.8453	0.8775	0.9090
7	0.7644	0.8325	0.8679	0.9183	0.9470
8	0.8118	0.8757	0.8850	0.9433	0.9607
9	0.8536	0.9157	0.8982	0.9654	0.9714
10	0.9028	0.9470	0.9130	0.9880	0.9990

Table 5.4 Values of coefficient 'b' in equations (5-43) for various bend angles

ρ	α				
	30-deg	45-deg	60-deg	90-deg	180-deg
2	0.2142	0.1866	0.1911	0.1716	0.1812
3	0.2000	0.1744	0.1593	0.1485	0.1624
4	0.1707	0.1565	0.1520	0.1560	0.1499
5	0.1558	0.1486	0.1421	0.1450	0.1397
6	0.1177	0.1201	0.1240	0.1364	0.1278
7	0.0912	0.1019	0.1120	0.1230	0.1180
8	0.0647	0.0837	0.1012	0.1120	0.1089
9	0.0382	0.0655	0.0914	0.1010	0.1005
10	0.0074	0.0433	0.0820	0.0774	0.0901

It can be seen from these equations that the flexibility factor is very much influenced by the bend angle. As can be inferred from the Tables, both terms in the square bracket could be neglected for elbows of large angle bend (90-deg and greater) and long radius bends. For all bend angles considered, and long radius, the second term

in the square bracket could also be neglected. It can be concluded that the asymptotic solution of Clark and Reissner [20] can be used only for elbows of large angle bend and long radius.

5.2.3 Pressure Reduction Effect

It was already shown in section 1 of this chapter that internal pressure reduces the ovalisation factor resulting from an in-plane closing bending loading. As a consequence, it also 'opens up' the bend. This phenomenon is known as the Bourdon Effect [Boyle, 115]. The theory of the Bourdon tube can be found in the paper of Wolf [16] and Jennings [28].

Typical pressure-end rotation plots are shown in Fig.5.32, plotted for a 90-deg pipe elbow and radius a ratio equals three. The abscissa value of 0.0 represents the final load step of moment loading and the start of the subsequent internal pressure loading.

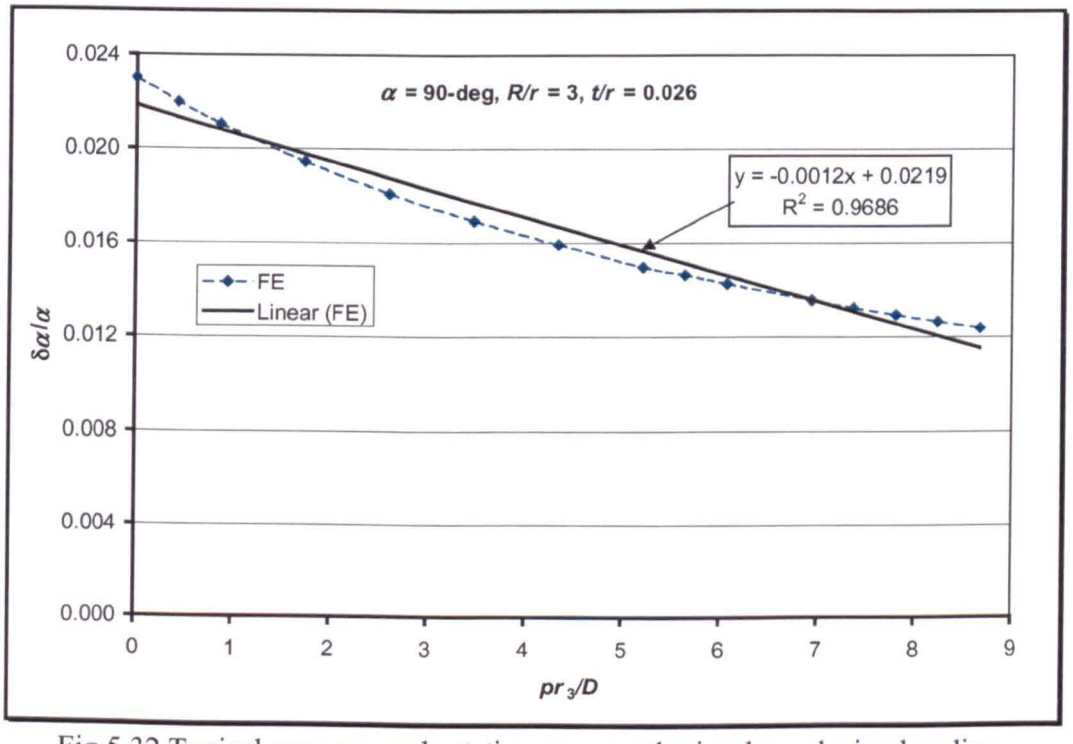

Fig.5.32 Typical pressure-end rotation curve under in-plane closing bending

It can be seen that the relation between internal pressure and end rotation is non-linear. Figure 5.32 shows the "Haigh effect" [11]: non-linearity is present whenever internal pressure acts on pipe of noncircular cross-section, (in this case, internal pressure acts on oval cross-section pipe bend due to in-plane bending).

Figure 5.33 through 5.36 show the flexibility factors of 90-deg pipe elbows plotted against pipe bend parameter, λ, for various radius ratio, ρ, under in-plane closing moment. It can be clearly seen that internal pressure acts to reduce the flexibility factor (open up the bend). The reduction is more pronounced for thin walled piping elbows (low pipe bend parameter). In the following, the effect of internal pressure on end rotation (flexibility factor) is evaluated and formulae developed. The procedure of Rodabaugh and George [30] is followed.

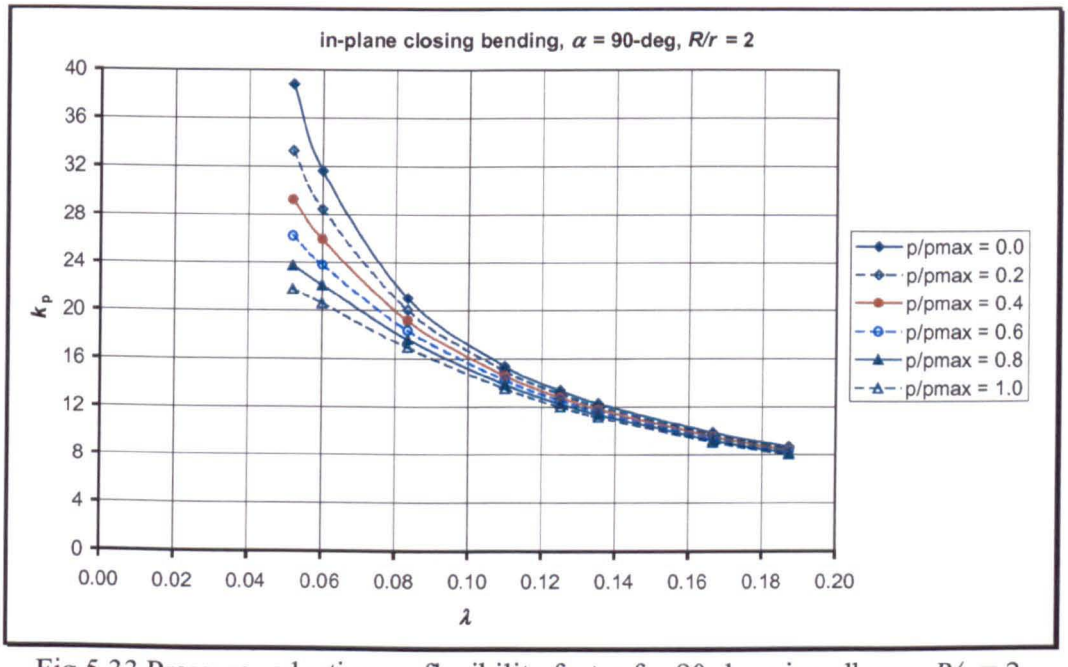

Fig.5.33 Pressure reduction on flexibility factor for 90-deg pipe elbows: $R/r = 2$

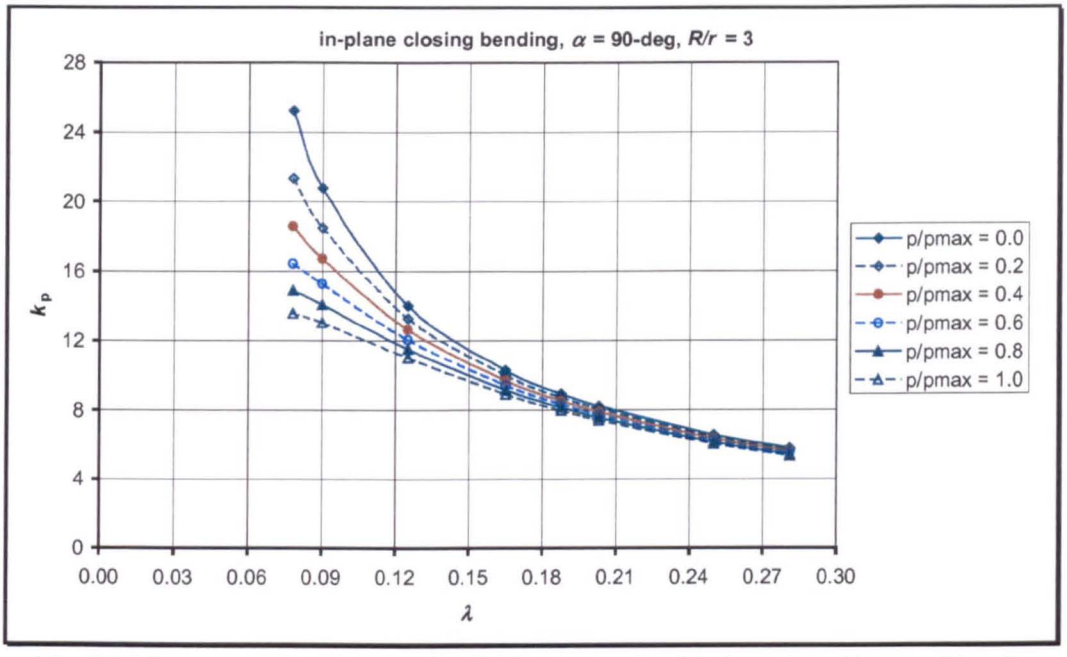

Fig.5.34 Pressure reduction on flexibility factor for 90-deg pipe elbows: $R/r = 3$

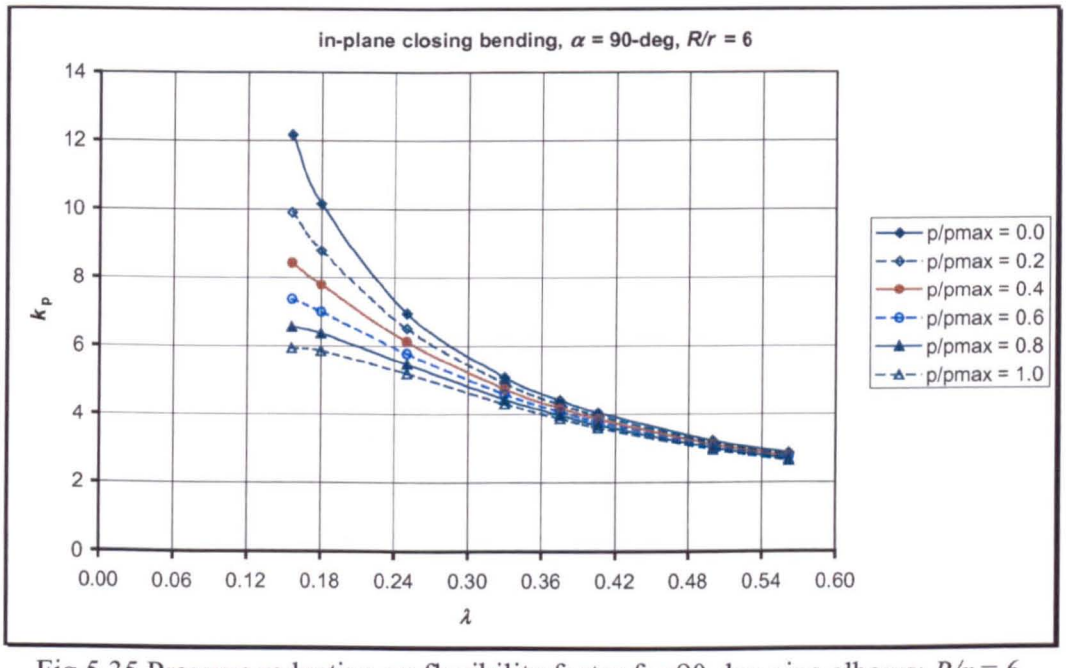

Fig.5.35 Pressure reduction on flexibility factor for 90-deg pipe elbows: $R/r = 6$

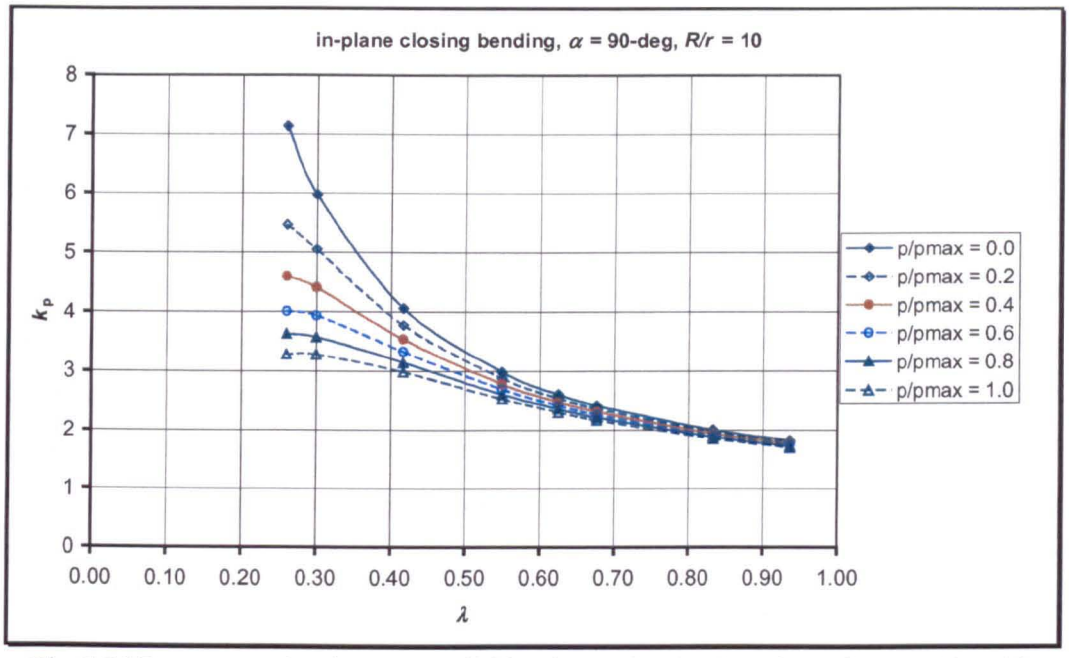

Fig.5.36 Pressure reduction on flexibility factor for 90-deg pipe elbows: $R/r = 10$

When internal pressure is included, the flexibility factor can be written in the following form:

$$k_p = \frac{k}{1 + X_k\left(\frac{p}{E}, \frac{r}{t}, \frac{R}{r}\right)} \qquad (5-44)$$

where, k is the flexibility factors in the absence of internal pressure, as given by Equations (5-43) and Table 5.3 and 54. The second term in the denominator represents the pressure reduction effect on the flexibility factor. It is a function of non-dimensional pressure p/E, non-dimensional thickness t/r, and radius ratio ρ.

To develop the expression for X_k, equation (5-44) is rewritten in the following form:

$$\frac{k}{k_p} - 1 = X_k\left(\frac{p}{E}, \frac{r}{t}, \frac{R}{r}\right) \qquad (5-45)$$

The left-hand side of equation (5-45) is obtained from finite element generated data as shown in Fig.5.33 through 5.36 for 90-deg pipe elbows. This quantity is plotted against p/E and r/t for a constant radius ratio ρ, and against p/E and ρ for a constant non-dimensional thickness t/r.

A typical pressure reduction effect on flexibility of 90-deg pipe elbows is plotted as a log-log graph in Fig.5.37 and 5.38 for a constant radius ratio and in Fig.5.39 and 5.40 for a constant thickness. Again linear relations are obtained if the pressure reduction is plotted against non-dimensional pressure p/E. Linear relations are also obtained if the pressure reduction is plotted against radius ratio ρ. Deviation from linearity can be seen if the pressure reduction is plotted against r/t. In this analysis, the pressure reduction coffcient, X_k, will be represented as straight lines and the error introduced in doing so will be discussed at the end of this chapter.

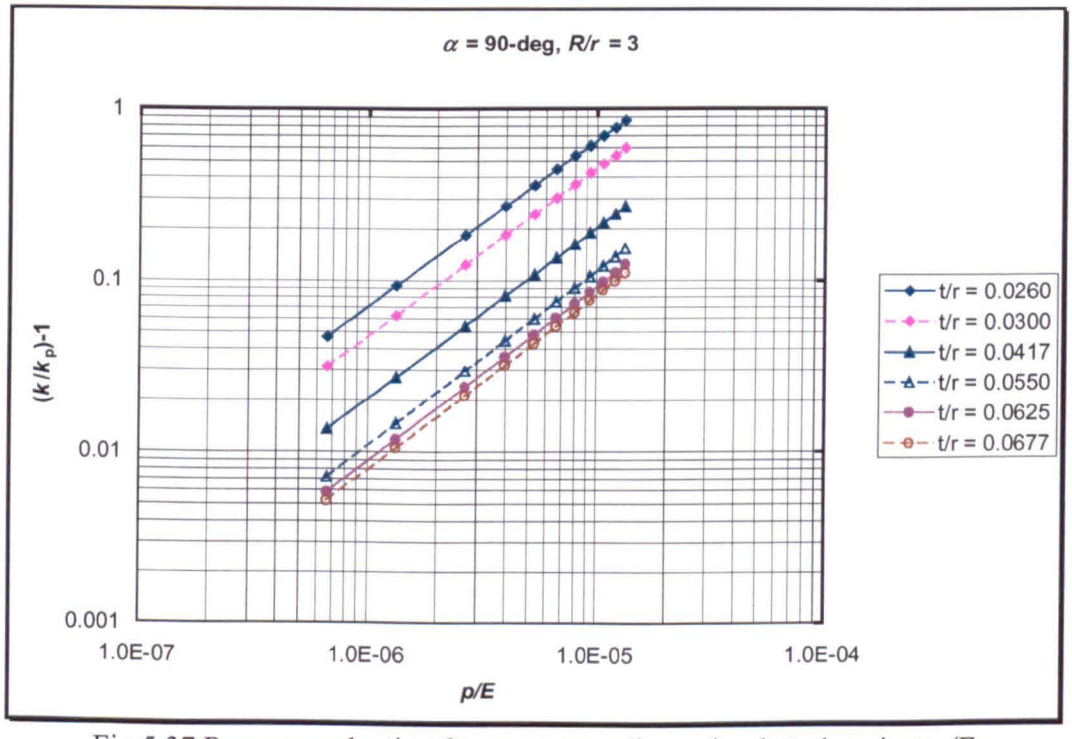

Fig.5.37 Pressure reduction for constant radius ratio plotted against p/E

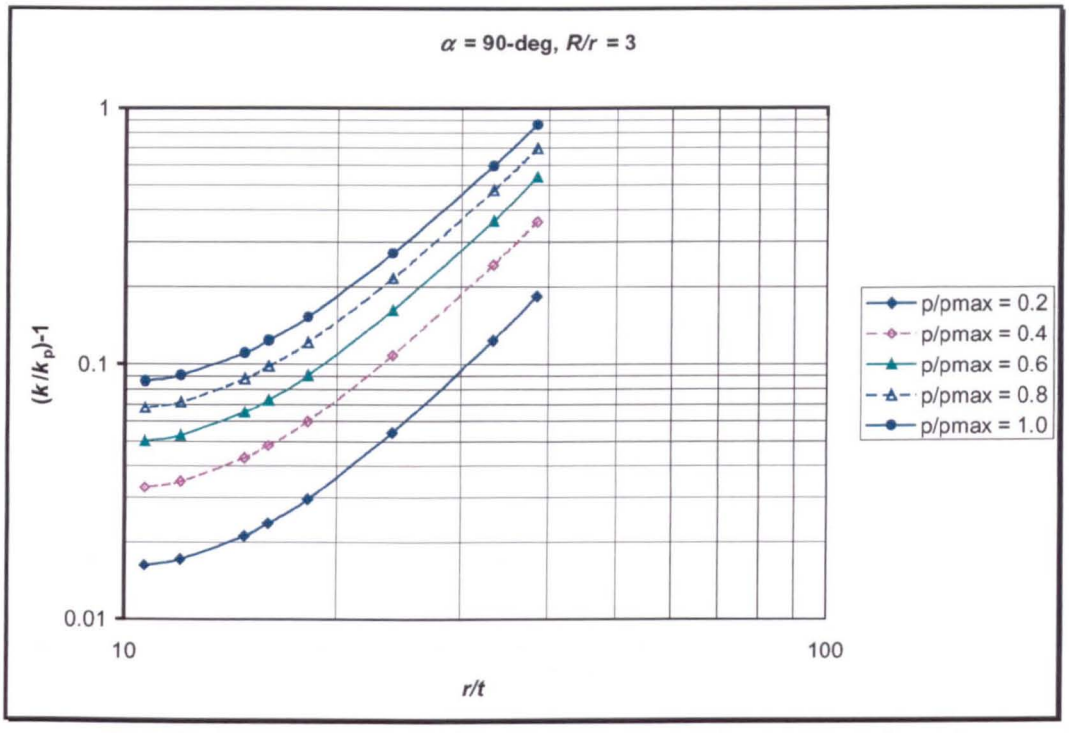

Fig.5.38 Pressure reduction for constant radius ratio plotted against r/t

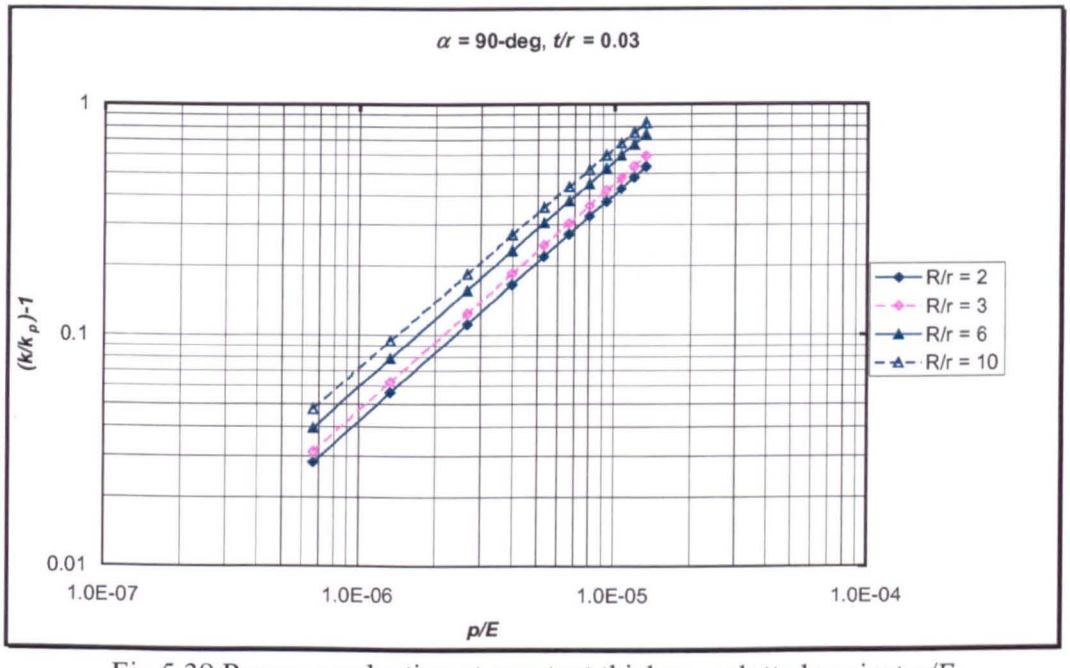

Fig.5.39 Pressure reduction at constant thickness plotted against p/E

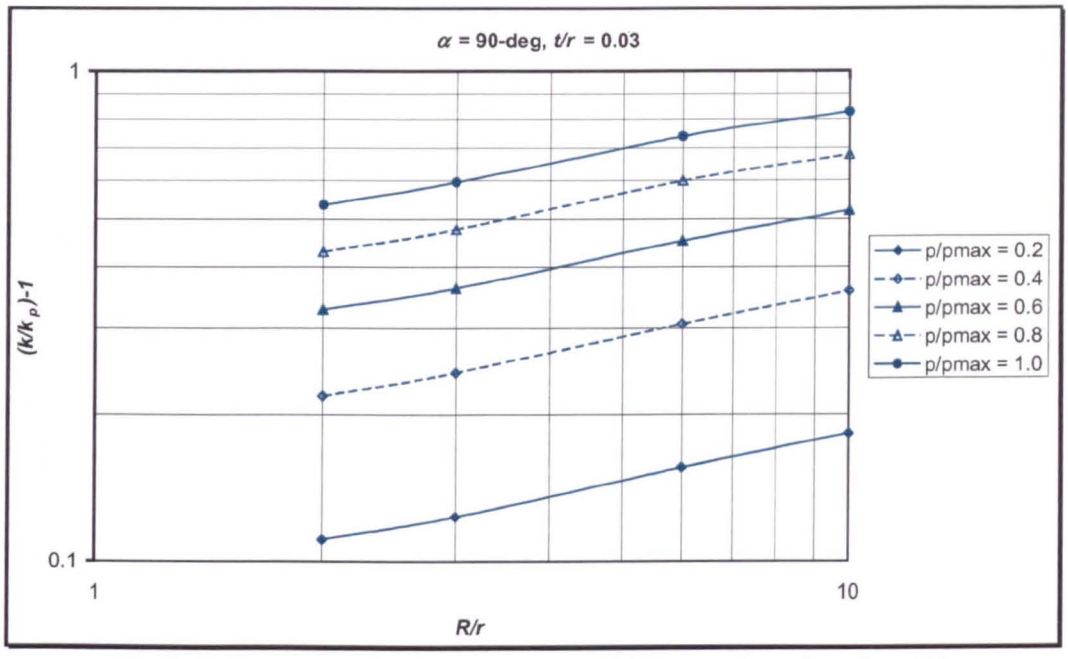

Fig.5.40 Pressure reduction at constant thickness plotted against *R/r*

Similar log-log plots for the pressure reduction (eqn (5-45)) to Fig.5.37 through 5.40 were obtained for all values of *R/t* and *r/t*. For brevity, again, those plots are not shown in this thesis, but can be easily derived (plotted) from Fig.A5.9 of Appendix AC5 for $\alpha = 90^0$. For all plots for different values of *R/r* and *r/t*, it has been found that the trends of all curves are similar. From all graphs, it has been found that the indices of *p/E*, *r/t*, and *R/r* are approximately 1, 2.25, and 0.31. Study of Fig.5.37 through 5.40 along with Fig.5.33 through 5.36, suggests the following equation for flexibility factor of 90-deg pipe elbows under in-plane bending and internal pressure:

$$k_p = \frac{k}{1+11.75\left(\frac{p}{E}\right)\left(\frac{r}{t}\right)^{9/4}\left(\frac{R}{r}\right)^{0.31}} \qquad (5-46)$$

where *k* is flexibility factor in the absence of internal pressure as given by equation (5-43) and Table 5.3 and 5.4. The value of the coefficient of 11.75 in equation (5-45) was obtained based on *R/r* = 10, p/pmax = 1, and *t/r* = 0.026. Equation (5-46) can be directly compared with the equation proposed by Rodabaugh and George [30] as adopted in the current design piping code [114, 120]. It can be seen that equation (5-

46) produces greater pressure reduction – marked by the coefficient 11.75 rather than 6 in equation (2-94).

5.2.4 Effect of Bend Angle on Pressure Reduction

It has been shown in section 5.2.1 that the flexibility factor in the absence of internal pressure is very much influenced by the bend angle. In this section, the effect of bend angle on the pressure reduction effect is studied and simple formulae proposed.

The same procedure is applied: by constructing log-log graphs for pressure reduction using the data of Fig.A5.6 through A5.10 of Appendix C5, the flexibility factor including internal pressure for various bend angles can be derived:

$$k_p = \frac{k}{1+18.5\left(\frac{p}{E}\right)\left(\frac{r}{t}\right)^{9/4}\left(\frac{R}{r}\right)^{0.096}} \qquad \text{for } \alpha = 30^0 \qquad (5-47)$$

$$k_p = \frac{k}{1+15.65\left(\frac{p}{E}\right)\left(\frac{r}{t}\right)^{9/4}\left(\frac{R}{r}\right)^{0.177}} \qquad \text{for } \alpha = 45^0 \qquad (5-48)$$

$$k_p = \frac{k}{1+13.5\left(\frac{p}{E}\right)\left(\frac{r}{t}\right)^{9/4}\left(\frac{R}{r}\right)^{0.247}} \qquad \text{for } \alpha = 60^0 \qquad (5-49)$$

$$k_p = \frac{k}{1+9.25\left(\frac{p}{E}\right)\left(\frac{r}{t}\right)^{9/4}\left(\frac{R}{r}\right)^{0.412}} \qquad \text{for } \alpha = 180^0 \qquad (5-50)$$

The pressure reduction coefficients in equation (5-46) through (5-50) are expressed in term of non-dimensional pressure *p/E*, non-dimensional thickness *r/t*, and radius ratio *R/r*. An alternative is to express the coefficient in term of the pipe bend parameter, λ, by noting that:

$$\frac{p}{E}\left(\frac{r}{t}\right)^{9/4} = \frac{p}{E}\left(\frac{r}{t}\right)^{3}\left(\frac{r}{R}\right)^{3/4}\lambda^{3/4}$$

Using this relation, flexibility factors under the action of in-plane closing bending and internal pressure can then be written in the following form:

$$k_p = \frac{k}{1+5.10\left(\frac{pr^3}{3D}\right)\lambda^{3/4}\left(\frac{r}{R}\right)^{0.654}} \qquad \text{for } \alpha = 30\text{-deg} \qquad (5\text{-}51)$$

$$k_p = \frac{k}{1+4.30\left(\frac{pr^3}{3D}\right)\lambda^{3/4}\left(\frac{r}{R}\right)^{0.573}} \qquad \text{for } \alpha = 45\text{-deg} \qquad (5\text{-}52)$$

$$k_p = \frac{k}{1+3.70\left(\frac{pr^3}{3D}\right)\lambda^{3/4}\left(\frac{r}{R}\right)^{0.503}} \qquad \text{for } \alpha = 60\text{-deg} \qquad (5\text{-}53)$$

$$k_p = \frac{k}{1+3.25\left(\frac{pr^3}{3D}\right)\lambda^{3/4}\left(\frac{r}{R}\right)^{0.440}} \qquad \text{for } \alpha = 90\text{-deg} \qquad (5\text{-}54)$$

$$k_p = \frac{k}{1+2.55\left(\frac{pr^3}{3D}\right)\lambda^{3/4}\left(\frac{r}{R}\right)^{0.338}} \qquad \text{for } \alpha = 180\text{-deg} \qquad (5\text{-}55)$$

where, D is the shell bending stiffness that can be found in any textbook of shell theory: see equation (2-75).

It can be seen from these equations that the contribution of the non-dimensional thickness r/t to the pressure reduction effect is not significantly influenced by the bend angle.

Equation (5-46) through (5-55) might be further simplified to find the general formula for other bend angles, however the range of bend angle considered in this study cover pipe elbows in practical usage.

5.3 Stress-Intensification Factors

In the foregoing sections of this chapter, the pressure reduction effect on ovalisation factor and flexibility factors (end rotation) has been studied and formulae have been developed. It has long been known that the cross-sectional ovalisation results in a stress distribution wholly different from that found in simple beam theory ($\sigma = My/I$). Von Karman [2] suggested that the maximum bending stress in a pipe bend could be written as:

$$\sigma_{max} = \gamma \frac{Mr}{I} \tag{5-56}$$

where γ is defined as the stress-intensification factor.

In this section the formula for stress-intensification factor under the action of bending alone will be first developed. The pressure reduction effect is then evaluated and formulae developed. The effect of bend angle is also investigated.

Typical stress contour plots for piping elbows under in-plane closing bending are shown in Fig.5.41 for longitudinal stress and in Fig.5.42 for hoop (circumferential) stress. These are obtained for a 90-deg elbow having a radius ratio, $\rho = 3$, and thickness to cross-section radius ratio, $t/r = 0.026$.

It can be seen from these plots that the maximum stresses in a piping elbow under in-plane closing bending occur at the mid-section of the elbow in the hoop direction. It is a compressive stress at the inner surface. In what follows, the hoop stresses at the mid-section of the elbow and the location of their maximum value in the circumferential direction is evaluated.

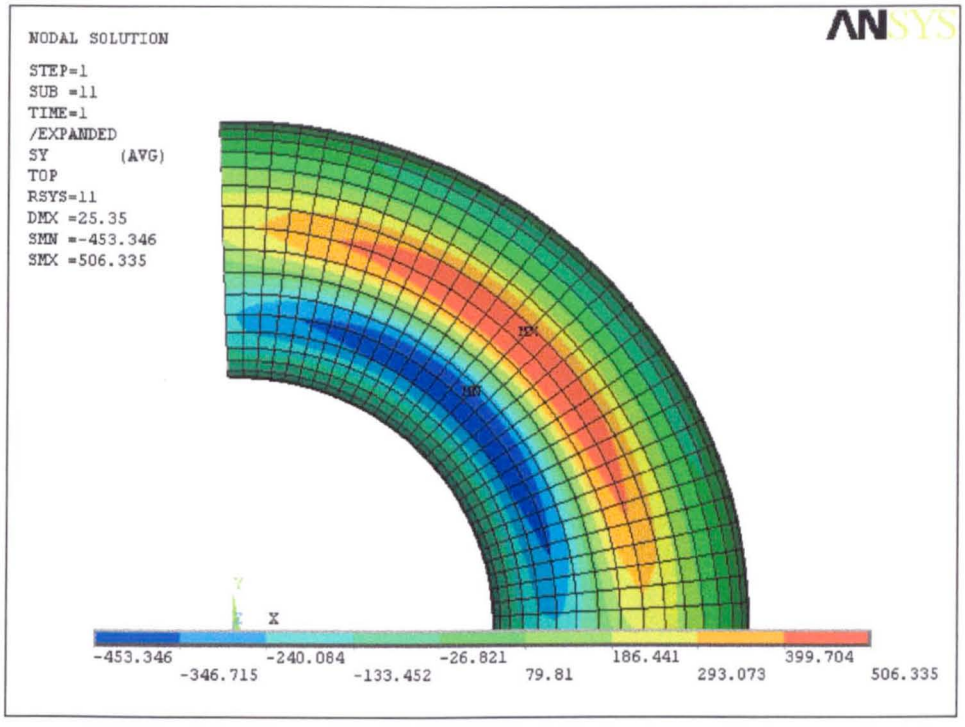

(a)

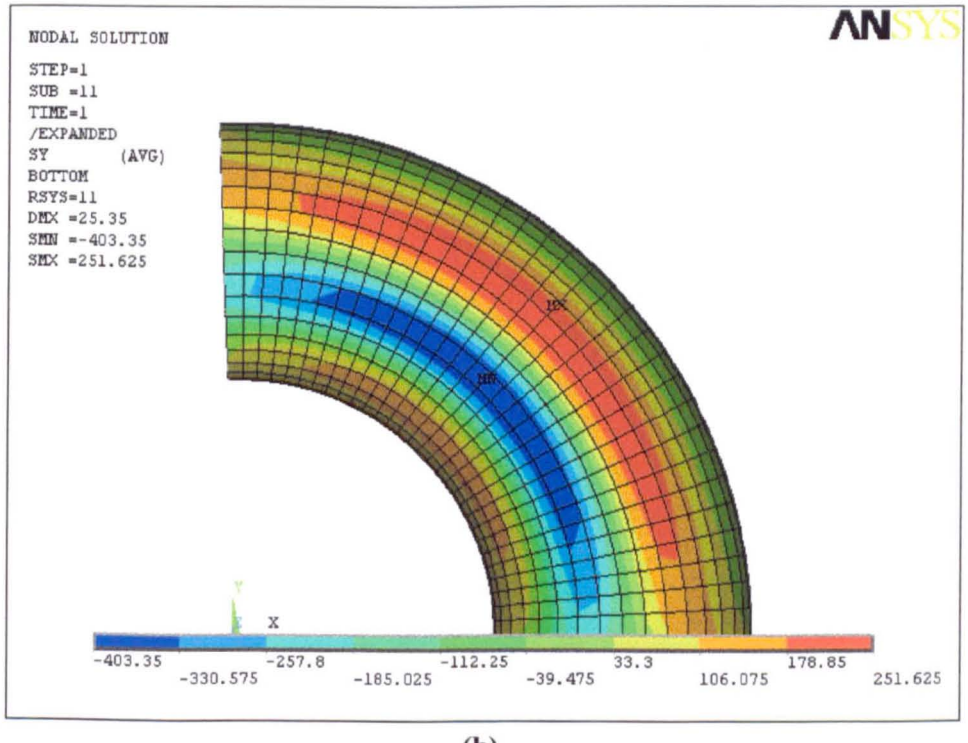

(b)

Fig.5.41 Typical longitudinal stress contour plot under in-plane closing moment for $\alpha = 90$-deg, $R/r = 3$, and $t/r = 0.026$ plotted for (a) outer surface, (b) inner surface

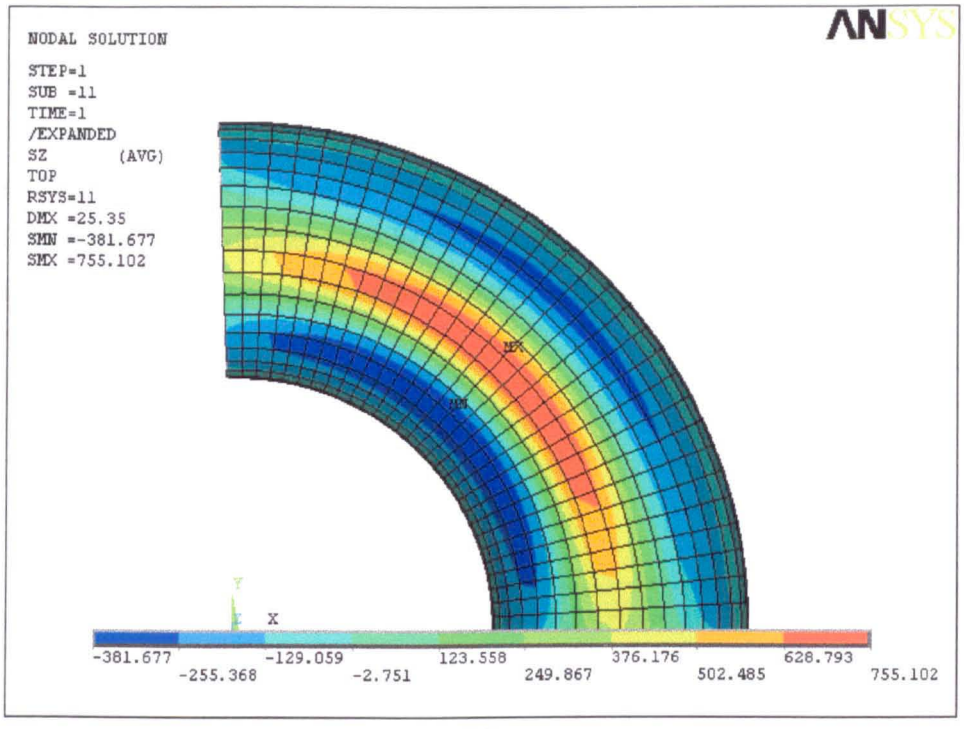

(a)

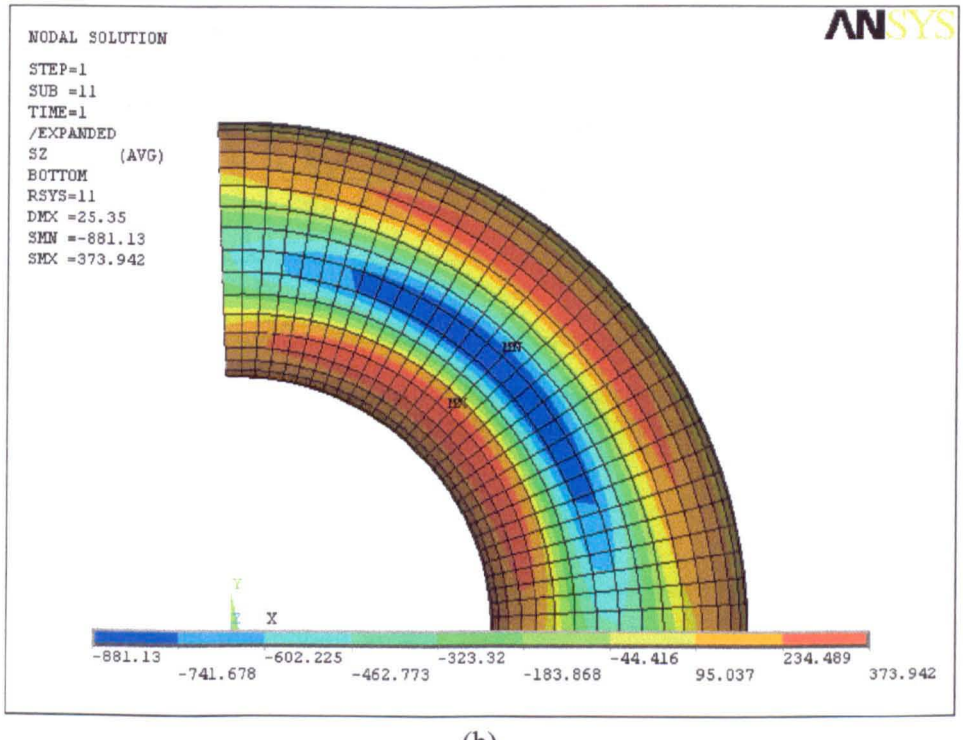

(b)

Fig.5.42 Typical hoop stress contour plot under in-plane closing moment for $\alpha = 90$-deg, $R/r = 3$, and $t/r = 0.026$ plotted for (a) outer surface, (b) inner surface

5.3.1 Stress Factors

Typical longitudinal and hoop stress distributions at the mid-section of the elbow are plotted for a 90-deg elbow in Fig.5.43. The stresses are plotted from the extrados to the intrados. The stresses have been normalized with respect to the nominal bending stress (in a straight pipe) calculated from simple beam bending:

$$\sigma_n = \frac{Mr}{I} \tag{5-57}$$

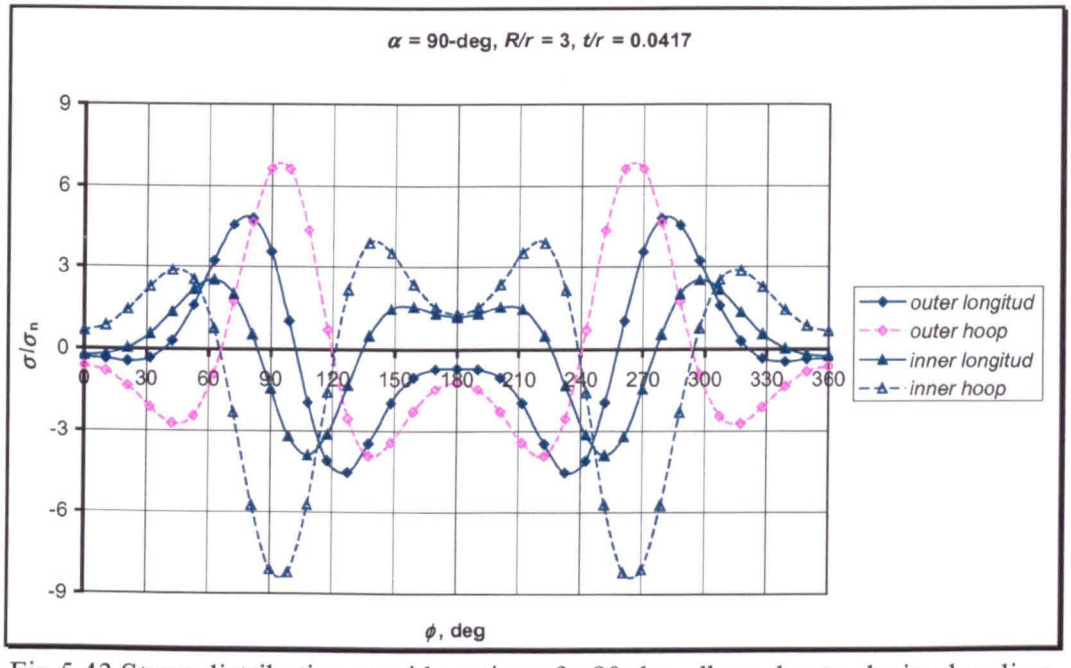

Fig.5.43 Stress distribution at mid-section of a 90-deg elbow due to closing bending

It can be clearly seen from Fig.5.43 that the maximum stress in a piping elbow is several times in magnitude greater than that predicted using equation (5-57). The maximum stress no longer occurs in the longitudinal direction, but in the hoop direction and is compressive under in-plane closing moment. The maximum stress also changes position from the furthest point from neutral axis, eqn (5-57) to a position near the neutral axis.

Figure 5.43 shows that the maximum compressive hoop stress for a 90-deg elbow located between 90 and 100-deg in the circumferential direction, measured from the extrados. For simplicity, the maximum stress factor (stress-intensification factor) will be evaluated at 90-deg position (crown) for 90-deg pipe elbows. Figure 5.44 shows a moment – stress (hoop) plot for an elbow subjected to in-plane closing moment plotted for a 90-deg elbow having $R/r = 3$ and $t/r = 0.026$.

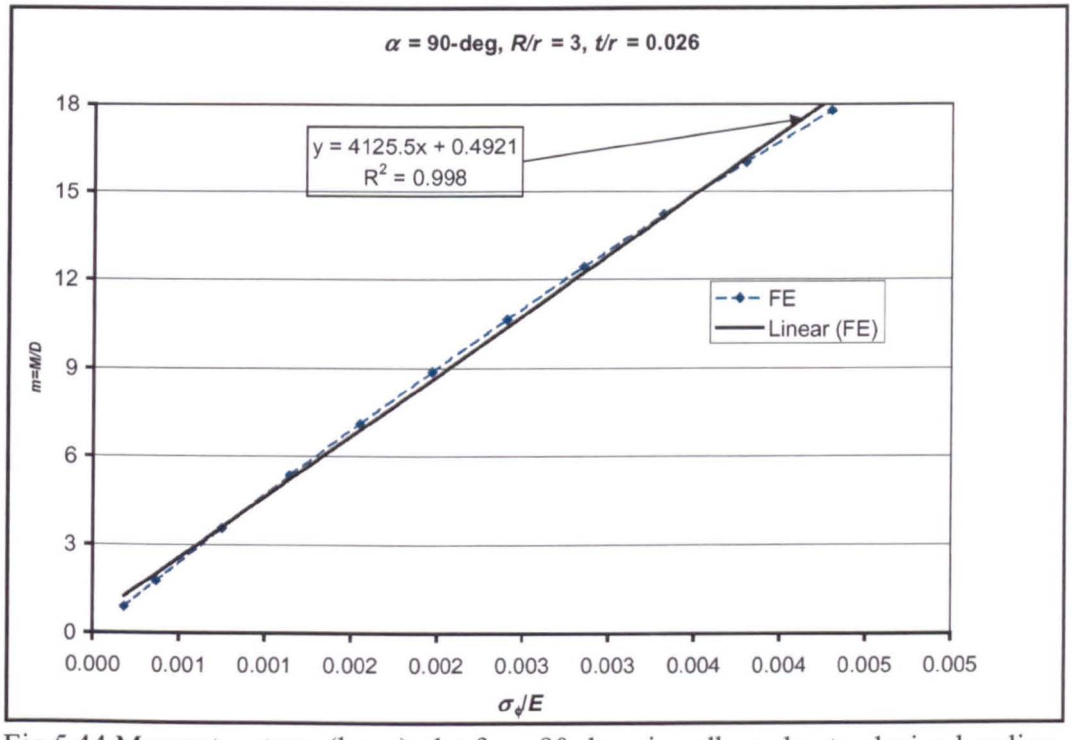

Fig.5.44 Moment – stress (hoop) plot for a 90-deg pipe elbow due to closing bending

The moment – stress plot in Fig 5.44 shows that a pipe elbow subjected to in-plane closing moment exhibits a structural softening behaviour. Fig 5.44 was plotted for a relatively thin-walled pipe to show the nonlinearirty. It can be seen that the nonlinearity is essentially small.

Figure 5.45 shows the stress-intensification factor for 90-deg pipe elbows subjected to in-plane closing bending. It can be clearly seen that the stress-intensification factor not only depends on the single parameter, λ, but also depend on the radius ratio, R/r.

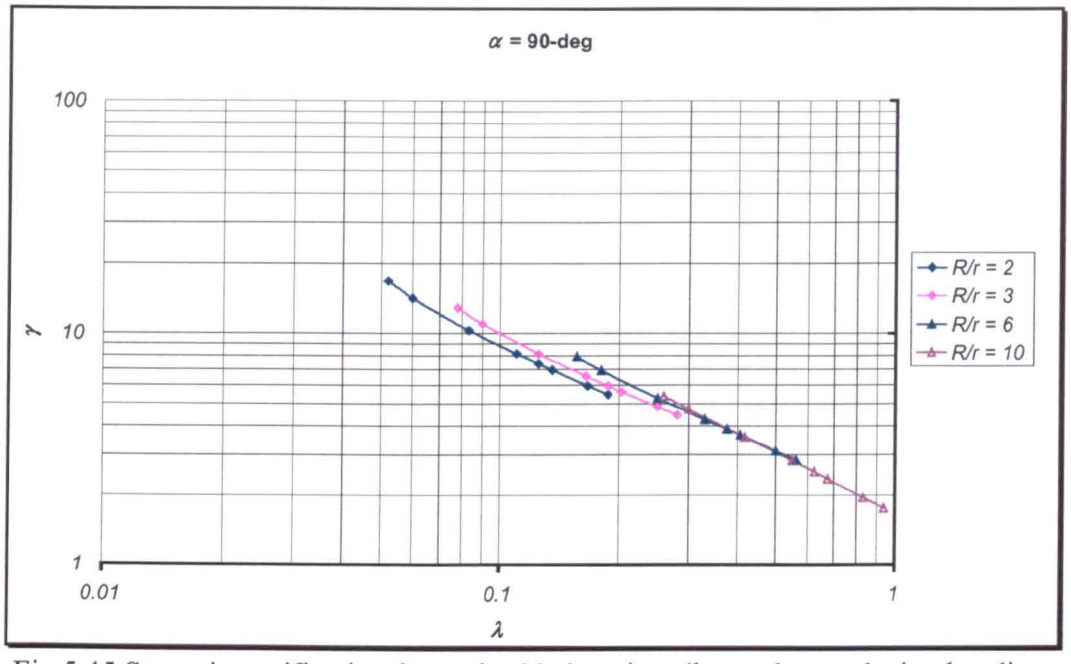

Fig.5.45 Stress-intensification factor for 90-deg pipe elbows due to closing bending

Figure 5.45 shows that the stress-intensification factor for 90-deg pipe elbow cannot be represented by a single function of pipe bend parameter, λ, but shows that the stress-intensification factor is also a function of radius ratio, R/r. As shown in Fig.5.45, the relation of stress-intensification factor, γ, and pipe bend parameter, λ, is essentially linear in a log-log plot. Accordingly the relation can be expressed in the following form:

$$\gamma = \frac{p}{\lambda^q} \tag{5-58}$$

In this thesis an attempt is again made to obtain empirical formulae for stress-intensification factors from finite element generated data. As shown in Fig.5.45, stress-intensification factors depend on pipe bend parameter, λ: higher stress-intensification factor is obtained for smaller pipe bend parameters. Taking the effect of radius ratio into account, expressions for the stress-intensification factor of 90-deg pipe elbows subjected to in-plane closing bending are obtained:

$$\gamma = \frac{1.240}{\lambda^{0.866}}; \qquad \text{for} \frac{R}{r} = 2 \tag{5-59}$$

$$\gamma = \frac{1.534}{\lambda^{0.818}}; \qquad \text{for} \frac{R}{r} = 3 \tag{5-60}$$

$$\gamma = \frac{1.786}{\lambda^{0.792}}; \qquad \text{for} \frac{R}{r} = 6 \tag{5-61}$$

$$\gamma = \frac{1.672}{\lambda^{0.867}}; \qquad \text{for} \frac{R}{r} = 10 \tag{5-62}$$

Equations (5-59) through (5-62) show that the stress-intensification factor as a function of pipe bend parameter, λ, is also depending on radius ratio, *R/r*. However, the above equations are not in suitable form for design purposes. It is intended to follow the suggestion of Fujimoto and Soh [92] to express the stress-intensification factor in term of the asymptotic solution of Clark and Reissner [20] as given in the following form:

$$\gamma = \frac{1.89}{\lambda^{2/3}}[f(\lambda)] \tag{5-63}$$

In equation (5-63), the term outside the square bracket is the asymptotic solution of Clark and Reissner [20] and the term inside the square bracket represents the dependence of stress-intensification factor on radius ratio (the function in the square would be different for every radius ratio).

Following the procedure of Fujimoto and Soh [92] as described in the previous sections, equations (5-59) through (5-62) can be rewritten in the following form:

$$\gamma = \frac{1.89}{\lambda^{2/3}}[0.5617 - 0.2092\ln(\lambda)] \qquad \text{for} \frac{R}{r} = 2 \tag{5-64}$$

$$\gamma = \frac{1.89}{\lambda^{2/3}}[0.7715 - 0.1650\ln(\lambda)] \qquad \text{for} \frac{R}{r} = 3 \tag{5-65}$$

$$\gamma = \frac{1.89}{\lambda^{2/3}}[0.9342 - 0.1390\ln(\lambda)] \qquad \text{for} \frac{R}{r} = 6 \tag{5-66}$$

$$\gamma = \frac{1.89}{\lambda^{2/3}}[0.8785 - 0.2054\ln(\lambda)] \qquad \text{for } \frac{R}{r} = 10 \qquad (5\text{-}67)$$

As shown in Fig.5.45, the stress-intensification factor is directly proportional to the inverse of radius ratio, but the first term in the square bracket in equation (5-67) for R/r = 10 is smaller than the corresponding term in equation (5-66) for R/r = 6. Figure 5.46 shows the stress-intensification factor obtained from finite element (FE), in comparison to those calculated using equations (5-59) through (5-62), and equations (5-64) through (5-67). It can be seen that the proposed equations fit well the results from finite element. In addition, the plot for the proposed design formulae, i.e., equations (5-64) through (5-67) coincide with those calculated using equations (5-59) through (5-62).

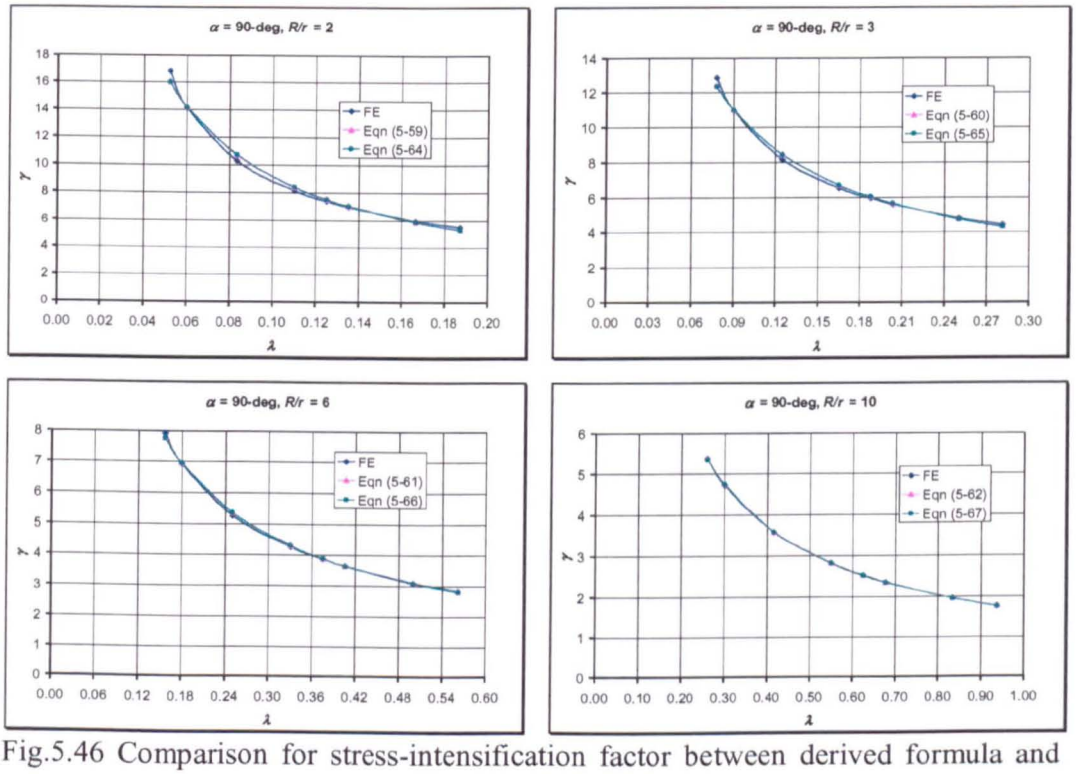

Fig.5.46 Comparison for stress-intensification factor between derived formula and FE results

5.3.2 Effect of Bend Angle on Stress-Intensification Factors

It can be seen once more that as the bend angle of a pipe elbow approaches a hypothetical zero, it tends to behave as a straight pipe. The location of maximum stress might be shifted from the crown toward the furthest location from the central axis as in a straight pipe. To account for the effect of bend angle on stress-intensification factor other than 90-deg, pipe elbows having bend angle of 30, 45, 60, and 180-deg has been studied.

Figure 5.47 through 5.50 show the stress distribution at the mid-section of a pipe elbows subjected to in-plane closing moment. These figures show that the maximum stress for the elbow again occurs in the hoop direction, but its position moves by 10-deg from crown toward intrados for elbow having bend angle of 30, 45, and 60-deg, while the location of maximum stress remain at the crown for a 180-deg pipe elbow.

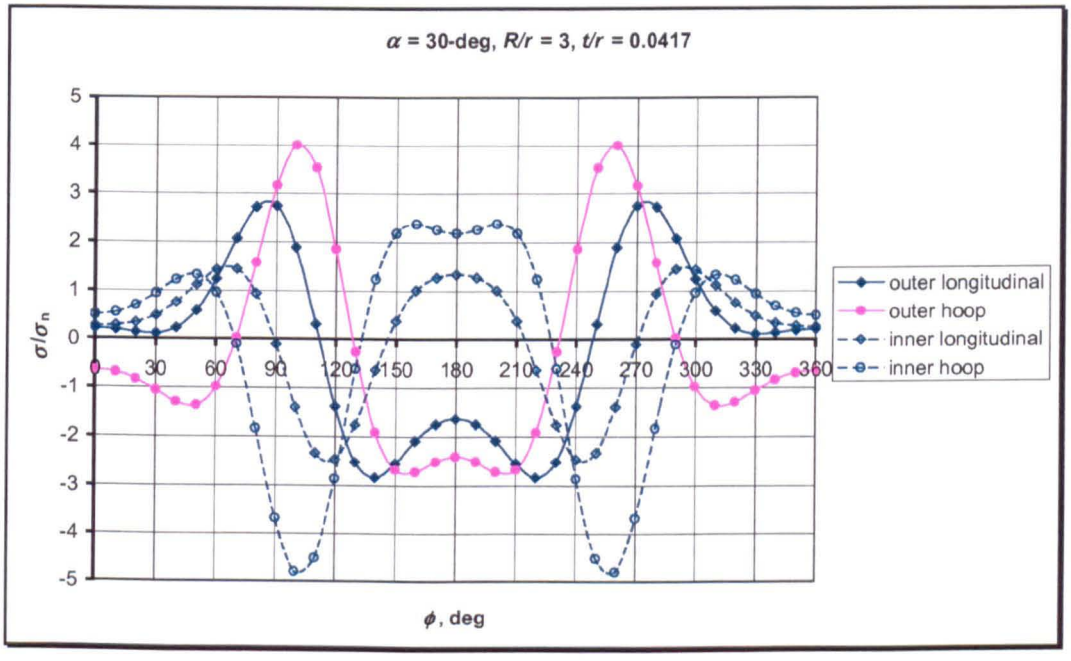

Fig.5.47 Stress-distribution for 30-deg pipe elbow under in-plane closing bending

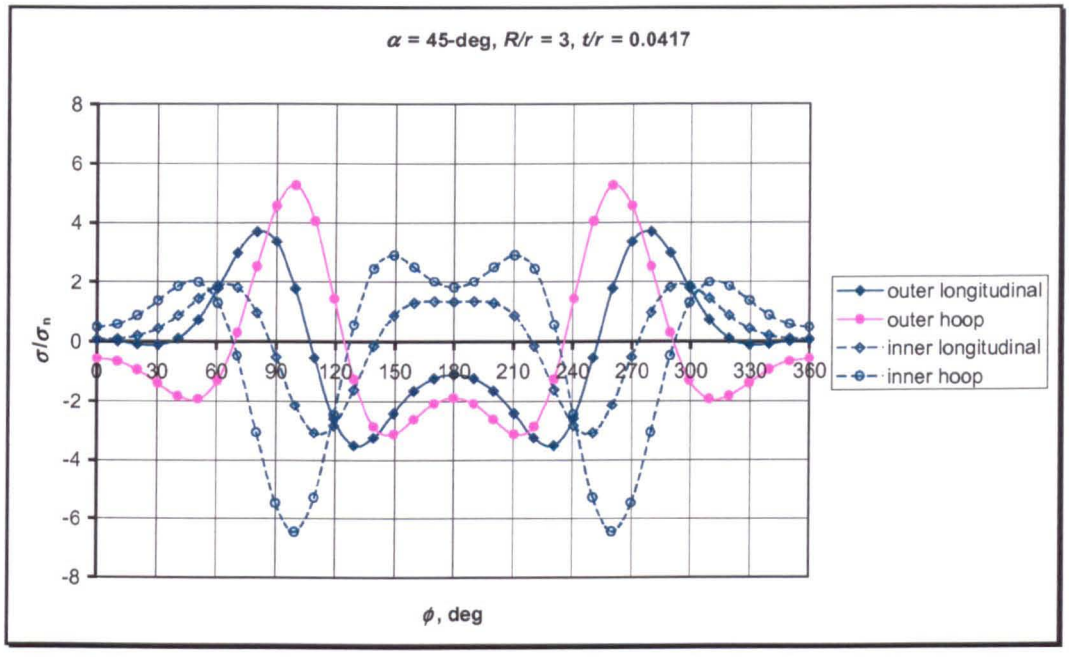

Fig.5.48 Stress-distribution for 45-deg pipe elbow under in-plane closing bending

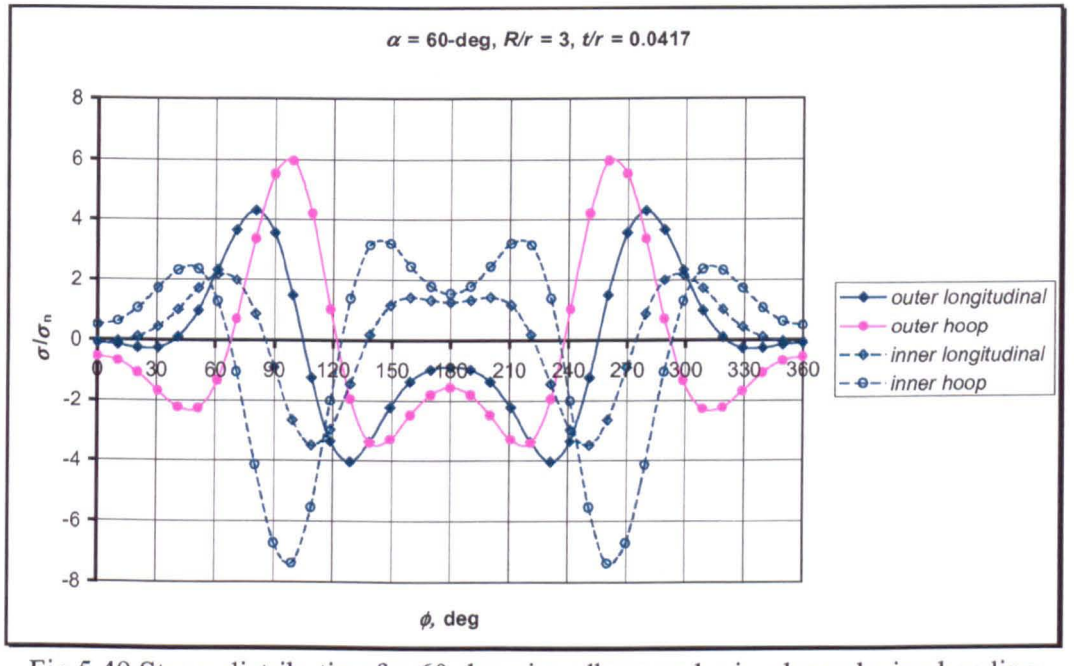

Fig.5.49 Stress-distribution for 60-deg pipe elbow under in-plane closing bending

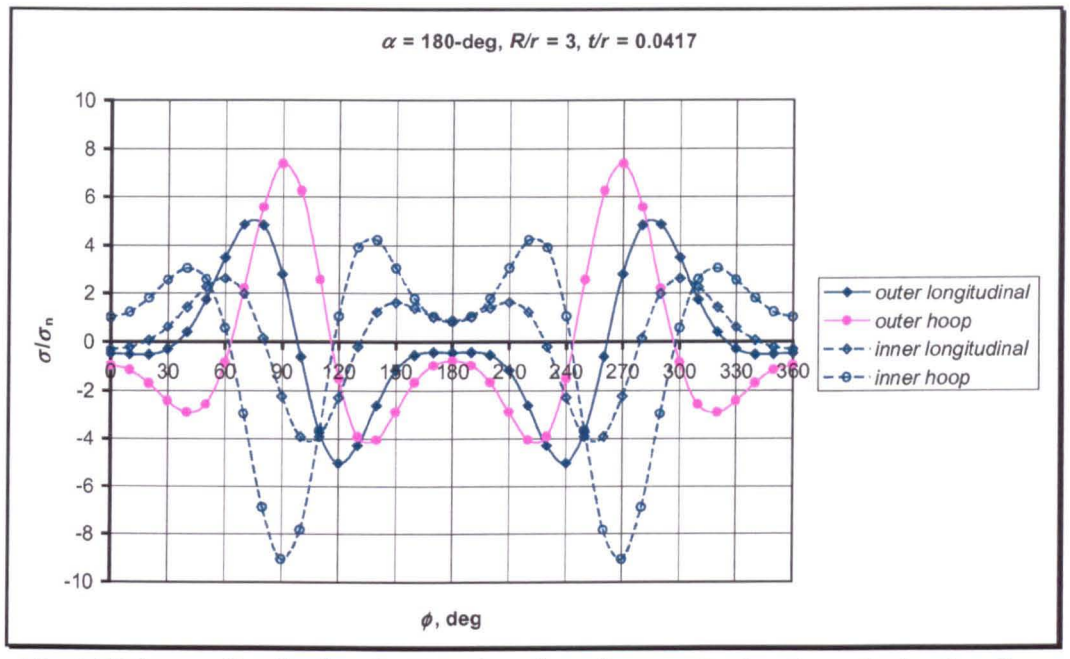

Fig.5.50 Stress-distribution for 180-deg pipe elbow under in-plane closing bending

In what follows, the maximum compressive hoop stress at the inner surface, defined as the '*stress-intensification factor*', is evaluated at any circumferential position, depending on bend angle. For the bend angles considered in this study, the locations of maximum stresses measured from the extrados are tabulated below:

Bend angle (α), deg	30	45	60	90	180
Position from extrados (ϕ), deg	100	100	100	90	90

Figure 5.51 through 5.54 show the stress-intensification factors for various bend angles of pipe elbows under in-plane closing moment. It can be seen that the stress-intensification factor not only depends on single parameter, λ, but also depends on radius ratio, R/r. The dependency of stress-intensification factor on radius ratio is more pronounced for pipe elbows of small angle and less significant for large bend angle.

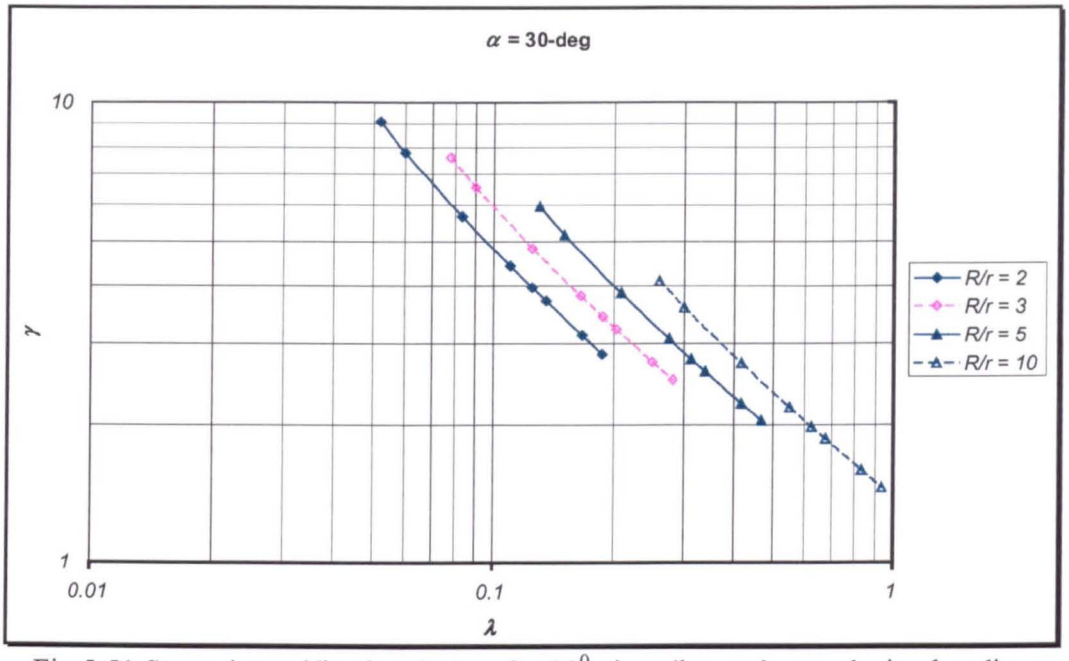

Fig.5.51 Stress-intensification factors for 30^0 pipe elbows due to closing bending

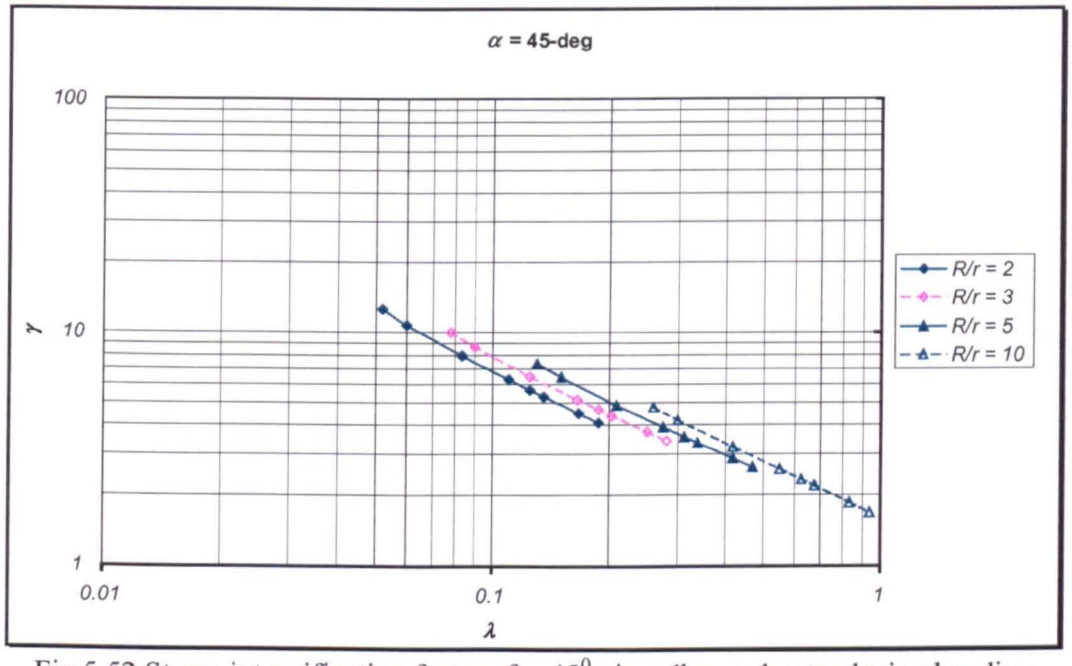

Fig.5.52 Stress-intensification factors for 45^0 pipe elbows due to closing bending

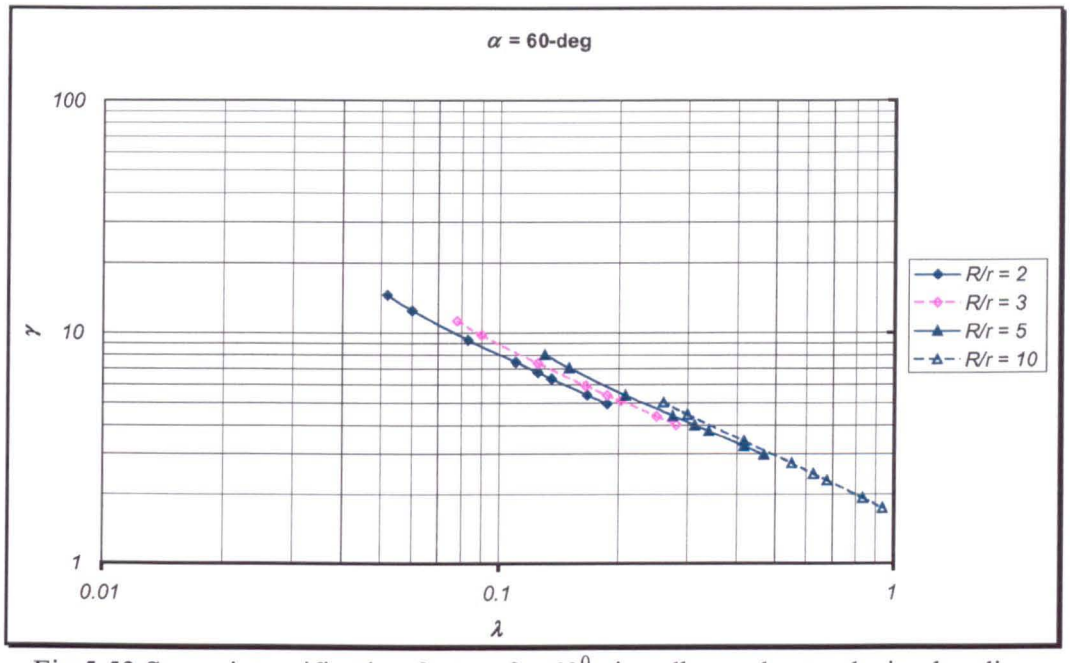

Fig.5.53 Stress-intensification factors for 60^0 pipe elbows due to closing bending

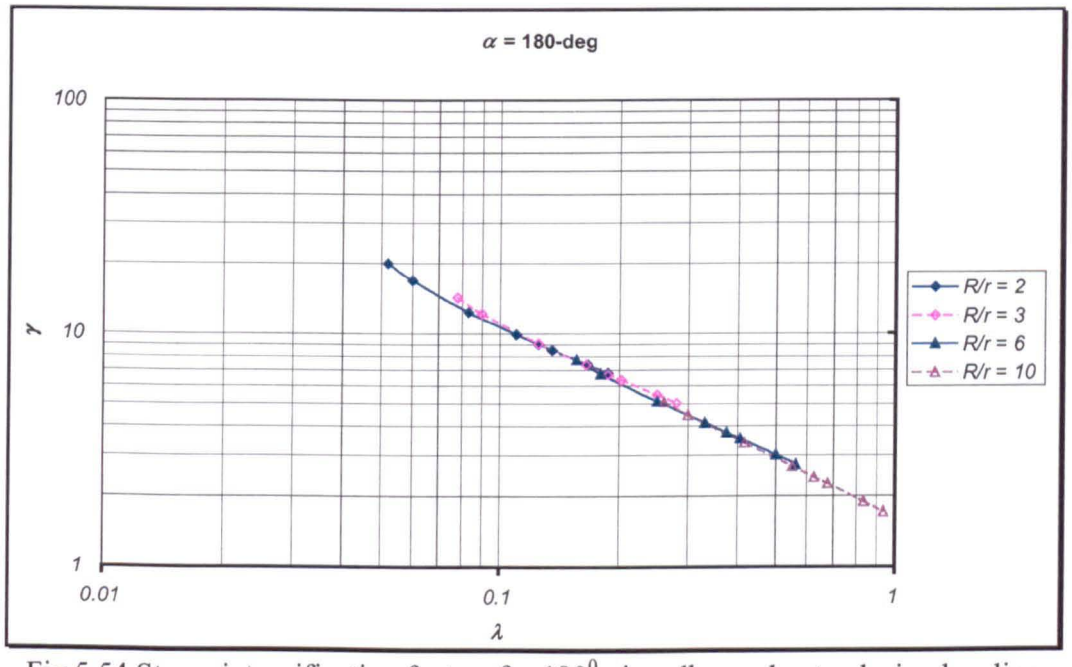

Fig.5.54 Stress-intensification factors for 180^0 pipe elbows due to closing bending

It can be seen from Fig.5.51 through 5.54 that as the bend angle becomes greater, the dependence of stresses on radius ratio becomes smaller. Figure 5.54 shows that the stress-intensification factor for 180-deg pipe elbows is less dependent on radius ratio.

The stress-intensification could be represented by a single line dependent only on pipe bend parameter.

An expression for the stress-intensification factors for pipe elbows under in-plane closing bending are obtained from these figures:

$$\gamma = \frac{1.89}{\lambda^{2/3}}[a - b\ln(\lambda)] \qquad (5\text{-}68)$$

where the coefficient 'a' and 'b' are functions of radius ratio R/r as given in Table 5.5 and 5.6 respectively for various bend angles.

Table 5-5 Values of coefficients 'a' in equation (5-68) for different bend angle

R/r	Bend angle				
	30-deg	45-deg	60-deg	90-deg	180-deg
2	0.2558	0.4175	0.5823	0.5617	0.7706
3	0.3932	0.5748	0.7312	0.7715	0.8953
4	0.4866	0.6576	0.7897	0.8617	0.9126
5	0.5476	0.7318	0.8287	0.9241	0.9087
6	0.6032	0.7620	0.8547	0.9342	0.8944
7	0.6414	0.7948	0.8733	0.9150	0.8826
8	0.6716	0.8203	0.8872	0.9019	0.8723
9	0.6961	0.8407	0.8980	0.9018	0.8633
10	0.7215	0.8410	0.9067	0.8785	0.8537

Table 5-6 Values of coefficients '*b*' in equation (5-68) for different bend angle

R/r	Bend angle				
	30-deg	45-deg	60-deg	90-deg	180-deg
2	0.1333	0.1637	0.1540	0.2092	0.2145
3	0.1256	0.1437	0.1276	0.1650	0.1674
4	0.1218	0.1298	0.1106	0.1550	0.1508
5	0.1180	0.1210	0.1010	0.1500	0.1427
6	0.1158	0.1128	0.0952	0.1390	0.1440
7	0.1137	0.1103	0.0977	0.1516	0.1501
8	0.1118	0.1118	0.1070	0.1656	0.1607
9	0.1102	0.1173	0.1231	0.1884	0.1636
10	0.1092	0.1311	0.1501	0.2054	0.1711

It is interesting to note that the stress-intensification factors for 180-deg elbows are less than stress-intensification factors for 90-deg elbows. This is contrary to the flexibility factors where 90-deg elbows are stiffer than 180-deg elbows. The variation of flexibility and stress-intensification factors with respect to total bend angle is given in Table 5.7. The values in Table 5.7 are factored by the flexibility and stress-intensification factors of 90-deg elbows.

Table 5.7 Summary of the effect of bend angle on flexibility and stresses

Bend angle, α	$k/k_{(90)}$	$\gamma/\gamma_{(90)}$
30-deg	< 1	< 1
45-deg	< 1	< 1
60-deg	< 1	< 1
90-deg	= 1	= 1
180-deg	> 1	< 1

5.3.3 Pressure Reduction Effect

For combined loading of bending and internal pressure, the total stresses from the finite element analysis results include the toroidal membrane pressure stresses. Recall that the definition of 'stress-intensification factor' adopted here is the maximum stress in a pipe bend (in the hoop direction) divided by the nominal bending stress in a straight pipe as given by equation (5-57). Because the stresses are factored by the nominal bending stress, the membrane stresses due to internal pressure as given in equation (2-15) should be subtracted from the total stresses obtained from finite element analysis (Fig.5.55). In the theoretical analysis developed by Rodabaugh and George [30], the toroidal membrane stresses resulting from internal pressure load were also excluded in calculation of the stress-intensification factor.

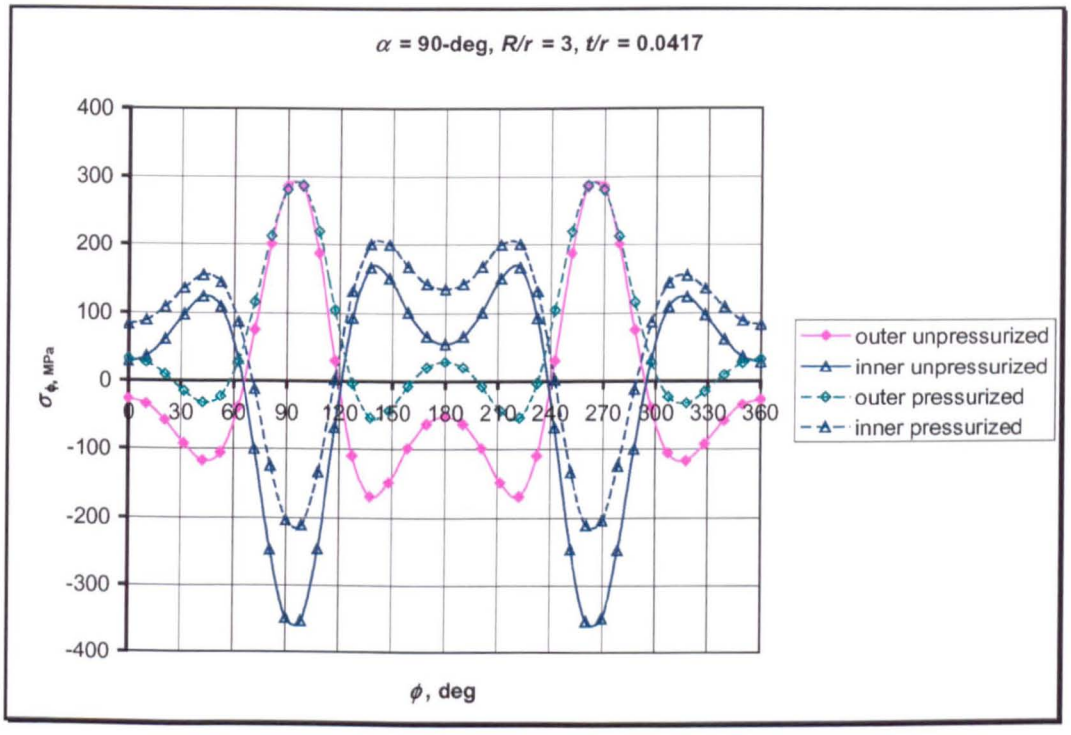

Fig.5.55 Hoop stress distribution under bending and internal pressure

Figure 5.55 shows the total hoop stress at the mid-section of an elbow under in-plane closing bending and internal pressure, plotted for α = 90-deg, R/r = 3, and t/r = 0.0417. It can be seen that internal pressure increases the total stress. It can bee seen from Fig.5.55 that internal pressure reduces the magnitude of compressive stress and increase the magnitude of tension stress due to bending alone.

Figure 5.56 shows the effect of internal pressure on stress-intensification factor of a pipe elbow under in-plane closing moment. Figure 5.56 was obtained by subtracting the toroidal hoop stress (eqn (2-15) from hoop stress in Fig.5.55. It can be clearly seen that the effect of internal pressure is to reduce the bending stresses. Figure 5.56 also shows that the system is bending dominated: this is indicated by the same characteristics of stress distribution under both unpressurized and pressurized condition. This trend was also found by Imamasa and Uragami [51] in their experimental analysis for pipe bends. It might be expected however that this characteristic would change if the internal pressure increased beyond a certain level [57].

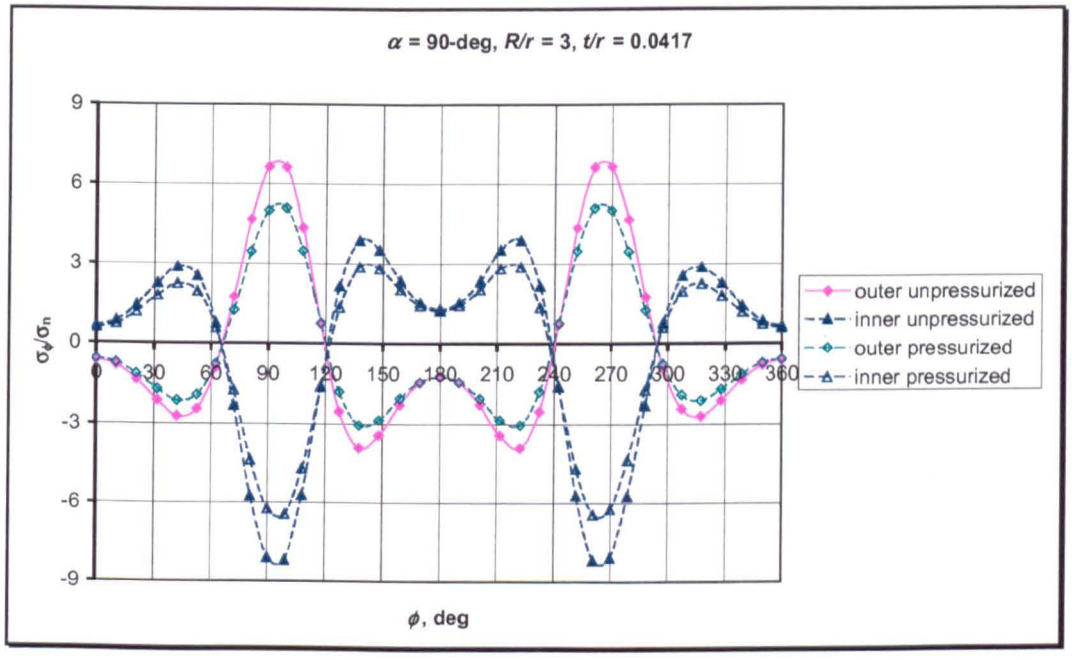

Fig.5.56 Typical pressure reduction effect on circumferential (hoop) stress

A typical pressure – stress (hoop) plot is shown in Fig.5.57, plotted for a 90-deg pipe elbow and a radius ratio equals three. The abscissa value of 0.0 represents the final load step of moment loading and the starting of the subsequent internal pressure loading. It can be seen that the relation between internal pressure and maximum hoop stress is non-linear. Figure 5.57 shows the 'Haigh effect' [11]: pipe subjected to internal pressure departs significantly from linear behaviour if the pipe cross-section is not circular. In Fig.5.57, internal pressure acts on oval cross-section pipe elbow due to applied bending moment.

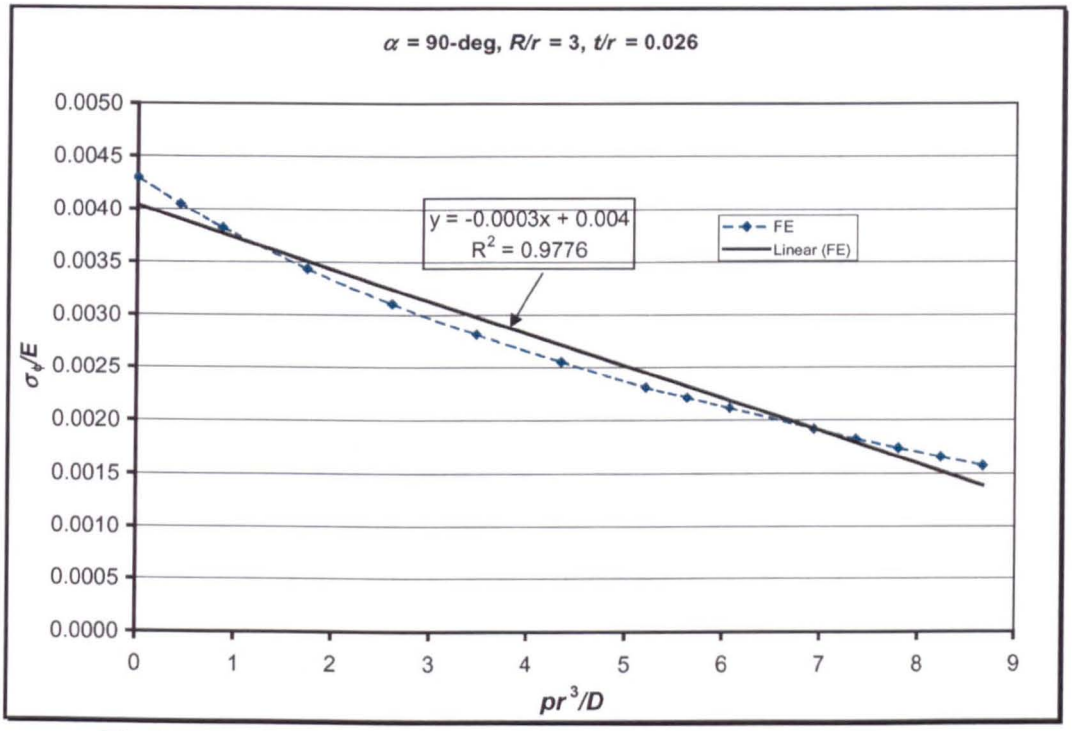

Fig.5.57 Typical pressure – stress plot under in-plane closing moment

Stress-intensification factors for 90-deg pipe elbows loaded by in-plane closing moment is shown in Fig.5.58 through 5.61 for various radius ratio. It can be clearly seen that the presence of internal pressure is to reduce the stress-intensification factor. The reduction is more pronounced for elbows having low pipe bend parameter, λ (small thickness and short radius bends). In this section, the effect of internal pressure on reducing stress-intensification factor is evaluated, and empirical

formulae for stress-intensification are proposed. The same procedure used in section 5.2.3 is followed.

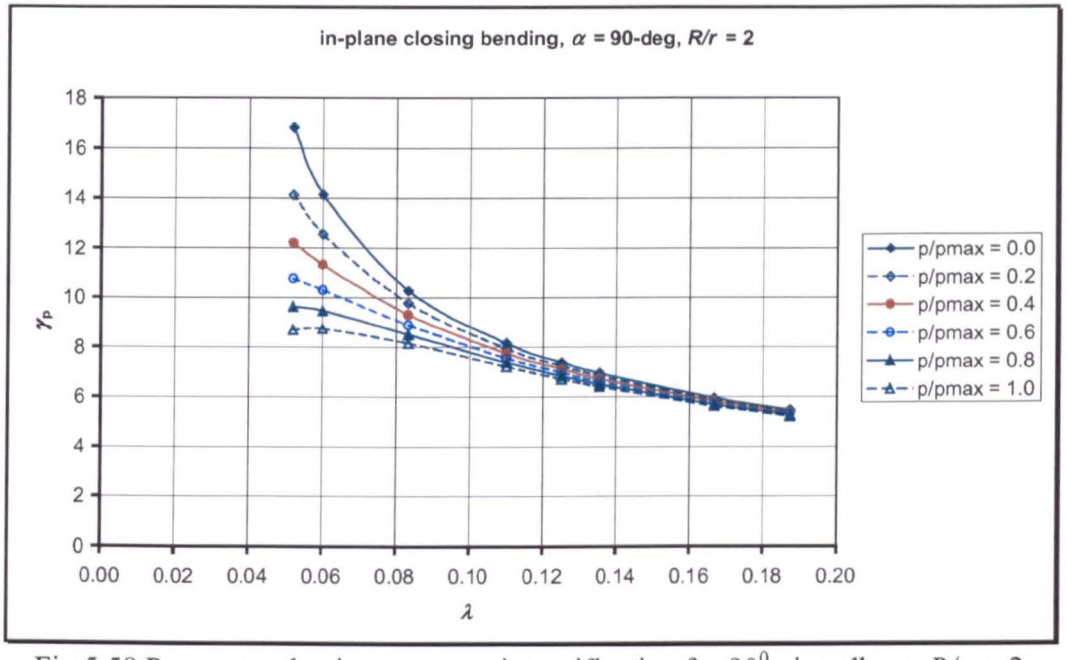

Fig.5.58 Pressure reduction on stress-intensification for 90^0 pipe elbow: $R/r = 2$

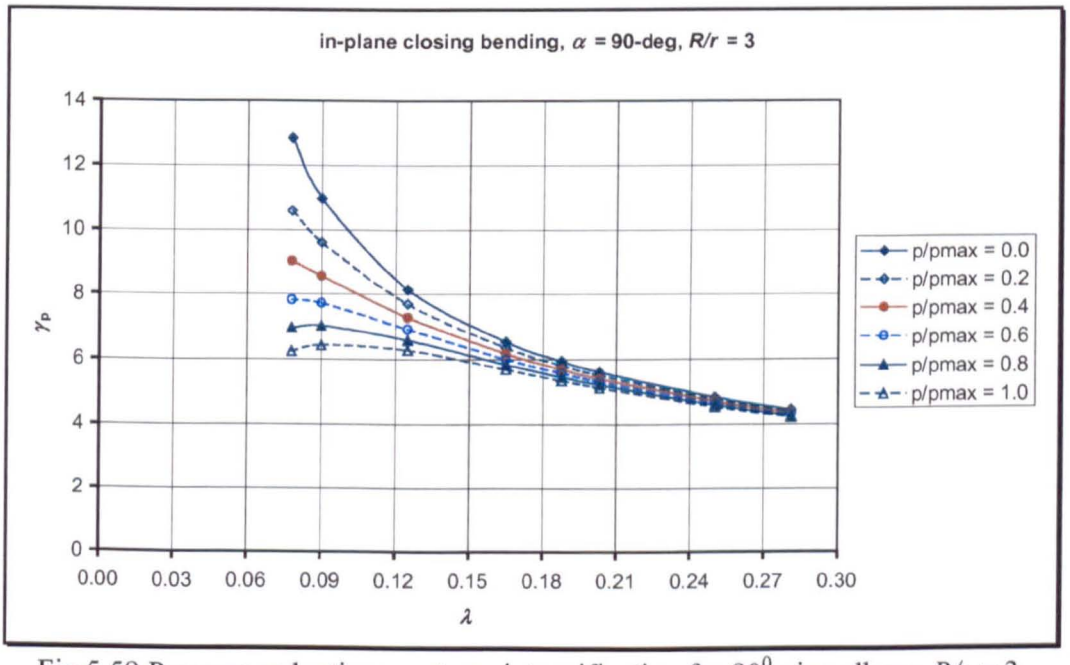

Fig.5.59 Pressure reduction on stress-intensification for 90^0 pipe elbow: $R/r = 3$

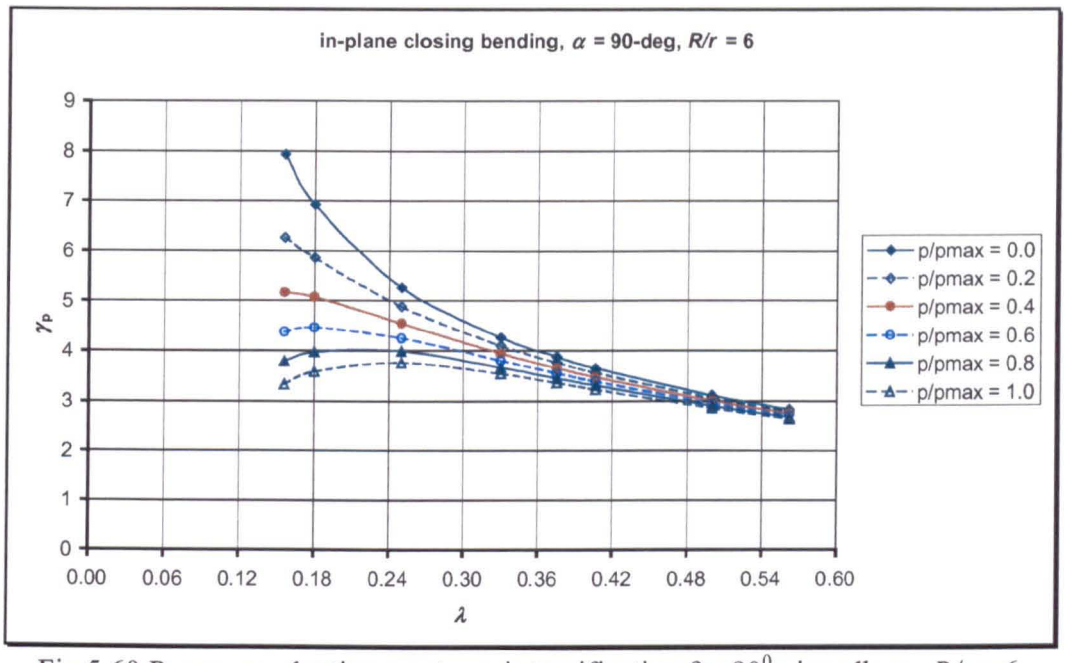

Fig.5.60 Pressure reduction on stress-intensification for 90^0 pipe elbow: $R/r = 6$

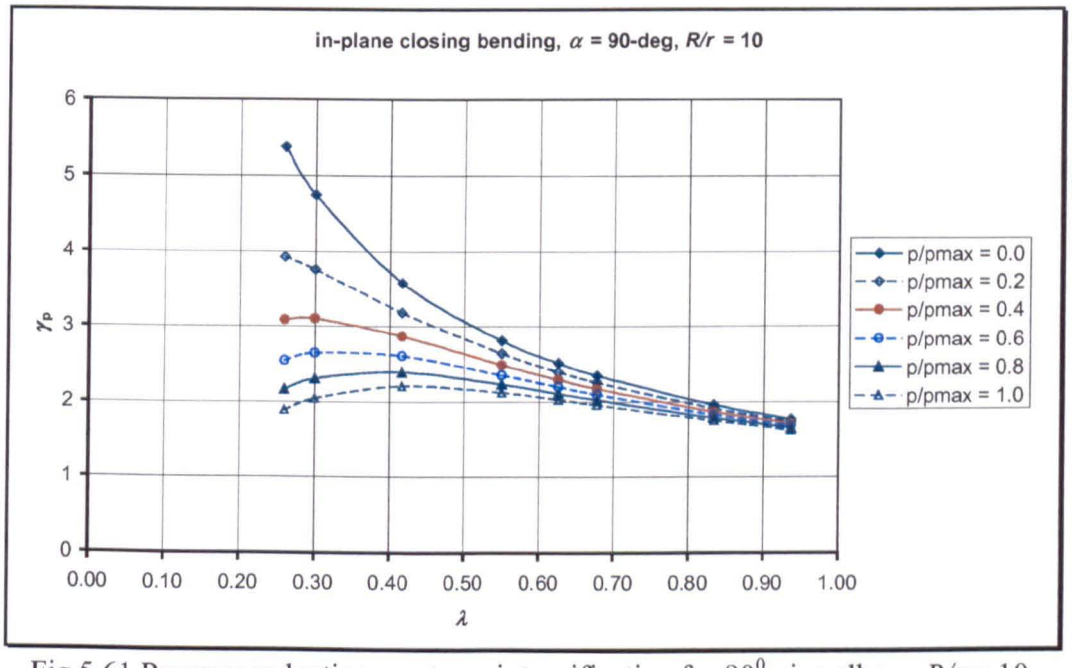

Fig.5.61 Pressure reduction on stress-intensification for 90^0 pipe elbow: $R/r = 10$

When internal pressure is included, the stress-intensification factor can be expressed in the following form:

$$\gamma_p = \frac{\gamma}{1 + X_i\left(\frac{p}{E}, \frac{r}{t}, \frac{R}{r}\right)} \qquad (5-69)$$

where, γ and γ_p are stress-intensification factors with and without internal pressure respectively.

To obtain the pressure reduction, i.e., the second term in the denominator, equation (5-69) is rewritten as:

$$\frac{\gamma}{\gamma_p} - 1 = X_i\left(\frac{p}{E}, \frac{r}{t}, \frac{R}{r}\right) \qquad (5-70)$$

The left-hand side of equation (5.70) is obtained from finite element generated data as given in Fig.5.58 through 5.61 for 90-deg pipe elbows, and the right hand side is the incremental pressure load and geometric parameter.

A typical pressure reduction effect on stress-intensification is plotted as a log-log graph in Fig.5.62 for constant radius ratio *R/r* and in Fig.5.63 for constant non-dimensional thickness *r/t*. These plots are obtained for 90-deg pipe elbows extracted from Fig.5.58 through 5.61. The pressure reduction effect is plotted as the ordinate and incremental internal pressure and geometric parameter are plotted as the abscissa.

It can be seen from these figures that straight lines are obtained if the pressure reduction is plotted against the non-dimensional pressure *p/E*. There is a slight deviation from a straight line if the pressure reduction is plotted against geometric parameter *r/t* and *R/r*. In this analysis, the pressure reduction will be fitted as straight lines and the error introduced will be discussed at the end of this chapter.

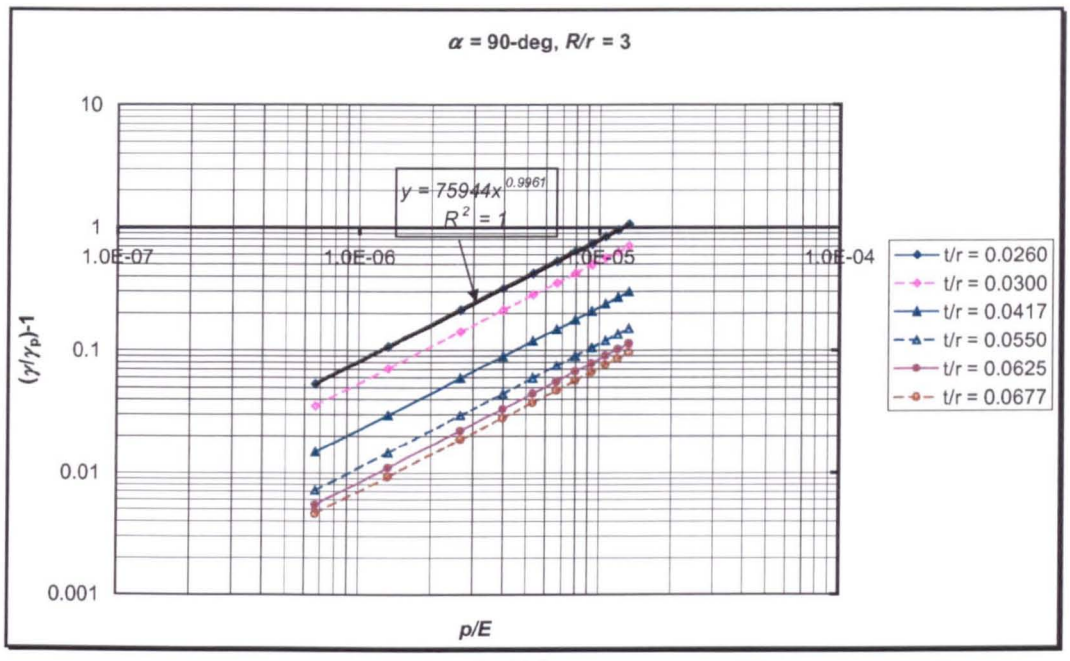

(a)

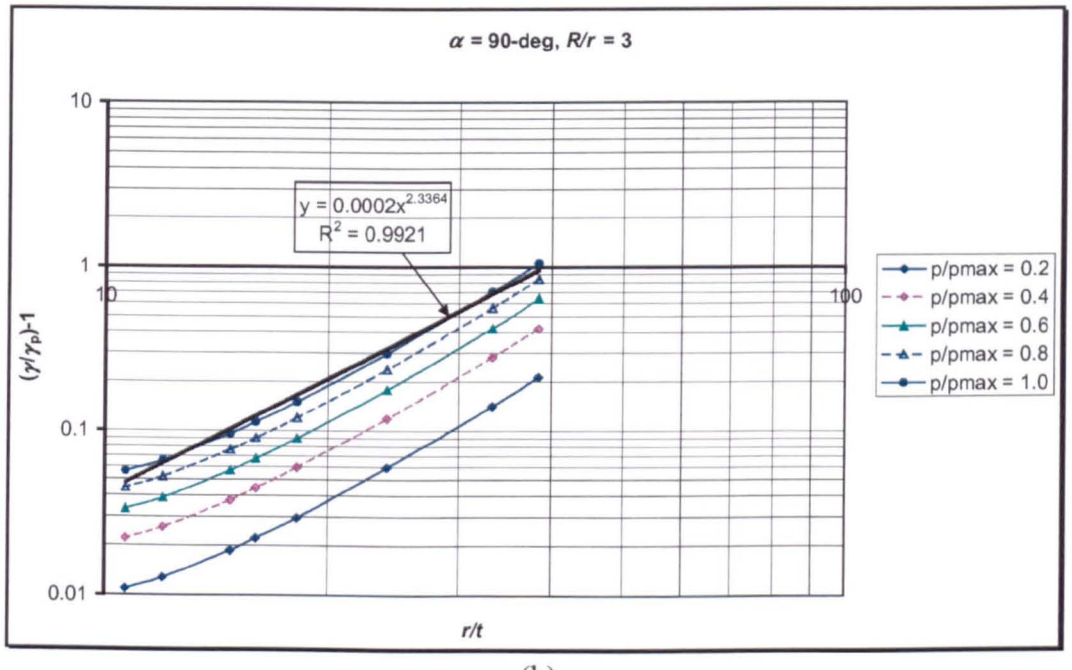

(b)

Fig.5.62 Pressure reduction for constant radius ratio plotted against (a) *p/E*, (b) *r/t*

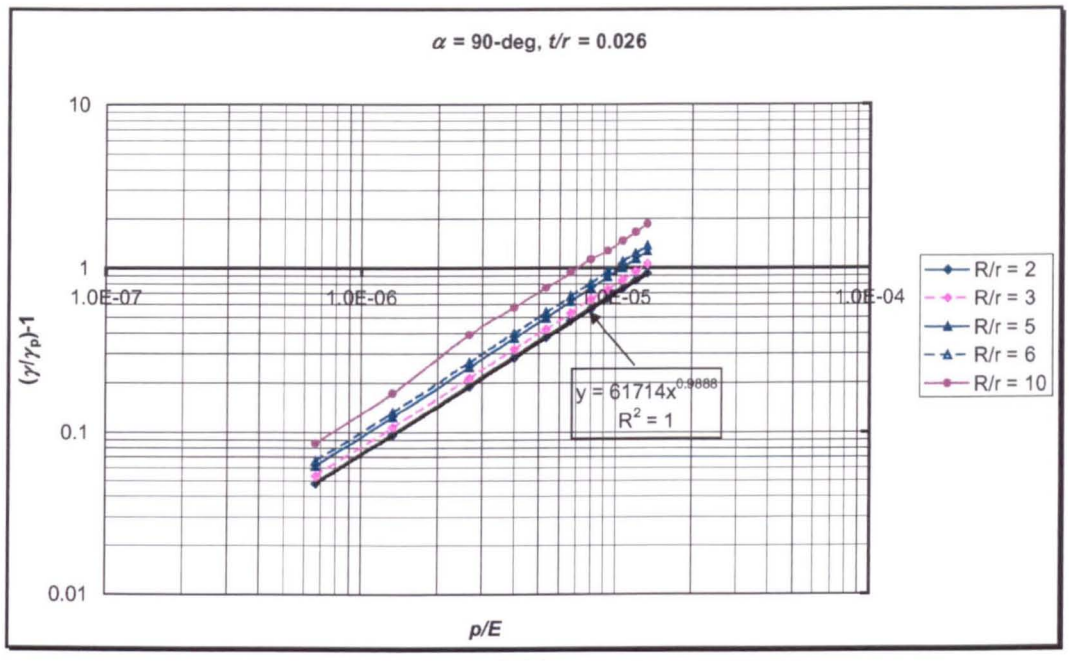

(a)

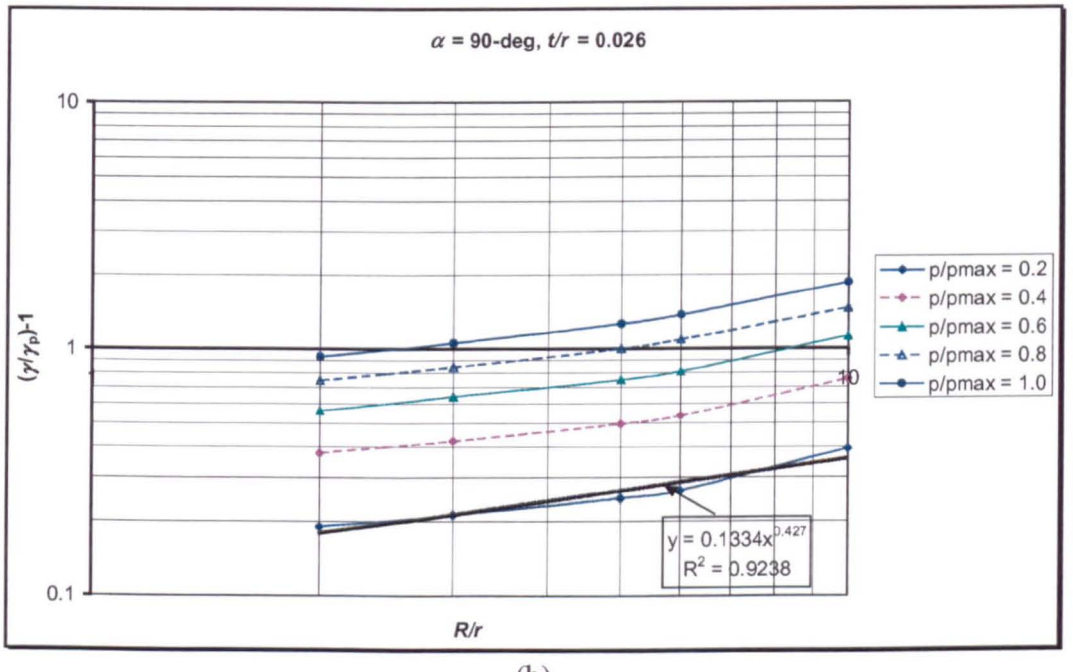

(b)

Fig.5.63 Pressure reduction for constant thickness plotted against (a) *p/E*, (b) *R/r*

Similar log-log plots for all geometry (radius ratio and thickness) was constructed, Again for brevity, these plots are not shown in this thesis, but it should be easily constructed from Fig.A5.14 of Appendix C5. From all the plots, it has been found that the index of *p/E*, *r/t*, and *R/r* is approximately equal to 1, 2.33, and 0.435 respectively.

From a careful observation of Fig.5.62 and 5.63 and similar plots for all geometry considered along with Fig.5.58 through 5.61, the following expression is proposed for stress-intensification factors of 90-deg elbows under in-plane closing moment and internal pressure:

$$\gamma_p = \frac{\gamma}{1+10.25\left(\frac{p}{E}\right)\left(\frac{r}{t}\right)^{7/3}\left(\frac{R}{r}\right)^{0.435}} \qquad (5-71)$$

where γ is stress-intensification factor in the absence of internal pressure as given by equation (5-53) and Table 5.7 and 5.8. The value of coefficient of 10.25 in equation (5-71) was established based on R/r = 10, t/r = 0.026, and p/pmax = 1.0. Eqn (5-71) can be directly compared with the equation proposed by Rodabaugh and George [30]. It can be seen that equation (5-56) produces greater pressure reduction – marked by the coefficient 10.25 rather than 3.25 in equation (2-98).

5.3.4 Effect of Bend Angle on Pressure Reduction

It has been shown in section 5.3.2 that the stress-intensification factor for unpressurized pipe elbows is very much influenced by the total angle of the bend. In this section the effect of bend angle on pressure reduction is studied and formulae again derived:

The same procedure can be applied for different bend angles. By constructing log-log graphs for pressure reduction for all geometry using the data from Fig.A5.11 through

A5.15 of Appendix C5, flexibility factors of pressurized elbows under in-plane closing moment are proposed as follows:

$$\gamma_p = \frac{\gamma}{1+16.90\left(\frac{p}{E}\right)\left(\frac{r}{t}\right)^{7/3}\left(\frac{R}{r}\right)^{0.197}} \qquad \text{for } \alpha = 30\text{-deg} \qquad (5\text{-}72)$$

$$\gamma_p = \frac{\gamma}{1+12.50\left(\frac{p}{E}\right)\left(\frac{r}{t}\right)^{7/3}\left(\frac{R}{r}\right)^{0.318}} \qquad \text{for } \alpha = 45\text{-deg} \qquad (5\text{-}73)$$

$$\gamma_p = \frac{\gamma}{1+10.25\left(\frac{p}{E}\right)\left(\frac{r}{t}\right)^{7/3}\left(\frac{R}{r}\right)^{0.407}} \qquad \text{for } \alpha = 60\text{-deg} \qquad (5\text{-}74)$$

$$\gamma_p = \frac{\gamma}{1+7.50\left(\frac{p}{E}\right)\left(\frac{r}{t}\right)^{7/3}\left(\frac{R}{r}\right)^{0.567}} \qquad \text{for } \alpha = 180\text{-deg} \qquad (5\text{-}75)$$

The pressure reduction in Equations (5-71) through (5-75) are expressed in terms of non-dimensional pressure *p/E*, non-dimensional thickness *r/t*, and radius ratio *R/r*. Again, an alternative can be obtained by noting that:

$$\left(\frac{p}{E}\right)\left(\frac{r}{t}\right)^{7/3} = \left(\frac{p}{E}\right)\left(\frac{r}{t}\right)^{3}\left(\frac{r}{R}\right)^{2/3}\lambda^{2/3}$$

Using this relation, the stress-intensification factors of piping elbows subjected to combined bending and in-plane closing moment can be written as:

$$\gamma_p = \frac{\gamma}{1+4.65\left(\frac{pr^3}{3D}\right)\lambda^{2/3}\left(\frac{r}{R}\right)^{0.47}} \qquad \text{for } \alpha = 30^0 \qquad (5\text{-}76)$$

$$\gamma_p = \frac{\gamma}{1+3.45\left(\frac{pr^3}{3D}\right)\lambda^{2/3}\left(\frac{r}{R}\right)^{0.35}} \qquad \text{for } \alpha = 45^0 \qquad (5\text{-}77)$$

$$\gamma_p = \frac{\gamma}{1+2.82\left(\frac{pr^3}{3D}\right)\lambda^{2/3}\left(\frac{r}{R}\right)^{0.26}} \qquad \text{for } \alpha = 60^0 \qquad (5-78)$$

$$\gamma_p = \frac{\gamma}{1+2.80\left(\frac{pr^3}{3D}\right)\lambda^{2/3}\left(\frac{r}{R}\right)^{0.23}} \qquad \text{for } \alpha = 90^0 \qquad (5-79)$$

$$\gamma_p = \frac{\gamma}{1+2.05\left(\frac{pr^3}{3D}\right)\lambda^{2/3}\left(\frac{r}{R}\right)^{0.10}} \qquad \text{for } \alpha = 180^0 \qquad (5-80)$$

The formulae in equations (5-71) through (5-80) if necessary can be further simplified into the following form:

$$\gamma_p = \frac{\gamma}{1+A\left(\frac{p}{E}\right)\left(\frac{r}{t}\right)^{7/3}\left(\frac{R}{r}\right)^{m}}$$

$$\gamma_p = \frac{\gamma}{1+B\left(\frac{pr^3}{3D}\right)\lambda^{2/3}\left(\frac{r}{R}\right)^{n}}$$

The simplification of the formulae aims to find the coefficient A and B, and the power m and n as a function of bend angle, α. This simplification will not be processed any further here as the bend angles considered in this study have covered pipe elbows dimension in practical usage.

5.4 Discussion

In the previous sections of this chapter, formulae for ovalisation, flexibility, and stress-intensification factors of piping elbows under in-plane closing moment have been developed. The pressure reduction effect corresponding to the work of

Rodabaugh and George [30] has also been developed. The formulae have been derived through simple curve fitting. Of course some error will be introduced, since the coefficient of the pressure reduction effects were obtained from one particular data set geometry and generalised for the whole data. The indices of p/E, r/t, and R/r were based on long radius bend (R/r = 10), thin pipe (t/r = 0.026), and p = 400 psi. The error introduced as a result of these approximations will be discussed in this section.

In developing the formula for unpressurised pipe elbows, the effect of radius ratio has been taken into account. In many theoretical developments, for example the work of von Karman [2], Rodabaugh and George [30] and others, the radius of the bend was assumed to be much greater than the cross-section radius and the result obtained then applied even to bends of short radius. As has been shown in the foregoing sections, there is a great influence of radius ratio on ovalisation, flexibility, and stress-intensification factors.

It is well known that an elbow's enhanced flexibility and stress-intensification arises from the cross-sectional ovalisation due to bending. However, the effect of various geometric parameters on ovalisation, flexibility, and stress-intensification factor is not necessarily identical either in trend or magnitude.

5.4.1 Unpressurized Conditions

For in-plane closing bending alone (without internal pressure), the ovalisation, flexibility, and stress-intensification factors have been expressed in the following form:

$$\xi = \frac{0.565}{\lambda^{2/3}}[a + b\ln(\lambda)] \tag{5-81}$$

$$k = \frac{1.65}{\lambda}[a - b\ln(\lambda)] \tag{5-82}$$

$$\gamma = \frac{1.89}{\lambda^{2/3}}[a - b\ln(\lambda)] \qquad (5\text{-}83)$$

where a and b are coefficients describing the dependence of ovalisation, flexibility and stress-intensification factors on the radius ratio, ρ: they are different for different bend angle for ovalisation, flexibility and stress-intensification factors. The term outside the square bracket for ovalisation factor was established based on the ovalisation for long-radius bend (R/r = 10), while the terms outside the square bracket for flexibility and stress-intensification factors are the asymptotic solution of Clark and Reissner [20].

It has been shown in the foregoing sections that a plot of ovalisation and stress-intensification factors against pipe bend parmeter, λ, show higher dependency on radius ratio, ρ, especially for large angle bends, compared to a similar plot for flexibility factor. The reason for this difference arises from the normalisation. Flexibility factor was obtained as the ratio of end rotation of a pipe bend to the end rotation of an equivalent straight pipe under the same bending load, as given by equation (5-31). It can be seen that the parameter R appears in equation (5-31) resulting in the flexibility factor being less dependent on radius ratio. The ovalisation and stress-intensification factor was obtained using equations (5-1) and (5-57) respectively for normalisation. It can be seen that there is no dependence on the parameter R in both equations and it has been defined as nominal ovalisation and nominal stress respectively. However for large angle bends (90-deg and greater), the effect of radius ratio on ovalisation, flexibility, and stress-intensification factors become less significant. This is expected since the difference of length between the extrados and the intrados become smaller.

Figure 5.64 shows the flexibility factor of 90-deg pipe elbows obtained from the present analysis as given by equation (5-40) for radius ratio ρ = 3, in comparison with the available theoretical results. It can be seen that the result from the present analysis is relatively higher than the asymptotic solution of Clark and Reissner [20] as adopted in the ASME B31.1 [114] and ASME B31.3 [120] and higher than the

von Karman third approximation. This is probably caused by the large deformation effect activated in the present analysis. The theoretical results in Fig.5.64 have been derived based on small deformation assumptions. The other sources of discrepancies are believed to result from the assumptions involved in the theoretical development.

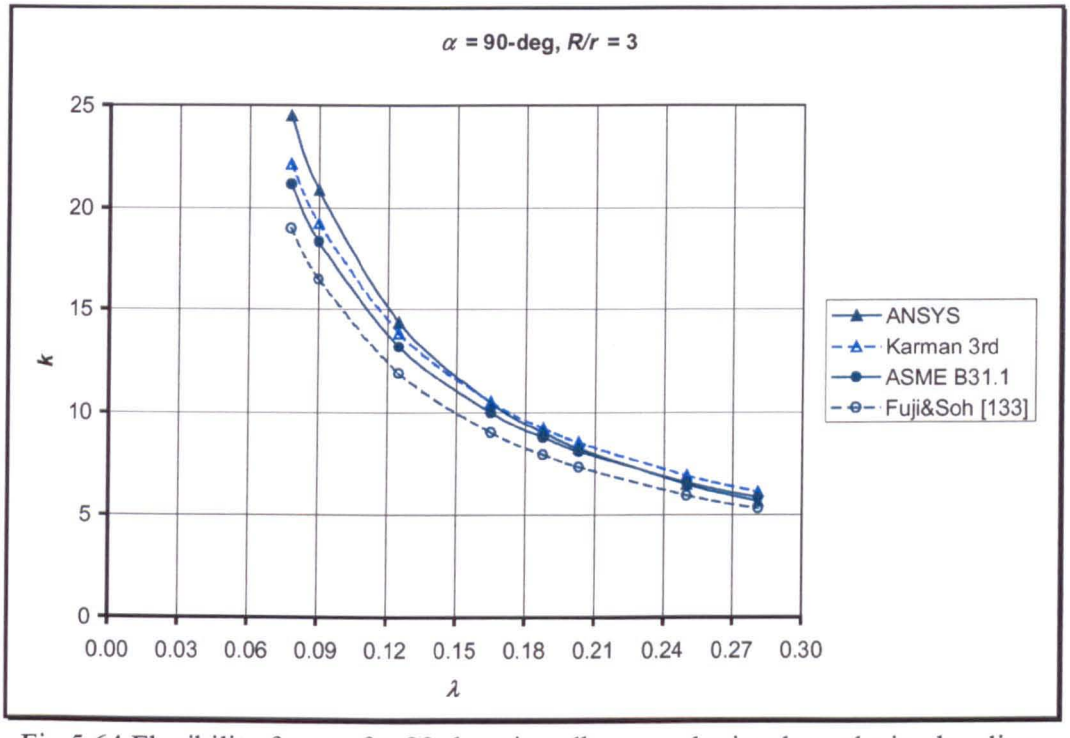

Fig.5.64 Flexibility factors for 90-deg pipe elbows under in-plane closing bending

Figure 5.65 shows the stress-intensification factor for 90-deg pipe elbows obtained from the present analysis as given by equation (5-65) for radius ratio $\rho = 3$, in comparison with the result of Markl's fatigue test as adopted in ASME B31.1 [114] and ASME B31.3 [120]. The figure also shows the stress-intensification factor obtained by Clark and Reissner [20] using the asymptotic solution. It can be seen that the result from the fatigue test due to Markl [23] is approximately half of the asymptotic solution of Clark and Reissner [20]. The results from the present finite element analysis using ANSYS are higher than the asymptotic solution of Clark and Reissner [20] for elbows of low pipe factors but slightly lower for elbows of high pipe factors. Again, it is argued that this discrepancy results from the large

deformation effect included in the present analysis, whereas small deformation assumption was made in the asymptotic solution of Clark and Reissner [20].

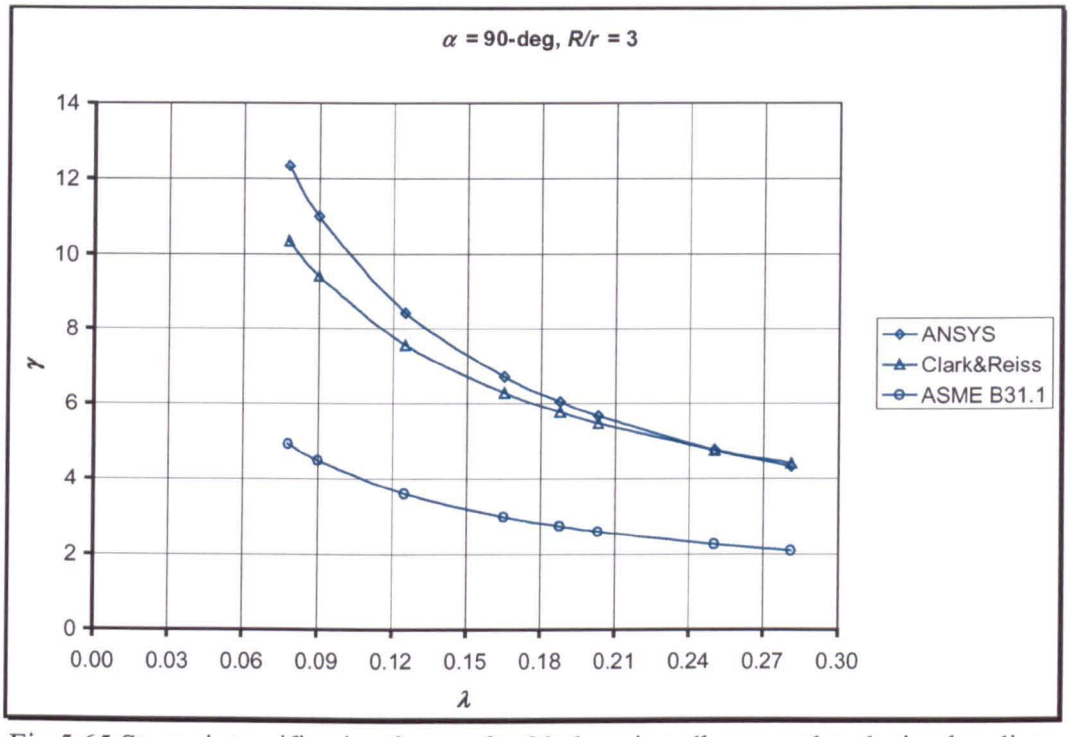

Fig.5.65 Stress-intensification factors for 90-deg pipe elbows under closing bending

5.4.2 Pressurized Conditions

In developing the formulae for the pressure reduction effect, the following approach has been applied:

(1) The relation of pressure reduction and nondimensional pressure p/E, nondimensional thickness r/t, and radius ratio R/r is linear in a log-log graph. Accordingly, the pressure reduction can be expressed as a power law.

(2) The index of non-dimensional pressure, p/E, non-dimensional thickness, r/t and radius ratio, R/r has been based on one-particular geometry.

Using this approach and taking the effect of bend angle into account, the following formula has been developed:

Ovalisation factor:

$$\xi_p = \frac{\xi}{1 + A\left(\frac{p}{E}\right)\left(\frac{r}{t}\right)^{10/3}\left(\frac{R}{r}\right)^m} \tag{5-84a}$$

$$\xi_p = \frac{\xi}{1 + B\left(\frac{pr^3}{3D}\right)\left(\frac{1}{\lambda}\right)^{1/3}\left(\frac{R}{r}\right)^n} \tag{5-84b}$$

Flexibility factor:

$$k_p = \frac{k}{1 + A\left(\frac{p}{E}\right)\left(\frac{r}{t}\right)^{9/4}\left(\frac{R}{r}\right)^m} \tag{5-85a}$$

$$k_p = \frac{k}{1 + B\left(\frac{pr^3}{3D}\right)\lambda^{3/4}\left(\frac{r}{R}\right)^n} \tag{5-85b}$$

Stress-intensification factor:

$$\gamma_p = \frac{\gamma}{1 + A\left(\frac{p}{E}\right)\left(\frac{r}{t}\right)^{7/3}\left(\frac{R}{r}\right)^m} \tag{5-86a}$$

$$\gamma_p = \frac{\gamma}{1 + B\left(\frac{pr^3}{3D}\right)\lambda^{2/3}\left(\frac{r}{R}\right)^n} \tag{5-86b}$$

where A, B, m, and n are a function of bend angle, α, as summarised in Table 5.8, 5.9, and 5.10 for ovalisation, flexibility, and stress-intensification respectively. Notice these values are different for ovalisation, flexibility, and stress-intensification factors.

Table 5.8 Values for *A, B, m,* and *n* in equation (5-84) for ovalisation factor

Bend angle, α	*A*	*B*	*m*	*N*
30-deg	0.405	0.110	0.165	0.530
45-deg	0.305	0.085	0.275	0.670
60-deg	0.255	0.070	0.355	0.765
90-deg	0.205	0.055	0.465	0.860
180-deg	0.155	0.045	0.590	0.970

Table 5.9 Values for *A, B, m,* and *n* in equation (5-85) for flexibility

Bend angle, α	*A*	*B*	*m*	*N*
30-deg	18.50	5.10	0.096	0.654
45-deg	15.65	4.30	0.177	0.573
60-deg	13.50	3.70	0.247	0.503
90-deg	11.75	3.25	0.310	0.440
180-deg	9.25	2.55	0.412	0.338

Table 5.10 Values for *A, B, m,* and *n* in equation (6-86) for stress-intensification

Bend angle, α	*A*	*B*	*m*	*N*
30-deg	16.90	4.65	0.197	0.47
45-deg	12.50	3.45	0.318	0.35
60-deg	10.25	2.82	0.407	0.26
90-deg	10.25	2.80	0.435	0.23
180-deg	7.50	2.05	0.567	0.10

Equation (5-84) applicable for pipe elbows of thin-walled. Equation (5-84) need to be modified for thick-walled pipe bends. This is subjected to further research. Figure A5.1 through A5.5 of Appendix C5 (appendix to this Chapter) shows roughly the value of *r/t* at which equation (5-84) applicable.

It is worth investigating the error introduced as a result of the two approaches used here. The error is calculated here as a percentage:

$$Err = \left|1 - \frac{fd}{fe}\right| x100\% \qquad (5\text{-}87)$$

where *fd* represents either ovalisation, flexibility, or stress-intensification obtained using the derived formula, and *fe* is data obtained directly from finite element results. Using this definition, the maximum error in percent is given in Table 5.11; 5.12; and 5.13 for ovalisation, flexibility, and stress-intensification respectively:

Table 5.11 Maximum error for ovalisation

α	*Err, %*				
	$R/r = 2$	$R/r = 3$	$R/r = 5$	$R/r = 6$	$R/r = 10$
30-deg	10.6	8.1	8.6	---	10.2
45-deg	4.9	4.6	4.3	---	6.4
60-deg	5.2	4.6	4.3	---	7.7
90-deg	5.0	4.5	---	4.0	7.6
180-deg	5.0	5.5		6.9	8.8

Table 5.12 Maximum error for flexibility

α	*Err, %*				
	$R/r = 2$	$R/r = 3$	$R/r = 5$	$R/r = 6$	$R/r = 10$
30-deg	7.6	5.9	4.2	---	6.1
45-deg	4.3	3.7	2.0	---	5.4
60-deg	3.2	3.0	1.9	---	5.1
90-deg	3.6	2.6	---	1.6	4.3
180-deg	4.5	3.5		3.8	4.7

Table 5.13 Maximum error stress-intensification

α	*Err, %*				
	$R/r = 2$	$R/r = 3$	$R/r = 5$	$R/r = 6$	$R/r = 10$
30-deg	2.5	3.9	4.5	---	4.7
45-deg	2.7	3.7	4.2	---	4.5
60-deg	2.9	4.1	4.5	---	4.5
90-deg	4.6	5.7	---	6.3	5.0
180-deg	4.5	5.9		2.9	4.9

It can be seen from these Tables that the error is relatively small from the practical point of view. Larger errors result from the formulae for ovalisation and flexibility can however be seen for elbow of short-radius bend. The error for stress however is very small. This is because the stresses were depicted directly from the ANSYS generated data without needing for any further derivation. Whereas, the flexibility factor was derived from the displacement of the extrados and intrados node in which plane cross-section before bending was assumed to remain plane after bending.

Figure 5.66 shows a comparison for flexibility factor between the result from the present analysis and the theoretical result due to Rodabaugh and George [30]. Figure 5.66 shows that in general the detailed finite element results lead to higher values than those of the simple Rodabaugh & George solution, but as the pressure increases, the latter results are (perhaps surprisingly) quite accurate. That the flexibility factor from a detailed finite element analysis is higher than the simple pure bending analysis may not be expected: it is usually argued that the presence of end effects should reduce the flexibility from a pure bending analysis [57, 84] even with long attached straight pipes. However it should be recalled that the present study includes large deformation effects – this is observed with small values of pipe bend parameter (that is large diameter, thin pipe) and it can also be argued that the attached straight pipes will have some flexibility close to the junction from a thin shell finite element analysis. The magnitude of the reduction due to pressure is not easy to compare since the basic flexibility factors for in-plane bending alone in the absence of internal pressure also differ. However it can be seen that the present results infer that the

pressure has a greater stiffening effect than obtained from the Rodabaugh and George analysis.

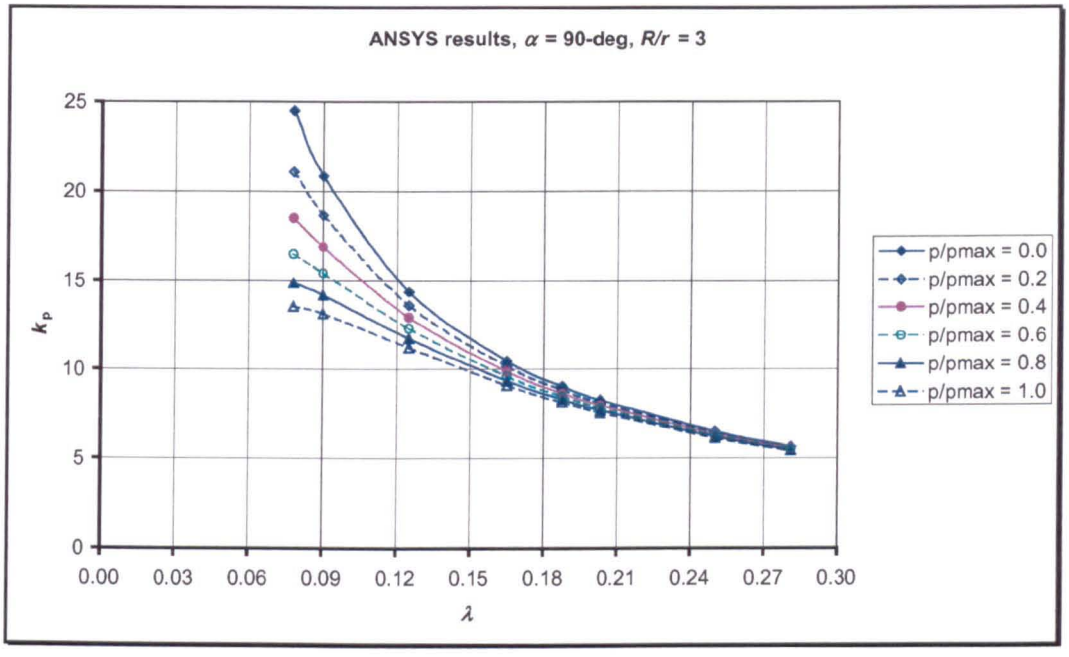

(a)

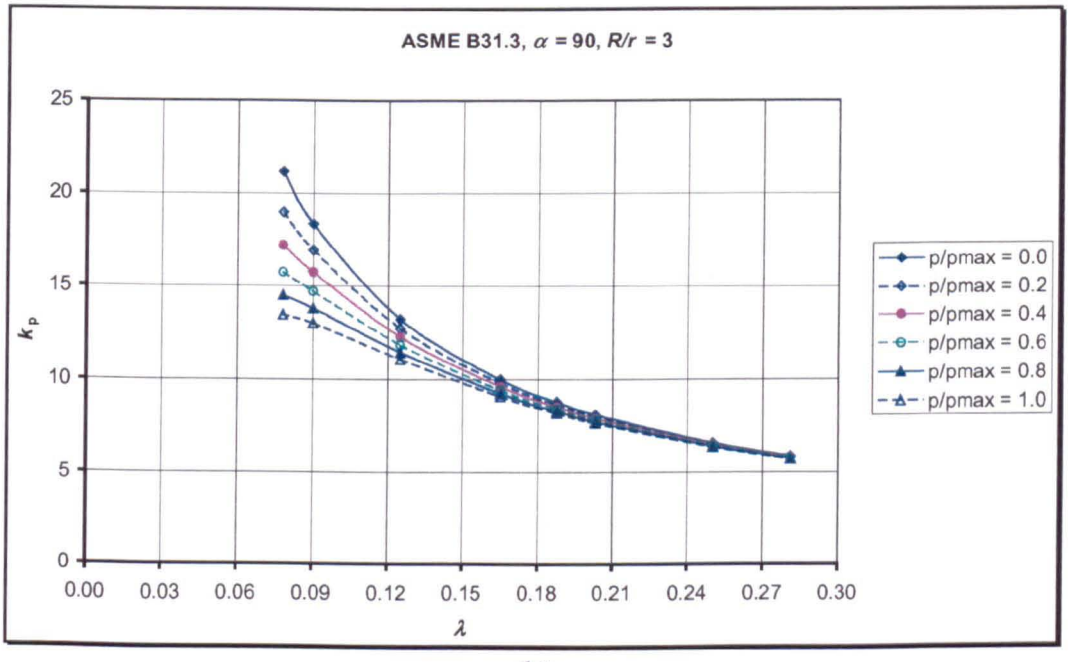

(b)

Fig.5.66 Flexibility factors for 90-deg elbows: (a) present analysis, (b) ASME B31.3

Recall the formula for flexibility factor for 90-deg pipe elbows from the present finite element analysis developed in equation (5-46):

$$k_p = \frac{k}{1+11.75\left(\frac{p}{E}\right)\left(\frac{r}{t}\right)^{9/4}\left(\frac{R}{r}\right)^{0.31}}$$

Also recall the formula developed by Rodabaugh & George [30] in equation (2-94):

$$k_p = \frac{k}{1+6\left(\frac{p}{E}\right)\left(\frac{r}{t}\right)^{7/3}\left(\frac{R}{r}\right)^{1/3}}$$

The form of equation (2-94) and (5-46) are the same but the values of the indices of (r/t) and (R/r) slightly differ. What is more marked is the coefficient (11.75 rather than 6) – this infers a greater pressure effect. (It should be noted these coefficients should be written in terms of $(1-\nu^2)$, but this factor is known to haunt the derivation of flexibility factors [43] and has been omitted here).

Figure 5.67 shows a comparison of stress-intensification factors for 90-deg pipe elbows obtained from the present analysis and the result of the Rodabaugh and George analysis [30]. Recall the formula developed in the present analysis, equation (5-71):

$$\gamma_p = \frac{\gamma}{1+10.25\left(\frac{p}{E}\right)\left(\frac{r}{t}\right)^{7/3}\left(\frac{R}{r}\right)^{0.435}}$$

And again recall the formula developed by Rodabaugh and George [30] as adopted in the ASME B31.3 process piping code [120], equation (2-98):

$$\gamma_p = \frac{\gamma}{1+3.25\left(\frac{p}{E}\right)\left(\frac{r}{t}\right)^{5/2}\left(\frac{R}{r}\right)^{2/3}}$$

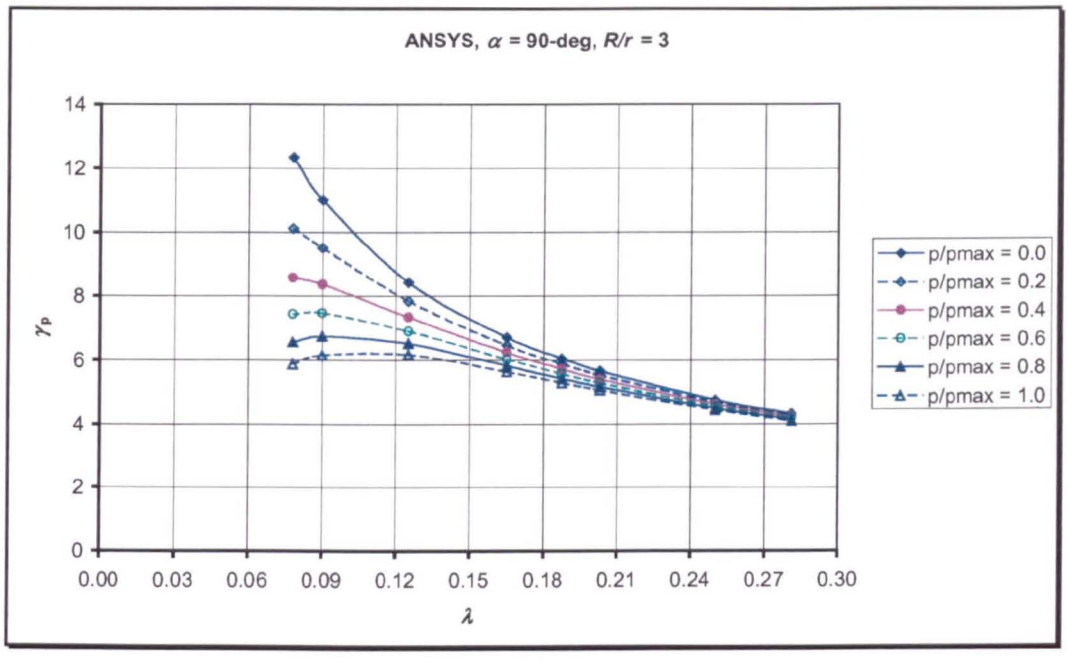

(a)

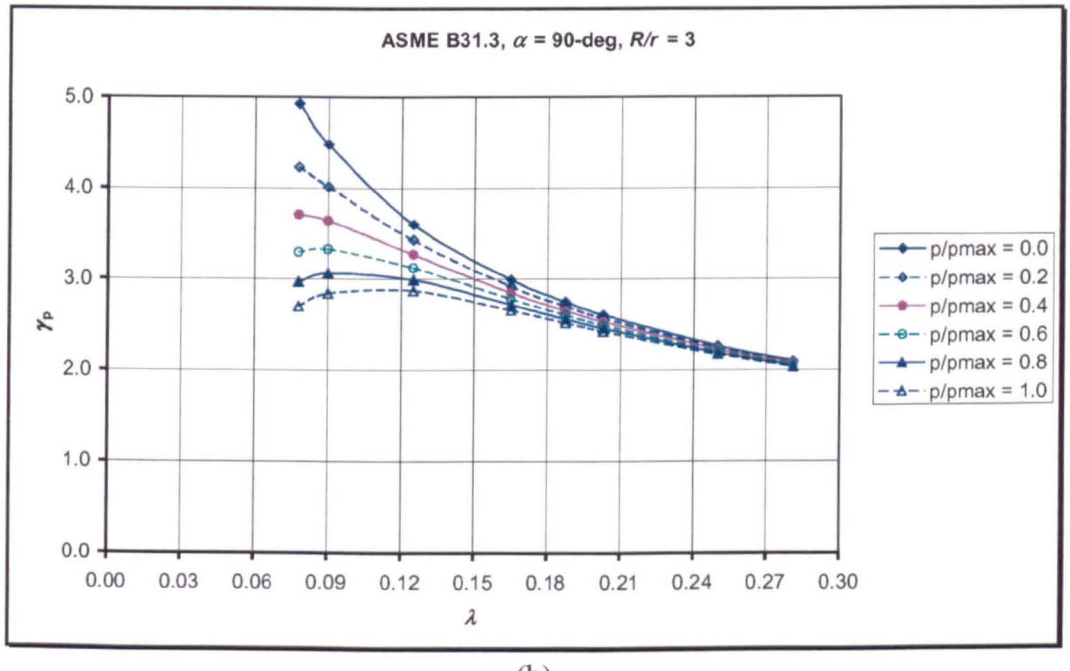

(b)

Fig.5.67 Stress-intensification factors of 90-deg elbows under in-plane closing moment, (a) present analysis, (b) ASME B31.3

Figure 5.73 shows that the present results predict a considerably more marked pressure reduction effect at lower values of pipe bend parameter. Again it may be expected that large deformations, couple with large diameter, have an effect. An exact comparison can not be seen clearly from Fig.5.67 since the basic stress-intensification factors for in-plane bending alone (in the absence of internal pressure) also differ.

5.4.3 Comparison with Other Theoretical and Experimental Results

To verify the accuracy of the formulae developed in this chapter, comparisons are made with theoretical and experimental results from other previous investigators.

In 1957, Turner and Ford [31] made attempt to eliminate some assumptions and approximation in the previous theories for in-plane bending without internal pressure. Using small deformation analysis, the long radius assumption was omitted. The theoretical analysis developed by Turner and Ford was considered as a more exact analysis at that time. Table 5.14 compares the hoop stress-intensification factor for typical pipe bend geometry: ($\lambda = 0.269$ and $R/r = 2.84$)*. It can be seen that the present result for short radius bend and thick-walled pipe predicts a lower stress-intensification factor compared to the theoretical analysis of Turner and Ford [31] and the asymptotic solution of Clark and Reissner [20]

Table 5.14 Comparison of stress-intensification factor with Turner and Ford [31]

Present analysis, Eqn (5-65)	**$\gamma = 4.476$**
Turner and Ford [31], theory	$\gamma = 4.750$
Clark and Reissner [20], theory	$\gamma = 4.535$

*Values from Turner and Ford [31] were read from graphs and not calculated form formulae

In 1966, Findlay and Spence [35] carried out an experimental analysis of 9ft 9in pipe elbow under in-plane bending. The geometry used is as follows:

$\alpha = 90$-deg

$r = 39.725$ in

$R = 117$ in

$t = 1.45$ in

$t/r = 0.036$

$R/r = 2.94$

$\lambda = 0.107$

For this particular geometry, the comparison for flexibility and stress-intensification factors are given in Table 5.15 and 5.16 respectively. These tables also present results from other investigateor [2, 20, 24, 31]*

Table 5.15 Comparison for flexibility factor with theoretical and experimental results

Present analysis, Eqn (5-40)	**17.12**
Findlay and Spence [35], experiment	12.8
1st Karman [2], theoretical	8.93
2nd Karman [2], theoretical	15.64
3rd Karman [2], theoretical	16.15
Clark & Reissner [20] theoretical	15.42
Turner and Ford [31, theoretical	15.5

*Values in Table 5.15 were quoted from Findlay and Spence [35] and not calculated from a formulae

Table 5.16 Comparison for stress-intensification factor with theory and experiment

Present analysis, Eqn (5-65)	**9.562**
Findlay and Spence [35], experiment	8.43
Gross [24], experiment	8.54
Clark & Reissner [20] theoretical	9.47
Turner and Ford [31, theoretical	8.73

*Values in Table 5.16 were quoted from Findlay and Spence [35] and not calculated from a formulae

It can be seen from Table 5.15 and 5.16 that the present result predicts higher flexibility and stress-intensification factor for a pipe bend of short-radius and thin-walled. This probably caused by large deformation effect especially for thin-walled pipe bend.

In 1975, Vrillon et al [56] carried out an in-plane bending test on a 180-deg pipe bends of short radius. Straight tangents pipe was attached at both ends of the bend but there was no specific information about its length. The geometry of the test is as follows:

$\alpha = 180$-deg

$t = 12$ mm

$r = 507$ mm

$R = 762$ mm

$t/r = 0.024$

$R/r = 1.5$

$\lambda = 0.036$

For this particular geometry, comparison for flexibility factor is given in Table 5.17

Table 5.17 Comparison for flexibility factor with ref [20] and [56]

Present analysis, eqn (5-43) and Table 5.3 and 5.4	**60.0**
Vrillon et al [56], experiment	10.4
Clark Reissner [20], theoretical	45.8

The experimental result obtained by Vrillon et al [56] should be doubted as it is about 400 percent lower than the asymptotic solution of Clark and Reissner [20]. It can be again seen from Table 5.17 that the present result produces higher flexibility for short-radius and thin-walled pipe bend. The explanation for this different is the large deformation effect which is more pronounced in thin-walled pipe.

In 1979, Brouard et al [62] carried out in-plane and out-of-plane bending test on carbon steel pipe bend without internal pressure. The geometry of pipe bend considered is as follows:

$\alpha = 90$ and 180-deg

$t = 7.1$ mm

$r = 125$ mm

$R = 190$ mm

$t/r = 0.057$

$R/r = 1.52$

$\lambda = 0.087$

$L = 565.7$ mm (for $\alpha = 90$-deg)

$L = 895$ mm (for $\alpha = 180$-deg)

For this particular geometry, comparison for flexibility factor is given in Table 5.18

Table 5.18 Comparison for flexibility factor with references [20] and [56]

	$\alpha = 180$-deg	$\alpha = 90$-deg
Present analysis, eqn (5-43) and Table 5.3 and 5.4	**21.82**	**20.67**
Brouard et al [62], experiment	5.1	2
Clark & Reissner [20], theoretical	18.96	18.96

The experimental result obtained by Brouard et al [62] again should be doubted as it is about 400 percent lower than the asymptotic solution of Clark and Reissner [20] for 180-deg bend. The difference is bigger for 90-deg bend. It can be again seen from Table 5.18 that the present result produces higher flexibility for short-radius and thin-walled pipe bend. The explanation for this different is again due to the large deformation effect, which is more pronounced in thin-walled pipe.

In 1972, Blomfield and Turner [47] updated a thin shell theory previously developed by Turner and Ford [31] to account for the pressure reduction effect on in-plane bending behaviour of pipe bends. Some numerical comparison was made with respect to the experimental result of Gross and Ford [25] and Rodabaugh and George [30]. The geometry for their numerical example is as follows:

$t/r = 0.035$

$R/r = 3.05$

$\lambda = 0.1068$

$p = 400$ psi

For this particular geometry and pressure loading, the flexibility factor is given in Table 5.19*

Table 5.19 Comparison for flexibility factor with theoretical and experimental

	$p = 0$	$p = 400$ psi	(k/k_p)-1
Present analysis	**17.1**	**12.12**	**0.41**
Blomfield & Turner [47] theoretical	15.5	12.54	0.24
Gross & Ford [25], experiment	15.0	11.0	0.36
Rodabaugh & George [20], experiment	15.5	12.0	0.29

*Values in Table 5.19 were quoted from Blomfield & Turner [47]

The numerical values in Table 5.19 shows that the present results produce greater pressure reduction. Large deformation effect could be an explanation for this difference.

5.5 Summary

Detailed non-linear large deformation finite element analysis of symmetric piping elbows of various geometry under in-plane closing moment and internal pressure have been carried out to derive a closed form solution of the cross-sectional

ovalisation, flexibility, and stress-intensification factors. The parametric results confirm the broad characteristics of the pressure reduction effect reported by Rodabaugh and George [30] for this simple loading case. Increased flexibility and stress-intensification factors are found for small values of pipe bend parameter. It has also been found that the broad format of the simple equation derived by Rodabaugh and George is acceptable, although there are differences in the values of various parameters. Although the Rodabaugh & George pressure reduction equations, widely used in piping design, have been broadly verified, the main problem is that the same equations are used for in-plane opening moment, and, with slight modification for out-of-plane bending. In the following chapter, a similar detailed finite element study is carried out for in-plane opening moment. Closed form solution of cross-sectional ovalisation, flexibility, and stress-intensification factors is presented. The difference structural behaviour of opening moment from closing moment is discussed.

Appendix C5

This appendix presented Figures obtained for in-plane closing bending. The approximate formulae presented in this Chapter have been obtained from these Figures:

Fig.A5.1 – A5.5: for Ovalisation factor
Fig.A5.6 – A5.10: for Flexibility factor
Fig.A5.11 – A5.15: for Stress-intensification factor

Continue to the next pages...→

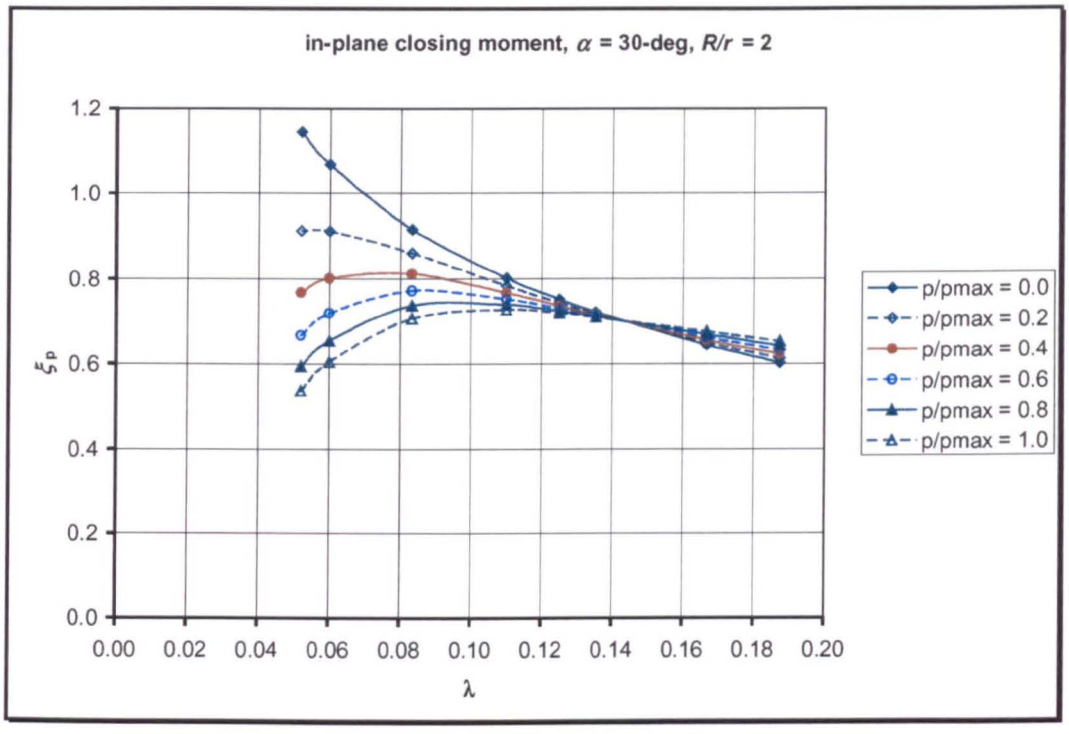

(a)

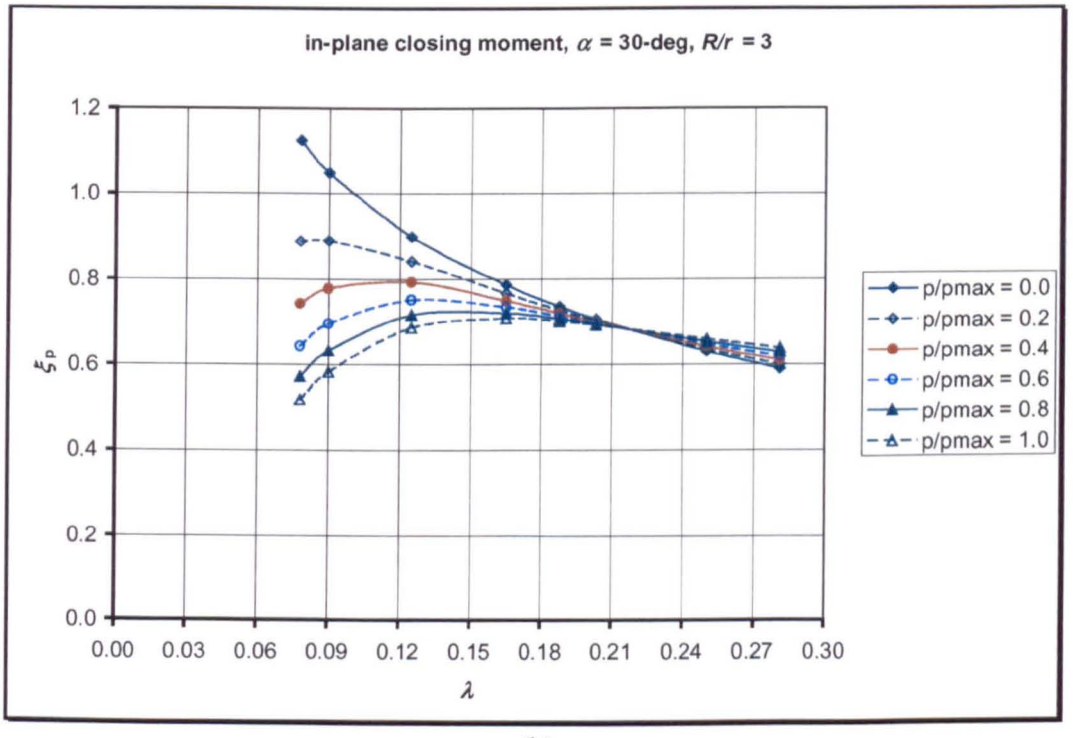

(b)

Fig.A5.1 Ovalisation factor under in-plane closing moment for bend angle of 30-deg: (a) $R/r = 2$, (b) $R/r = 3$

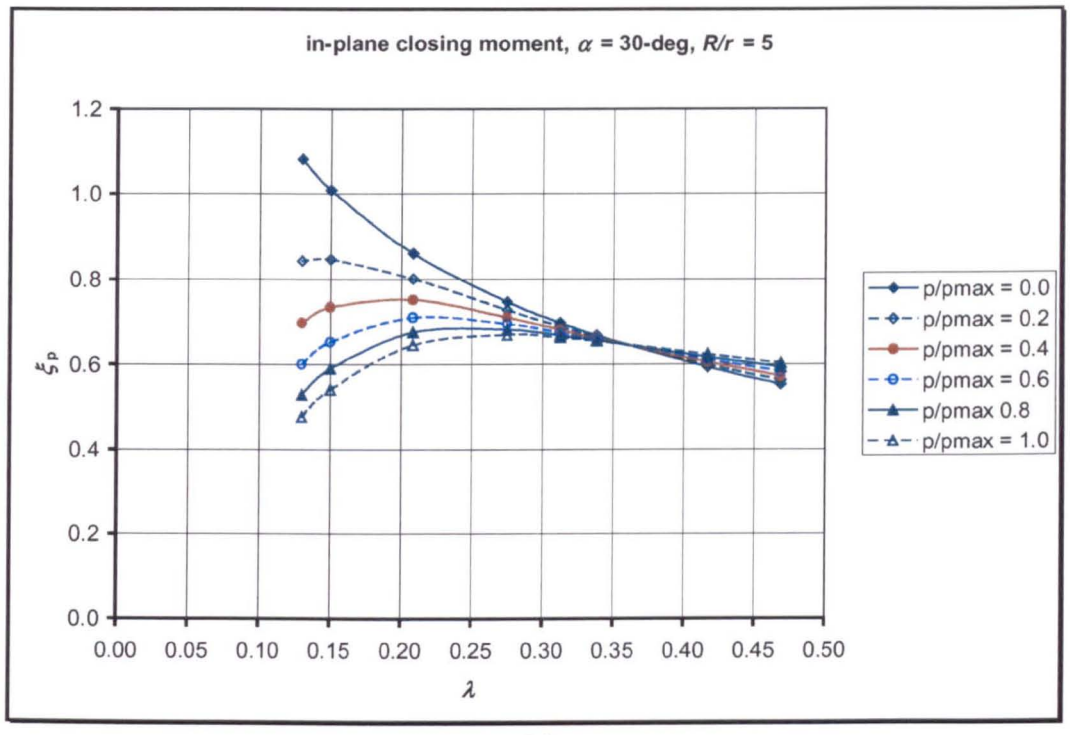

(c)

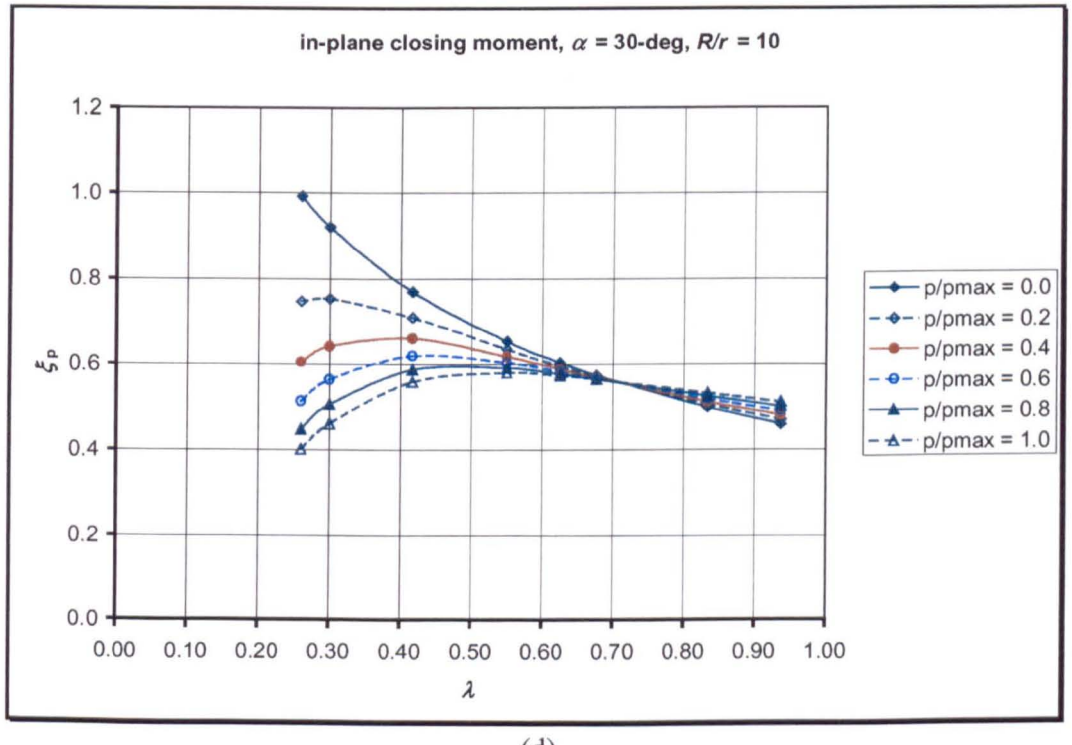

(d)

Fig.A5.1 Ovalisation factor under in-plane closing moment for bend angle of 30-deg: (c) $R/r = 5$, (d) $R/r = 10$

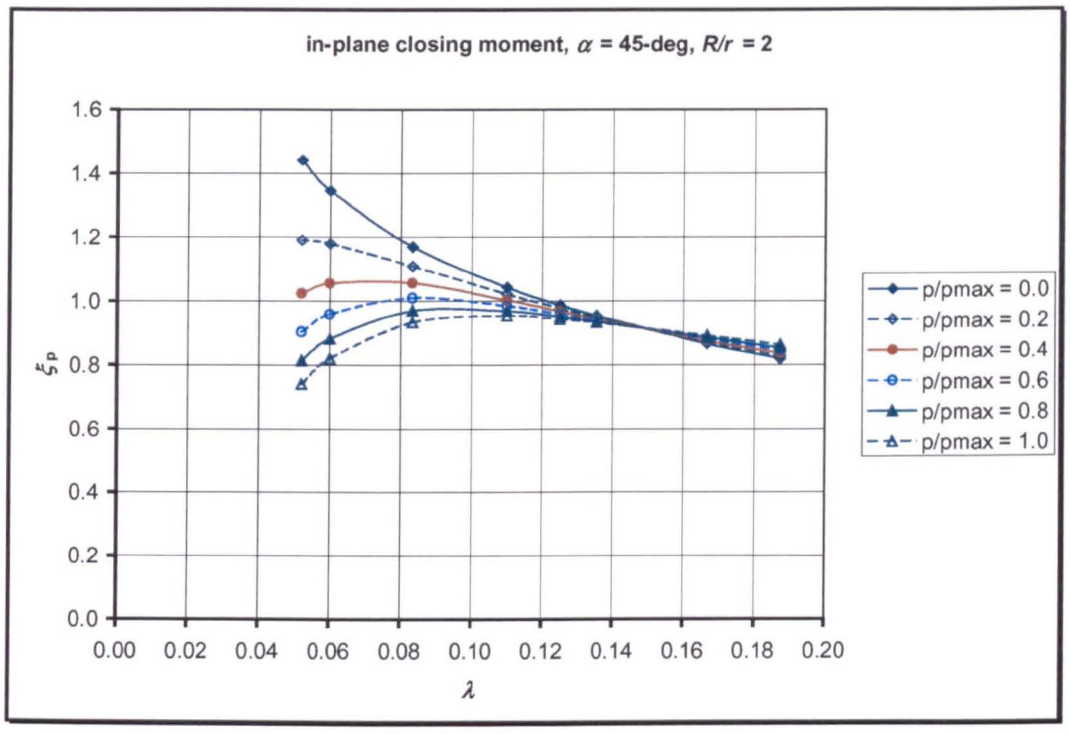

(a)

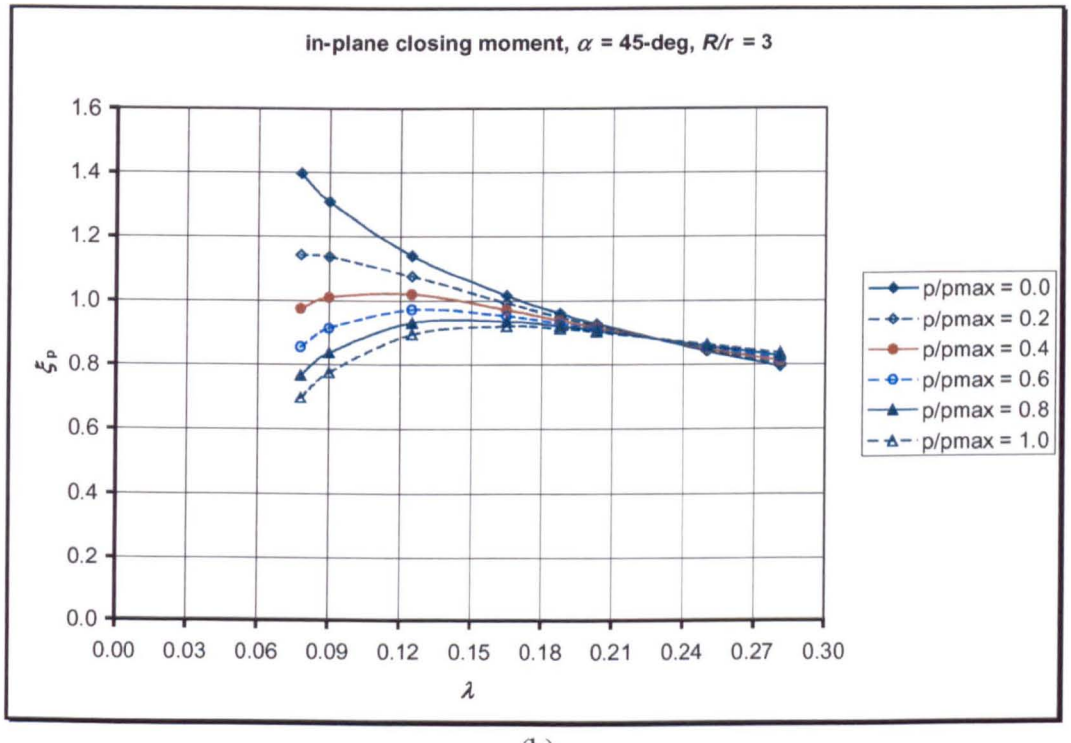

(b)

Fig.A5.2 Ovalisation factor under in-plane closing moment for bend angle of 45-deg: (a) $R/r = 2$, (b) $R/r = 3$

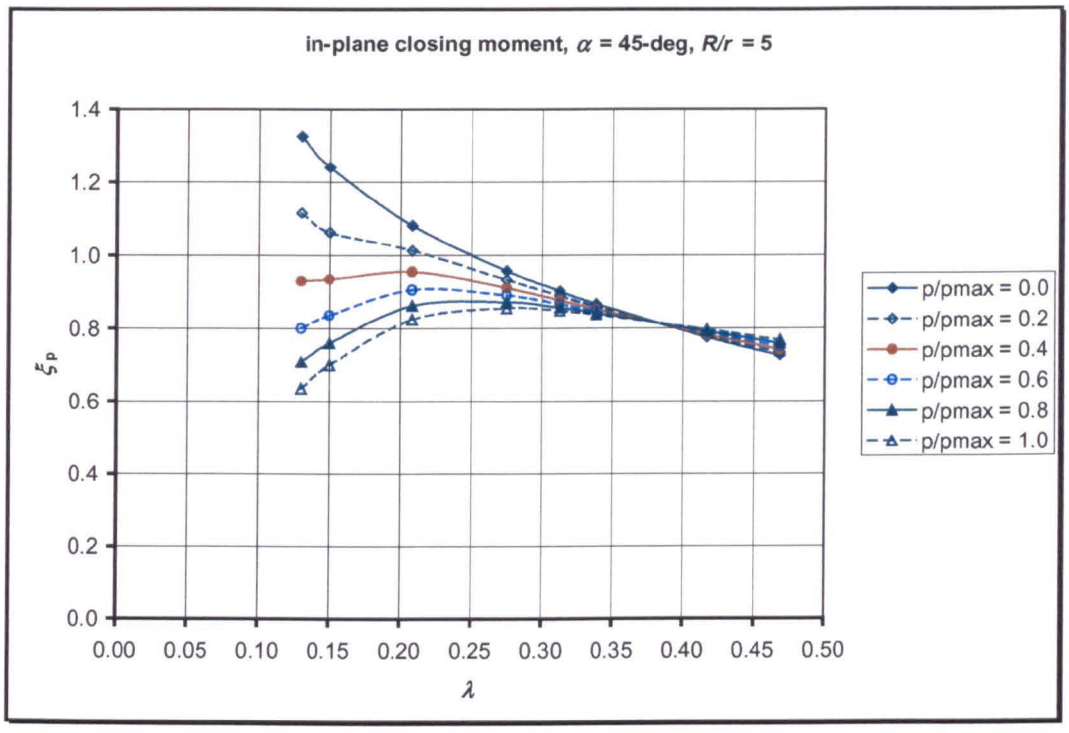

(c)

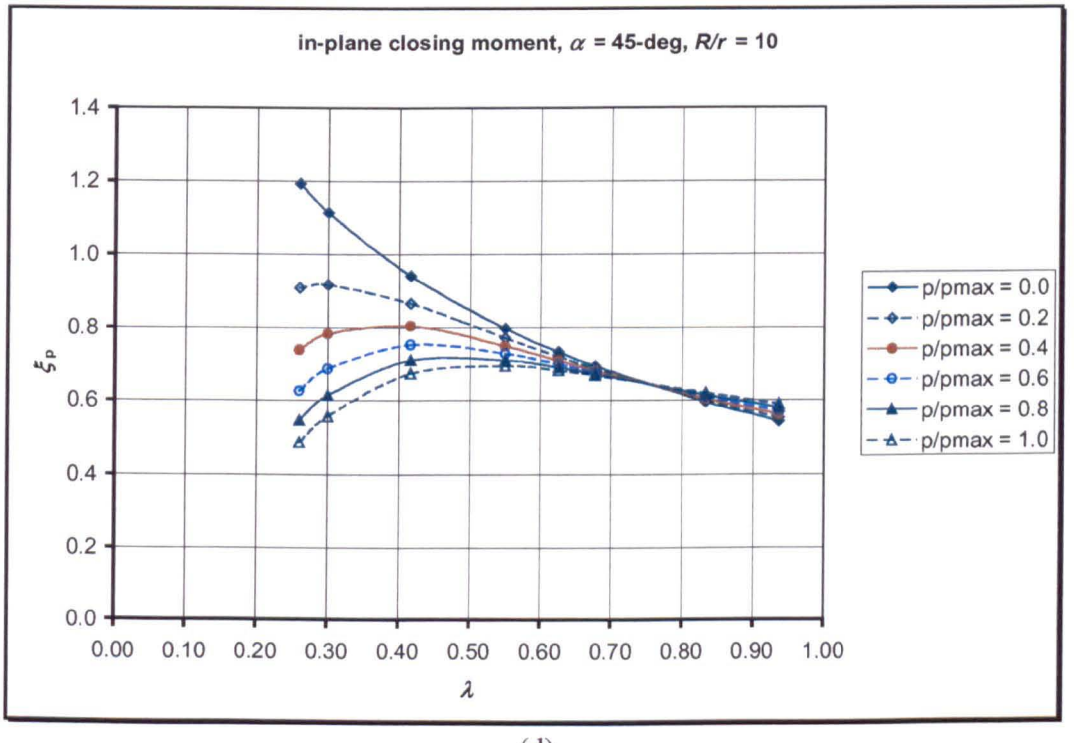

(d)

Fig.A5.2 Ovalisation factor under in-plane closing moment for bend angle of 45-deg: (c) $R/r = 5$, (d) $R/r = 10$

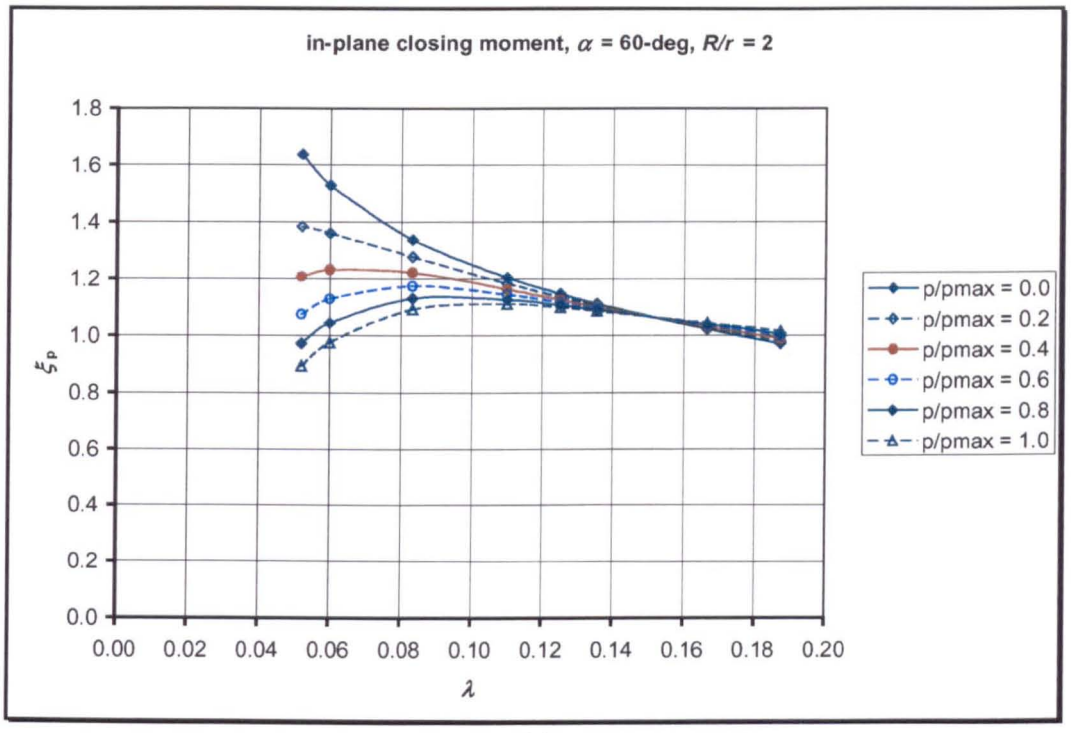

(a)

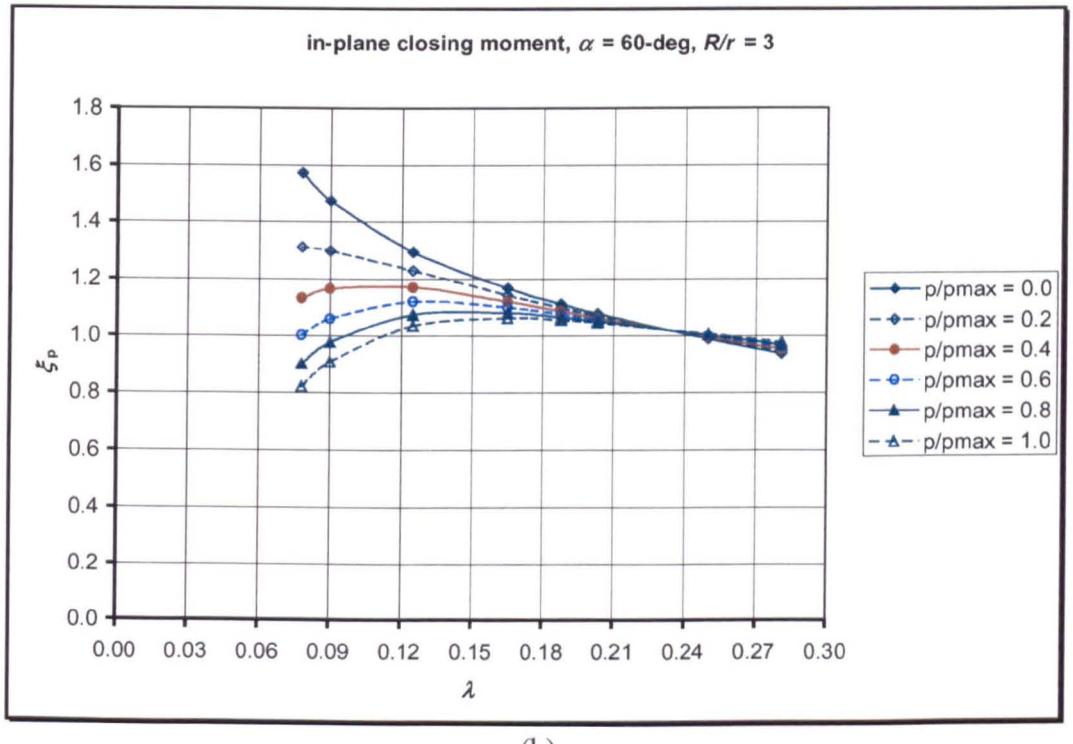

(b)

Fig.A5.3 Ovalisation factor under in-plane closing moment for bend angle of 60-deg: (a) $R/r = 2$, (b) $R/r = 3$

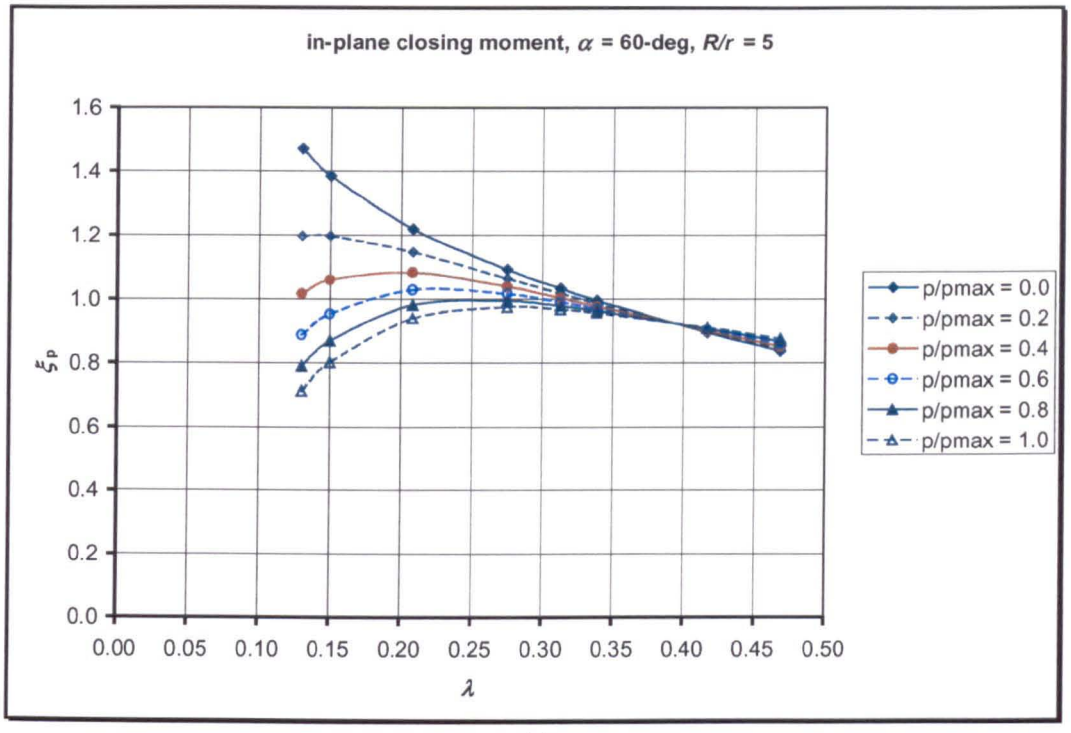

(c)

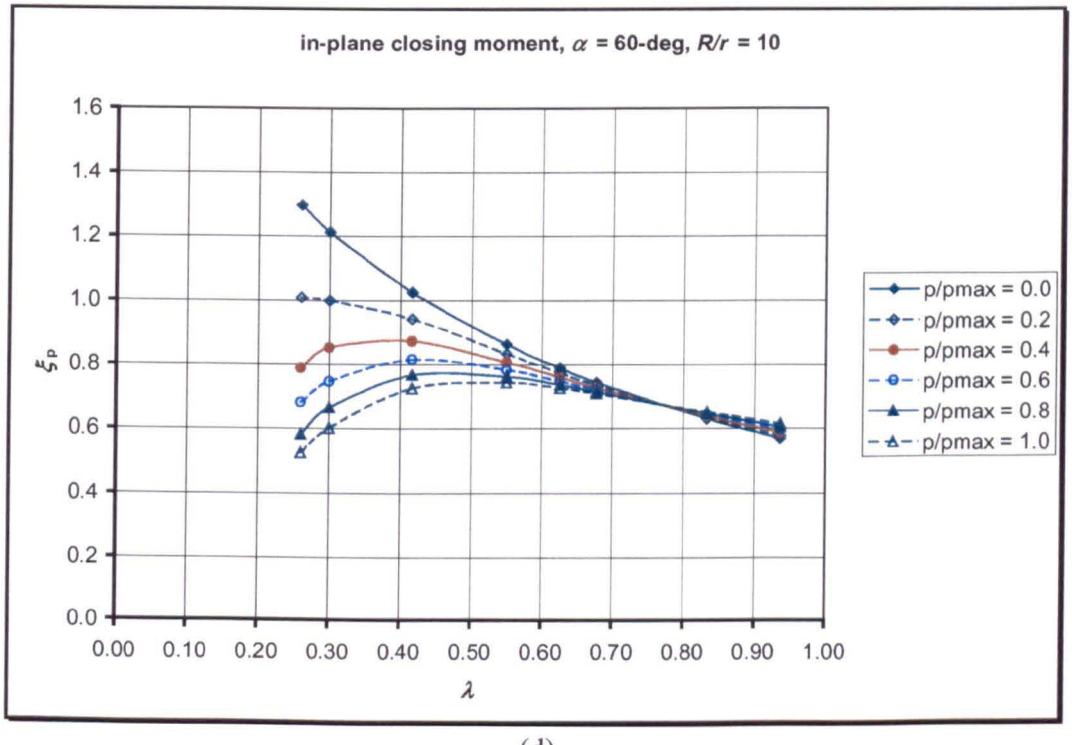

(d)

Fig.A5.3 Ovalisation factor under in-plane closing moment for bend angle of 60-deg: (c) $R/r = 5$, (d) $R/r = 10$

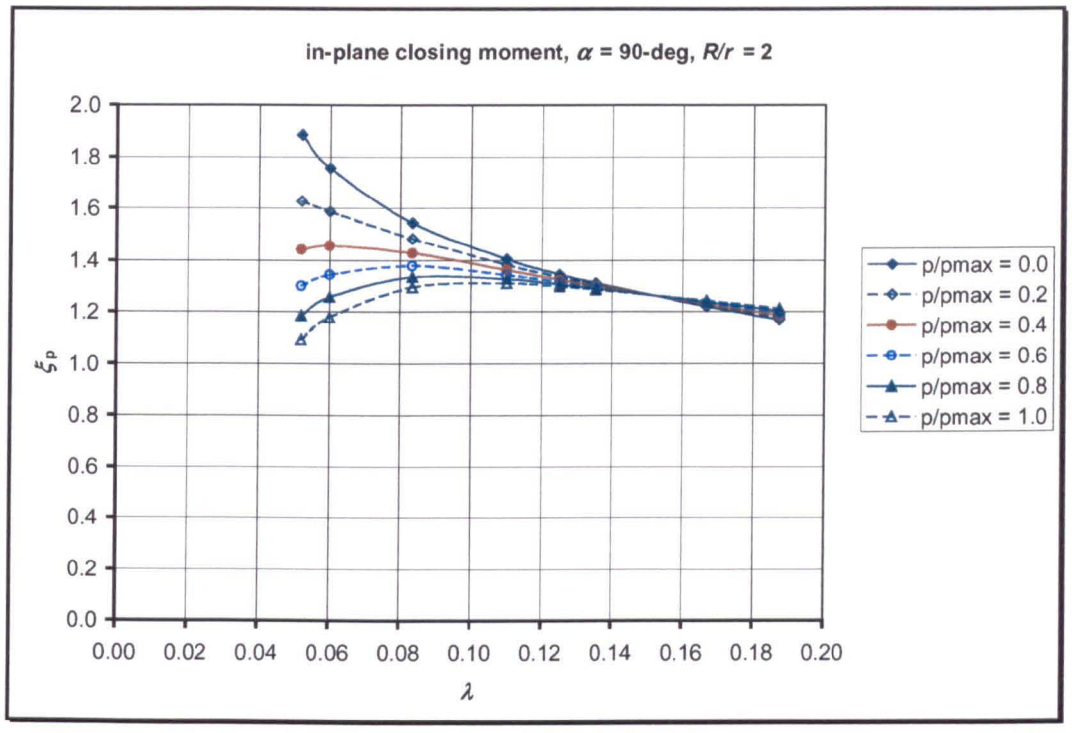

(a)

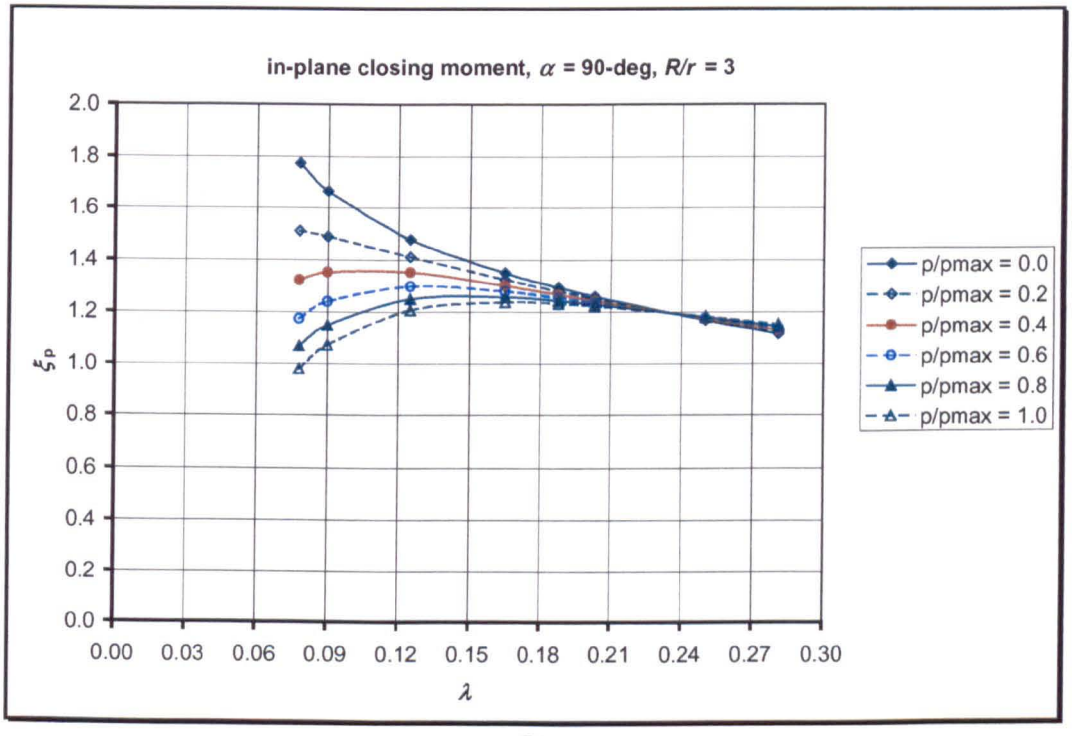

(b)

Fig.A5.4 Ovalisation factor under in-plane closing moment for bend angle of 90-deg: (a) $R/r = 2$, (b) $R/r = 3$

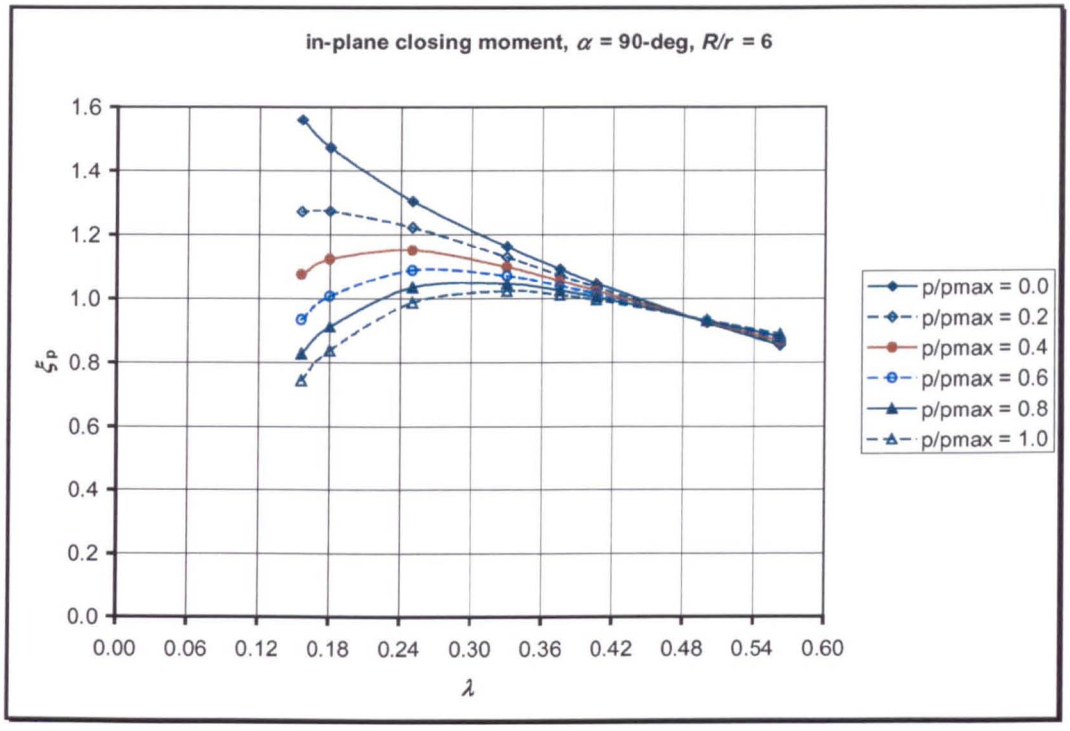

(c)

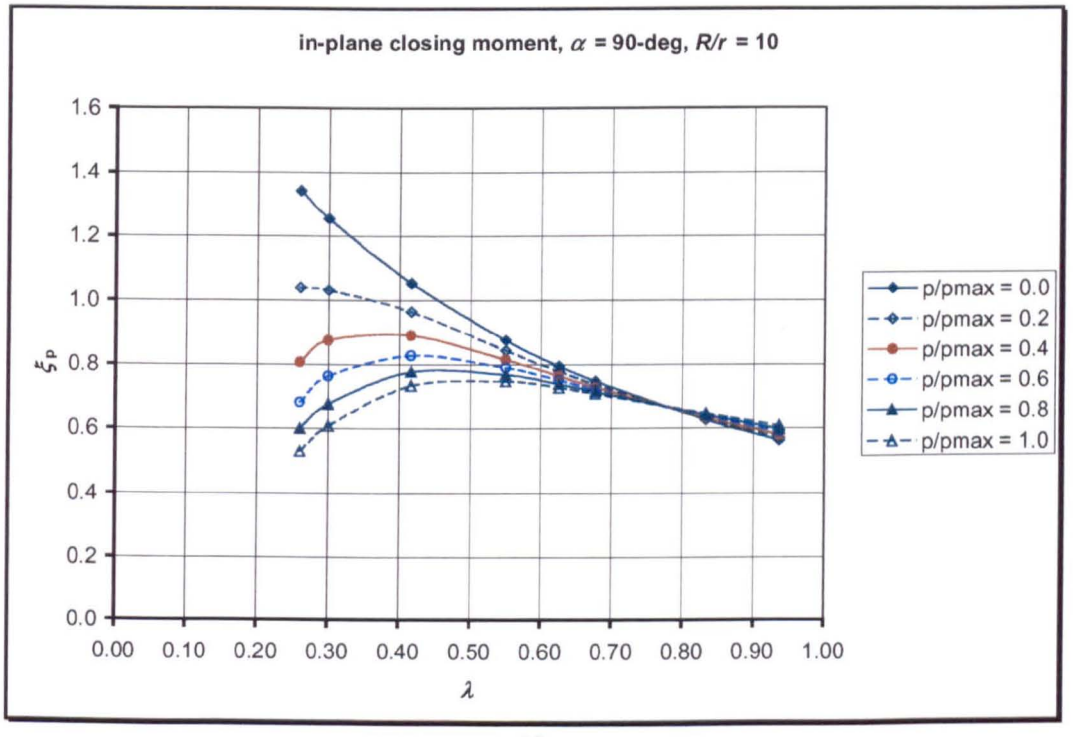

(d)

Fig.A5.4 Ovalisation factor under in-plane closing moment for bend angle of 90-deg: (c) $R/r = 6$, (d) $R/r = 10$

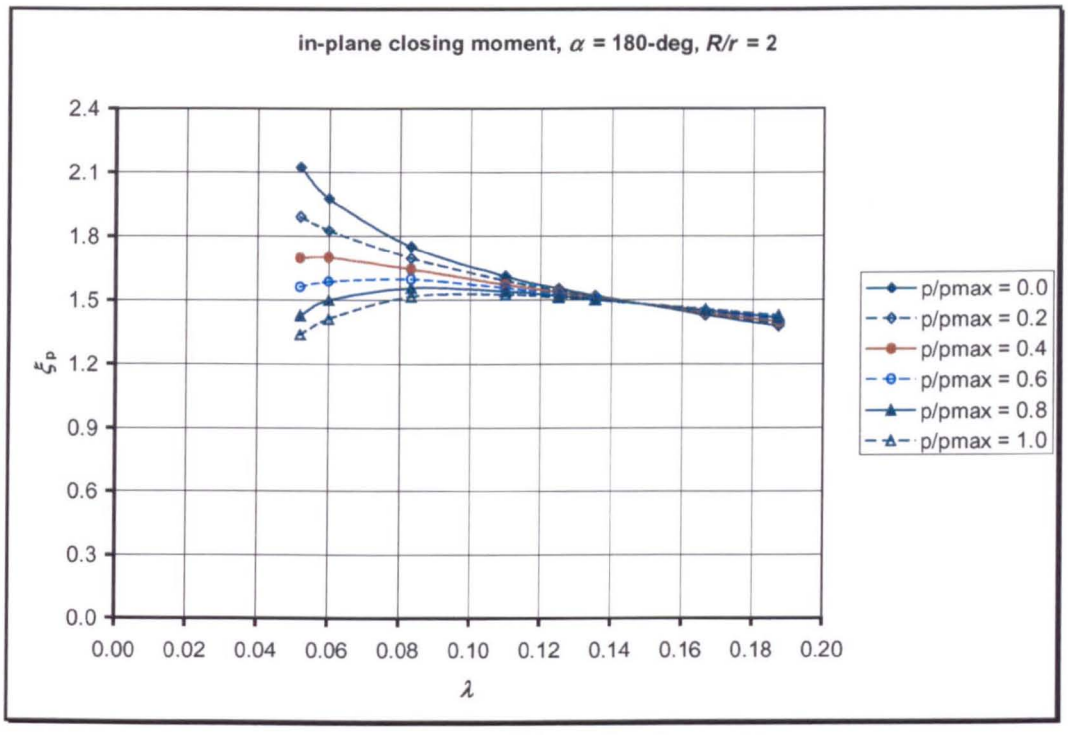

(a)

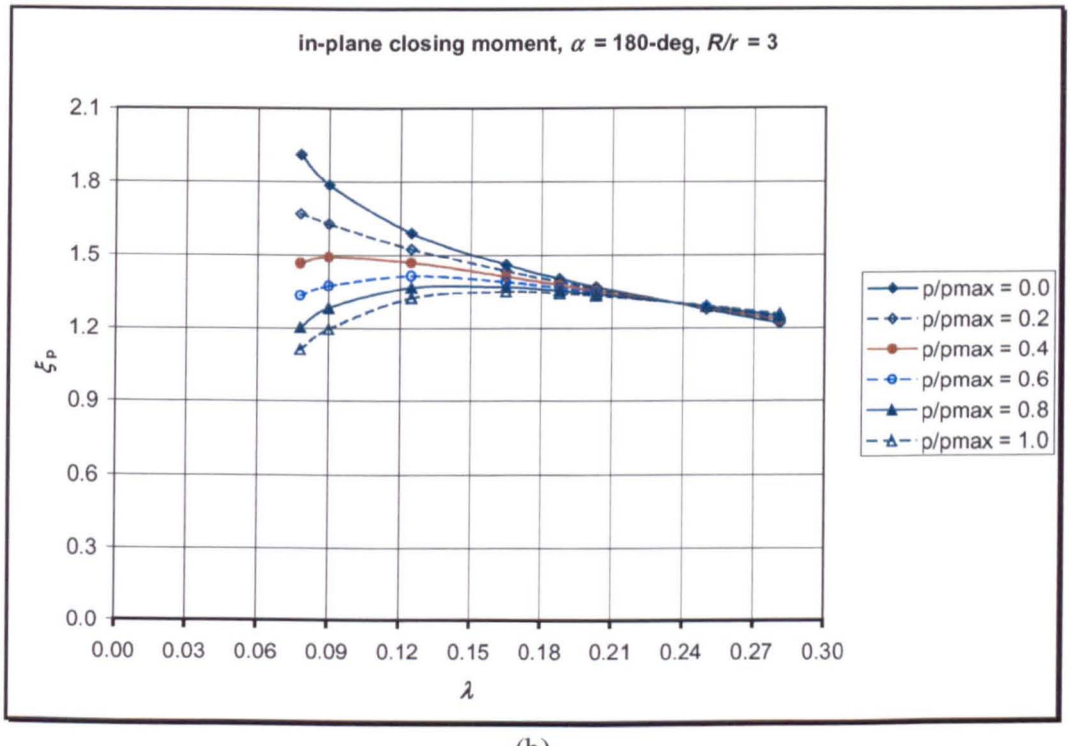

(b)

Fig.A5.5 Ovalisation factor under in-plane closing moment for bend angle of 180-deg: (a) $R/r = 2$, (b) $R/r = 3$

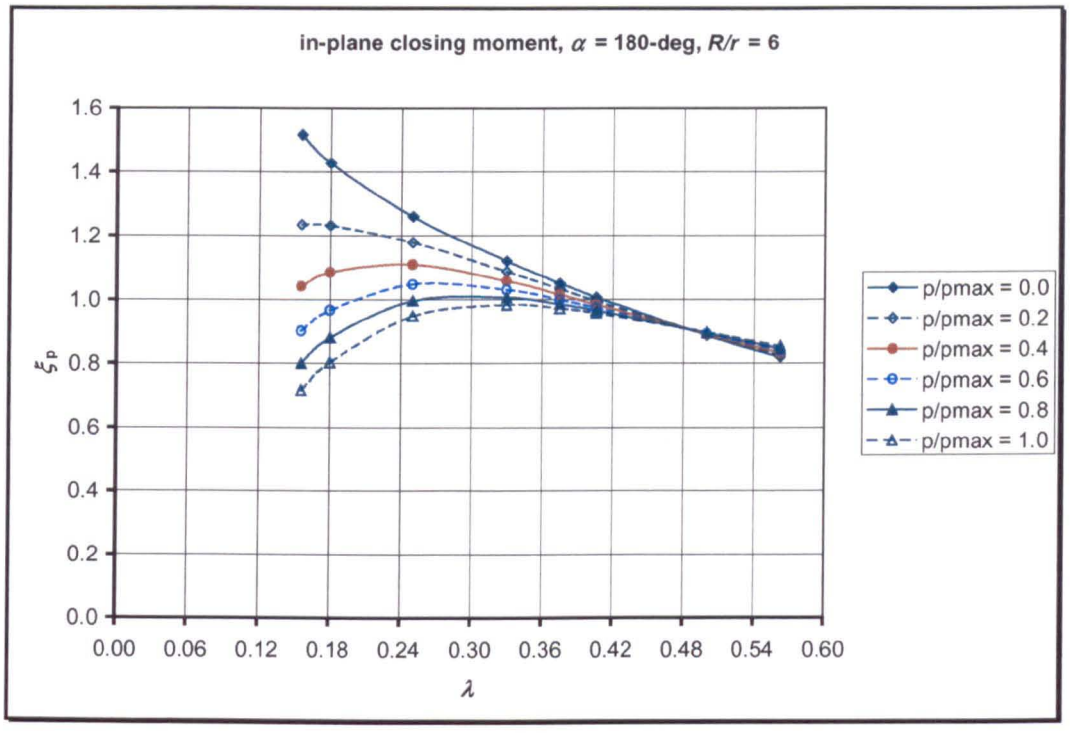

(c)

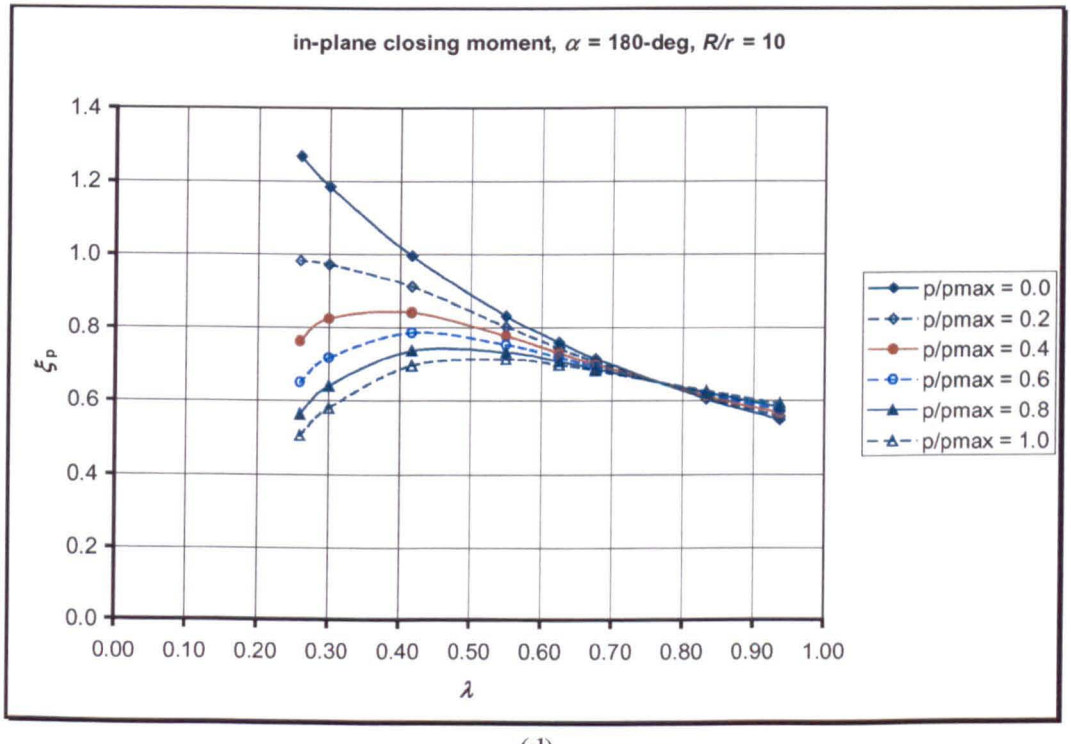

(d)

Fig.A5.5 Ovalisation factor under in-plane closing moment for bend angle of 180-deg: (c) $R/r = 6$, (b) $R/r = 10$

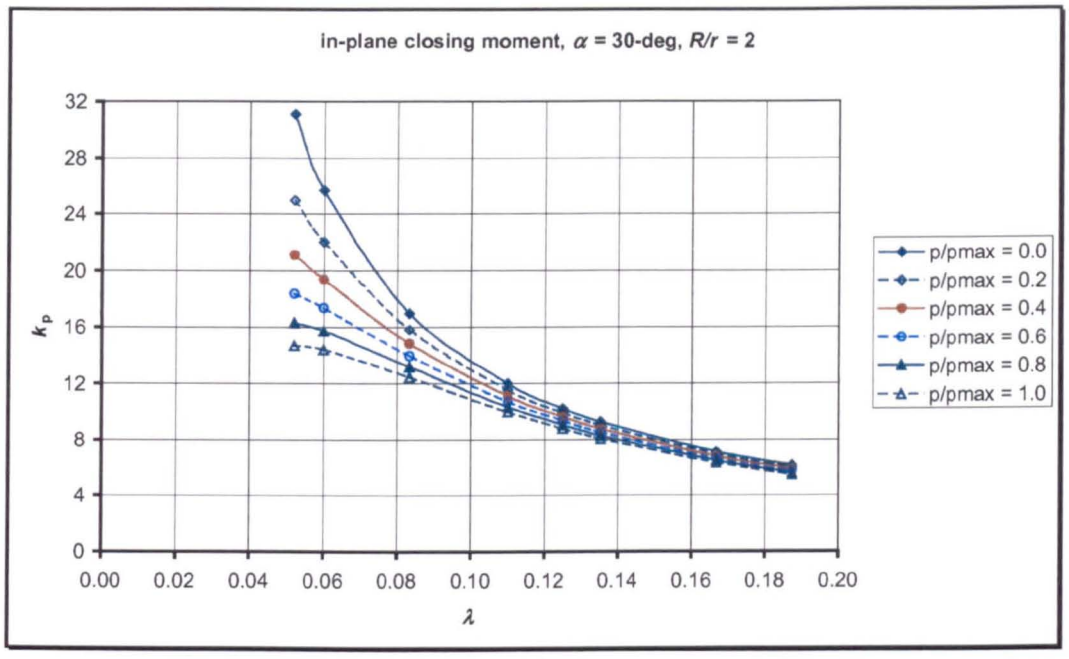

(a)

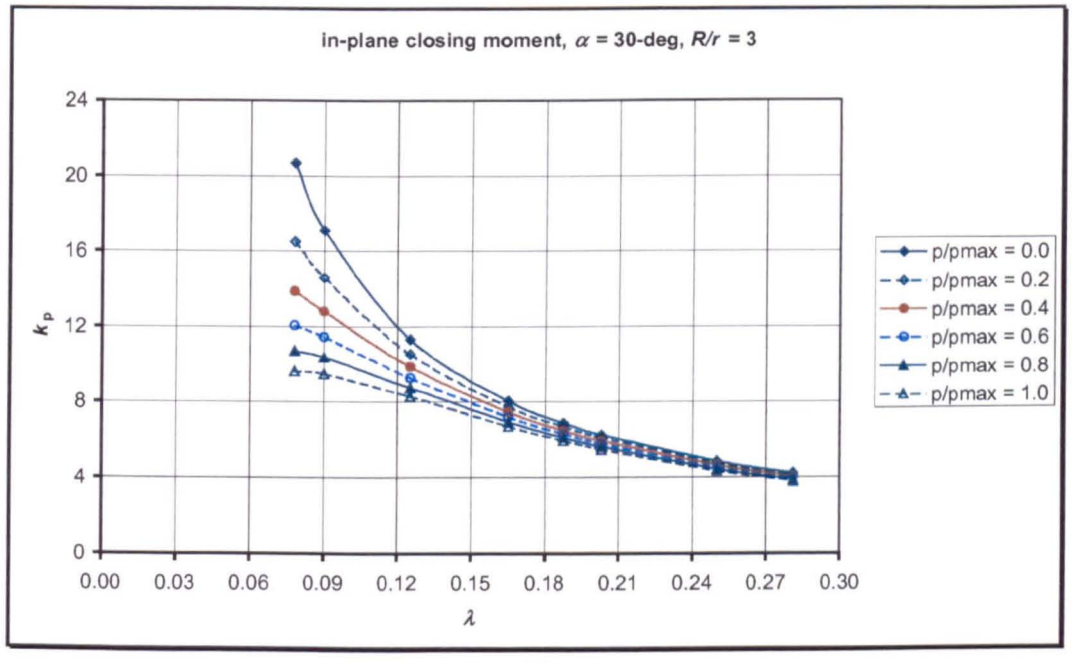

(b)

Fig.A5.6 Flexibility factor of pipe elbows under in-plane closing moment for bend angle of 30-deg: (a) $R/r = 2$, (b) $R/r = 3$

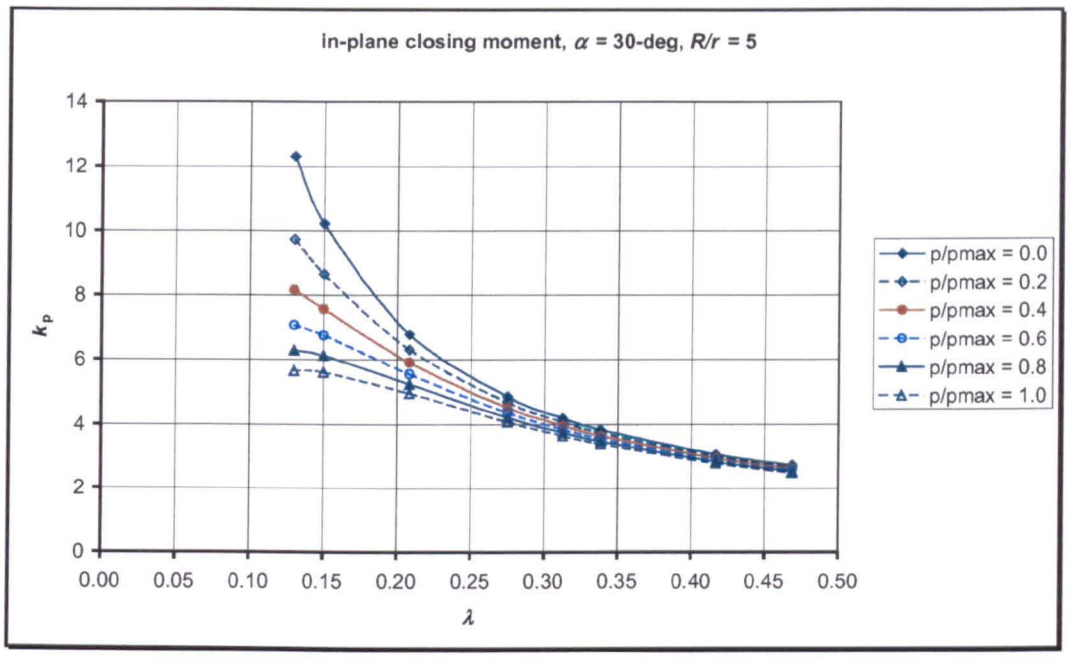

(c)

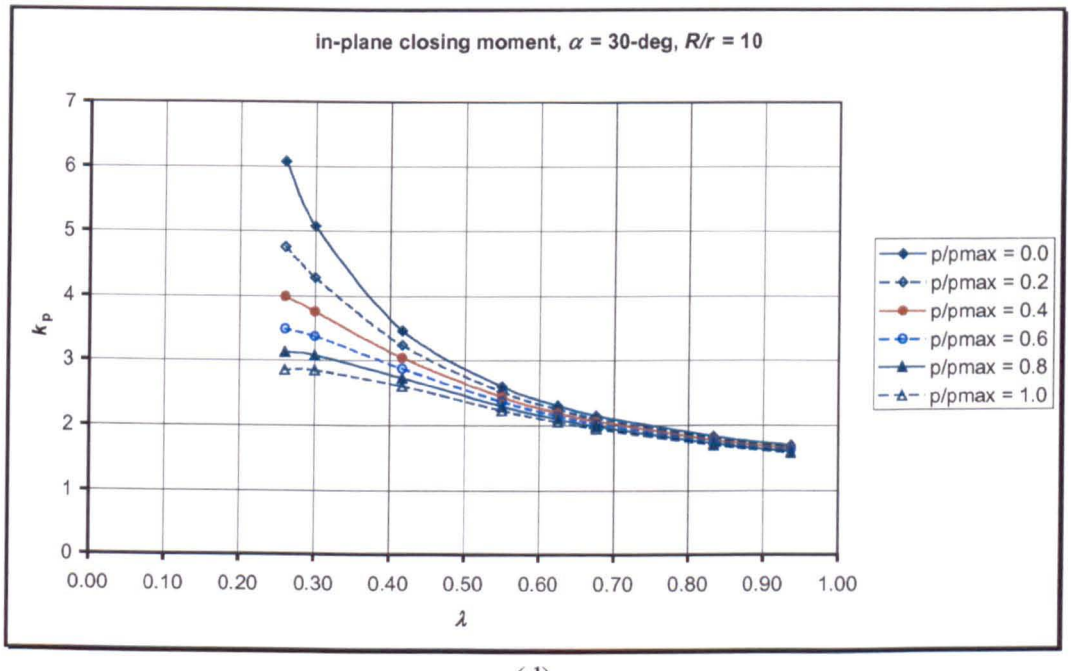

(d)

Fig.A5.6 Flexibility factors of pipe elbows under in-plane closing moment for bend angle of 30-deg: (c) $R/r = 5$, (d) $R/r = 10$

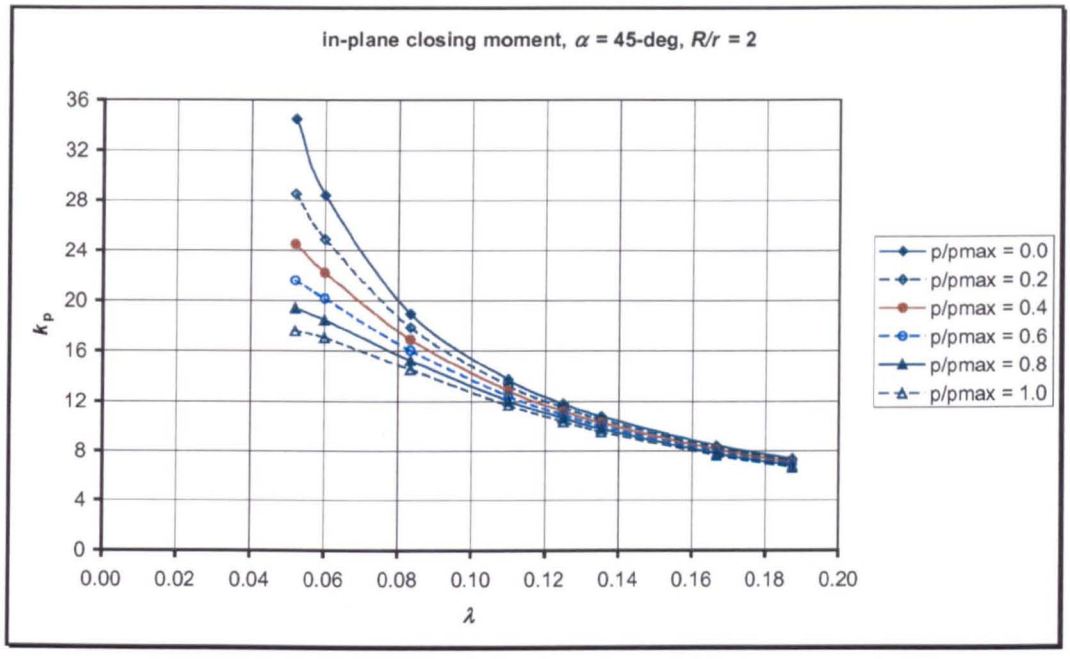

(a)

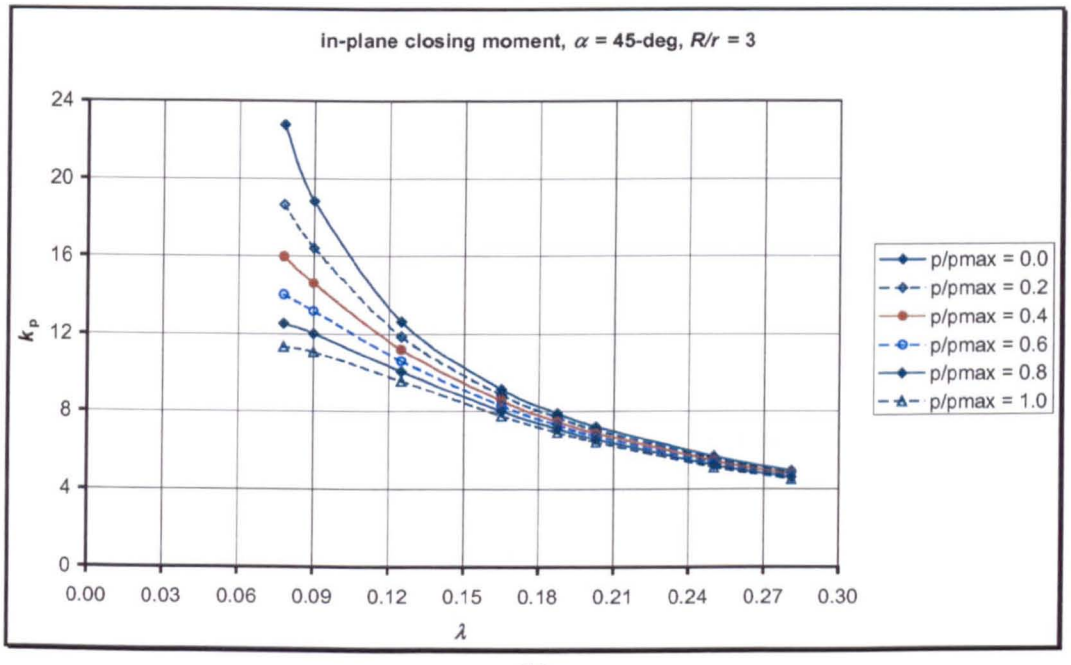

(b)

Fig.A5.7 Flexibility factors of pipe elbows under in-plane closing moment for bend angle of 45-deg: (a) $R/r = 2$, (b) $R/r = 3$

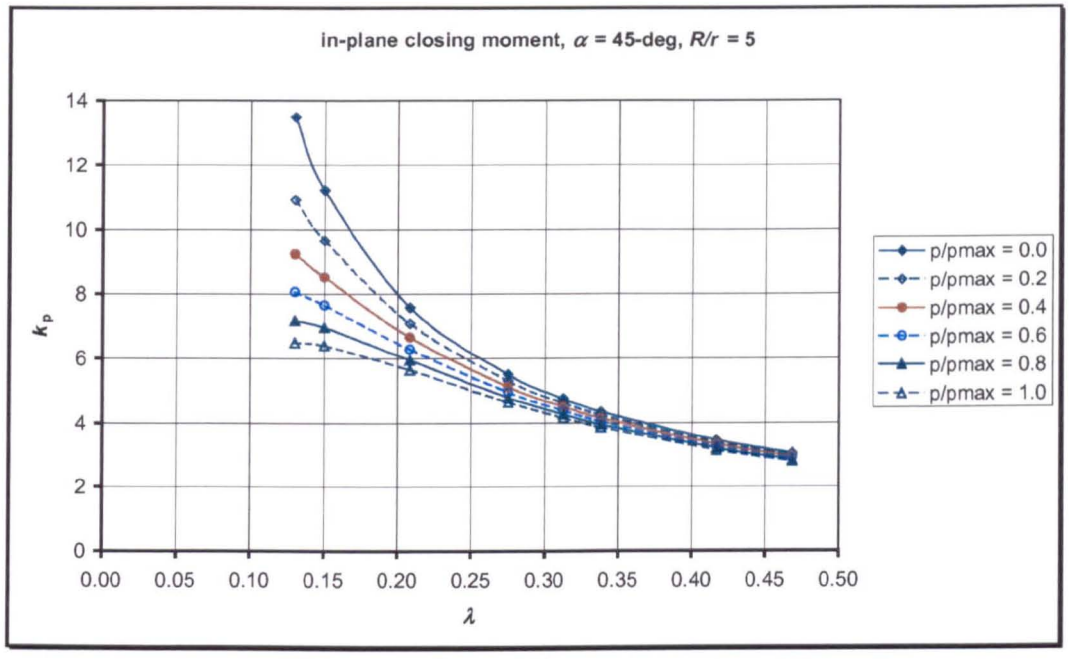

(c)

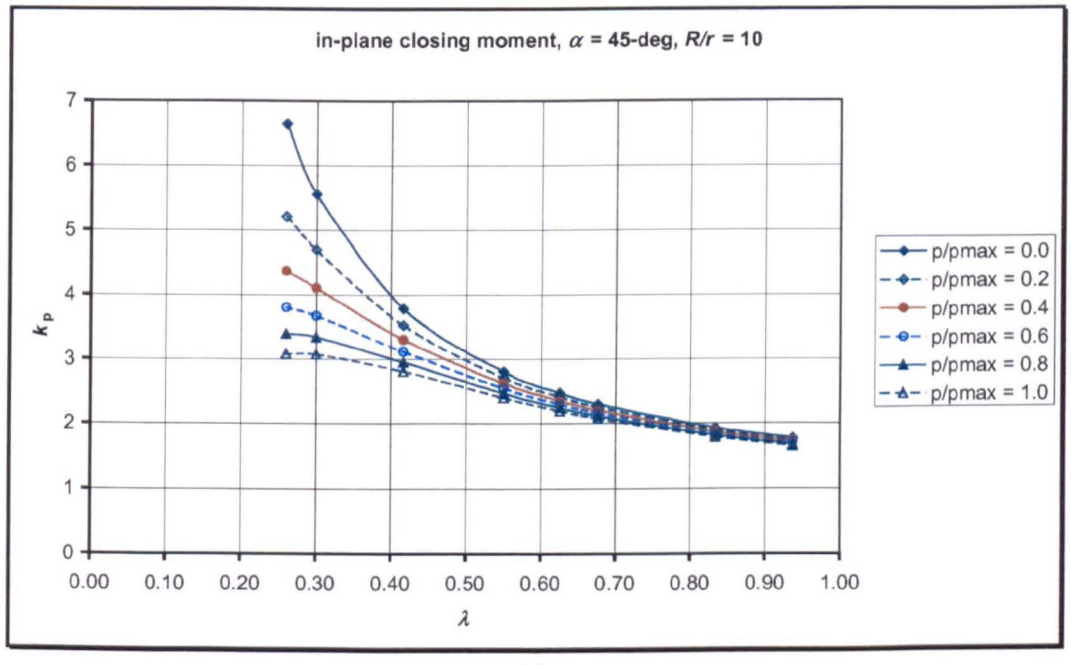

(d)

Fig.A5.7 Flexibility factors of pipe elbows under in-plane closing moment for bend angle of 45-deg: (c) $R/r = 5$, (d) $R/r = 10$

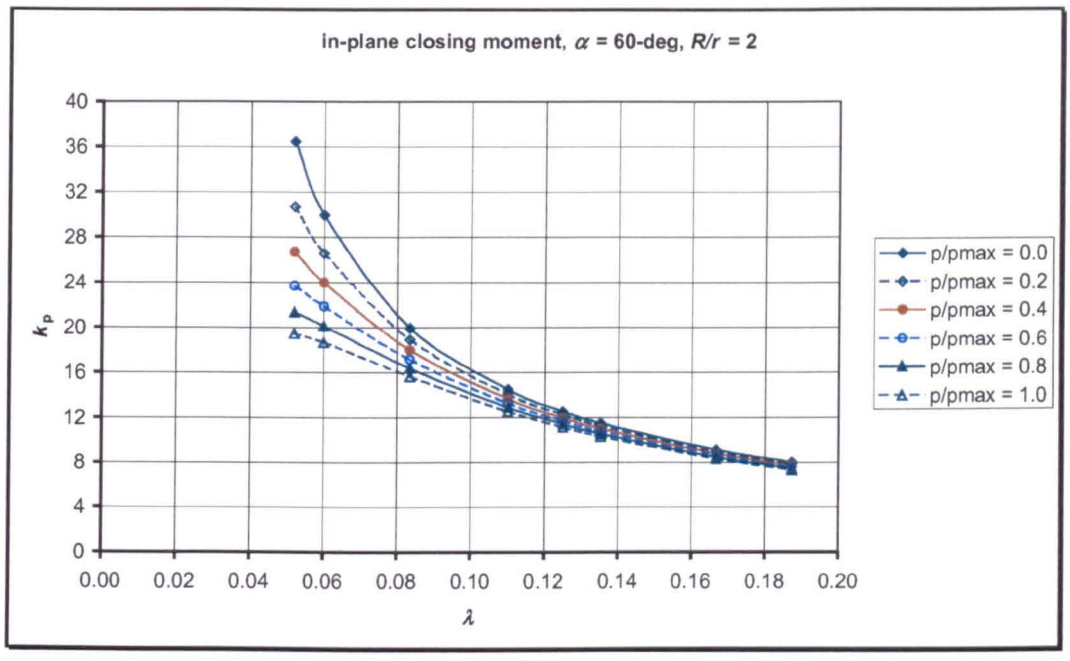

(a)

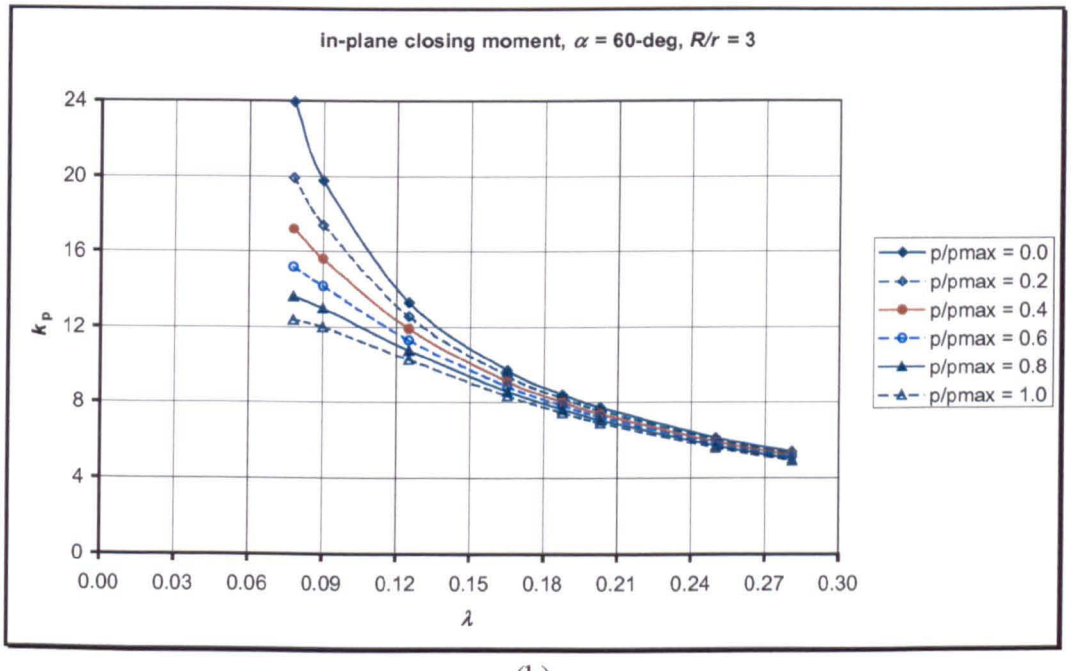

(b)

Fig.A5.8 Flexibility factors of pipe elbows under in-plane closing moment for bend angle of 60-deg: (a) $R/r = 2$, (b) $R/r = 3$

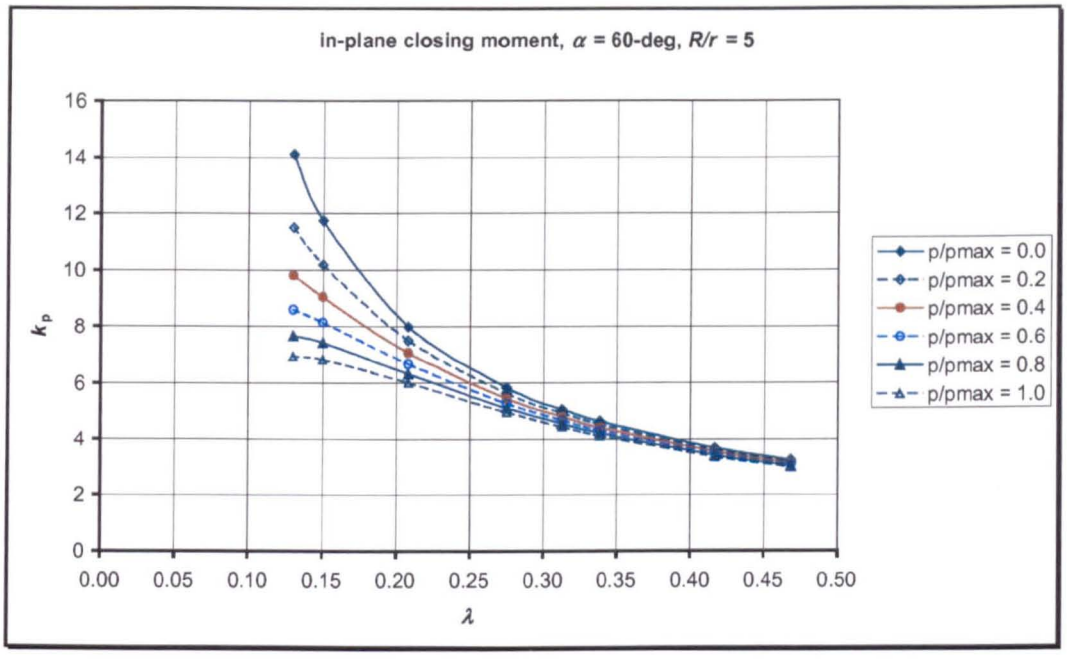

(c)

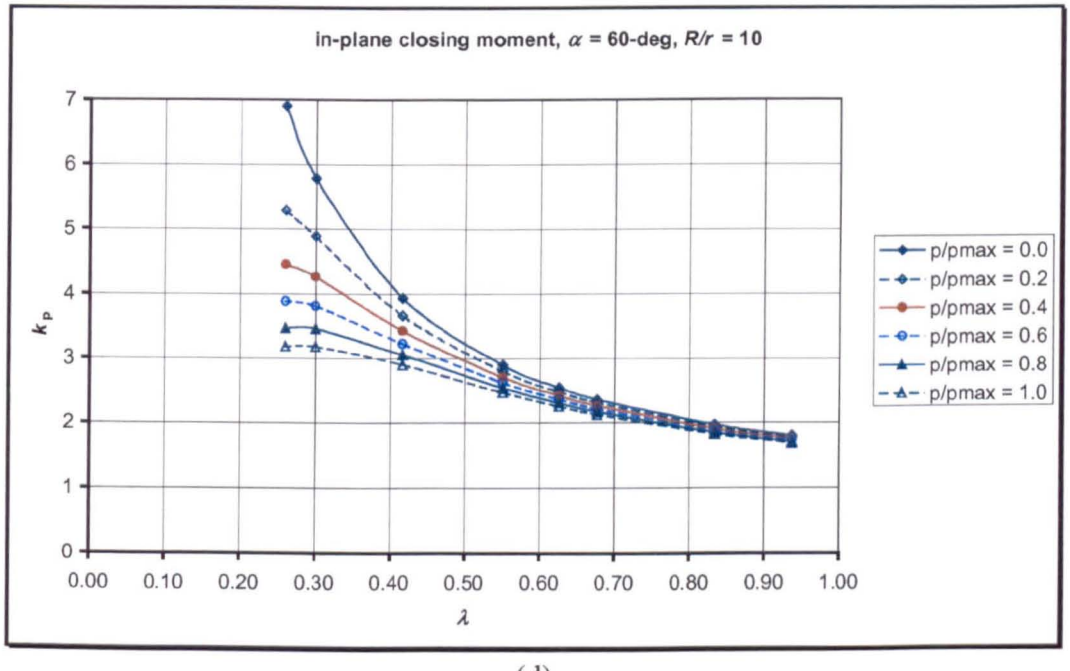

(d)

Fig.A5.8 Flexibility factors of pipe elbows under in-plane closing moment for bend angle of 60-deg: (c) $R/r = 5$, (d) $R/r = 10$

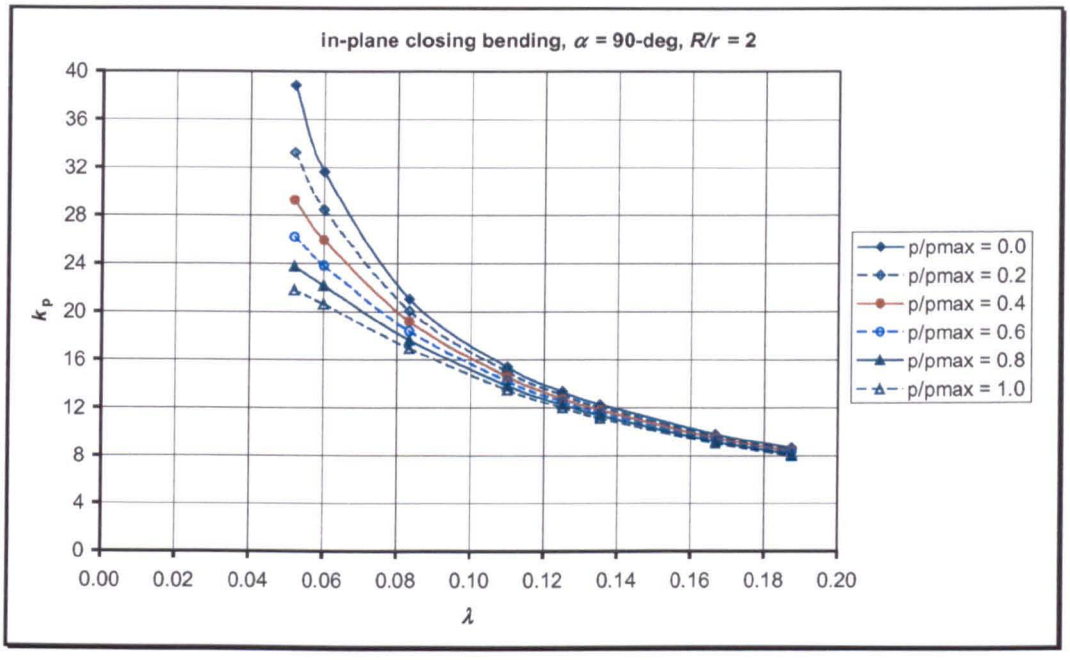

(a)

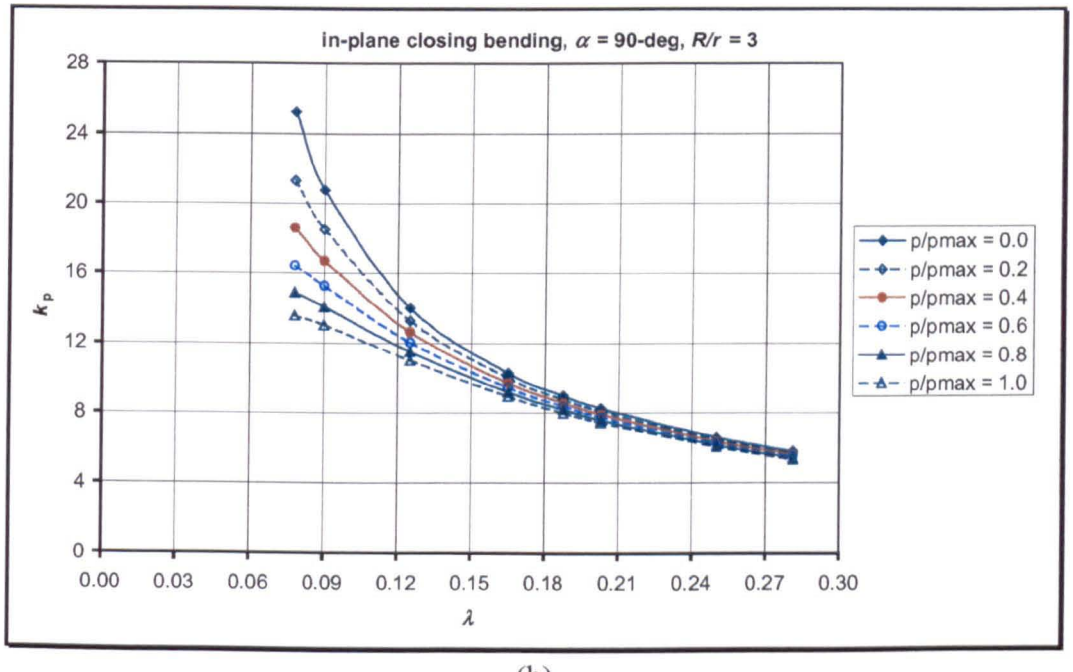

(b)

Fig.A5.9 Flexibility factors of pipe elbows under in-plane closing moment for bend angle of 90-deg: (a) $R/r = 2$, (b) $R/r = 3$

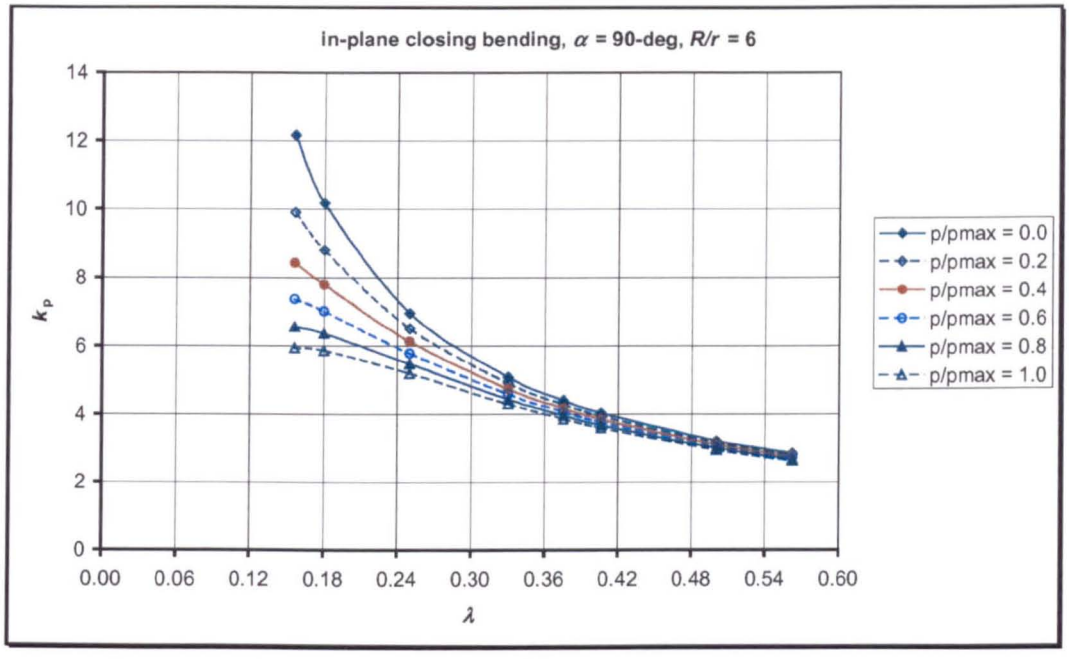

(c)

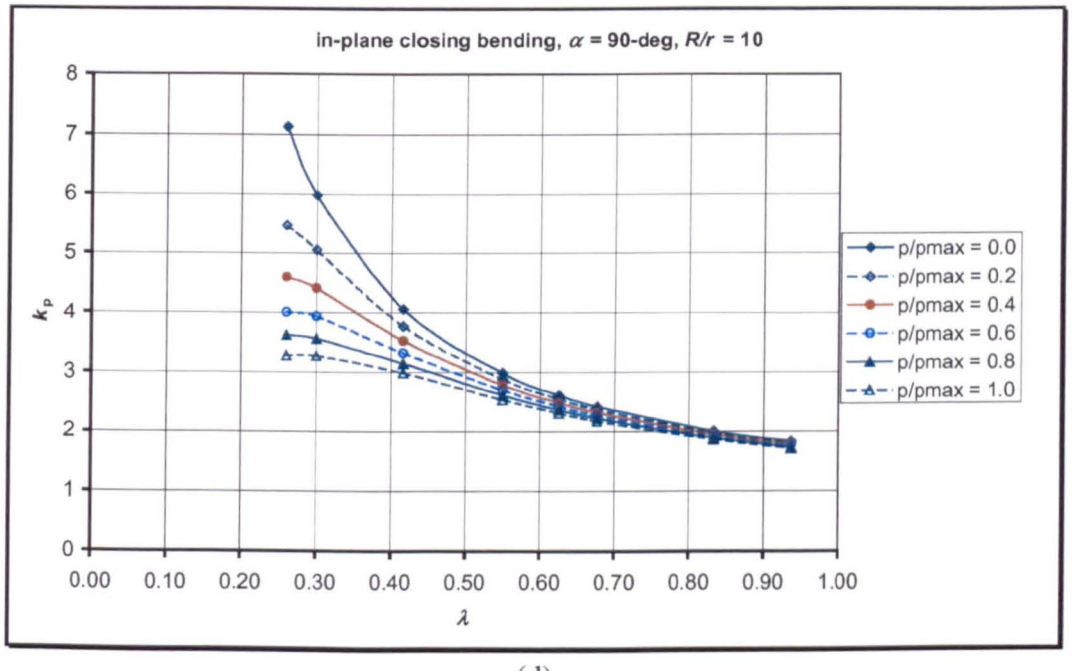

(d)

Fig.A5.9 Flexibility factors of pipe elbows under in-plane closing moment for bend angle of 90-deg: (c) $R/r = 6$, (d) $R/r = 10$

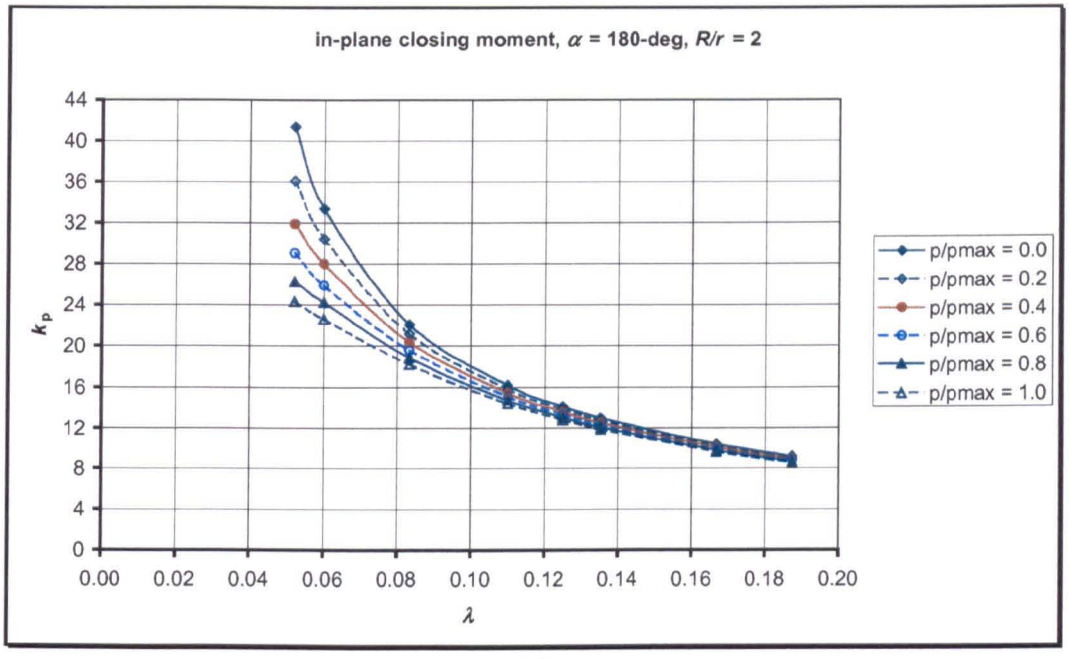

(a)

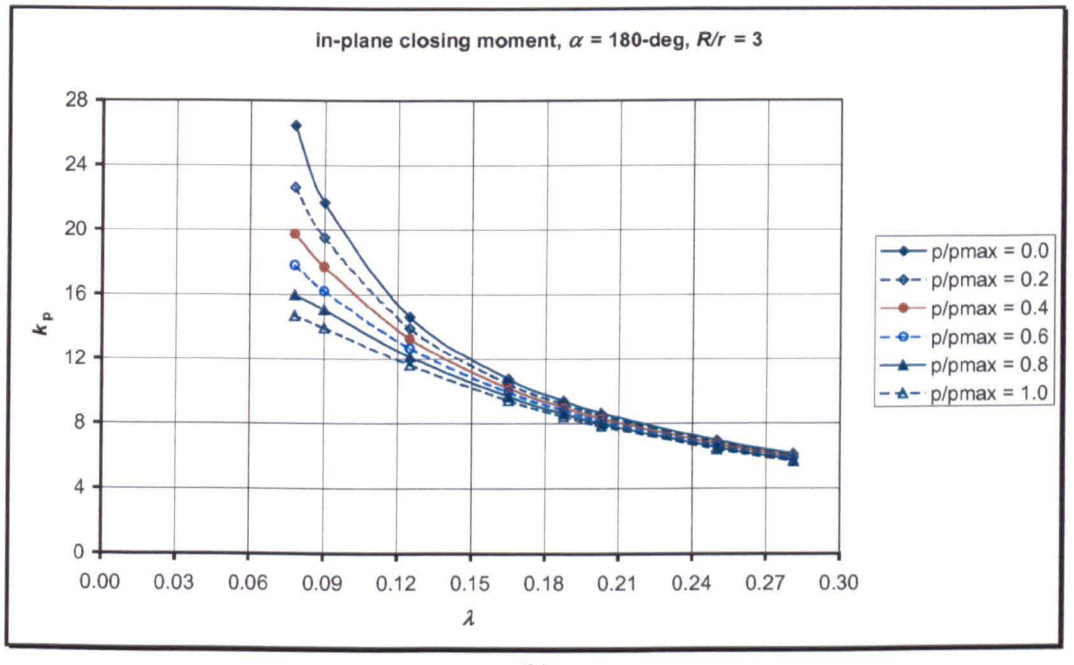

(b)

Fig.A5.10 Flexibility factors of pipe elbows under in-plane closing moment for bend angle of 180-deg: (a) $R/r = 2$, (b) $R/r = 3$

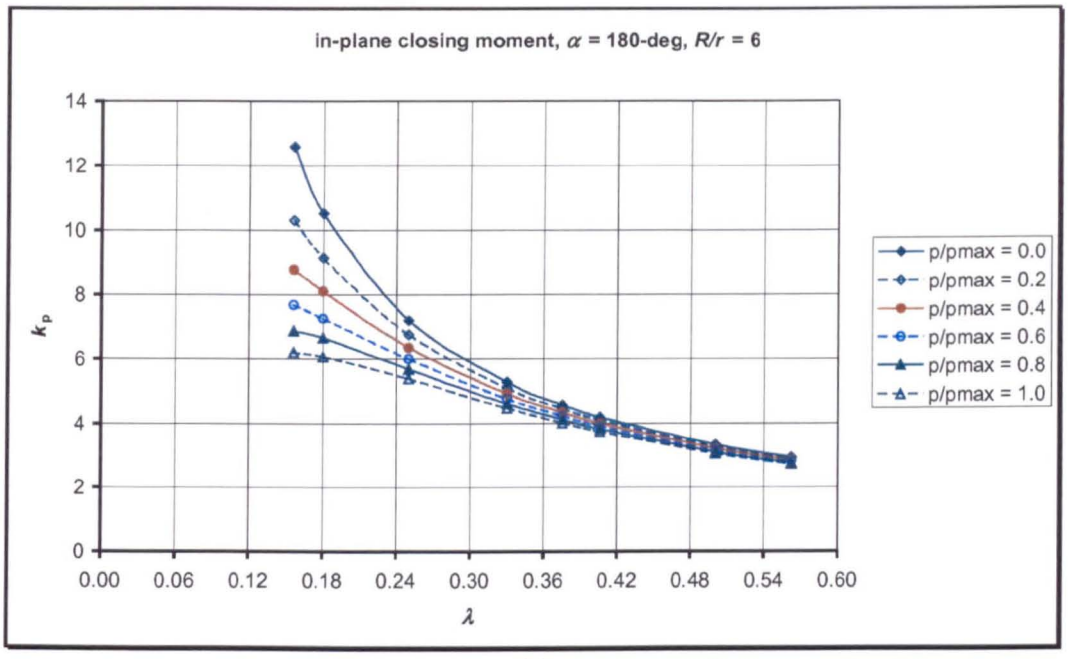

(c)

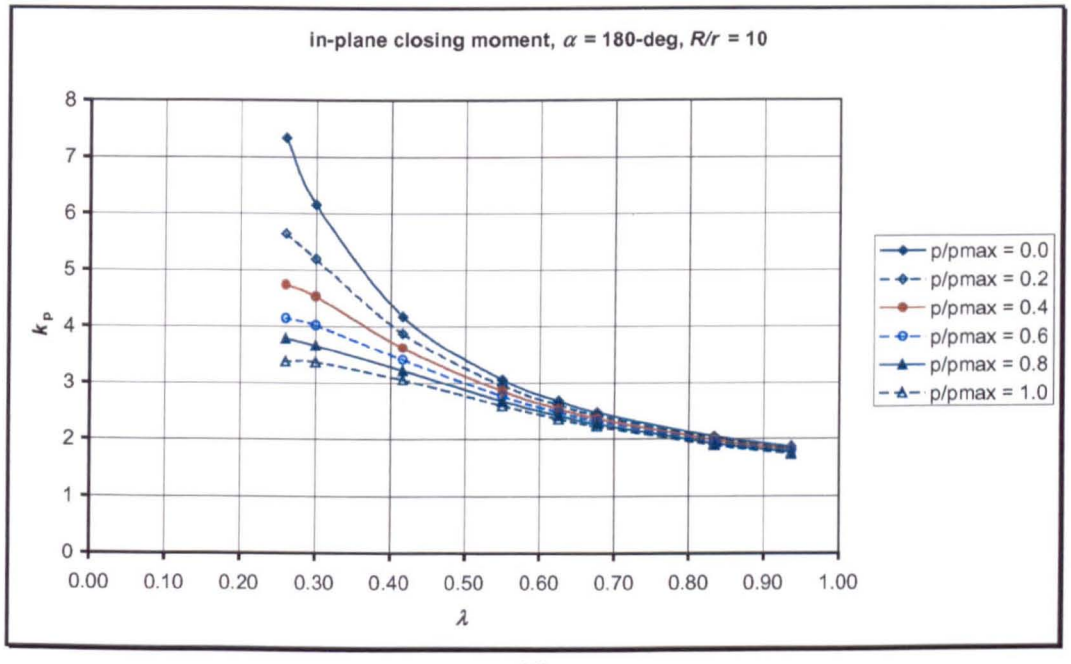

(d)

Fig.A5.10 Flexibility factors of pipe elbows under in-plane closing moment for bend angle of 180-deg: (c) $R/r = 6$, (d) $R/r = 10$

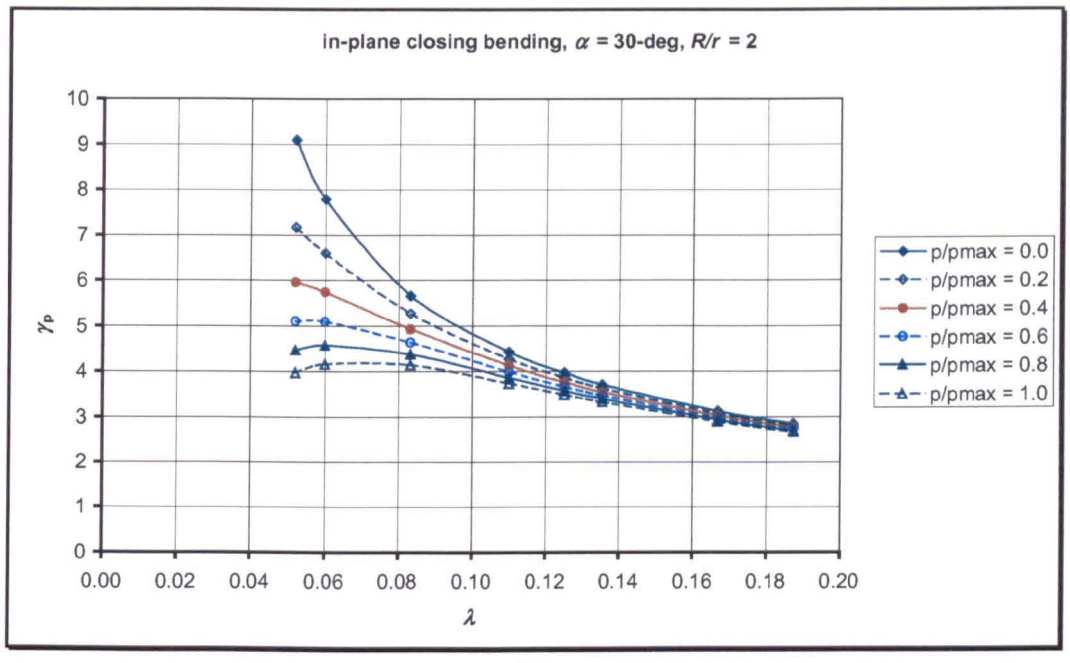

(a)

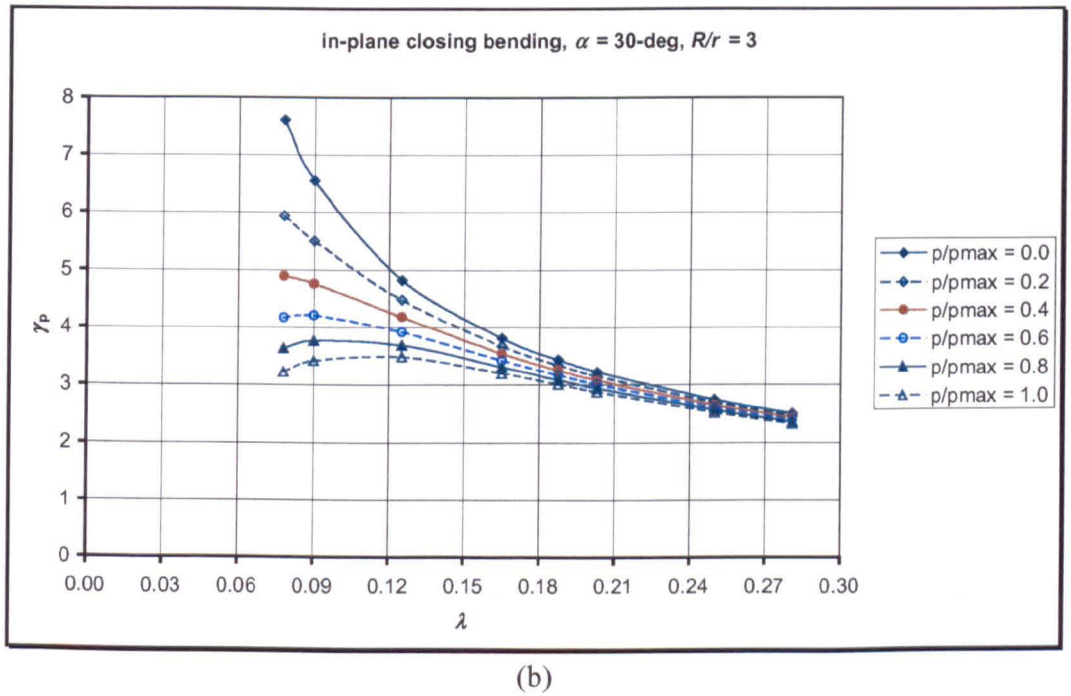

(b)

Fig.A5.11 Stress-intensification factor of 30-deg pipe elbows under in-plane closing moment: (a) $R/r = 2$, (b) $R/r = 3$

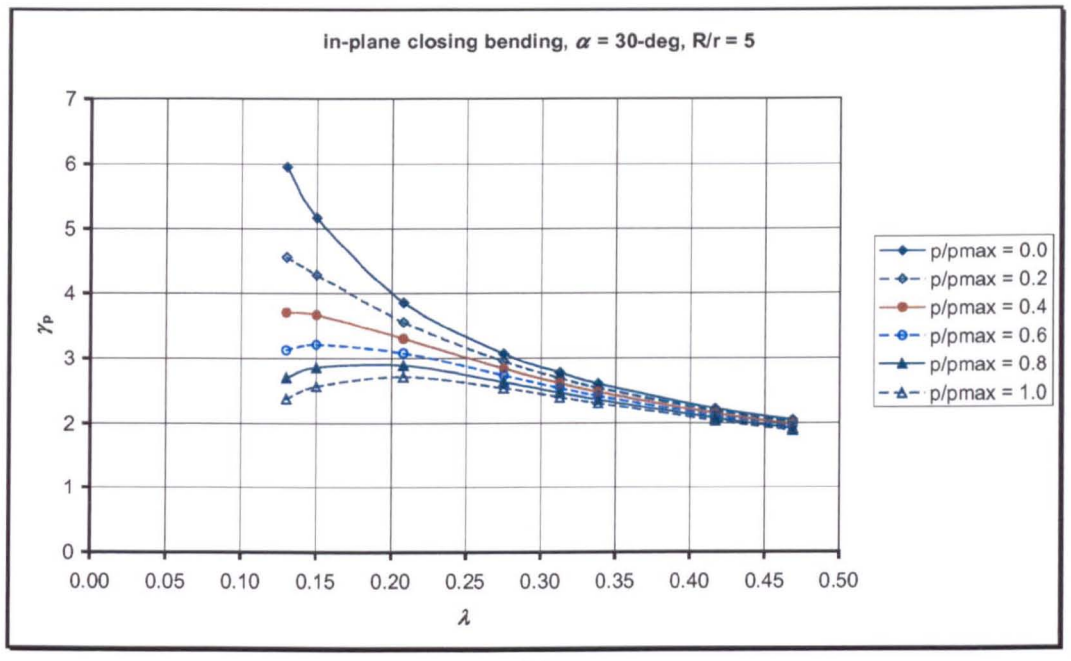

(c)

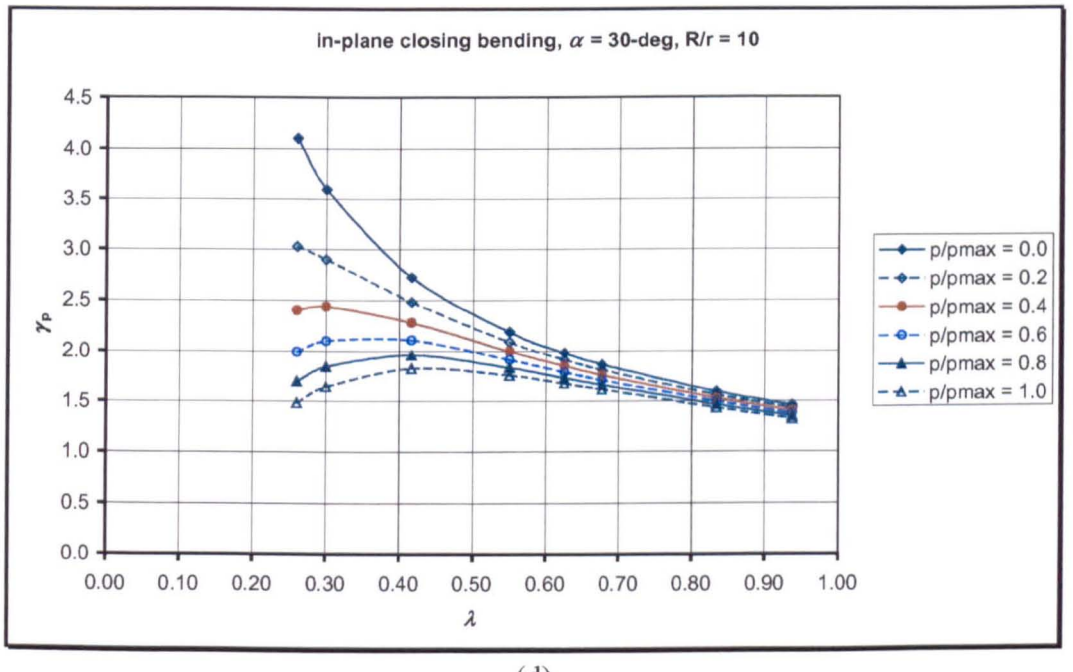

(d)

Fig.A5.11 Stress-intensification factor of 30-deg pipe elbows under in-plane closing moment: (c) $R/r = 5$, (d) $R/r = 10$

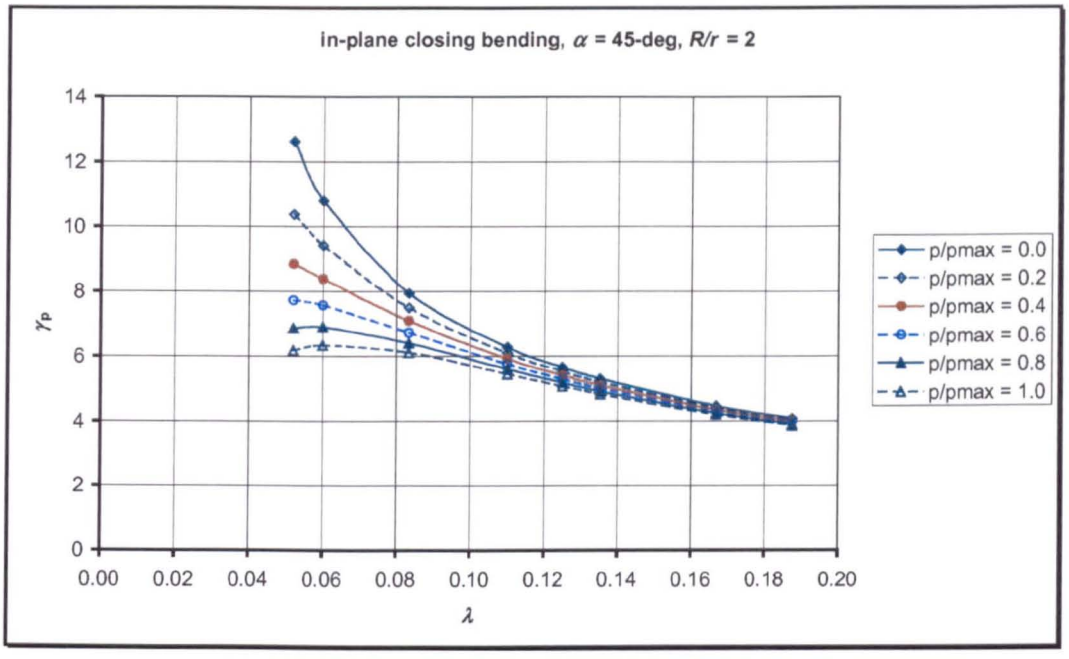

(a)

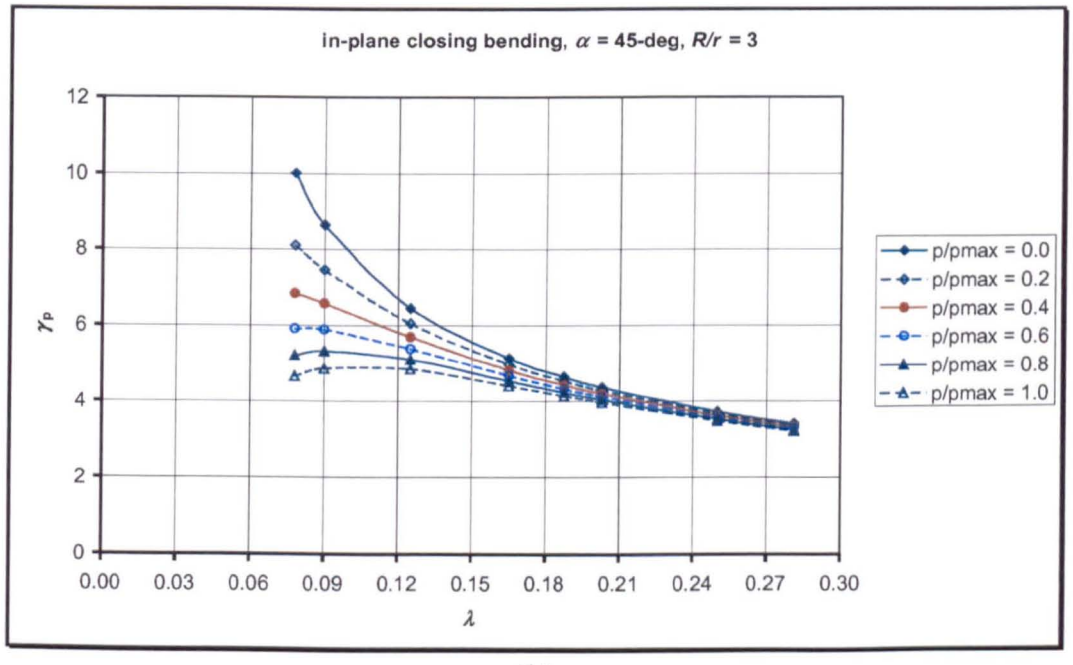

(b)

Fig.A5.12 Stress-intensification factor of 45-deg pipe elbows under in-plane closing moment: (a) $R/r = 2$, (b) $R/r = 3$

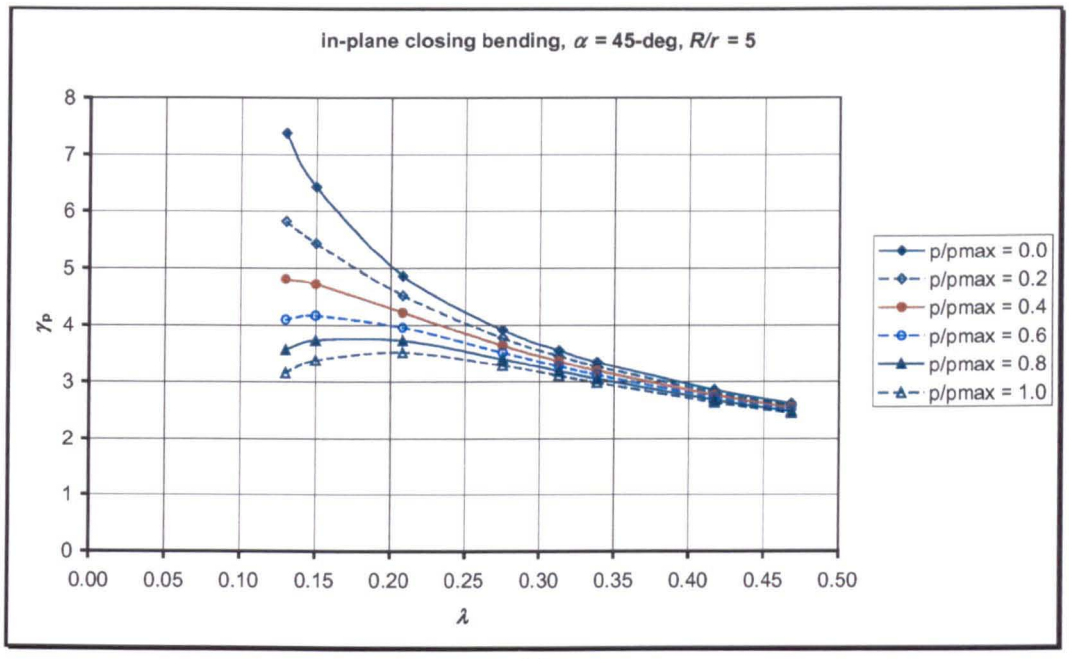

(c)

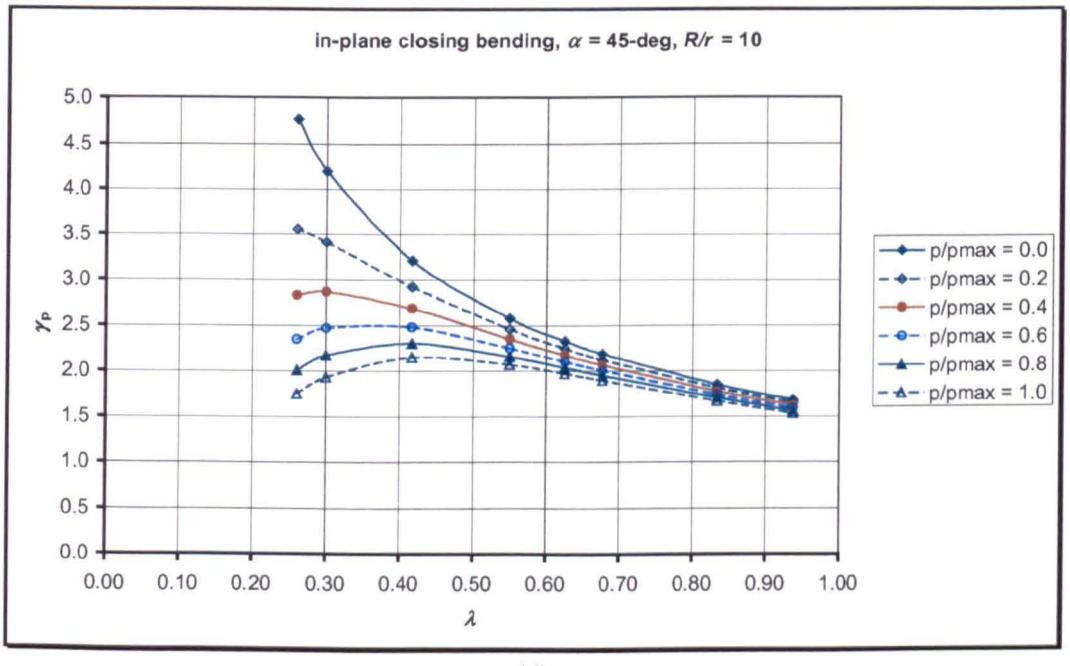

(d)

Fig.A5.12 Stress-intensification factor of 45-deg pipe elbows under in-plane closing moment: (c) $R/r = 5$, (d) $R/r = 10$

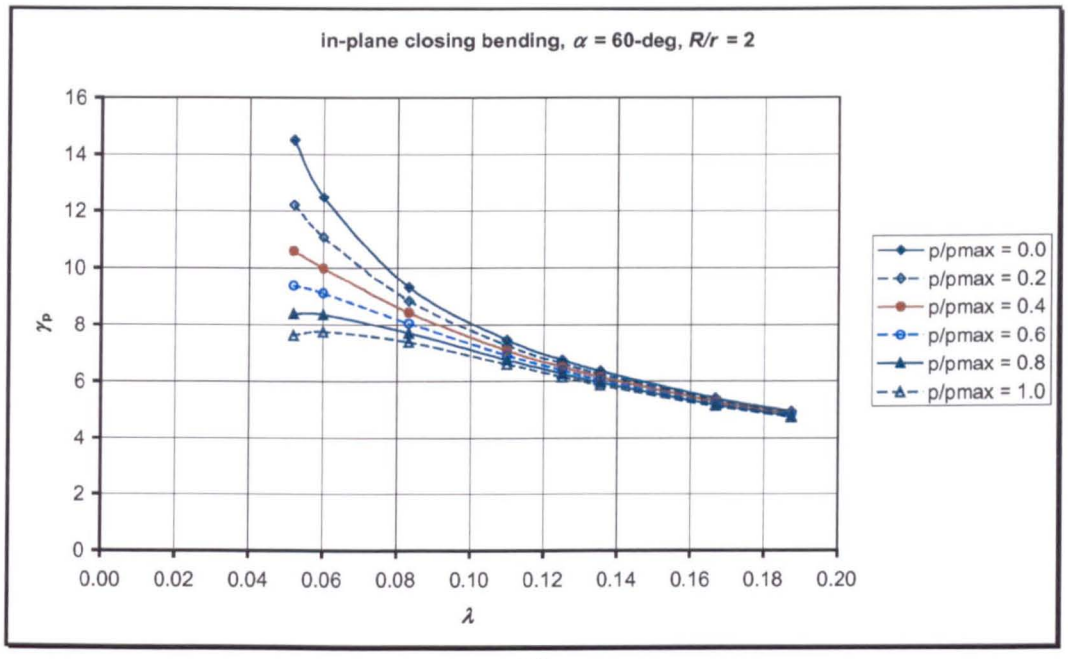

(a)

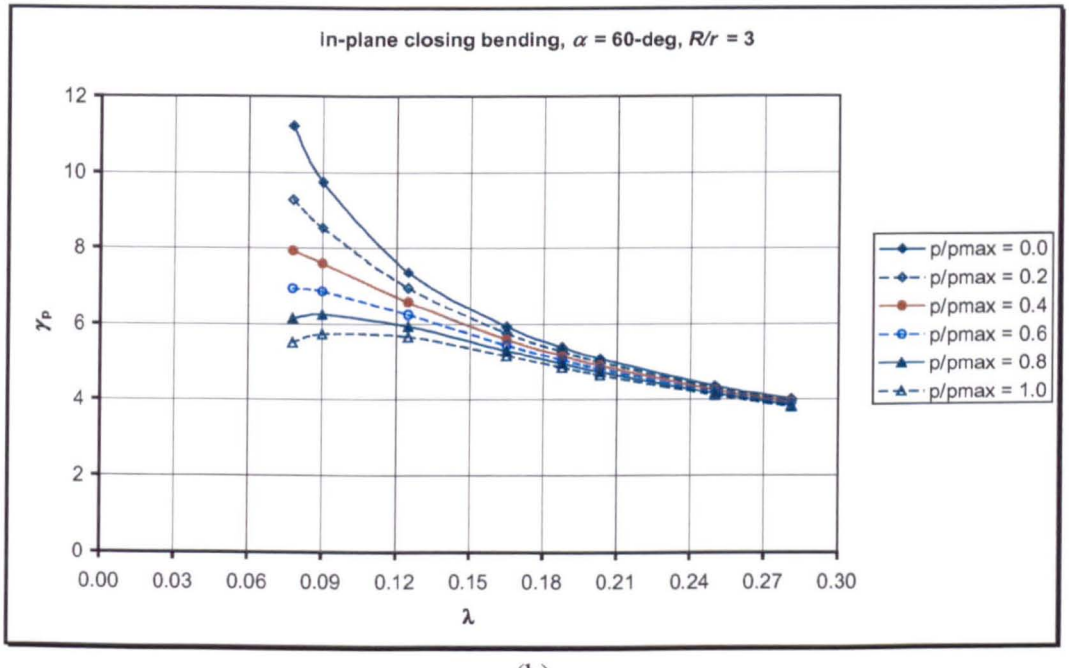

(b)

Fig.A5.13 Stress-intensification factor of 60-deg pipe elbows under in-plane closing moment: (a) $R/r = 2$, (b) $R/r = 3$

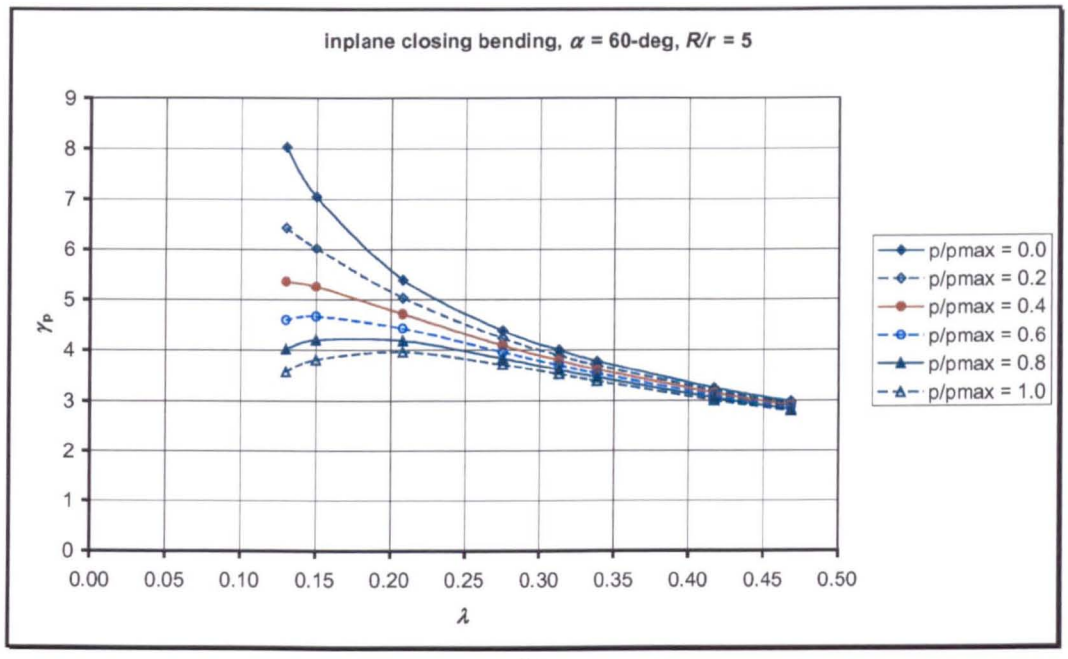

(c)

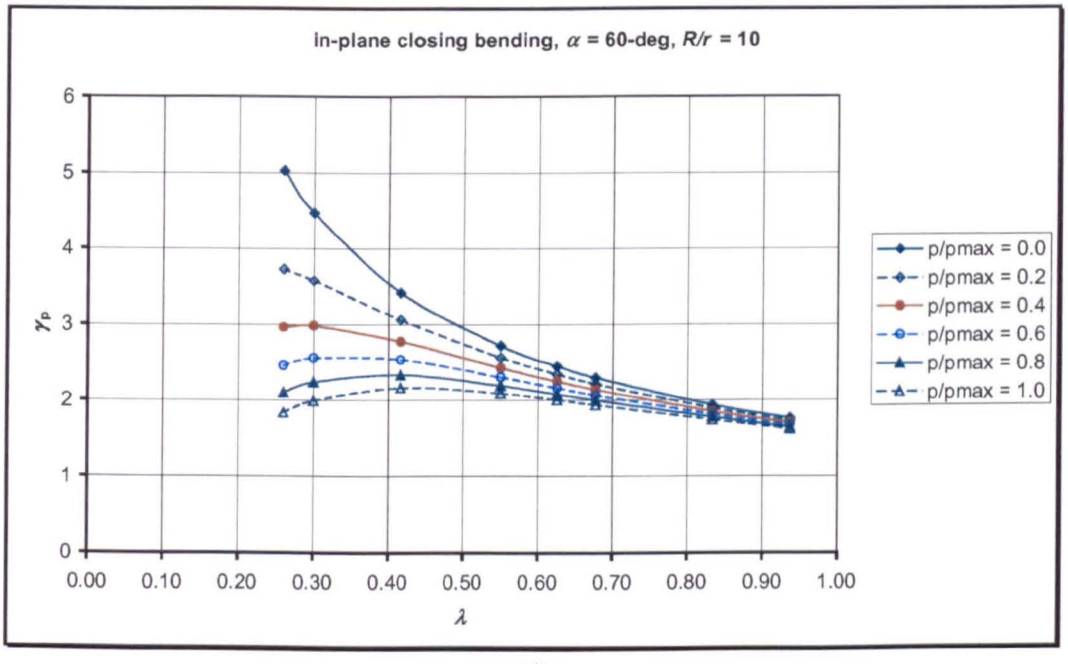

(d)

Fig.A5.13 Stress-intensification factor of 60-deg pipe elbows under in-plane closing moment: (c) $R/r = 5$, (d) $R/r = 10$

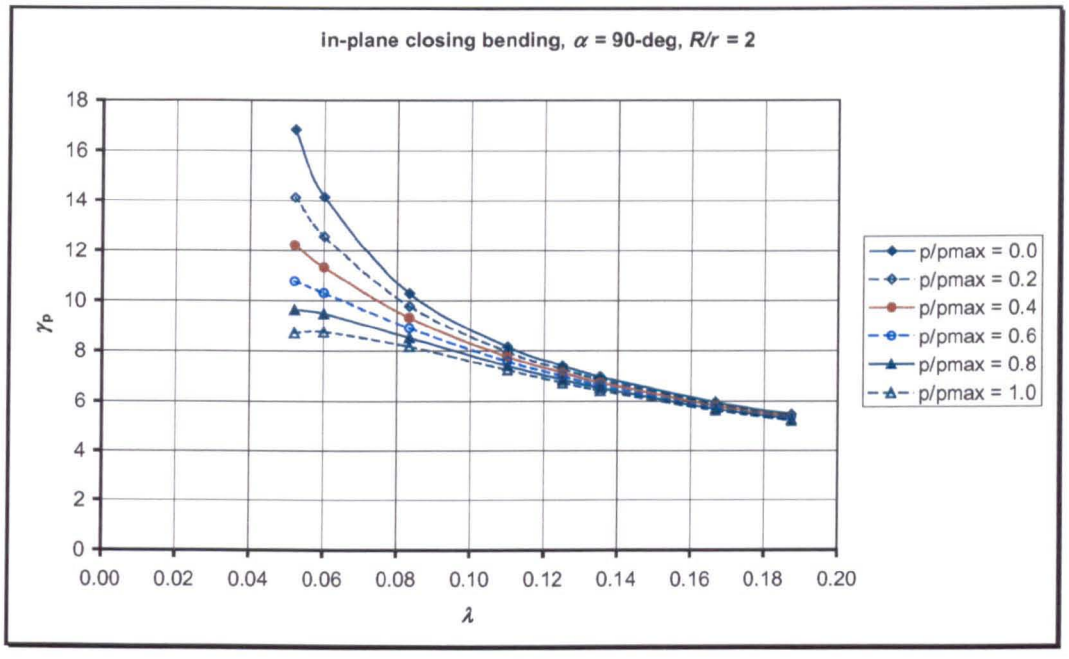

(a)

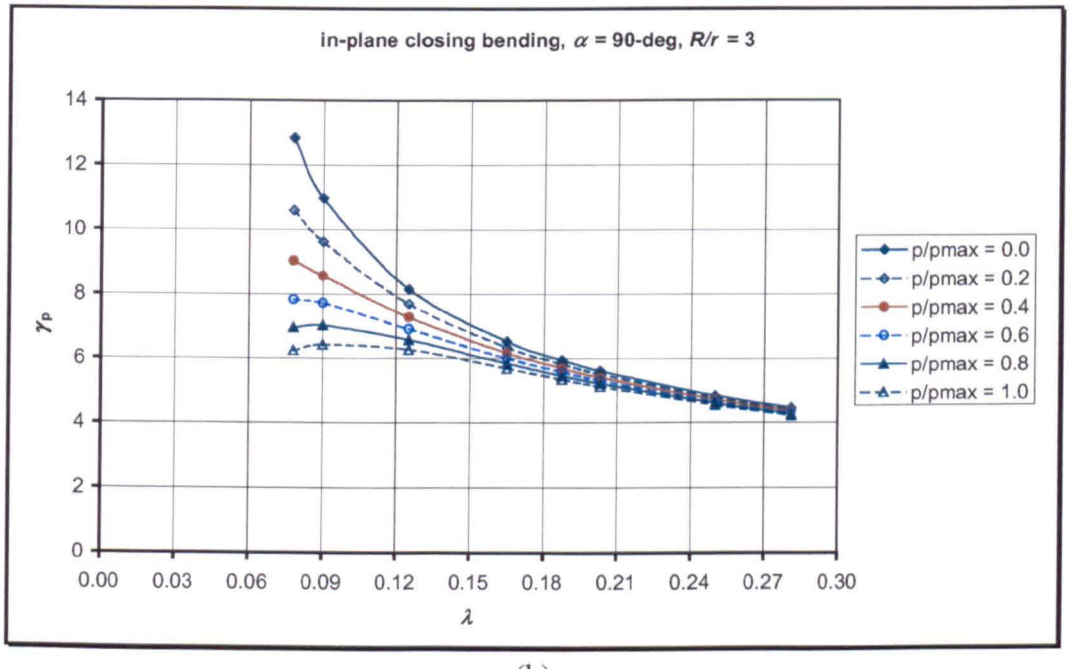

(b)

Fig.A5.14 Stress-intensification factor of 90-deg pipe elbows under in-plane closing moment: (a) $R/r = 2$, (b) $R/r = 3$

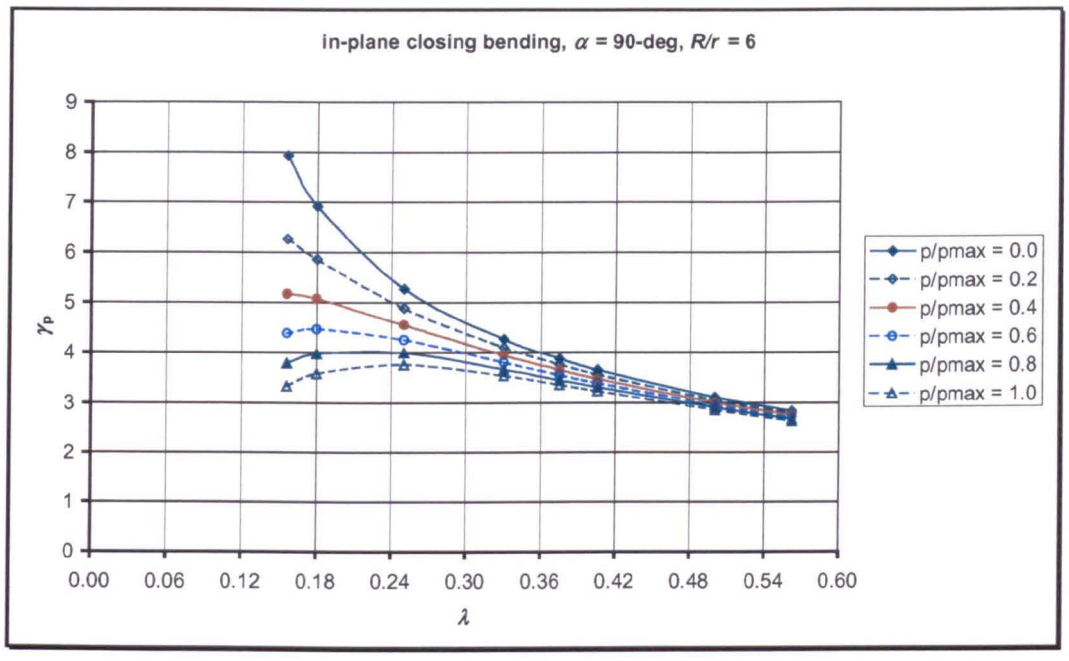

(c)

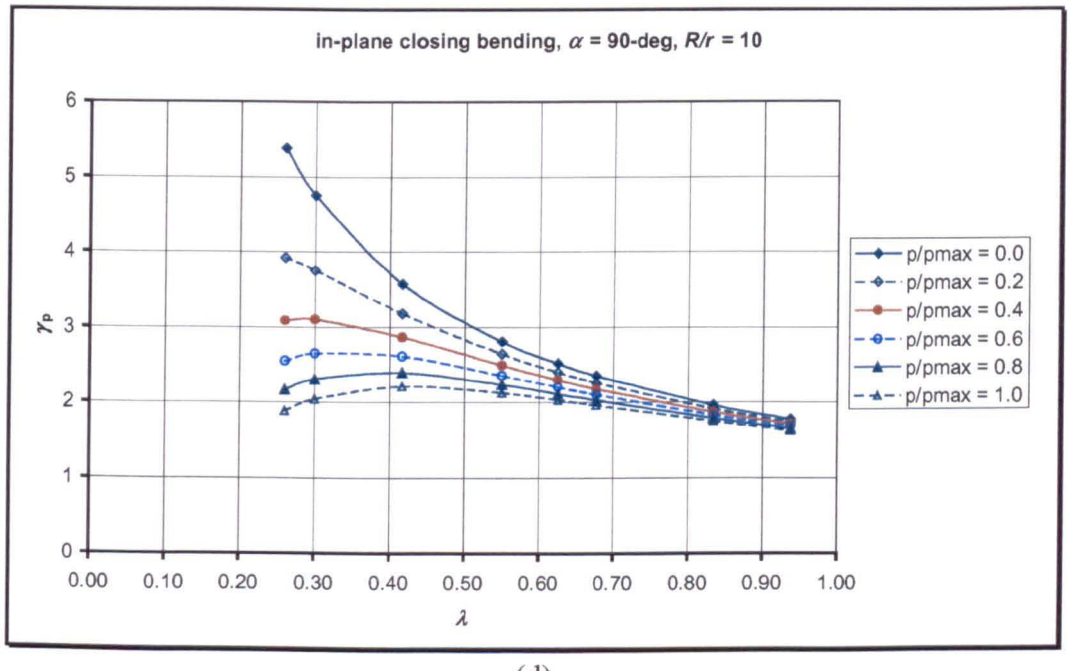

(d)

Fig.A5.14 Stress-intensification factor of 90-deg pipe elbows under in-plane closing moment: (c) $R/r = 6$, (d) $R/r = 10$

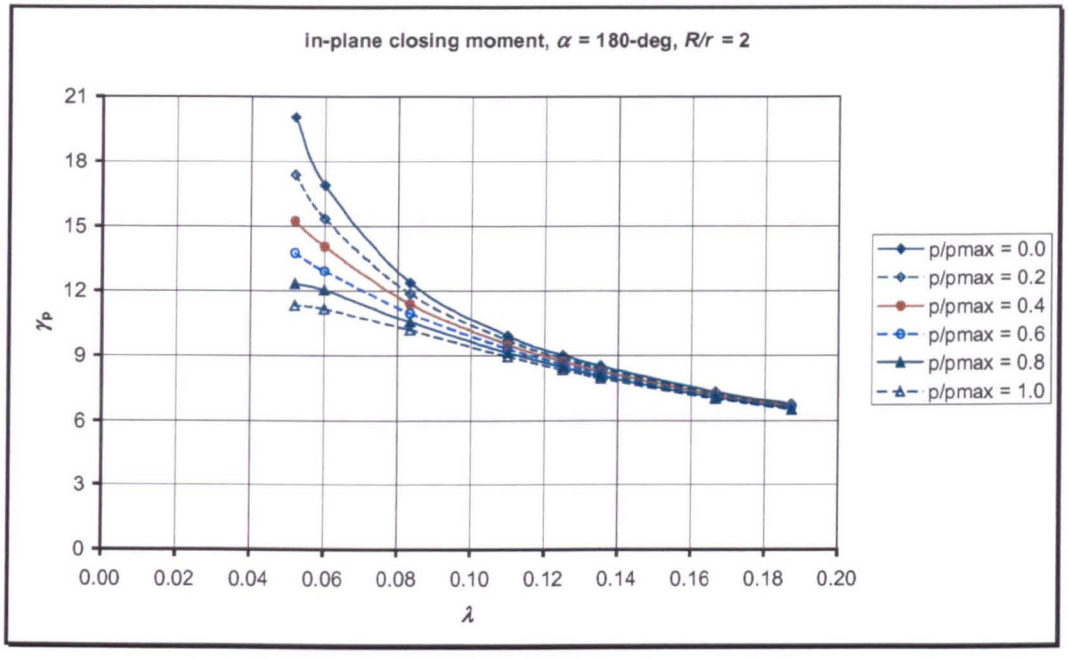

(a)

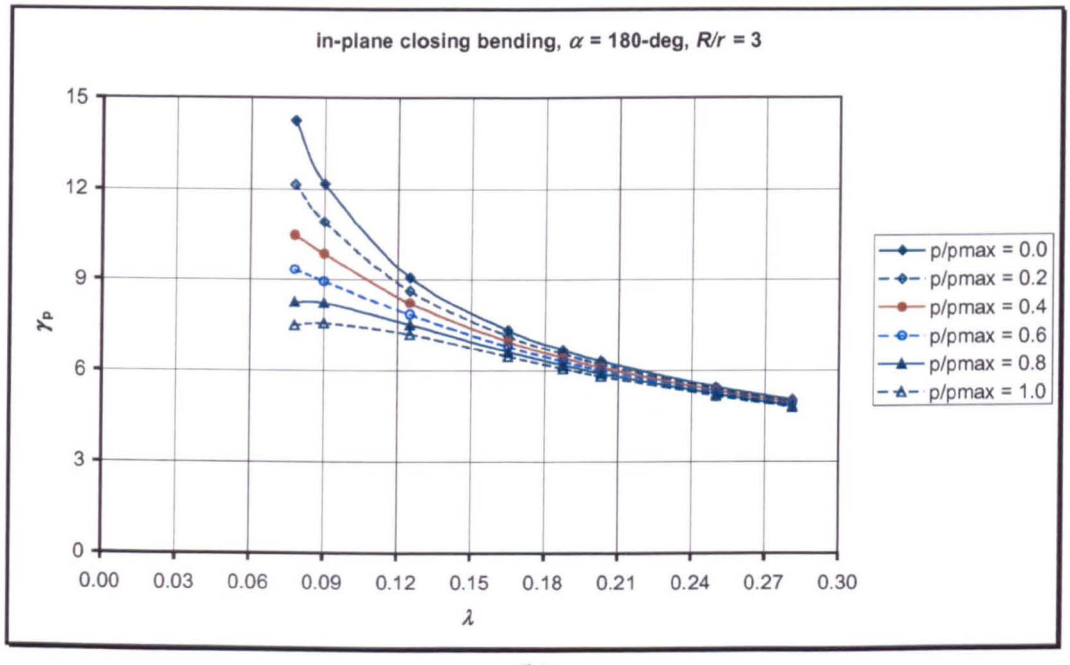

(b)

Fig.A5.15 Stress-intensification factor of 180-deg pipe elbows under in-plane closing moment: (a) $R/r = 2$, (b) $R/r = 3$

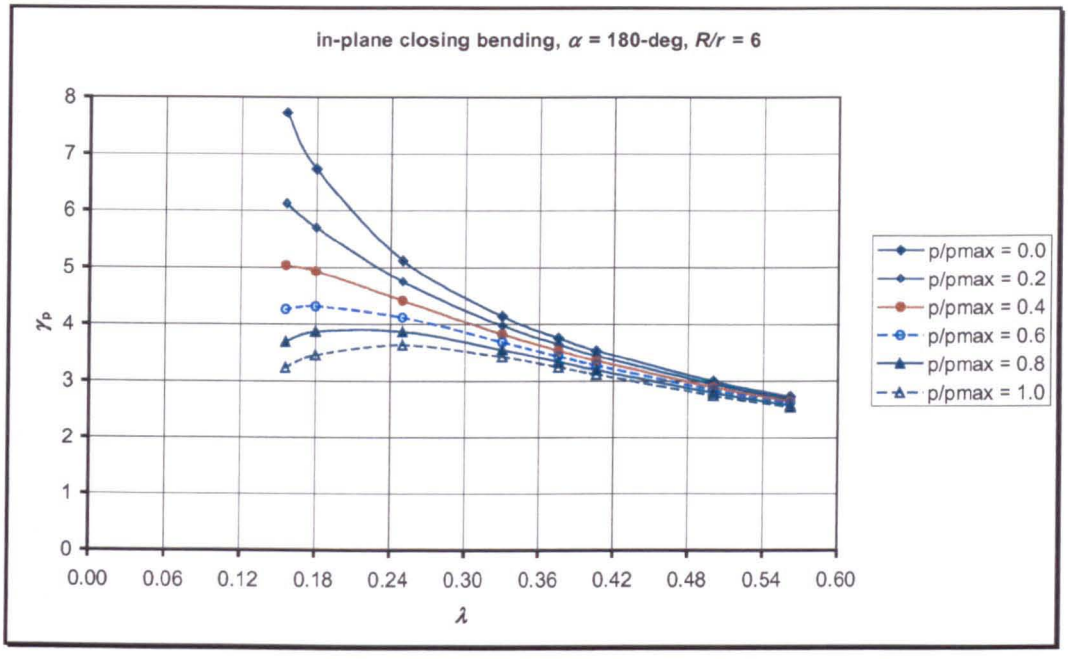

(c)

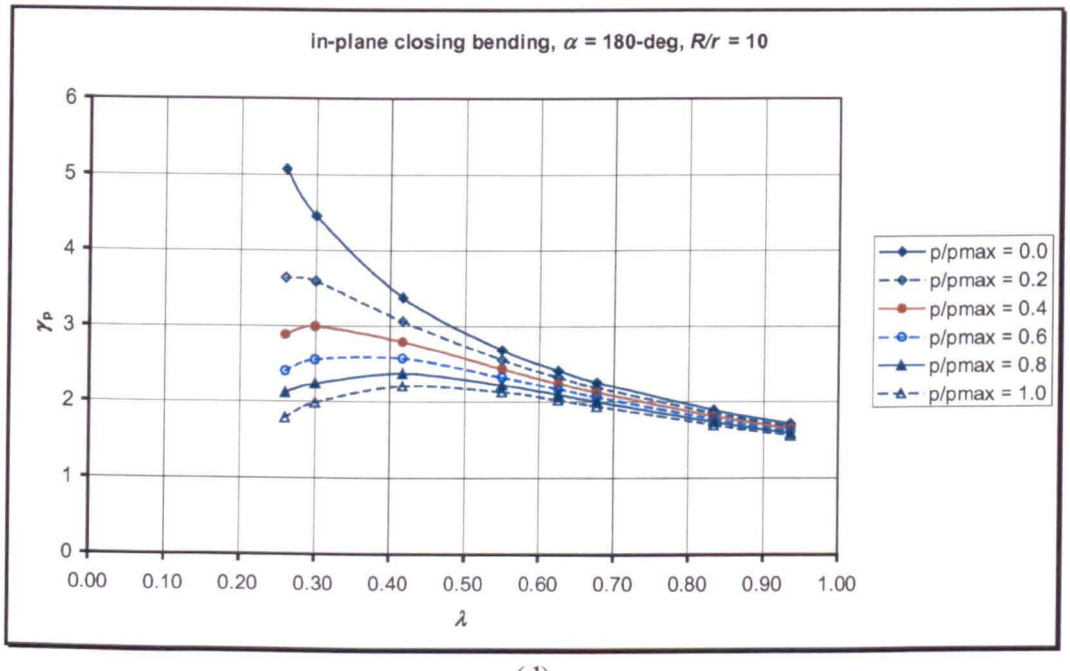

(d)

Fig.A5.15 Stress-intensification factor of 180-deg pipe elbows under in-plane closing moment: (c) $R/r = 6$, (d) $R/r = 10$

CHAPTER 6

IN-PLANE OPENING BENDING

The behaviour of piping elbows subjected to in-plane closing moment combined with internal pressure has been analysed in Chapter 5. The new formulae for unpressurised and pressurised piping elbows for ovalisation, flexibility, and stress-intensification factors have been developed. In this chapter, the behaviour of piping elbows under combined loading of in-plane *opening* moment and internal pressure is analysed. To the writer's knowledge, this loading case has been rarely studied in the literature. As has been done in Chapter 5 for in-plane closing moment, formulae suitable for incorporation in conventional piping design and analysis software for cross-sectional ovalisation, flexibility and stress-intensification are developed.

6.1 Ovalisation Factors

Under the action of an in-plane opening moment, the cross-section deforms into an oval shape with major axis lying on the plane of the bend. This type of deformation is called "*negative flattening*". Negative flattening is defined as the diameter contraction from crown to crown at the mid-section of the bend.

Typical negative flattening of a cross-section is shown in Fig.6.1. This figure is plotted for a 90-deg elbow having radius ratio R/r = 3 and a thickness to cross-section radius ratio t/r = 0.026.

Figure 6.2 shows a typical moment vs. negative flattening curve plotted for the same geometry as figure 6.1. It can be seen that the moment – negative flattening curve is represented well by a straight line. It can also be seen from the curve that piping

elbows exhibit a 'structural hardening' behaviour under an in-plane moment, contrary to the 'structural softening' when subjected to in-plane closing moment.

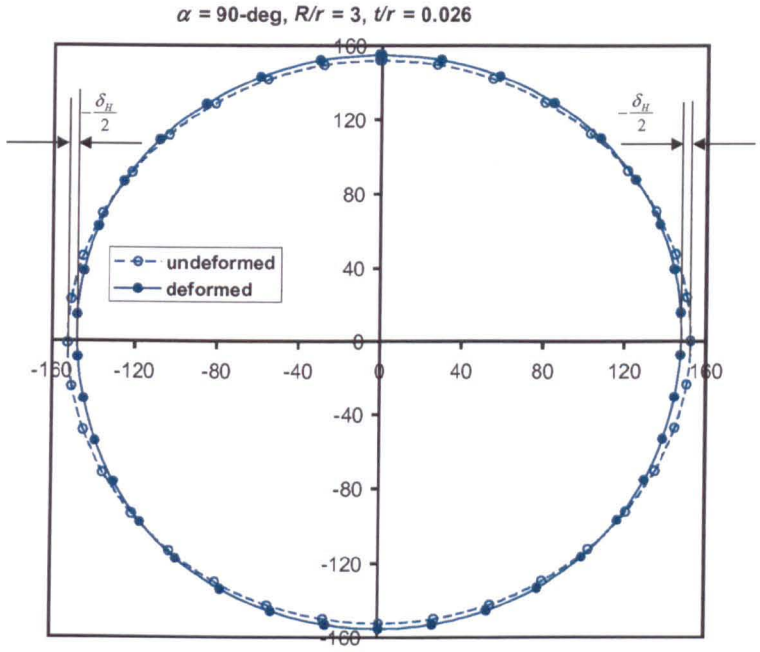

Fig.6.1 Typical cross-sectional ovalisation under in-plane opening bending

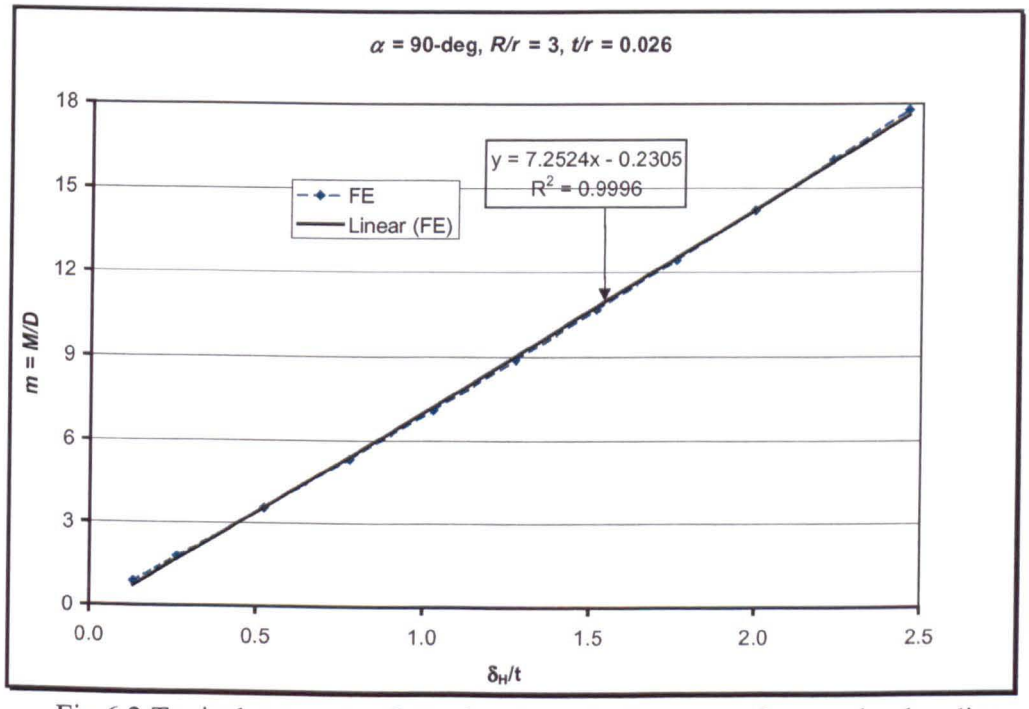

Fig.6.2 Typical moment – flattening (negative) curve under opening bending

Ovalisation factor for an in-plane opening moment has the same definition as for an in-plane closing moment, but they are different in sign (positive for closing bending and negative for opening bending). Since negative values cannot be plotted in a logarithm curve, the minus sign will be omitted.

Figure 6.3 shows the ovalisation factor for 90-deg pipe elbows plotted against pipe bend parameters, λ, for various radius ratios, ρ: it was plotted in a semi log graph. At first, an attempt was made to plot the ovalisation factor in a log-log graph, but a straight line was not obtained. Accordingly, the ovalisation factor as a function of pipe bend parameter cannot be accurately expressed by a power relation, as given by equation (5-3). Instead, straight lines were obtained for the relation between ovalisation factor and pipe bend parameter in a semi-log graph as shown in Fig.6.3.

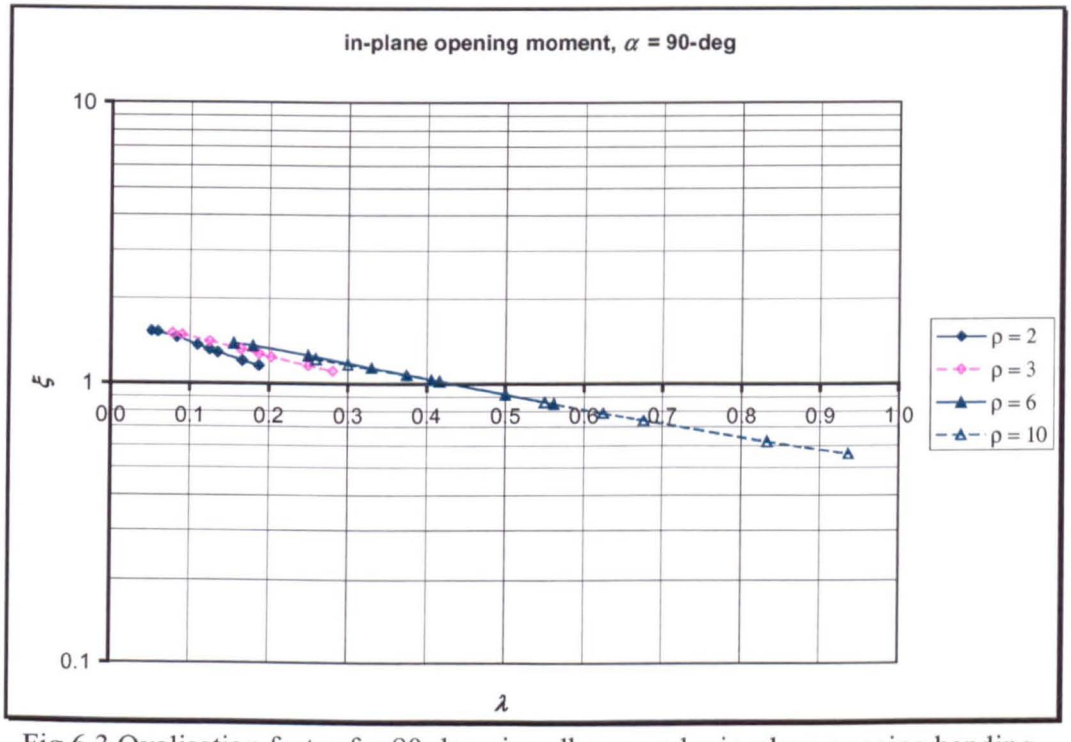

Fig.6.3 Ovalisation factor for 90-deg pipe elbows under in-plane opening bending

According to Fig.6.3, the ovalisation factor can be expressed in the following form:

$$\xi = p\exp(-q\lambda) \tag{6-1}$$

where p and q are coefficients to be determined.

By curve fitting to, ovalisation factor for 90-deg pipe elbows due to in-plane opening bending can be expressed as follows:

$$\xi = 1.730\exp(-2.142\lambda) \quad \text{for } \rho = 2 \tag{6-2}$$
$$\xi = 1.701\exp(-1.533\lambda) \quad \text{for } \rho = 3 \tag{6-3}$$
$$\xi = 1.696\exp(-1.221\lambda) \quad \text{for } \rho = 6 \tag{6-4}$$
$$\xi = 1.656\exp(-1.175\lambda) \quad \text{for } \rho = 10 \tag{6-5}$$

The above equations are not suitable for design purpose. Based on ovalisation factor for a long radius bend (R/r = 10), equations (6-2) through (6-5) can be expressed in the following form:

$$\xi = 1.656\exp(-1.175\lambda)[f(\lambda)] \tag{6-6}$$

where $f(\lambda)$ represents the dependence of ovalisation factor on radius ratio, R/r. This function would be different for every radius ratio. Following the procedure of Fujimoto and Soh [92], equations (6-2) through (6-5) can be expressed in the following form:

$$\xi = 1.656\exp(-1.175\lambda)[1.0393 - 0.9026\lambda] \quad \text{for } \rho = 2 \tag{6-7}$$
$$\xi = 1.656\exp(-1.175\lambda)[1.0254 - 0.3452\lambda] \quad \text{for } \rho = 3 \tag{6-8}$$
$$\xi = 1.656\exp(-1.175\lambda)[1.0239 - 0.04666\lambda] \quad \text{for } \rho = 6 \tag{6-9}$$
$$\xi = 1.656\exp(-1.175\lambda)[1.0 - 0.0002\lambda] \quad \text{for } \rho = 10 \tag{6-10}$$

Figure 6.4 shows the ovalisation factor obtained directly from finite element (FE), using equation (6-2) through (6-5) and using equation (6-7) through (6-10). It can be seen that the proposed equation fit well to the results from finite element.

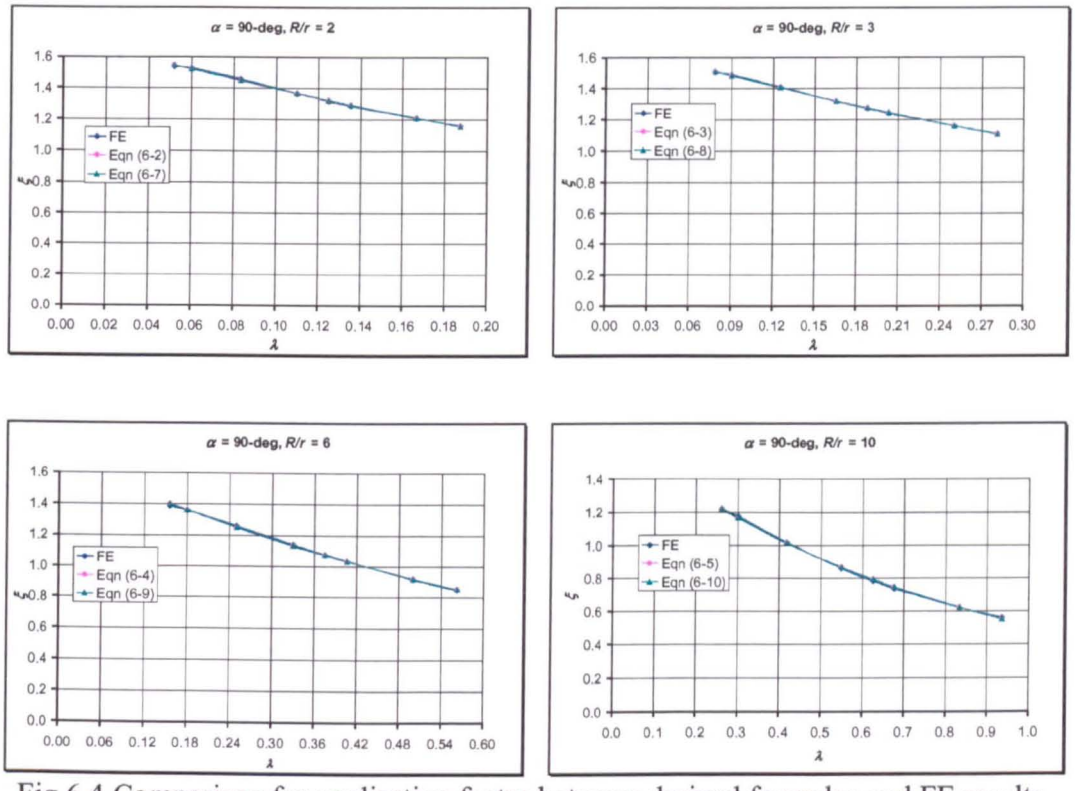

Fig.6.4 Comparison for ovalisation factor between derived formulae and FE results

6.1.1 Effect of Bend Angle on Ovalisation Factor

To account for the effect of bend angle on ovalisation factor due to in-plane opening bending, pipe elbows of bend angles 30, 45, 60, 90, and 180-deg have been investigated. It is expected that the effect of bend angle on ovalisation factor is of significance, since it would tend to behave as a straight pipe as the bend angle approaches hypothetically zero. Figure 6.5 through 6.8 show the ovalisation factor for pipe elbows of various bend angles:

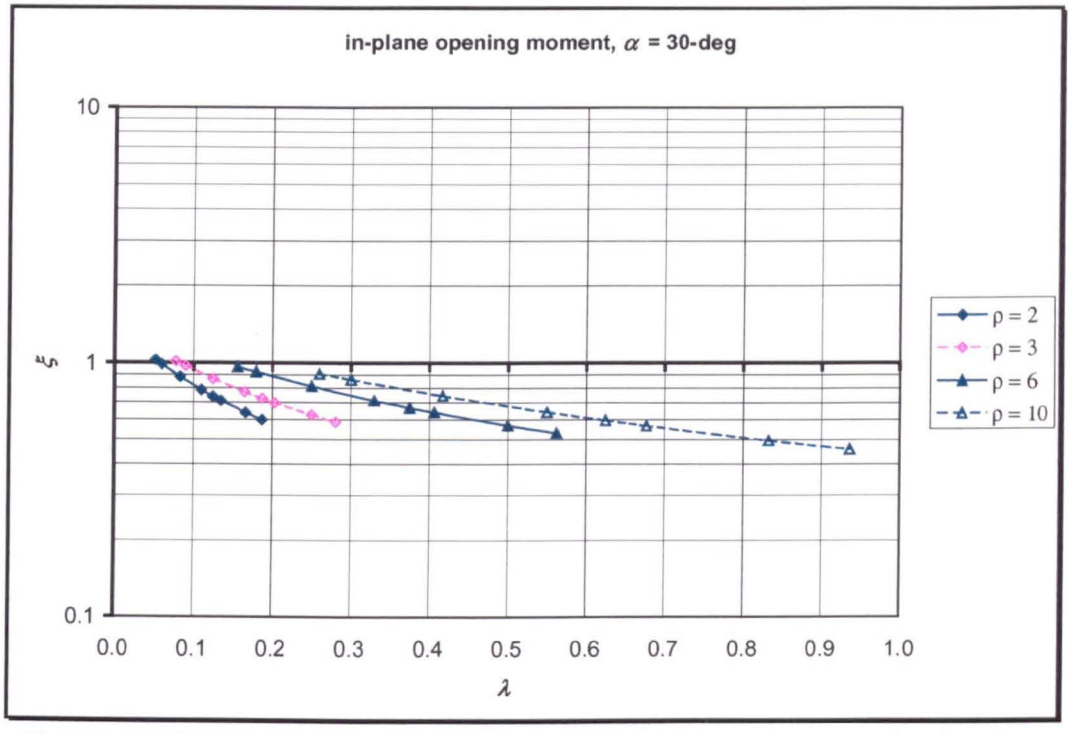

Fig.6.5 Ovalisation factor for 30-deg pipe elbows due to in-plane opening bending

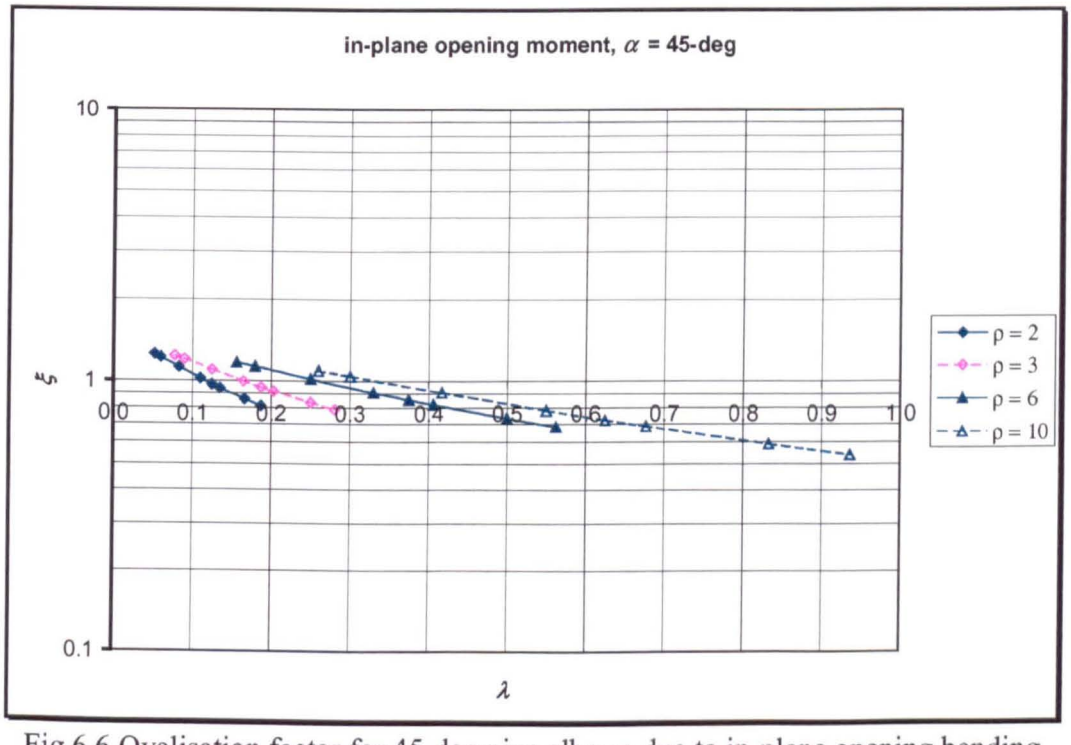

Fig.6.6 Ovalisation factor for 45-deg pipe elbows due to in-plane opening bending

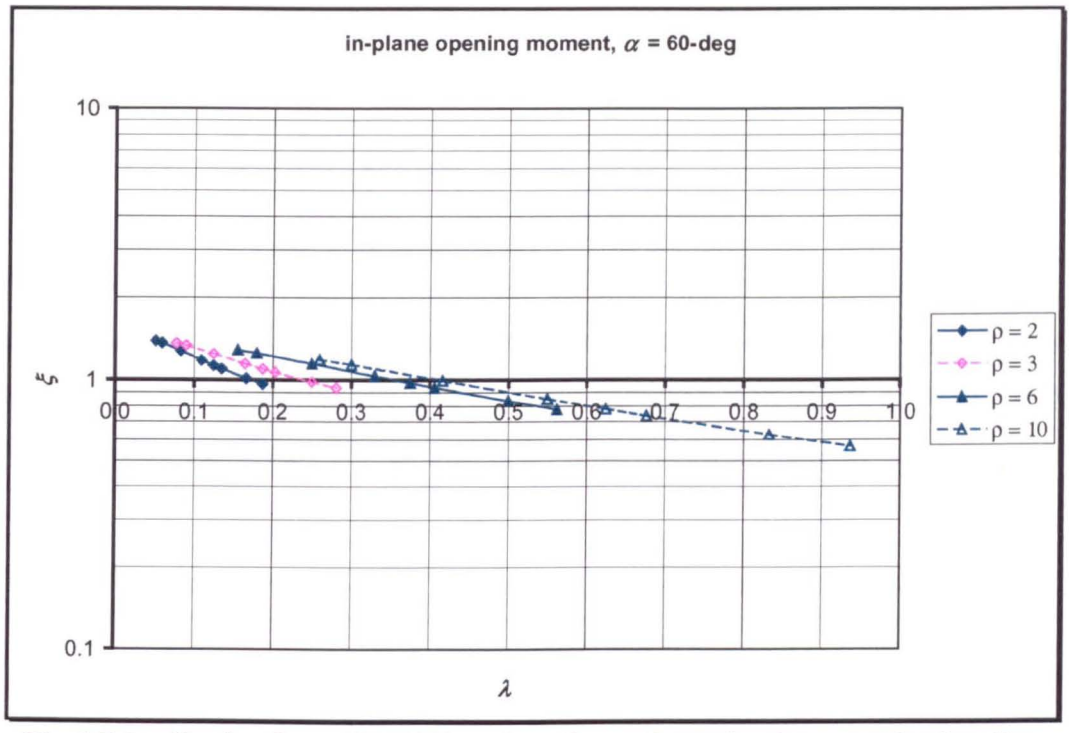

Fig.6.7 Ovalisation factor for 60-deg pipe elbows due to in-plane opening bending

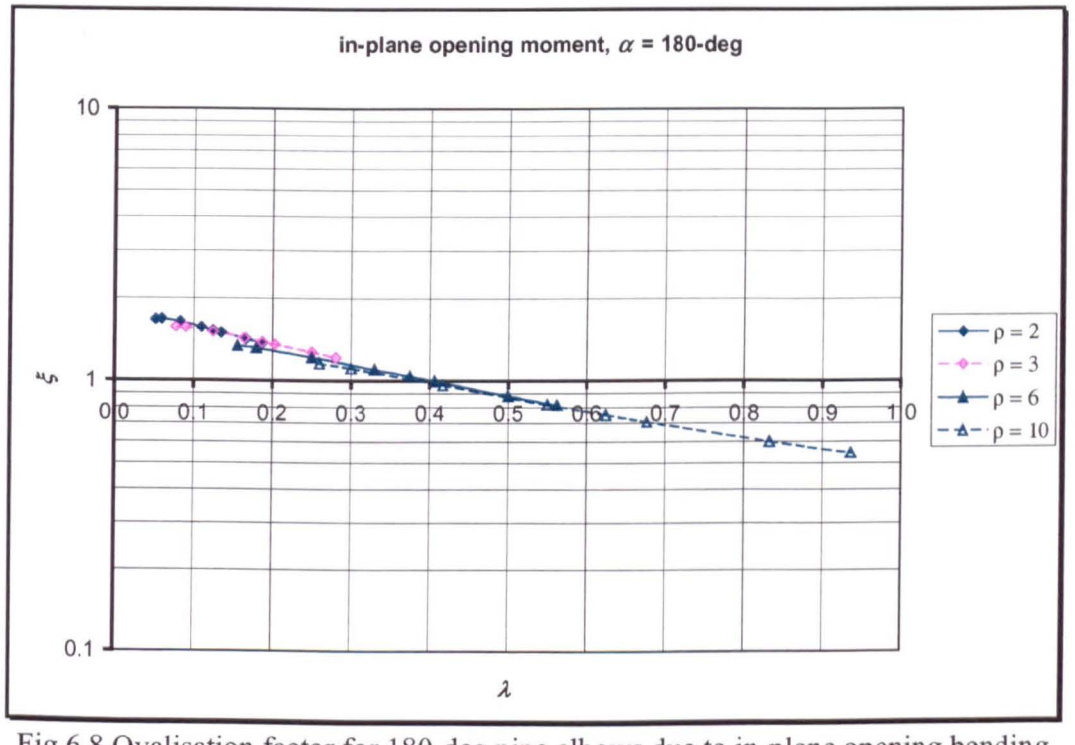

Fig.6.8 Ovalisation factor for 180-deg pipe elbows due to in-plane opening bending

From these figures, the ovalisation factor for various bend angles can be expressed in the following form:

$$\xi = 1.656\exp(-1.175\lambda)[a - b\lambda] \qquad (6\text{-}11)$$

It can be seen from equation (6-11) that the dependence of ovalisation factor on radius ratio can be represented by a linear relation in terms of pipe bend parameter, λ, with a and b the coefficients of the straight lines with their values given in Table 6.1 and 6.2 respectively:

Table 6.1 Values of coefficient "a" in equation (6-11) for various bend angles

R/r	Bend angle, α				
	30-deg	45-deg	60-deg	90-deg	180-deg
2	0.7216	0.8675	0.9507	1.0393	1.1102
3	0.7194	0.8624	0.9421	1.0254	1.0557
4	0.7172	0.8602	0.9406	1.0244	1.0280
5	0.7140	0.8580	0.9414	1.0242	1.0035
6	0.7108	0.8561	0.9425	1.0239	0.9882
7	0.7076	0.8547	0.9435	1.0147	0.9676
8	0.7044	0.8533	0.9445	1.0105	0.9538
9	0.7012	0.8522	0.9453	1.0062	0.9417
10	0.6954	0.8513	0.9469	1.0000	0.9291

Table 6.2 Values of coefficient "*b*" in equation (6-11) for various bend angles

R/r	Bend angle, α				
	30-deg	45-deg	60-deg	90-deg	180-deg
2	1.5307	1.4318	1.2443	0.9026	0.4071
3	0.8669	0.7529	0.5938	0.3452	0.1146
4	0.5185	0.4516	0.3747	0.1502	0.1075
5	0.3144	0.2582	0.2086	0.0535	0.0557
6	0.1998	0.1229	0.0644	0.0466	0.0553
7	0.0811	0.0372	0.0188	0.0068	-0.0034
8	0.0082	-0.0319	-0.0405	0.0024	-0.0219
9	-0.0485	-0.0856	-0.0866	0.0009	-0.0363
10	-0.1149	-0.1142	-0.1236	0.0002	-0.0431

It can be inferred from these Tables that the terms in the square bracket must be taken into account except for 90-deg pipe elbows of long radius bend.

6.1.2 The Pressure Reduction Effect

When internal pressure acts on an ovalised cross-section resulting from in-plane bending load, it tries to push the deformed cross-section back to its original circular shape. However, the deformed cross section of pipe elbows under an in-plane opening bending is again in oval shape but with the major axis lying on the plane of the bend. Subsequent internal pressure loading will decrease the length of the major axis. This type of deformation is shown in Fig.6.9:

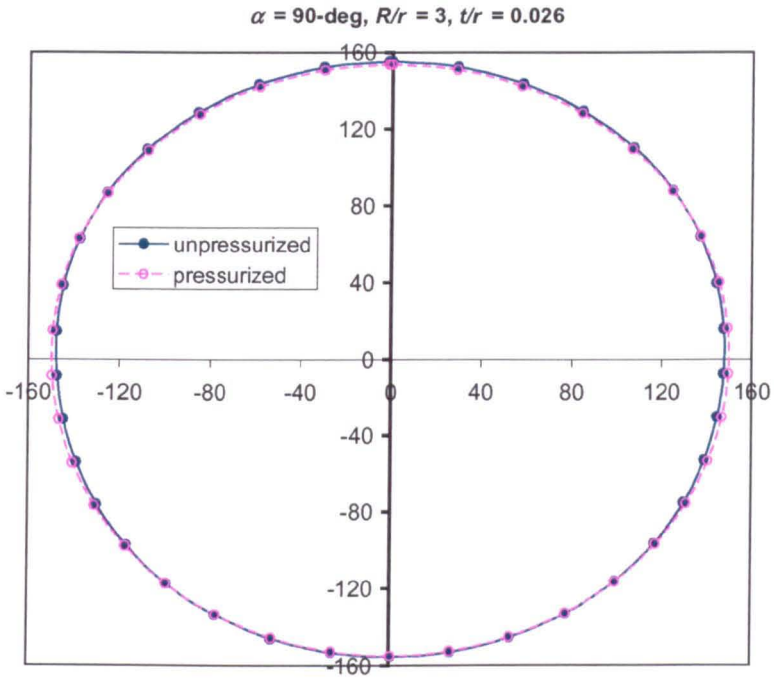

Fig.6.9 Typical pressure reduction effect on cross-sectional negative flattening

Similar to the positive flattening exhibited in Chapter 5, pressure reduction is evaluated here on the radial displacement of the crown node at the mid-section of the bend, where the maximum value is expected to be located. Figure 6.10 shows a typical pressure – negative flattening curve plotted for 90-deg elbow under in-plane opening moment.

In Fig.6.10, the abscissa of 0.0 represents the final load step of moment loading and the start of subsequent internal pressure load. It can be seen that the relation between internal pressure loading and negative flattening is non-linear. This graph again shows the "Haigh effect" [11] where non-linearity is present whenever internal pressure load acts on straight or curved pipes of noncircular cross-section. In this study, internal pressure was applied to pipe elbows with oval cross-section resulting from an in-plane opening moment.

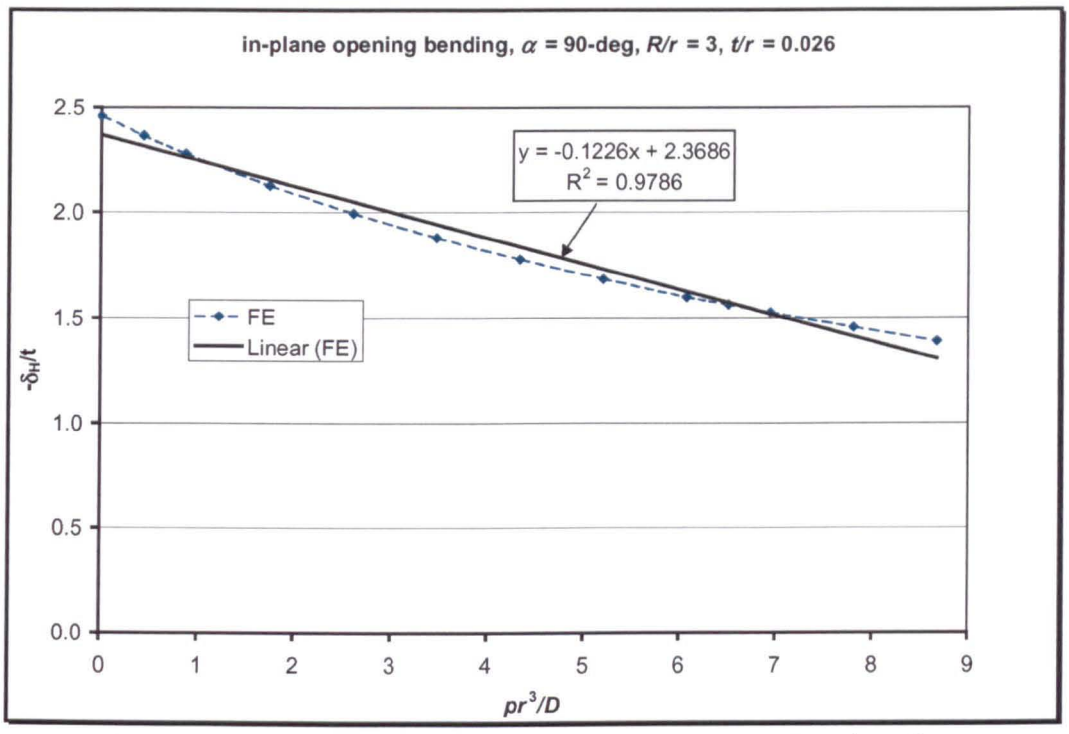

Fig.6.10 Pressure – flattening (negative) curve for a 90-deg pipe elbow

Figure 6.11 through 6.14 show the ovalisation factor for 90-deg pipe elbows plotted against pipe bend parameters for various radius ratios. These figures again show clearly that the effect of the presence of internal pressure is to reduce the ovalisation factor resulting from the in-plane opening moment. The pressure reduction is more pronounced in thin walled piping elbows (low pipe bend parameter). In what follows, the pressure reduction effect on negative ovalisation factor is comprehensively evaluated and empirical formulae are developed and proposed. The procedure of Rodabaugh and George [30] followed in Chapter 5 is again adopted in this section.

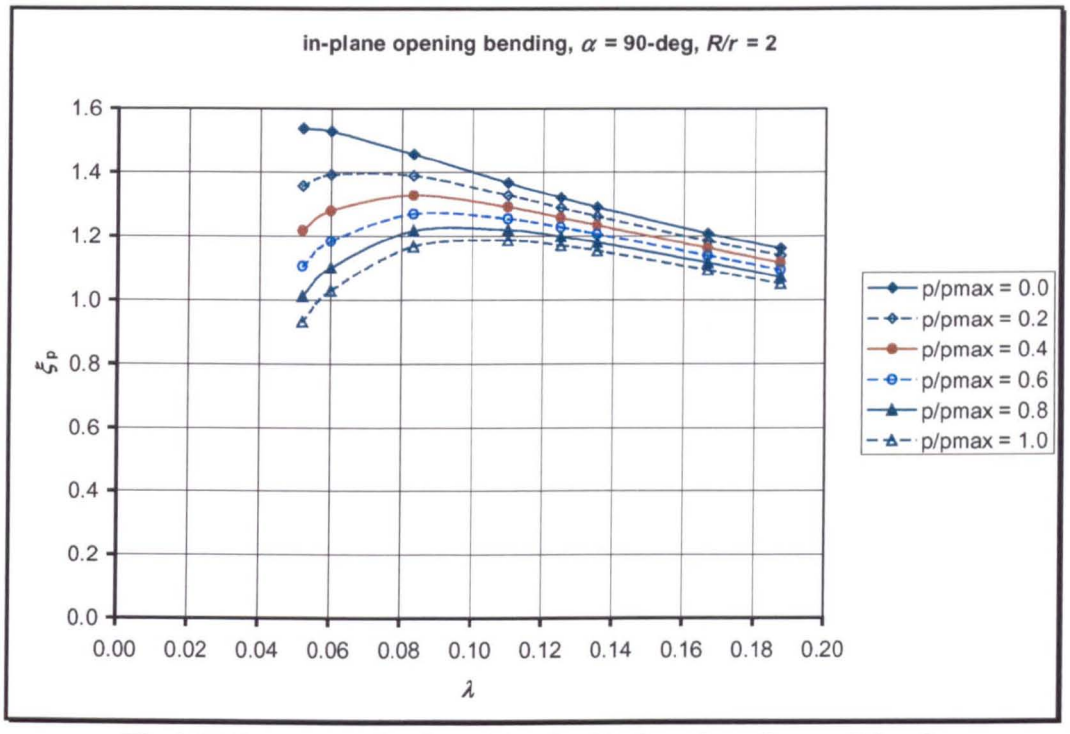

Fig.6.11 Pressure reduction effect for 90-deg pipe elbows: $R/r = 2$

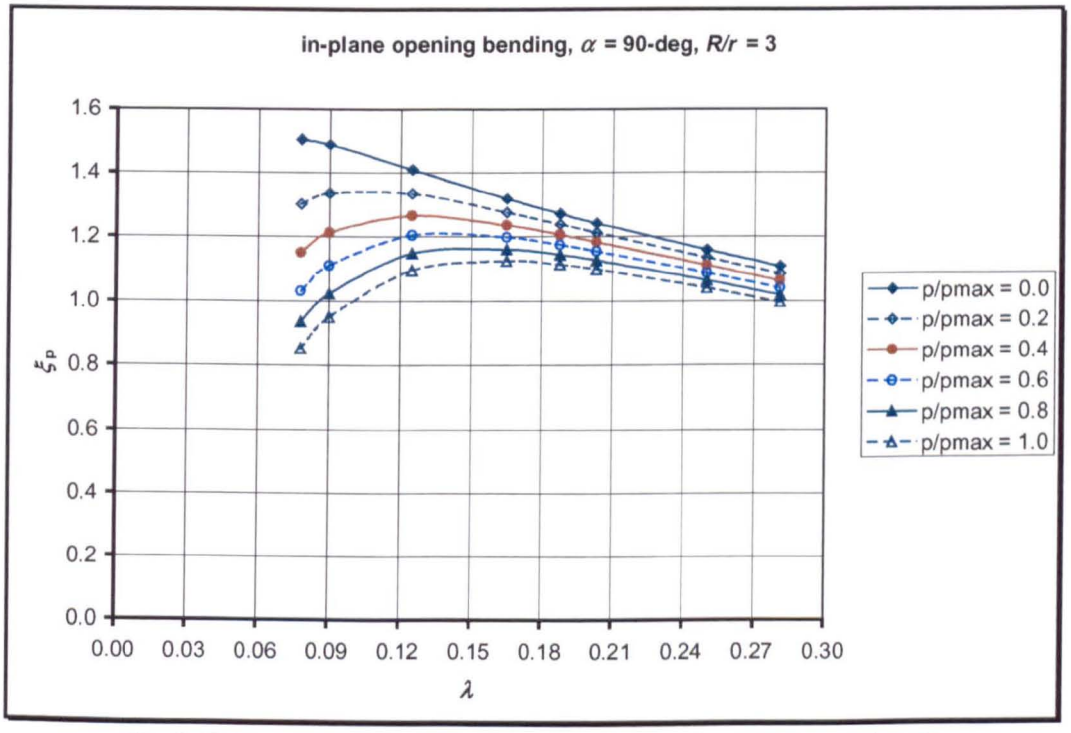

Fig.6.12 Pressure reduction effect for 90-deg pipe elbows: $R/r = 3$

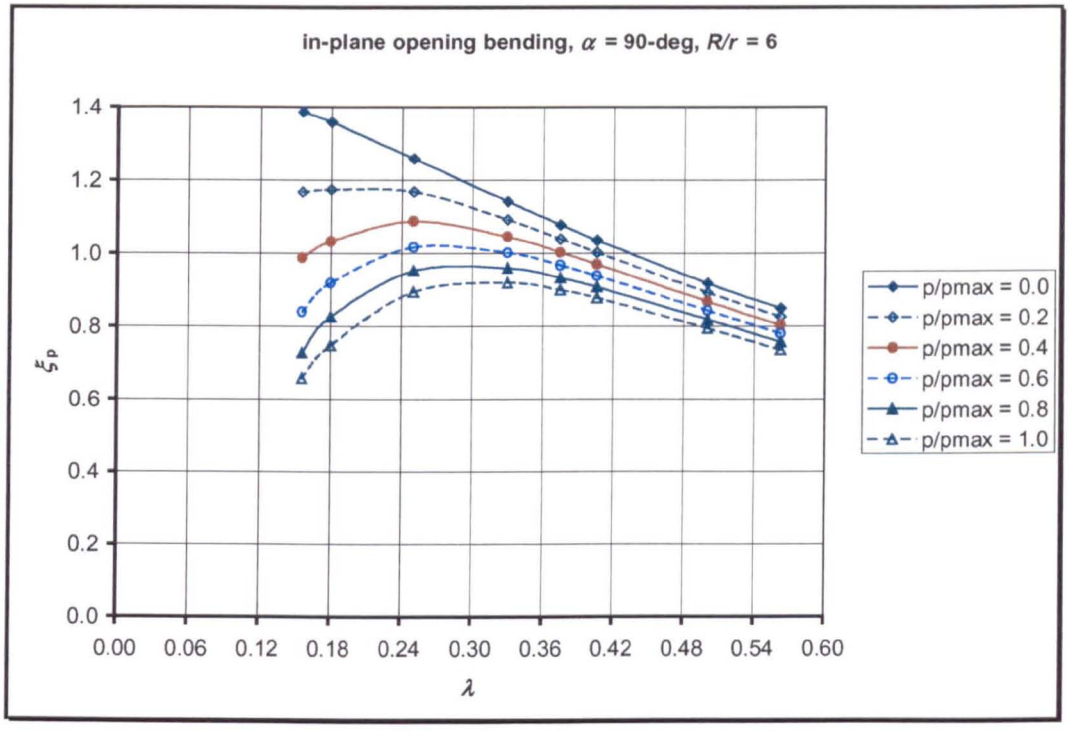

Fig.6.13 Pressure reduction effect for 90-deg pipe elbows: $R/r = 6$

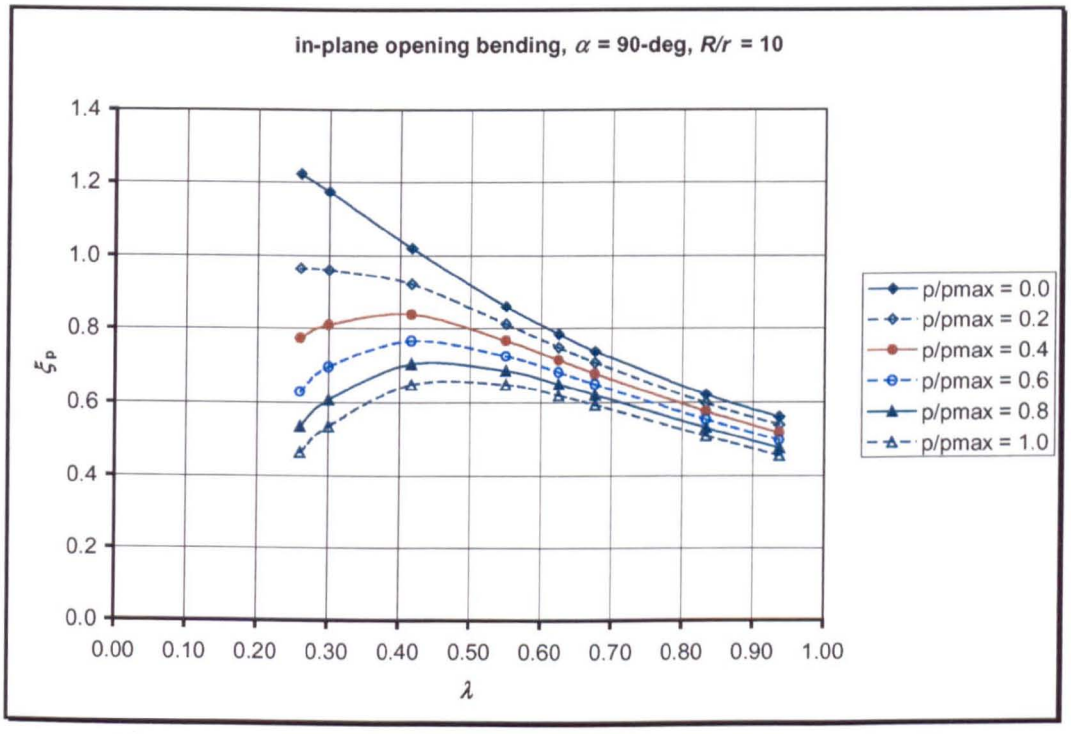

Fig.6.14 Pressure reduction effect for 90-deg pipe elbows: $R/r = 10$

Figure 6.15 and 6.16 show typical pressure reduction effects on the ovalisation factor of 90-deg pipe elbows under in-plane opening moment. These figures are constructed using the relation in equation (5-15) where the pressure reduction effect is written as a function of nondimensionl pressure *p/E,* nondimensional thickness *r/t*, and radius ratio *R/r*.

It can be seen from Fig.6.15 and 6.16 that straight lines in log-log graphs are obtained if the pressure reduction is plotted against non-dimensional pressure *p/E*. There is a slight departure from linearity if the pressure reduction is plotted against nondimensional thickness *r/t* and radius ratio *R/r*. In this study, the pressure reduction effect is approximated by a linear relationship and any error introduced as a result will be assessed and discussed at the end of this chapter. Following careful study of Fig.6.15 and 6.16 and similar plots for all radius ratio and wall thickness (not shown) along with Fig.6.11 through 6.14, the following equation is proposed for the negative ovalisation factor for 90-deg pipe elbows under in-plane opening moment:

$$\xi_p = \frac{\xi}{1 + 76\left(\frac{p}{E}\right)\left(\frac{r}{t}\right)^{5/3}\left(\frac{R}{r}\right)^{0.570}} \qquad \text{for } \alpha = 90\text{-deg} \qquad (6\text{-}12)$$

Equation (6-12) can be directly compared with the corresponding equation for in-plane closing moment as given by equation (5-16) for 90-deg pipe elbows. It can be seen that these equations are markedly different from one to another. They are also markedly different in the coefficient of the pressure reduction – 76 rather than 0.205. Of course, they are also different in the index for *r/t* and *R/r*. By comparing Fig.6.11 through 6.14 with corresponding figures for in-plane closing moment, it can be quickly noted that the magnitude of pressure reduction is bigger for in-plane closing moment.

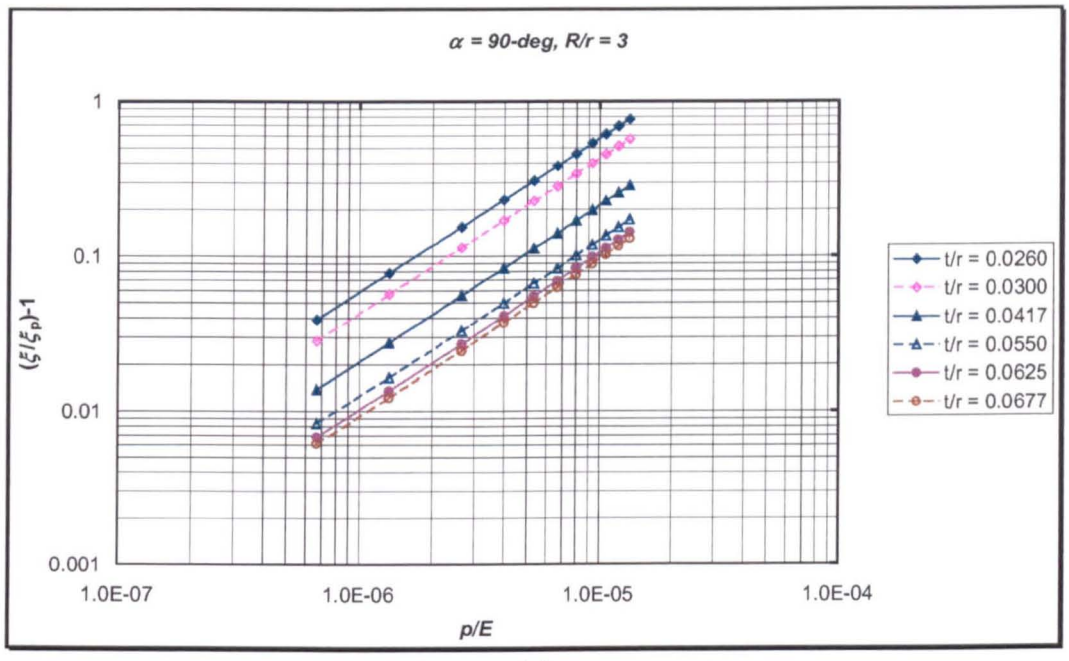

(a)

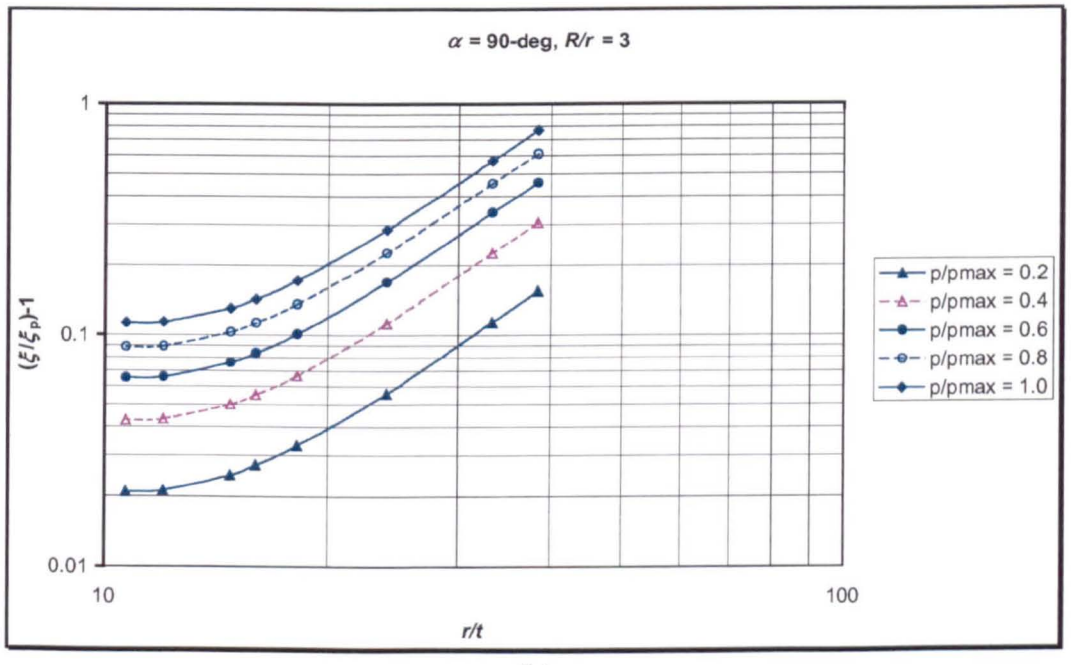

(b)

Fig.6.15 Pressure reduction for constant radius ratio plotted against (a) *p/E*, (b) *r/t*

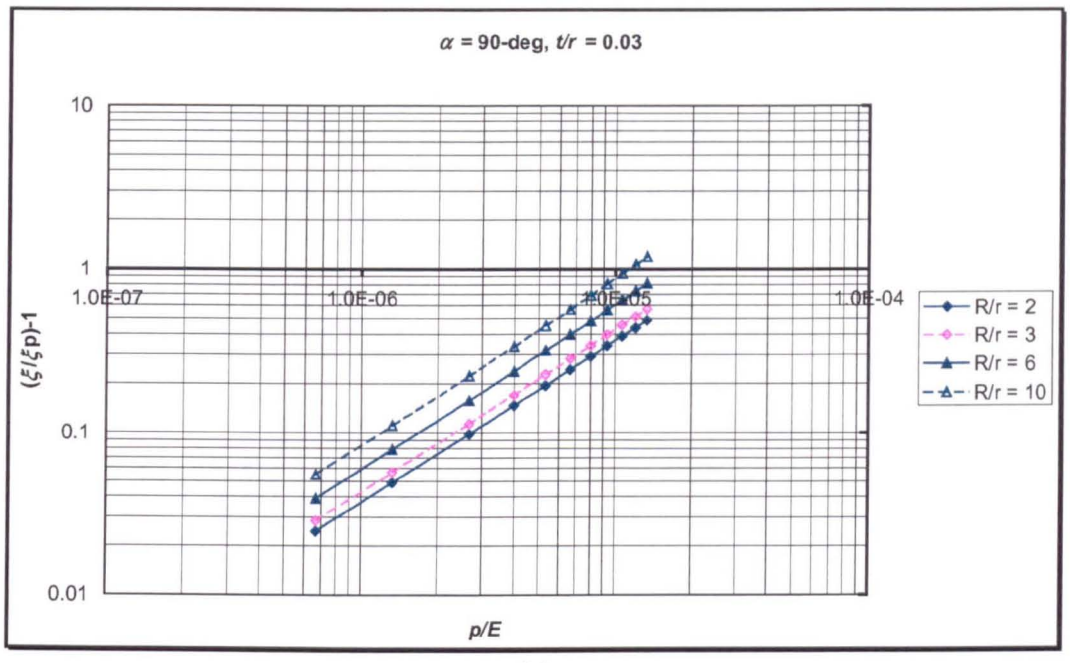

(a)

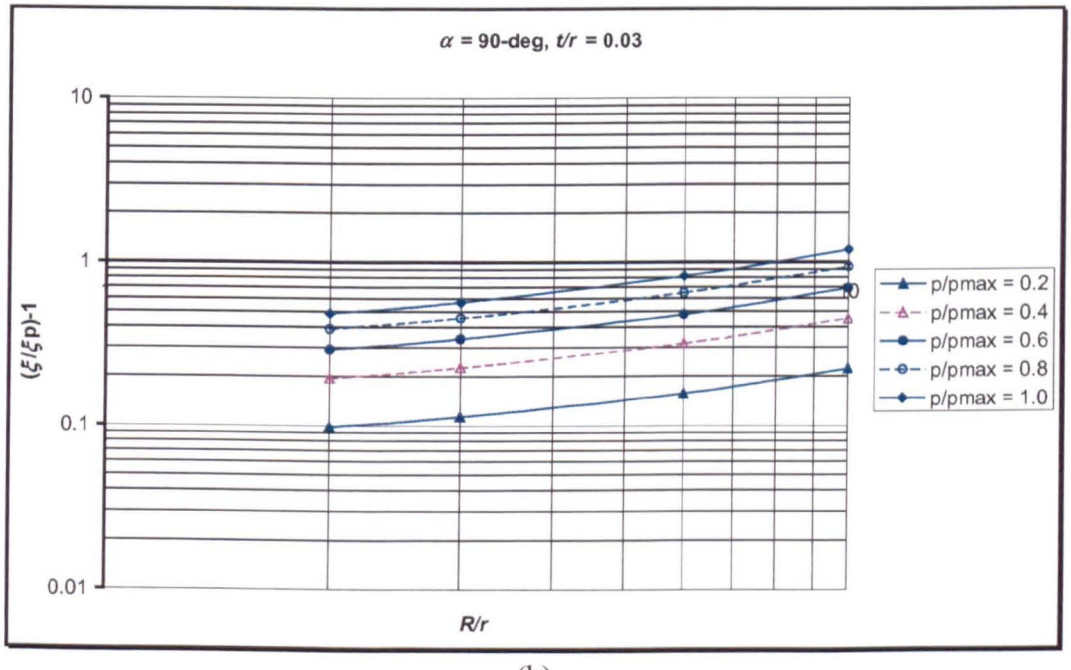

(b)

Fig.6.16 Pressure reduction for constant radius ratio plotted against (a) *p/E*, (b) *R/r*

6.1.3 Effect of Bend Angle on Pressure Reduction

The pressure reduction effect on the ovalisation factor for pipe elbows with different bend angles other than 90-deg can be derived from Fig.A6.1 through A6.5 of Appendix C6. By constructing similar log-log graphs, the following formulae for negative flattening of elbow cross section are proposed:

$$\xi_p = \frac{\xi}{1+175\left(\frac{p}{E}\right)\left(\frac{r}{t}\right)^{5/3}\left(\frac{R}{r}\right)^{0.206}} \qquad \text{for } \alpha = 30\text{-deg} \qquad (6\text{-}13)$$

$$\xi_p = \frac{\xi}{1+126\left(\frac{p}{E}\right)\left(\frac{r}{t}\right)^{5/3}\left(\frac{R}{r}\right)^{0.333}} \qquad \text{for } \alpha = 45\text{-deg} \qquad (6\text{-}14)$$

$$\xi_p = \frac{\xi}{1+100\left(\frac{p}{E}\right)\left(\frac{r}{t}\right)^{5/3}\left(\frac{R}{r}\right)^{0.430}} \qquad \text{for } \alpha = 60\text{-deg} \qquad (6\text{-}15)$$

$$\xi_p = \frac{\xi}{1+52\left(\frac{p}{E}\right)\left(\frac{r}{t}\right)^{5/3}\left(\frac{R}{r}\right)^{0.725}} \qquad \text{for } \alpha = 180\text{-deg} \qquad (6\text{-}16)$$

Equations (6-12) through (6-16) can be expressed in an alternative form by noting that:

$$\left(\frac{r}{t}\right)^{5/3} = \left(\frac{r}{t}\right)^{3} \lambda^{4/3} \left(\frac{r}{R}\right)^{4/3}$$

Using this relation, the negative ovalisation factor of pipe elbows under in-plane opening and internal pressure can be approximated as:

$$\xi_p = \frac{\xi}{1+48.0\left(\frac{pr^3}{3D}\right)\lambda^{4/3}\left(\frac{r}{R}\right)^{1.125}} \qquad \text{for } \alpha = 30\text{-deg} \qquad (6\text{-}17)$$

$$\xi_p = \frac{\xi}{1+34.5\left(\frac{pr^3}{3D}\right)\lambda^{4/3}\left(\frac{r}{R}\right)^{1.005}} \qquad \text{for } \alpha = 45\text{-deg} \qquad (6\text{-}18)$$

$$\xi_p = \frac{\xi}{1+27.5\left(\frac{pr^3}{3D}\right)\lambda^{4/3}\left(\frac{r}{R}\right)^{0.905}} \qquad \text{for } \alpha = 60\text{-deg} \qquad (6\text{-}19)$$

$$\xi_p = \frac{\xi}{1+21.0\left(\frac{pr^3}{3D}\right)\lambda^{4/3}\left(\frac{r}{R}\right)^{0.765}} \qquad \text{for } \alpha = 90\text{-deg} \qquad (6\text{-}20)$$

$$\xi_p = \frac{\xi}{1+14.5\left(\frac{pr^3}{3D}\right)\lambda^{4/3}\left(\frac{r}{R}\right)^{0.610}} \qquad \text{for } \alpha = 180\text{-deg} \qquad (6\text{-}21)$$

Equations (6-12) through (6-21) if necessary might be further simplified with the aims to find the coefficient and the power of radius ratio of the denominator. This simplification will not be processed any further here, since the bend angles considered in this study have covered the need in practical usage.

6.2 Flexibility Factors

The procedure for determining the flexibility factors of piping elbows under in-plane opening moment is similar to those used for in-plane closing moment. The end rotation is obtained from the axial displacement of the extrados and the intrados nodes at the junctions of the bends with the loaded tangent and the fixed tangent. The end rotation of an elbow at the junction with the loaded tangent is defined again as φ_1 and the end rotation of an elbow at the junction with fixed tangent is defined as φ_2. Typical deflection of piping elbows showing end rotation under in-plane opening moment is shown in Fig.6.17.

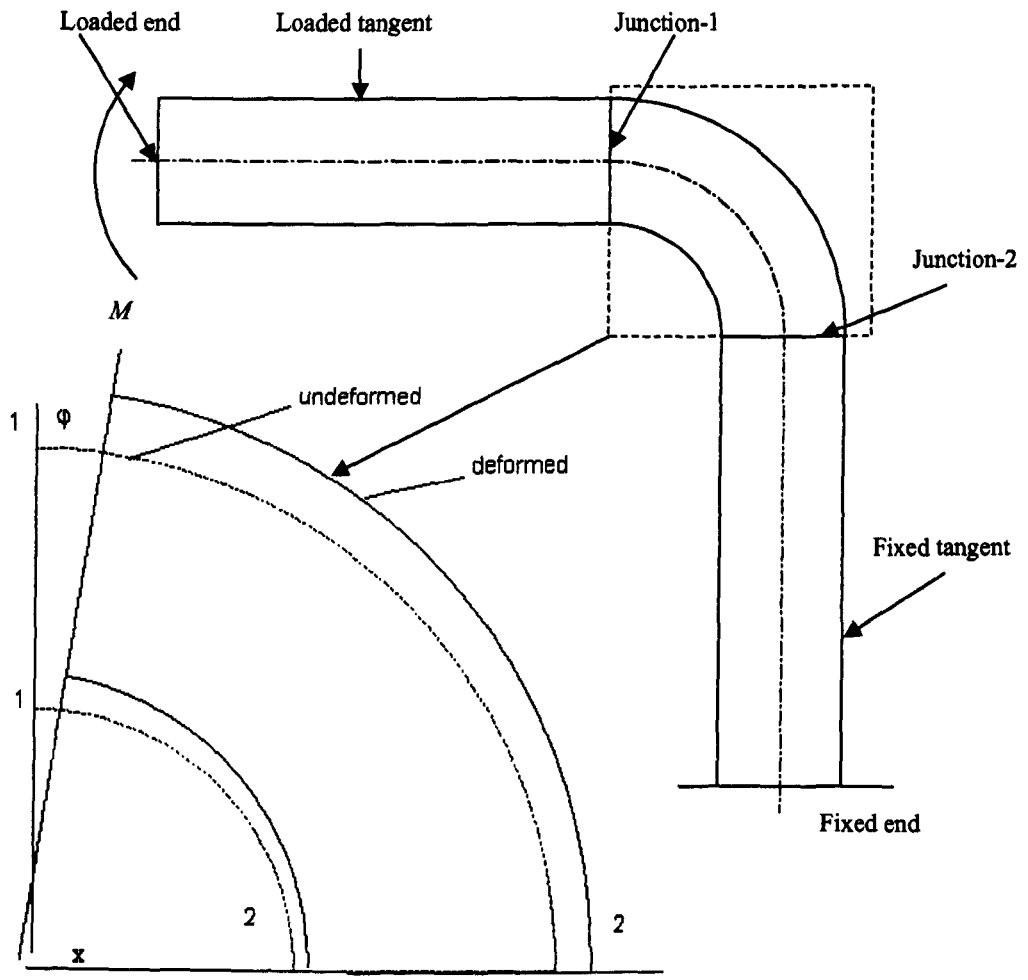

Fig.6.17 Deflection of a pipe elbow under in-plane opening bending

The procedure for determining the end rotation of an elbow under in-plane moment has been fully described in chapter 5. The total end rotation is obtained by subtracting the rotation of section-2 as given by equation (5-29b) from the rotation of section-1as given by equation (5-29a). Typical moment-end rotation curve of an elbow under in-plane opening moment is shown in Fig.6.18.

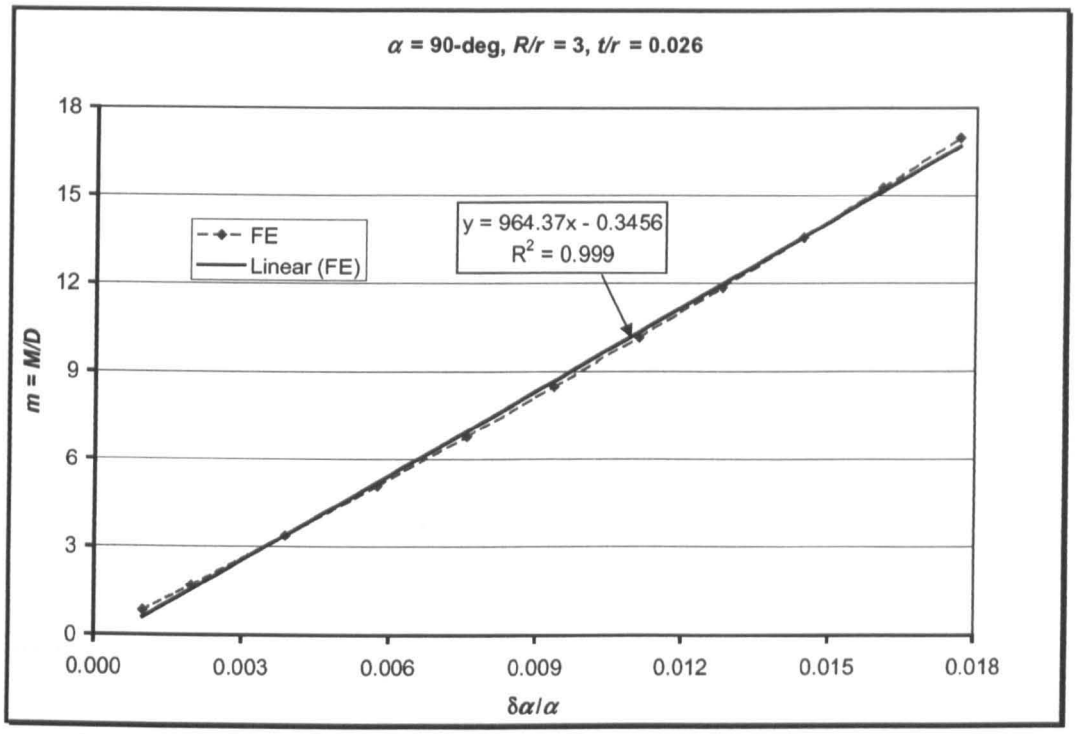

Fig.6.18 Typical moment end rotation curve under in-plane opening bending

Fig.6.18 shows that an elbow subjected to in-plane opening moment exhibits the behaviour of non-linear 'hardening' structures. This figure can be directly compared with Fig.5.25 of chapter 5, where an elbow subjected to an in-plane closing moment exhibits the behaviour of non-linear 'softening' structures.

The flexibility factor is further determined using equation (5-32). Figure 6.19 shows the flexibility factors for 90-deg pipe elbows under an in-plane opening bending. It can be seen from Fig.6.19 that the relation between flexibility factor, k, and pipe bend parameter, λ, is essentially linear in a log-log plot. Accordingly the flexibility factor for in-plane opening bending can be expressed in form of equation (5-33). Figure 6.19 also shows that the flexibility factor can be represented accurately by a single curve as only a function of pipe bend parameter, λ, and less dependent on radius ratio, R/r.

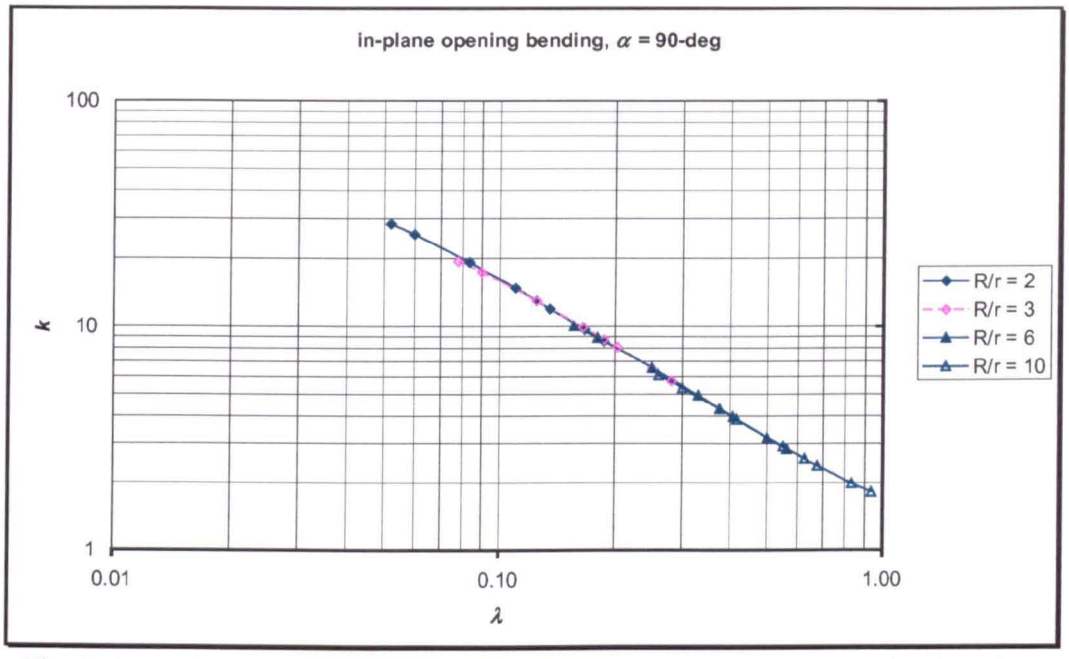

Fig.6.19 Flexibility factor for 90-deg pipe elbows under in-plane opening bending

An expression for the flexibility factor of 90-deg pipe elbows under in-plane opening moment can be derived from Fig.6.19. By curve fitting, the flexibility factor for 90-deg pipe elbows under an in-plane opening moment can be approximated by:

$$k = \frac{1.82}{\lambda^{0.94}} \qquad \text{for } \rho = 2 \qquad (6-22)$$

$$k = \frac{1.75}{\lambda^{0.95}} \qquad \text{for } \rho = 3 \qquad (6-23)$$

$$k = \frac{1.62}{\lambda^{0.99}} \qquad \text{for } \rho = 6 \qquad (6-24)$$

$$k = \frac{1.66}{\lambda^{0.96}} \qquad \text{for } \rho = 10 \qquad (6-25)$$

Equations (6-22) through (6-25) are not suitable for design purposes. However these equations can be expressed in form of equation (5-38). Following the procedure of Fujimoto and Soh [92], equations (6-22) through (6-25) can be written in the following form:

$$k = \frac{1.65}{\lambda}[1.0926 + 0.0584\ln(\lambda)] \qquad \text{for } \rho = 2 \qquad (6\text{-}26)$$

$$k = \frac{1.65}{\lambda}[1.058 + 0.0475\ln(\lambda)] \qquad \text{for } \rho = 3 \qquad (6\text{-}27)$$

$$k = \frac{1.65}{\lambda}[0.98 + 0.0077\ln(\lambda)] \qquad \text{for } \rho = 6 \qquad (6\text{-}28)$$

$$k = \frac{1.65}{\lambda}[1.0084 + 0.0385\ln(\lambda)] \qquad \text{for } \rho = 10 \qquad (6\text{-}29)$$

The term outside the square bracket is the asymptotic solution of Clark and Reissner [20] as adopted in the current design piping code [114, 120], while the terms in the square bracket show the dependency of flexibility factor on radius ratio. It can be quickly noted from these equations that the term in the square bracket for 90-deg pipe elbow is not significant. Figure 6.20 shows plots of flexibility factor obtained from finite element in comparison with the derived formulae. It can be seen that the proposed equations fit well the results from finite element.

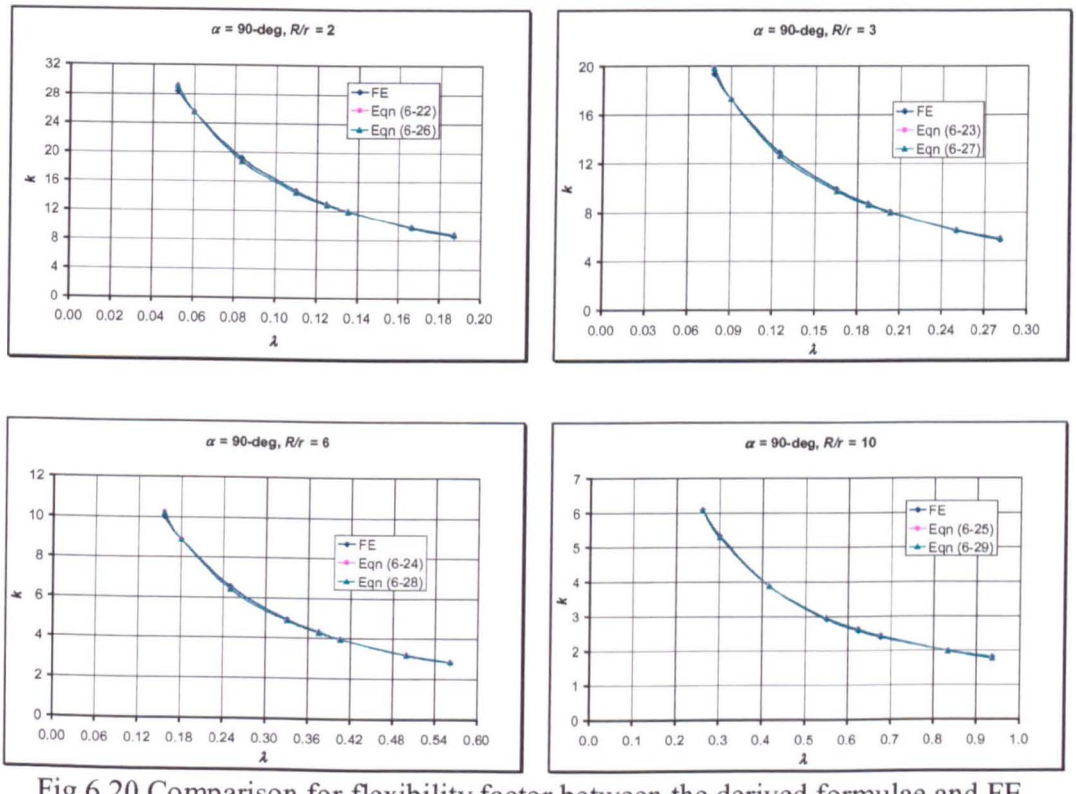

Fig.6.20 Comparison for flexibility factor between the derived formulae and FE

6.2.1 Effect of Bend Angle on Flexibility Factors

To account for the effect of bend angle on flexibility factor due to in-plane opening bending, pipe elbows of bend angles 30, 45, 60, 90, and 180-deg have been investigated. It is expected that the effect of bend angle on flexibility factor is of significance, since a pipe elbow would tend to behave as a straight pipe as the bend angle approaches hypothetically zero. Figure 6.21 through 6.24 show the flexibility factor for pipe elbows of various bend angles:

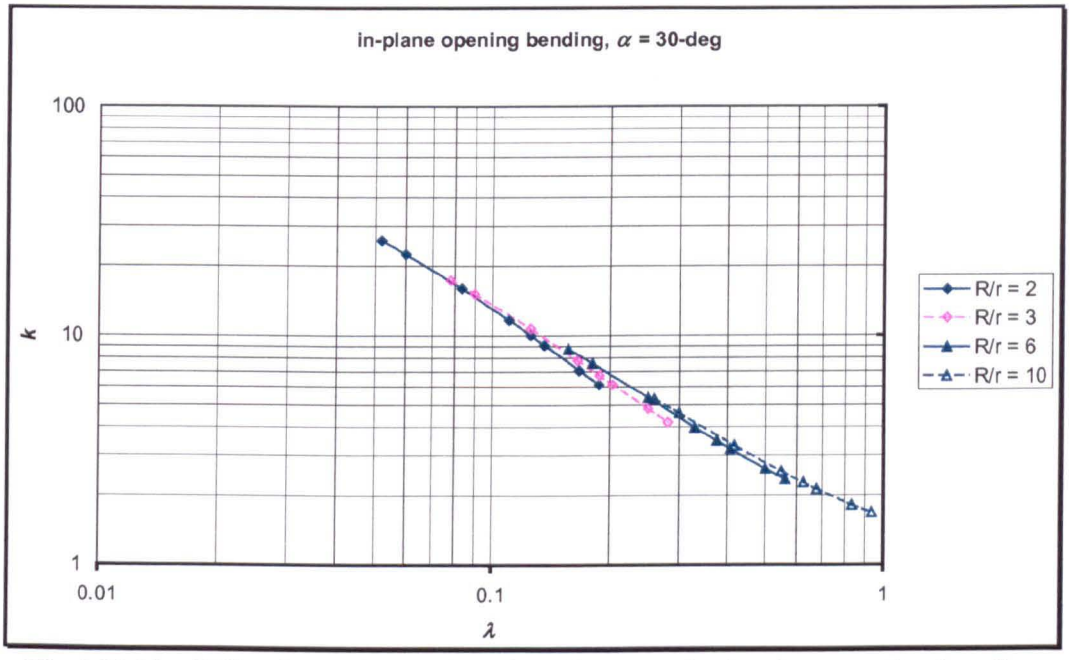

Fig.6.21 Flexibility factor for 30-deg pipe elbows under in-plane opening bending

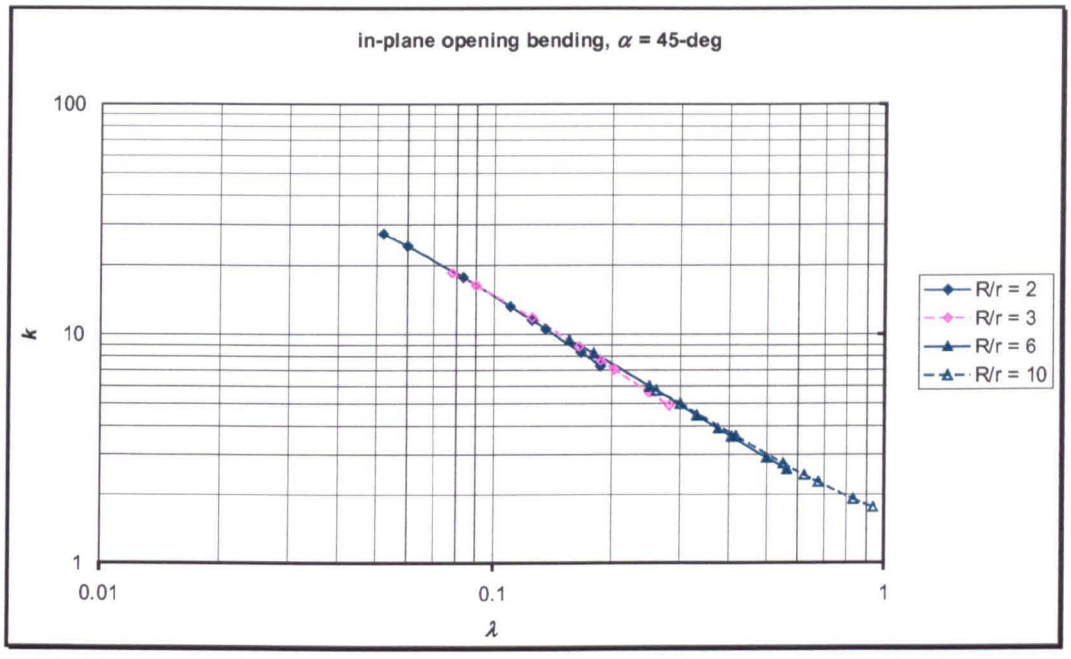

Fig.6.22 Flexibility factor for 45-deg pipe elbows under in-plane opening bending

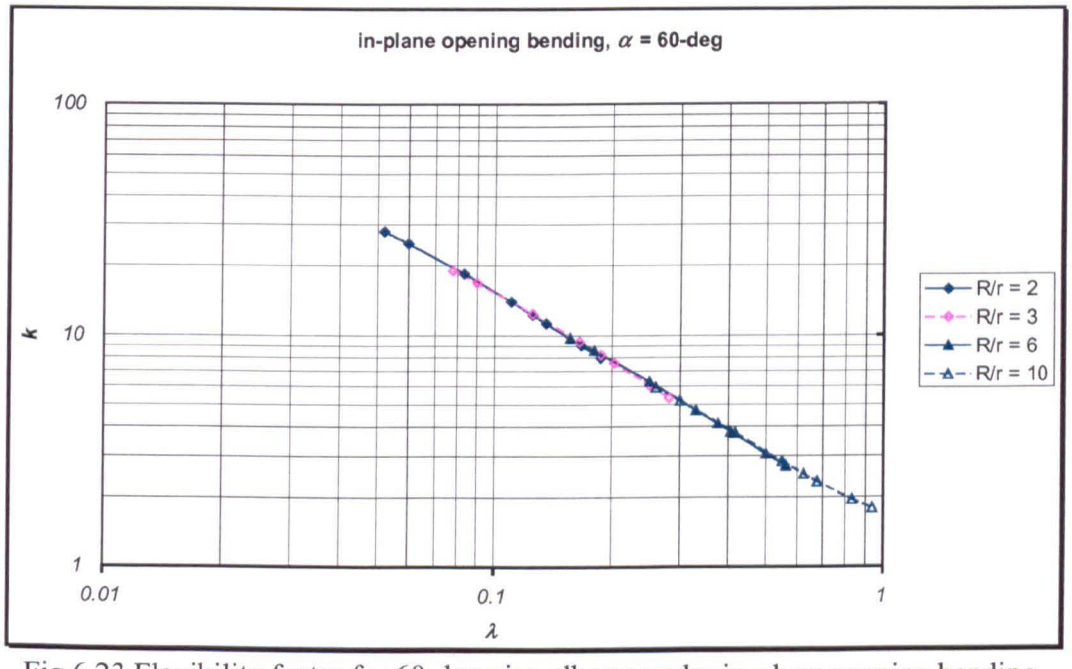

Fig.6.23 Flexibility factor for 60-deg pipe elbows under in-plane opening bending

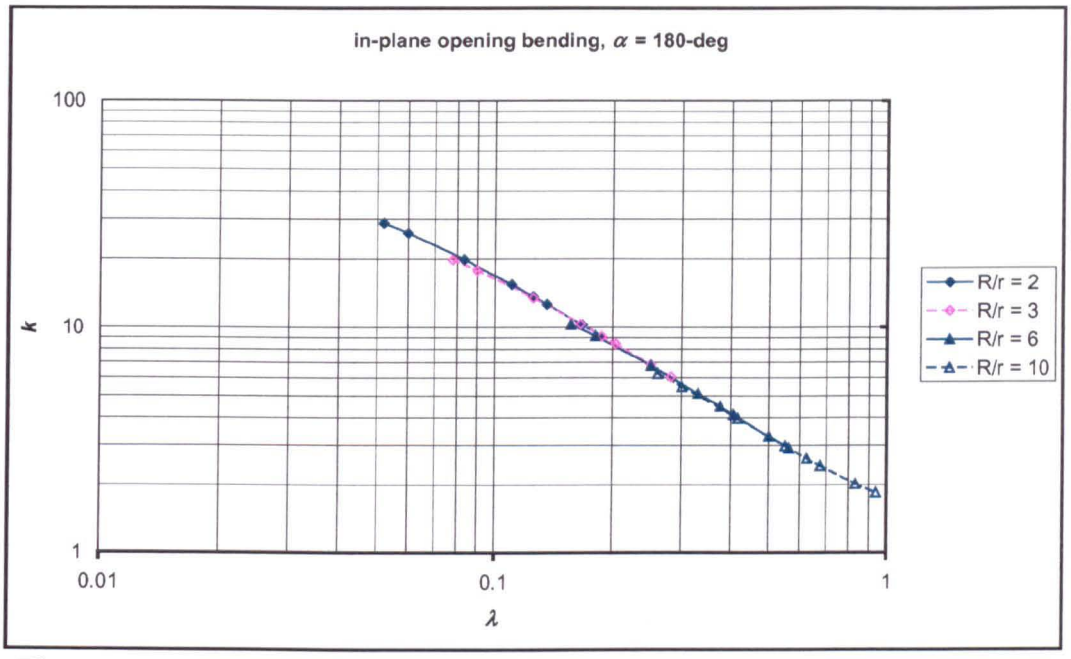

Fig.6.24 Flexibility factor for 180-deg pipe elbows under in-plane opening bending

Approximate formulae for flexibility factors can now be obtained from these figures by curve fitting and the results are given in the following form:

$$k = \frac{1.65}{\lambda}[a - b\ln(\lambda)] \qquad (6\text{-}30)$$

where the coefficient 'a' and 'b' are a functions of radius ratio R/r as summarised in Table 6.3 and 6.4 respectively.

Table 6.3 Values for coefficient '*a*' in equation (6-30) for various bend angles

R/r	*Bend angle, α*				
	30-deg	45-deg	60-deg	90-deg	180-deg
2	0.5483	0.8000	0.9438	1.0926	1.2190
3	0.6131	0.8140	0.9352	1.0580	1.1480
4	0.6797	0.8360	0.9268	1.0217	1.0931
5	0.7307	0.8566	0.9250	0.9980	1.0497
6	0.7690	0.8735	0.9280	0.9800	1.0215
7	0.8149	0.8993	0.9358	0.9770	1.0007
8	0.8509	0.9214	0.9484	0.9797	0.9951
9	0.8840	0.9440	0.9658	0.9912	1.0021
10	0.9220	0.9700	0.9900	1.0084	1.0266

Table 6.4 Values for coefficient '*b*' in equation (6-30) for various bend angles

R/r	*Bend angle, α*				
	30-deg	45-deg	60-deg	90-deg	180-deg
2	0.0961	0.0286	-0.0135	-0.0584	-0.0970
3	0.0865	0.0304	-0.0076	-0.0475	-0.0750
4	0.0613	0.0300	0.0009	-0.0261	-0.0466
5	0.0391	0.0247	0.0029	-0.0156	-0.0290
6	0.0305	0.0120	0.0020	-0.0077	-0.0144
7	-0.0053	0.0039	-0.0051	-0.0096	-0.0124
8	-0.0275	-0.0116	-0.0151	-0.0141	-0.0134
9	-0.0497	-0.0305	-0.0291	-0.0236	-0.0206
10	-0.0719	-0.0581	-0.0472	-0.0385	-0.0316

It can be inferred from these Tables that the terms in the square bracket of equation (6-30) could be neglected for pipe elbows of large angle and long radius bend without any significant loss in accuracy.

6.2.2 Pressure Reduction Effect

It has been shown in Chapter 5 that pipe elbows subjected to in-plane closing moment exhibit non-linear structural 'softening' behaviour. The pressure reduction effect was studied and various formulae developed. It has also been shown earlier in this chapter that pipe elbows subjected to in-plane opening moment exhibit non-linear structural 'hardening' behaviour. It is expected that the pressure reduction effect would be different for the in-plane closing and opening cases. In this section, the pressure reduction effect on the flexibility factor for pipe elbows subjected to opening moment is studied and once more approximate formulae developed. The same procedure as in previous sections for assessing the pressure reduction effect is also followed.

A typical pressure-end rotation curve is shown in Fig.6.25. It has been plotted for a 90-deg pipe elbow having a radius ratio of three. The abscissa of 0.0 represents the final load step of opening moment loading and the start of the subsequent internal pressure loading.

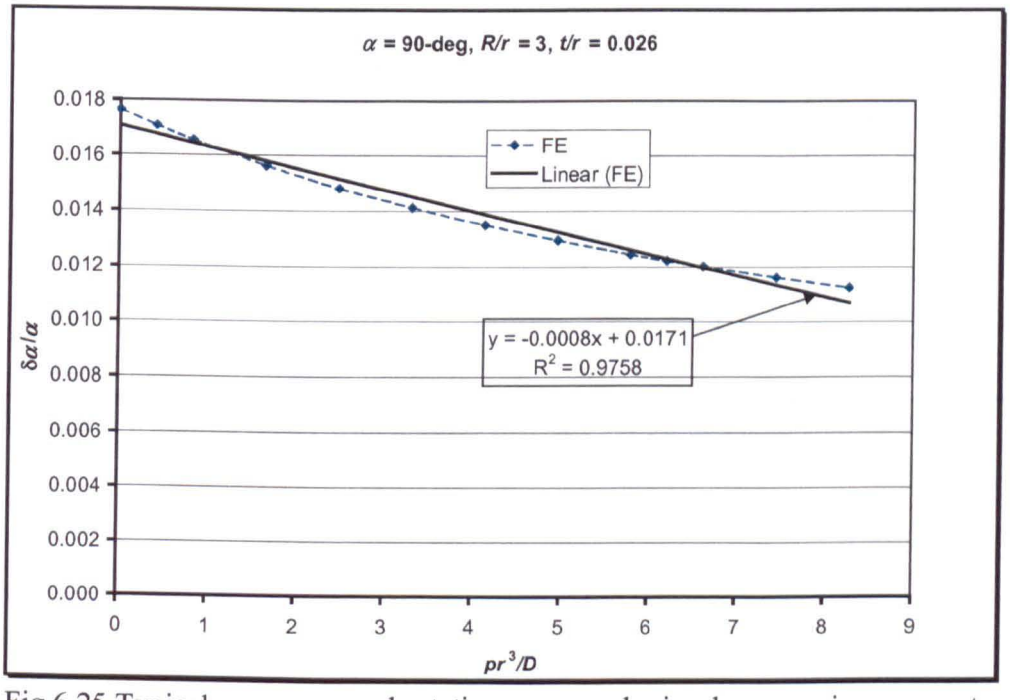

Fig.6.25 Typical pressure – end rotation curve under in-plane opening moment

It can be seen from Fig.6.25 that the relation between internal pressure and end rotation is again non-linear. This figure clearly shows the Haigh effect [11] where high non-linearity apparent when internal pressure acts on a pipe of noncircular cross section. In this case, the internal pressure loading has been applied to an elbow ovalised due to in-plane opening moment.

Figure 6.26 through 6.29 show the flexibility factor for 90-deg pipe elbows plotted against pipe bend parameters for various radius ratios. Once more it can be seen that internal pressure reduces the flexibility factor (stiffening effect) for thin-walled pipe elbows and increasing the flexibility factors (weakening effect) for thick-walled pipe elbows.

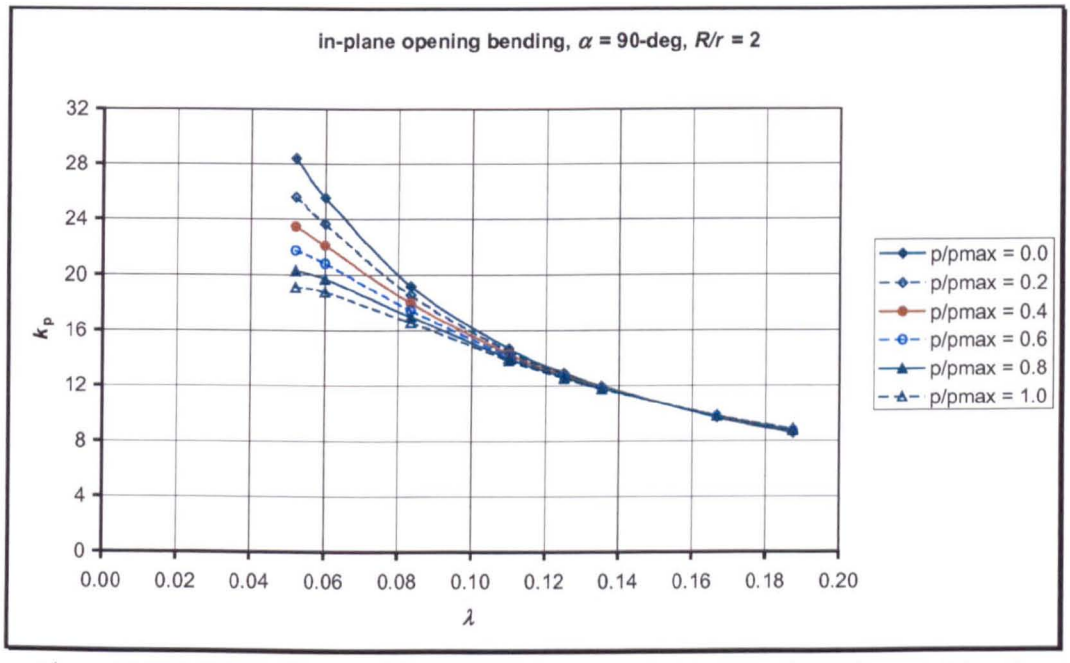

Fig.6.26 Flexibility factor with internal pressure for 90-deg pipe elbows: $R/r = 2$

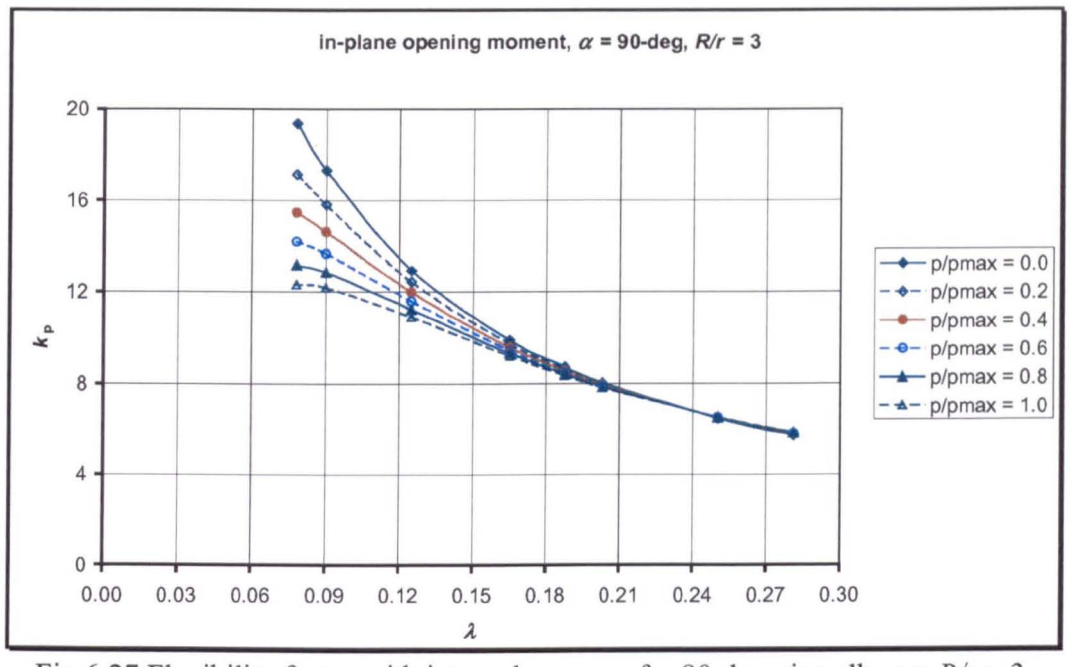

Fig.6.27 Flexibility factor with internal pressure for 90-deg pipe elbows: $R/r = 3$

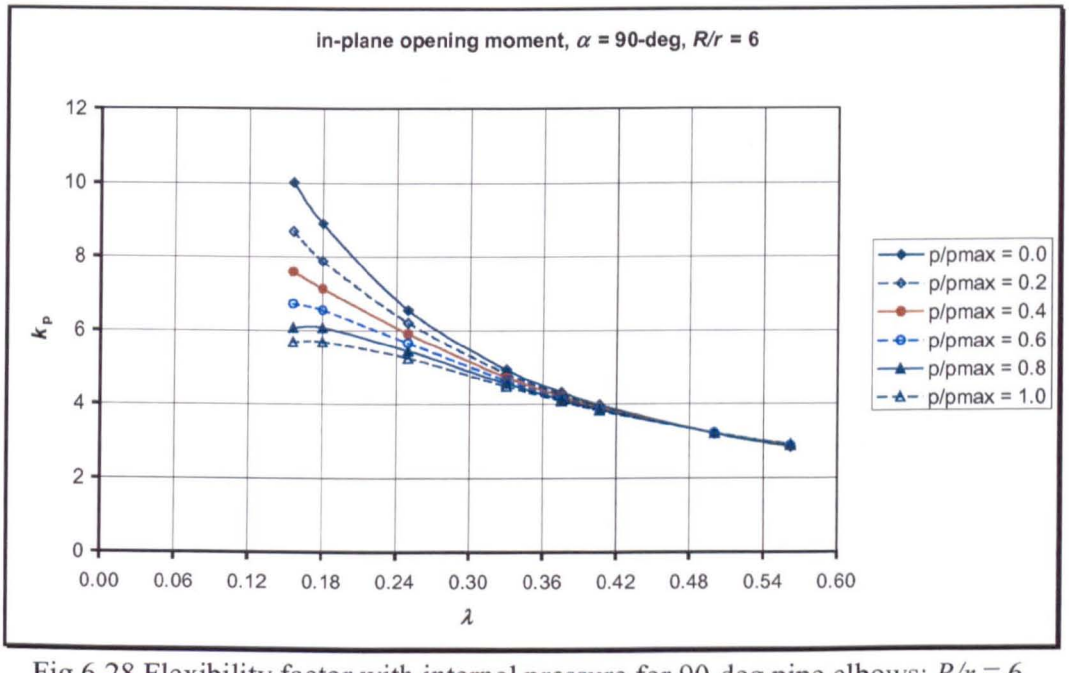

Fig.6.28 Flexibility factor with internal pressure for 90-deg pipe elbows: $R/r = 6$

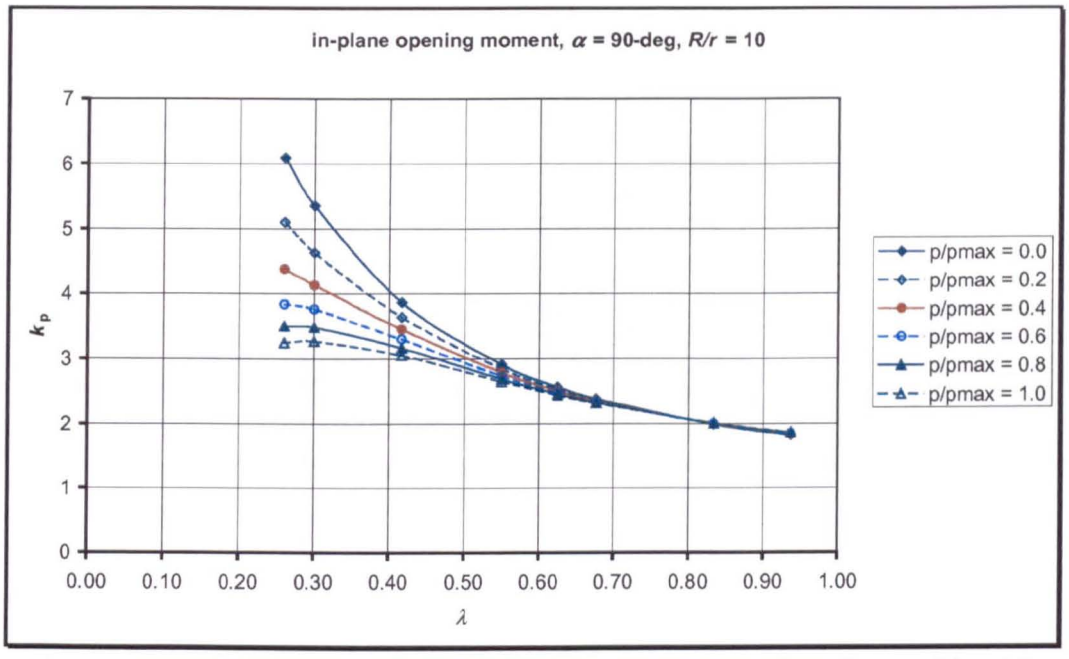

Fig.6.29 Flexibility factor with internal pressure for 90-deg pipe elbows: $R/r = 10$

Pressure reduction effect in line with equation (5-45) can be obtained from Fig.6.26 through 6.29. If the pressure reductions are plotted against p/E and r/t for a constant radius ratio, similar plots to Fig.5.17 will be obtained. For certain value of thickness to cross-section radius ratio, equation (5-45) produces negative values.

A typical plot of flexibility factor against pressure, in line with equation (5-45) is shown for 90-deg pipe elbows using a log-log graph in Fig.6.30 for constant radius ratio and in Fig.6.31 for constant thickness. Straight lines are again obtained. Linear relations are also obtained for the plot of pressure reduction effect against radius ratio, R/r. A small deviation from linearity can be seen if the pressure reduction is plotted against r/t. It should be noted that only positive values produced by equation (5-45) are plotted in these Figures, because negative values cannot be plotted in a log-log graph. As indicated by Fig.6.26 through 6.29, there is a value of r/t where internal pressure no longer reduces the flexibility factor but increases it, produces a negative value of equation (5-45). For 90-deg pipe elbows as shown in Fig.6.26 through 6.29, the values of r/t where internal pressure effect on flexibility factor changes from reduction effect to increasing effect is at about 12.35.

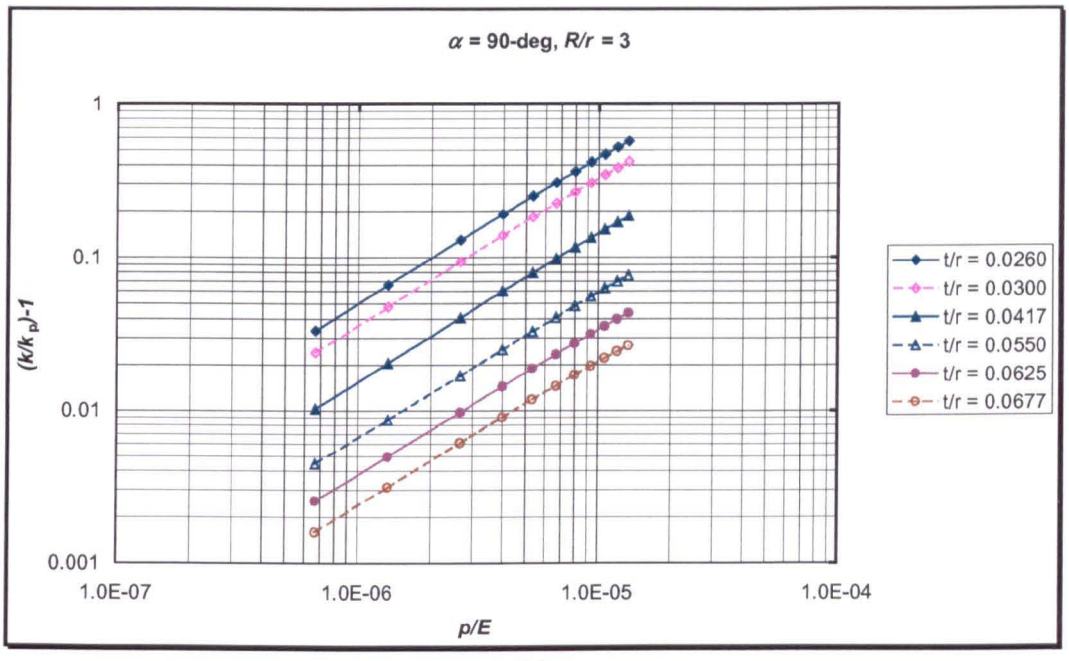

(a)

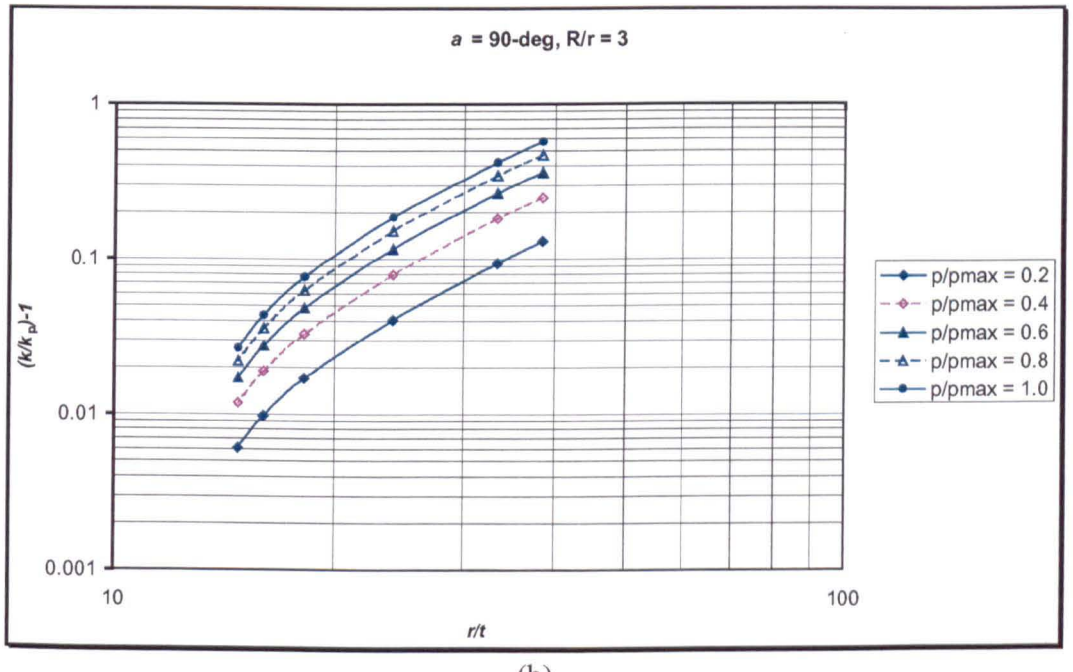

(b)

Fig.6.30 Pressure reduction for constant radius ratio plotted against (a) *p/E*, (b) *r/t*

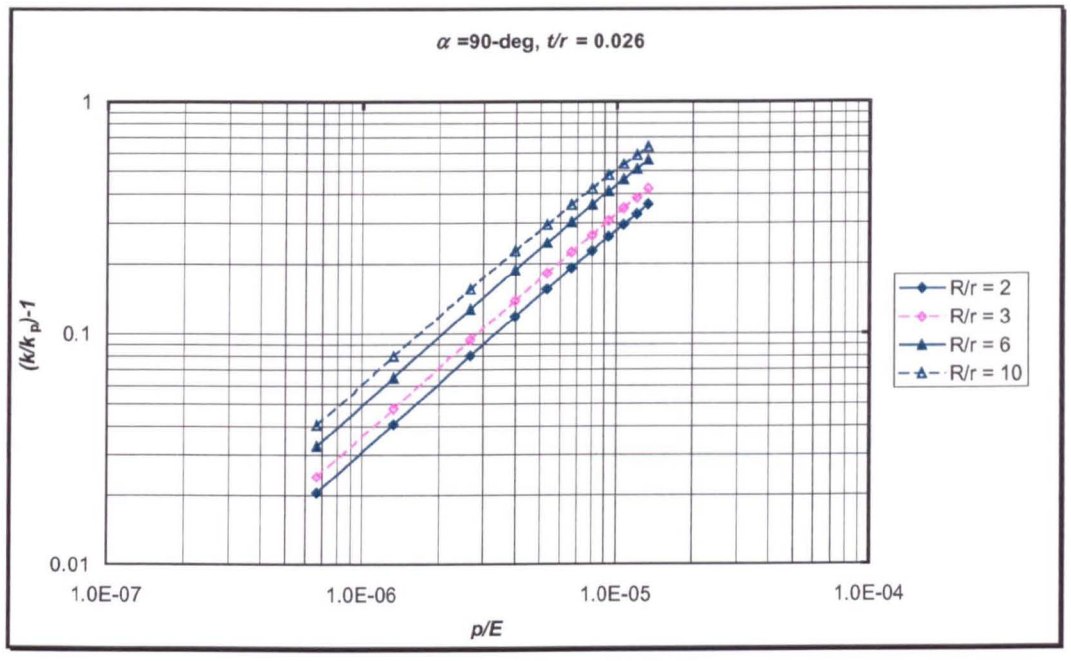

(a)

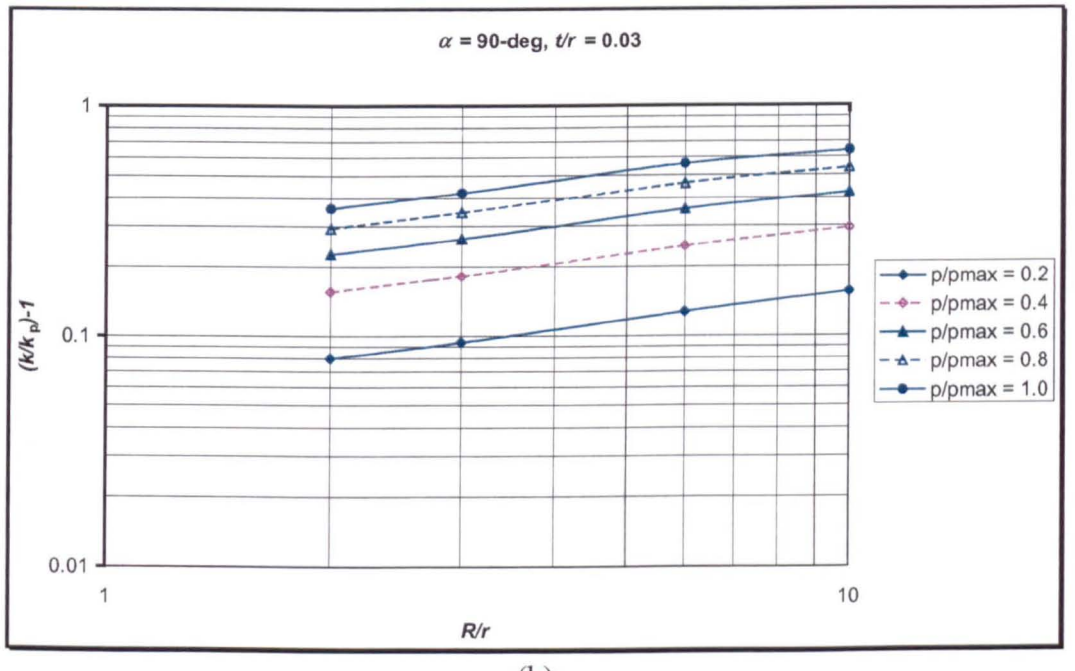

(b)

Fig.6.31 Pressure reduction at constant thickness plotted against (a) p/E, (b) R/r

Study of Fig.6.30 and 6.31 and similar plots for all radius ratio and thickness (not shown) along with Fig.6.26 through 6.29, suggests the following formula for the flexibility factors for 90-deg pipe elbows under in-plane opening moment:

$$k_p = \frac{k}{1+0.145\left(\frac{p}{E}\right)\left(\frac{r}{t}\right)^{10/3}\left(\frac{R}{r}\right)^{0.376}} \qquad \text{for} \frac{r}{t} > 12.35 \qquad (6\text{-}31)$$

where k is flexibility factor in the absence of internal pressure as given by equation (6-30) for in-plane opening moment. The limitation of equation (6-31) obtained from Fig.6.26 through 6.29. Equation (6-31) need to be modified for values of r/t less than 12.35. This will be subjected to further research.

6.2.3 Effect of Bend Angle on Pressure Reduction

It has been shown in Chapter 5 that the pressure reduction effect on flexibility factors is very much influenced by the angle of the bend for the case of in-plane closing moment. This effect is investigated as before for in-plane opening moment.

The same procedure is applied for all bend angles. By constructing log-log graphs for pressure reduction corresponding to equation (5-45) using the data of Fig.A6.6 through A6.10 of Appendix C6, flexibility factors which include internal pressure effect for various bend angles are proposed as follows:

$$k_p = \frac{k}{1+0.300\left(\frac{p}{E}\right)\left(\frac{r}{t}\right)^{10/3}\left(\frac{R}{r}\right)^{0.037}} \qquad \text{for} \begin{cases} \alpha = 30\text{-deg} \\ \frac{r}{t} > 13.11 \end{cases} \qquad (6\text{-}32)$$

$$k_p = \frac{k}{1+0.225\left(\frac{p}{E}\right)\left(\frac{r}{t}\right)^{10/3}\left(\frac{R}{r}\right)^{0.174}} \qquad \text{for} \begin{cases} \alpha = 45-\text{deg} \\ \frac{r}{t} > 12.47 \end{cases} \qquad (6\text{-}33)$$

$$k_p = \frac{k}{1+0.185\left(\frac{p}{E}\right)\left(\frac{r}{t}\right)^{10/3}\left(\frac{R}{r}\right)^{0.266}} \quad \text{for} \begin{cases} \alpha = 60-\text{deg} \\ \frac{r}{t} > 12.42 \end{cases} \tag{6-34}$$

$$k_p = \frac{k}{1+0.115\left(\frac{p}{E}\right)\left(\frac{r}{t}\right)^{10/3}\left(\frac{R}{r}\right)^{0.481}} \quad \text{for} \begin{cases} \alpha = 180-\text{deg} \\ \frac{r}{t} > 12.22 \end{cases} \tag{6-35}$$

As previously, an alternative expression can be obtained by noting that:

$$\left(\frac{r}{t}\right)^{10/3} = \left(\frac{r}{t}\right)^{3}\left(\frac{1}{\lambda}\right)^{1/3}\left(\frac{R}{r}\right)^{1/3}$$

Using this relation, flexibility factors for piping elbows under the action of bending and internal pressure can be further written in the following form:

$$k_p = \frac{k}{1+0.084\left(\frac{pr^3}{3D}\right)\left(\frac{1}{\lambda}\right)^{1/3}\left(\frac{R}{r}\right)^{0.370}} \quad \text{for} \begin{cases} \alpha = 30-\text{deg} \\ \frac{r}{t} > 13.11 \end{cases} \tag{6-36}$$

$$k_p = \frac{k}{1+0.062\left(\frac{pr^3}{3D}\right)\left(\frac{1}{\lambda}\right)^{1/3}\left(\frac{R}{r}\right)^{0.507}} \quad \text{for} \begin{cases} \alpha = 45-\text{deg} \\ \frac{r}{t} > 12.47 \end{cases} \tag{6-37}$$

$$k_p = \frac{k}{1+0.051\left(\frac{pr^3}{3D}\right)\left(\frac{1}{\lambda}\right)^{1/3}\left(\frac{R}{r}\right)^{0.599}} \quad \text{for} \begin{cases} \alpha = 60-\text{deg} \\ \frac{r}{t} > 12.42 \end{cases} \tag{6-38}$$

$$k_p = \frac{k}{1+0.040\left(\frac{pr^3}{3D}\right)\left(\frac{1}{\lambda}\right)^{1/3}\left(\frac{R}{r}\right)^{0.709}} \quad \text{for} \begin{cases} \alpha = 90-\text{deg} \\ \frac{r}{t} > 12.35 \end{cases} \tag{6-39}$$

$$k_p = \frac{k}{1+0.031\left(\frac{pr^3}{3D}\right)\left(\frac{1}{\lambda}\right)^{1/3}\left(\frac{R}{r}\right)^{0.814}} \quad \text{for} \begin{cases} \alpha = 180-\text{deg} \\ \frac{r}{t} > 12.22 \end{cases} \tag{6-40}$$

The formulae in equation (6-22) through (6-31) if necessary, can be further simplified into the following forms:

$$k_p = \frac{k}{1 \pm A(\alpha)\left(\frac{p}{E}\right)\left(\frac{r}{t}\right)^{10/3}\left(\frac{R}{r}\right)^{m(\alpha)}}$$

$$k_p = \frac{k}{1 \pm B(\alpha)\left(\frac{pr^3}{3D}\right)\left(\frac{1}{\lambda}\right)^{1/3}\left(\frac{R}{r}\right)^{n(\alpha)}}$$

where A, B, m, and n are a function of bend angle α. This simplification will not be processed further here, as the bend angles considered have covered the pipe elbows in practical usage.

6.3 Stress-Intensification Factors

Stress-intensification factors for unpressurized and pressurized pipe elbows under in-plane closing moment have been studied in chapter 5 and simple design formulae were developed. In this section, similar formulae for stress-intensification factor for pipe elbows under in-plane opening moment are derived. The nature of the pressure reduction effect is then assessed. The effect of bend angle on stress-intensification factors of unpressurized and pressurized elbows is once more specifically examined.

Typical stress contour plots of pipe elbows under in-plane opening moment are shown in Fig.6.32 for longitudinal stress and Fig.6.33 for circumferential (hoop) stress. These figures are obtained for a 90-deg pipe elbow having radius ratio R/r equals three and thickness to cross-section radius ratio t/r equal to 0.026.

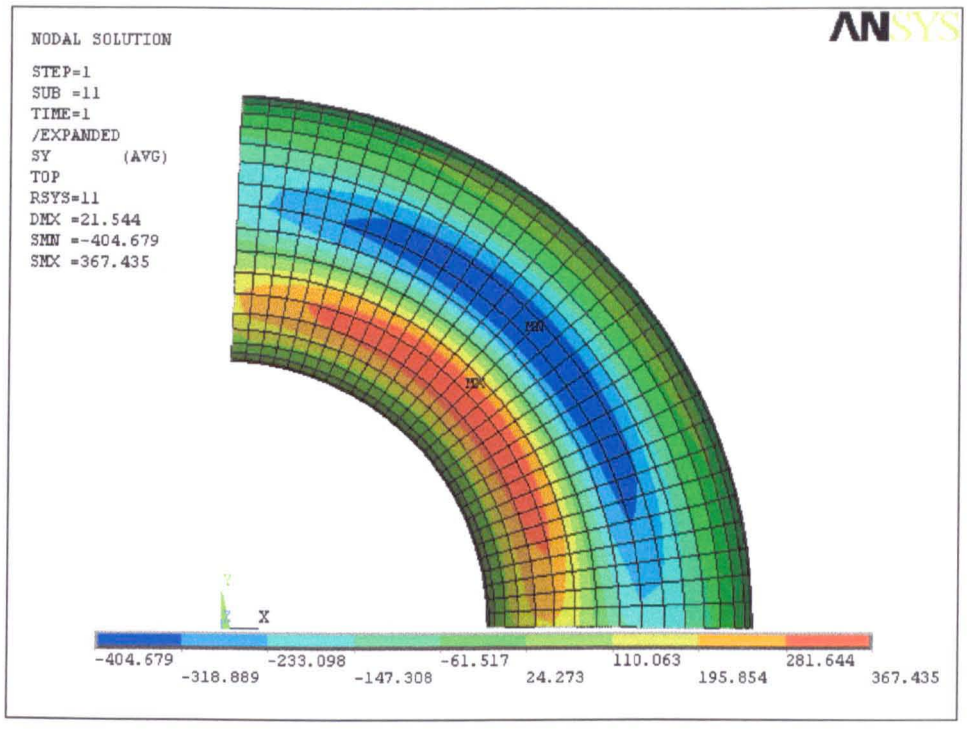

(a)

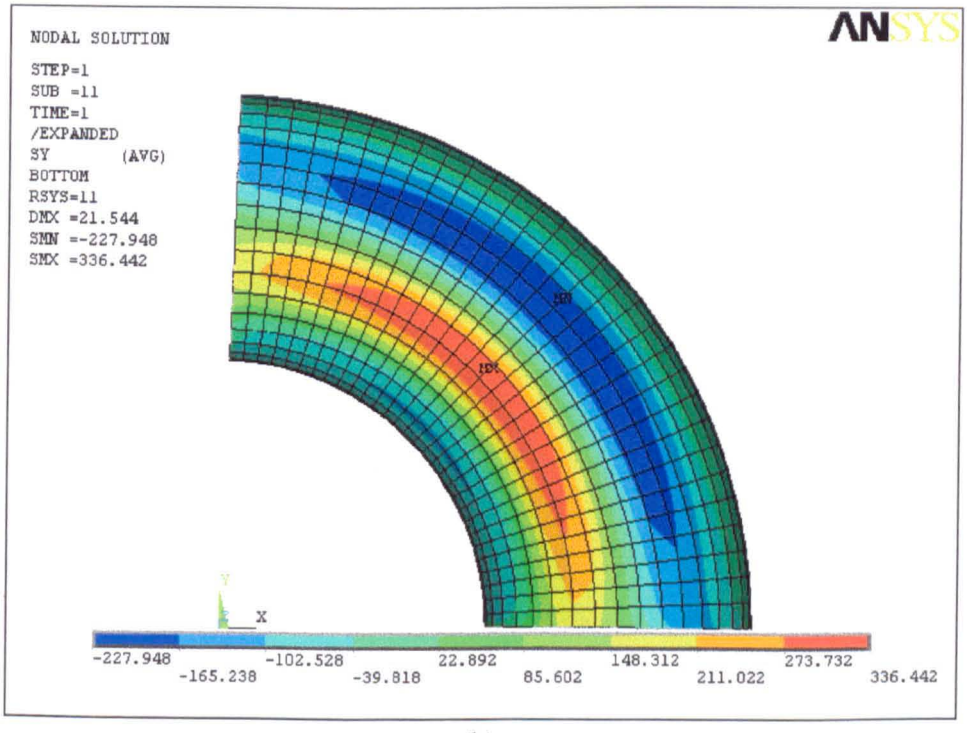

(b)

Fig.6.32 Typical longitudinal stress contour plot of piping elbows under in-plane opening moment, (a) outer surface, (b) inner surface

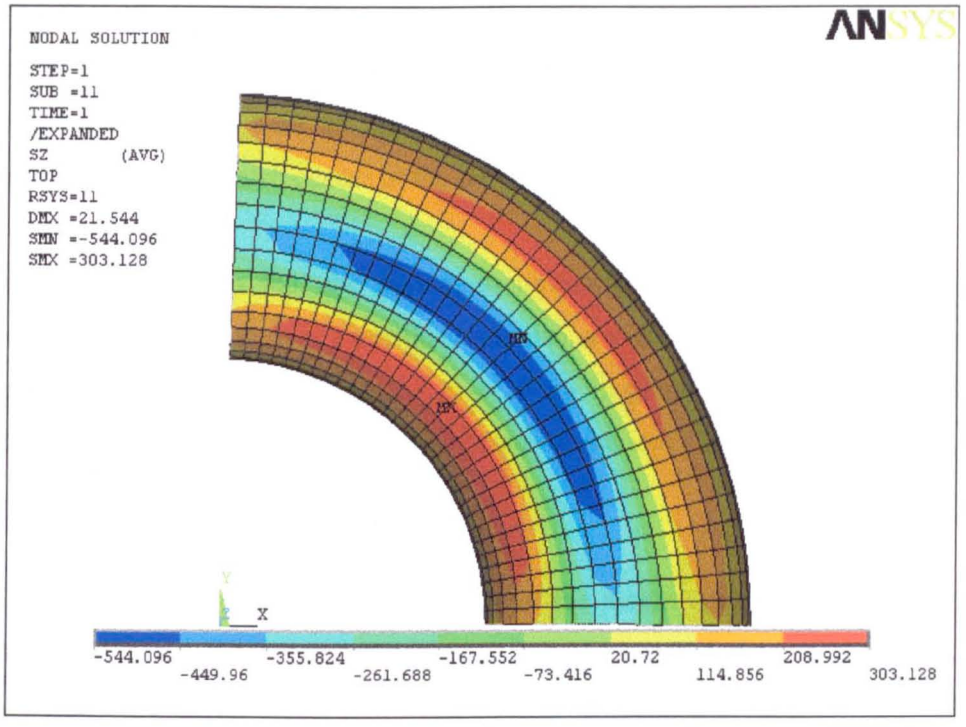

(a)

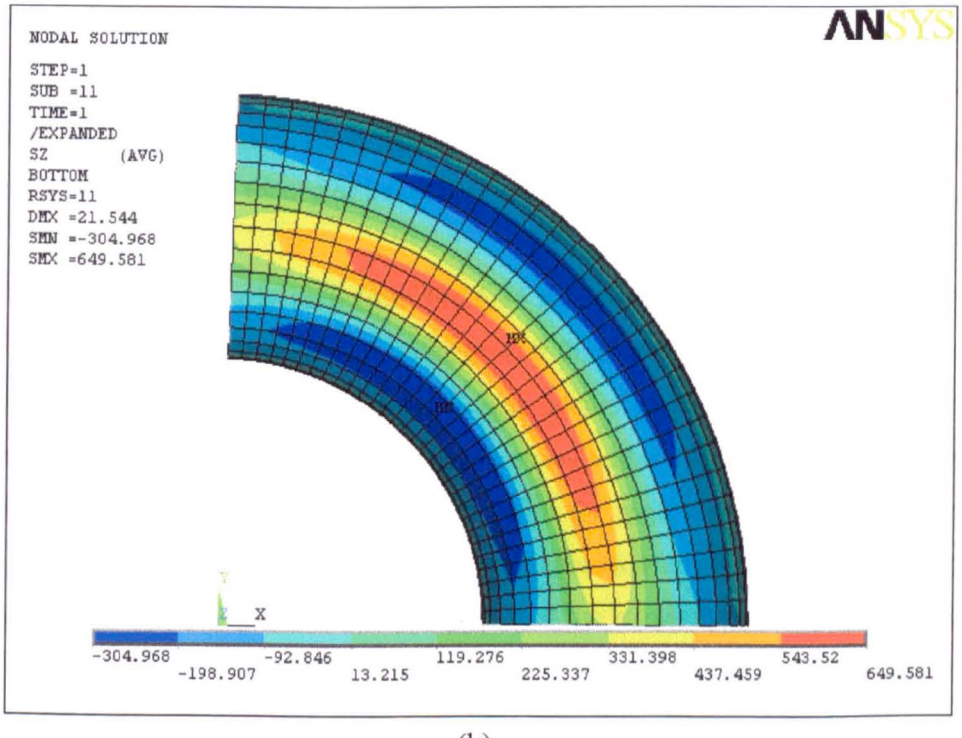

(b)

Fig.6.33 Typical circumferential stress contour plot of piping elbows under in-plane opening moment, (a) outer surface, (b) inner surface

Figure 6.32 shows that the maximum longitudinal stress occurs at the outer surface of the elbow. It is a compressive stress at the mid-section of the elbow. This can be compared to the case of an in-plane closing moment where the maximum longitudinal stress also occurs at the outer surface but it is in tension.

Figure 6.33 shows that the maximum circumferential stress occurs at the inner surface of the elbow. It is a tensile stress also at mid section of the bend. Again, this can be directly compared to the case of an in-plane closing moment where the maximum circumferential stress also occurs at the inner surface of the elbow, but is a compressive stress.

It can be seen from Fig.6.32 and 6.33 that the maximum stresses in piping elbows under an in-plane opening moment is the circumferential stress at the inner surface. In what follows, the maximum hoop stresses at the mid-section of the bend and its location in the circumferential direction is studied.

Typical longitudinal and hoop stress distributions at mid-section of a 90-deg pipe elbow is shown in Fig.6.34. The stresses are plotted from the extrados toward the intrados. The stresses have been normalised with the nominal bending stress calculated from the theory of beam bending as given by equation (5-57).

It again can be clearly seen from Fig.6.34 that the maximum stress in a pipe elbow subjected to bending is several times greater than predicted using the theory of beam bending. The maximum stress no longer occurs in the longitudinal direction but occurs in the hoop direction. It is tensile stress under in-plane opening moment. The maximum stress also changes position from the most distant from the neutral axis according to the beam bending theory to a position close to the neutral axis in the present analysis. Figure 6.34 also shows that the maximum compressive hoop stress for a 90-deg pipe elbow is located at crown (90-deg circumferentially measured from the extrados). This stress will be evaluated as stress-intensification factor.

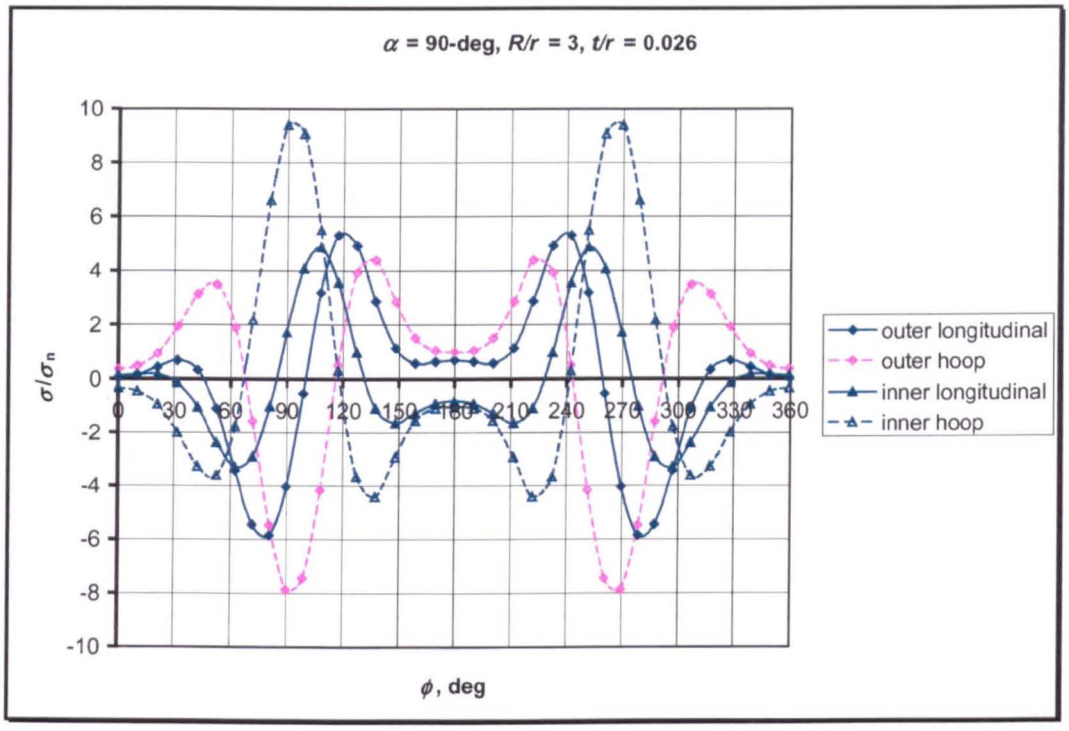

Fig.6.34 Stress distribution for a 90-deg pipe elbow under in-plane opening bending

Figure 6.35 shows a typical moment – stress (hoop) curve for a pipe elbow subjected to an in-plane opening moment plotted for a 90-deg pipe elbow with *R/r* and *t/r* equal 3 and 0.26 respectively.

It can be seen from Fig.6.35, that a pipe elbow subjected to an in-plane opening moment again exhibits non-linear structural hardening behaviour. Figure 6.35 was plotted for a relatively thin-walled pipe to show the non-linearity. It can be seen from Fig.6.35 that the non-linearity is essentially small.

Figure 6.36 shows the stress-intensification factor for 90-deg pipe elbows with various radius ratios subjected to in-plane opening moment. It can be seen that stress-intensification factor depends on pipe bend parameter λ - higher values are obtained for small pipe bend parameter. Figure 6.36 also shows that stress-intensification factor is not very influenced by radius ratio – the straight lines almost coincide with each other.

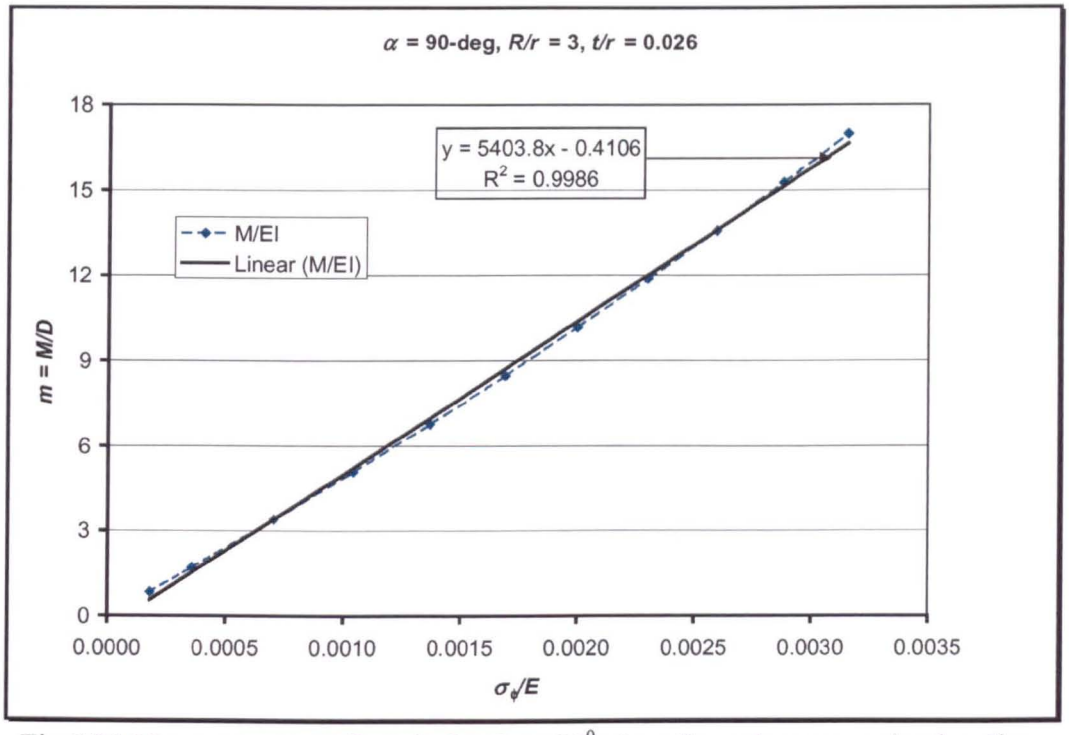

Fig.6.35 Moment – stress (hoop) plot for a 90^0 pipe elbow due to opening bending

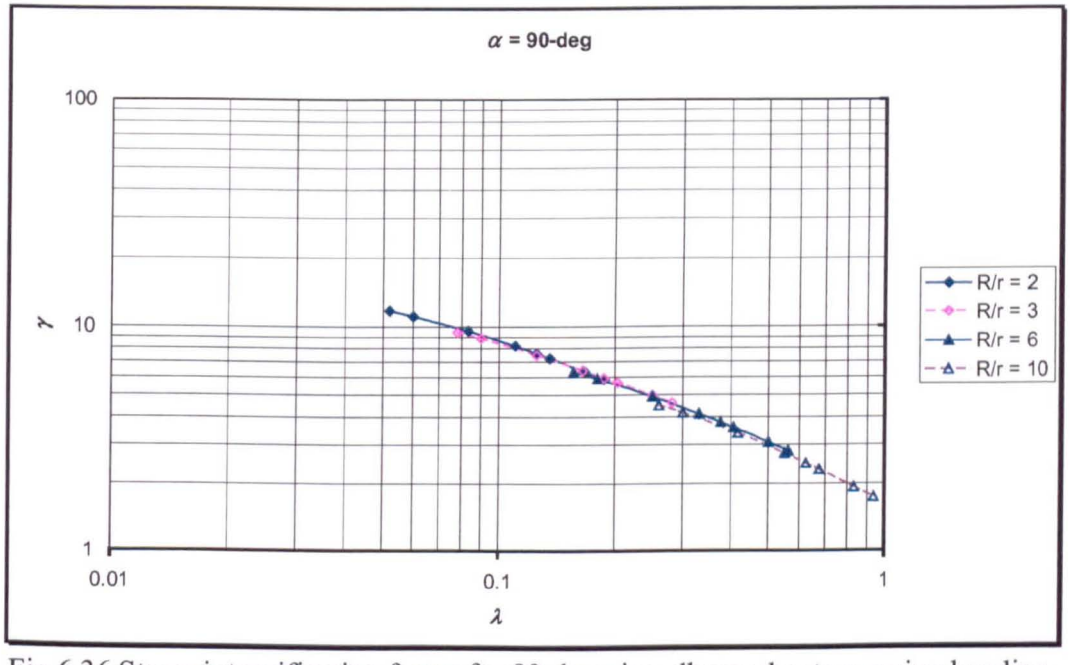

Fig.6.36 Stress-intensification factor for 90-deg pipe elbows due to opening bending

As shown in Fig.6.36, the relation between stress-intensification factor, γ, and pipe bend parameter, λ, is essentially linear in a log-log plot. Accordingly, the relation can be expressed in the form of equation (5-58). By curve fitting, expressions for the stress-intensification factor for 90-deg pipe elbows subjected to in-plane opening moment are obtained:

$$\gamma = \frac{2.463}{\lambda^{0.536}}; \qquad \text{for} \frac{R}{r} = 2 \tag{6-41}$$

$$\gamma = \frac{2.307}{\lambda^{0.56}}; \qquad \text{for} \frac{R}{r} = 3 \tag{6-42}$$

$$\gamma = \frac{2.006}{\lambda^{0.632}}; \qquad \text{for} \frac{R}{r} = 6 \tag{6-43}$$

$$\gamma = \frac{1.717}{\lambda^{0.74}}; \qquad \text{for} \frac{R}{r} = 10 \tag{6-44}$$

These equations are not suitable for design purposes. Following the procedure of Fujimoto and Soh [92], equations (6-41) through (6-44) can be written in form of equation (5-63):

$$\gamma = \frac{1.89}{\lambda^{2/3}}[1.2553 + 0.1259\ln(\lambda)] \qquad \text{for} \frac{R}{r} = 2 \tag{6-45}$$

$$\gamma = \frac{1.89}{\lambda^{2/3}}[1.1992 + 0.1062\ln(\lambda)] \qquad \text{for} \frac{R}{r} = 3 \tag{6-46}$$

$$\gamma = \frac{1.89}{\lambda^{2/3}}[1.0606 + 0.0355\ln(\lambda)] \qquad \text{for} \frac{R}{r} = 6 \tag{6-47}$$

$$\gamma = \frac{1.89}{\lambda^{2/3}}[0.9078 - 0.0706\ln(\lambda)] \qquad \text{for} \frac{R}{r} = 10 \tag{6-48}$$

In the above equations, the term outside the square bracket is the asymptotic solution of Clark and Reissner [20] and the term in the square bracket represents the dependence of stress-intensification factor on radius ratio. Figure 6.37 shows the stress-intensification calculated using the derived formula in comparison with those obtained from finite element. It can be seen that the plots for the proposed design

formulae, i.e., equations (6-45) through (6-48) coincide with those calculated using equations (6-41) through (6-44).

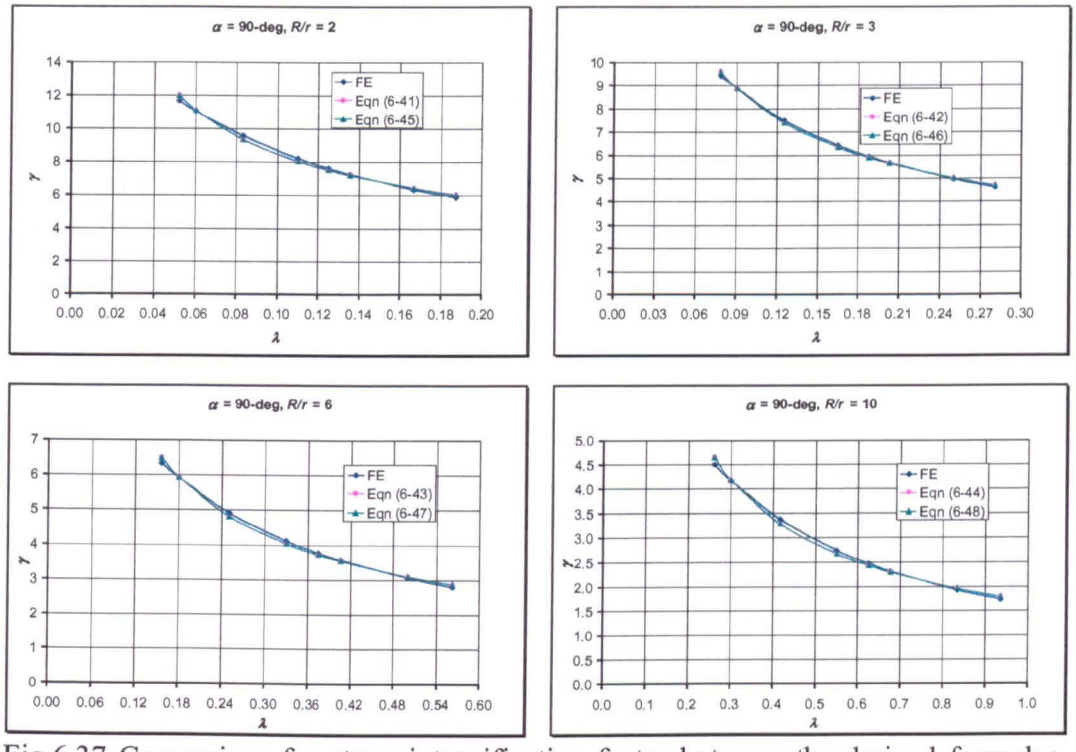

Fig.6.37 Comparison for stress-intensification factor between the derived formulae and finite element results

6.3.1 Effect of Bend Angle on Stress-Intensification Factor

It can be generally understood that as the bend angle of a pipe elbow becomes smaller, it tends to behave as a straight pipe. The location and direction of maximum stress might be shifted from crown toward the furthest location from the neutral axis. To account for the effect of bend angle on stress-intensification factor pipe elbows having bend angle of 30, 45, 60, as well as 180-deg subjected to opening bending have been studied. Figure 6.38 through 6.41 show the stress-distributions at the mid-section of the bend for pipe elbows of different bend angle subjected to in-plane opening moment.

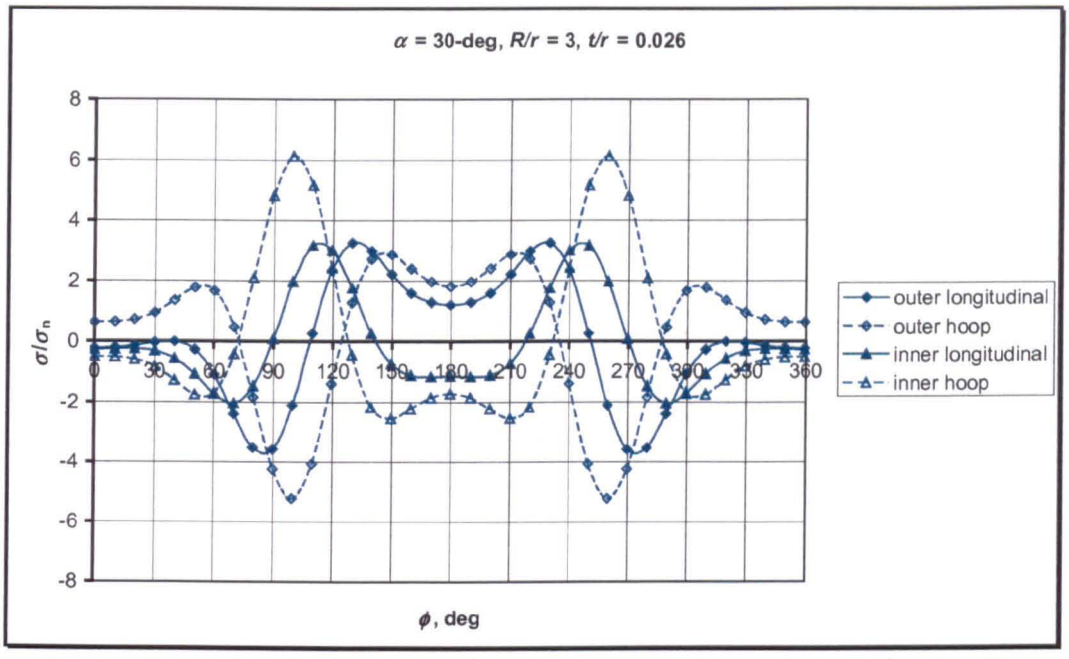

Fig.6.38 Stress-distribution for 30-deg pipe elbows subjected to opening bending

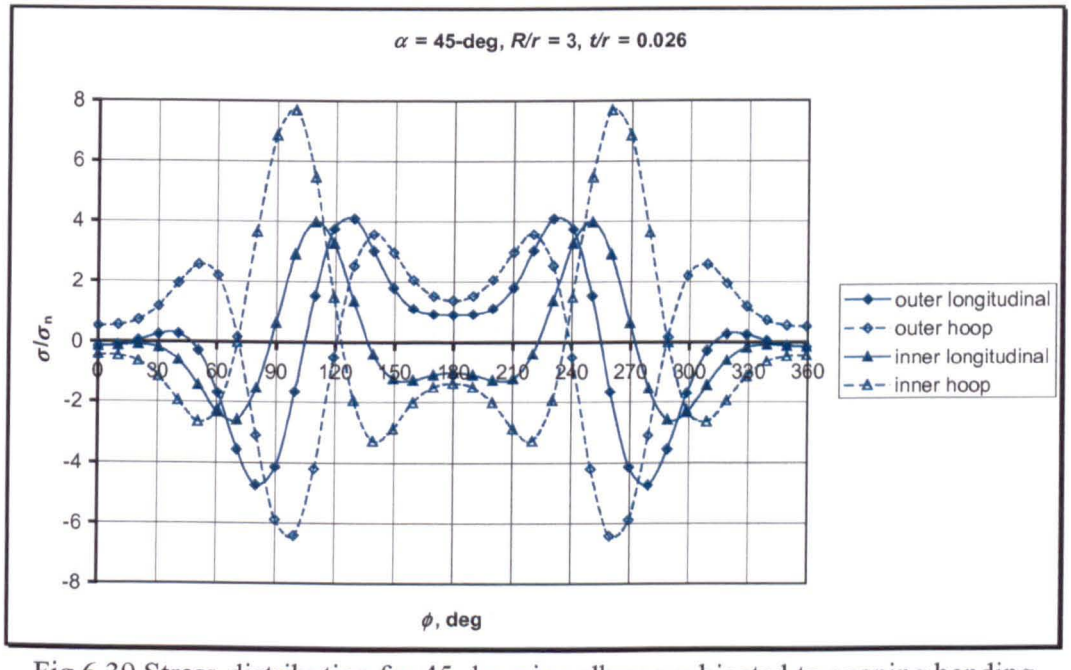

Fig.6.39 Stress-distribution for 45-deg pipe elbows subjected to opening bending

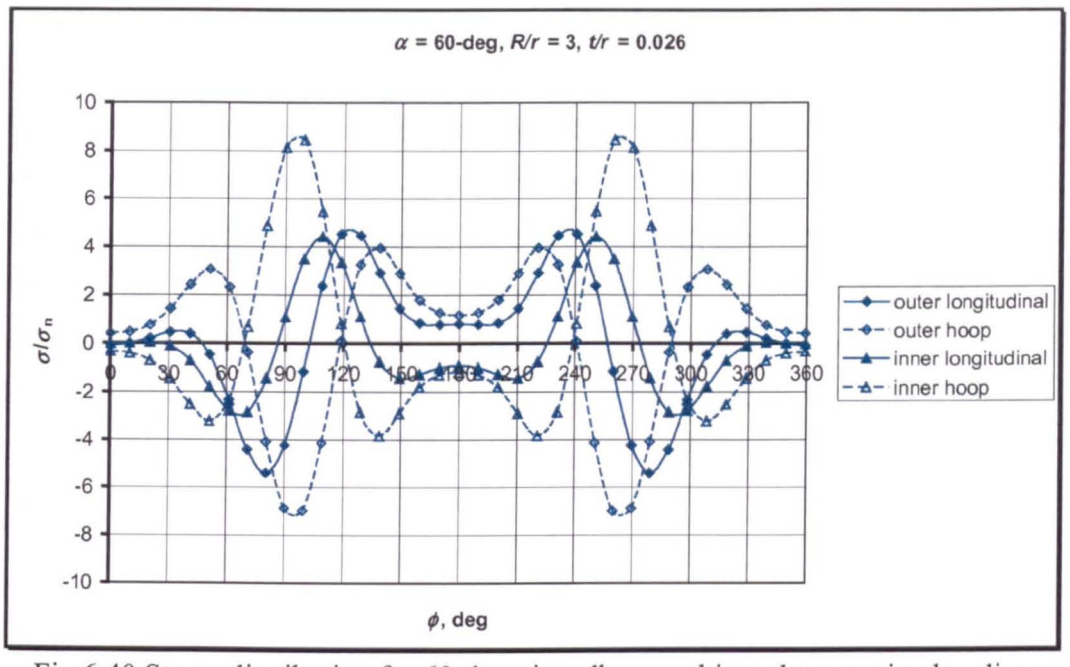

Fig.6.40 Stress-distribution for 60-deg pipe elbows subjected to opening bending

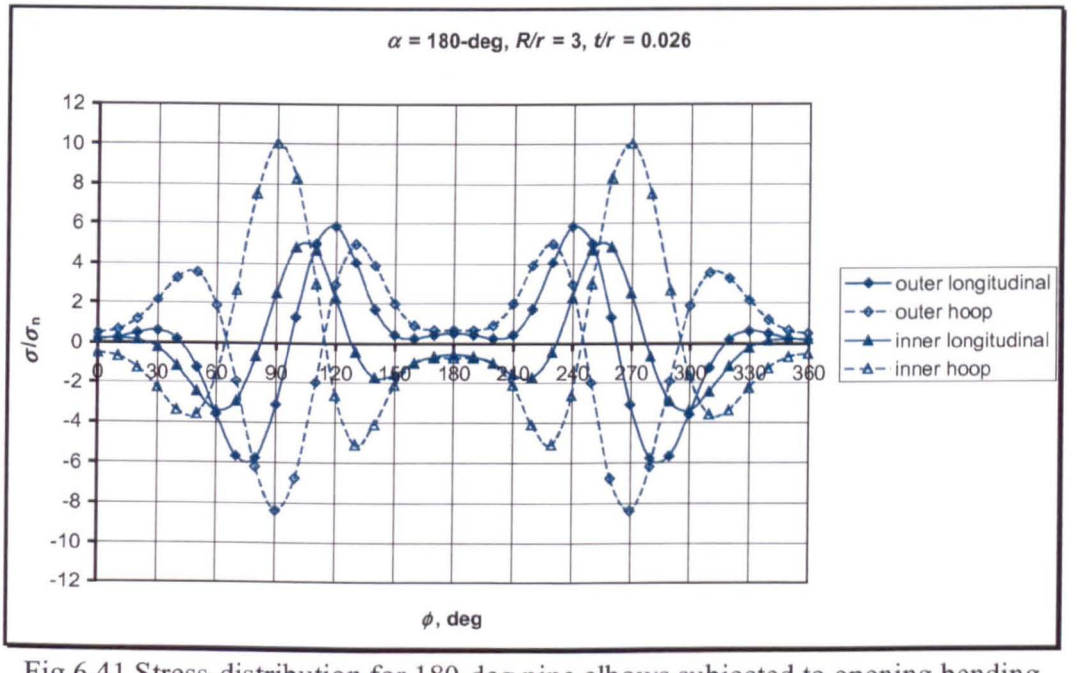

Fig.6.41 Stress-distribution for 180-deg pipe elbows subjected to opening bending

It is interesting to note that the maximum tensile hoop stress occurs at the inner surface of the wall, located at the crown (90-deg from extrados), for pipe elbows having bend angle of 180-deg as shown in Fig.6.41. For pipe elbows of bend angle

30, 45, and 60-deg, the maximum hoop stress is located at 100-deg from the extrados towards the intrados as shown in Fig.6.38, 6.39, and 6.40. It might be concluded that the maximum hoop stress in the circumferential direction is located at the crown for pipe elbows of bend angle 90-deg and greater and shifted by 10-deg from the crown toward the intrados for bend angles less than 90-deg and greater than 30-deg. In what follows, the maximum tensile hoop stress at the inner surface of the pipe wall is evaluated at any circumferential position, depending on the bend angle. For the elbows considered in this study, the location of maximum stress is tabulated below:

Bend angle (α), deg	30	45	60	90	180
Position from extrados (ϕ), deg	100	100	100	90	90

Figure 6.42 through 6.45 show plots of stress-intensification factors for various bend angles under in-plane opening moment. It can be seen that the stress-intensification factor for 30, 45, and 60-deg pipe elbows not only depends on the parameter, λ, but also depends on the radius ratio: as the bend angle becomes greater, the dependence of stress-intensification factor on radius ratio becomes smaller. Figure 6.45 shows that the stress-intensification factor for 180-deg pipe elbows is less dependent on radius ratio.

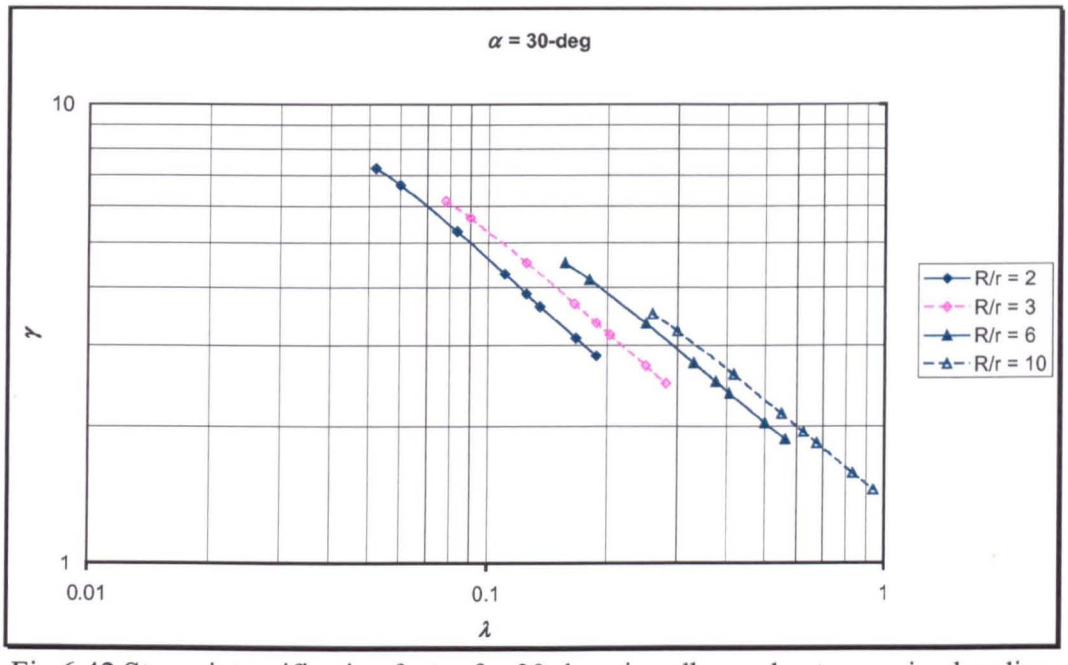

Fig.6.42 Stress-intensification factor for 30-deg pipe elbows due to opening bending

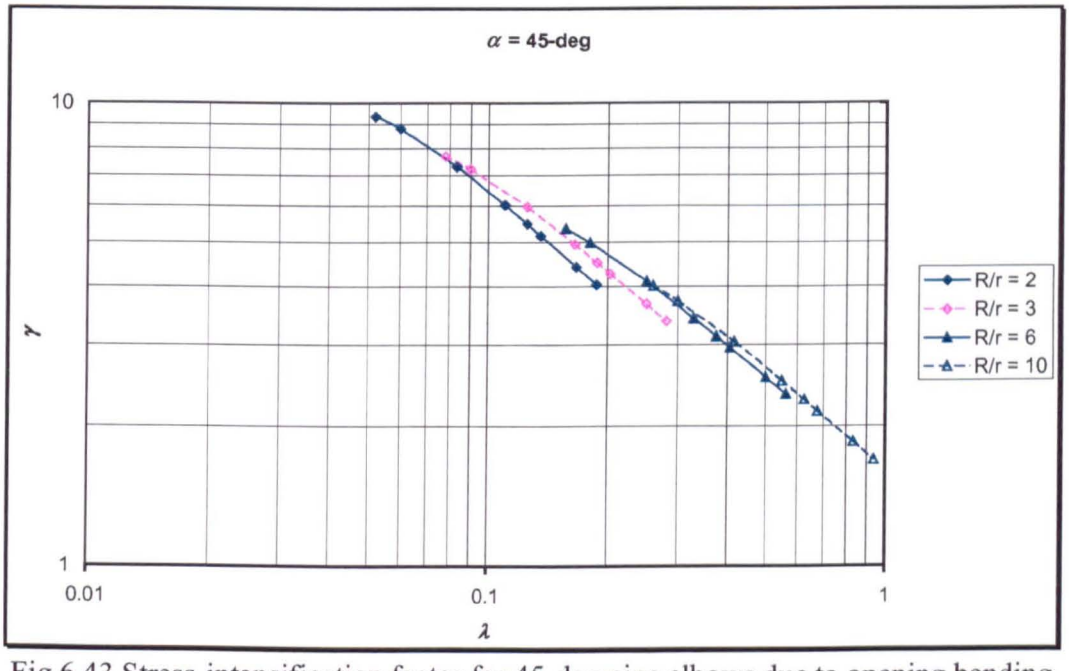

Fig.6.43 Stress-intensification factor for 45-deg pipe elbows due to opening bending

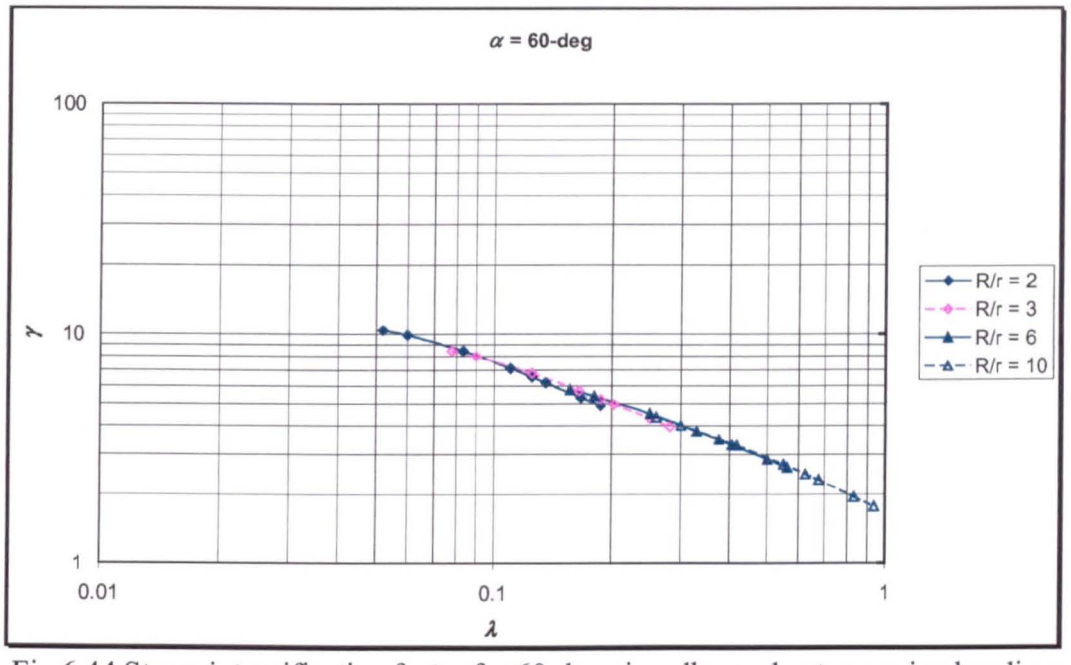

Fig.6.44 Stress-intensification factor for 60-deg pipe elbows due to opening bending

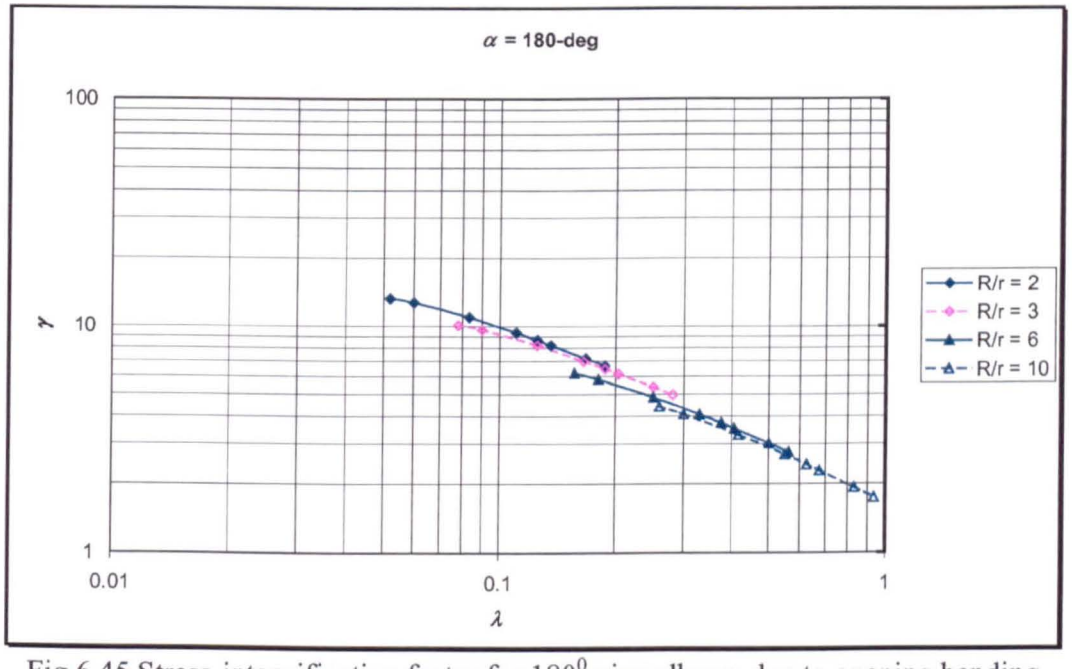

Fig.6.45 Stress-intensification factor for 180^0 pipe elbows due to opening bending

Expressions for the stress-intensification factor can be derived as an approximation from these figures by means of a curve fitting. The stress-intensification factor for pipe elbows subjected to in-plane opening moment can be written in a similar form to equation (5-68).

$$\gamma = \frac{1.89}{\lambda^{2/3}}[a - b\ln(\lambda)] \qquad (6\text{-}49)$$

As in equation (5-68), the term outside the square bracket is the asymptotic solution of Clark and Reissner [20]. The term in the square bracket represents the dependence of stress-intensification factor on pipe bend parameter as well as on radius ratio: the coefficient '*a*' and '*b*' are functions of radius ratio as given in Table 6.5 and 6.6 respectively for various bend angles.

Table 6.5 Approximate values for coefficient "*a*" in equation (6-49)

R/r	*α*				
	30-deg	45-deg	60-deg	90-deg	180-deg
2	0.4320	0.7277	0.9776	1.2553	1.4185
3	0.5314	0.7992	1.0033	1.1992	1.3031
4	0.6005	0.8266	1.0045	1.1541	1.1765
5	0.6422	0.8452	1.0017	1.1085	1.1033
6	0.6685	0.8692	0.9931	1.0606	1.0413
7	0.6934	0.8666	0.9861	1.0227	1.0014
8	0.7102	0.8733	0.9699	0.9823	0.9636
9	0.7236	0.8785	0.9481	0.9435	0.9314
10	0.7400	0.8826	0.9217	0.9078	0.9029

Table 6.6 Approximate values for coefficient "*b*" in equation (6-49)

R/r	α				
	30-deg	45-deg	60-deg	90-deg	180-deg
2	0.0380	-0.0052	-0.0616	-0.1259	-0.1389
3	0.0283	-0.0140	-0.0638	-0.1062	-0.1182
4	0.0246	-0.0166	-0.0627	-0.0802	-0.0896
5	0.0220	-0.0181	-0.0573	-0.0555	-0.0651
6	0.0203	-0.0155	-0.0476	-0.0355	-0.0330
7	0.0191	-0.0139	-0.0345	-0.0061	-0.0161
8	0.0182	-0.0082	-0.0171	0.0186	0.0084
9	0.0175	-0.0001	0.0043	0.0433	0.0329
10	0.0169	0.0129	0.0309	0.0706	0.0539

It is not easy to draw a comprehensive conclusion from these Tables unless the results are checked for some extreme values of λ and *R/r*. The reason for this is that if the stress intensification factors are expressed in form of equation (5-58), the corresponding value of '*index q*' in some cases is greater than 2/3, but smaller than 2/3 in other cases. Consequently, if the term outside the square bracket of equation (5-63) is the asymtotic solution of Clark and Reissner (q = 2/3), the sign of the second term in the square bracket could be positive and negative. In addition, the sign of the second term in the square bracket will further depend on the value of λ, whether it is greater or smaller than 1. The mixing sign of the second term in the square bracket (value of coefficient *b* in Table 6.6) however can be avoided by changing the term outside the square bracket, but the results can not be directly compared to the results of in-plane closing bending case. More discussion of this problem and comparison with the closing bending case will be presented at the end of this Chapter.

6.3.2 The Pressure Reduction Effect

The pressure reduction effect on ovalisation (negative flattening) and flexibility factors of piping elbows under in-plane opening moment has been examined in the previous sections of this chapter. In this section, the pressure reduction effect on the stress-intensification factor is studied and simple formulae in a similar way to previous Chapter is derived.

Figure 6.46 shows a typical hoop stress distribution at the mid-section of an elbow under an in-plane opening bending. It can be seen that the maximum hoop stress occurs at the inner surface as tension stresses. In Fig.6.46, the toroidal membrane stress due to internal pressure is included in the total stresses for pressurized condition. Because the stresses are factored by nominal bending stress (to obtained stress-intensification factor), the membrane stress due to internal pressure as given by equation (2-15) should be subtracted from finite element result (Fig.6.46)

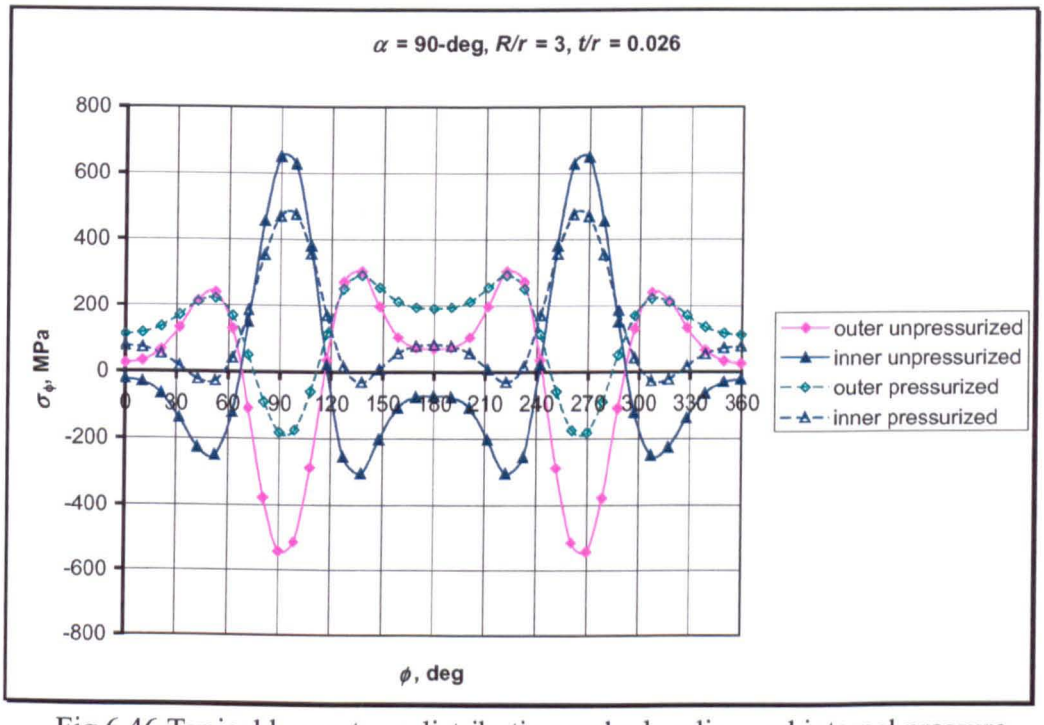

Fig.6.46 Typical hoop stress distribution under bending and internal pressure

Figure 6.47 shows stress-intensification factor for pipe elbows under combined in-plane opening moment and internal pressure. It can be clearly seen that the effect of internal pressure is to reduce the stress. Figure 6.47 also shows that the elbow under consideration is bending dominated. This is indicated by the same trend of stress distributions and location of maximum stress under unpressurized and pressurized conditions. It is expected that this tendency would change if the internal pressure increased beyond a certain level [57].

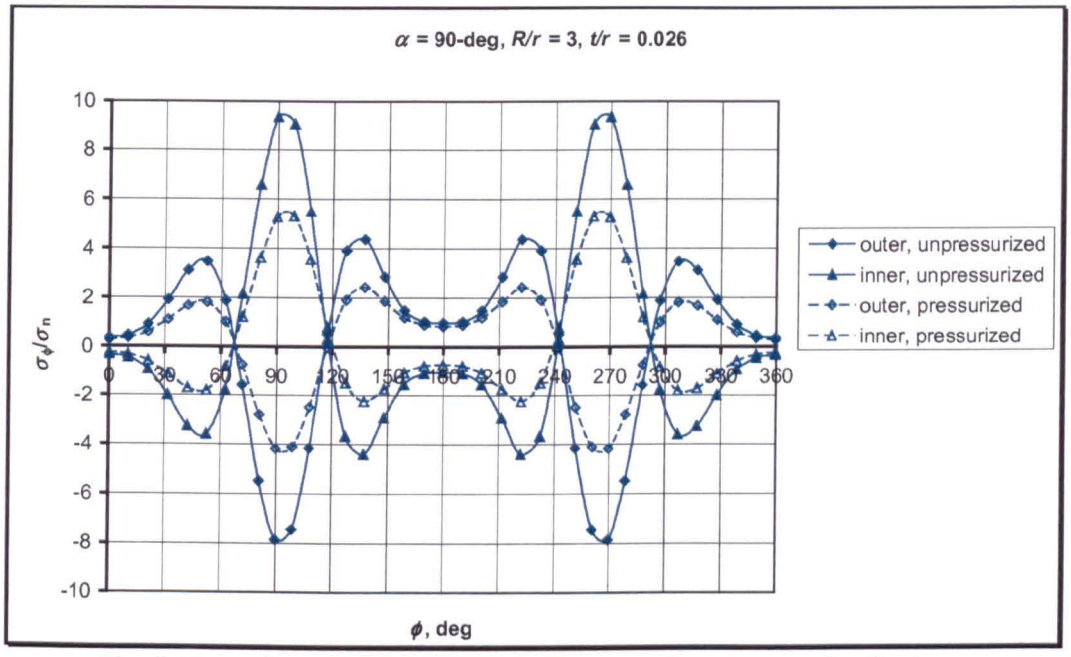

Fig.6.47 Typical pressure reduction effect on hoop stress distributions

A typical pressure – stress (hoop) plot is shown in Fig. 6.48, plotted for a 90-deg piping elbow having radius ratio $R/r = 3$. The abscissa of 0.0 represents the final load step of moment loading and the starting of the subsequent internal pressure loading. It can be seen that the relation between internal pressure and maximum hoop stress is non-linear. Figure 6.48 again shows the 'Haigh effect' [11]: pipe subjected to internal pressure departs significantly from linear behaviour if the pipe cross-section is not perfectly circular. In Fig.6.48, internal pressure acts on an oval cross-section due to applied in-plane opening moment.

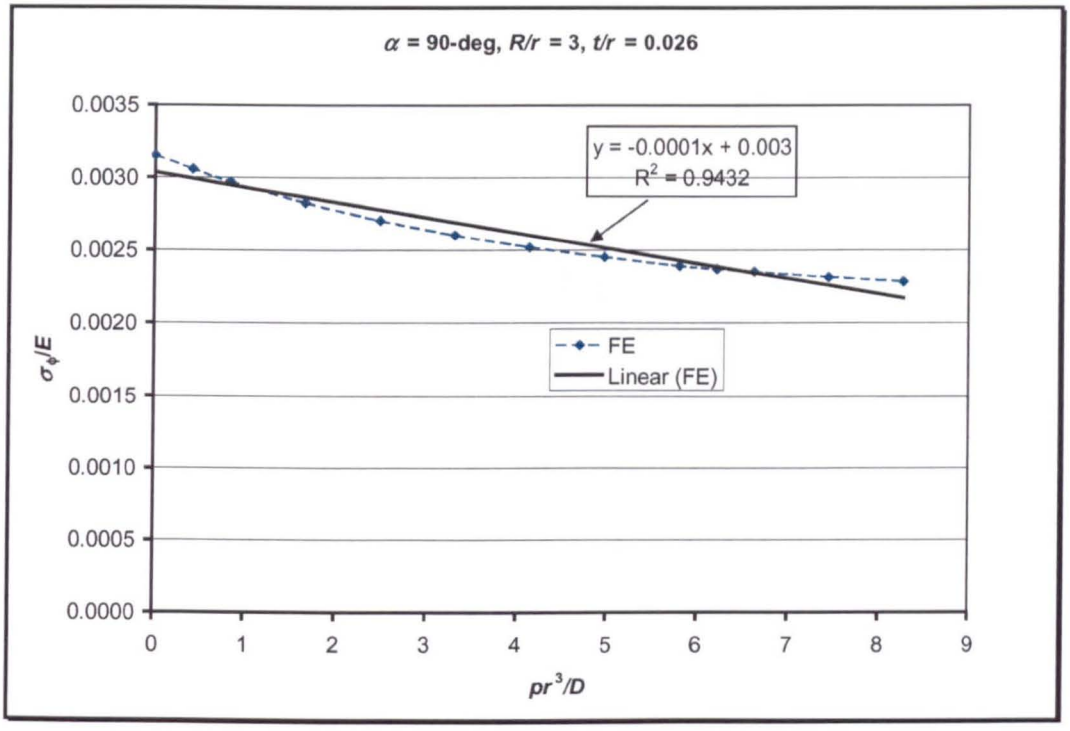

Fig.6.48 Typical pressure – stress plot for in-plane opening bending

Figure 6.49 through 6.52 show the stress-intensification factor for 90-deg pipe elbows for various radius ratios loaded by an in-plane opening moment and internal pressure. It can be again clearly seen that internal pressure reduces the stress-intensification factor for piping elbows under in-plane opening moment. The magnitude of the reduction is more pronounced for elbows having low pipe factors λ.

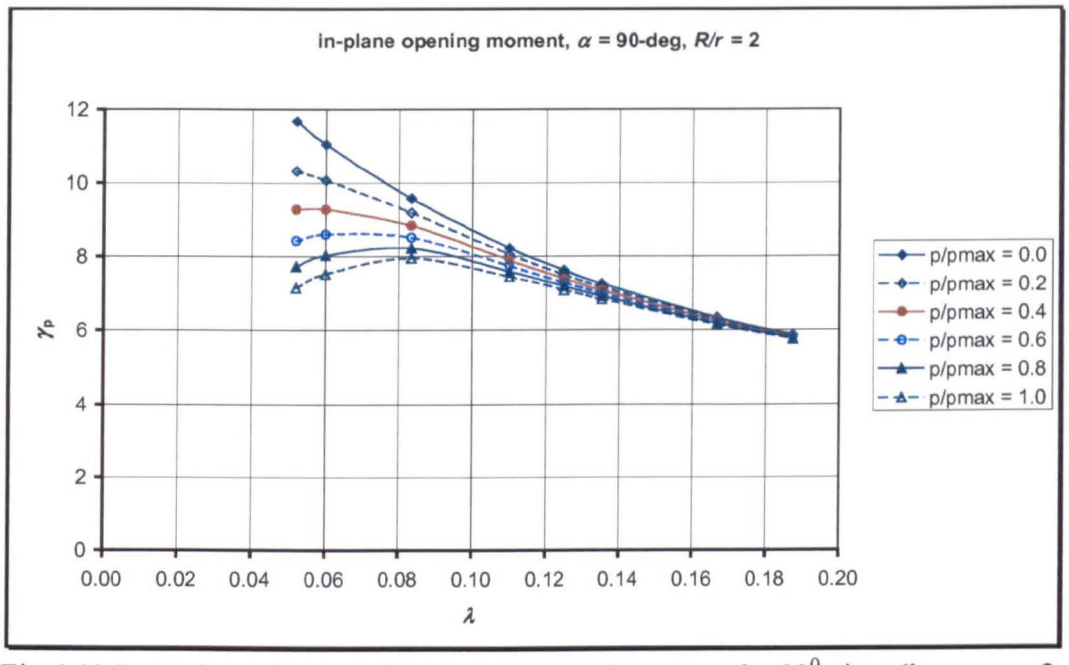

Fig.6.49 Stress-intensification factor with internal pressure for 90^0 pipe elbows: $\rho = 2$

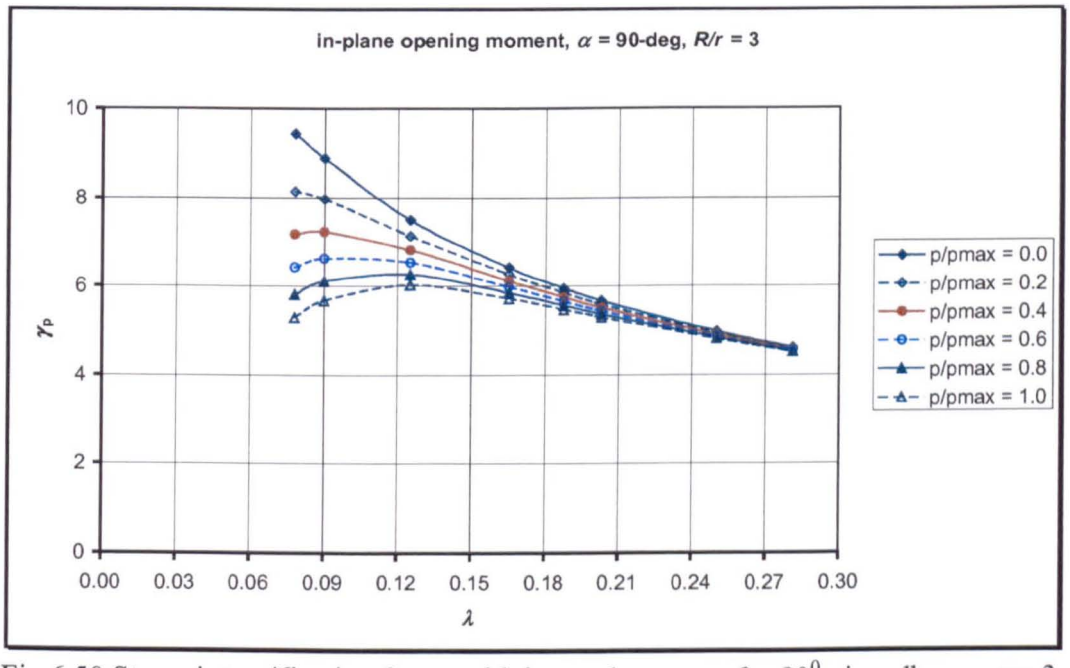

Fig.6.50 Stress-intensification factor with internal pressure for 90^0 pipe elbows: $\rho = 3$

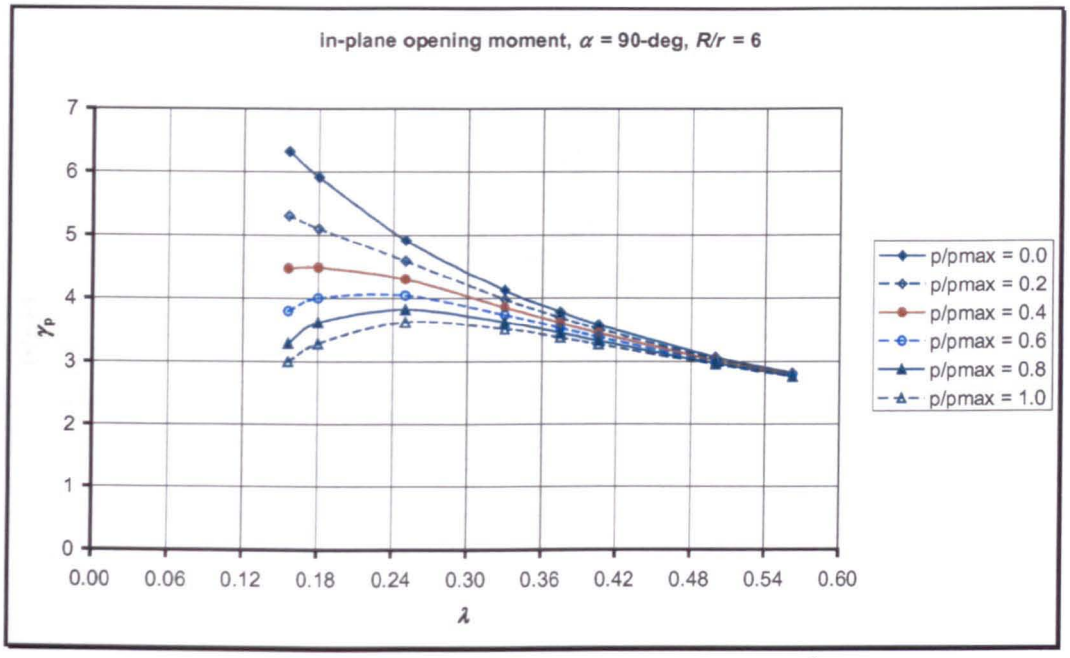

Fig.6.51 Stress-intensification factor with internal pressure for 90^0 pipe elbows: $\rho = 6$

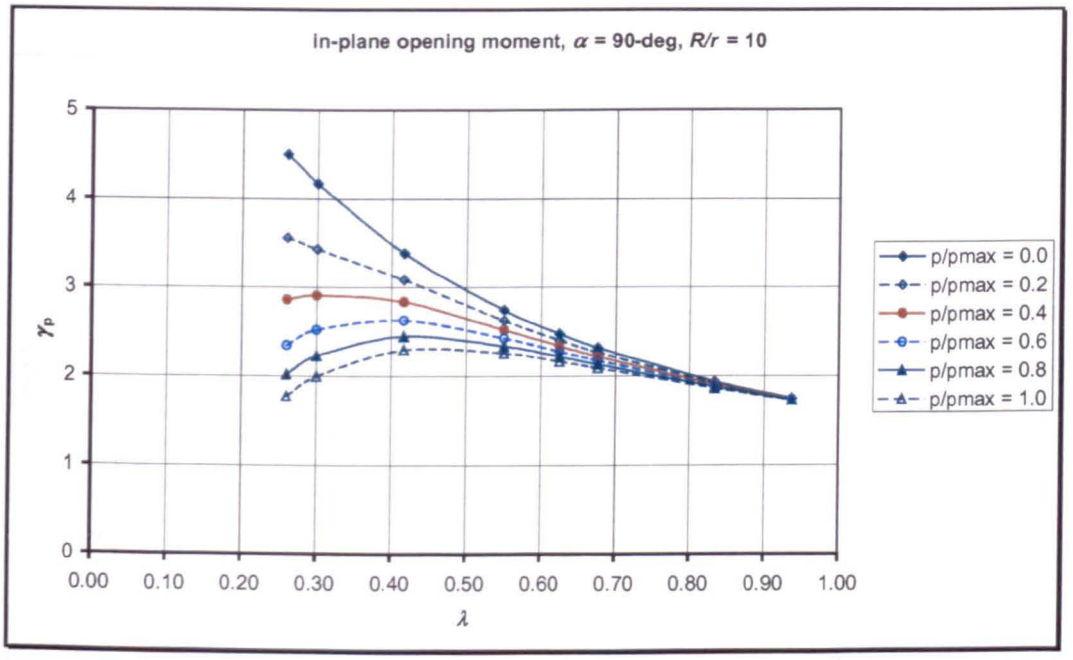

Fig.6.52 Stress-intensification factor with internal pressure for 90^0 elbows: $\rho = 10$

Pressure reduction for the stress-intensification factor (equation 5-70)) for 90-deg pipe elbows can be derived from Fig.6.49 through 6.52. It is plotted as a log-log graph in Fig.6.53 for constant radius ratio *R/r* and in Fig.6.54 for constant non-dimensional thickness *r/t*.

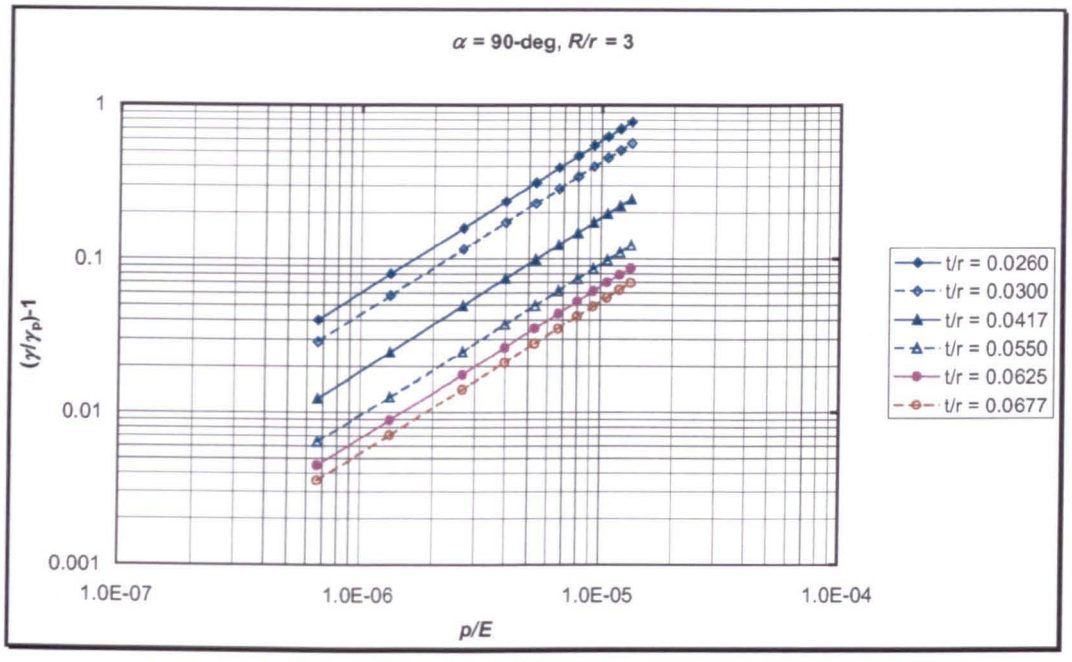

(a)

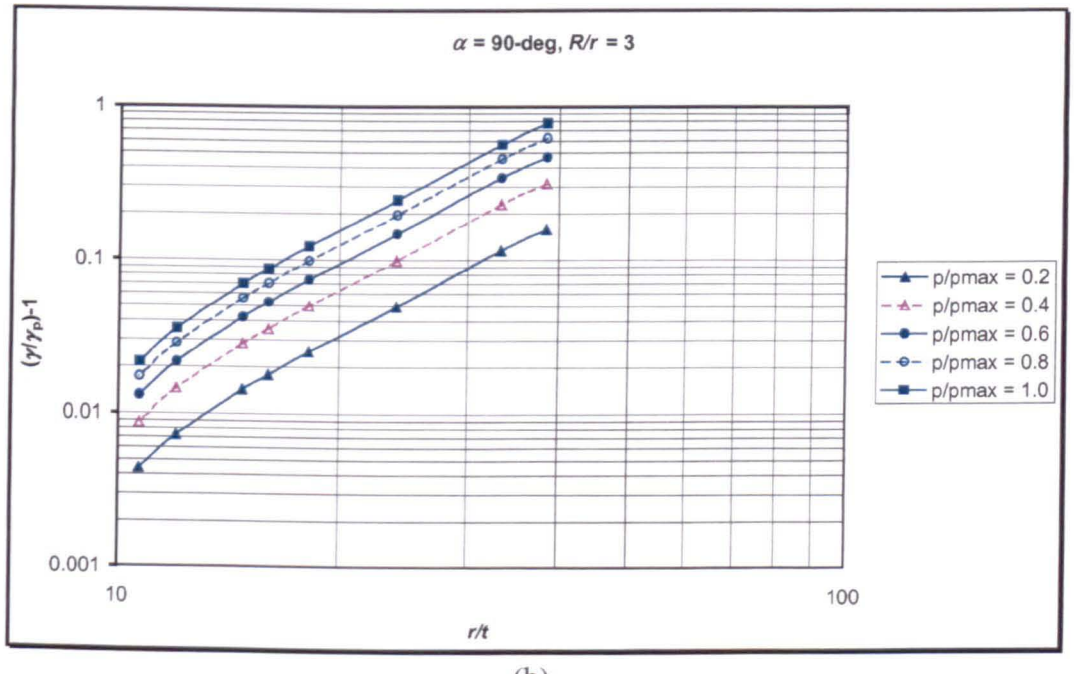

(b)

Fig.6.53 Pressure reduction for constant radius ratio plotted against (a) *p/E*, (b) *r/t*

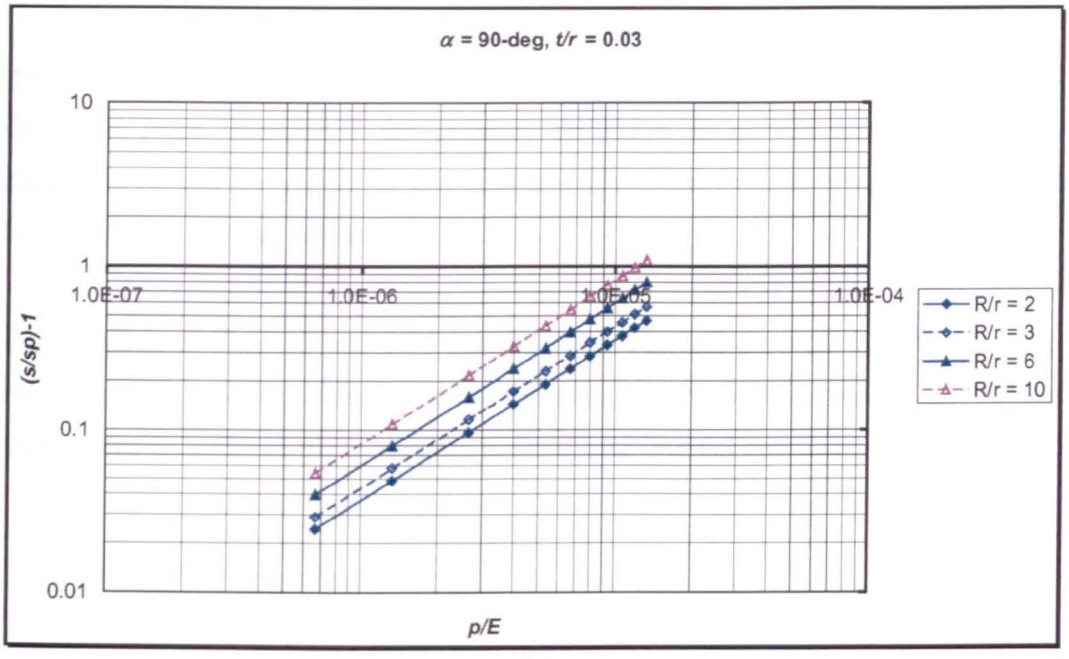

(a)

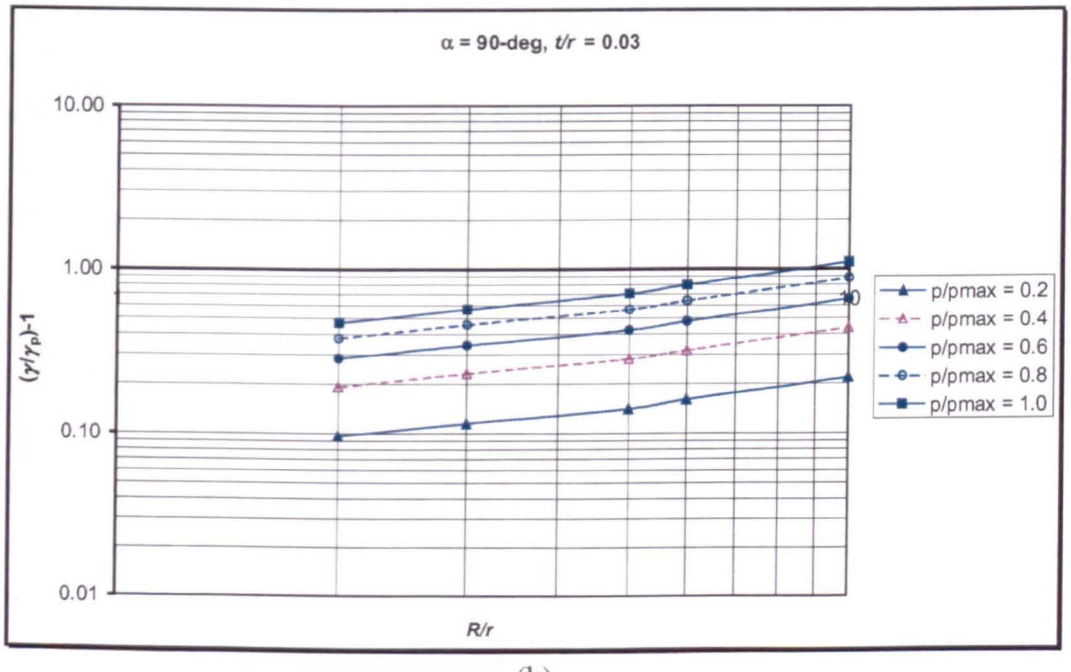

(b)

Fig.6.54 Pressure reduction for constant thickness plotted against (a) *p/E*, (b) *R/r*

It can be seen from these figures that the relation between pressure reduction and non-dimensional pressure p/E is once more linear in a log-log plot. There is a small deviation from linearity if the pressure reduction is plotted against geometric parameter r/t and R/r. Again the development of the approximate design formula will be based on this linear relation.

Examination of Fig.6.53 and 6.54 together with Fig.6.49 through 6.52 leads to the following approximate expression for the stress-intensification factors for 90-deg piping elbows under in-plane opening moment and internal pressure:

$$\gamma_p = \frac{\gamma}{1+0.172\left(\frac{p}{E}\right)\left(\frac{r}{t}\right)^{10/3}\left(\frac{R}{r}\right)^{0.546}} \qquad (6-50)$$

where γ is stress-intensification factor in the absence of internal pressure as given by equation (6-49) and along with Table 6.5 and 6.6. Equation (6-50) can be directly compared with equation (5-71) for closing bending case. Comparison also can be made with the equation proposed by Rodabaugh and George [30]. The difference will be clearer if the comparison is made using numerical data. This will be checked later in the discussion to this chapter.

6.3.3 Effect of Bend Angle on Pressure Reduction

It has been shown in Section 6.3.1 that the stress-intensification factor for unpressurized piping elbows is very much influenced by the bend angle. This is investigated further here for the current loading cases.

By constructing log-log graphs for pressure reduction (eqn. (5-70)) using the data of Fig.A6.11 through A6.15 of Appendix C6, stress-intensification factors for pressurised piping elbows under in-plane opening moment are obtained:

$$\gamma_p = \frac{\gamma}{1+0.330\left(\frac{p}{E}\right)\left(\frac{r}{t}\right)^{10/3}\left(\frac{R}{r}\right)^{0.245}} \qquad \text{for } \alpha = 30\text{-deg} \qquad (6\text{-}51)$$

$$\gamma_p = \frac{\gamma}{1+0.230\left(\frac{p}{E}\right)\left(\frac{r}{t}\right)^{10/3}\left(\frac{R}{r}\right)^{0.393}} \qquad \text{for } \alpha = 45\text{-deg} \qquad (6\text{-}52)$$

$$\gamma_p = \frac{\gamma}{1+0.183\left(\frac{p}{E}\right)\left(\frac{r}{t}\right)^{10/3}\left(\frac{R}{r}\right)^{0.502}} \qquad \text{for } \alpha = 60\text{-deg} \qquad (6\text{-}53)$$

$$\gamma_p = \frac{\gamma}{1+0.124\left(\frac{p}{E}\right)\left(\frac{r}{t}\right)^{10/3}\left(\frac{R}{r}\right)^{0.685}} \qquad \text{for } \alpha = 180\text{-deg} \qquad (6\text{-}54)$$

Using the relation:

$$\left(\frac{r}{t}\right)^{10/3} = \left(\frac{r}{t}\right)^{3}\left(\frac{1}{\lambda}\right)^{1/3}\left(\frac{R}{r}\right)^{1/3}$$

Equation (6-50) through (6-54) can be further written as:

$$\gamma_p = \frac{\gamma}{1+0.091\left(\frac{pr^3}{3D}\right)\left(\frac{1}{\lambda}\right)^{1/3}\left(\frac{R}{r}\right)^{0.578}} \qquad \text{for } \alpha = 30\text{-deg} \qquad (6\text{-}55)$$

$$\gamma_p = \frac{\gamma}{1+0.063\left(\frac{pr^3}{3D}\right)\left(\frac{1}{\lambda}\right)^{1/3}\left(\frac{R}{r}\right)^{0.726}} \qquad \text{for } \alpha = 45\text{-deg} \qquad (6\text{-}56)$$

$$\gamma_p = \frac{\gamma}{1+0.050\left(\frac{pr^3}{3D}\right)\left(\frac{1}{\lambda}\right)^{1/3}\left(\frac{R}{r}\right)^{0.835}} \qquad \text{for } \alpha = 60\text{-deg} \qquad (6\text{-}57)$$

$$\gamma_p = \frac{\gamma}{1+0.047\left(\frac{pr^3}{3D}\right)\left(\frac{1}{\lambda}\right)^{1/3}\left(\frac{R}{r}\right)^{0.879}} \qquad \text{for } \alpha = 90\text{-deg} \qquad (6\text{-}58)$$

$$\gamma_p = \frac{\gamma}{1+0.034\left(\frac{pr^3}{3D}\right)\left(\frac{1}{\lambda}\right)^{1/3}\left(\frac{R}{r}\right)^{1.019}} \qquad \text{for } \alpha = 180\text{-deg} \qquad (6\text{-}59)$$

Equations (6-50) through (6-59) if necessary can be further simplified to:

$$\gamma_p = \frac{\gamma}{1+A(\alpha)\left(\frac{p}{E}\right)\left(\frac{r}{t}\right)^{10/3}\left(\frac{R}{r}\right)^{m(\alpha)}}$$

$$\gamma_p = \frac{\gamma}{1+B(\alpha)\left(\frac{pr^3}{3D}\right)\left(\frac{1}{\lambda}\right)^{1/3}\left(\frac{R}{r}\right)^{n(\alpha)}}$$

where A, B, m, and n are functions of bend angle α. However as the bend angle considered in this study have covered the most general requirements in practice, this simplification will not be processed any further.

6.4 Discussion

In this chapter, alternative design formulae have been developed for cross-sectional ovalisation, flexibility, and stress-intensification factors for unpressurised piping elbows under an in-plane opening moment. The pressure reduction effect following Rodabaugh and George [30] has also been re-examined. All the formulae developed here have been obtained by curve fitting. Of course errors are introduced during this approximation. It will be seen however that the errors introduced are surprisingly small from a practical point of view.

A comparison of results between in-plane closing bending and some fundamental theoretical development has been made in Chapter 5. In the present discussion for in-plane opening bending, comparisons will not be made with respect to the theoretical development as reviewed in Chapter 2, because most of the theoretical development refers to closing bending. Throughout the following discussion, comparison will be made for results between in-plane closing bending as have been developed in Chapter 5 and in-plane opening bending as developed in the present Chapter.

6.4.1 Unpressurized Conditions

In developing the formulae for unpressurised piping elbows, the effect of radius ratio has been taken in to account. In many theoretical developments, for example the initial work of von Karman [2], Rodabaugh and George [30] and others, the radius of the bend was assumed to be much greater than the cross-section radius – a long radius assumption. Flexibility and stress-intensification factors for short-radius pipe bends has been developed theoretically by Gross and Ford [25] and also by Cheng and Thailer [41]. As will be seen in what follows, there is a substantial influence of radius ratio on cross-section ovalisation, flexibility, and stress-intensification factors.

It is well known that the flexibility and stress-intensification factors are modified due to cross-sectional ovalisation. However the effects of the various geometric parameter on cross-sectional ovalisation, flexibility and stresses are not identical either in trend or in magnitude.

Ovalisation, flexibility, and stress-intensification factors have been expressed in the following forms:

$$\xi = 1.656\exp(-1.175\lambda)[a - b\lambda] \qquad (6\text{-}6)$$

$$k = \frac{1.65}{\lambda}[a - b\ln(\lambda)] \qquad (6\text{-}30)$$

$$\gamma = \frac{1.89}{\lambda^{2/3}}[a - b\ln(\lambda)] \qquad (6-49)$$

In the above equations, the term in the square bracket represents their dependence on pipe bend parameter, λ, as well as on radius ratio: the coefficient a and b are functions of radius ratio.

Figure 6.55 shows ovalisation factor for sort radius pipe elbows under in-plane opening bending calculated using equation (6-6). It can be seen that for short radius piping elbows, the ovalisation factors are directly proportional to the bend angle.

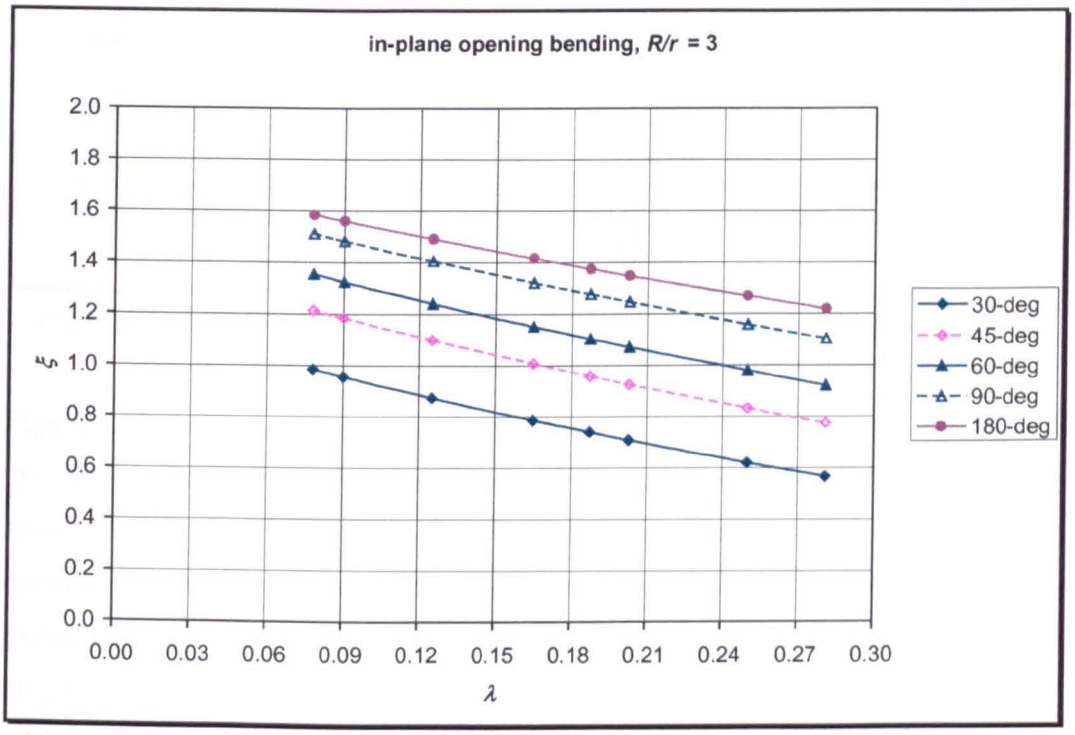

Fig.6.55 Ovalisation factor for short radius piping elbows under opening bending

Figure 6.56 shows ovalisation factor for long radius piping elbows. It can be seen that the ovalisation factors are directly proportional to the bend angle for bend angle less than 90-deg. It can be seen that the ovalisation factor for 90-deg pipe elbows of high pipe bend parameter, lies between the value for 45 and 60-deg pipe elbows, but over the value for 60-deg for low pipe bend parameter. Figure 6.56 shows that the

ovalisation factors for 180-deg pipe elbows are less than those for 60 and 90-deg, but greater than those for 45-deg.

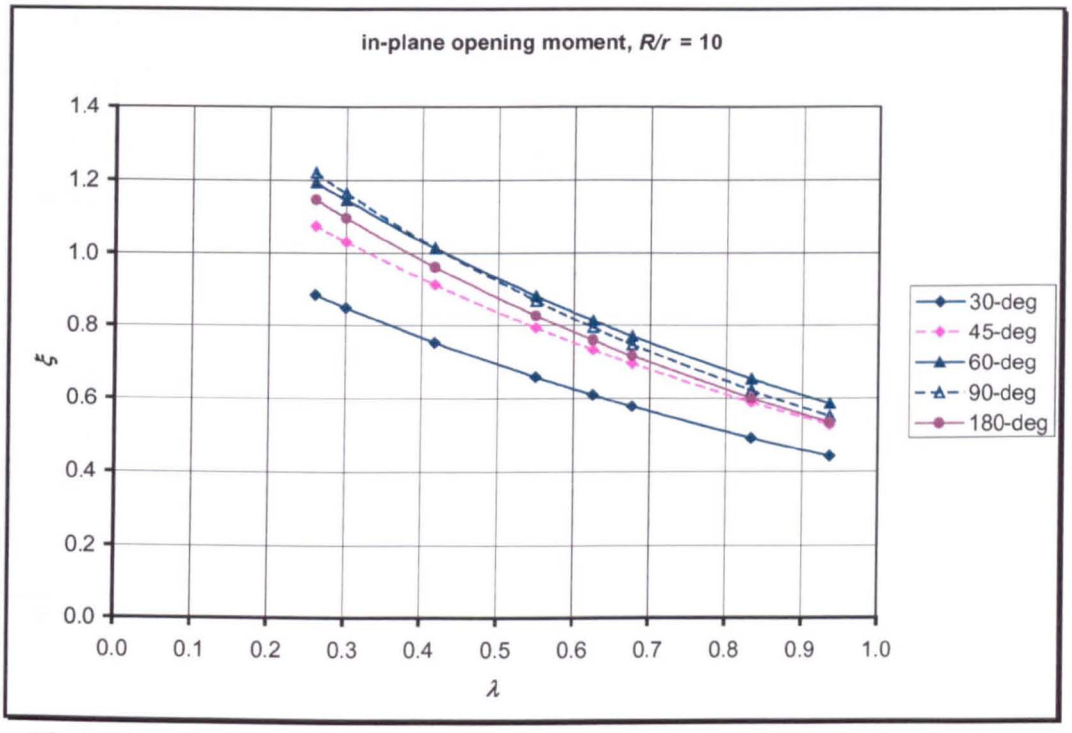

Fig.6.56 Ovalisation factor for long radius piping elbows under opening bending

Figure 6.57 shows a comparison of ovalisation factor between in-plane closing and opening bending, plotted for pipe elbows having radius ratio equals three. It can be seen overall that the ovalisation factor under closing bending is greater than under opening bending, especially for low pipe bend parameter. The difference in ovalisation between closing and opening bending mode is not significant for pipe elbows of high pipe bend parameter.

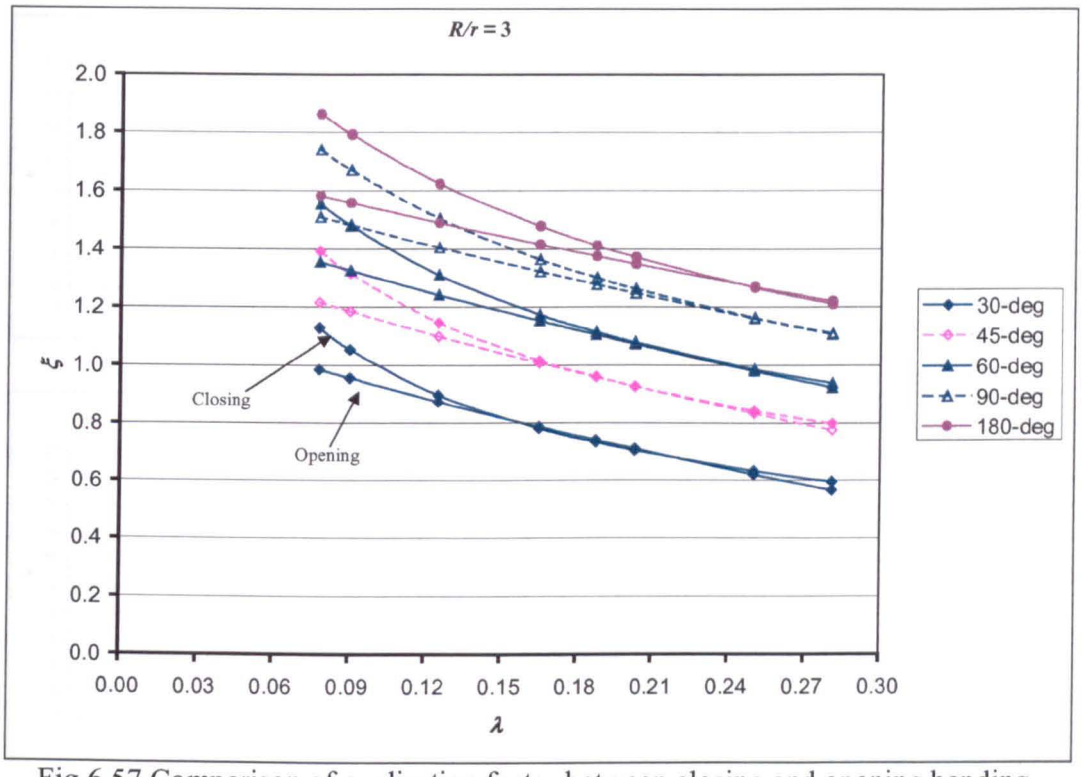

Fig.6.57 Comparison of ovalisation factor between closing and opening bending

Figure 6.58 shows flexibility factor for short-radius piping elbows under in-plane opening bending calculated using equation (6-30) in comparison with the flexibility factor for piping elbows under in-plane closing bending. Figure 6.58 shows that flexibility factors for piping elbows are not in the same magnitude for in-plane closing and opening moment, but lower for opening case especially for low pipe bend parameters. This trend can be found for small and large angle bend piping elbows. This difference arises from the structural behaviour, where piping elbows exhibits the behaviour of non-linear structural 'softening' under in-plane closing moment and non-linear structural 'hardening' under opening moment. Experimental investigation by Smith and Ford [38] also shows that pipe bends are more flexible under closing bending than under opening bending.

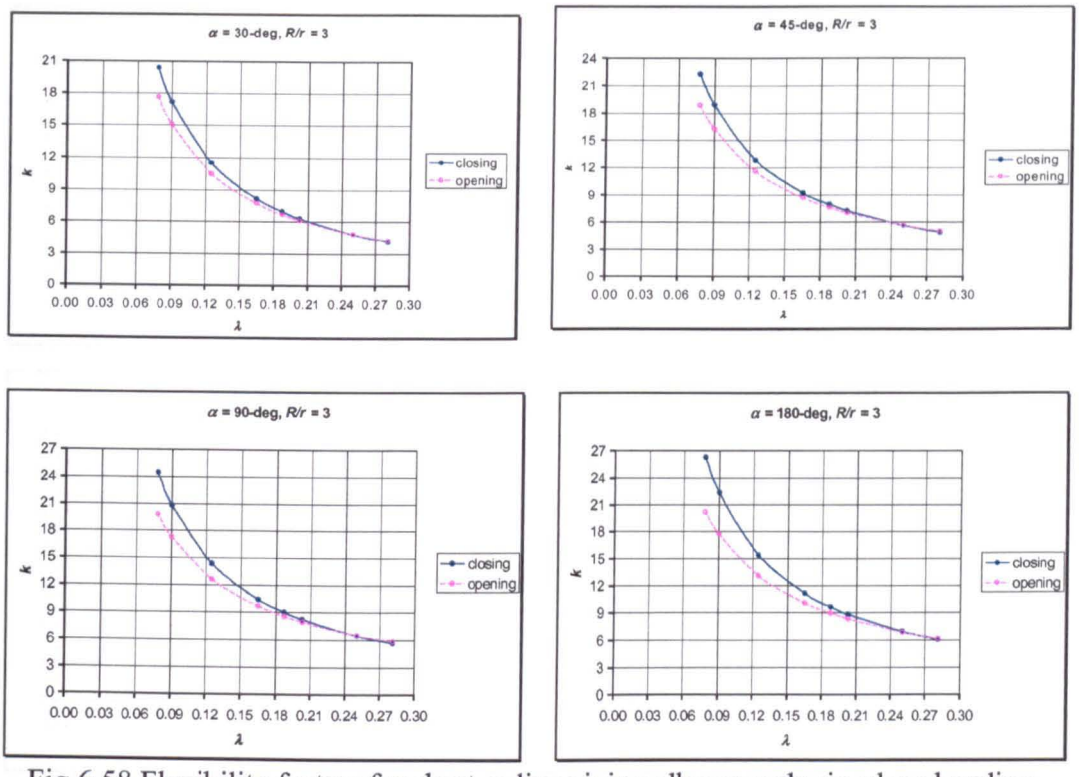

Fig.6.58 Flexibility factors for short-radius piping elbows under in-plane bending

Figure 6.59 shows the flexibility factor for long-radius piping elbows under in-plane opening bending calculated using equation (6-30) in comparison with the flexibility factor for piping elbows under in-plane closing bending. It can be seen again for long radius piping elbows that the flexibility factor under in-plane opening bending is lower than those for in-plane closing bending especially for low pipe bend parameters. This trend can be found for small and large angle bend piping elbows.

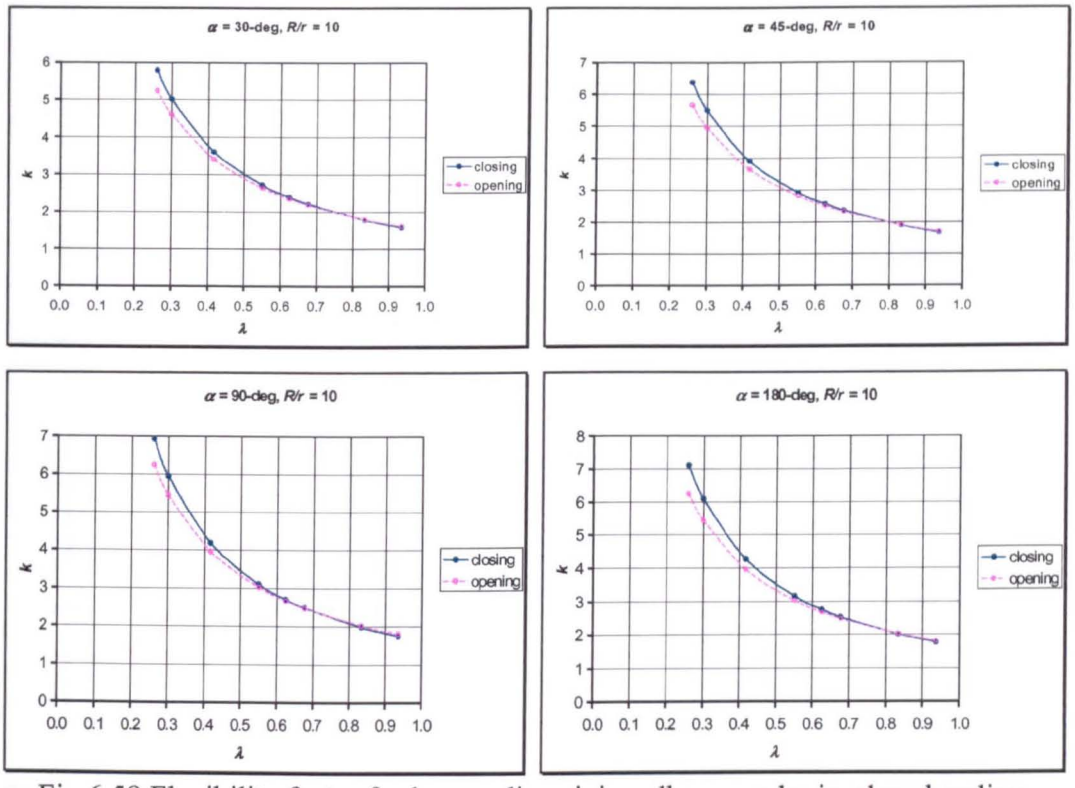

Fig.6.59 Flexibility factor for long-radius piping elbows under in-plane bending

Figure 6.60 shows the stress-intensification factor for short-radius piping elbows subjected to in-plane opening bending in comparison with those under in-plane closing bending. It can be seen from this figure that the stress-intensification factor of piping elbows under in-plane opening moment is lower than those for in-plane closing moment for elbows of low pipe bend parameter. The Stress-intensification factor under in-plane opening bending is slightly higher than those for in-plane closing bending for high pipe bend parameter.

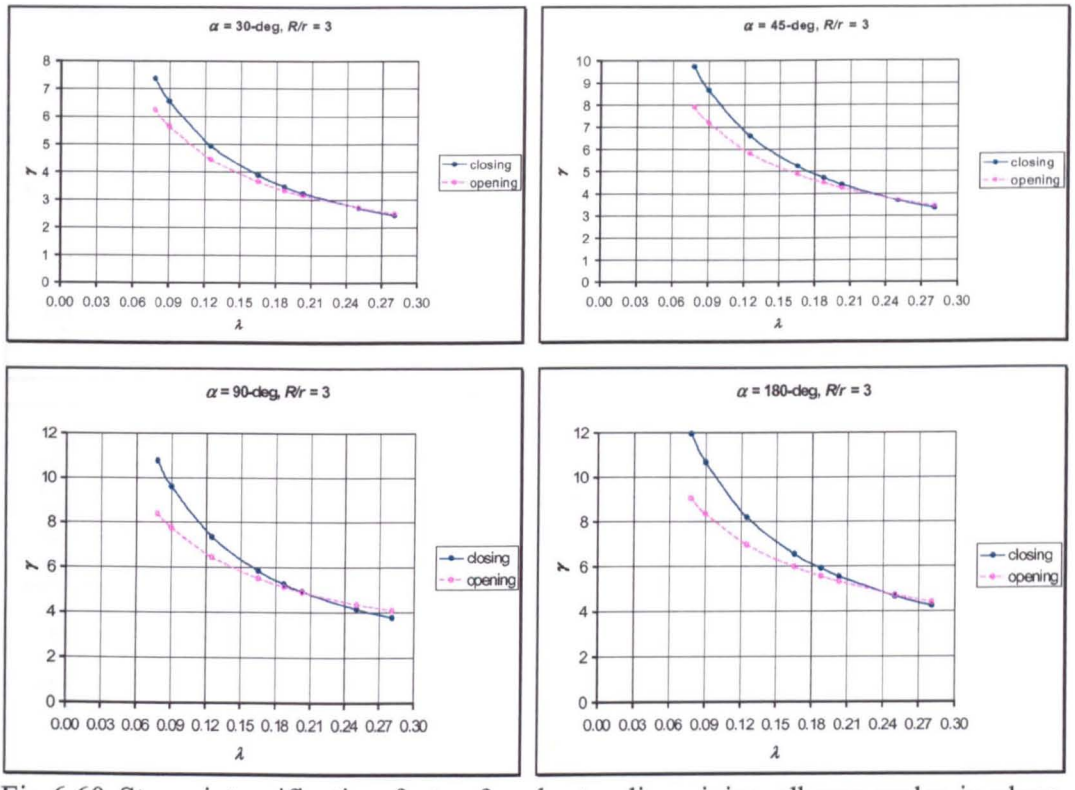

Fig.6.60 Stress-intensification factor for short-radius piping elbows under in-plane bending

Figure 6.61 shows the stress-intensification factor for long-radius piping elbows subjected to in-plane opening bending in comparison with those under in-plane closing bending. Again it can be seen that the stress-intensification factor of piping elbows under in-plane opening moment is much lower than those for in-plane closing moment for elbows of low pipe bend parameter, but slightly greater for high pipe bend parameter and large angle bend.

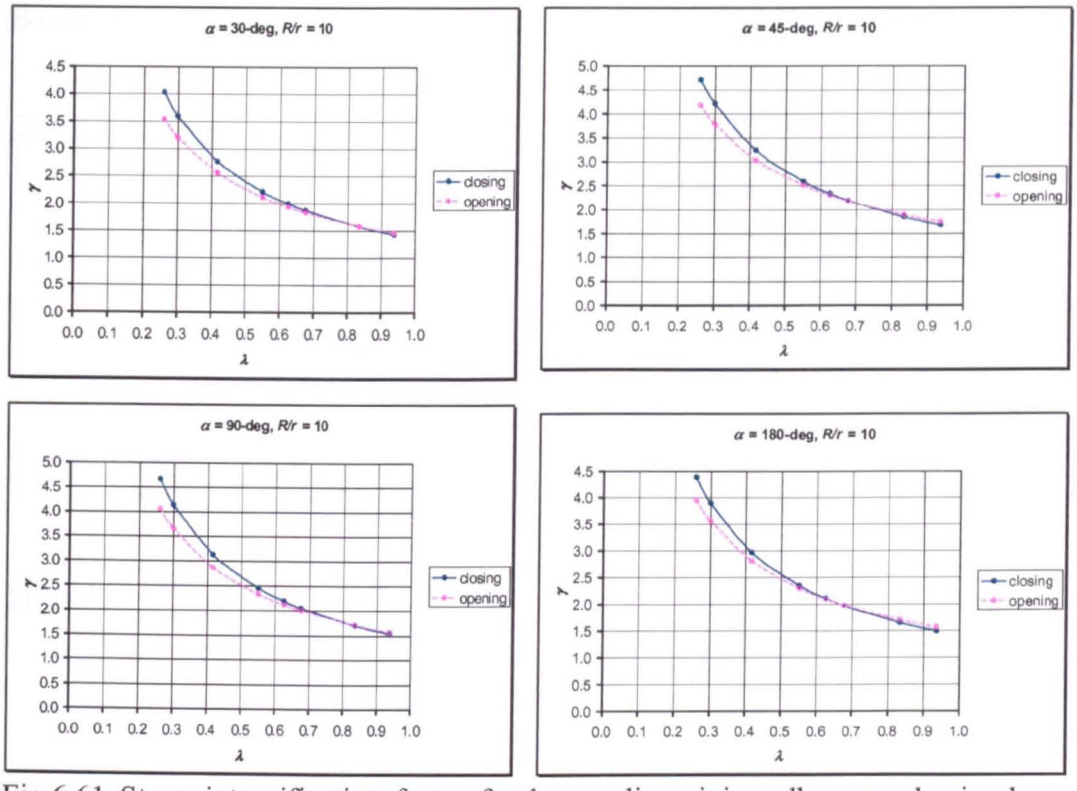

Fig.6.61 Stress-intensification factor for long-radius piping elbows under in-plane bending

6.4.2 Pressurized Conditions

In developing the formulae for the pressure reduction effect, the following approximations have been made:

(1) The pressure reduction is related linearly to the non-dimensional pressure paremater, p/E, nondimensional thickness r/t, and radius ratio R/r in a log-log plot. Accordingly, the pressure reduction effect can be approximated by a power law.

(2) The index in the power law for non-dimensional pressure, p/E, non-dimensional thickness, r/t, and radius ratio, R/r, has been based on results for the following particular data: $p = p_{\max}$, $R/r = 2$, $t/r = 0.026$.

Based on these observations, the following formulae have been developed:

Ovalisation factor

$$\xi_p = \frac{\xi}{1 + A\left(\frac{p}{E}\right)\left(\frac{r}{t}\right)^{5/3}\left(\frac{R}{r}\right)^m} \tag{6-60a}$$

$$\xi_p = \frac{\xi}{1 + B\left(\frac{pr^3}{3D}\right)\lambda^{4/3}\left(\frac{r}{R}\right)^n} \tag{6-60b}$$

Flexibility factor

$$k_p = \frac{k}{1 + A\left(\frac{p}{E}\right)\left(\frac{r}{t}\right)^{10/3}\left(\frac{R}{r}\right)^m} \tag{6-61a}$$

$$k_p = \frac{k}{1 + B\left(\frac{pr^3}{3D}\right)\left(\frac{1}{\lambda}\right)^{1/3}\left(\frac{r}{R}\right)^n} \tag{6-61b}$$

Stress-intensification factor

$$\gamma_p = \frac{\gamma}{1 + A\left(\frac{p}{E}\right)\left(\frac{r}{t}\right)^{10/3}\left(\frac{R}{r}\right)^m} \tag{6-62a}$$

$$\gamma_p = \frac{\gamma}{1 + B\left(\frac{pr^3}{3D}\right)\left(\frac{1}{\lambda}\right)^{1/3}\left(\frac{r}{R}\right)^n} \tag{6-62b}$$

where A, B, m, and n are functions of the bend angle and are summarised in the following Tables. The values are different for ovalisation, flexibility and stress-intensification factors.

Table 6.7 Values for A, B, m, and n in equation (6-60) for ovalisation factor

Bend angle (α)	*$A(\alpha)$*	*$B(\alpha)$*	*$m(\alpha)$*	*$n(\alpha)$*
30-deg	175	48.0	0.206	1.125
45-deg	126	34.5	0.333	1.005
60-deg	100	27.5	0.430	0.905
90-deg	76	21.0	0.570	0.765
180-deg	52	14.5	0.725	0.610

Table 6.8 Values for A, B, m, and n in equation (6-61) for flexibility factor

Bend angle (α)	*$A(\alpha)$*	*$B(\alpha)$*	*$m(\alpha)$*	*$n(\alpha)$*
30-deg	0.300	0.084	0.037	0.370
45-deg	0.225	0.062	0.174	0.507
60-deg	0.185	0.051	0.266	0.599
90-deg	0.145	0.040	0.376	0.709
180-deg	0.115	0.031	0.481	0.814

Table 6.9 Values of A, B, m, and n in eqn (6-62) for stress-intensification factor

Bend angle (α)	*$A(\alpha)$*	*$B(\alpha)$*	*$m(\alpha)$*	*$n(\alpha)$*
30-deg	0.330	0.091	0.245	0.578
45-deg	0.236	0.063	0.393	0.726
60-deg	0.183	0.050	0.502	0.835
90-deg	0.172	0.047	0.546	0.879
180-deg	0.124	0.034	0.685	1.019

It is worthwhile examining the error introduced as a result of the two approximations described above. The percentage is calculated here as:

$$Err = \left|1 - \frac{fd}{fe}\right| x100\%$$

where *fd* represents either ovalisation, flexibility, or stress-intensification factor obtained using the derived formula and *fe* represents the data obtained directly from the finite element analyses.

Using this definition of error, the maximum percentage is summarised in the following Tables:

Table 6.10 Maximum error for ovalisation factor, %

Bend angle (α)	*R/r* = 2	*R/r* = 3	*R/r* = 6	*R/r* = 10
30-deg	9.9	11.3	13.0	13.4
45-deg	8.0	9.9	12.6	13.4
60-deg	7.4	9.3	12.6	13.7
90-deg	6.1	8.5	13.0	14.4
180-deg	6.2	6.1	9.3	13.5

Table 6.11 Maximum error for flexibility factor, %

Bend angle (α)	*R/r* = 2	*R/r* = 3	*R/r* = 6	*R/r* = 10
30-deg	7.1	7.5	7.7	6.7
45-deg	5.8	6.4	6.5	6.7
60-deg	5.1	5.2	6.5	6.7
90-deg	5.1	5.0	7.1	6.8
180-deg	4.1	5.6	8.6	7.0

Table 6.12 Maximum error for stress-intensification factor, %

Bend angle (α)	*R/r* = 2	*R/r* = 3	*R/r* = 6	*R/r* = 10
30-deg	6.9	7.2	7.4	7.8
45-deg	6.2	6.3	7.3	7.9
60-deg	5.7	5.4	6.9	8.2
90-deg	5.5	5.2	7.0	8.3
180-deg	5.2	5.1	8.7	8.7

It can be seen from these Tables that there is a relatively large error in the approximate equations as compared to the finite element results, especially for the ovalisation factor. As indicated previously, this error results from the two approximations used. This error could be reduced by trial-and error curve fitting to find more appropriate indices for *r/t* and *R/r*. However the maximum error for flexibility and stress-intensification factor from Table 6.11 and 6.12 is less than 10% and deemed appropriate for design purposes.

Figure 6.62 shows a comparison of ovalisation factor between in-plane opening and closing bending for short-radius 90-deg pipe elbows. Recalling the formulae for ovalisation factor for short-radius (*R/r* = 3), 90-deg pipe elbows:

$$\left.\begin{aligned} \xi_p &= \frac{\xi}{1+76\left(\frac{p}{E}\right)\left(\frac{r}{t}\right)^{5/3}\left(\frac{R}{r}\right)^{0.57}} \\ \xi &= 1.656\exp(-1.175\lambda)[1.0254-0.3452\lambda] \end{aligned}\right\} \quad \text{in - plane opening bending}$$

$$\left.\begin{aligned} \xi_p &= \frac{\xi}{1+0.205\left(\frac{p}{E}\right)\left(\frac{r}{t}\right)^{10/3}\left(\frac{R}{r}\right)^{0.464}}; \text{for} \frac{r}{t} > 13.33 \\ \xi &= \frac{0.565}{\lambda^{2/3}}[1.1179+0.2177\ln(\lambda)] \end{aligned}\right\} \quad \text{in - plane closing bending}$$

It can be seen from Fig.6.62 that there is a marked difference for the pressure reduction effect on ovalisation factor between in-plane opening and closing bending. Overall it can be seen that the magnitude of the pressure reduction is higher for in-plane opening bending, even for relatively thick-walled pipe, whereas internal pressure increases the ovalisation factor for thick-walled pipes.

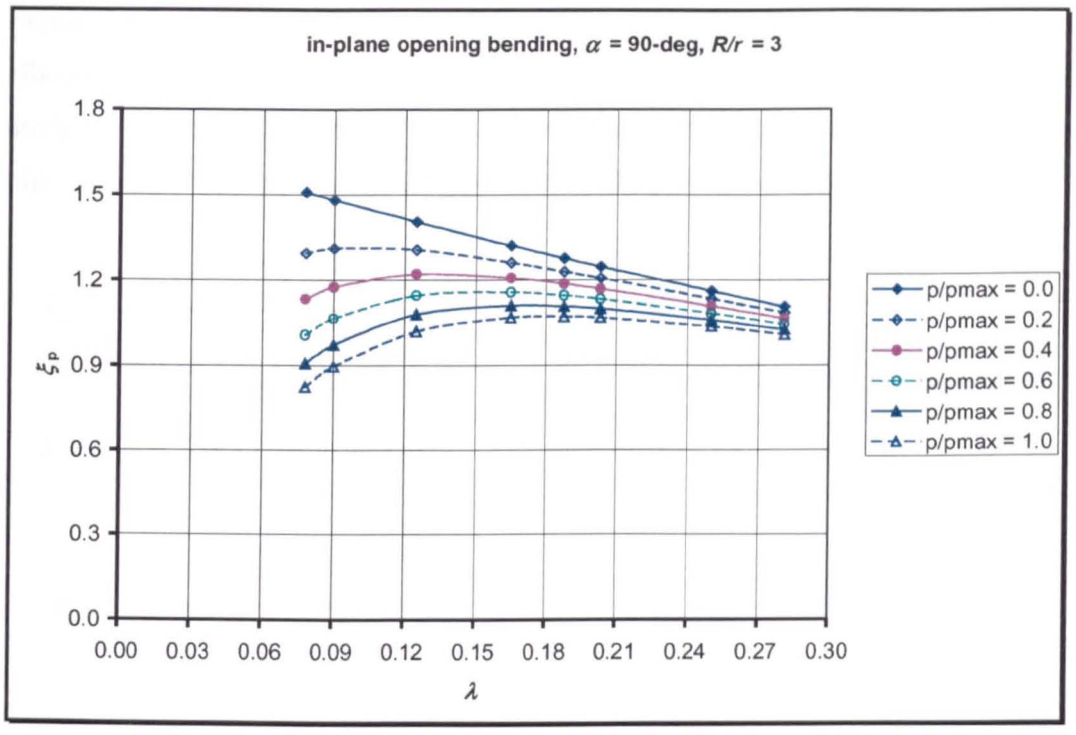

(a)

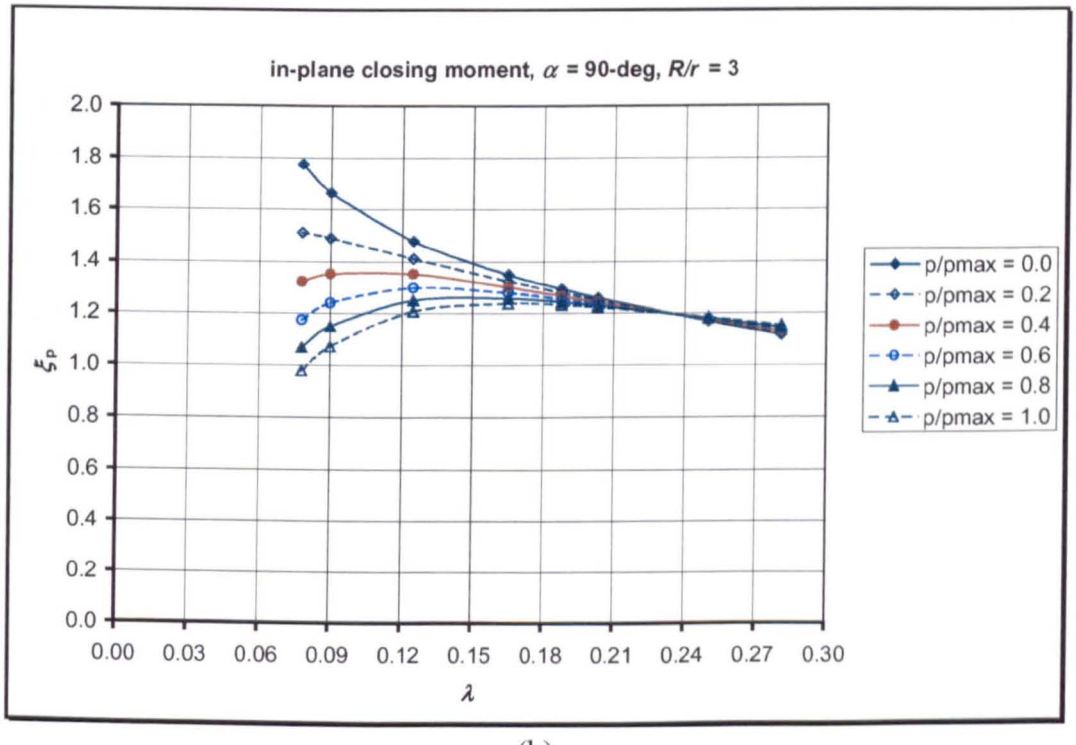

(b)

Fig.6.62 Pressure reduction effect for ovalisation factor of piping elbows under in-plane bending: (a) opening mode, (b) closing mode

Figure 6.63 shows a comparison of flexibility factor for short-radius 90-deg pipe elbows under in-plane opening and closing bending obtained from the present analysis. Recalling the formulae for flexibility factor of short-radius (R/r = 3), 90-deg pipe elbows under in-plane bending obtained in the present analysis:

$$\left.\begin{aligned} k_p &= \frac{k}{1+0.145\left(\frac{p}{E}\right)\left(\frac{r}{t}\right)^{10/3}\left(\frac{R}{r}\right)^{0.376}}; \quad \text{for} \frac{r}{t} > 12.35 \\ k &= \frac{1.65}{\lambda}[1.058+0.0475\ln(\lambda)] \end{aligned}\right\} \quad \text{in - plane opening bending}$$

$$\left.\begin{aligned} k_p &= \frac{k}{1+11.75\left(\frac{p}{E}\right)\left(\frac{r}{t}\right)^{9/4}\left(\frac{R}{r}\right)^{0.31}} \\ k &= \frac{1.65}{\lambda}[0.78-0.1485\ln(\lambda)] \end{aligned}\right\} \quad \text{in - plane closing bending}$$

It can be seen from these equations that the index of r/t and R/r of the pressure reduction are bigger for opening bending, but the coefficient of the pressure reduction is bigger for closing bending. In addition there is a marked difference in the coefficient – much lower for opening bending. Overall, the magnitude of the pressure reduction for flexibility factor is bigger for closing bending as shown in Fig.6.63.

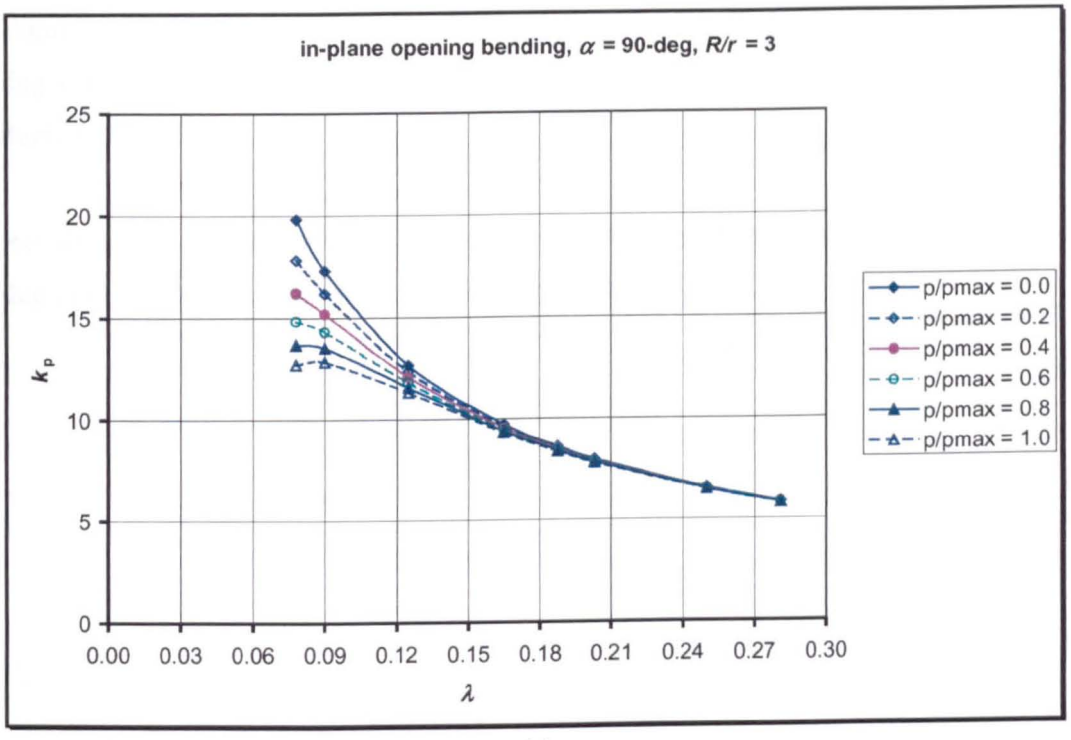

(a)

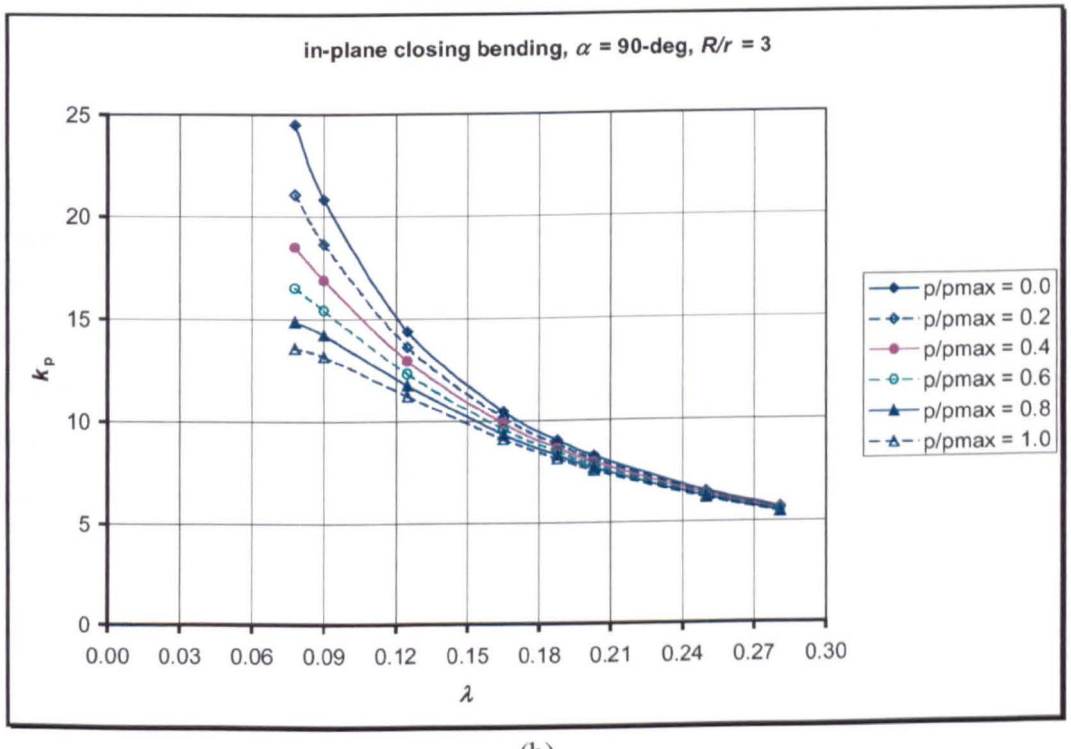

(b)

Fig.6.63 Flexibility factors for short-radius 90-deg pipe elbows under in-plane bending: (a) opening bending, (b) closing bending

Figure 6.64 shows a comparison of stress-intensification factor for short-radius, 90-deg pipe elbows under in-plane opening and closing bending calculated using the derived formula.

Recalling the formulae for stress-intensification factor of short-radius (R/r = 3), 90-deg pipe elbows under in-plane bending obtained previously:

$$\left.\begin{aligned} \gamma_p &= \frac{\gamma}{1+0.172\left(\frac{p}{E}\right)\left(\frac{r}{t}\right)^{10/3}\left(\frac{R}{r}\right)^{0.546}} \\ \gamma &= \frac{1.89}{\lambda^{2/3}}[1.1992+0.1062\ln(\lambda)] \end{aligned}\right\} \quad \text{in - plane opening bending}$$

$$\left.\begin{aligned} \gamma_p &= \frac{\gamma}{1+10.25\left(\frac{p}{E}\right)\left(\frac{r}{t}\right)^{7/3}\left(\frac{R}{r}\right)^{0.435}} \\ \gamma &= \frac{1.89}{\lambda^{2/3}}[0.7715-0.165\ln(\lambda)] \end{aligned}\right\} \quad \text{in - plane closing bending}$$

Again it can be seen that the indices are very different, being much bigger for opening bending and again followed by a significant difference in the coefficient (0.172 for opening bending and 10.25 for closing bending). It can be seen from Fig.6.64 that the magnitude of the pressure reduction is much bigger for closing bending, implying that pipe elbows under opening bending are stiffer than under closing bending.

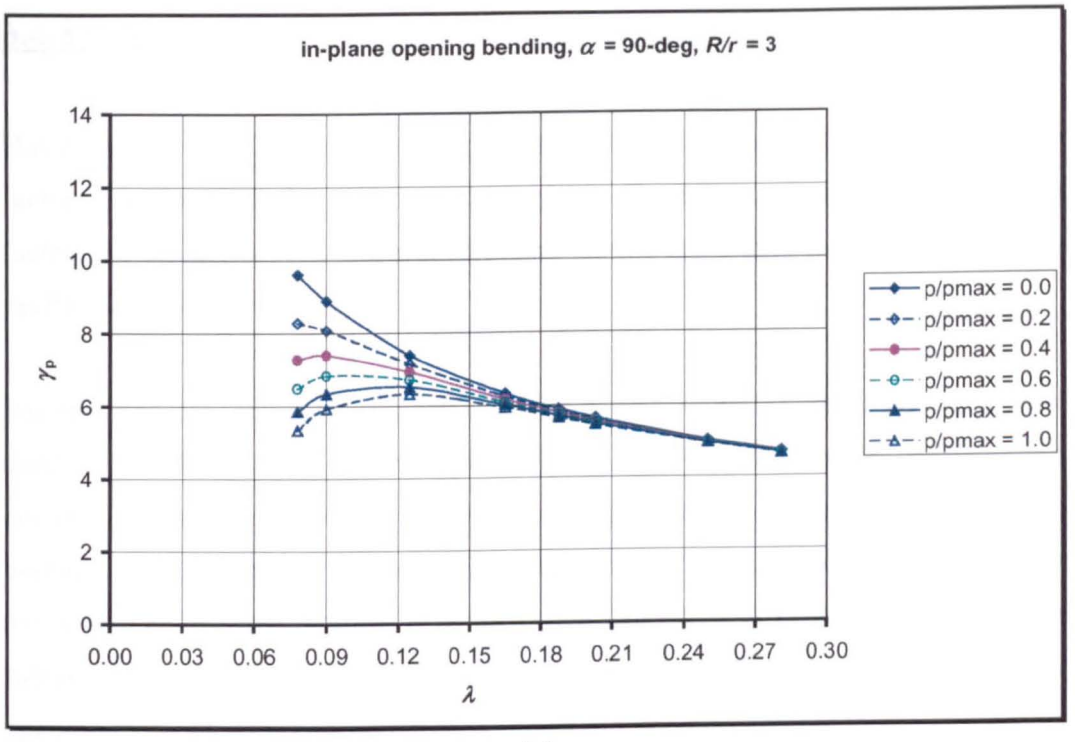

(a)

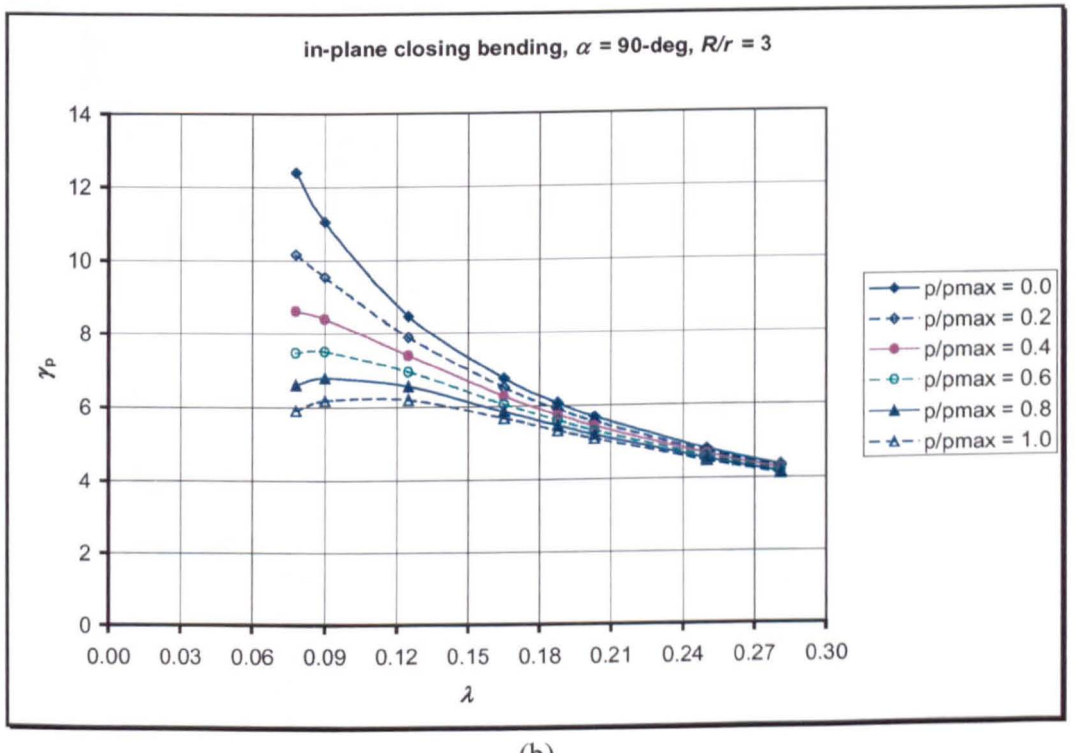

(b)

Fig.6.64 Stress-intensification factor short-radius, 90-deg pipe elbows under in-plane bending: (a) pening bending, (b) closing bending

6.4.3 S-Shaped Back-to-Back 90-deg Piping Elbows

Having established approximate formulae for flexibility and stress-intensification factors for piping elbows with straight tangents, flexibility and stress-intensification factors for closely-spaced thin-walled piping elbows are briefly examined in order to verify their accuracy.

For this purpose, (model 2, model 3, model 4, and model 5) elbow configurations used by Glickstein and Schmitz [93, 96] are checked. The basic configuration consists of two-90-deg elbows with various lengths of tangent and is arranged in an S-shape. One end of the model is fixed and another end is loaded by an in-plane moment. The in-plane moment is applied such that elbow-A (lower quarter bend) is subjected to a closing bending and elbow-B (upper quarter bend) is subjected to an opening moment. This configuration is shown in Fig.6.65

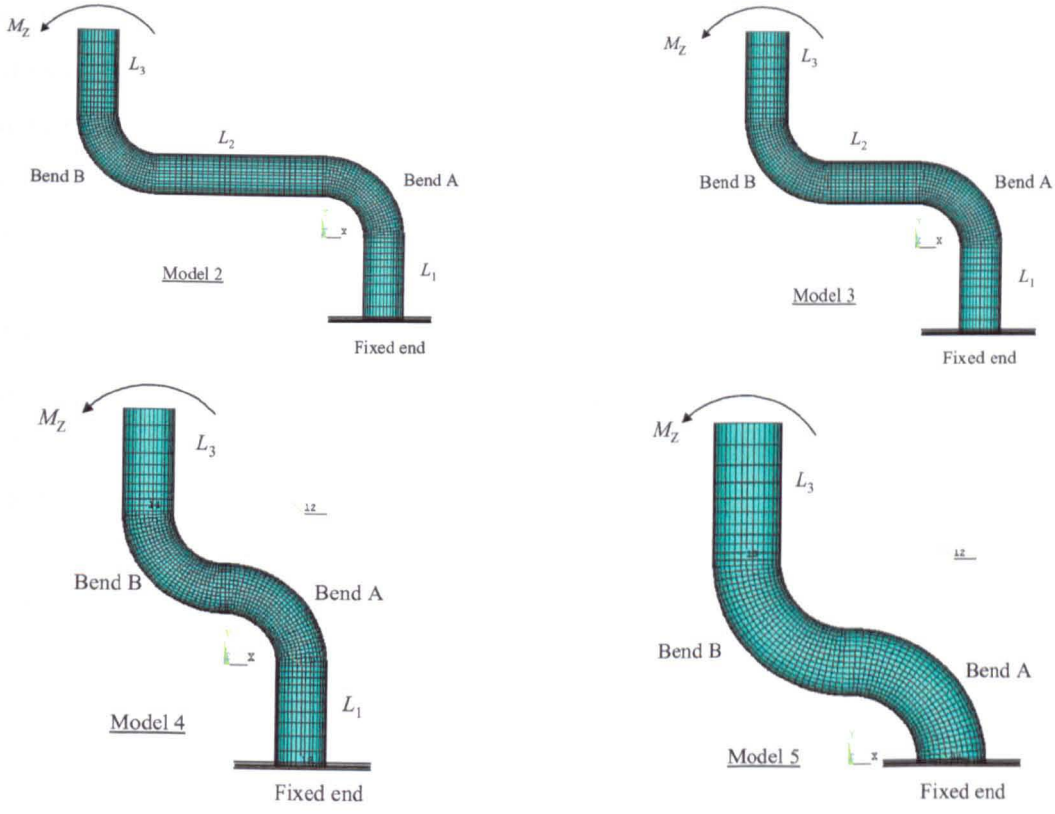

Fig.6.65 Glicstein & Schmitz's model elbow configurations

Key to Fig.6.65:

Wall thickness (t) = 0.245 in = 6.223 mm

Cross-section radius (r) = 7.96 in = 202.25 mm

Radius ratio (R/r) = 3.05

Thickness ratio (r/t) = 32.5

Pipe bend parameter (λ) = 0.0904

Length of tangents: Model 2: $L1 = L3 = 32$ in, $L2 = 64$ in

Model 3: $L1 = L2 = L3 = 32$ in

Model 4: $L1 = L3 = 32$ in, $L2 = 0$

Model 5: $L1 = L2 = 0$, $L3 = 32$ in

Glickstein and Schmitz [93, 96] analysis these model using ABAQUS finite element program. The elbow and pipe tangents were modelled using the S8R quadratic 8-node thick shell element. Geometry and finite element modelling was described in section 3.2. In-plane bending was applied as concentrated force to simulate a linear stress distribution in the pipe due to in-plane bending. The end rotation was determined from the axial displacement of nodes at the ends of the elbows as described in section 5.2.1 of this thesis. This procedure was also implemented by Thomas [78].

Table 6.13 gives a summary of flexibility factors from the present analysis in comparison with the result presented by Glickstein & Schmith in their original paper. The appropriate approximate formulae for unpressurised pipe elbows derived in this study are:

(a) In-plane closing moment:

$$k = \frac{1.65}{\lambda}[0.78 - 0.1485\ln(\lambda)] \qquad (5-40)$$

(b) In-plane opening moment:

$$k = \frac{1.65}{\lambda}[1.058 + 0.0475\ln(\lambda)] \qquad (6\text{-}27)$$

(c) The asymptotic solution of Clark and Reissner [20]:

$$k = \frac{1.65}{\lambda}$$

For the geometries considered in Glickstein and Schmitz's study ($\lambda = 0.0904$), the flexibility factor is:

$k_{ic} = 20.75$ (in - plane closing moment)
$k_{io} = 17.22$ (in - plane opening moment)
$k_{C\&R} = 18.25$ (Clark and Reissner)

Table 6.13 Summary of flexibility factors for S-shaped pipe bends

Elbow model (see figures)	Flexibility factor, k			
	ANSYS	G&S [93]	Formulae	C&R [20]
2A (closing moment)	18.33	16.24	20.75	18.25
2B (opening moment)	12.83	17.33	17.22	
3A (closing moment)	18.32	16.24	20.75	18.25
3B (opening moment)	11.47	17.33	17.22	
4A (closing moment)	14.19	12.96	20.75	18.25
4B (opening moment)	5.67	13.87	17.22	
5A (closing moment)	5.59	5.11	20.75	18.25
5B (opening moment)	3.15	13.87	17.22	

In Table 6.13 the results under the column heading marked as ANSYS is obtained from a new finite element solution. Comparison of results for model-2 and -3 between FE result (ANSYS) and those calculated using the derived formulae indicated that the length of tangent ($L = 4r$) was not sufficiently long enough to eliminate end effect. For an S-shaped pipe bends without intermediate tangent

(model –4 and –5), the flexibility factor reduces significantly. The results from Table 6.13 confirm the major conclusion of Glickstein & Schmitz [93] that the restraining effect of an S-shaped back-to-back piping elbow results in a significant reduction in flexibility.

It is interesting to note from Table 6.13 that the result from the present analysis is consistent: the flexibility factor under closing moment is always larger than under opening. Recall the reason for this is that elbows under in-plane closing moment exhibit non-linear softening structural behaviour, while elbows loaded by in-plane opening moment exhibit non-linear hardening structural behaviour. This is contrary to the results presented by Glickstein & Schmitz [93] where elbows under closing moment are stiffer than under an opening moment. The reason for this difference is probably caused by the large deformation effect. It should be noted that the analysis of Glickstein and Schmitz [93] does not take large deformation effects into account, while in the present analysis does.

Table 6.14 summarises the comparison for stress-intensification factor, their direction, surface and location. The location is expressed as (θ, ϕ), where θ and ϕ are the longitudinal and circumferential directions respectively. The longitudinal position is measured from the junction with the fixed tangent for elbows-A (closing moment) and from the junction with the loaded tangent for elbows-B (opening moment). The circumferential position is measured from the extrados.

Table 6.14 Summary of stress-intensification factors, their direction, surface, and locations

Model	present analysis				Glickstein & Schmitz			
	SIFs	Dir	Surf	Loc	SIFs	Dir	Surf	Loc
2A	9.83	Hoop	Inner	51, 100	8.26	Hoop	Inner	60, 80
2B	9.13	Hoop	Inner	51, 100	9.83	Hoop	Inner	45, 80
3A	10.12	Hoop	Inner	48, 100	9.45	Hoop	Inner	50, 100
3B	9.41	Hoop	Inner	48, 100	10.28	Hoop	Inner	50, 80
4A	9.3	Hoop	Inner	33, 100	6.83	Hoop	Inner	30, 100
4B	9.7	Hoop	Inner	33, 100	8.88	Hoop	Inner	60, 80
5A	7.14	Long	Outer	0, 0	5.40	Hoop	Inner	0, 80
5B	8.01	Hoop	Inner	33, 100	8.13	Hoop	Inner	60, 80

Recalling the formulae developed for stress-intensification factor for 90-deg pipe elbows having $R/r = 3$ with long tangents:

(a) In-plane closing moment:

$$\gamma = \frac{1.89}{\lambda^{2/3}}[0.7715 - 0.165\ln(\lambda)] \qquad (5\text{-}65)$$

(b) In-Plane opening moment:

$$\gamma = \frac{1.89}{\lambda^{2/3}}[1.1992 + 0.1062\ln(\lambda)] \qquad (6\text{-}46)$$

From the asymptotic solution of Clark and Reissner [20]:

$$\gamma = \frac{1.892}{\lambda^{2/3}} + \frac{0.48}{\lambda^{1/3}}$$

and from the fatigue test result of Markl [23]

$$\gamma = \frac{0.9}{\lambda^{2/3}}$$

For the geometries considered in Glickstein & Schmitz's [96] analysis, the stress-intensification factors are:

$\gamma_{close} = 12.22$	(in-plane closing moment)
$\gamma_{open} = 9.87$	(in-plane opening moment)
$\gamma_{C\&R} = 10.46$	(Clark and Reissner's asymptotic solution)
$\gamma_{Markl} = 4.47$	(Markl's fatigue test)

These values can now be compared with Table 6.14 obtained directly from a new finite element solution.

Comparison using the formulae derived here and the results in Table 6.14 once more confirms the conclusion of Glickstein & Schmitz [96] that the restraining effect of an S-shaped back-to-back elbow causes a significant reduction in stress-intensification.

It is interesting to note that the results given by Glickstein & Schmitz for stress-intensification of all the models considered is higher under in-plane opening moment than under in-plane closing moment. Contrary, the present analysis shows that the stress-intensification factor is higher under a closing moment than under an opening moment if there is intermediate tangent present between two elbows (model-2 & model-3). If there is no intermediate tangent between the two elbows, the maximum stress is higher under an opening moment than under a closing moment. The reason for this difference again believed to be caused by large deformation effects, which are not included by Glickstein & Schmitz.

The pressure reduction effect was not included in both Glickstein and Schmitz' paper [93, 96]. This effect is now considered here, focusing on how the pressure reduction

is influenced by the spacing tangent. The various formulae developed in the previous section summarising:

- Flexibility factors:

$$k_p = \frac{k}{1+11.75\left(\frac{p}{E}\right)\left(\frac{r}{t}\right)^{9/4}\left(\frac{R}{r}\right)^{0.31}} \quad \text{closing bending} \qquad (5-46)$$

$$k_p = \frac{k}{1+0.145\left(\frac{p}{E}\right)\left(\frac{r}{t}\right)^{10/3}\left(\frac{R}{r}\right)^{0.37}}; \text{for} \frac{r}{t} > 12.35, \text{ opening bending} \qquad (6-31)$$

- Stress-intensification factors:

$$\gamma_p = \frac{\gamma}{1+10.25\left(\frac{p}{E}\right)\left(\frac{r}{t}\right)^{7/3}\left(\frac{R}{r}\right)^{0.43}} \quad \text{closing bending} \qquad (5-71)$$

$$\gamma_p = \frac{\gamma}{1+0.172\left(\frac{p}{E}\right)\left(\frac{r}{t}\right)^{10/3}\left(\frac{R}{r}\right)^{0.54}} \quad \text{opening bending} \qquad (6-50)$$

Using these equations and the value for unpressurized elbows from Table.6.13 and 6.14, the pressure reduction effect on flexibility and stress-intensification is shown in Fig.6.66 and 6.67 respectively.

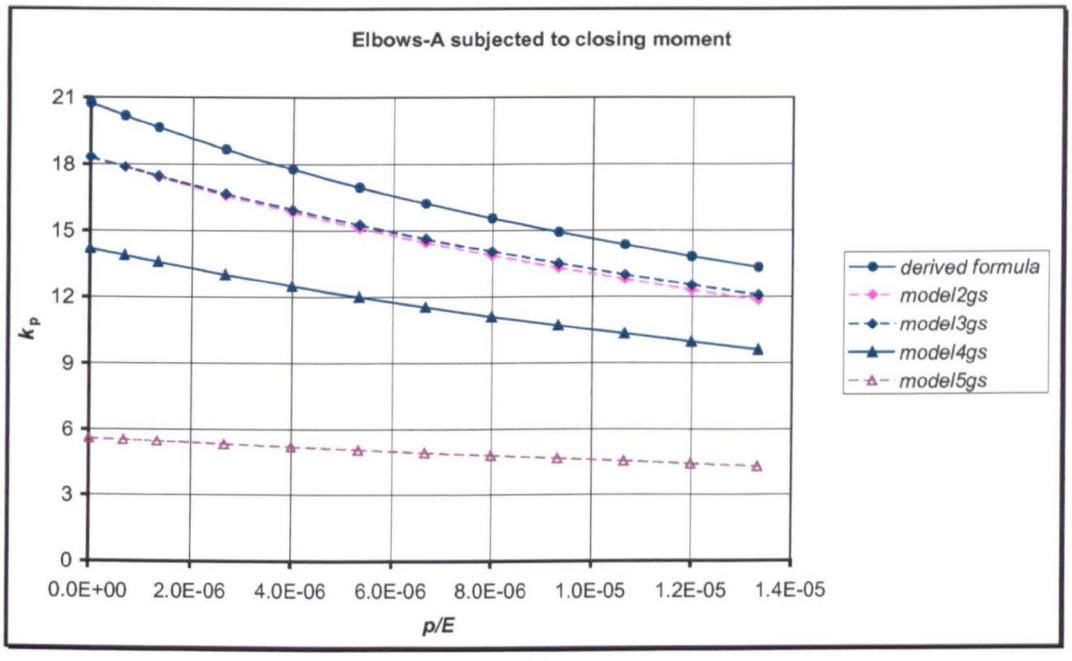

(a)

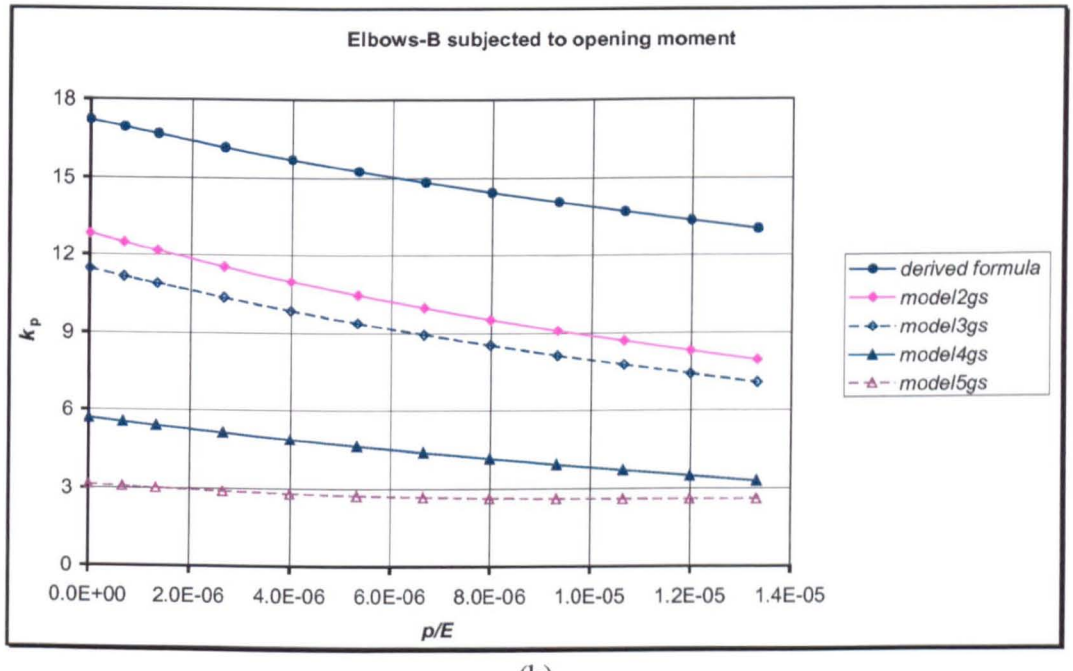

(b)

Fig.6.66 Flexibility factors for (a) Elbow-A under closing moment, (b) Elbow-B under opening moment

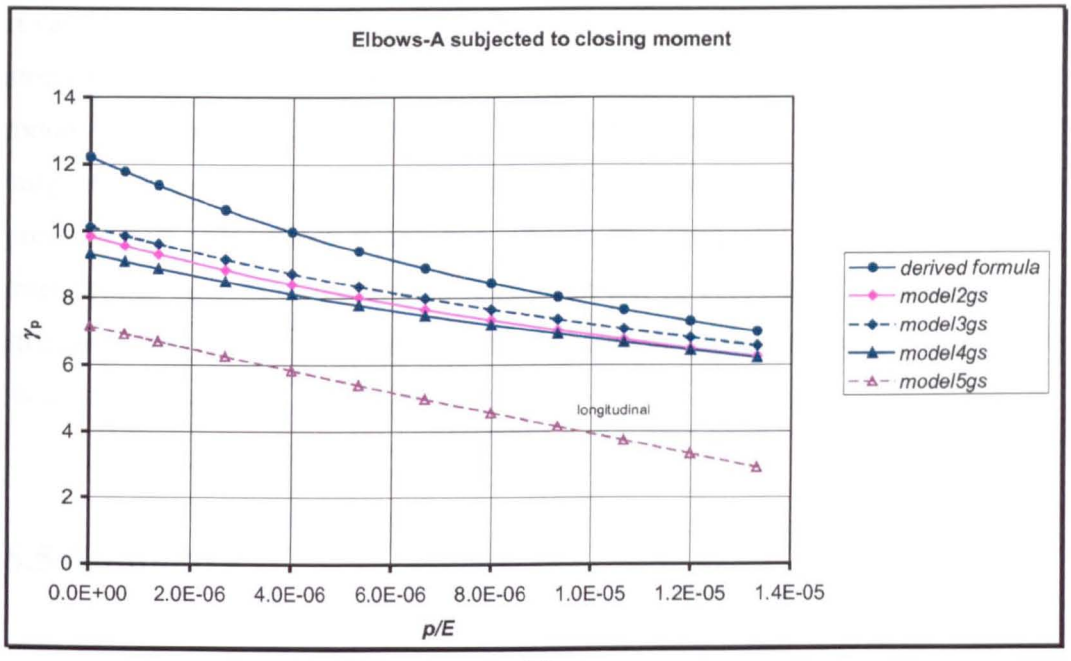

(a)

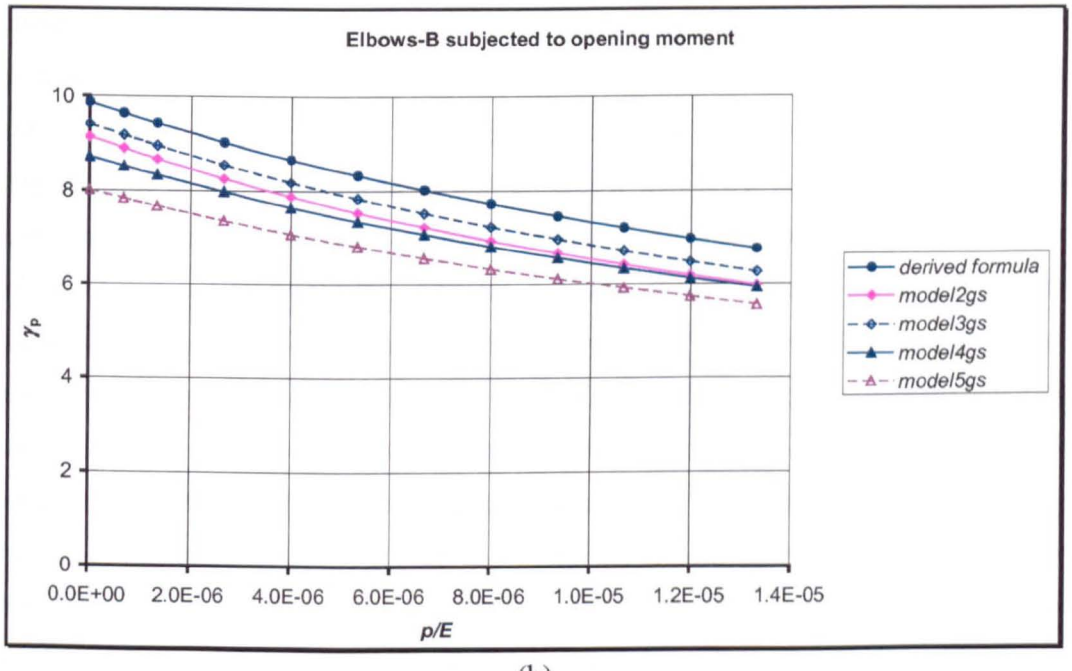

(b)

Fig.6.67 Stress-intensification factors for (a) Elbow-A under closing moment, (b) Elbow-B under opening moment

It can be seen from these figures that the pressure reduction effect on flexibility and stress-intensification developed in the present analysis has the same trend as that for model-2 and model-3 in the Glickstein and Schmitz study [93, 96] if an intermediate tangent is present between the two elbows. There is a significant difference in the pressure reduction effect if the two elbows are connected together without an intermediate tangent between them. Overall, it can be concluded that attachment of straight tangent at both ends of a pipe bend should be sufficiently length to eliminate its restraining effects.

6.5 Summary

Detailed non-linear large deformation finite element analysis of symmetrical piping elbows of various geometries under in-plane opening moment and internal pressure have been carried out to develop approximate formulae for the cross-sectional ovalisation, flexibility, and stress-intensification factor. It has been found that a piping elbow is stiffer under opening moment than under closing moment. The explanation to this phenomena is that an elbow subjected to an opening moment exhibits non-linear hardening structural behaviour (geometric stiffening), whereas an elbow subjected to a closing moment exhibits a non-linear softening structural behaviour (geometric weakening). The accuracy of the formulae developed in Chapter 5 for in-plane closing bending and in Chapter 6 for in-plane opening bending are checked for piping elbow configuration of type *S-shaped back-to-back* arrangement where closing and opening mode are exhibited under an in-plane bending. Comparison of results for unpressurised conditions obtained directly from finite element analysis and the derived formulae confirm the major conclusion drawn by Glickstein and Schmitz [93, 96] that the restraining effect of an S-shaped back-to-back piping elbow result in a significant reduction in flexibility and stress-intensification. However, the study carried out-out-by Glickstein and Schmitz show that elbows are stiffer under in-plane closing bending than under in-plane opening bending, whereas the present analysis give a contradict conclusion. The reason for this contradiction is caused by large deformation effects, which were not included in

Glickstein and Schmitz's study. Now that the pressure reduction effect is found to be different for in-plane closing and opening moment, it is of interest to investigate the pressure reduction effect for elbows subjected to out-of-plane bending. The following Chapter will dealt with this problem.

Appendix C6

This appendix present Figures for in-plane opening bending. All the approximate formula presented in this Chapter have been derived from these Figures:

Fig.A6.1 – A6.5: for Ovalisation factor

Fig.A6.6 – A6.10: for Flexibility factor

Fig.A6.11 – A6.15: for Stress-intensification factor

Continue to the next pages...→

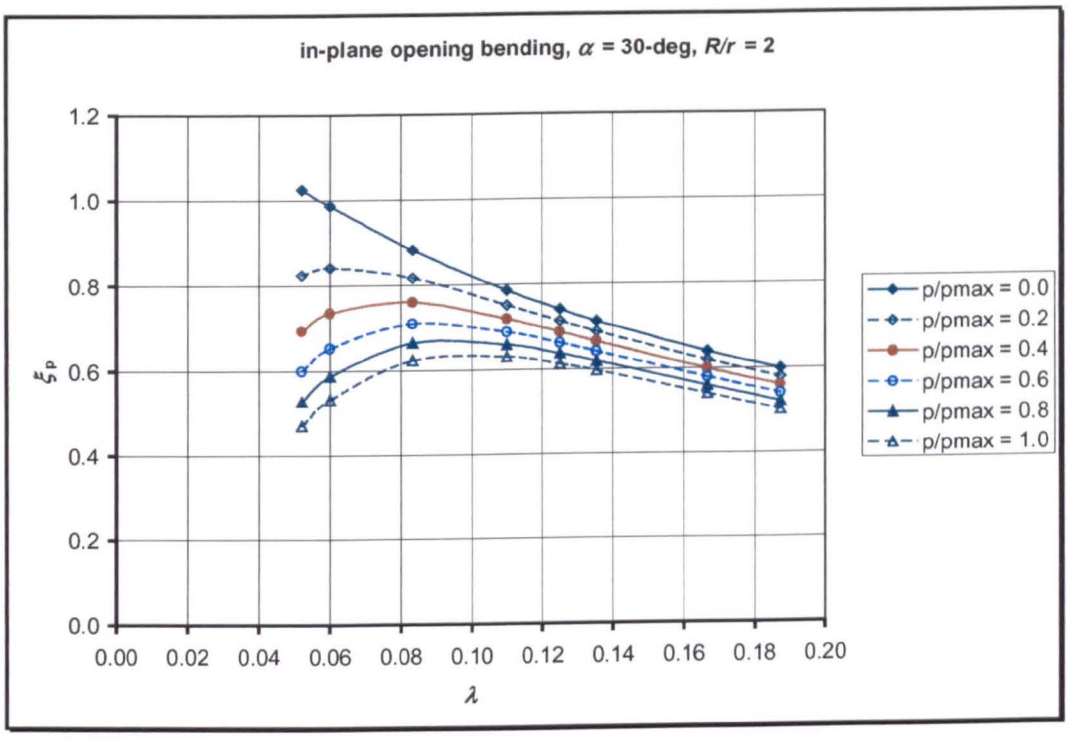

(a)

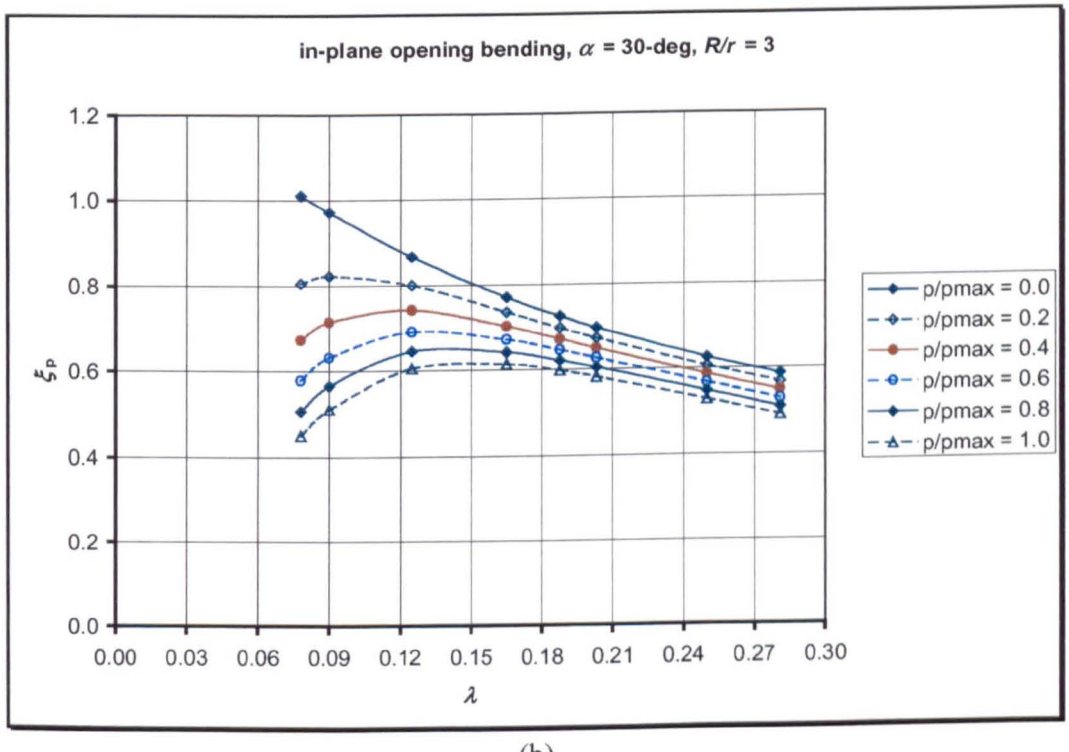

(b)

Fig.A6.1 Ovalisation factor for 30-deg pipe elbows under in-plane opening bending: (a) $R/r = 2$, (b) $R/r = 3$

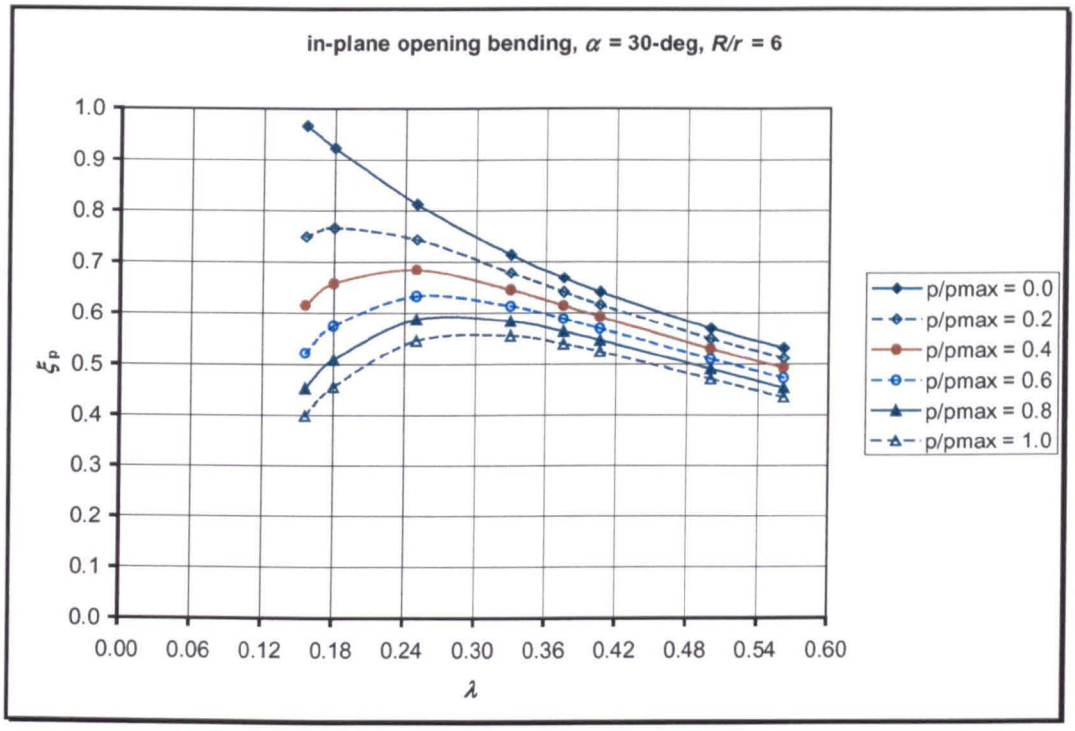

(c)

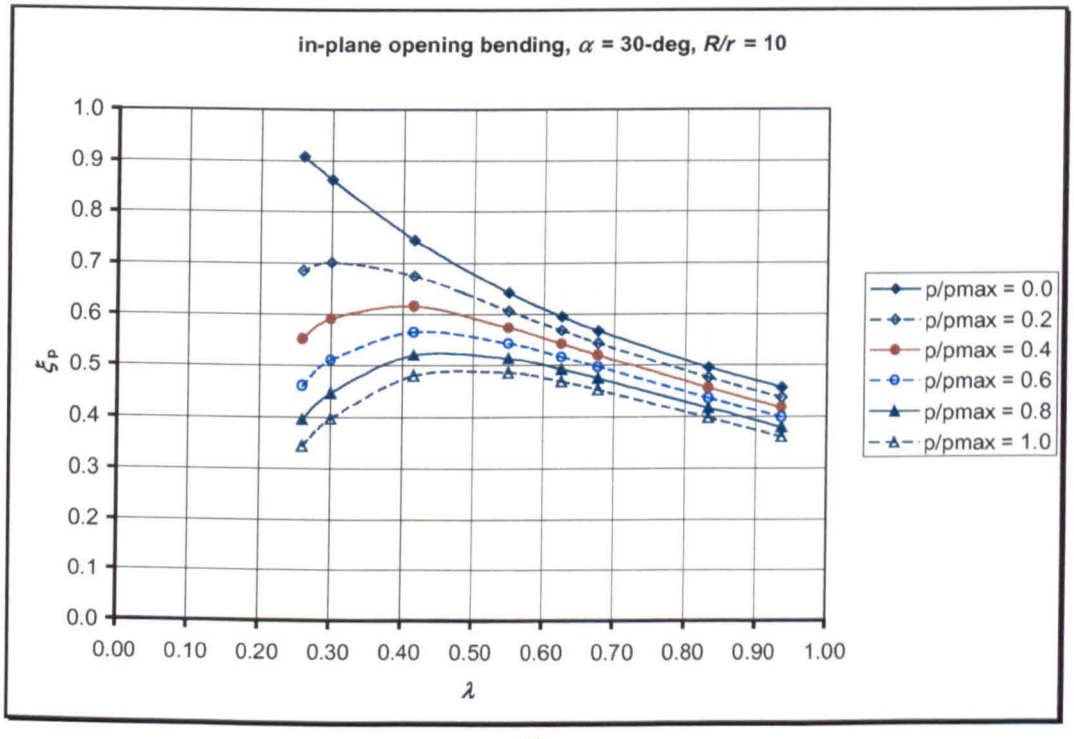

(d)

Fig.A6.1 Ovalisation factor for 30-deg pipe elbows under in-plane opening bending: (c) $R/r = 6$, (d) $R/r = 10$

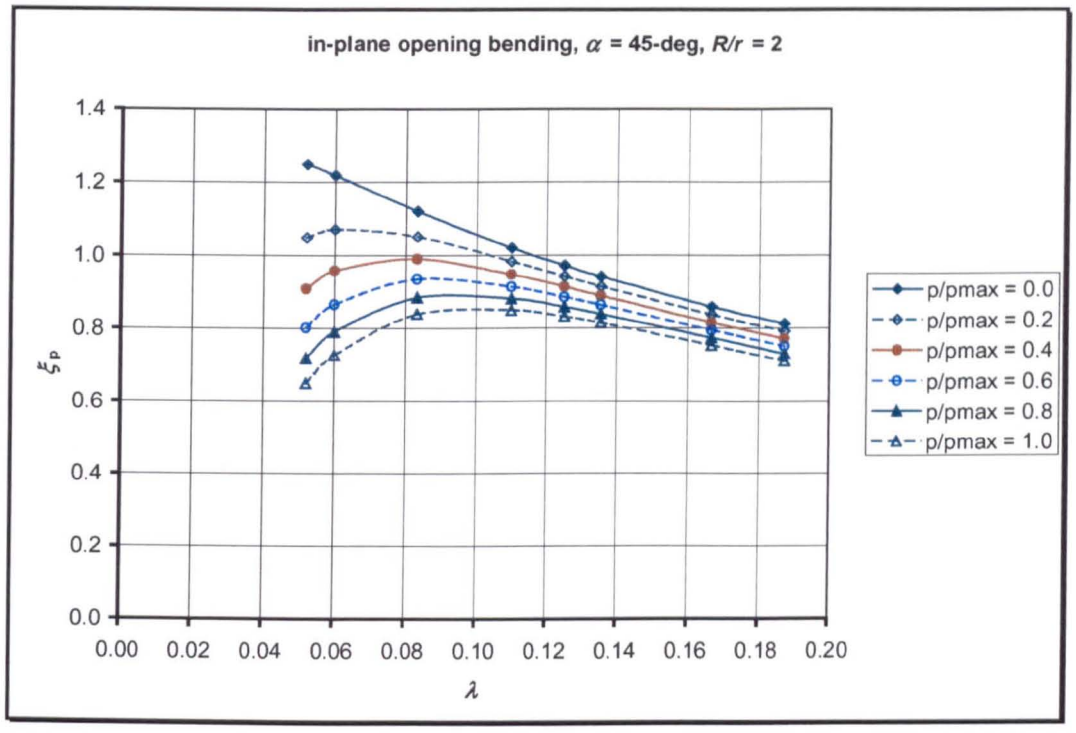

(a)

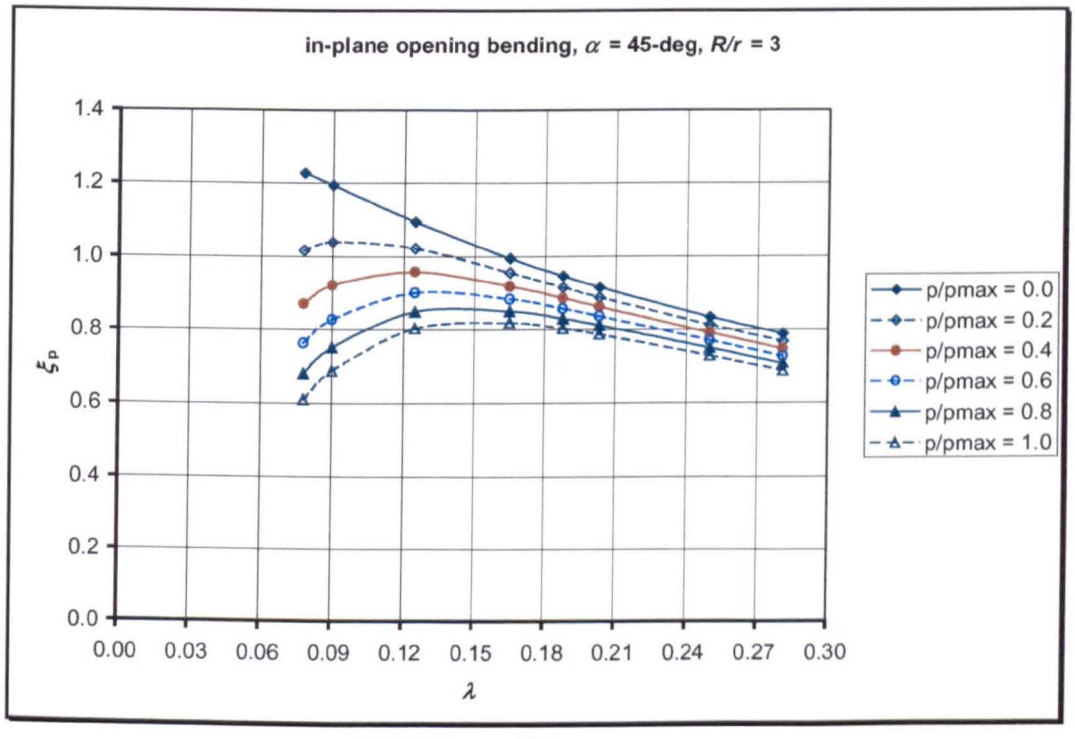

(b)

Fig.A6.2 Ovalisation factor of 45-deg pipe elbows under in-plane opening bending: (a) $R/r = 2$, (b) $R/r = 3$

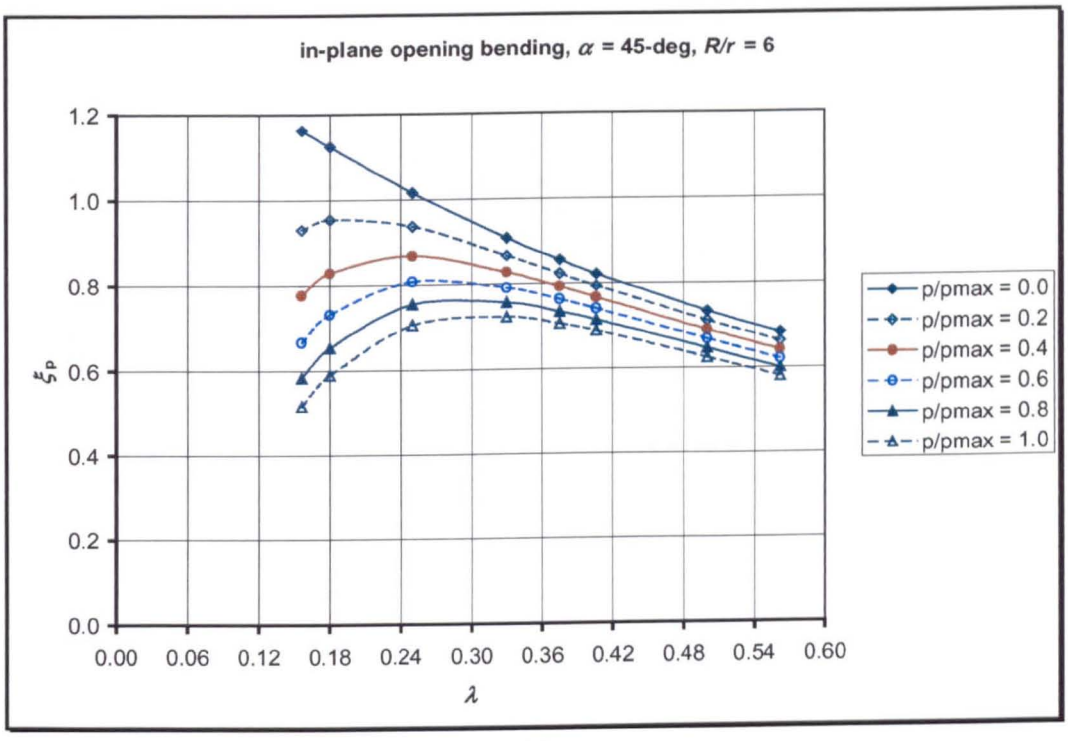

(c)

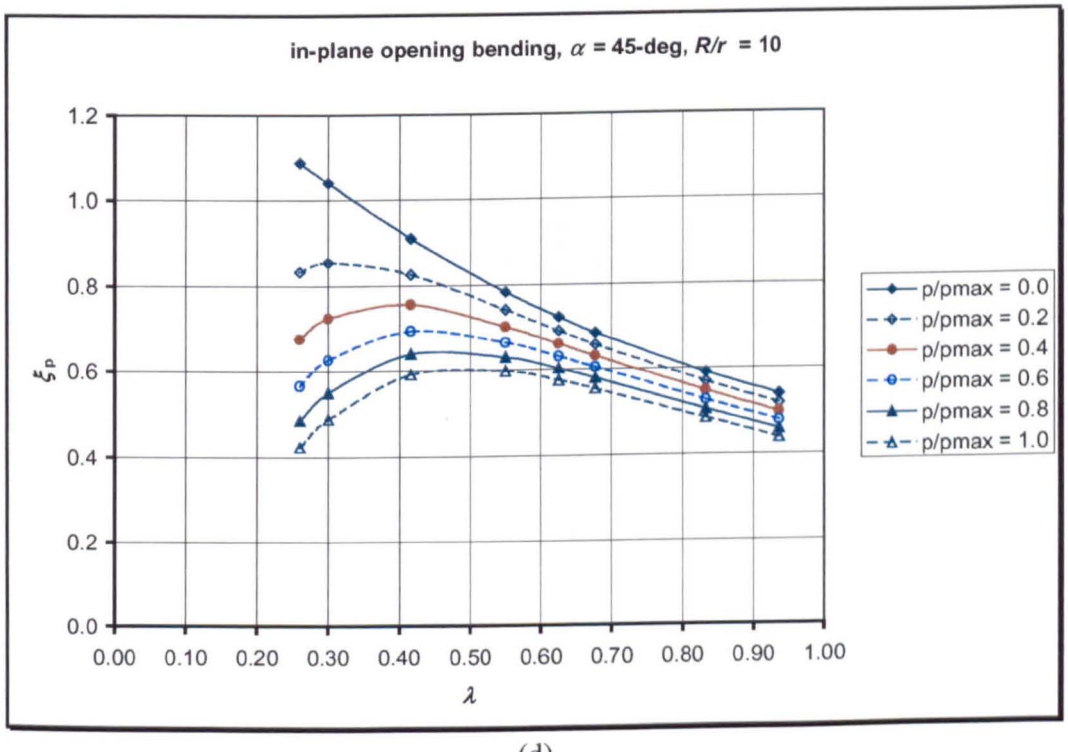

(d)

Fig.A6.2 Ovalisation factor of 45-deg pipe elbows under in-plane opening bending: (c) $R/r = 6$, (d) $R/r = 10$

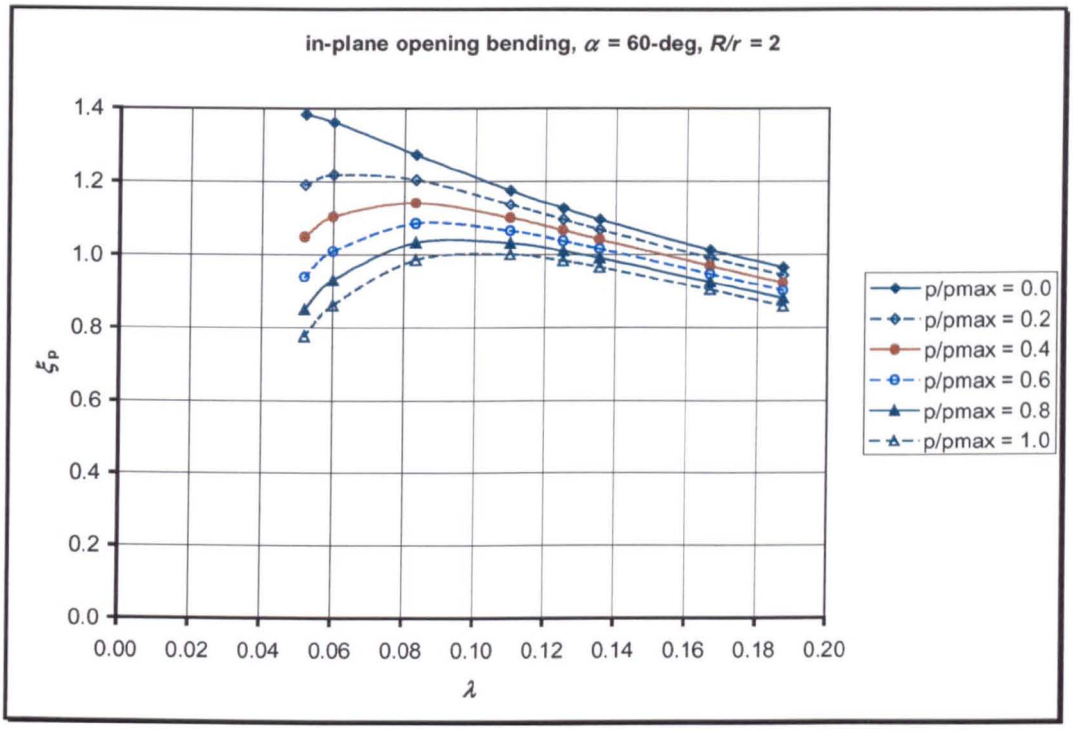

(a)

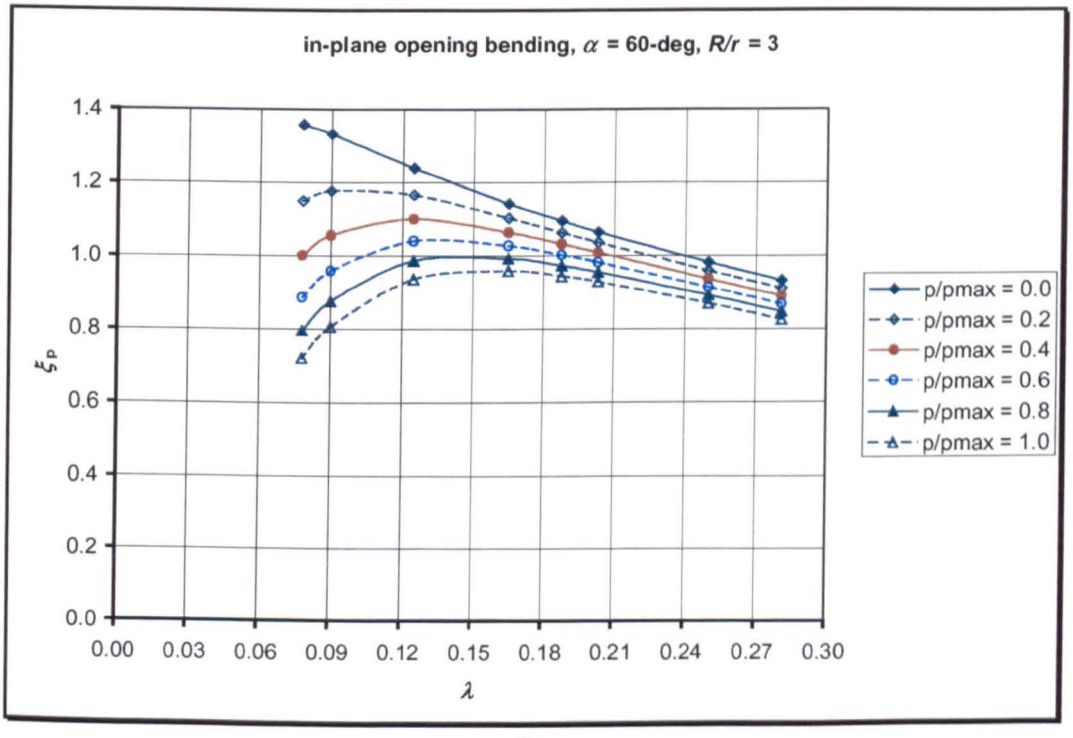

(b)

Fig.A6.3 Ovalisation factor for 60-deg pipe elbows under in-plane opening bending: (a) $R/r = 2$, (b) $R/r = 3$

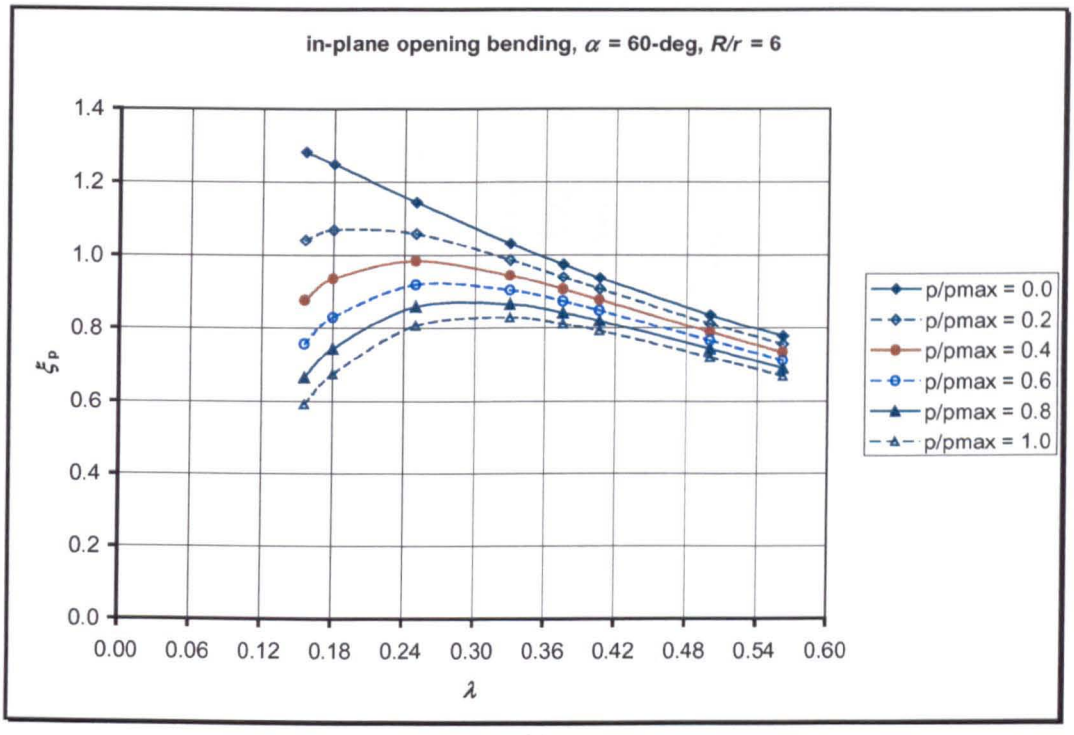

(c)

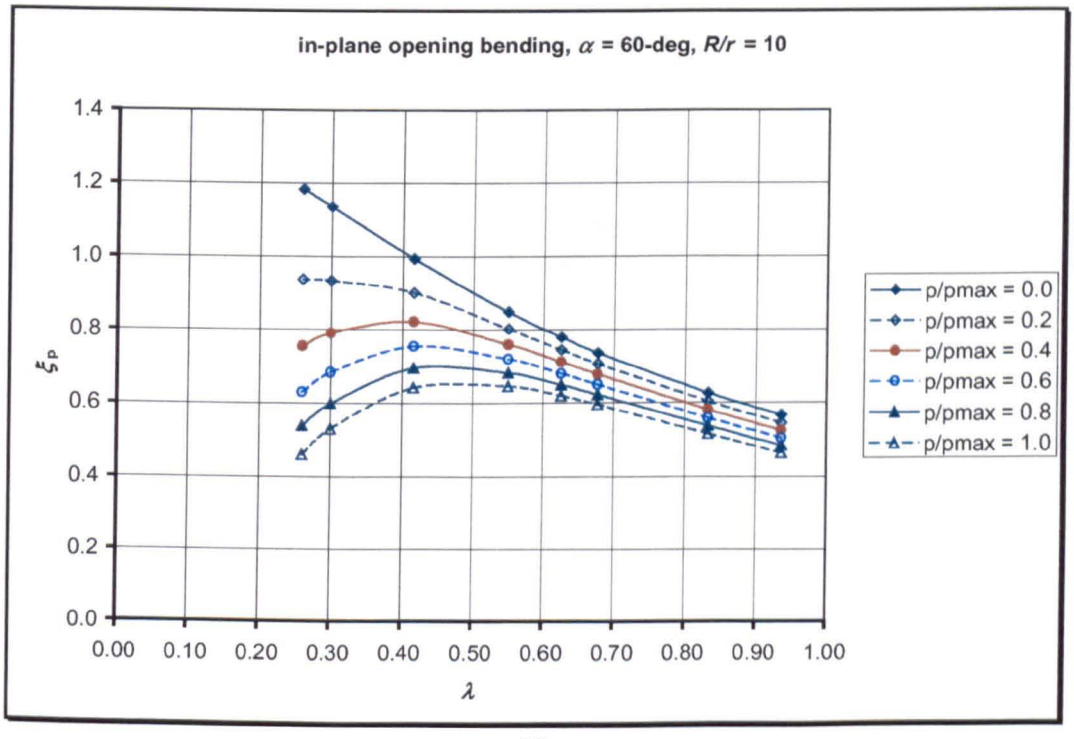

(d)

Fig.A6.3 Ovalisation factor for 60-deg pipe elbows under in-plane opening bending: (c) $R/r = 6$, (d) $R/r = 10$

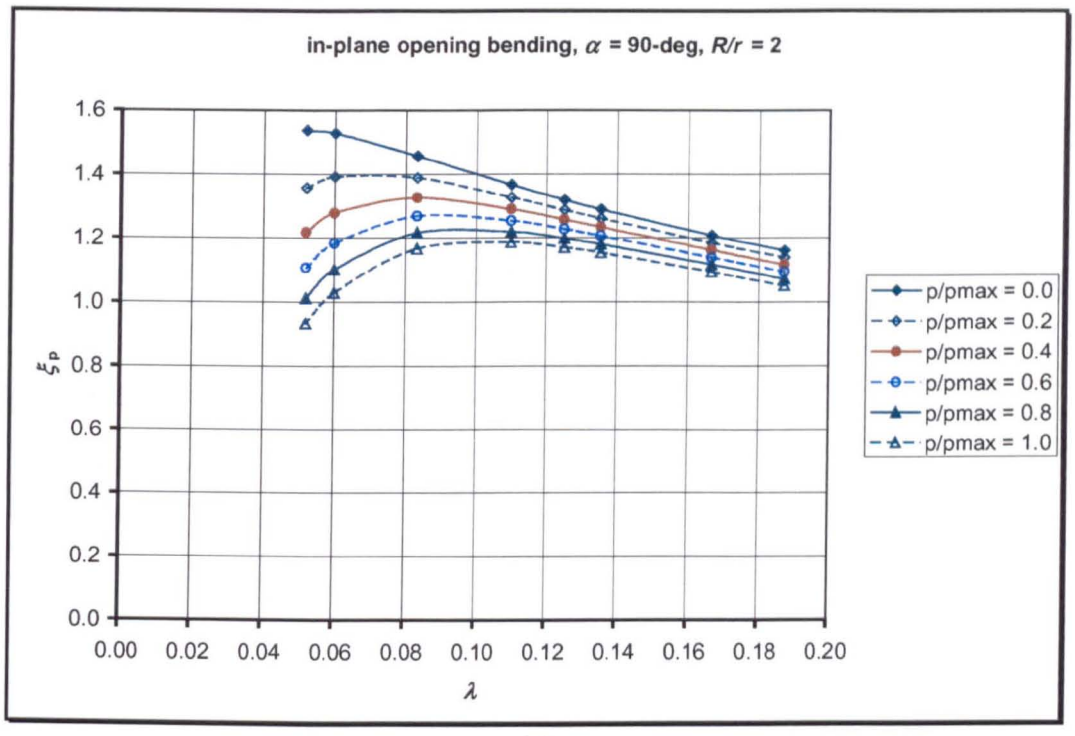

(a)

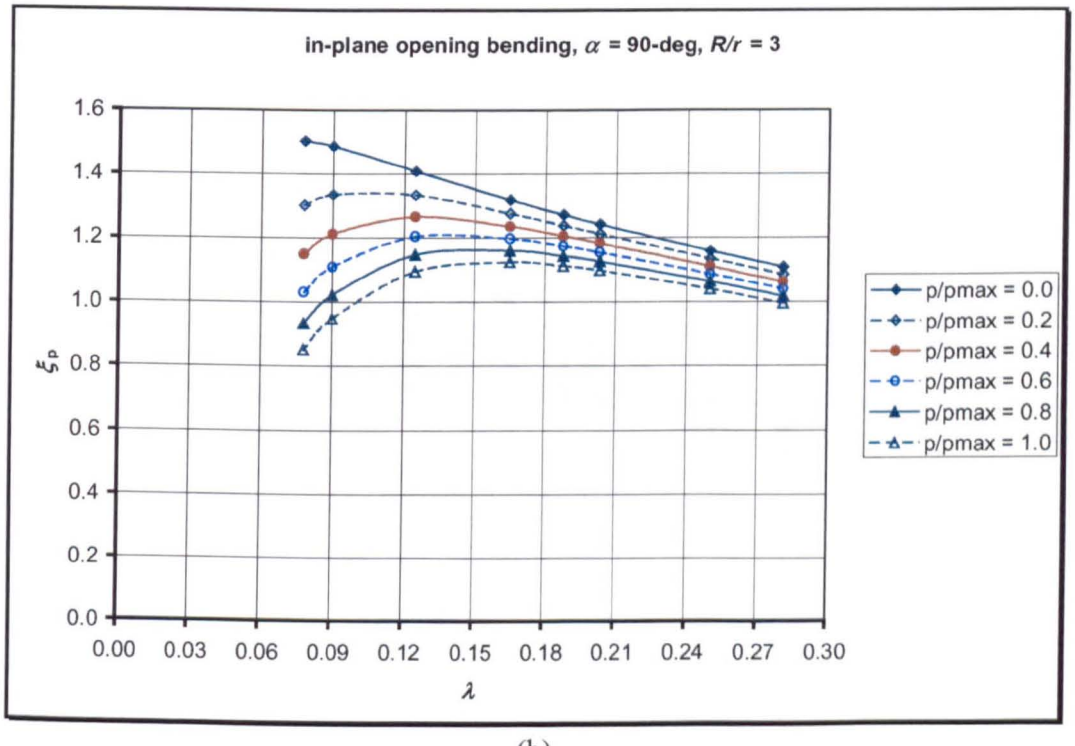

(b)

Fig.A6.4 Ovalisation factor for 90-deg pipe elbows under in-plane opening bending: (a) $R/r = 2$, (b) $R/r = 3$

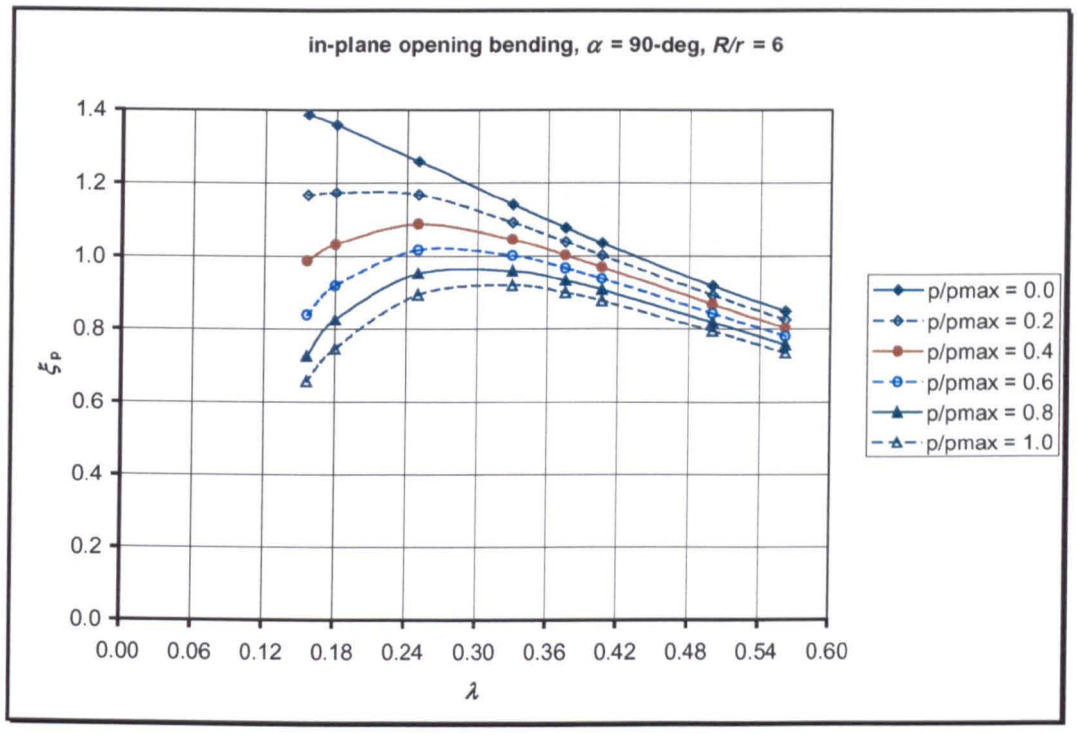

(c)

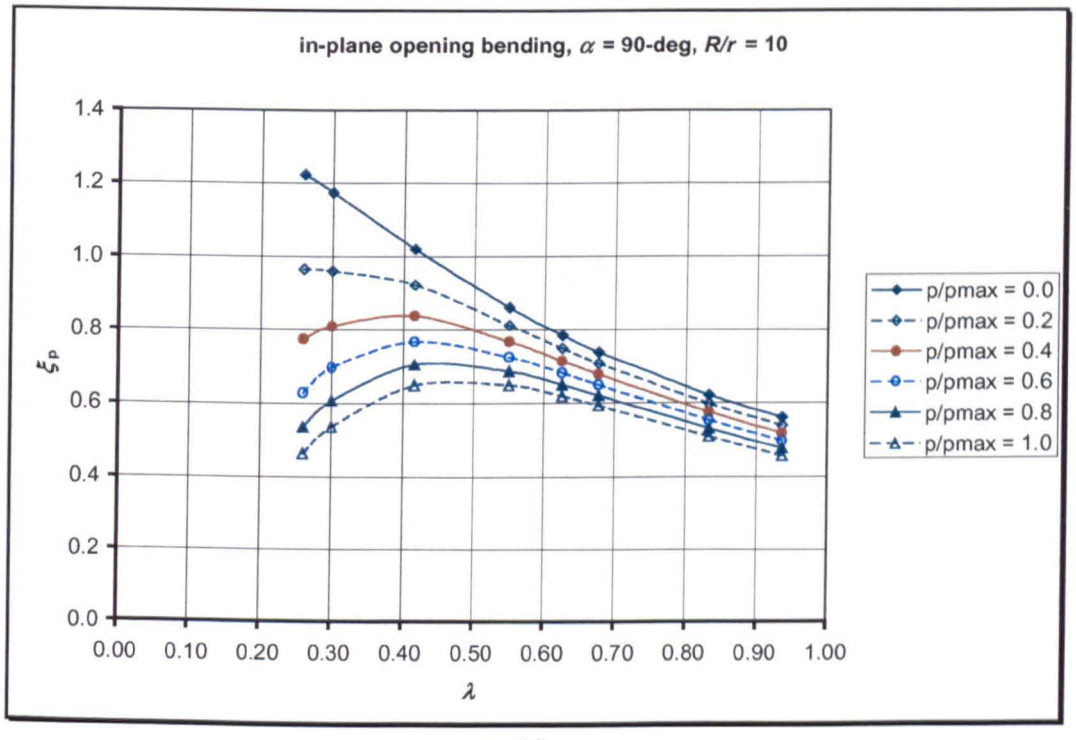

(d)

Fig.A6.4 Ovalisation factor for 90-deg pipe elbows under in-plane opening bending: (c) $R/r = 6$, (d) $R/r = 10$

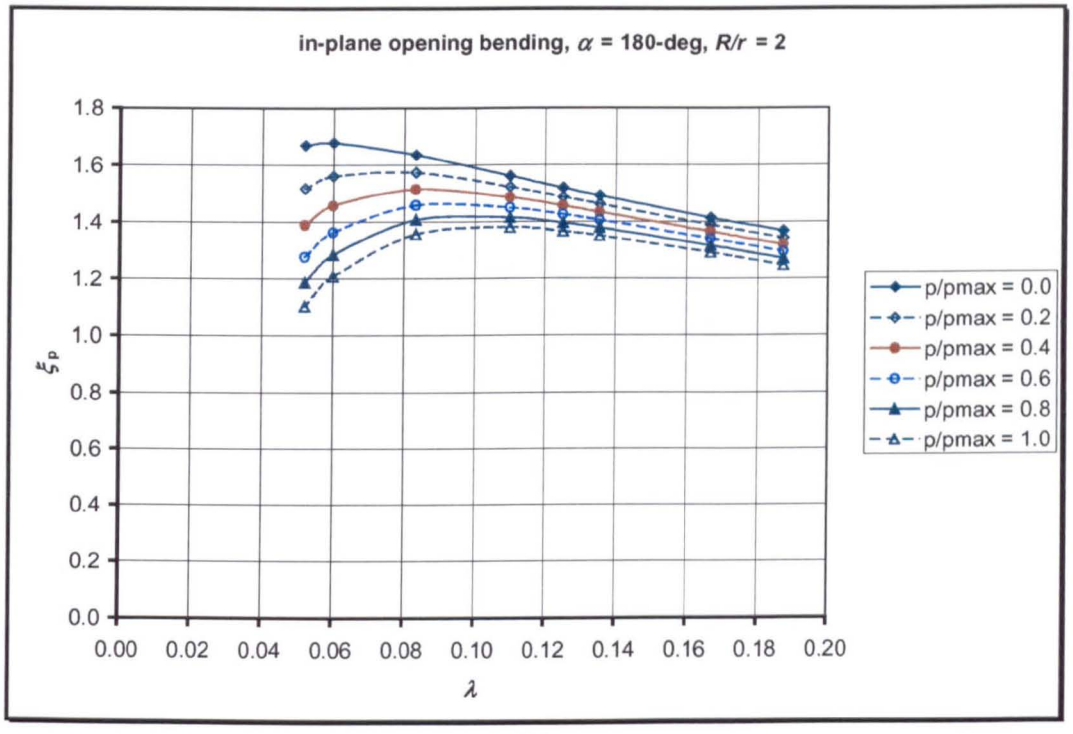

(a)

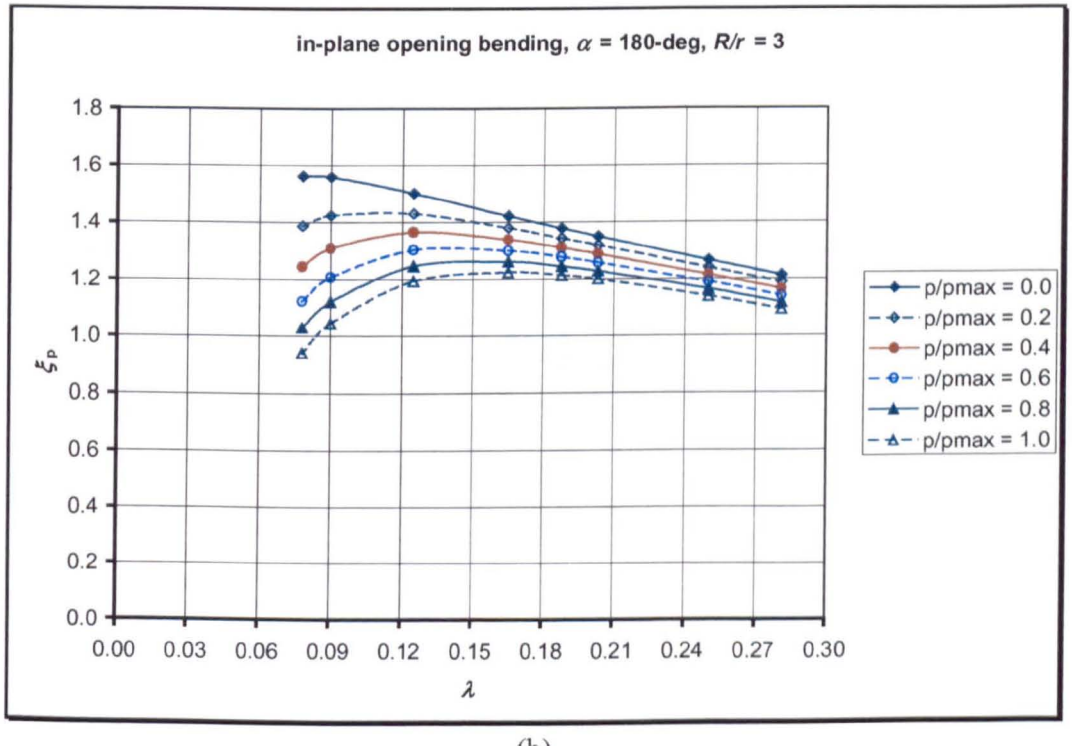

(b)

Fig.A6.5 Ovalisation factor for 180-deg pipe elbows under in-plane opening bending: (a) $R/r = 2$, (b) $R/r = 3$

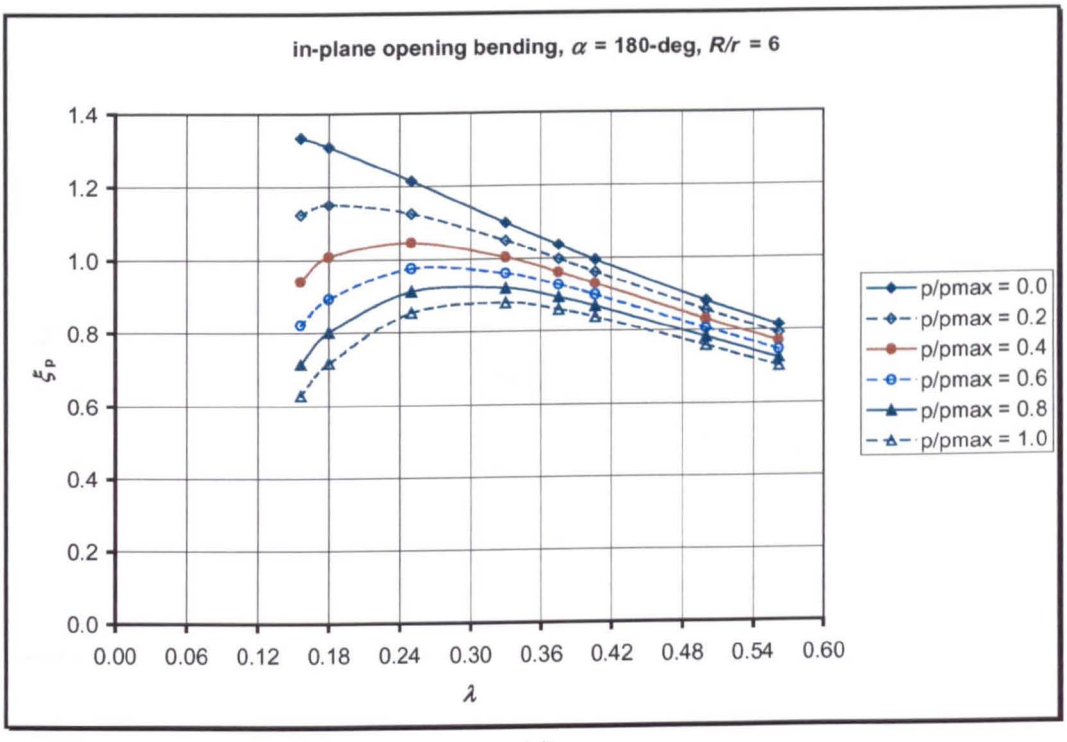

(c)

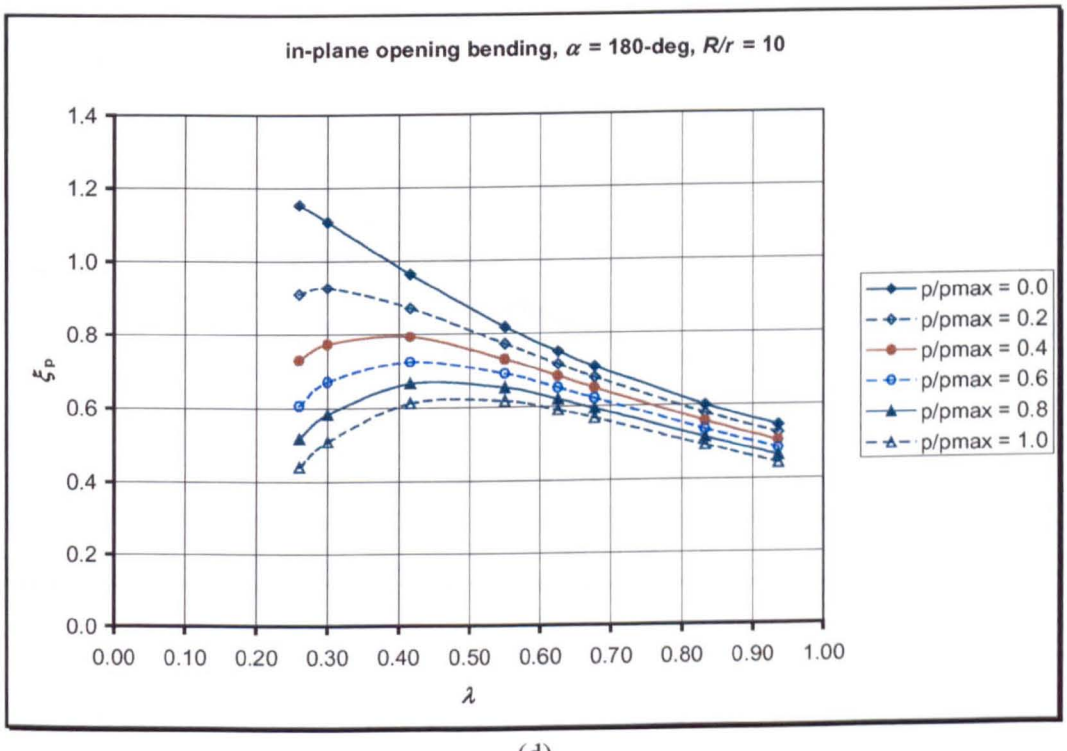

(d)

Fig.A6.5 Ovalisation factor for 180-deg pipe elbows under in-plane opening bending: (c) $R/r = 6$, (d) $R/r = 10$

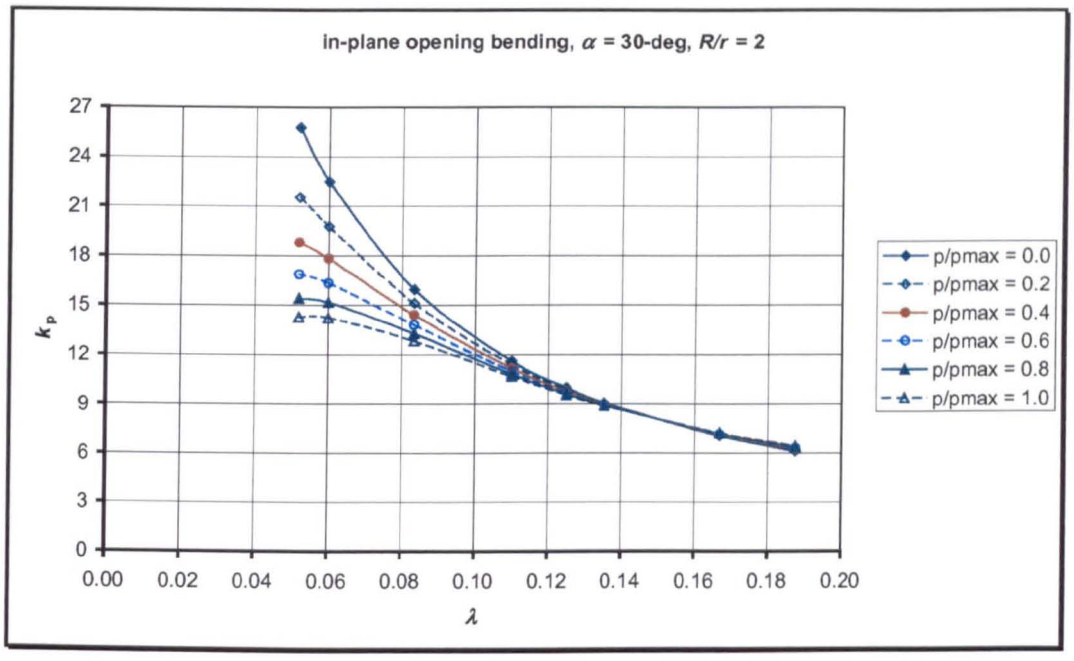

(a)

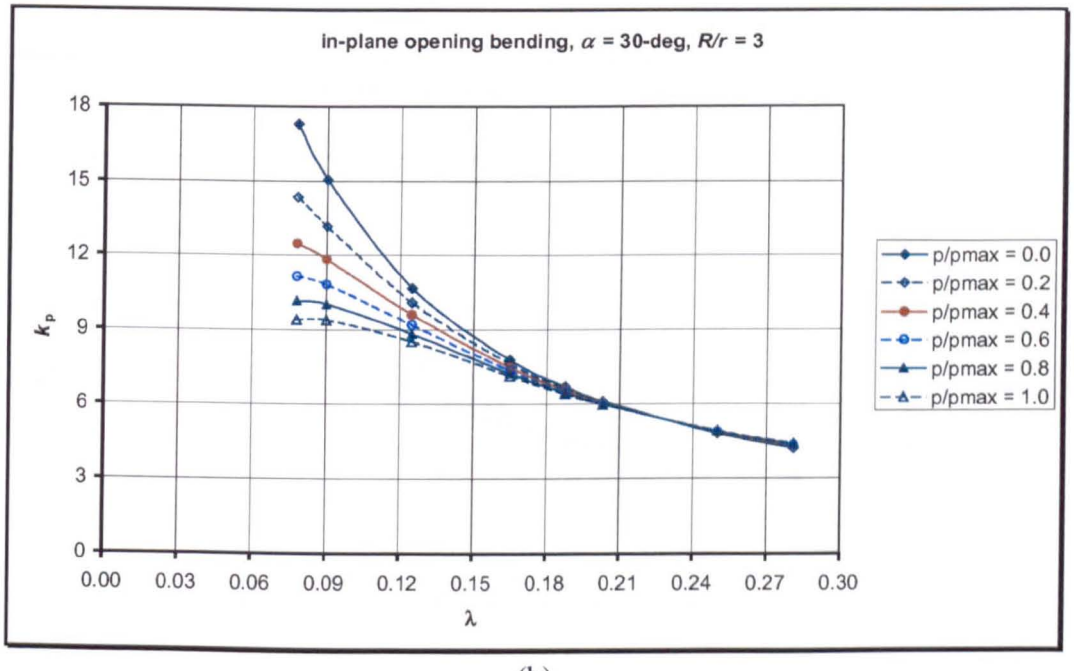

(b)

Fig.A6.6 Flexibility factor for 30-deg pipe elbows subjected to in-plane opening bending: (a) $R/r = 2$, (b) $R/r = 3$

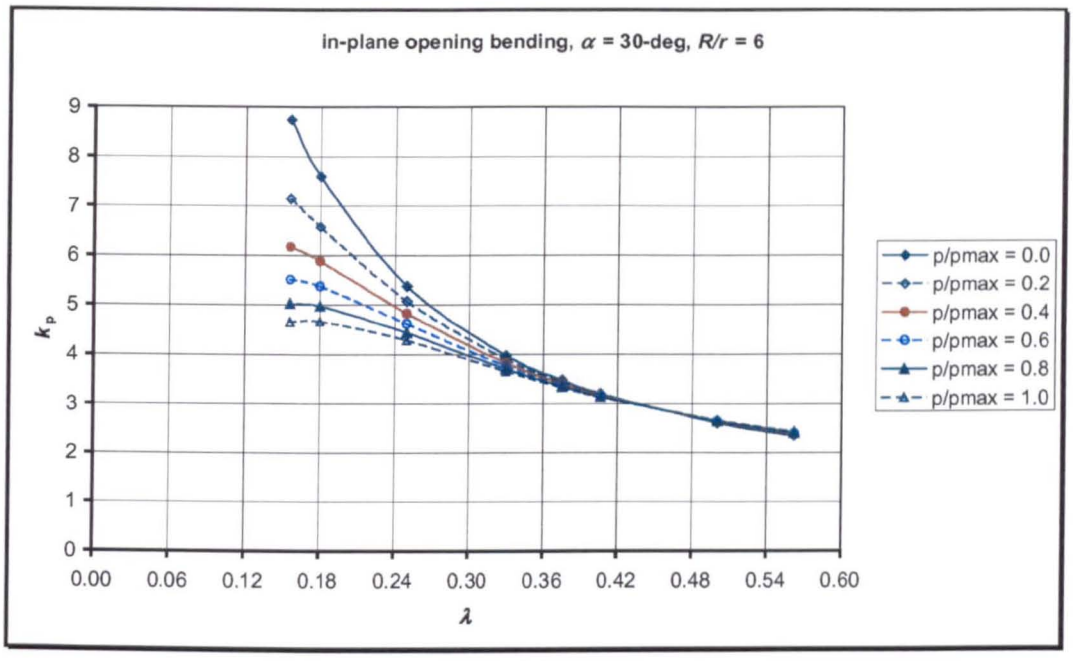

(c)

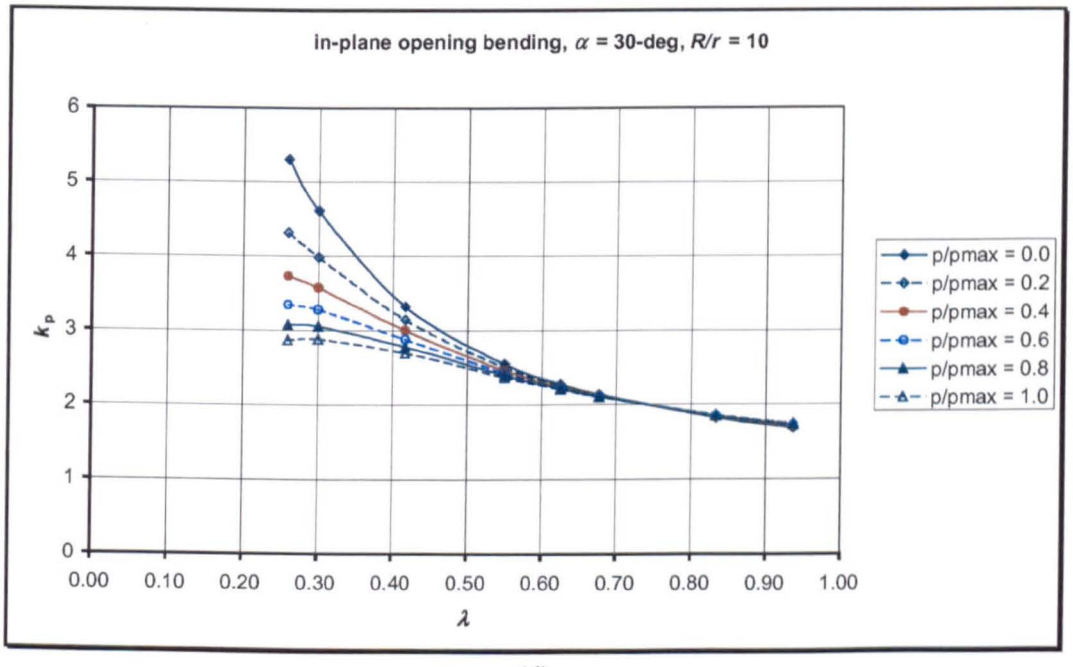

(d)

Fig.A6.6 Flexibility factor for 30-deg pipe elbows subjected to in-plane opening bending: (c) $R/r = 6$, (d) $R/r = 10$

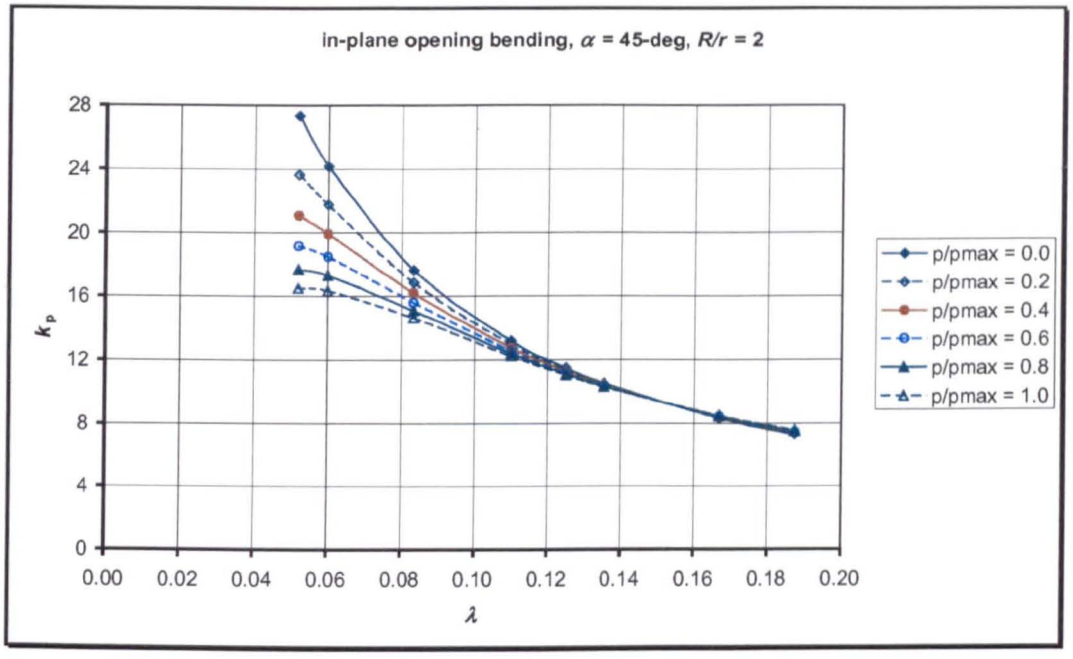

(a)

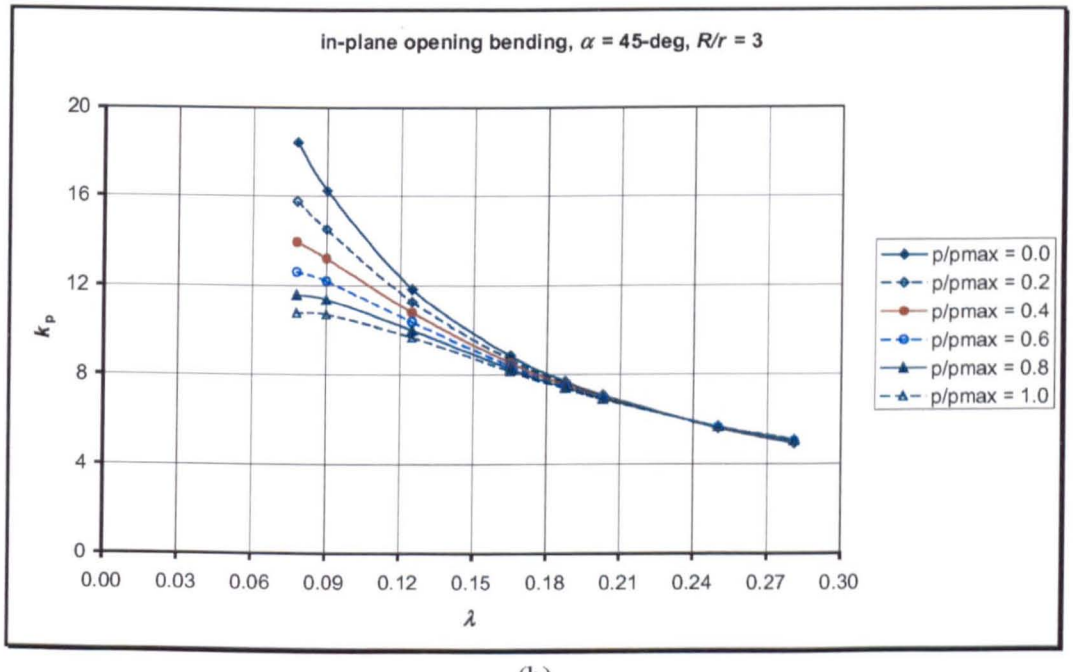

(b)

Fig.A6.7 Flexibility factor for 45-deg pipe elbows subjected to in-plane opening bending: (a) $R/r = 2$, (b) $R/r = 3$

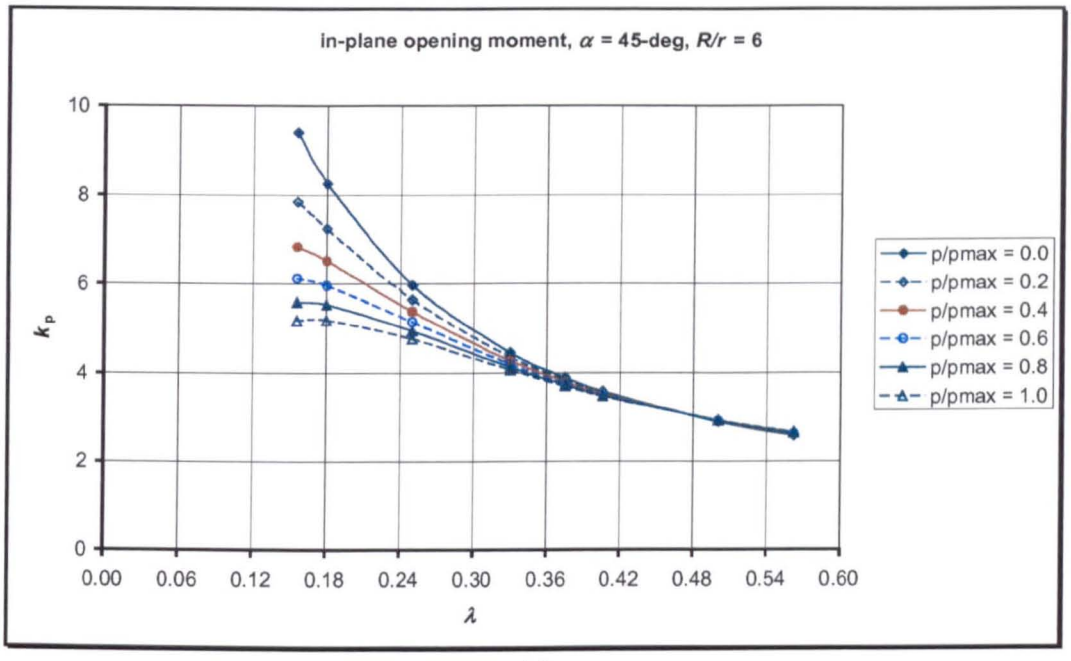

(c)

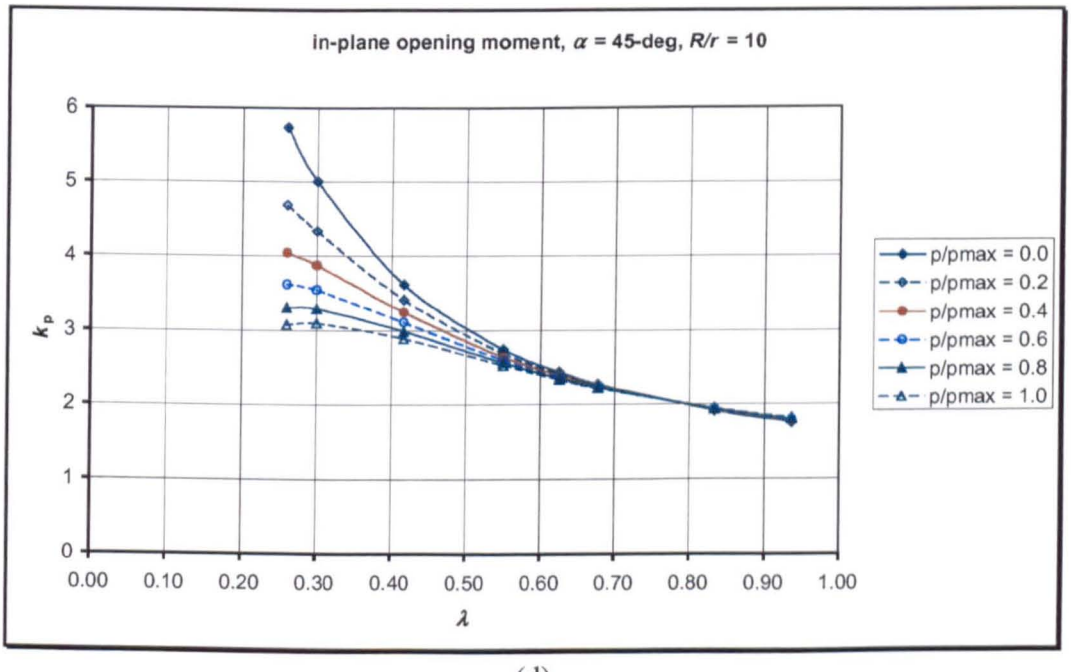

(d)

Fig.A6.7 Flexibility factor for 45-deg pipe elbows subjected to in-plane opening bending: (c) $R/r = 6$, (d) $R/r = 10$

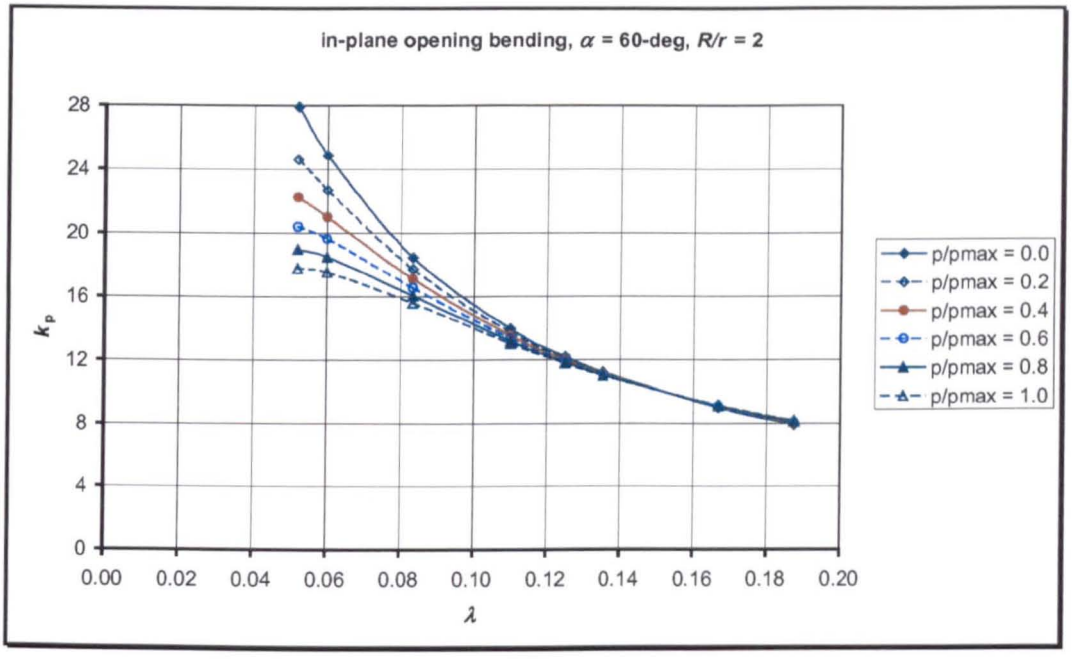

(a)

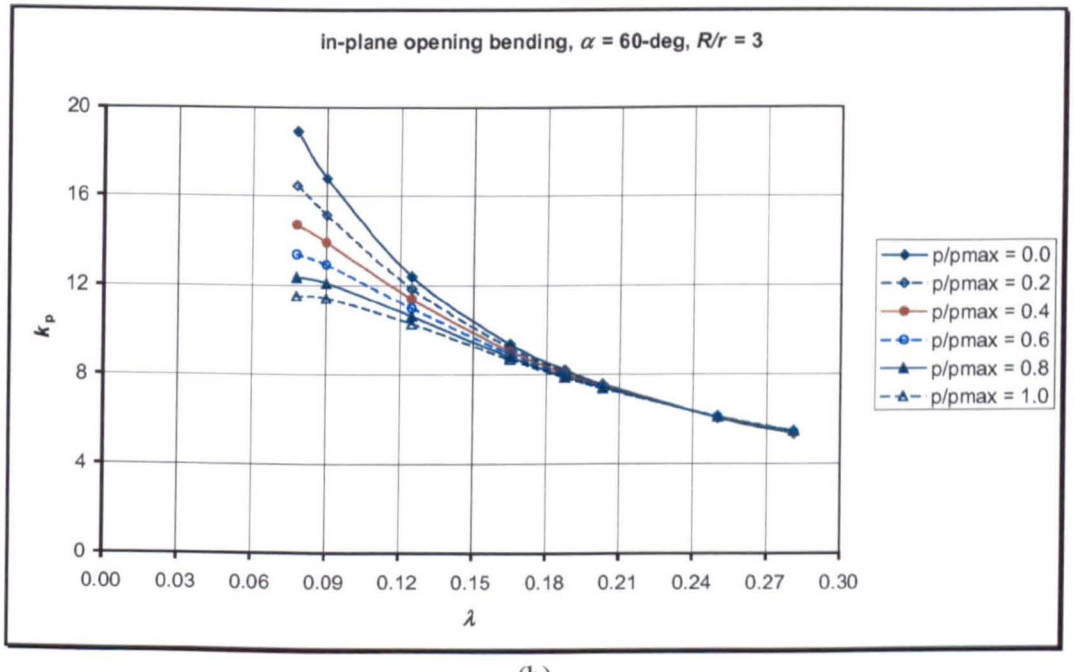

(b)

Fig.A6.8 Flexibility factor for 60-deg pipe elbows subjected to in-plane opening bending: (a) $R/r = 2$, (b) $R/r = 3$

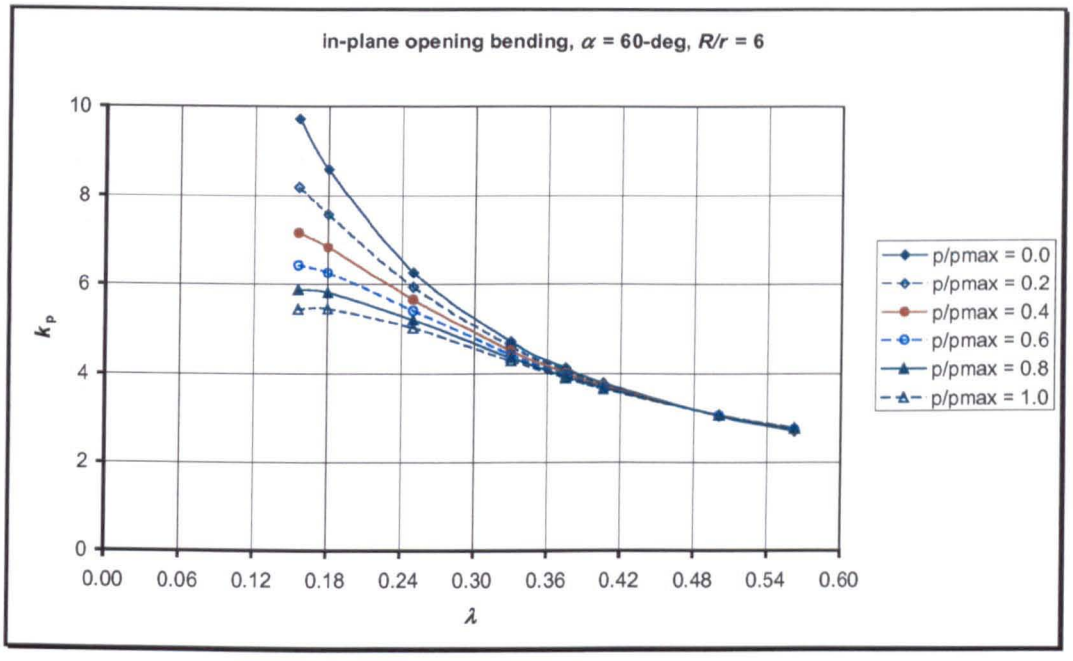

(c)

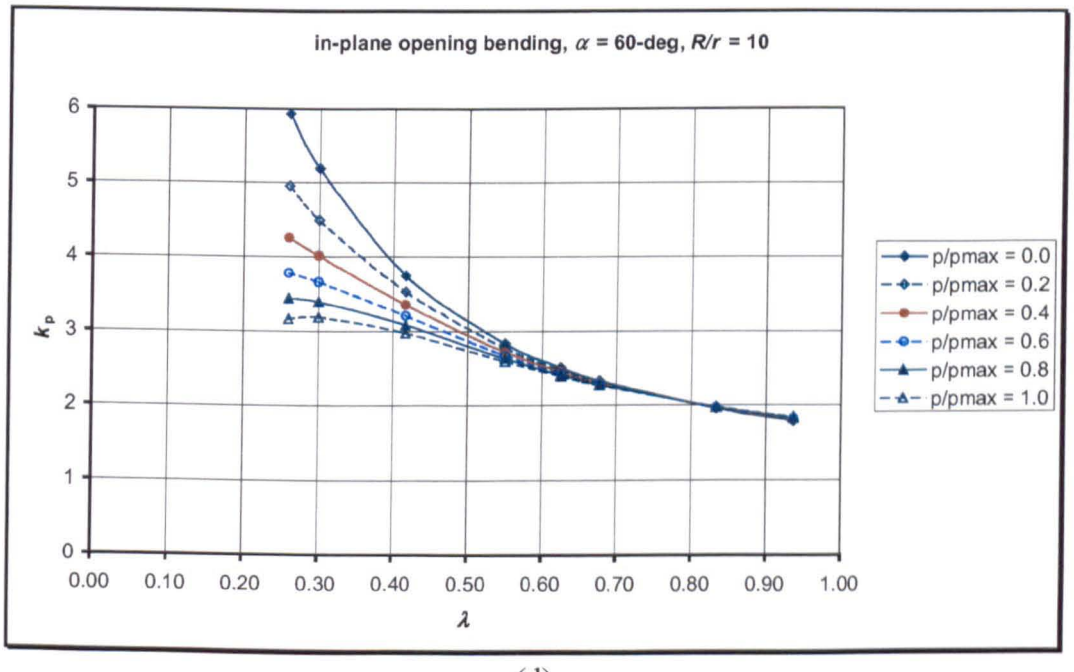

(d)

Fig.A6.8 Flexibility factor for 60-deg pipe elbows subjected to in-plane opening bending: (c) $R/r = 6$, (d) $R/r = 10$

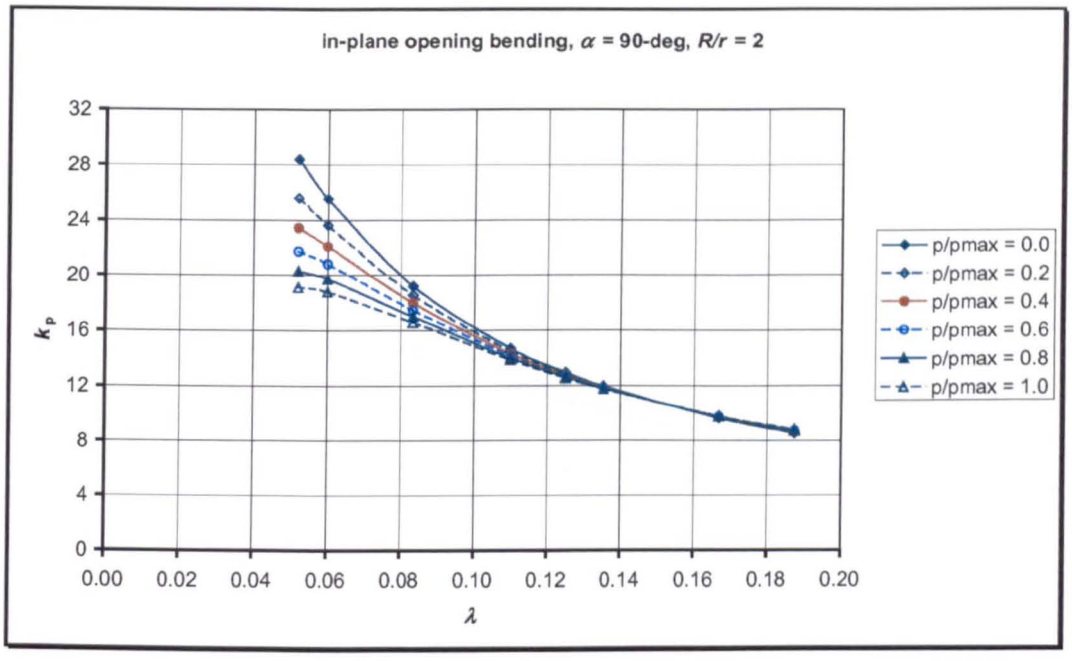

(a)

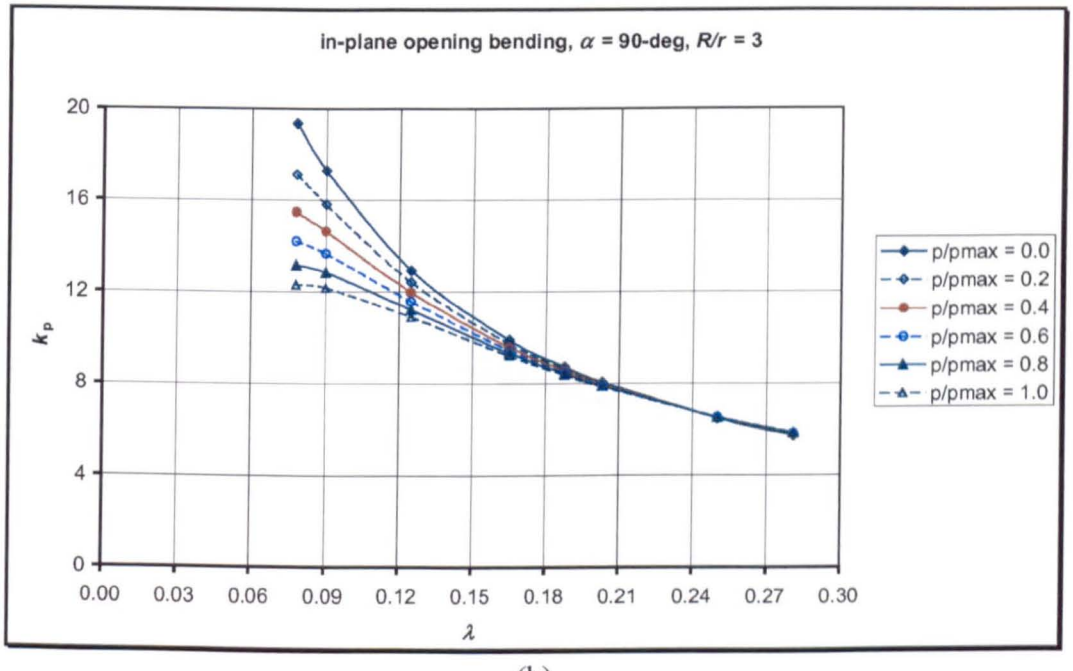

(b)

Fig.A6.9 Flexibility factor for 90-deg pipe elbows subjected to in-plane opening bending: (a) $R/r = 2$, (b) $R/r = 3$

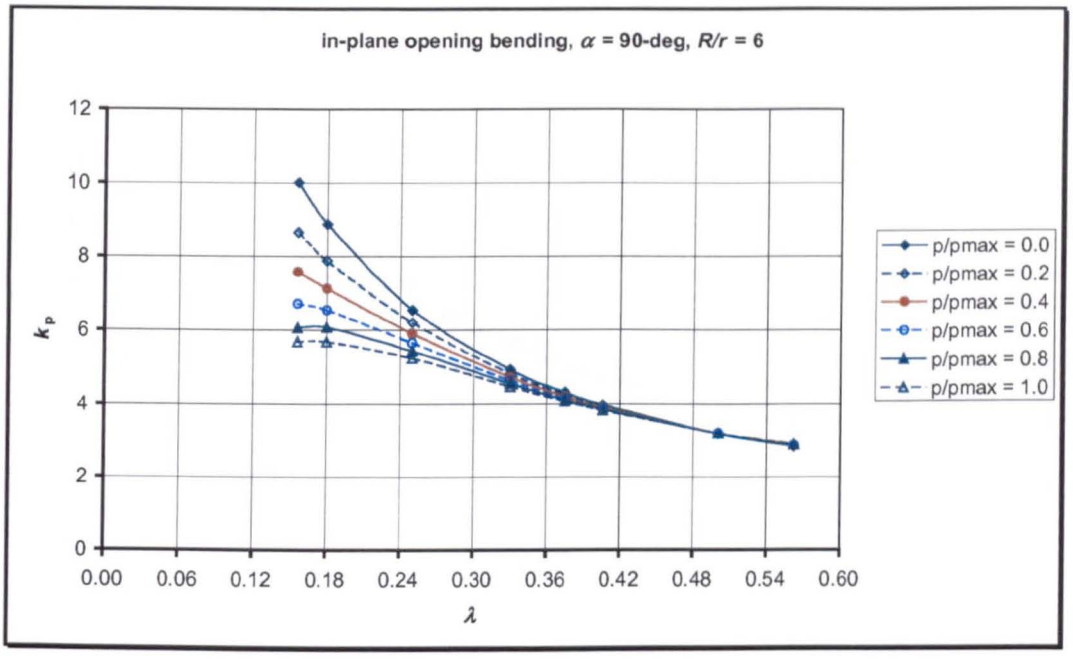

(c)

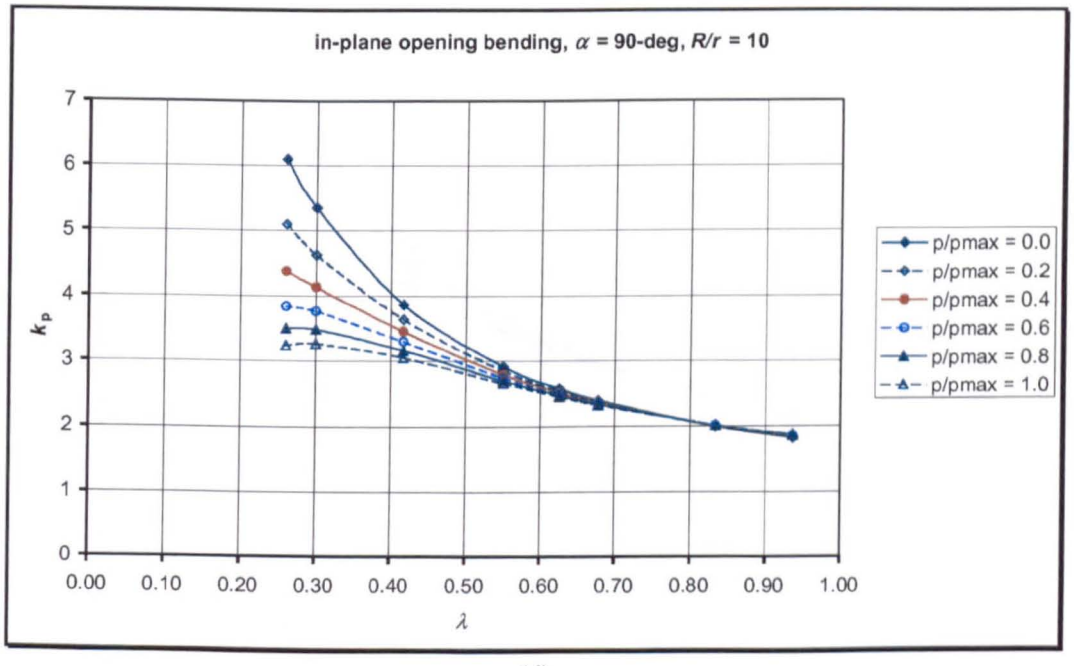

(d)

Fig.A6.9 Flexibility factor for 90-deg pipe elbows subjected to in-plane opening bending: (c) $R/r = 6$, (d) $R/r = 10$

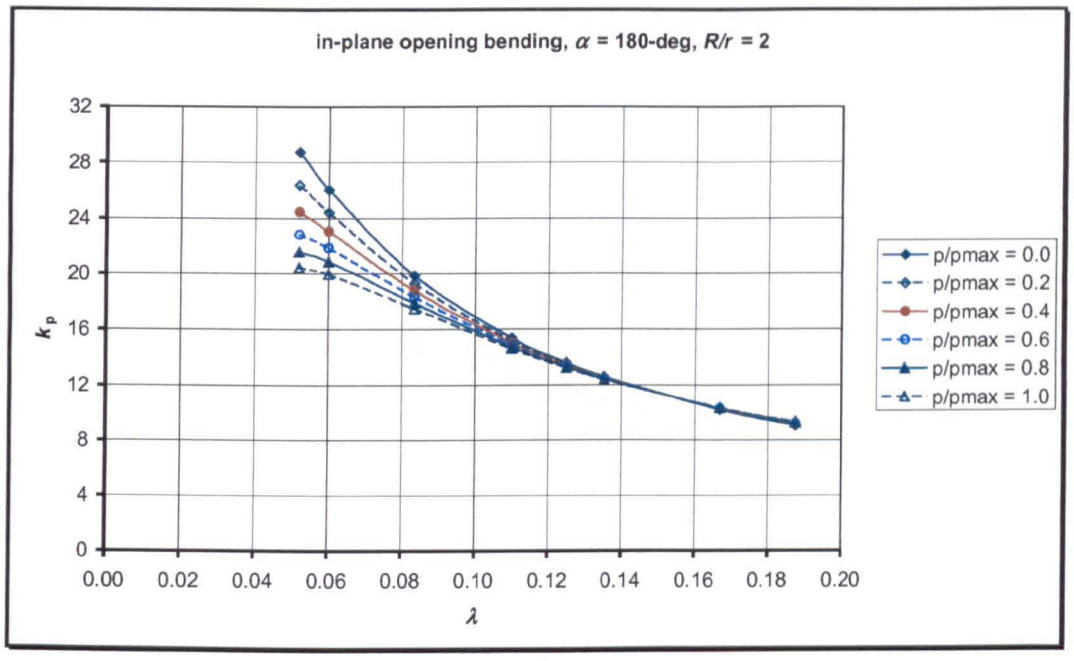

(a)

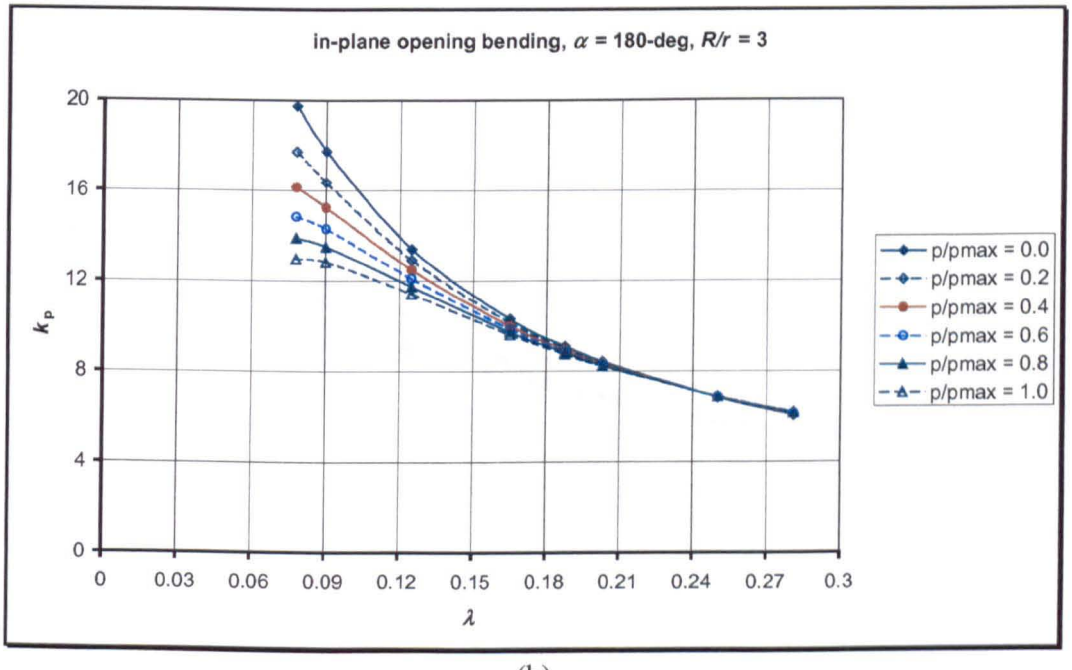

(b)

Fig.A6.10 Flexibility factor for 180-deg pipe elbows subjected to in-plane opening bending: (a) $R/r = 2$, (b) $R/r = 3$

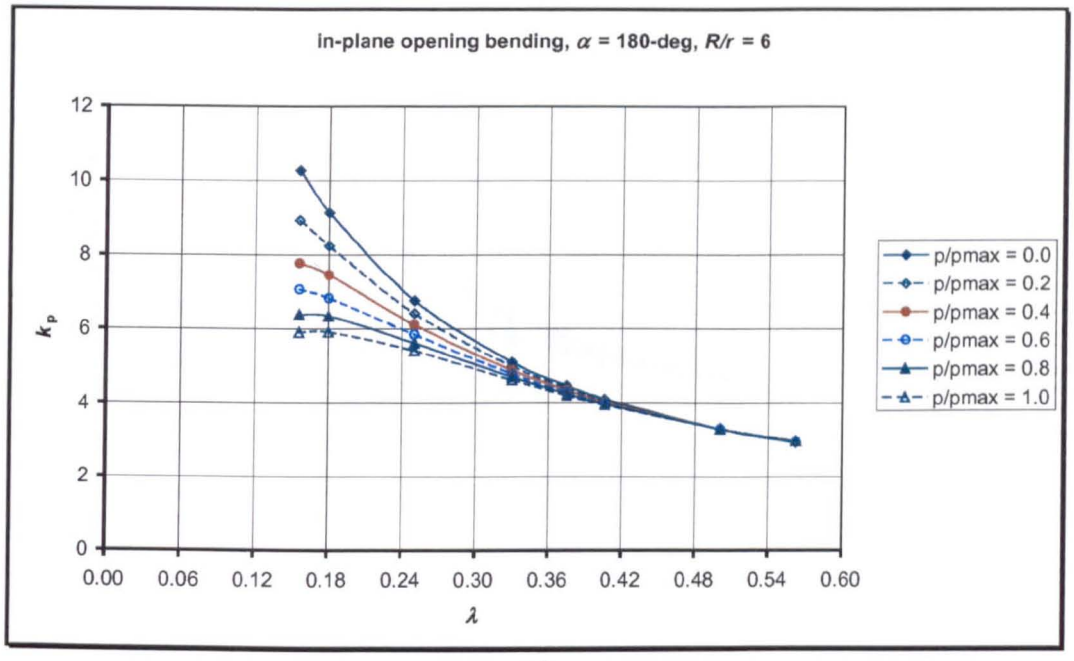

(c)

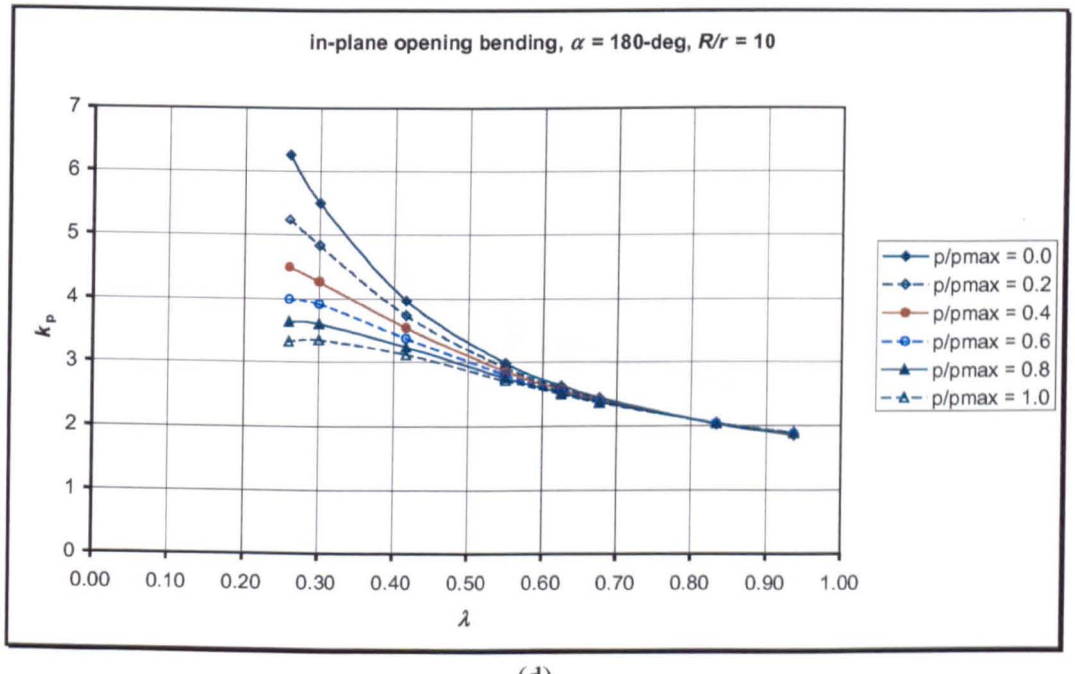

(d)

Fig.A6.10 Flexibility factor for 180-deg pipe elbows subjected to in-plane opening bending: (c) $R/r = 6$, (d) $R/r = 10$

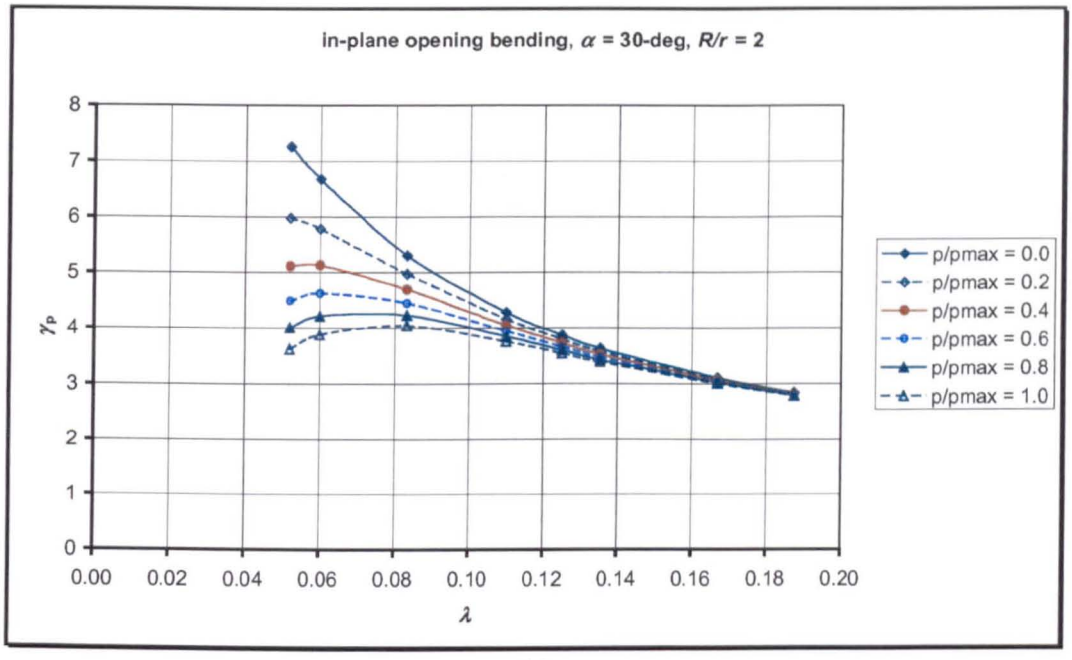

(a)

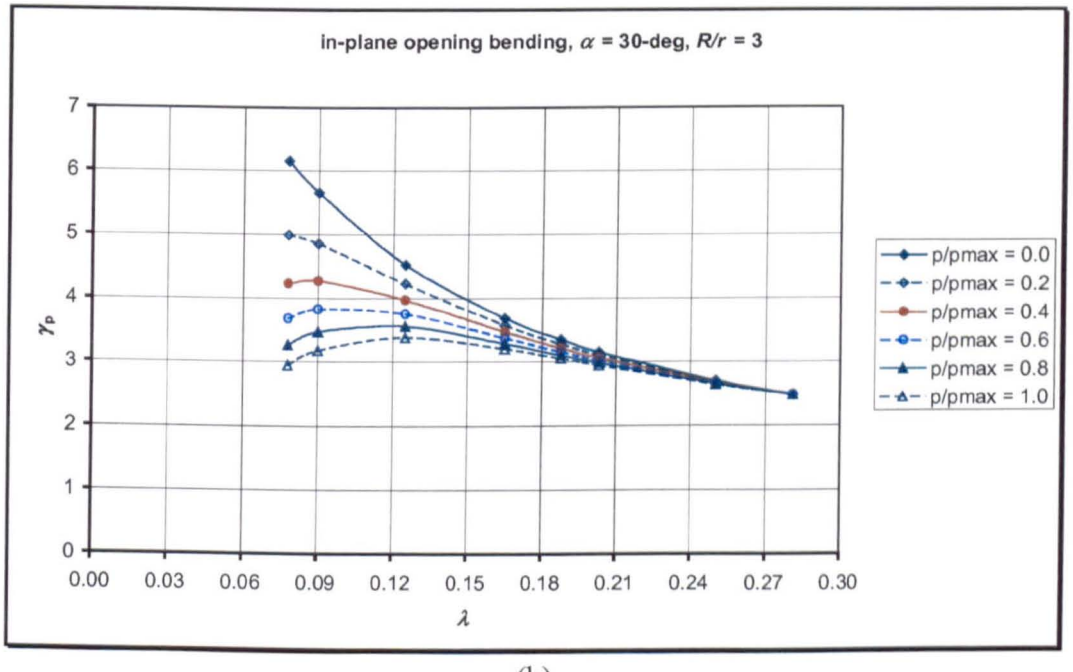

(b)

Fig.A6.11 Stress-intensification factor for 30-deg pipe elbows subjected to in-plane opening bending: (a) $R/r = 2$, (b) $R/r = 3$

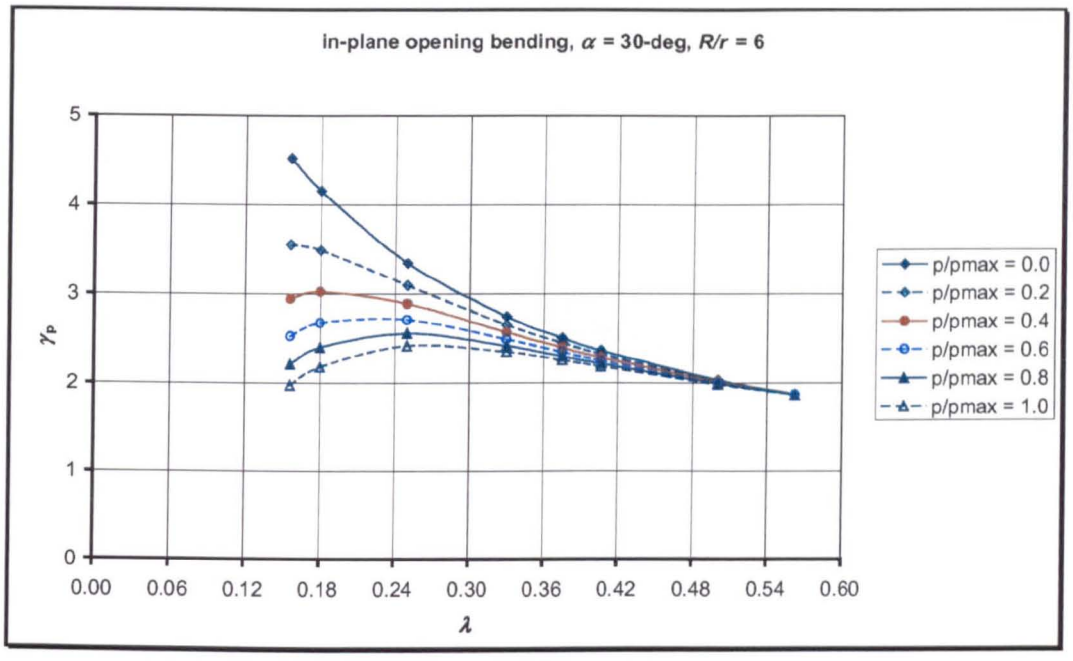

(c)

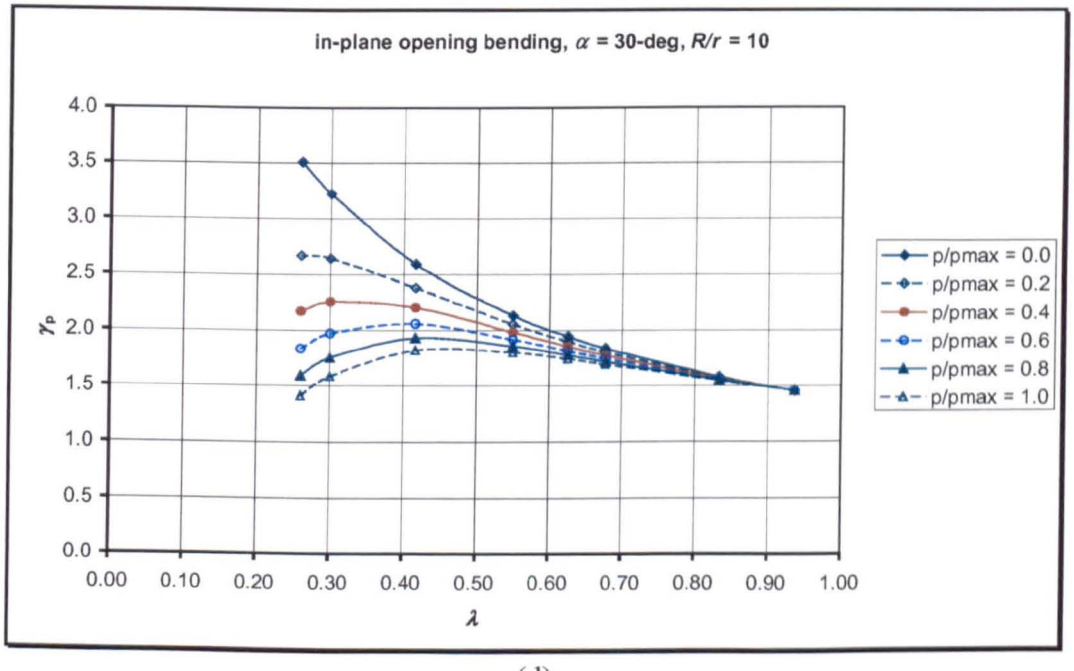

(d)

Fig.A6.11 Stress-intensification factor for 30-deg pipe elbows subjected to in-plane opening bending: (c) $R/r = 6$, (d) $R/r = 10$

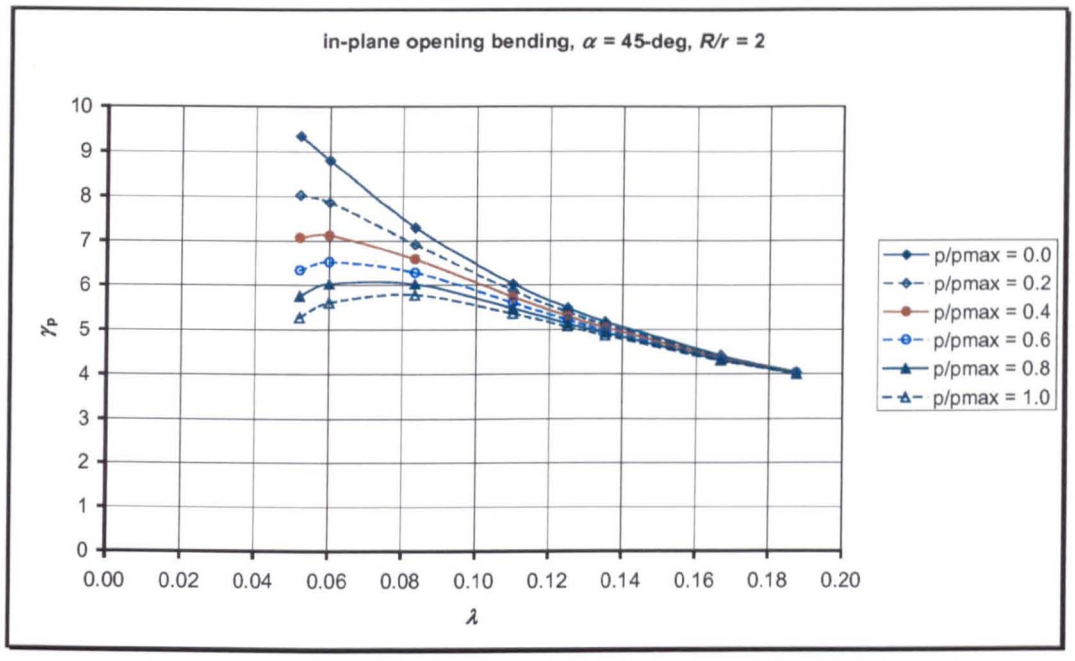

(a)

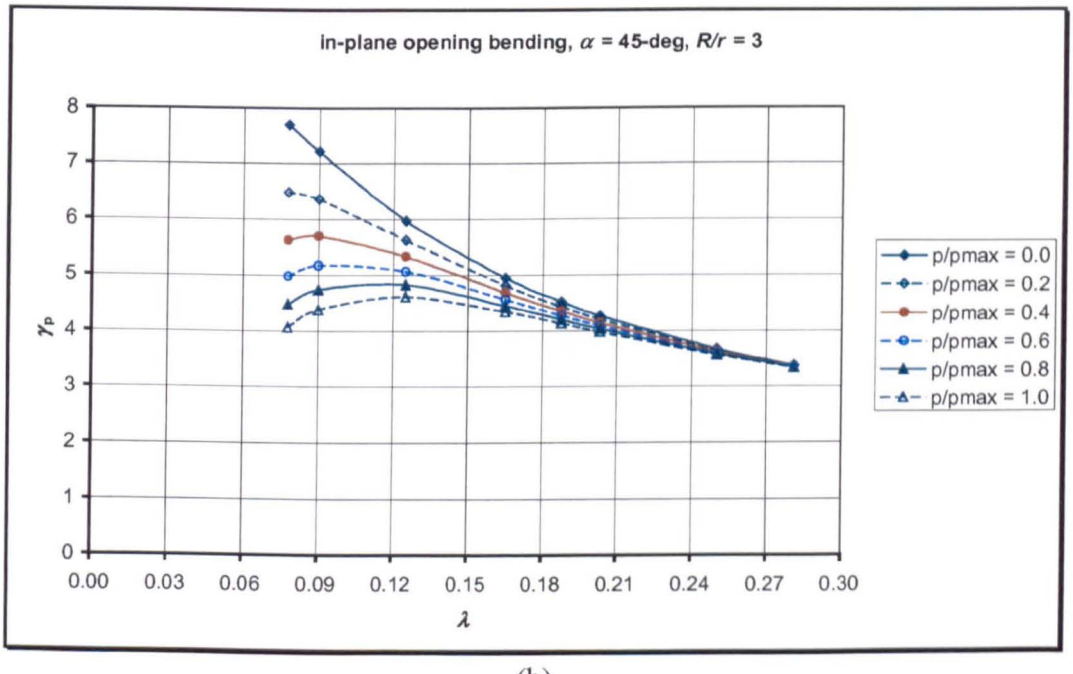

(b)

Fig.A6.12 Stress-intensification factor for 45-deg pipe elbows subjected to in-plane opening bending: (a) $R/r = 2$, (b) $R/r = 3$

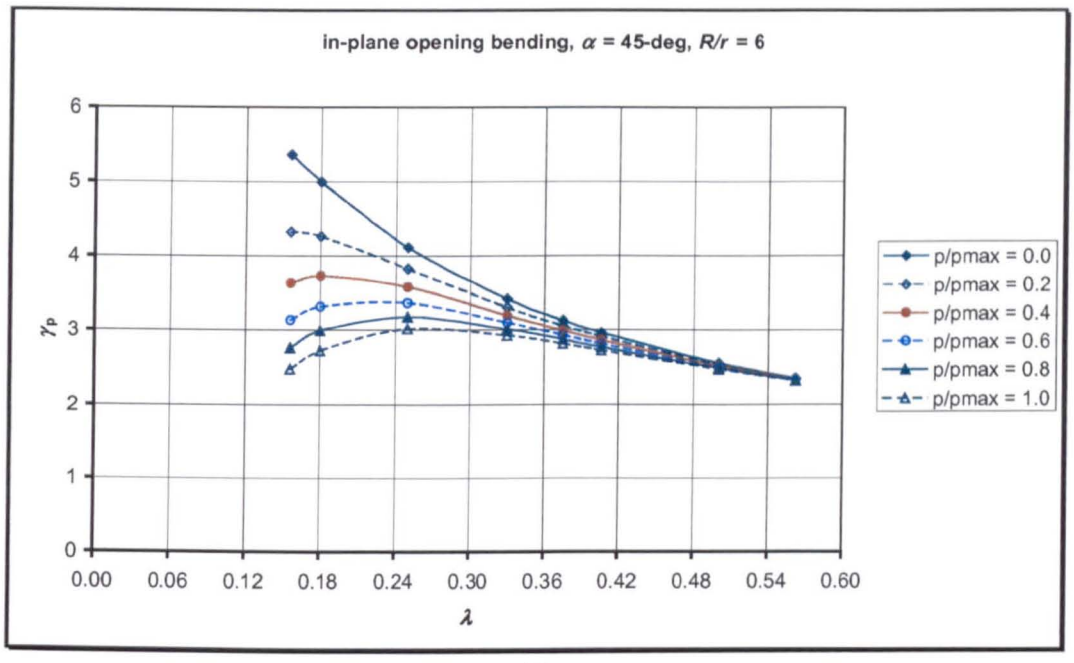

(c)

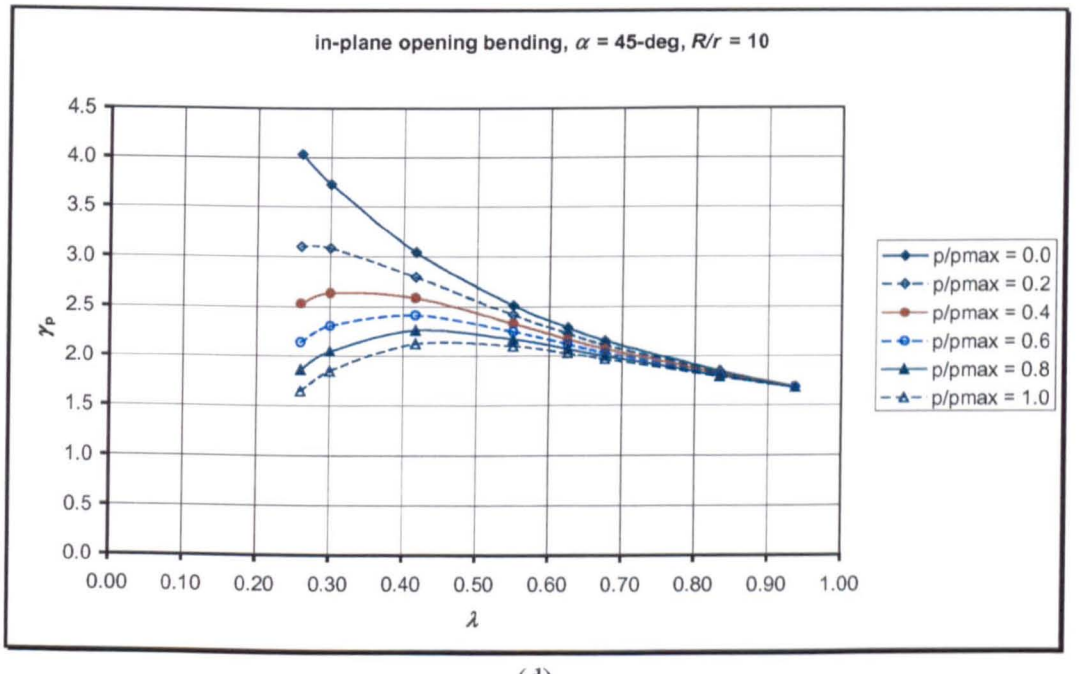

(d)

Fig.A6.12 Stress-intensification factor for 45-deg pipe elbows subjected to in-plane opening bending: (c) $R/r = 6$, (d) $R/r = 10$

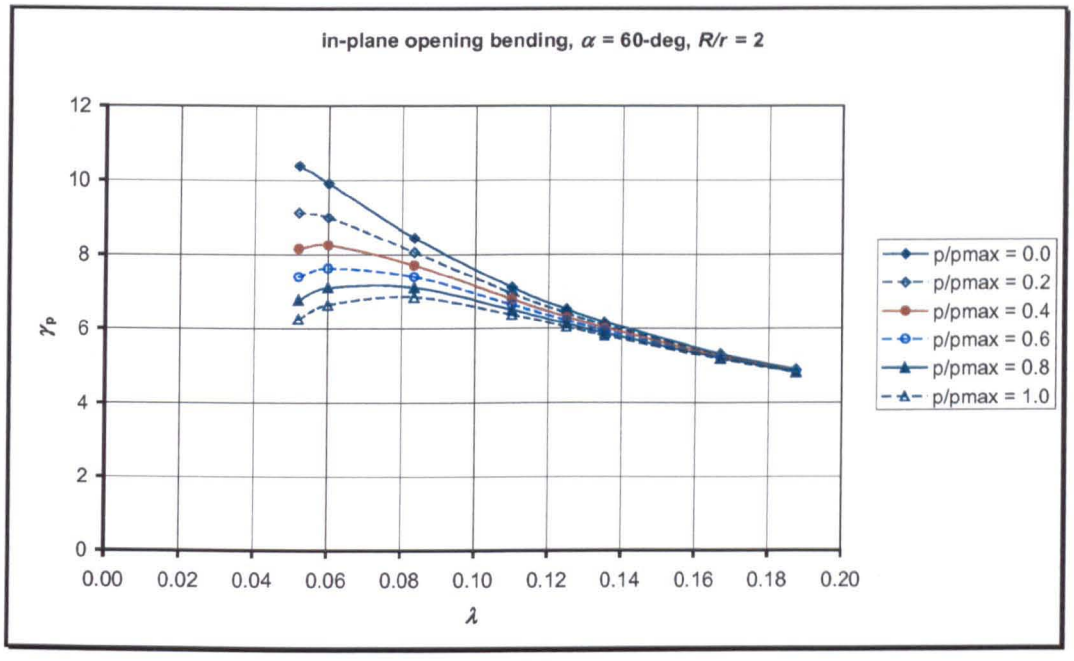

(a)

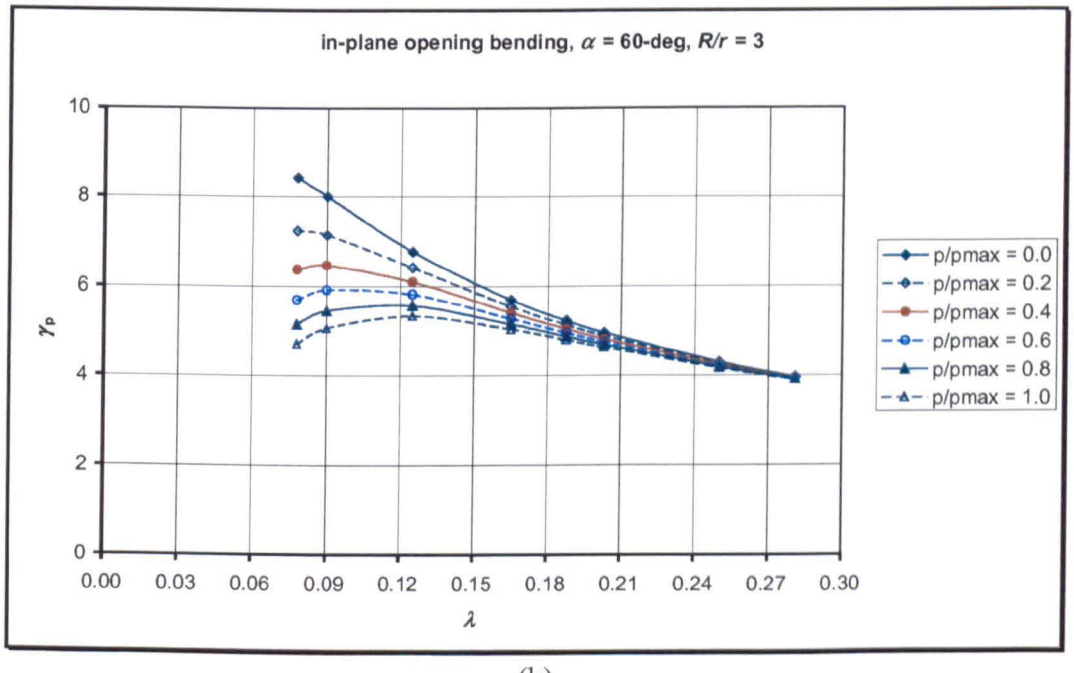

(b)

Fig.A6.13 Stress-intensification factor for 60-deg pipe elbows subjected to in-plane opening bending: (a) $R/r = 2$, (b) $R/r = 3$

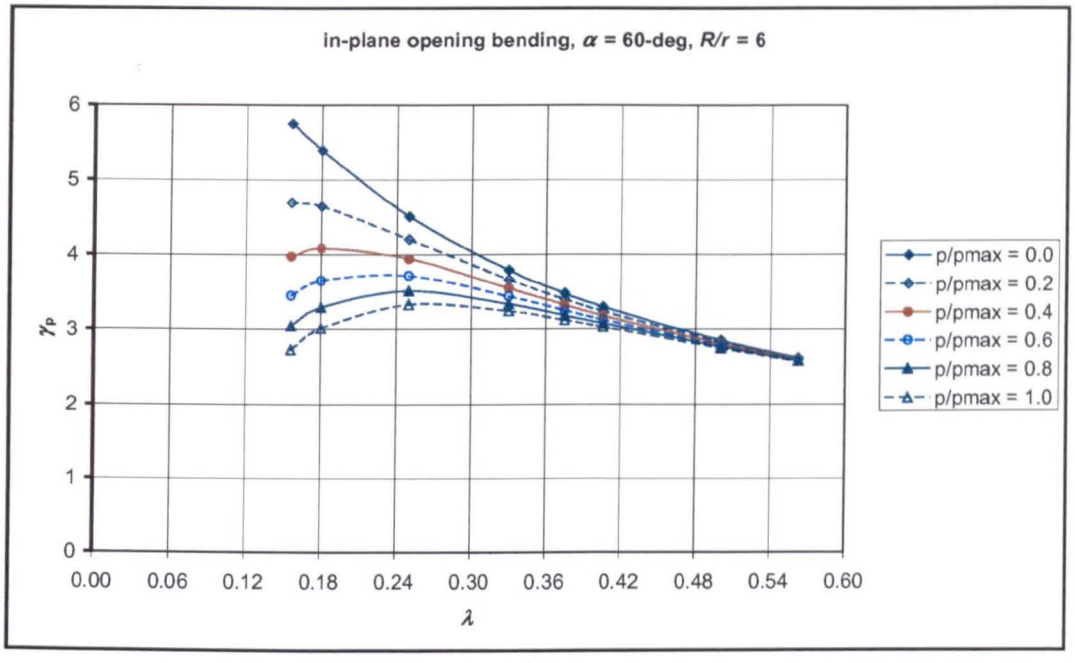

(c)

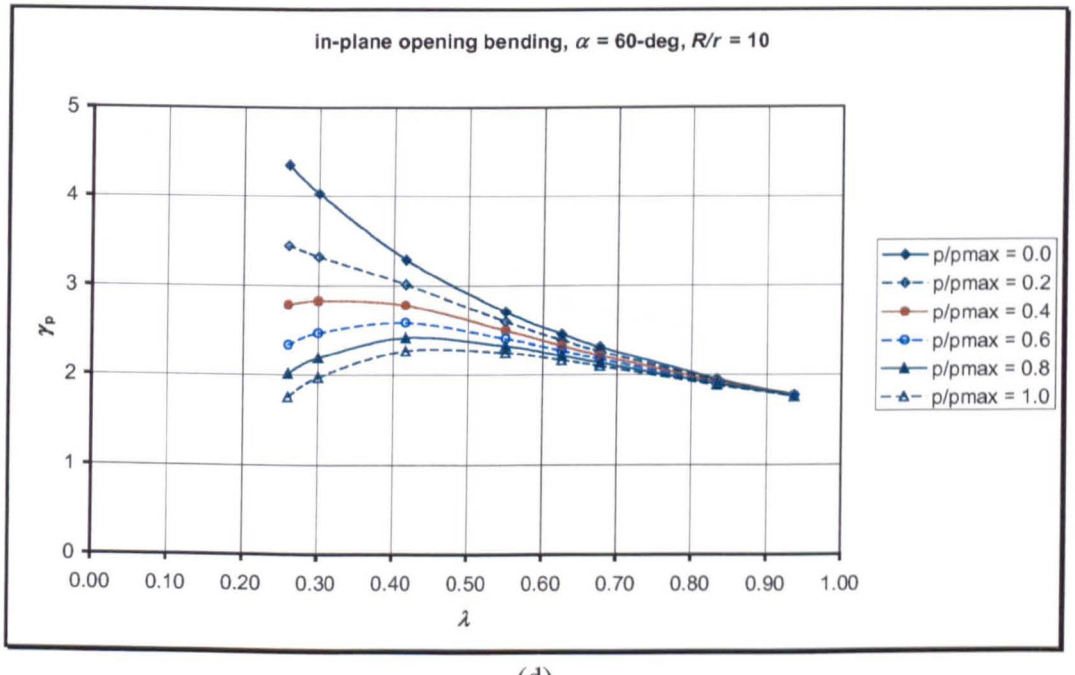

(d)

Fig.A6.13 Stress-intensification factor for 60-deg pipe elbows subjected to in-plane opening bending: (c) $R/r = 6$, (d) $R/r = 10$

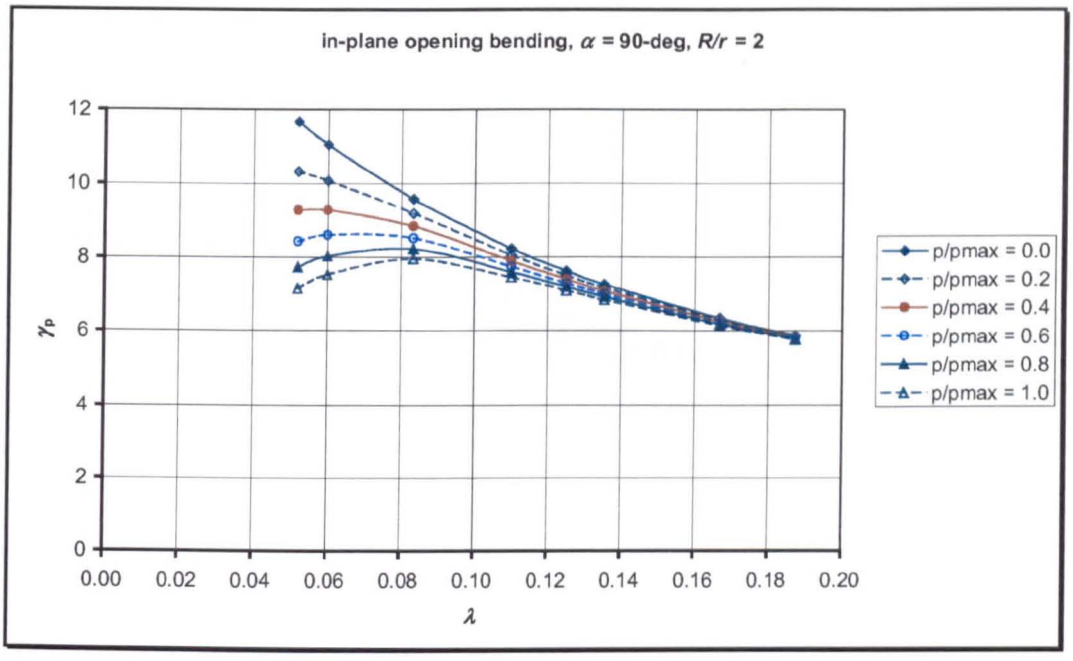

(a)

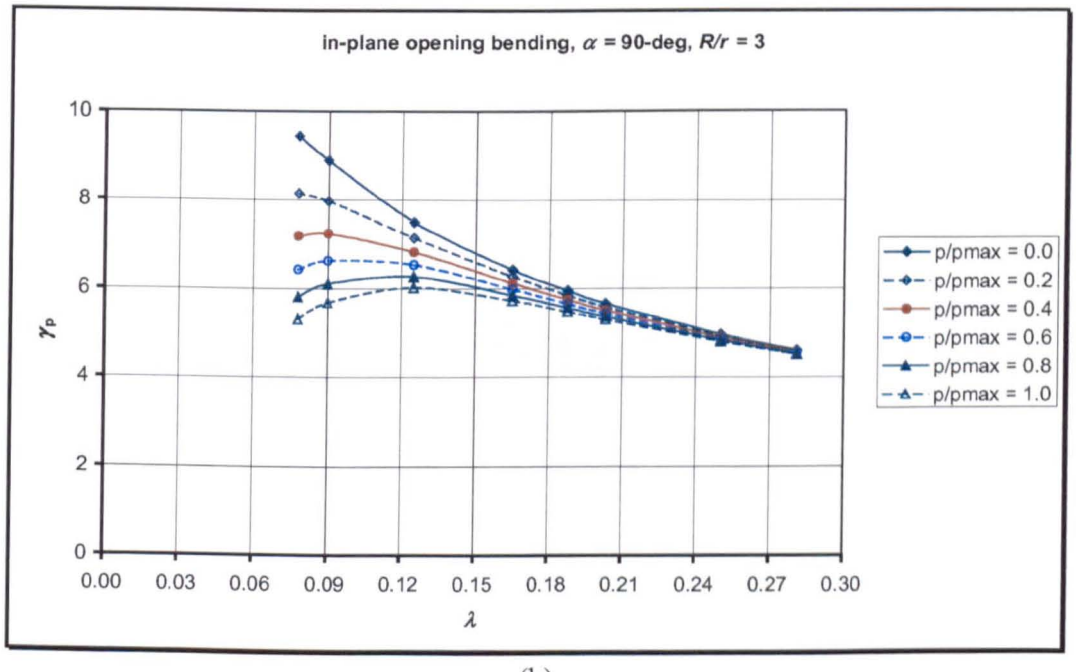

(b)

Fig.A6.14 Stress-intensification factor for 90-deg pipe elbows subjected to in-plane opening bending: (a) $R/r = 2$, (b) $R/r = 3$

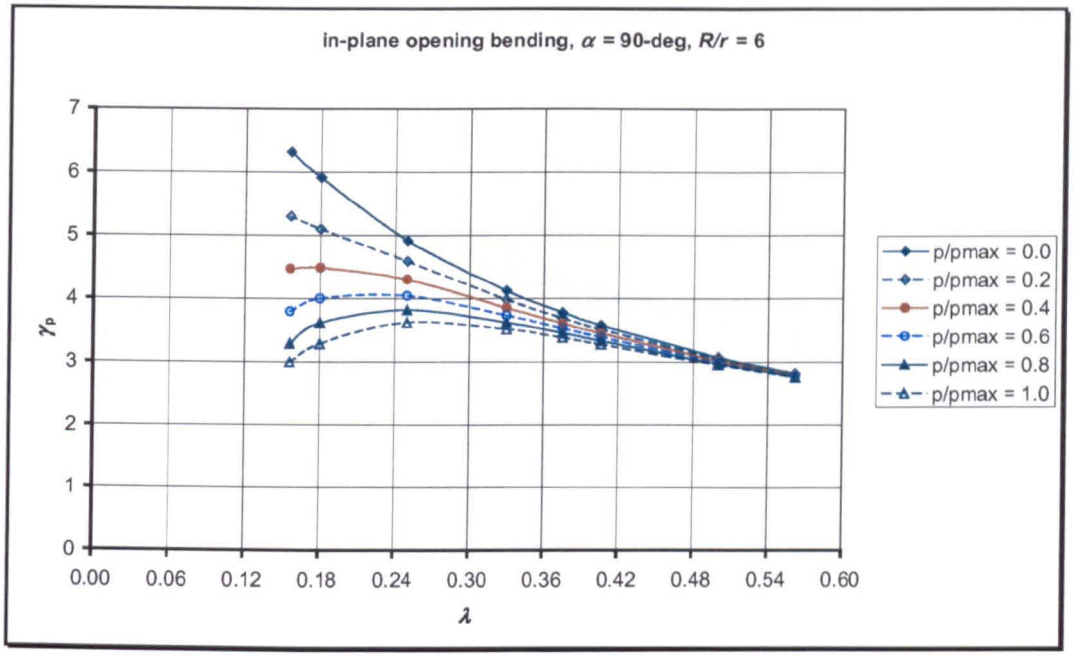

(c)

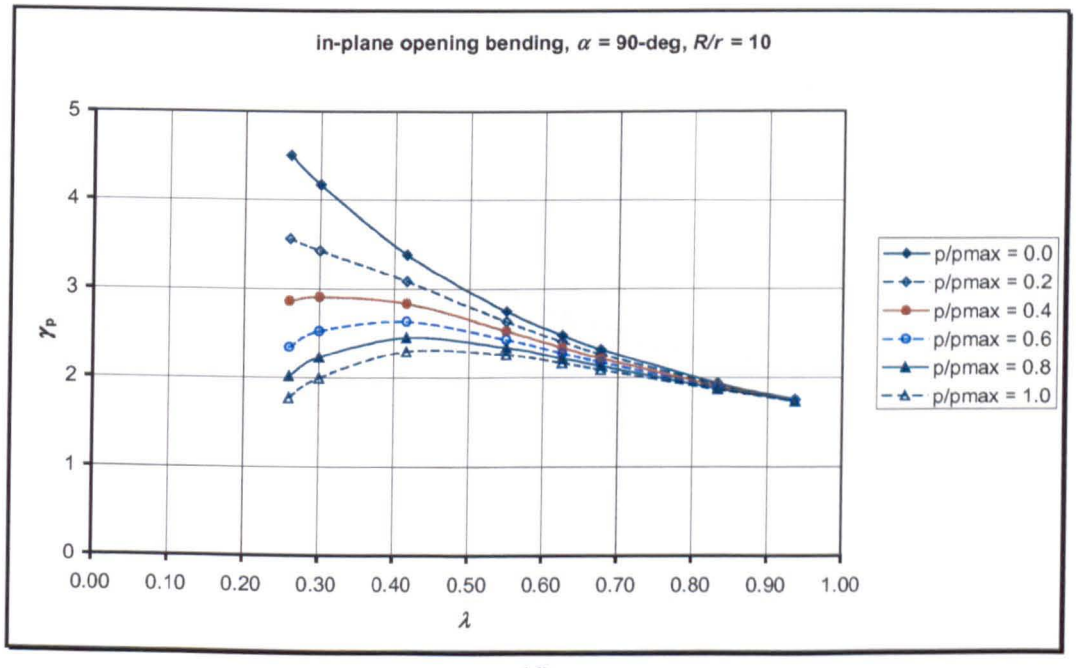

(d)

Fig.A6.14 Stress-intensification factor for 90-deg pipe elbows subjected to in-plane opening bending: (c) $R/r = 6$, (d) $R/r = 10$

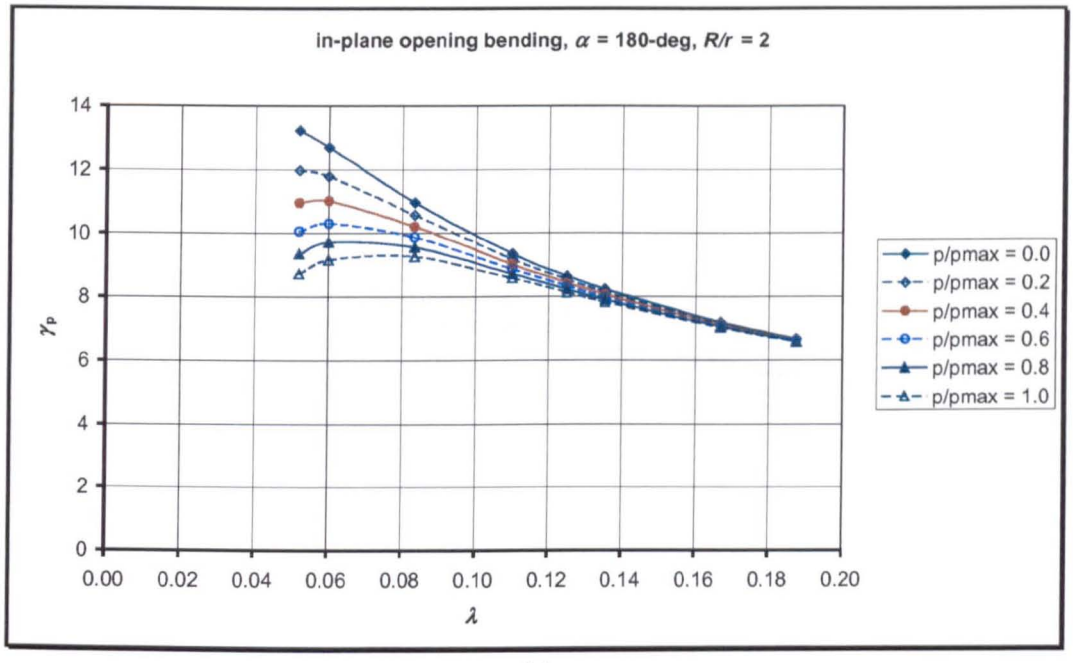

(a)

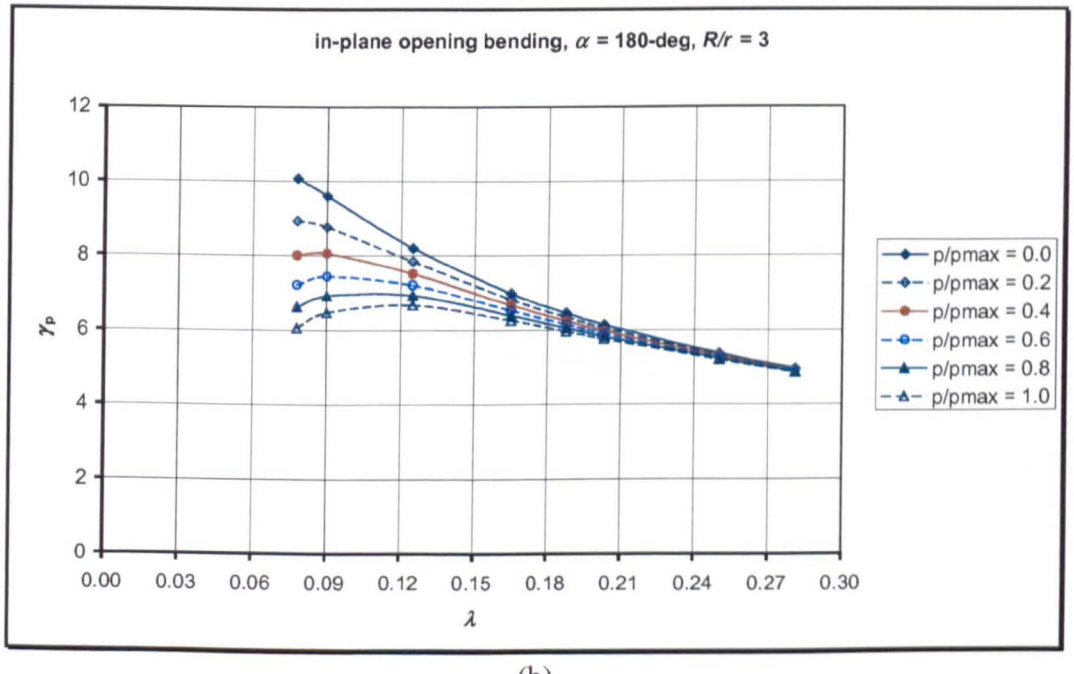

(b)

Fig.A6.15 Stress-intensification factor for 90-deg pipe elbows subjected to in-plane opening bending: (a) $R/r = 2$, (b) $R/r = 3$

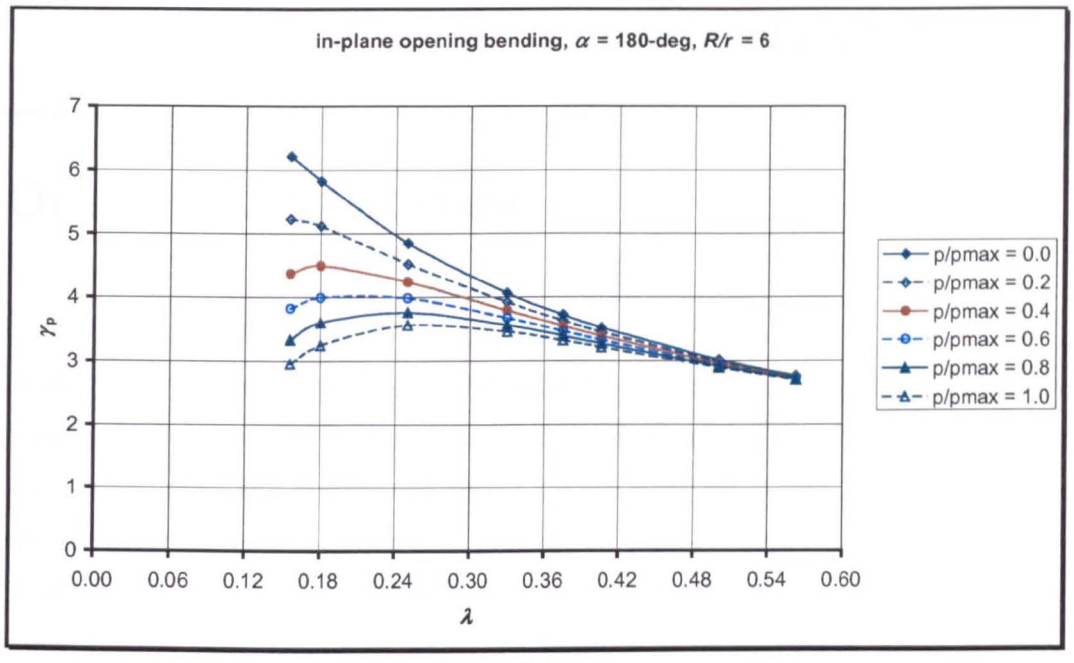

(c)

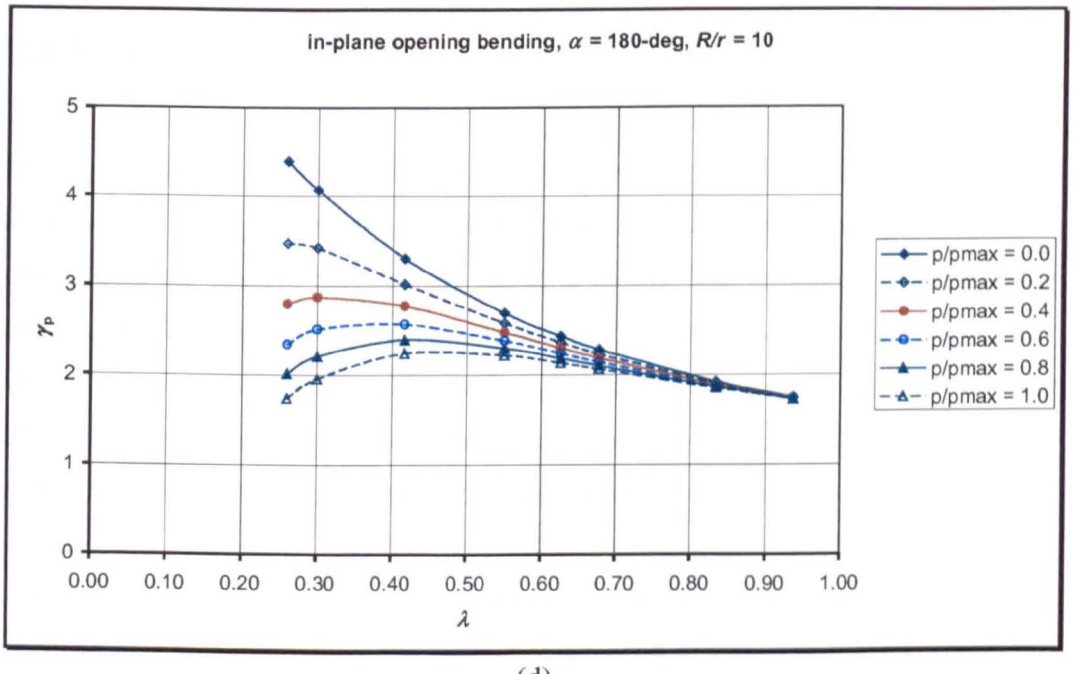

(d)

Fig.A6.15 Stress-intensification factor for 90-deg pipe elbows subjected to in-plane opening moment: (c) $R/r = 6$, (d) $R/r = 10$

CHAPTER 7

OUT-OF-PLANE BENDING

In the previous two chapters, the cross-sectional ovalisation, flexibility and stresses for piping elbows under in-plane bending have been studied. Approximate formulae for unpressurised and pressurised piping elbows were developed. In this chapter, a similar study of unpressurised and pressurised piping elbows under *out-of-plane bending* is developed. A formula for cross-sectional ovalisation is not presented here, since there is some ambiguity about the location of its maximum, being strongly dependent on the geometry of the pipe elbow.

7.1 Flexibility Factors

In the previous study of in-plane bending, the flexibility factor was derived from the axial and radial displacement of the extrados and intrados nodes at the junction of the elbow with the straight tangent, see equation (5-29). The definition of a flexibility factor used for in-plane bending is also adopted here for out-of-plane bending, i.e., through the concept of end rotation, although there may be alternatives. For the case of out-of-plane bending, the out-of-plane rotation will be derived from the displacement of the crown nodes at the elbow-straight pipe junction.

An out-of-plane bending load, M_o, is applied on the free end of the loaded tangent about an axis perpendicular to the tangent of the bend as shown in Fig.7.1. Under this load, end of the elbow at junction-1 will be subjected to pure bending, and the other end at junction-2 will be subjected to bending and torsion, depending on the bend angle. Definition of junction-1 and junction-2 is shown in Fig.7.2. For bend angles of 90 and 180-deg, the end of the elbow at junction-2 (corresponding to Fig.7.2) is

subjected to pure torsion and pure bending respectively. For other bend angle, this end is subjected to both bending and torsion.

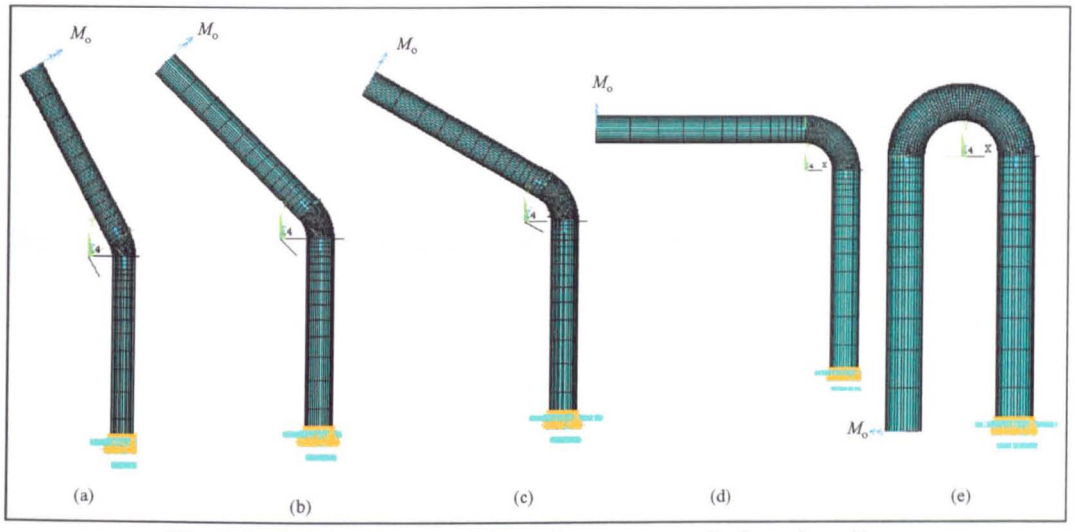

Fig.7.1 Piping elbows subjected to an out-of-plane bending

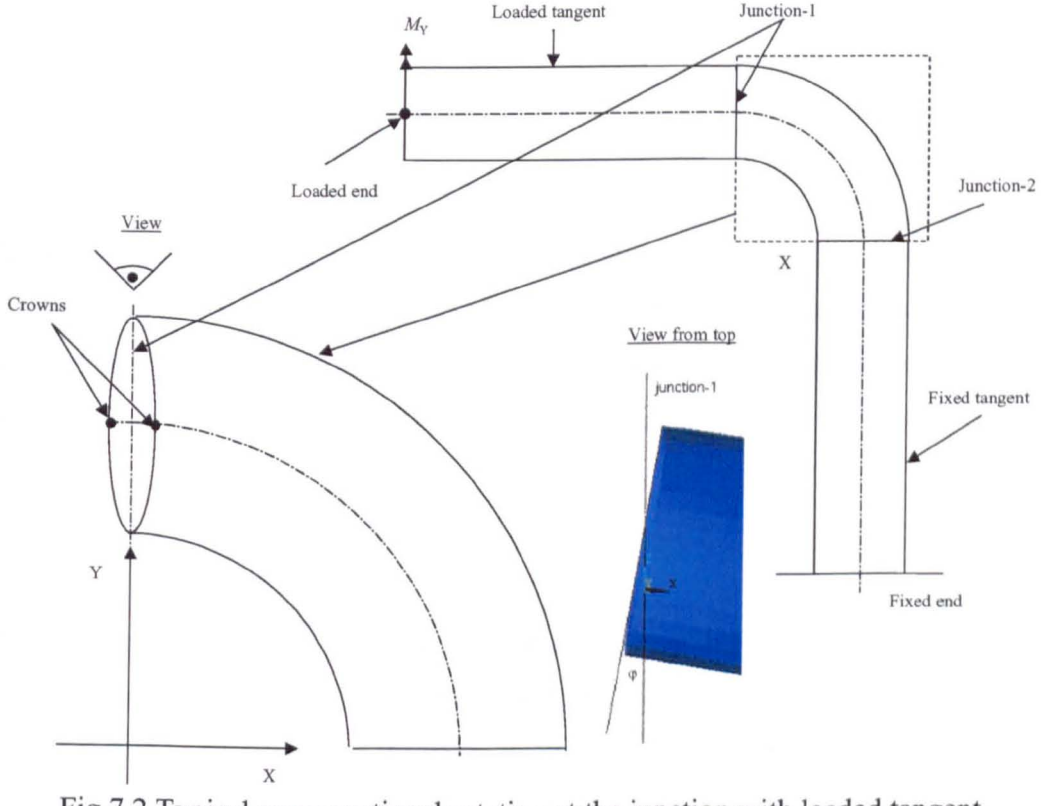

Fig.7.2 Typical cross-sectional rotation at the junction with loaded tangent

The out-of-plane rotation of section-1 is obtained from the axial and radial displacement of crown nodes. Accordingly, the rotation of this end is obtained from the following relation:

$$\varphi_1 = \tan^{-1}\left(\frac{dz_1}{2r + dr_1}\right) \tag{7-1}$$

The rotation of section-2 is obtained in a similar way from the following:

$$\varphi_{2m} = \tan^{-1}\left(\frac{dz_2}{2r + dr_2}\right) \tag{7-2}$$

Section-2 is also subjected to torsion. The angle of twist is obtained from the tangential and radial displacement of crown nodes at this section. Accordingly, the angle of twist is obtained as:

$$\varphi_{2t} = \tan^{-1}\left(\frac{dy_2}{2r + dr_2}\right) \tag{7-3}$$

It should be noted that for a Cartesian co-ordinate system, the rotation of section-2 according to equation (7-2) occurs in YZ-plane and the axis of twist in equation (7-3) is the axis of the fixed tangent. The total end rotation about an axis perpendicular to the loaded tangent is therefore obtained from the following geometric relation:

$$\varphi = \varphi_1 - \varphi_{2m}\cos\alpha - \varphi_{2t}\sin\alpha \tag{7-4}$$

A typical moment – end rotation ($\delta\alpha/\alpha$) curve is shown in Fig.7.3 using the equation (7-4). It can be seen that the relationship between bending and out-of-plane rotation is linear. The flexibility factor is finally obtained by dividing the derived end rotation produced by the end rotation of an equivalent straight pipe as given by eqn (5-31).

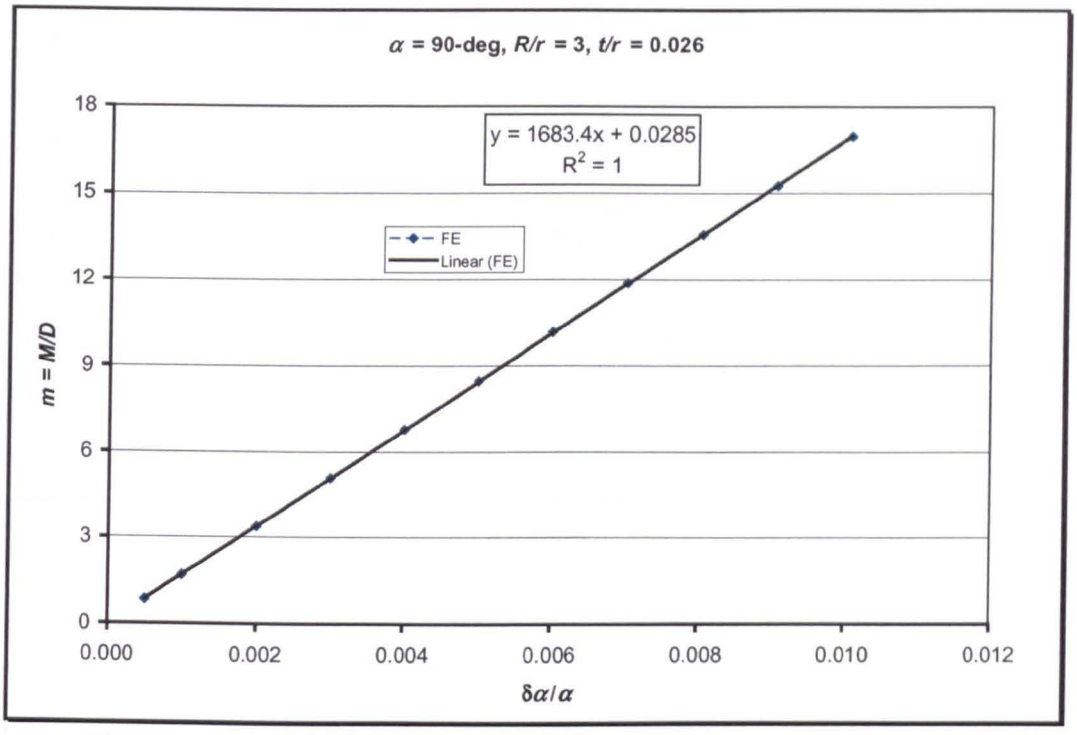

Fig.7.3 Typical moment – end rotation curve under out-of-plane bending

Figure 7.4 shows the flexibility factor for 90-deg piping elbows plotted against pipe bend parameter, λ, for various value of radius ratios, R/r. It can be seen that a high value of flexibility factor is obtained for a small value of pipe bend parameter. Figure 7.4 also shows a dependency of flexibility on radius ratio. As shown in Fig.7.4 the relationship between flexibility factor k, and pipe bend parameter, λ, is approximately linear in a log-log plot. Accordingly, the relation can be expressed in form of equation (5-33).

As before, it is required to obtain approximate formulae for the flexibility factor from finite element generated data. It can be seen from Fig.7.4 that the flexibility factor under out-of-plane bending depends on the pipe bend parameter as well as on radius ratio. By curve fitting, flexibility factors for 90-deg piping elbows under out-of-plane bending are summarised in the following equations:

$$k = \frac{2.605}{\lambda^{0.57}}; \qquad \text{for} \frac{R}{r} = 2 \tag{7-5}$$

$$k = \frac{2.39}{\lambda^{0.59}}; \qquad \text{for} \frac{R}{r} = 3 \tag{7-6}$$

$$k = \frac{2.19}{\lambda^{0.58}}; \qquad \text{for} \frac{R}{r} = 6 \tag{7-7}$$

$$k = \frac{2.11}{\lambda^{0.53}}; \qquad \text{for} \frac{R}{r} = 10 \tag{7-8}$$

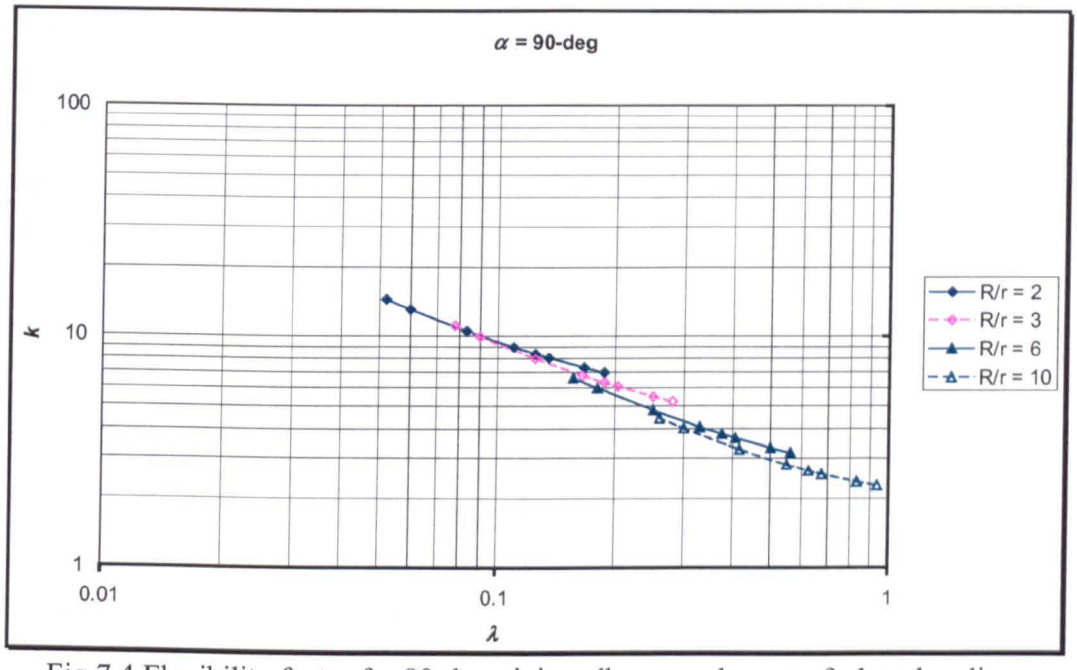

Fig.7.4 Flexibility factor for 90-deg piping elbows under out-of-plane bending

As has been done for in-plane bending case, the derivation of flexibility factor following the form of equations proposed by Fujimoto and Soh [92], where the flexibility factor is expressed in term of the asymptotic solution of Clark and Reissner [20] and multiplying it with a factor representing the dependence of flexibility factor on pipe bend parameter, λ, as well as on radius ratio, *R/r*. Equation (7-5) through (7-8) can be further written in the following form:

$$k = \frac{1.65}{\lambda}[1.176 + 0.252\ln(\lambda)] \qquad \frac{R}{r} = 2 \qquad (7-9)$$

$$k = \frac{1.65}{\lambda}[1.193 + 0.2727\ln(\lambda)] \qquad \frac{R}{r} = 3 \qquad (7-10)$$

$$k = \frac{1.65}{\lambda}[1.218 + 0.3341\ln(\lambda)] \qquad \frac{R}{r} = 6 \qquad (7-11)$$

$$k = \frac{1.65}{\lambda}[1.244 + 0.4348\ln(\lambda)] \qquad \frac{R}{r} = 10 \qquad (7-12)$$

It can be inferred from these equations that the flexibility factor under an out-plane bending is much smaller than the asymptotic solution of Clark and Reissner [20] as adopted in current design piping code [114, 120]. Fig.7.5 shows the flexibility factor calculated using the formulae of Equations (7-9) through (7-12) in comparison with the finite element results. It can be seen that the proposed formulae fit the results obtained from finite element, but not as good as for in-plane bending case.

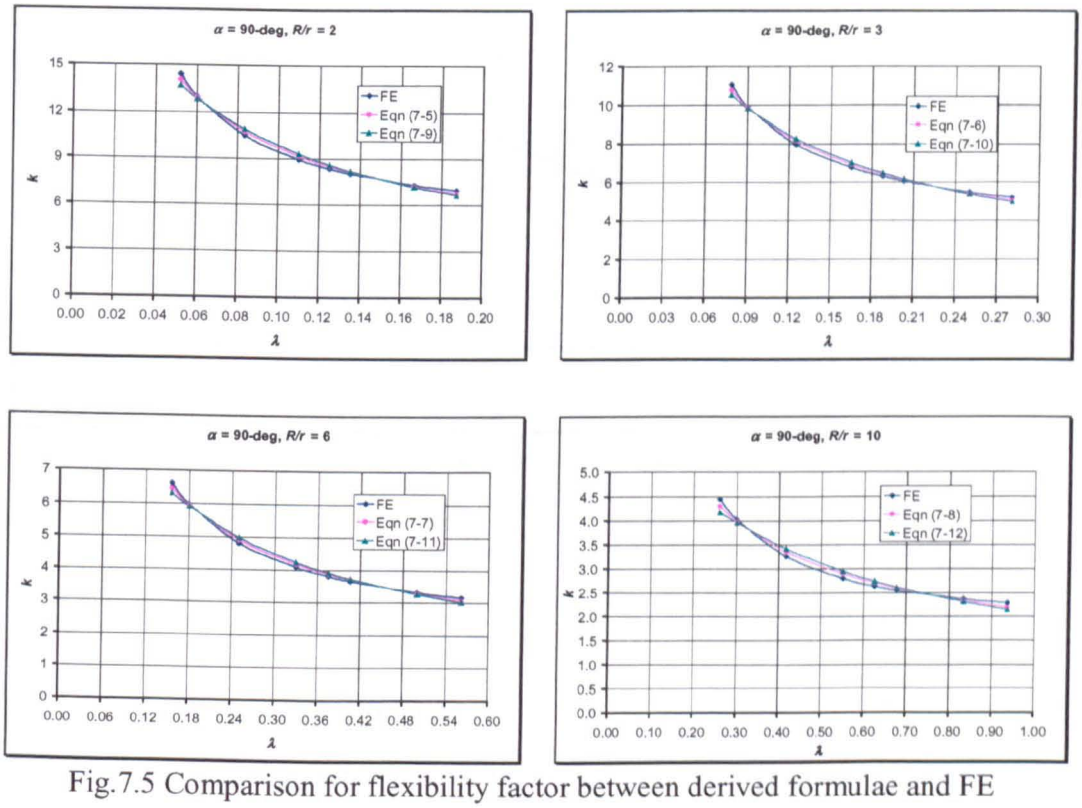

Fig.7.5 Comparison for flexibility factor between derived formulae and FE

7.1.1 Effect of Bend Angle on Flexibility Factor

As has been done for in-plane bending case, the effect of bend angle on flexibility factor under out-of-plane bending will continue be taken into account. For this purpose, piping elbows of bend angle 30, 45, 60, and 180-deg have been studied. Figure 7.6 through 7.9 show plots of flexibility factor against pipe bend parameter. It can be seen from these plots that the relationship between flexibility factor and pipe bend parameter is once more approximately linear in log-log plot for all the bend angles considered.

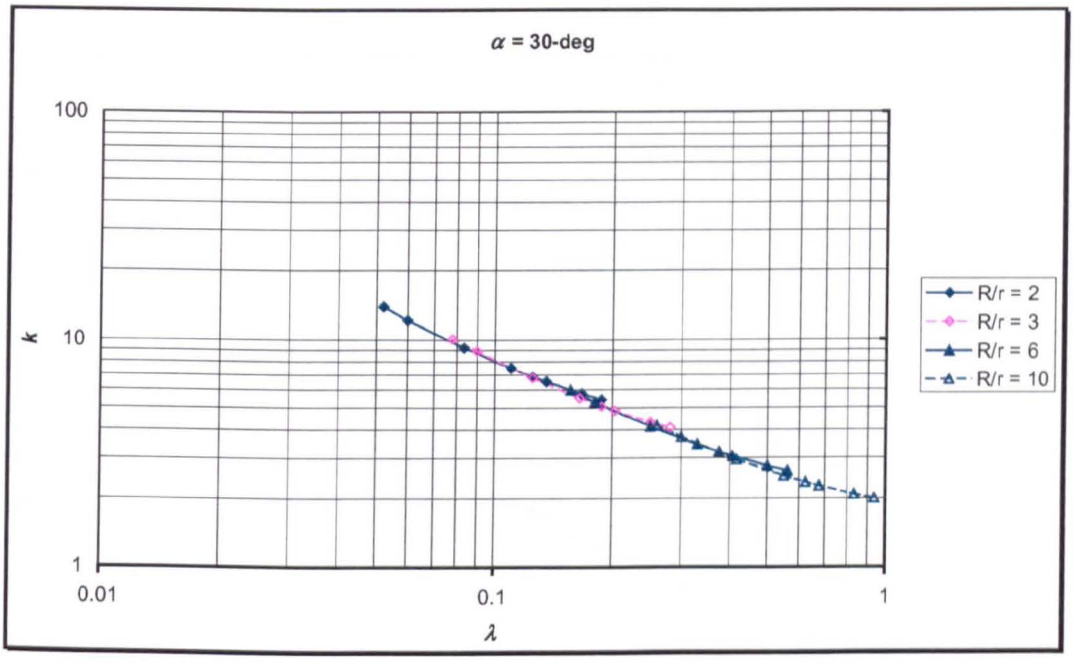

Fig.7.6 Flexibility factor for 30-deg pipe elbows under out-of-plane bending

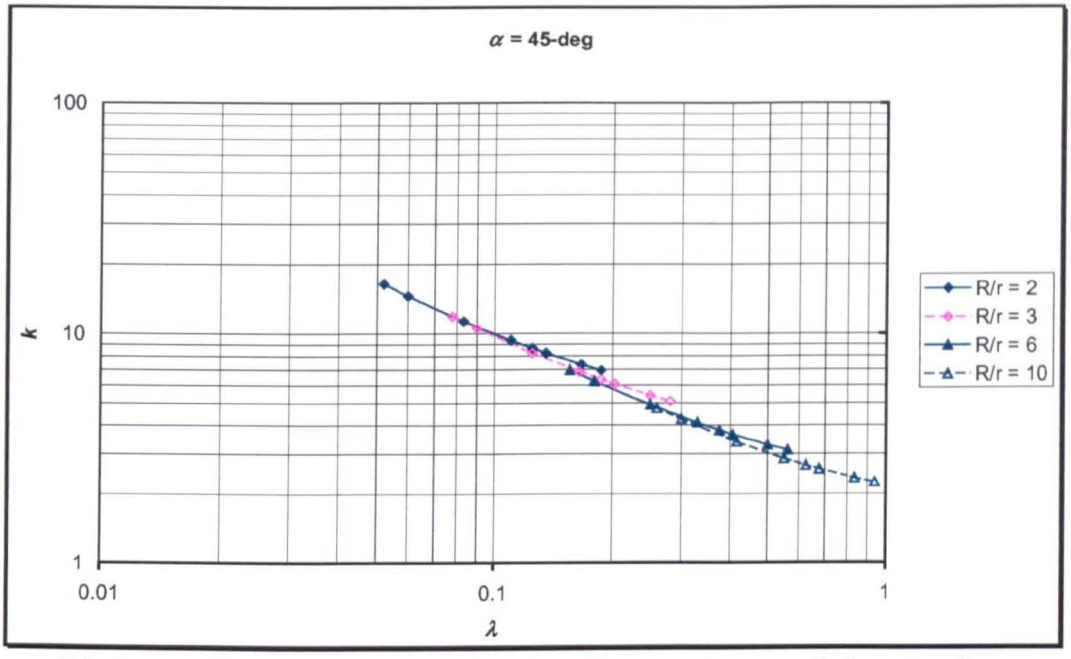

Fig.7.7 Flexibility factor for 45-deg pipe elbows under out-of-plane bending

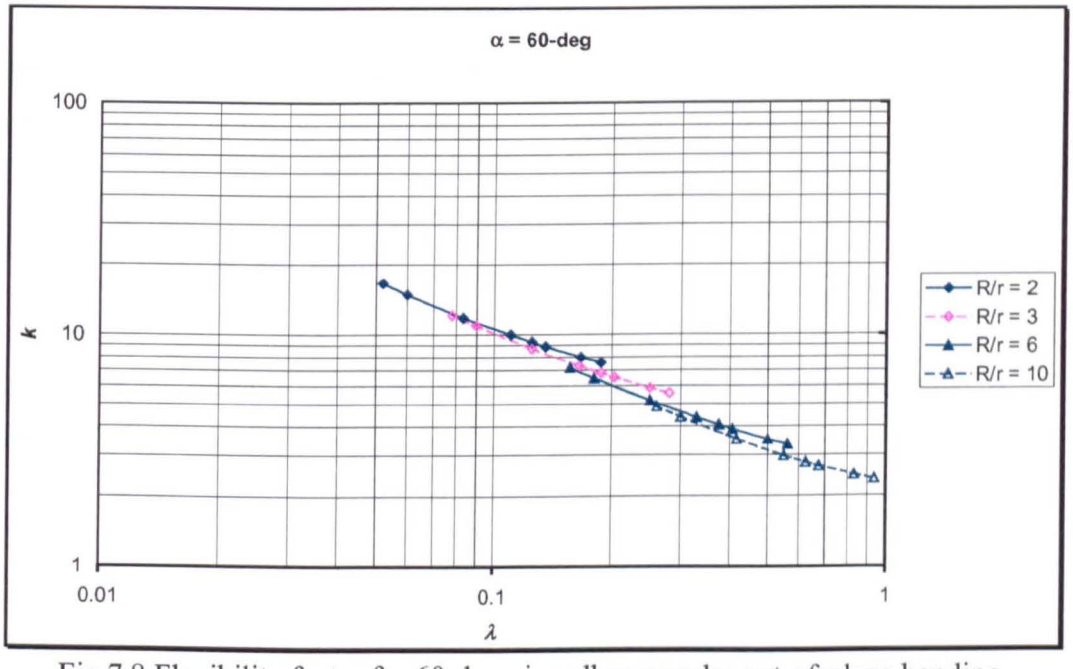

Fig.7.8 Flexibility factor for 60-deg pipe elbows under out-of-plane bending

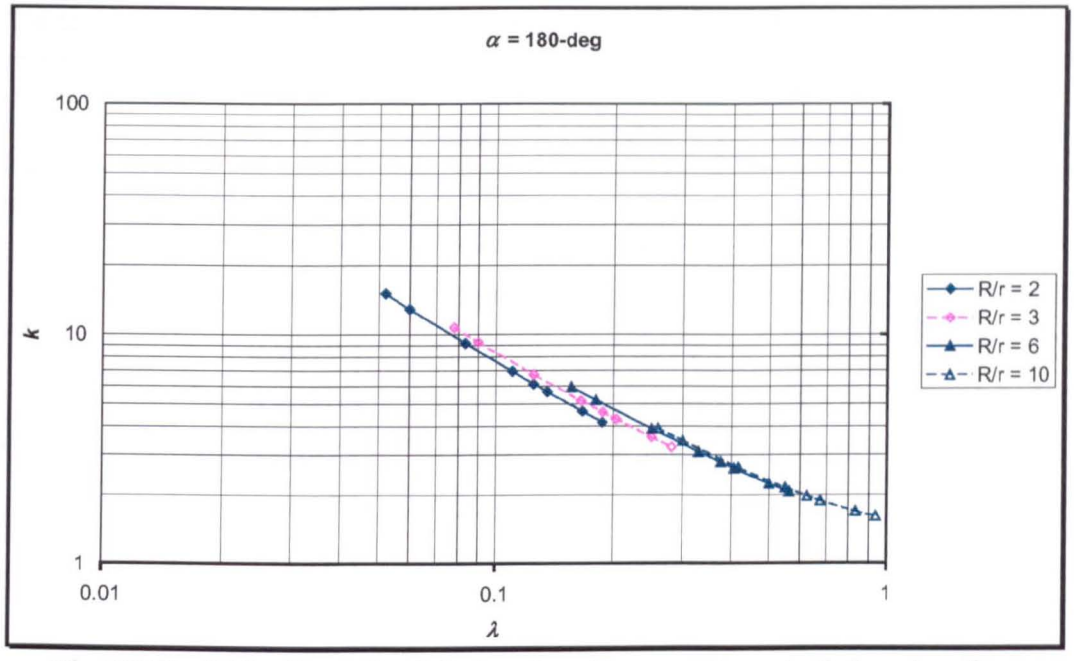

Fig.7.9 Flexibility factor for 180-deg pipe elbows under out-of-plane bending

By curve fitting, flexibility factors for piping elbows under out-of-plane bending can now be derived as before and the results are expressed in form:

$$k = \frac{1.65}{\lambda}[a + b\ln(\lambda)] \qquad (7\text{-}13)$$

where the coefficient a and b are functions of radius ratio, R/r, and bend angle, α, and are summarised in Table 7.1 and 7.2 respectively.

Table 7.1 Values of coefficient "*a*" in equation (7-13) for various bend angles

R/r	*Bend Angle, α*				
	30-deg	45-deg	60-deg	90-deg	180-deg
2	0.8110	1.0880	1.2427	1.1760	0.4617
3	0.8650	1.1224	1.2618	1.1930	0.5860
4	0.9181	1.1440	1.2714	1.2039	0.6468
5	0.9570	1.1633	1.2772	1.2132	0.7037
6	0.9890	1.1850	1.2800	1.2180	0.7480
7	1.0187	1.1930	1.2840	1.2272	0.7894
8	1.0443	1.2050	1.2861	1.2328	0.8234
9	1.0674	1.2157	1.2877	1.2378	0.8535
10	1.0910	1.2322	1.2900	1.2440	0.8788

Table 7.2 Values of coefficient "*b*" in equation (7-13) for various bend angles

R/r	*Bend Angle, α*				
	30-deg	45-deg	60-deg	90-deg	180-deg
2	0.1320	0.2001	0.2510	0.2520	0.0020
3	0.1603	0.2300	0.2800	0.2727	0.0346
4	0.1871	0.2404	0.2967	0.2904	0.0552
5	0.2143	0.2636	0.3179	0.3107	0.0818
6	0.2424	0.3000	0.3385	0.3341	0.1062
7	0.2687	0.3100	0.3603	0.3558	0.1350
8	0.2959	0.3332	0.3815	0.3807	0.1616
9	0.3231	0.3564	0.4027	0.4074	0.1882
10	0.3501	0.3880	0.4242	0.4348	0.2146

Figure 7.10 and 7.11 show flexibility factor for various bend angles calculated using equation (7-13) and Table 7.1 and 7.2. It can be seen for both short radius and long radius piping elbows that the flexibility factor is directly proportional to the bend angle for bend angle between 30 and 60-deg. There is a significant drop in value of

flexibility for 90-deg bend angle compared to the flexibility for 60-deg elbows. It can be seen that the flexibility factor for 90-deg elbows lying between the value for 45 and 60-deg for high pipe bend parameter and between the value for 30 and 45-deg for low pipe bend parameter. For short-radius 180-deg piping elbows, the flexibility factor is less than the value for 30-deg for high pipe bend parameter but approximately equal to the flexibility for 90-deg for low pipe bend parameter. Figure 7.11 shows that the flexibility factor for long radius 180-deg piping elbows is less than the value for 30-deg pipe elbows.

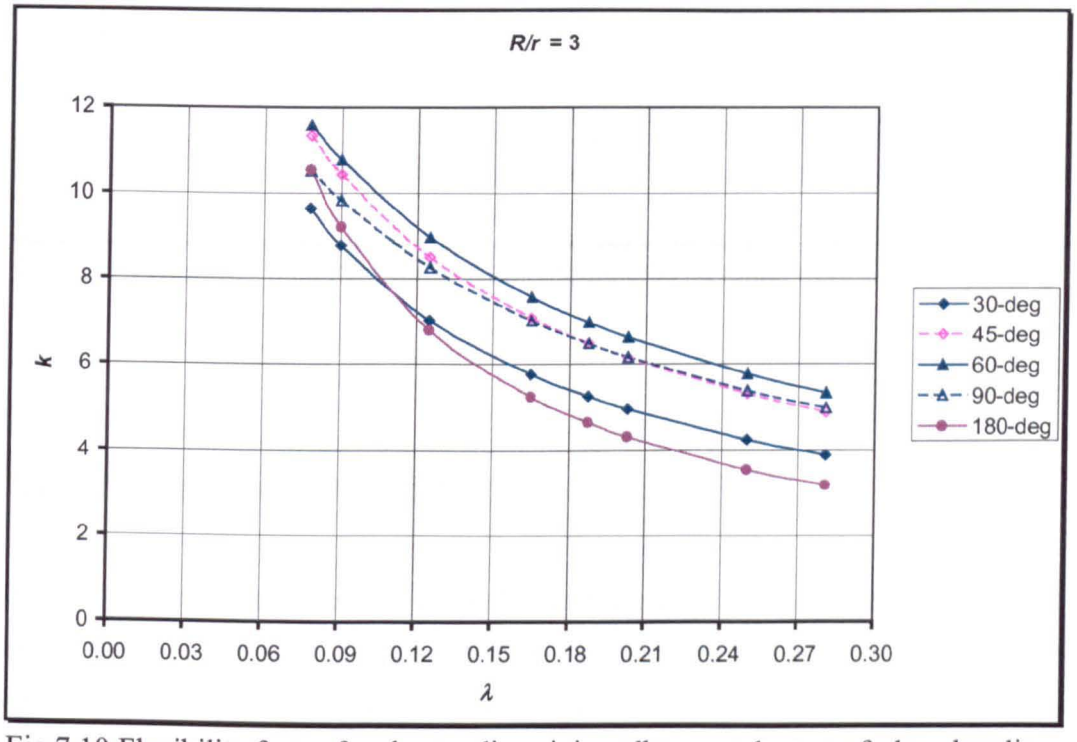

Fig.7.10 Flexibility factor for short-radius piping elbows under out-of-plane bending

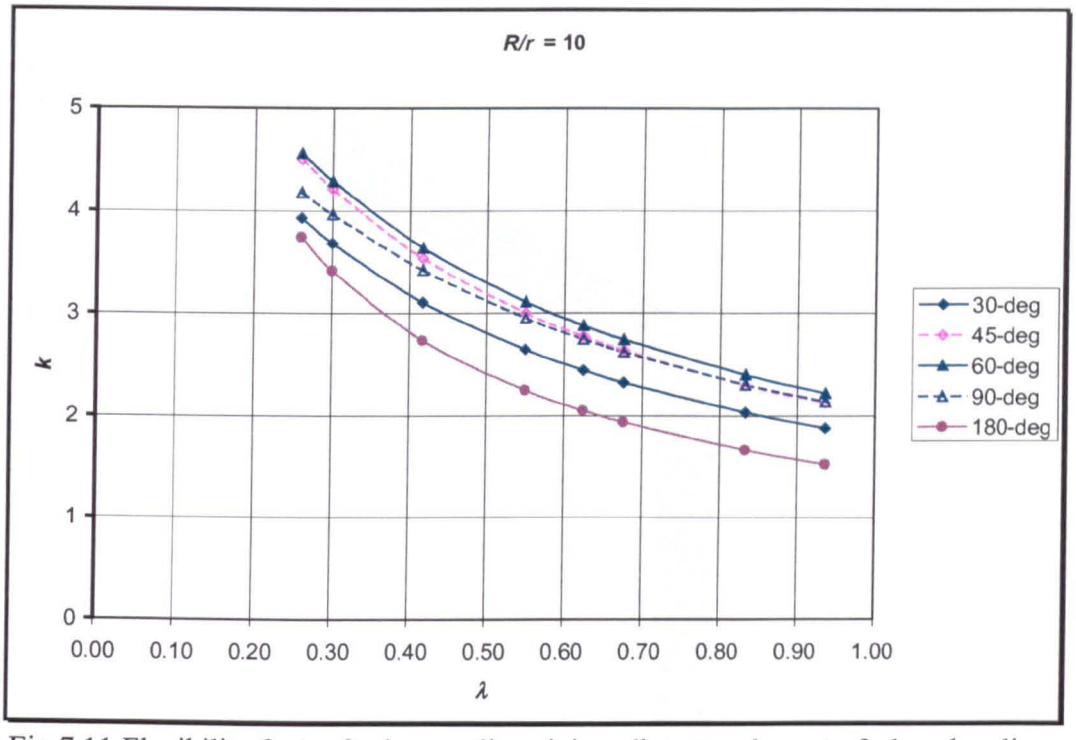

Fig.7.11 Flexibility factor for long-radius piping elbows under out-of-plane bending

7.1.2 Pressure Reduction Effect

It was confirmed in the previous chapters that internal pressure reduces the flexibility of piping elbows under in-plane bending. In this section the pressure reduction effect on flexibility for piping elbows under out-of-plane bending is examined.

The closed-end effect of internal pressure is modelled in usual way, i.e., acting on the edge of the loaded end as shown in Fig.7.12. As a family of surface load, ANSYS always treats the pressure (either it acting on a surface or on an edge) as follower force. See ANSYS on-line help section 8.1.2.3 [119].

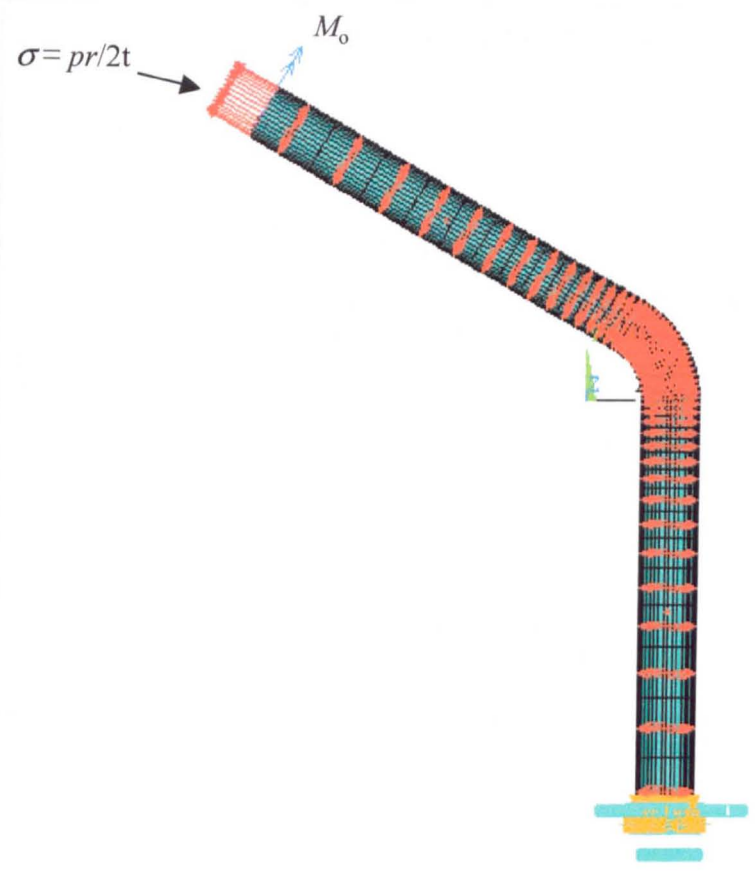

Fig.7.12 Piping elbow subjected to out-of-plane bending and internal pressure

As usual a typical pressure – end rotation curve is shown in Fig.7.13 plotted for a 90-deg elbow having radius ratio equals three where the abscissa 0.0 represents the final load step of moment loading and the start of the subsequent internal pressure loading. It can be seen that the relation between internal pressure and the end rotation is non-linear as compared to the linear relation in the moment – end rotation curve.

Figure 7.14 through 7.17 show the flexibility factor for 90-deg pipe elbows plotted against pipe bend parameters for various radius ratios. Once more it can be clearly seen that internal pressure reduces the flexibility and the reduction is more pronounced for thin walled piping elbows (elbows of low pipe factors). The pressure reduction effect corresponding to equation (5-45) can be further derived from these Figures.

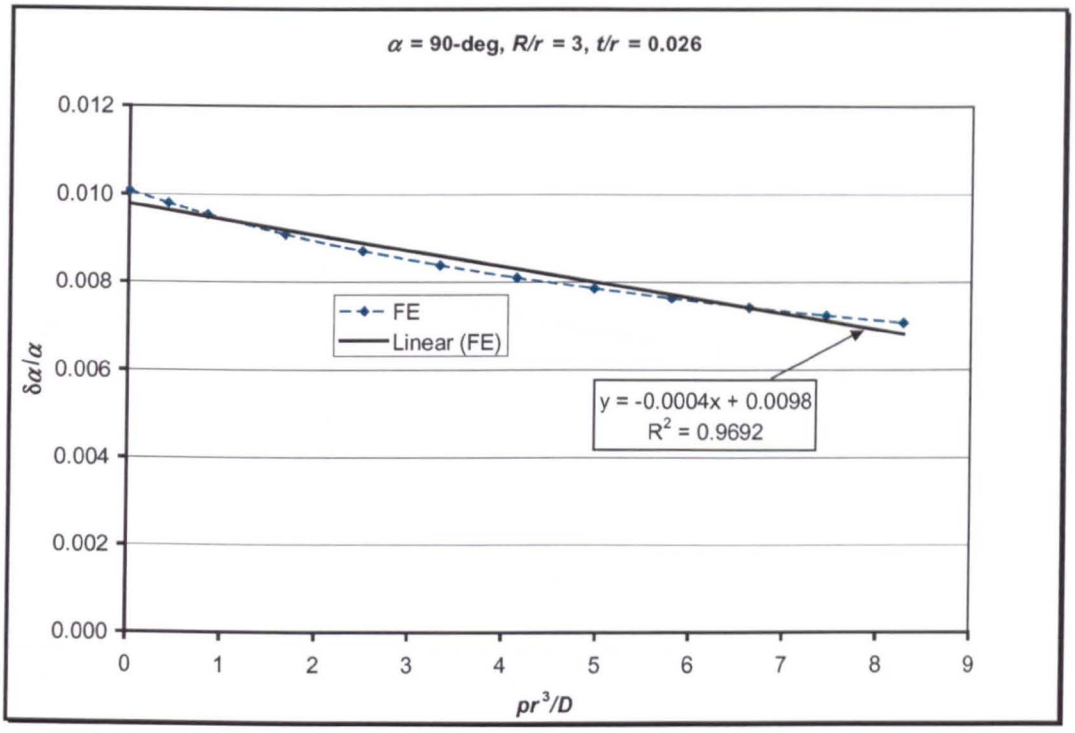

Fig.7.13 Typical pressure – end rotation curve under out-of-plane bending

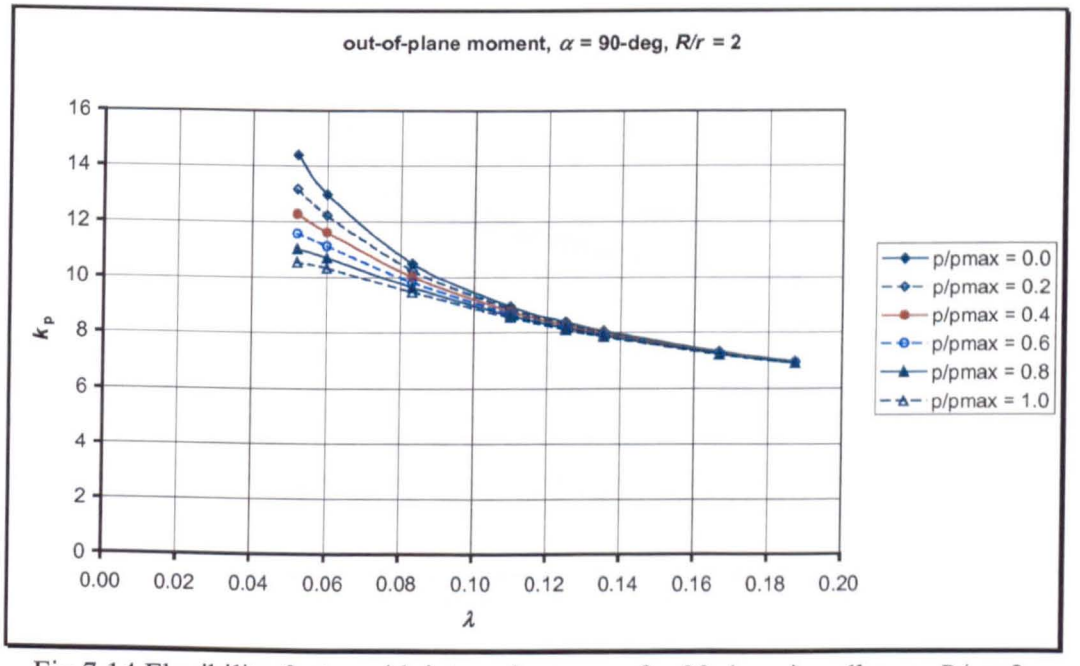

Fig.7.14 Flexibility factor with internal pressure for 90-deg pipe elbows: $R/r = 2$

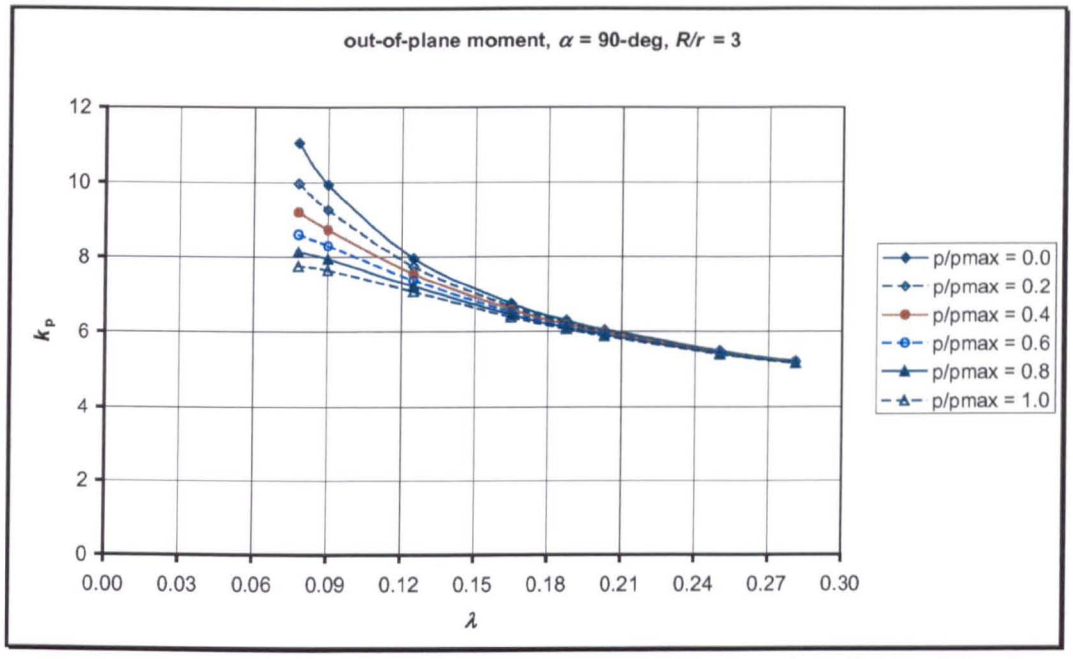

Fig.7.15 Pressure reduction on flexibility factor for 90-deg pipe elbows: $R/r = 3$

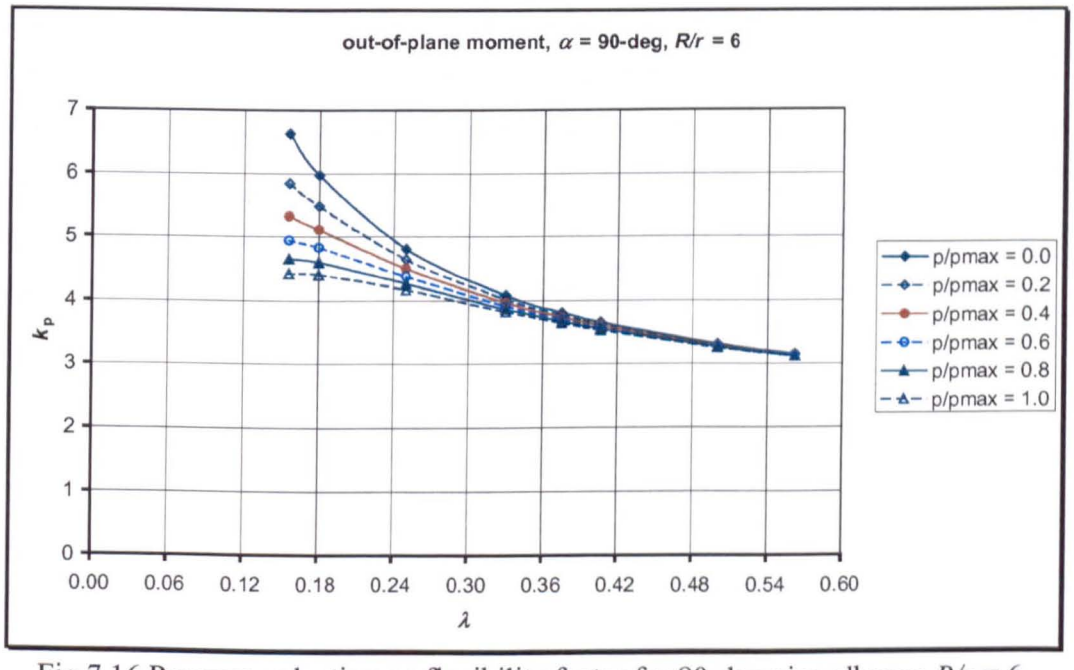

Fig.7.16 Pressure reduction on flexibility factor for 90-deg pipe elbows: $R/r = 6$

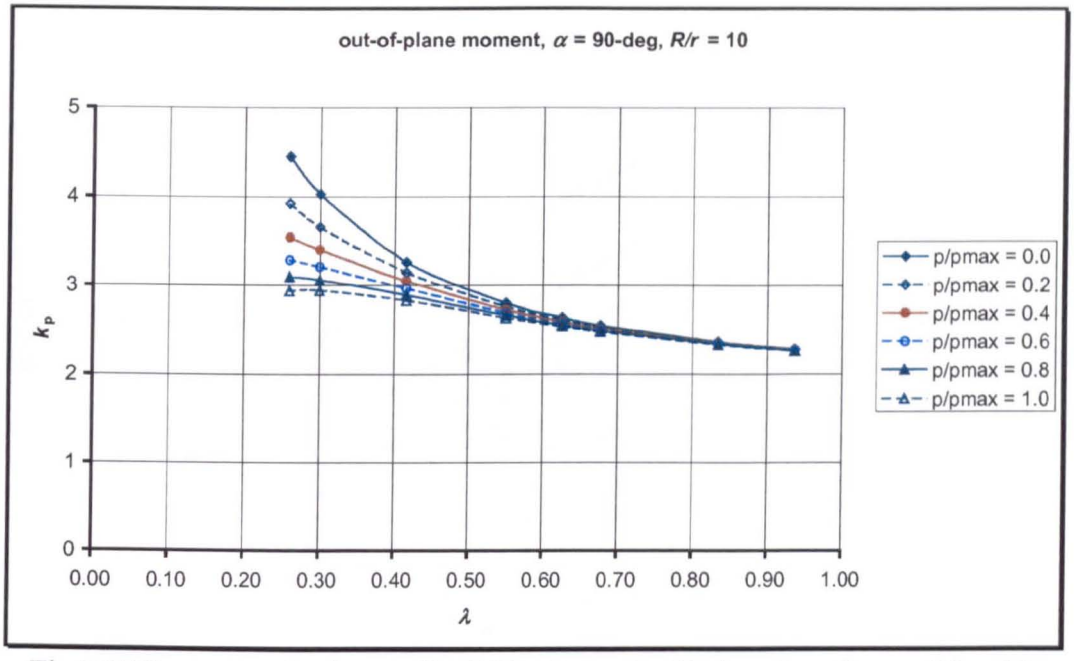

Fig.7.17 Pressure reduction on flexibility factor for 90-deg pipe elbows: $R/r = 10$

Again, a typical example of the pressure reduction effect on out-of-plane flexibility for 90-deg pipe elbows is shown as a log-log plot in Fig.7.18 and 7.19, and it can be seen that the relations are linear. There is a small deviation from linearity for the relation between pressure reduction and radius ratio (R/r). Throughout the development of approximate formula in what follows, this linear behaviour will again be adopted as the basis for approximation.

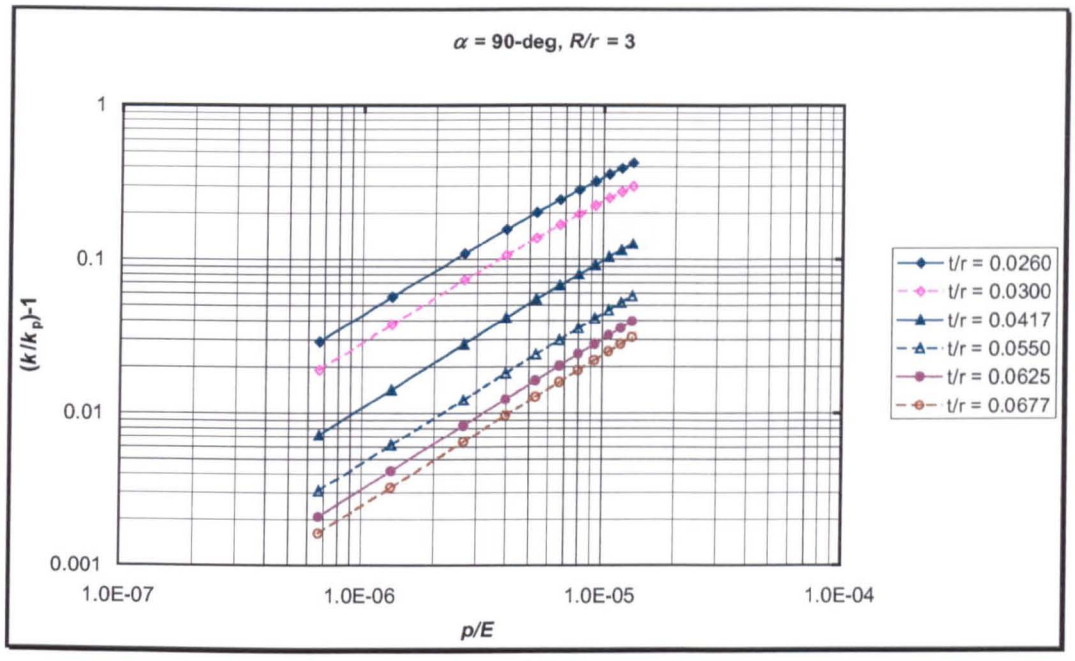

(a)

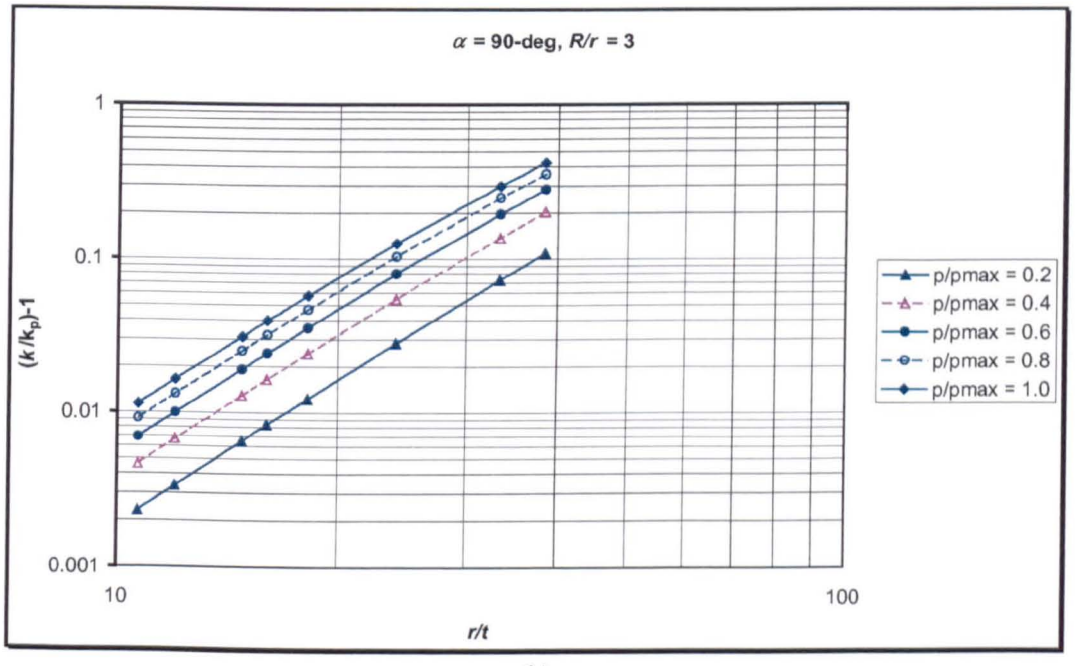

(b)

Fig.7.18 Pressure reduction for constant radius ratio plotted against (a) *p/E*, (b) *r/t*

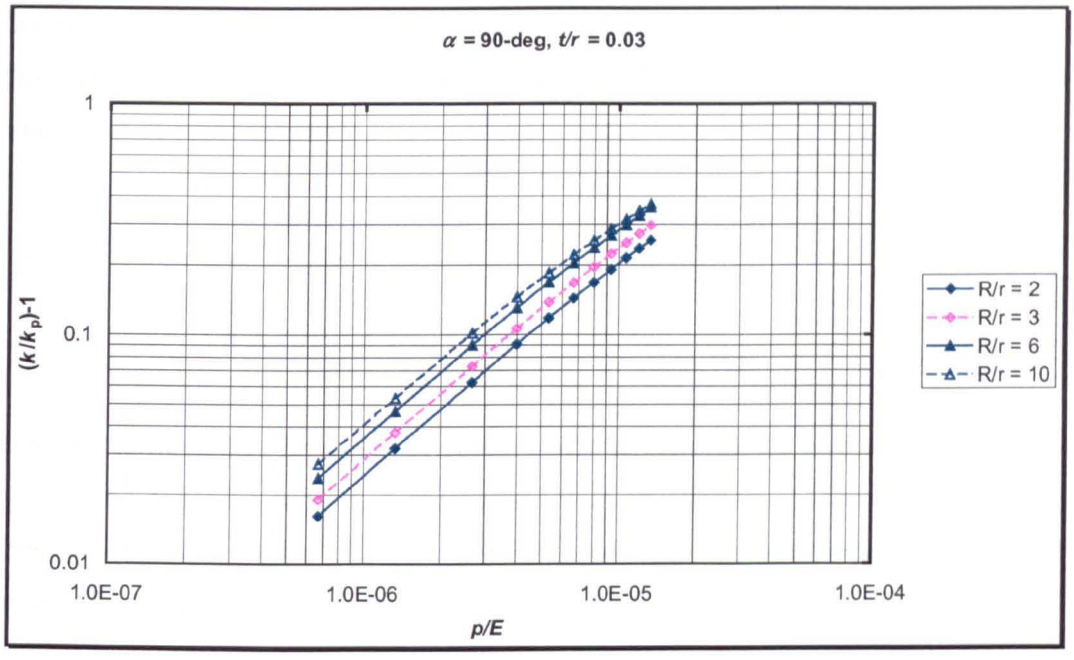

(a)

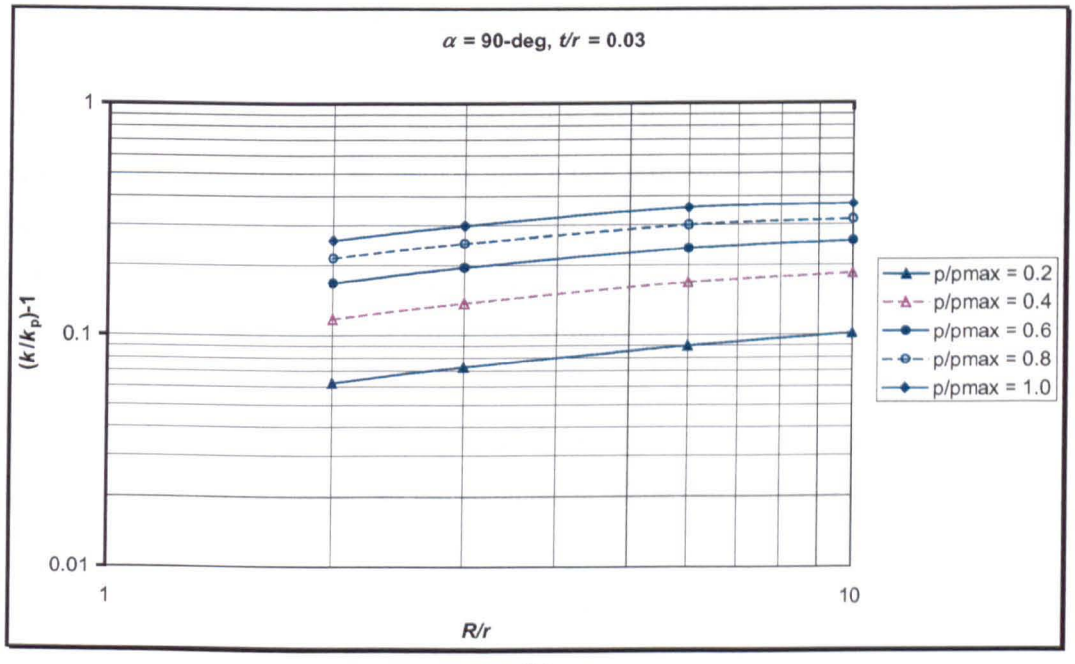

(b)

Fig.7.19 Pressure reduction for constant thickness plotted against (a) *p/E*, (b) *R/r*

Examination of Fig.7.18 and 7.19 together with Fig.7.14 through 7.17 results in the following approximate equation is proposed for the flexibility 90-deg pipe elbows under out-of-plane moment:

$$k_p = \frac{k}{1+0.175\left(\frac{p}{E}\right)\left(\frac{r}{t}\right)^{19/6}\left(\frac{R}{r}\right)^{0.322}} \qquad (7\text{-}14)$$

where k is flexibility factor in the absence of internal pressure as given by equation (7-13) and Table 7.1 and 7.2. A comparison with equation (6-31) for in-plane closing bending shows roughly that the pressure reduction in both equations are not markedly different in magnitude.

7.1.3 Effect of Bend Angle on Pressure Reduction

It has been shown elsewhere in this thesis that the flexibility for unpressurised piping elbows under out-of-plane moment is very much influenced by the bend angle. It has been found however that the flexibility is not directly proportional to the bend angle if the bend angle approached 90-deg and greater. In what follows, the effect of bend angle on the pressure reduction effect is examined.

Using the data of Fig.A7.1 through A7.5 in Appendix C7, flexibility factors for pressurised piping elbows under out-of-plane bending can be derived as before:

$$k_p = \frac{k}{1+0.385\left(\frac{p}{E}\right)\left(\frac{r}{t}\right)^{19/6}\left(\frac{R}{r}\right)^{0.033}} \qquad \text{for } \alpha = 30\text{-deg} \qquad (7\text{-}15)$$

$$k_p = \frac{k}{1+0.295\left(\frac{p}{E}\right)\left(\frac{r}{t}\right)^{19/6}\left(\frac{R}{r}\right)^{0.149}} \qquad \text{for } \alpha = 45\text{-deg} \qquad (7\text{-}16)$$

$$k_p = \frac{k}{1+0.225\left(\frac{p}{E}\right)\left(\frac{r}{t}\right)^{19/6}\left(\frac{R}{r}\right)^{0.244}} \qquad \text{for } \alpha = 60\text{-deg} \qquad (7\text{-}17)$$

$$k_p = \frac{k}{1+0.300\left(\frac{p}{E}\right)\left(\frac{r}{t}\right)^{19/6}\left(\frac{R}{r}\right)^{0.231}} \qquad \text{for } \alpha = 180\text{-deg} \qquad (7\text{-}18)$$

Noting that:

$$\left(\frac{r}{t}\right)^{19/6} = \left(\frac{r}{t}\right)^{3}\left(\frac{1}{\lambda}\right)^{1/6}\left(\frac{R}{r}\right)^{1/6}$$

equations (7-14) through (7-18) can be written as:

$$k_p = \frac{k}{1+0.106\left(\frac{pr^3}{3D}\right)\left(\frac{1}{\lambda}\right)^{1/6}\left(\frac{R}{r}\right)^{0.199}} \qquad \text{for } \alpha = 30\text{-deg} \qquad (7\text{-}19)$$

$$k_p = \frac{k}{1+0.080\left(\frac{pr^3}{3D}\right)\left(\frac{1}{\lambda}\right)^{1/6}\left(\frac{R}{r}\right)^{0.316}} \qquad \text{for } \alpha = 45\text{-deg} \qquad (7\text{-}20)$$

$$k_p = \frac{k}{1+0.062\left(\frac{pr^3}{3D}\right)\left(\frac{1}{\lambda}\right)^{1/6}\left(\frac{R}{r}\right)^{0.411}} \qquad \text{for } \alpha = 60\text{-deg} \qquad (7\text{-}21)$$

$$k_p = \frac{k}{1+0.048\left(\frac{pr^3}{3D}\right)\left(\frac{1}{\lambda}\right)^{1/6}\left(\frac{R}{r}\right)^{0.489}} \qquad \text{for } \alpha = 90\text{-deg} \qquad (7\text{-}22)$$

$$k_p = \frac{k}{1+0.057\left(\frac{pr^3}{3D}\right)\left(\frac{1}{\lambda}\right)^{1/6}\left(\frac{R}{r}\right)^{0.553}} \qquad \text{for } \alpha = 180\text{-deg} \qquad (7\text{-}23)$$

It can be seen from these equations that for elbows having bend angle of 90-deg and smaller, the pressure reduction effect is directly proportional to bend angle.

Following previous practice, equations (7-14) through (7-19) if required can be further simplified:

$$k_p = \frac{k}{1 + A\left(\frac{p}{E}\right)\left(\frac{r}{t}\right)^{19/6}\left(\frac{R}{r}\right)^m}$$

$$k_p = \frac{k}{1 + B\left(\frac{pr^3}{3D}\right)\left(\frac{1}{\lambda}\right)^{1/6}\left(\frac{R}{r}\right)^n}$$

where A, B, m, and n are function of bend angle, α. This simplification will not be processed further.

7.2 Stress-Intensification Factors

The formulae for the stress-intensification factor for unpressurised and pressurised piping elbows under in-plane moment have been developed in Chapters 5 and 6 for closing and opening bending respectively, where it was found that the cross-section deformed into an oval shape with major axis perpendicular to the plane of the bend for the closing case and lying in the plane of the bend for the opening case. For the out-of-plane bending case, ovalisation occurs close to an axis inclined at about 45-deg to the plane of the elbow and is maximum at a section between the junction with the loaded tangent at the mid-section of the bend. Due to this behaviour different flexibility and stress factors will be expected.

Figure 7.20 shows a typical cross-sectional ovalisations of a pipe elbow under out-of-plane bending for a radius ratio equal R/r equal to 3 and thickness to cross-section radius t/r equal to 0.03 (pipe schedule 10s). These are plotted for ovalisation at the

junction with the loaded tangent, at a section where the hoop stress has its maximum value, and at mid-section of the bend. The results are approximately anti-symmetric with respect to the elbow plane of symmetry. It can be seen that the maximum radial displacement (ovalisation) does not occur at the section where the stresses are maximum. It is understood that the cross-sectional ovalisation is due to bending and the maximum bending along the elbow is at the junction of the elbow with the loaded tangent. Recall that the out-of-plane moment is applied about an axis perpendicular to the loaded tangent as shown in Fig.7.1 ($M = M_Y$). In this sense, the moment loading diminishes as we move toward the junction with the fixed tangent. For a 90-deg elbow, the loading at the junction with the fixed tangent is pure torsion and there no 'ovalisation' occurs at this section.

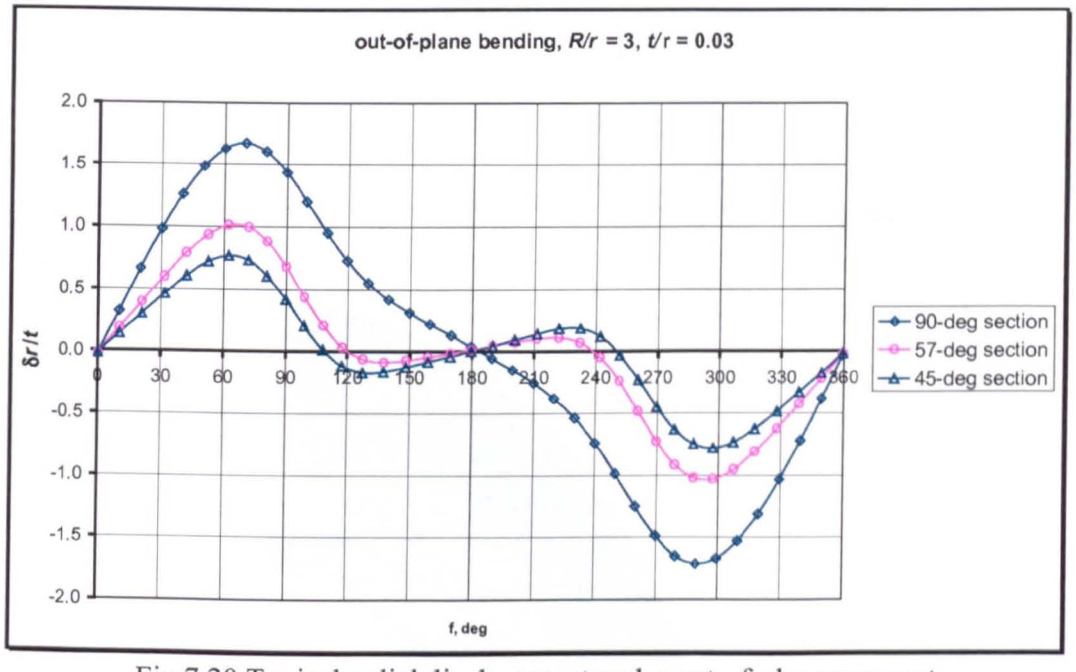

Fig.7.20 Typical radial displacement under out-of-plane moment

Figure 7.21 and 7.22 respectively show typical longitudinal and circumferential stress contour plots plotted for a 90-deg pipe elbow. It can be seen from these figures that the location of the maximum stress in a pipe elbow under an out-of-plane moment occurs not at mid-section of the bend, but between the mid-section and the junction of the elbow with the loaded tangent; it is a compressive stress at the inner surface of the wall.

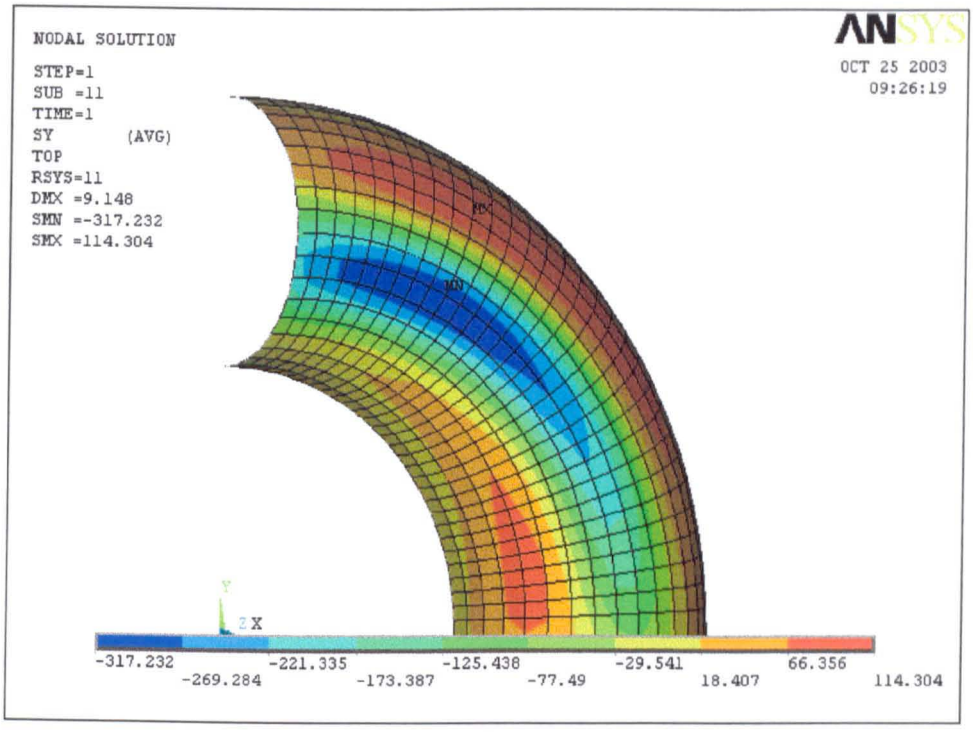

(a)

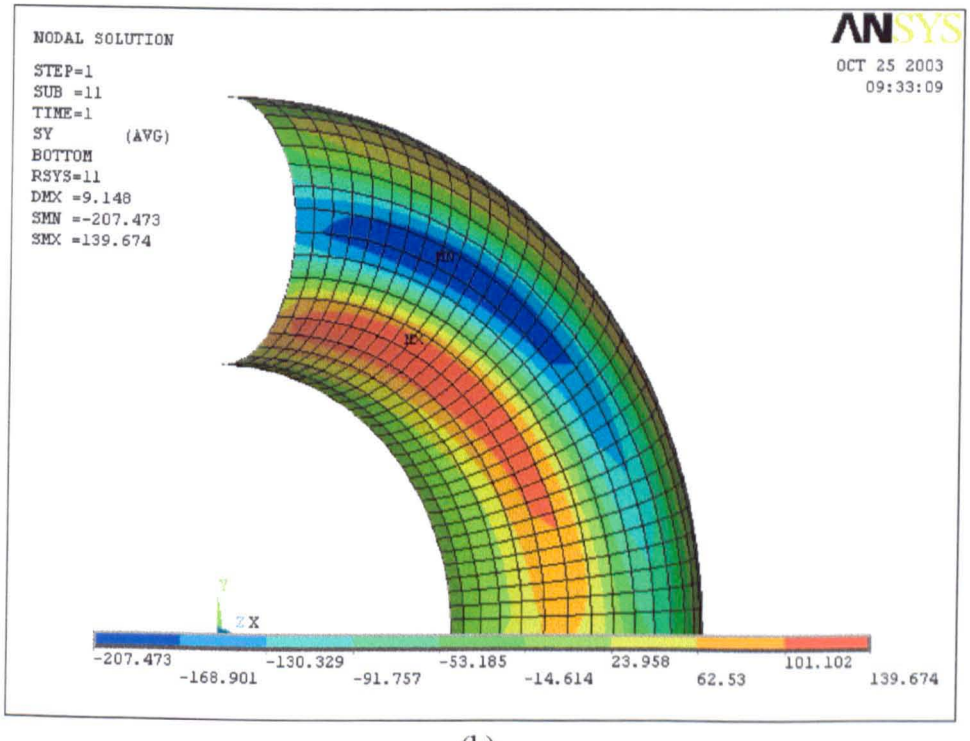

(b)

Fig.7.21 Typical longitudinal stress contour plot under out-of-plane bending (a) outer surface, (b) inner surface

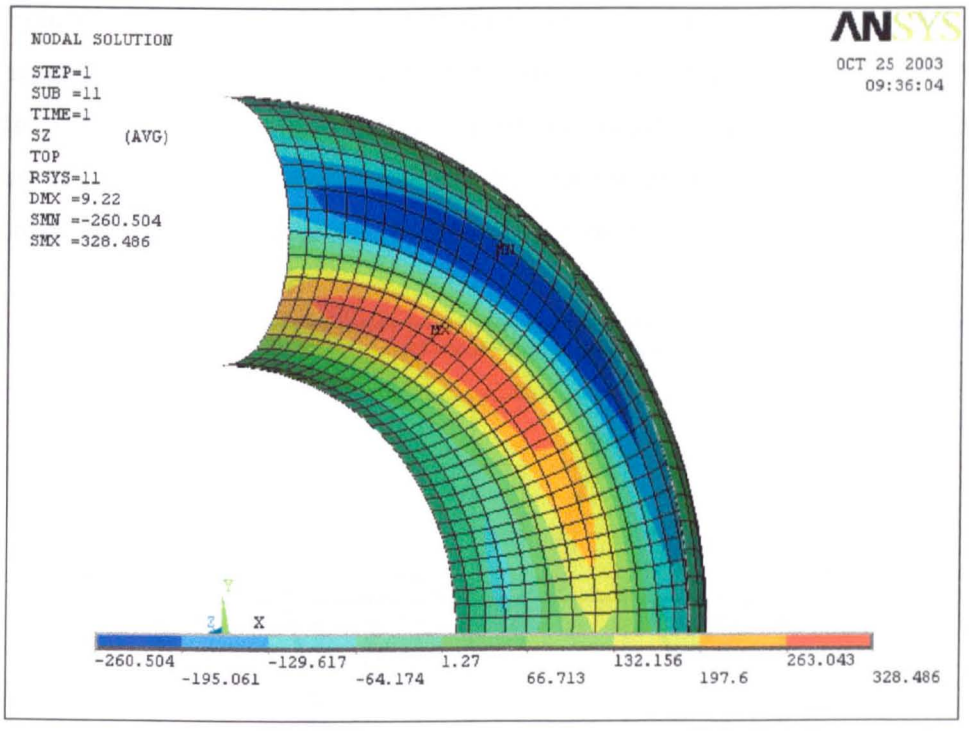

(a)

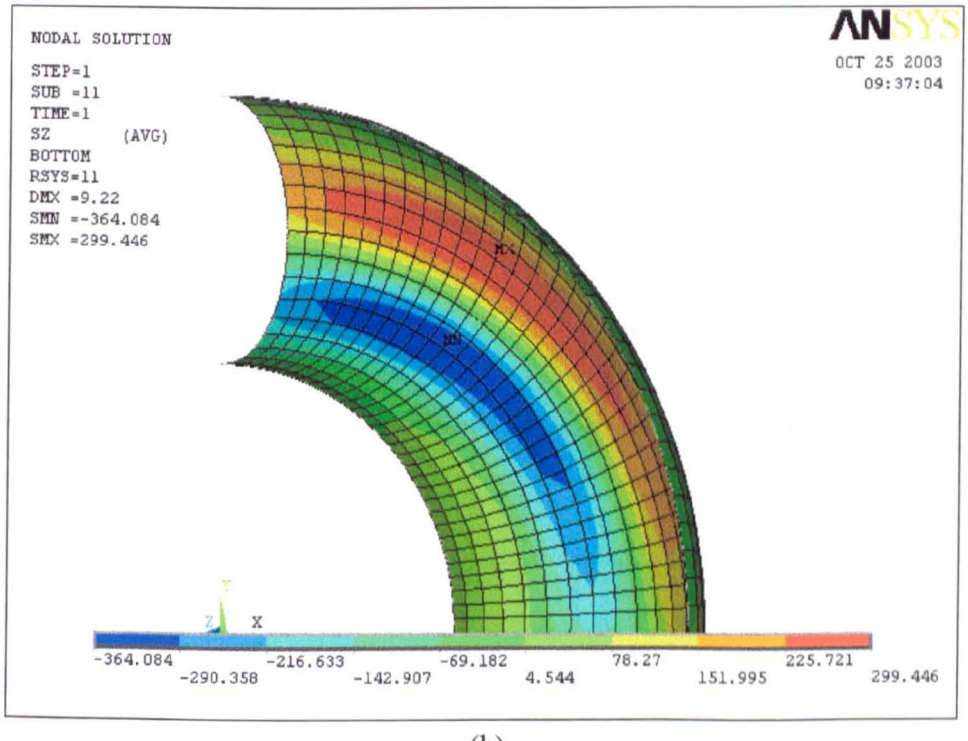

(b)

Fig.7.22 Typical circumferential stress contour plot under out-of-plane bending (a) outer surface, (b) inner surface

Figure 7.23 shows typical longitudinal stress factor at the loaded end (90-deg section), 57-deg section where the hoop stress is maximum, and at the mid-section of the elbow. It can be seen that the maximum longitudinal stress occurs at the outer surface as compressive stresses; the circumferential location of maximum longitudinal stress is at about 10-deg from the crown toward the intrados.

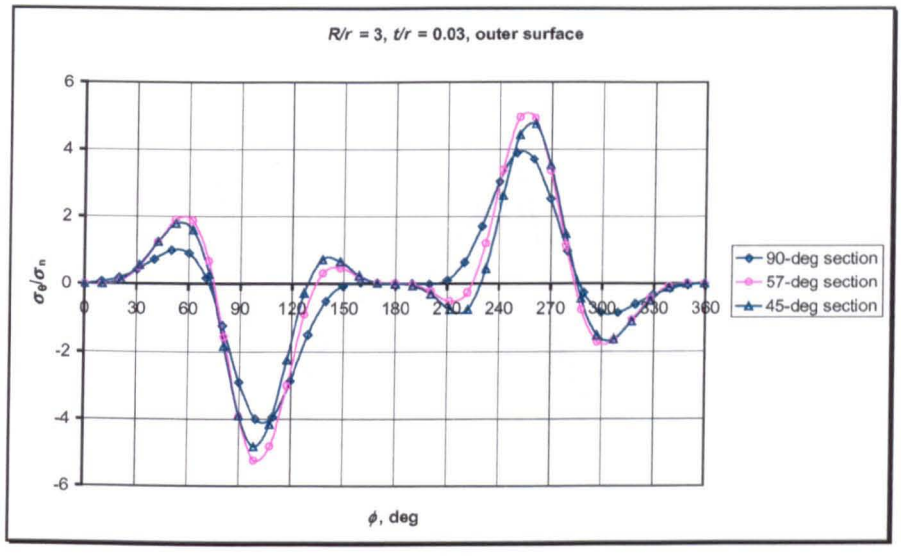

(a)

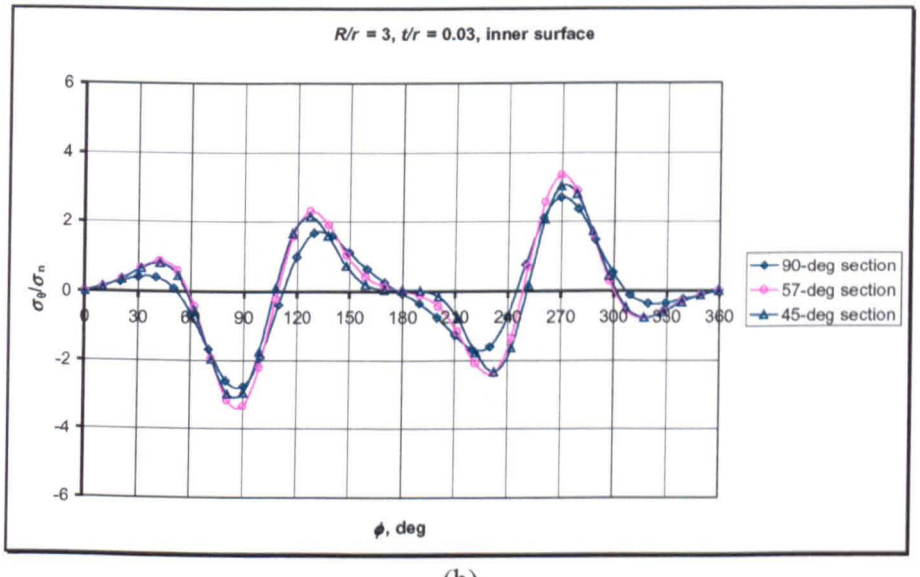

(b)

Fig.7.23 Typical longitudinal stress factor for a 90-deg pipe elbow under out-of-plane bending (a) outer surface, (b) inner surface

Figure 7.24 shows typical circumferential stress factor at the loaded end section, 57-deg section where the stresses are maximum and at mid-section of the bend. It can be seen that the maximum hoop stress occurs at the inner surface as compressive stress; the circumferential location of maximum hoop stress is at about 30-deg from the crown toward the intrados.

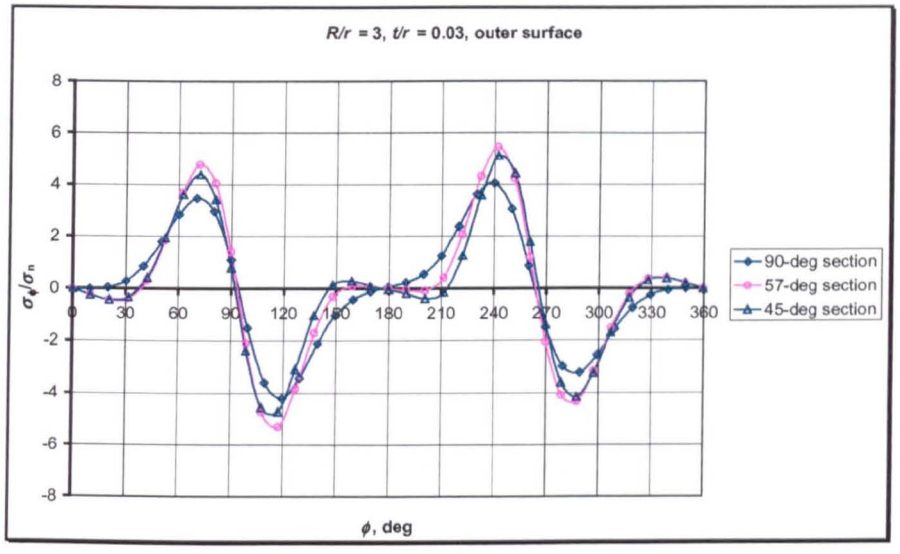

(a)

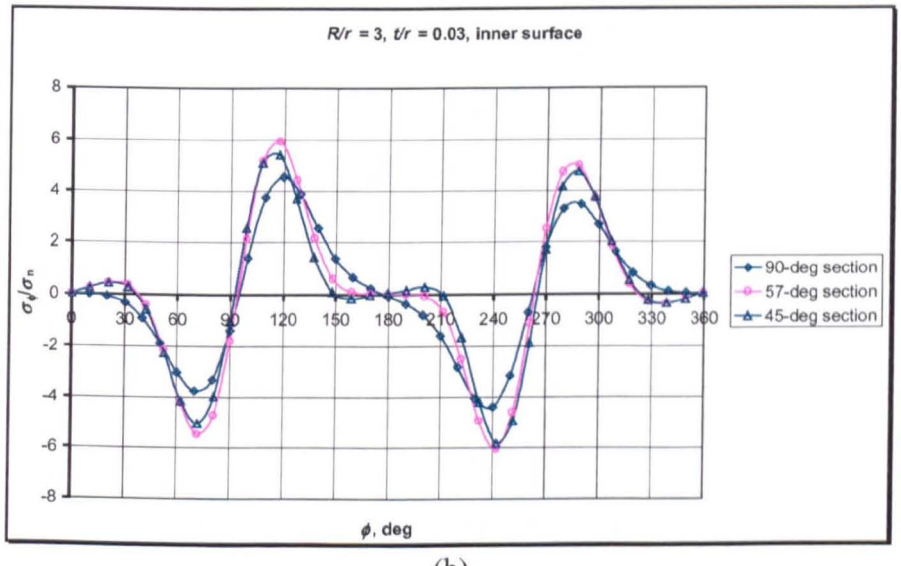

(b)

Fig.7.24 Typical circumferential stress factor for a 90-deg pipe elbow under out-of-plane bending (a) outer surface, (b) inner surface

Overall, it has been found that the maximum stress for elbows having bend angle of 30-deg and greater occurs in the hoop direction as compressive stresses at the inner surface. Its location is not always at the same location for all pipe bends parameters, but depends on bend angle, radius ratio and wall thickness. In what follows, the maximum hoop stress is evaluated regardless of its location longitudinally and circumferentially.

Figure 7.25 shows a typical moment-stress curve for a piping elbow under out-of-plane bending for a 90-deg elbow having radius of 3 and thickness to cross-section radius ratio of 0.026. It can be clearly seen that the relation of applied bending and resulting stress is essentially linear. It will be seen that this is not the case when internal pressure is further applied and the pressure reduction included.

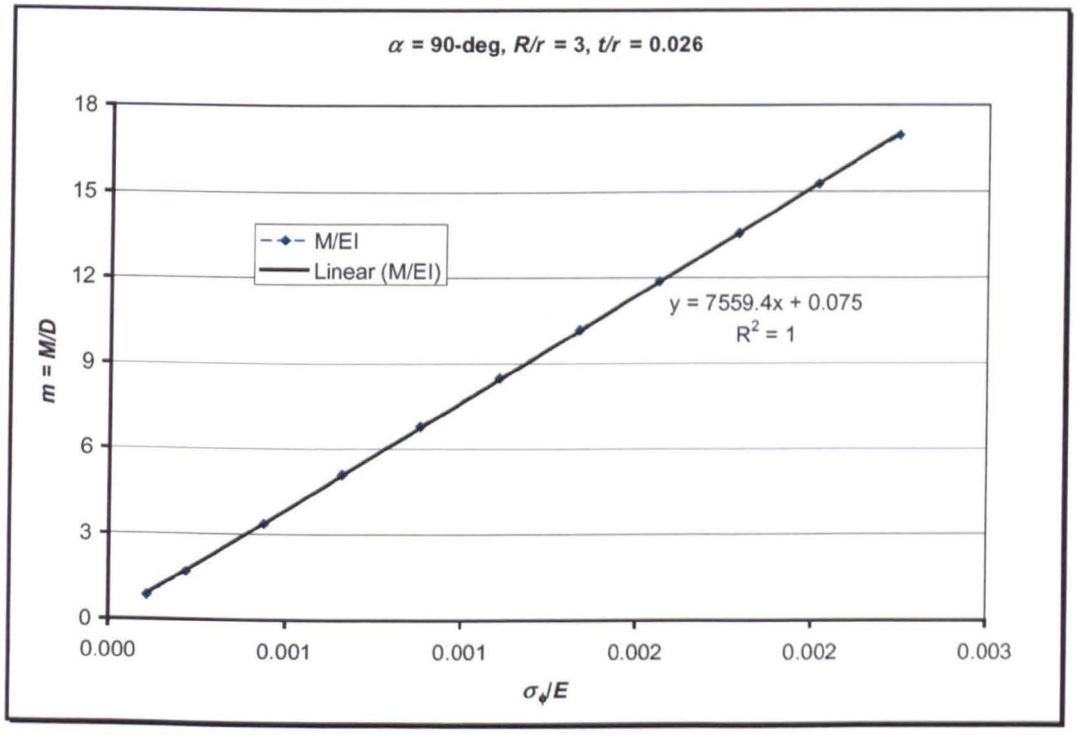

Fig.7.25 Typical moment – stress (hoop) curve under out-plane moment

Figure 7.26 shows the stress-intensification factor for 90-deg piping elbows plotted for various radius ratios. It can be seen that high stress-intensification factor is obtained for low pipe bend parameter. Figure 7.26 also shows that the stress-intensification factor is influenced by radius ratio. Figure 7.26 again shows that the relationship between stress-intensification factor, γ, and pipe bend parameter, λ, is approximately linear in a log-log plot and can be expressed in form of equation (5-58).

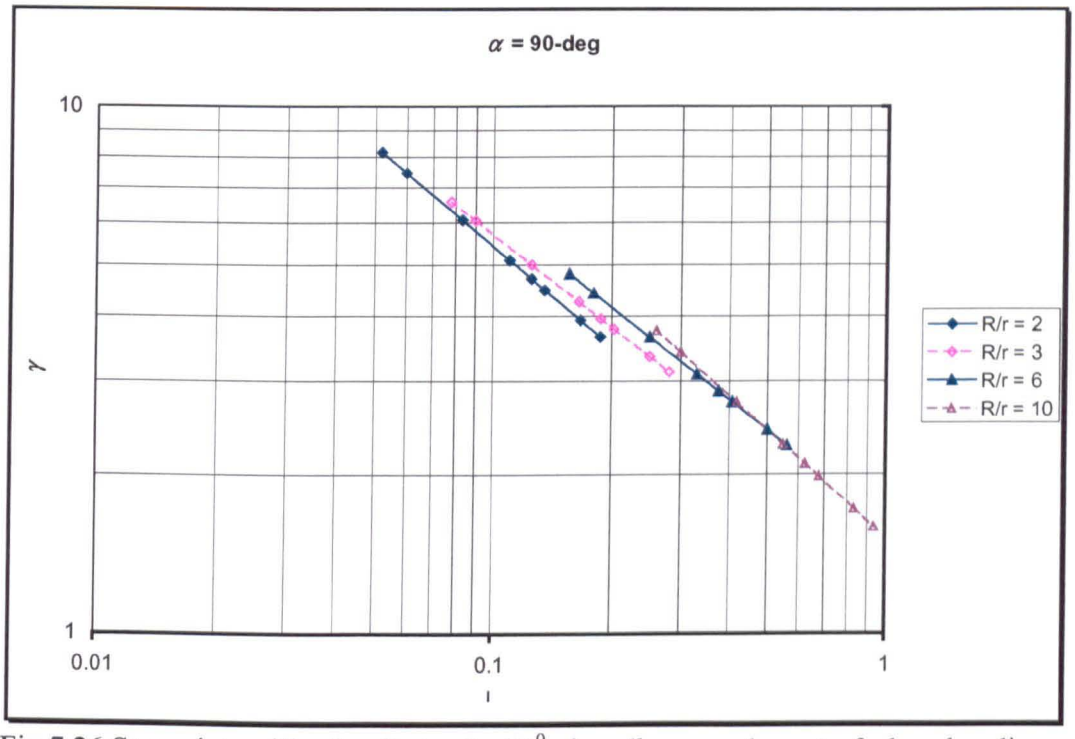

Fig.7.26 Stress-intensification factor for 90^0 pipe elbows under out-of-plane bending

Approximate formula for stress-intensification factor for 90-deg piping elbows under an out-of-plane bending can be derived from Fig.7.26:

$$\gamma = \frac{1.50}{\lambda^{0.58}}; \qquad \text{for} \frac{R}{r} = 2 \qquad (7-24)$$

$$\gamma = \frac{1.60}{\lambda^{0.59}}; \qquad \text{for} \frac{R}{r} = 3 \qquad (7-25)$$

$$\gamma = \frac{1.61}{\lambda^{0.59}}; \qquad \text{for} \frac{R}{r} = 6 \tag{7-26}$$

$$\gamma = \frac{1.52}{\lambda^{0.67}}; \qquad \text{for} \frac{R}{r} = 10 \tag{7-27}$$

Following the procedure of Fujimoto and Soh [92], equations (7-24) through (7-27) can be written in form of equations (5-63):

$$\gamma = \frac{1.89}{\lambda^{2/3}}[0.6726 + 0.0236\ln(\lambda)] \qquad \text{for} \frac{R}{r} = 2 \tag{7-28}$$

$$\gamma = \frac{1.89}{\lambda^{2/3}}[0.7818 + 0.0573\ln(\lambda)] \qquad \text{for} \frac{R}{r} = 3 \tag{7-29}$$

$$\gamma = \frac{1.89}{\lambda^{2/3}}[0.8509 + 0.061\ln(\lambda)] \qquad \text{for} \frac{R}{r} = 6 \tag{7-30}$$

$$\gamma = \frac{1.89}{\lambda^{2/3}}[0.8065 - 0.0029\ln(\lambda)] \qquad \text{for} \frac{R}{r} = 10 \tag{7-31}$$

In the above equations, the term outside the square bracket again is the asymptotic solution of Clark and Reissner [20] and the term inside the square bracket represents the dependence of stress-intensification on pipe bend parameter, λ, as well as on radius ratio, R/r. The change in sign for the second term in the square bracket implies that the value of 'index q' corresponding to equation (5-58) could be either smaller or greater than 2/3.

Figure 7.27 shows plots for stress-intensification factor for 90-deg pipe elbows calculated using the derived formulae in comparison with those obtained directly from finite element solution. It can be seen that the proposed equation fit well the result from finite element solution. In addition, plots for the proposed formulae, i.e., equations (7-28) through (7-31) coincide with those calculated using equation (7-24) through (7-27).

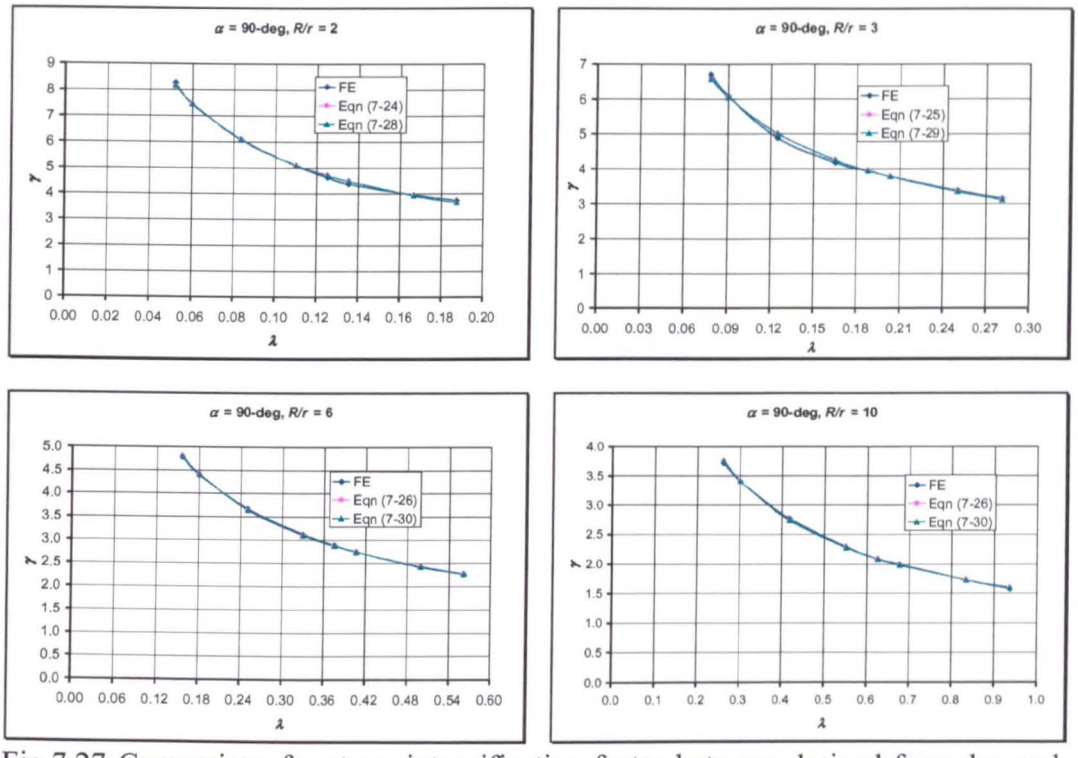

Fig.7.27 Comparison for stress-intensification factor between derived fprmulae and finite element solution

7.2.1 Effect of Bend Angle on Stress-Intensification Factor

As before, the effect of bend angle on stress-intensification factor is again considered here. For this purpose, pipe elbows having bend angles of 30, 45, 60, 90, and 180-deg have been studied. Figure 7.28 through 7.31 show stress-intensification factor for out-of-plane bending. It can be seen again that straight lines are obtained in a log-log graph for all bend angles considered. These Figures show that the stress-intensification factor not only depends on the parameter, λ, but also depends on the radius ratio, R/r: as the bend angle becomes greater, the dependence of stress-intensification on radius ratio becomes smaller. Figure 7.31 shows that the stress-intensification factor for 180-deg pipe elbows less dependent on radius ratio.

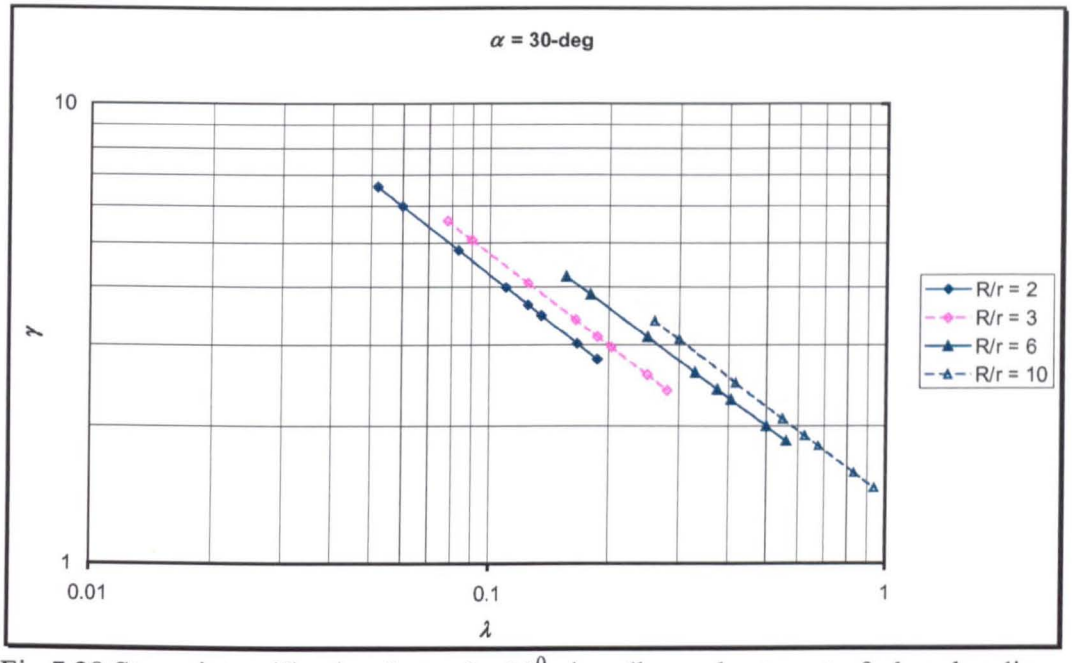

Fig.7.28 Stress-intensification factor for 30^0 pipe elbows due to out-of-plane bending

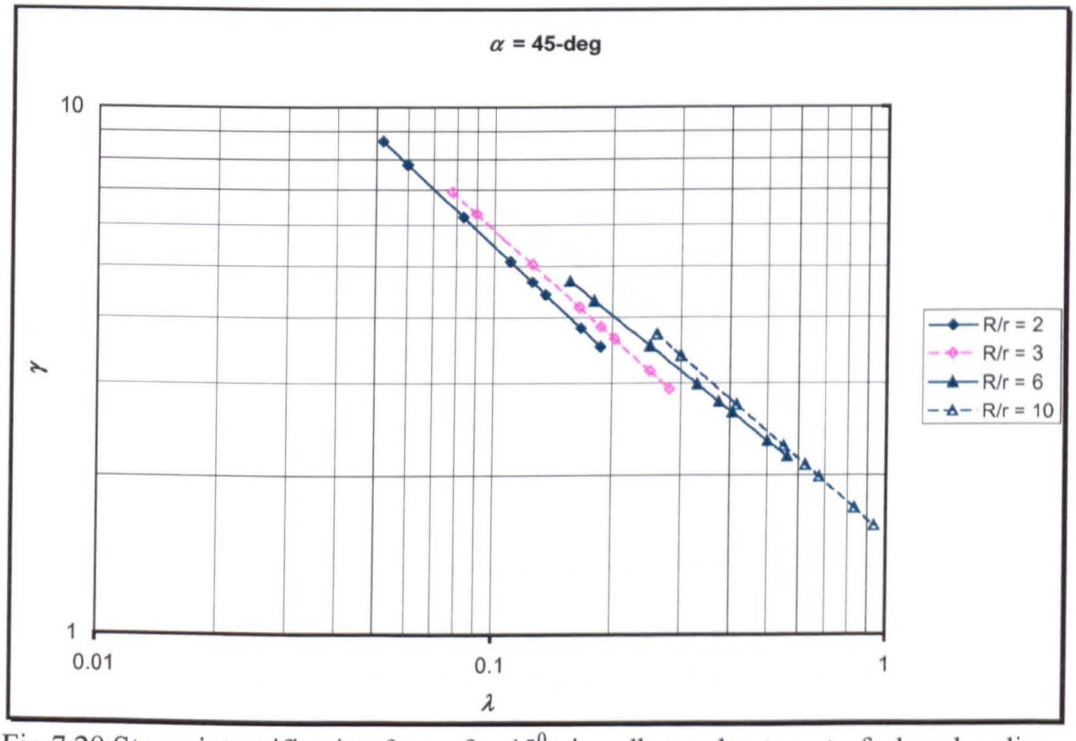

Fig.7.29 Stress-intensification factor for 45^0 pipe elbows due to out-of-plane bending

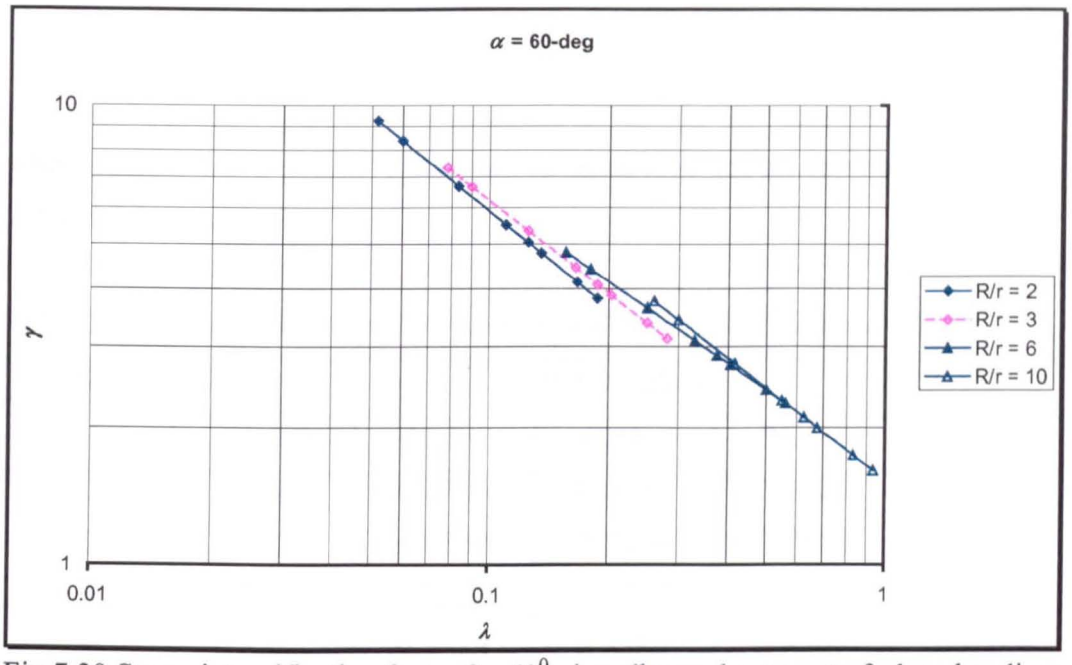

Fig.7.30 Stress-intensification factor for 60^0 pipe elbows due to out-of-plane bending

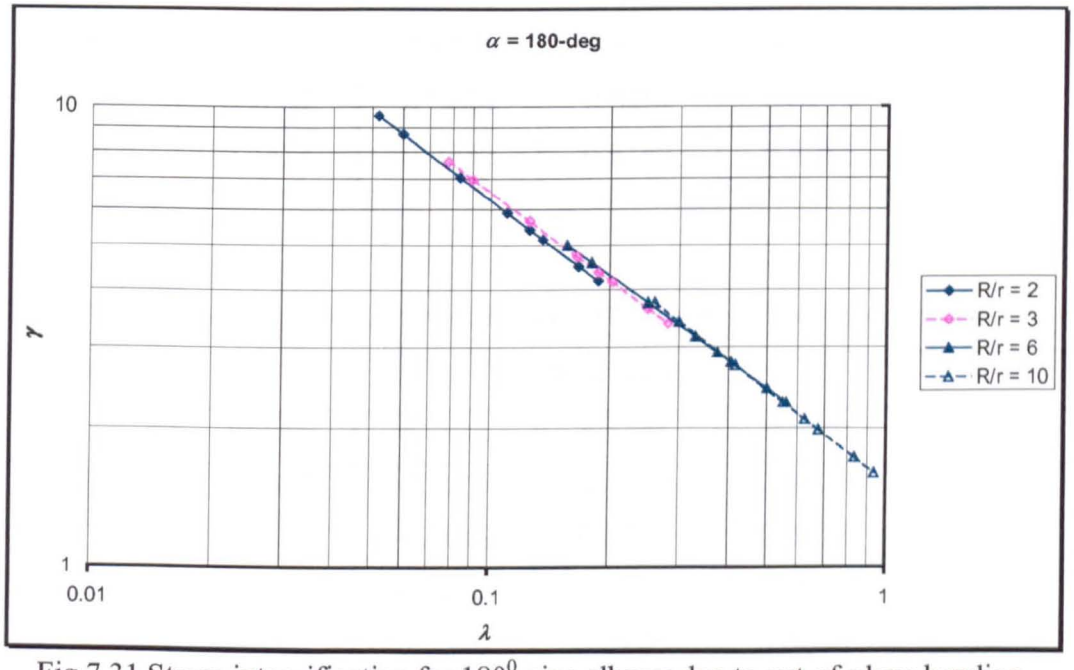

Fig.7.31 Stress-intensification for 180^0 pipe elbows due to out-of-plane bending

Approximate formula can be derived from the above figures and written in the following form:

$$\gamma = \frac{1.89}{\lambda^{2/3}}[a + b\ln(\lambda)] \qquad (7-32)$$

where coefficients '*a*' and '*b*' a functions of radius ratio and are summarised in Table 7.3 and 7.4 respectively:.

Table 7.3 Values of coefficient "*a*" in equation (7-32) for various bend angles

R/r	Bend angle, α				
	30-deg	45-deg	60-deg	90-deg	180-deg
2	0.4749	0.5725	0.6331	0.6726	0.7468
3	0.5473	0.6564	0.7074	0.7818	0.7964
4	0.5965	0.7227	0.7707	0.8229	0.8159
5	0.6343	0.7578	0.8168	0.8297	0.8352
6	0.6793	0.8096	0.8494	0.8509	0.8461
7	0.6913	0.8100	0.8622	0.8276	0.8486
8	0.7140	0.8136	0.8615	0.8248	0.8427
9	0.7339	0.8244	0.8452	0.8219	0.8284
10	0.7424	0.8332	0.8167	0.8065	0.8081

Table 7.4 Values of coefficient "*b*" in equation (7-32) for various bend angles

R/r	Bend angle, α				
	30-deg	45-deg	60-deg	90-deg	180-deg
2	-0.0031	-0.0217	-0.0163	0.0236	0.0143
3	0.0038	-0.0049	0.0001	0.0573	0.0239
4	0.0103	0.0239	0.0335	0.0650	0.0353
5	0.0145	0.0390	0.0491	0.0648	0.0403
6	0.0176	0.0493	0.0620	0.0610	0.0404
7	0.0175	0.0494	0.0551	0.0554	0.0383
8	0.0163	0.0447	0.0455	0.0408	0.0313
9	0.0133	0.0334	0.0275	0.0196	0.0203
10	0.0099	0.0114	0.0041	-0.0029	0.0005

It can be seen from these Tables that values of coefficient '*b*' given in Table 7.4 is small and the second term in the square bracket in of equation (7-32) can be neglected without significant loss in accuracy. Figure 7.32 shows plots of stress-intensification factor for short radius pipe elbows and various bend angles. Similar plot for long-radius pipe elbows is shown in Fig.7.33.

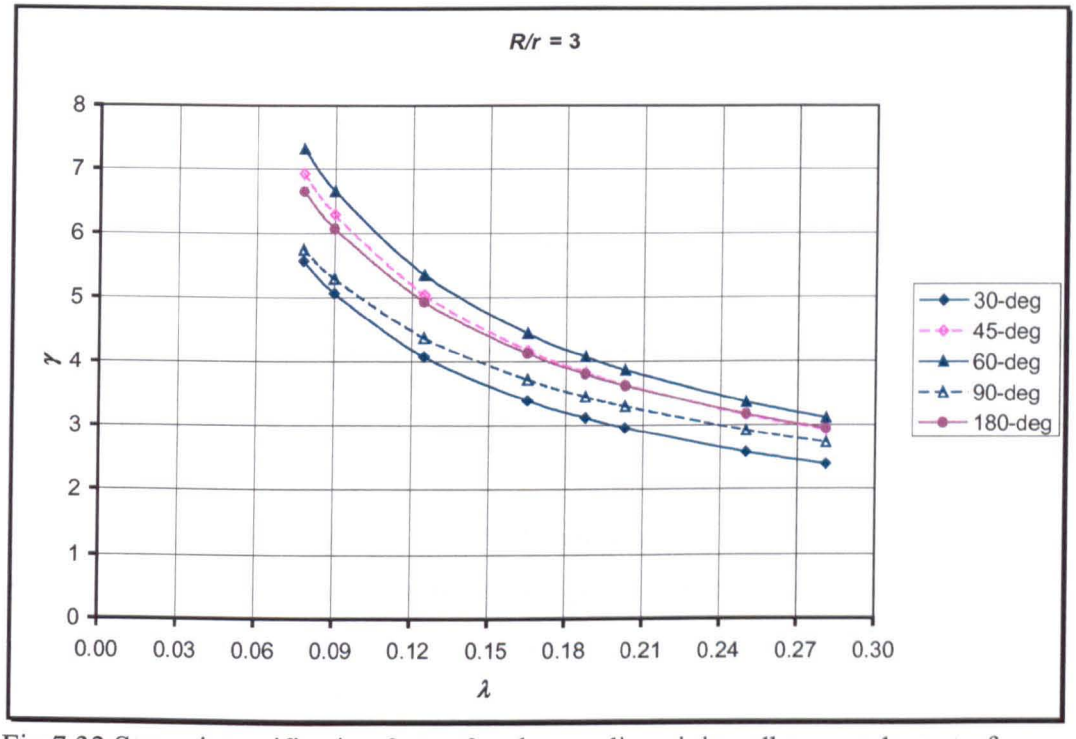

Fig.7.32 Stress-intensification factor for short-radius piping elbows under out-of-plane bending

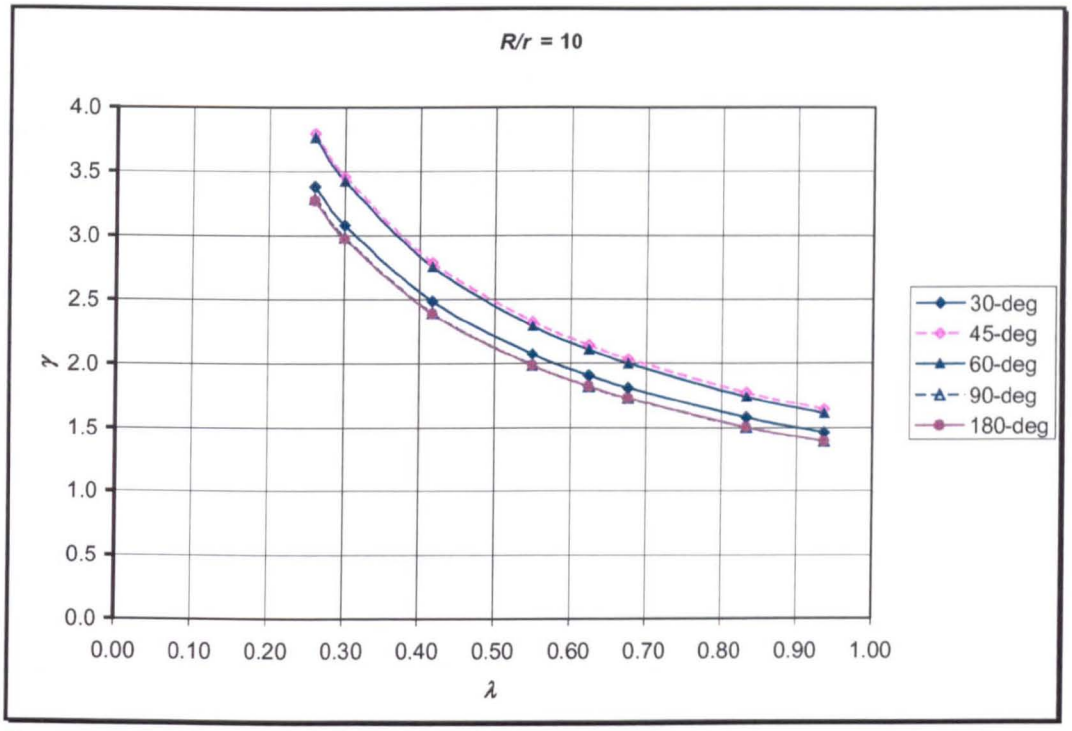

Fig.7.33 Stress-intensification factor for long-radius piping elbows under out-of-plane bending

It can be seen from Fig.7.32 and 7.33 that stress-intensification is not directly proportional to the bend angle for out-of-plane bending case. Table 7.5 below summarises the trend of stress-intensification factor with respect to the stress-intensification for 90-deg pipe elbows:

Table 7.5 Trend of stress-intensification under out-of-plane bending

α	γ/γ_{90}	
	Short-radius elbows	Long-radius elbows
30-deg	< 1	> 1
45-deg	> 1	> 1
60-deg	> 1	> 1
90-deg	$= 1$	$=1$
180-deg	> 1	≈ 1

It can be inferred from Table 7.5 that the stress-intensification for 90-deg pipe elbows is smaller than for other bend angle, except for short-radius and small bend angle. It can be said that stress states in 90-deg elbows is very different from those for other bend angle. A 90-deg elbow under out-of-plane bending produced smallest ovalisation leading to smallest flexibility and stresses, because the loading in one end becomes pure torsion where no ovalisation occurs. It is interesting to note from Table 7.5 that the stress-intensification factor for 90 and 180-deg pipe elbows are about level for long-radius bends.

7.2.2 The Pressure Reduction Effect

Previously, it has been found that the internal pressure always reduces the maximum stresses for all pipe bend parameters. It has long been known that the cross-sectional distortion of a pipe bend under out-of-plane bending is different from that of in-plane bending. It is expected that the pressure reduction effect will also be different.

Figure 7.34 shows typical hoop stress distribution under unpressurized and pressurized condition plotted for a 90-deg elbow having R/r = 3 and t/r = 0.03. Figure 7.34 is plotted at 23-deg section from junction with loaded tangent (refer to Fig.7.2) where maximum stress located at this section.

To obtain stress-intensification factor under bending and internal pressure, the toroidal membrane hoop stress (eqn (2-15)) must be subtracted from the total hoop stress for the pressurized condition in Fig.7.34. Figure 7.35 shows typical pressure reduction on hoop stress factors under an out-of-plane bending after subtracting the toroidal stress (eqn(2-15)) from the stresses for unpressurized condition in Fig.7.34. It can be seen that internal pressure reduce the stress. Figure 7.35 also shows that the system under consideration is bending dominated, characterised by the same location of maximum stresses under unpressurised and pressurised condition. It is however expected that the tendency for this stress distribution to change if internal pressure load increase beyond a certain level [57].

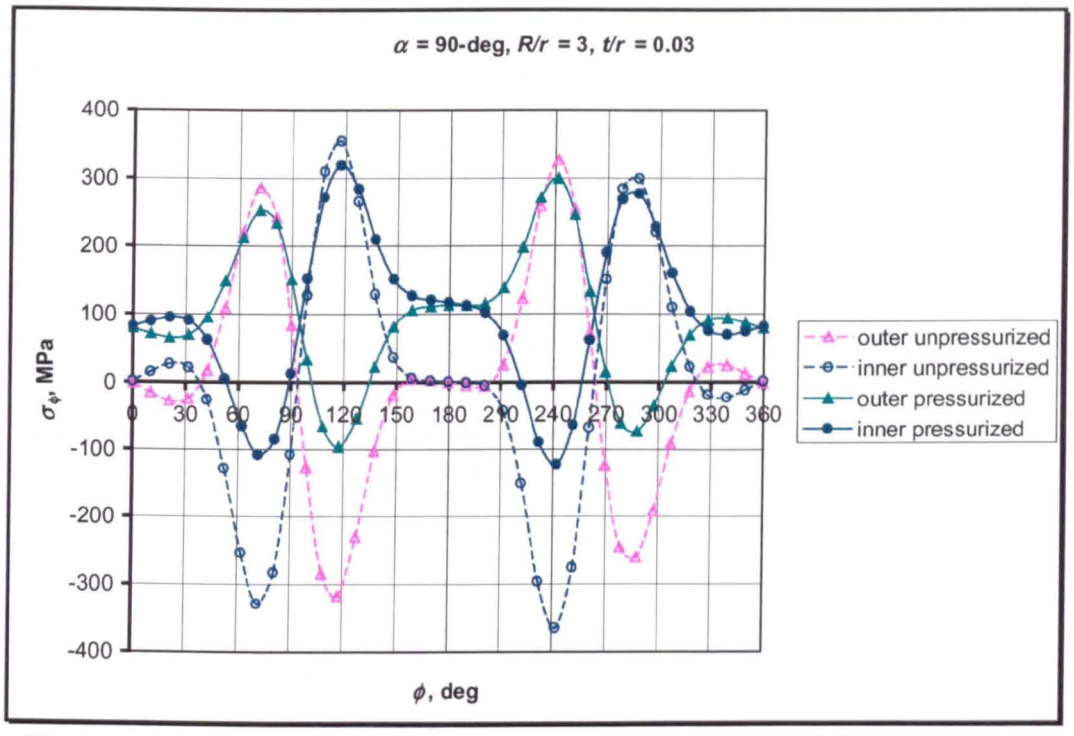

Fig.7.34 Hoop stress distribution under out-of-plane bending and internal pressure

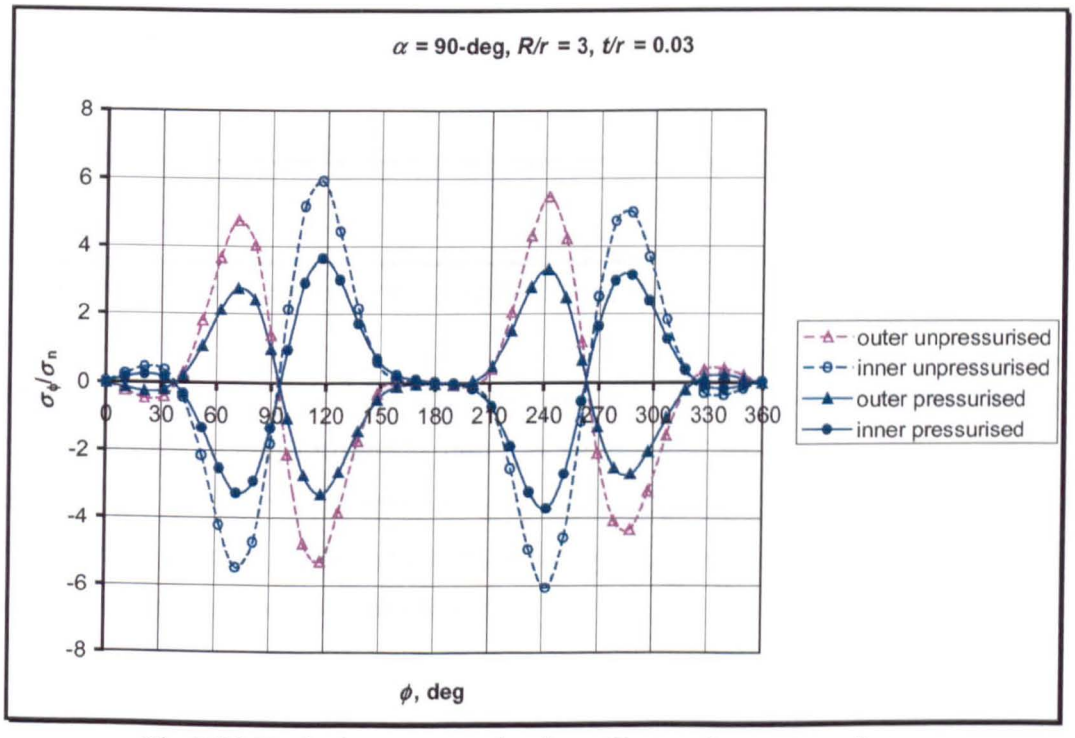

Fig.7.35 Typical pressure reduction effect on hoop stress factor

A typical pressure – stress (hoop) plot is shown in Fig.7.36, plotted for the same elbow geometry as Fig.7.34. The abscissa 0.0 represents the final load step of bending load and the start of the subsequent internal pressure load. It can be seen that the relationship between the internal pressure and hoop stress in non-linear. Figure 7.36 can be directly compared with Fig.7.252, where the relationship between moment and hoop stress is linear. Again, Fig.7.36 shows the 'Haigh effect' as a result of applying internal pressure on ovalized cross-section piping elbow.

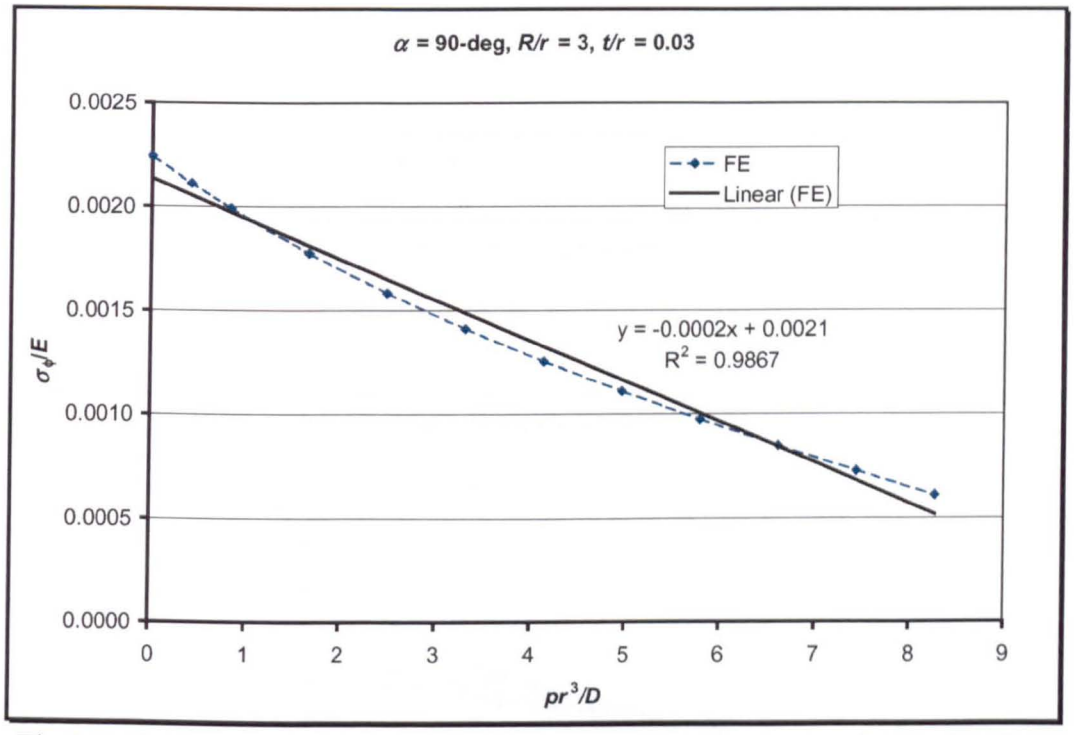

Fig.7.36 Typical pressure – stress plot for a pipe elbow due to out-of-plane bending

Figure 7.37 through 7.40 show stress-intensification factors for 90-deg pipe elbows for various radius ratios loaded by out-of-plane bending and internal pressure. It can be seen that the effect of internal pressure is to reduce the stress-intensification. As before, the reduction is more pronounced in elbows having low pipe bend parameter (small thickness and short-radius bend).

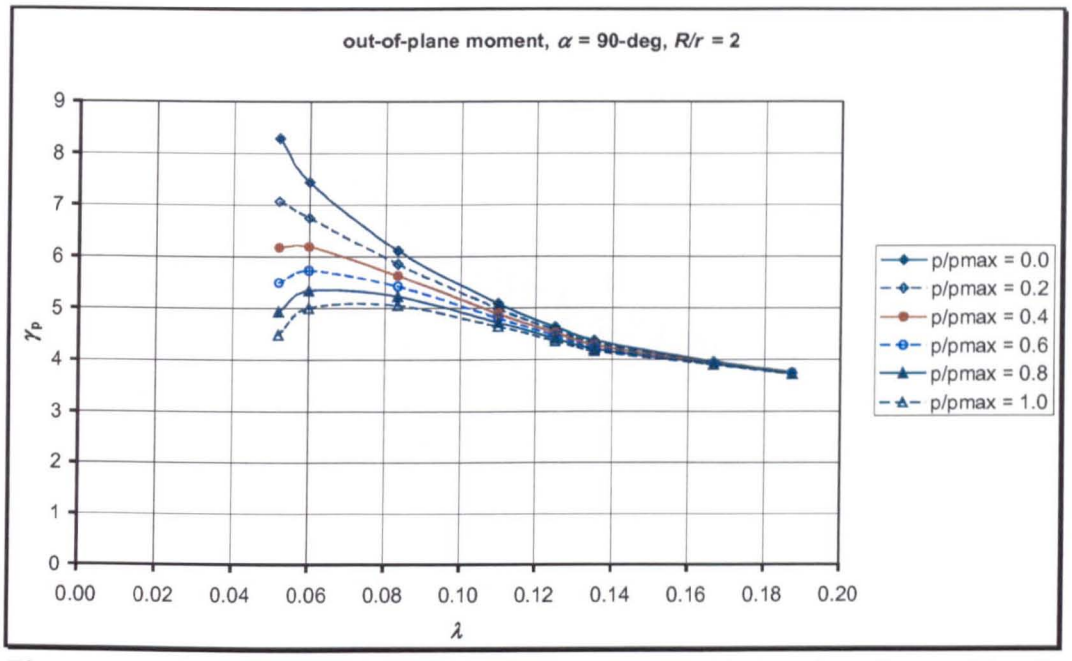

Fig.7.37 Stress-intensification with internal pressure for 90-deg pipe elbows: $R/r = 2$

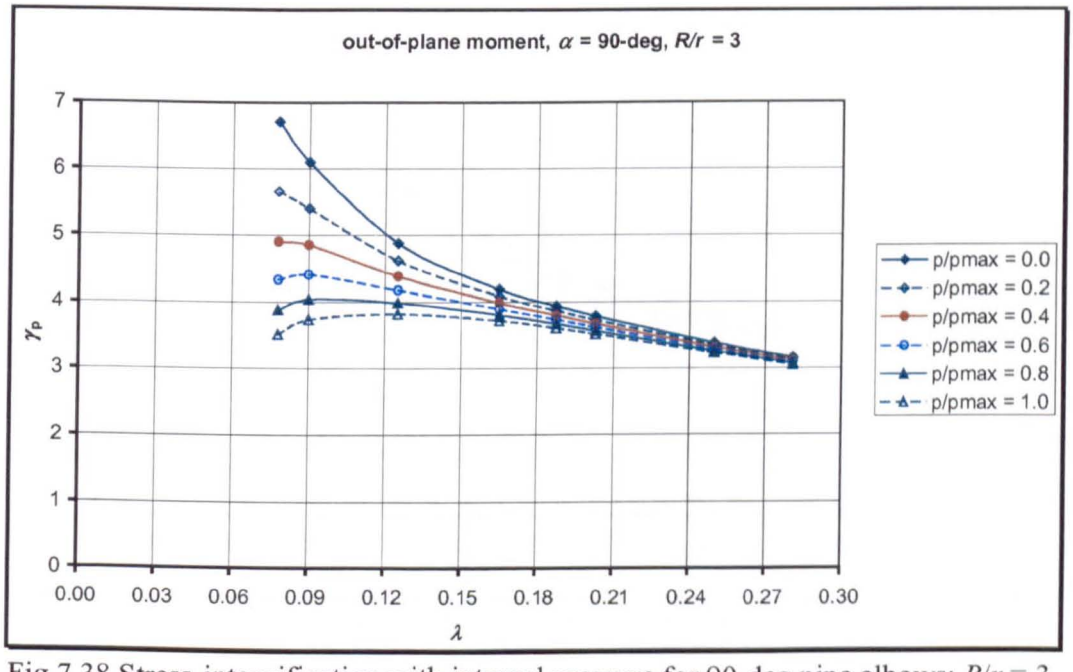

Fig.7.38 Stress-intensification with internal pressure for 90-deg pipe elbows: $R/r = 3$

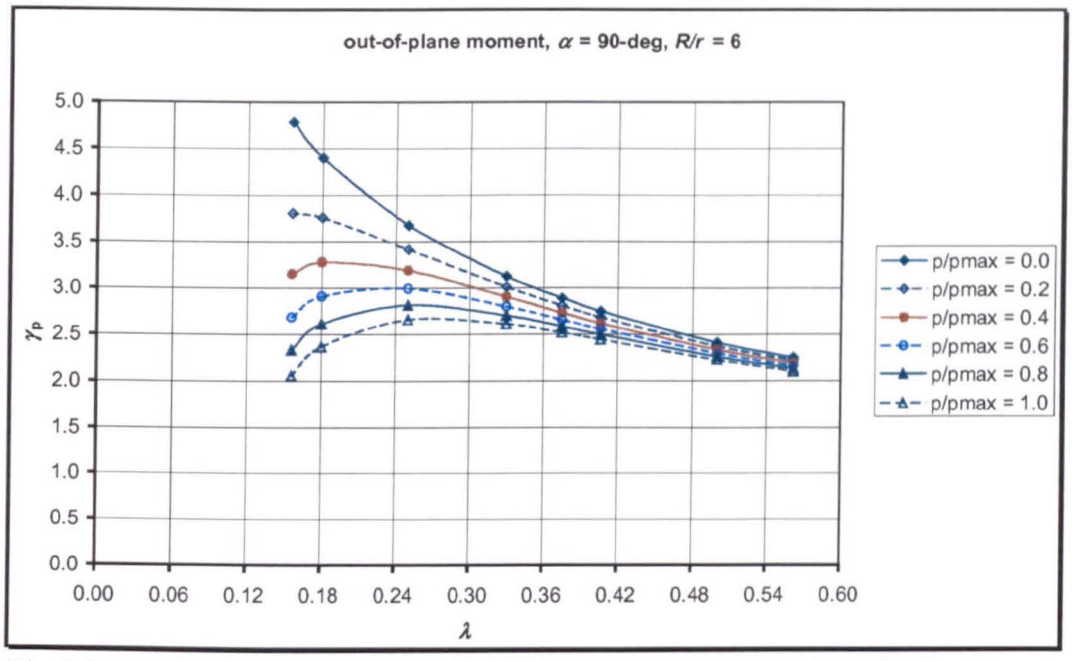

Fig.7.39 Stress-intensification with internal pressure for 90-deg pipe elbows: $R/r = 6$

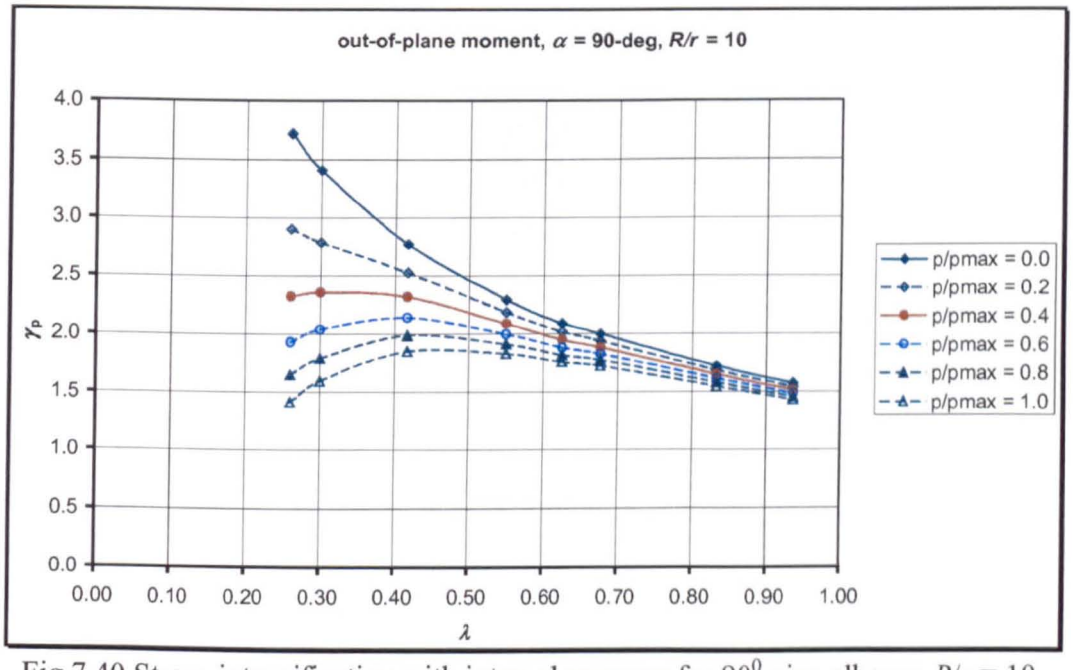

Fig.7.40 Stress-intensification with internal pressure for 90^0 pipe elbows: $R/r = 10$

Pressure reduction for stress-intensification factor corresponding to equation (5-70) for 90-deg piping elbows can be derived from Fig.7.37 through 7.40. It is plotted as log-log graph in Fig.7.41 for constant value of R/r and in Fig.7.42 for constant value of r/t.

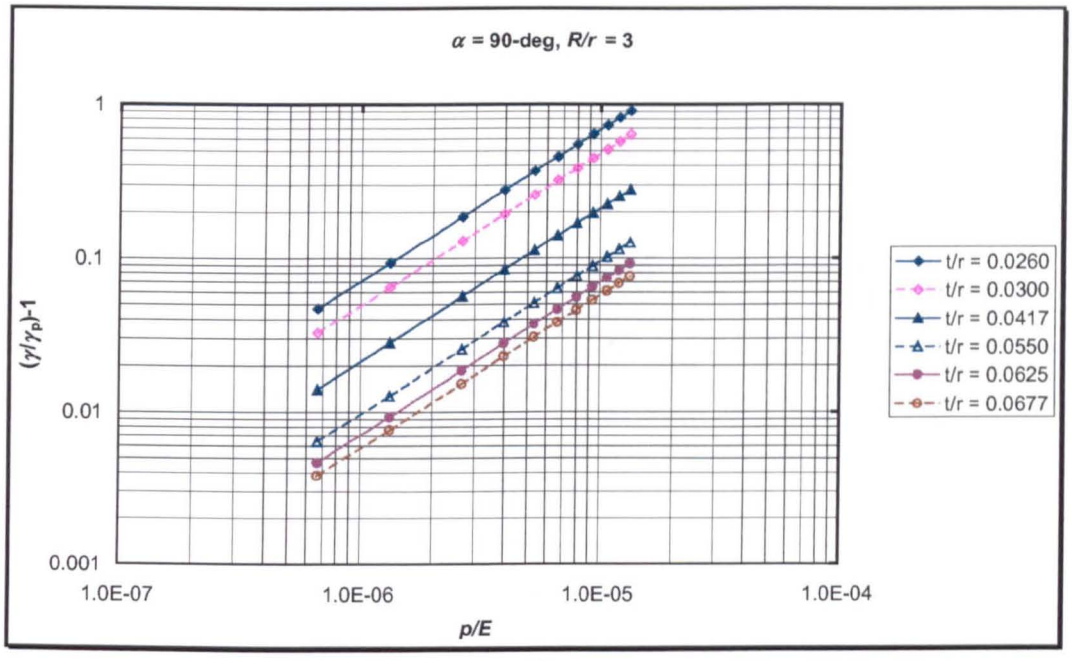

(a)

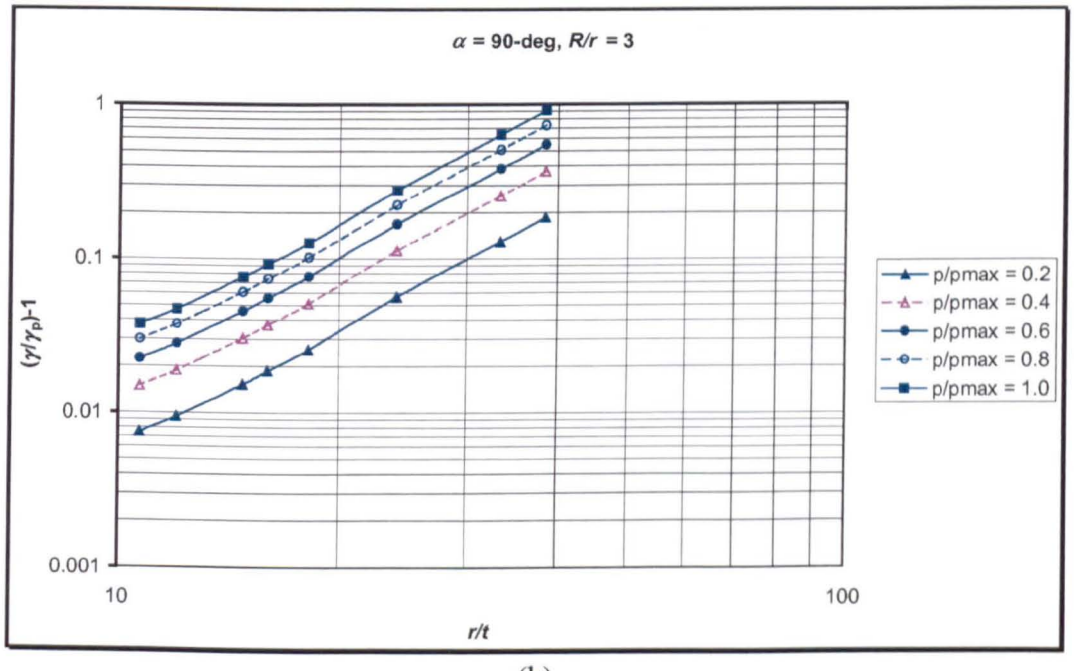

(b)

Fig.7.41 Pressure reduction on stress-intensification for R/r = constant plotted against: (a) p/E, (b) r/t

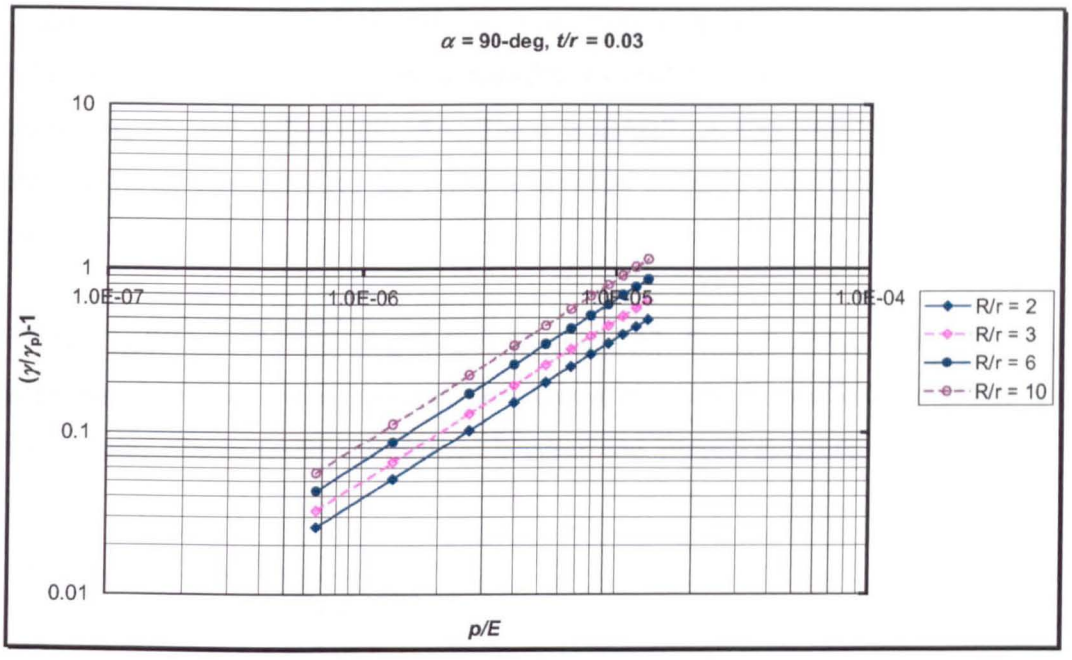

(a)

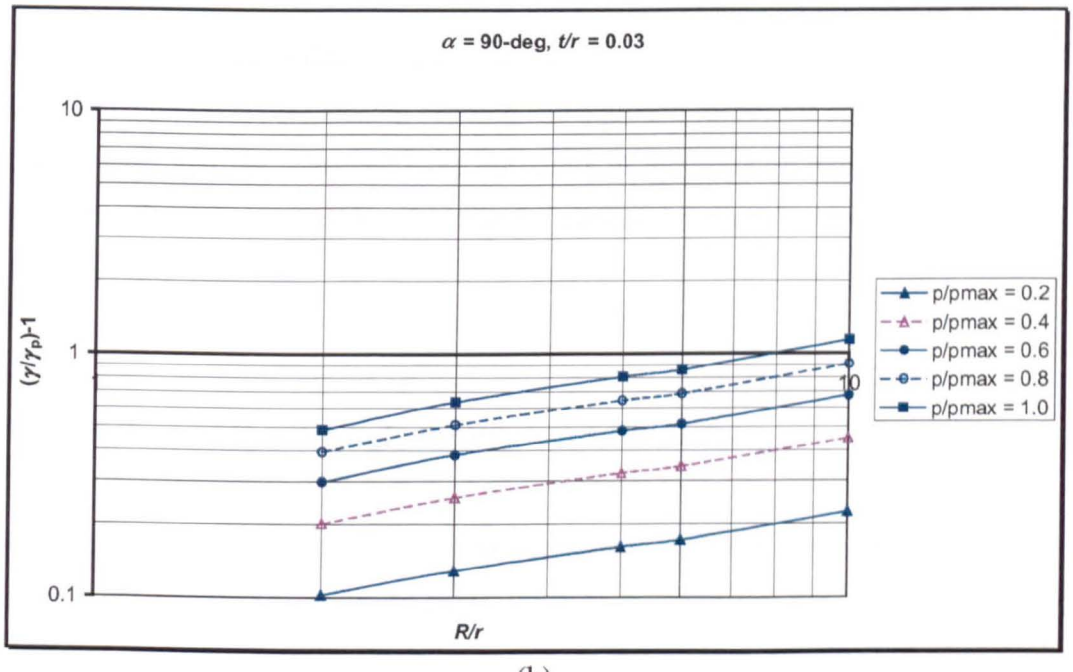

(b)

Fig.7.42 Pressure reduction on stress-intensification for t/r = constant plotted against: (a) p/E, (b) r/t

It can be seen from Fig.7.41 and 7.42 that linear plots are again obtained for the relation between pressure reduction, non-dimensional pressure, p/E, non-dimensional thickness, r/t, and radius ratio, R/r. There is actually a very small deviation from straight lines, especially for the relation between pressure reduction and geometric parameters.

From Fig.7.41 and 7.42 together with Fig.7.37 through 7.40, the following approximate expression is proposed for calculating stress-intensification factors for 90-deg pipe elbows under out-of-plane bending and internal pressure:

$$\gamma_p = \frac{\gamma}{1+9.25\left(\frac{p}{E}\right)\left(\frac{r}{t}\right)^{7/3}\left(\frac{R}{r}\right)^{0.426}} \qquad (7-33)$$

where γ is stress-intensification factor in the absence of internal pressure as given by equation (7-32) and Table 7.3 and 7.4. Equation (7-33) can be directly compared with equation (5-71) for closing bending and equation (6-50) for opening bending. It can be seen that the coefficient and the index of the pressure reduction for out-of-plane bending is comparable with that for closing bending, but markedly different from opening bending.

7.2.3 Effect of Bend Angle on Pressure Reduction

It has been shown in section 7.2.1 that stress-intensification factor of unpressurised elbows is influenced by the bend angle. It has been found also that the stress- state is different markedly for different bend angles. In this section, the effect of bend angle on pressure reduction is studied and approximate formulae again proposed.

By constructing log-log plots for pressure reduction using the data of Fig.A7.6 through A7.10 of Appendix C7, stress-intensification factors for pressurised pipe elbows under out-of-plane bending can be written as:

$$\gamma_p = \frac{\gamma}{1+19\left(\frac{p}{E}\right)\left(\frac{r}{t}\right)^{7/3}\left(\frac{R}{r}\right)^{0.120}} \qquad \text{for } \alpha = 30\text{-deg} \qquad (7\text{-}34)$$

$$\gamma_p = \frac{\gamma}{1+12.3\left(\frac{p}{E}\right)\left(\frac{r}{t}\right)^{7/3}\left(\frac{R}{r}\right)^{0.290}} \qquad \text{for } \alpha = 45\text{-deg} \qquad (7\text{-}35)$$

$$\gamma_p = \frac{\gamma}{1+9.7\left(\frac{p}{E}\right)\left(\frac{r}{t}\right)^{7/3}\left(\frac{R}{r}\right)^{0.394}} \qquad \text{for } \alpha = 60\text{-deg} \qquad (7\text{-}36)$$

$$\gamma_p = \frac{\gamma}{1+8.3\left(\frac{p}{E}\right)\left(\frac{r}{t}\right)^{7/3}\left(\frac{R}{r}\right)^{0.466}} \qquad \text{for } \alpha = 180\text{-deg} \qquad (7\text{-}37)$$

Again noting that:

$$\left(\frac{r}{t}\right)^{7/3} = \left(\frac{r}{t}\right)^{3}\left(\frac{r}{R}\right)^{2/3}\lambda^{2/3}$$

Stress-intensification factors for piping elbows under combined out-of-plane moment and internal pressure can be written in the alternative form:

$$\gamma_p = \frac{\gamma}{1+5.22\left(\frac{pr^3}{3D}\right)\lambda^{2/3}\left(\frac{r}{R}\right)^{0.548}} \qquad \text{for } \alpha = 30\text{-deg} \qquad (7\text{-}38)$$

$$\gamma_p = \frac{\gamma}{1+3.40\left(\frac{pr^3}{3D}\right)\lambda^{2/3}\left(\frac{r}{R}\right)^{0.378}} \qquad \text{for } \alpha = 45\text{-deg} \qquad (7\text{-}39)$$

$$\gamma_p = \frac{\gamma}{1+2.67\left(\frac{pr^3}{3D}\right)\lambda^{2/3}\left(\frac{r}{R}\right)^{0.273}} \qquad \text{for } \alpha = 60\text{-deg} \qquad (7\text{-}40)$$

$$\gamma_p = \frac{\gamma}{1+2.53\left(\frac{pr^3}{3D}\right)\lambda^{2/3}\left(\frac{r}{R}\right)^{0.240}} \qquad \text{for } \alpha = 90\text{-deg} \qquad (7\text{-}41)$$

$$\gamma_p = \frac{\gamma}{1+2.29\left(\frac{pr^3}{3D}\right)\lambda^{2/3}\left(\frac{r}{R}\right)^{0.201}} \qquad \text{for } \alpha = 180\text{-deg} \qquad (7\text{-}42)$$

which can be further simplified as:

$$\gamma_p = \frac{\gamma}{1+A\left(\frac{p}{E}\right)\left(\frac{r}{t}\right)^{7/3}\left(\frac{R}{r}\right)^{m}}$$

$$\gamma_p = \frac{\gamma}{1+B\left(\frac{pr^3}{3D}\right)\lambda^{2/3}\left(\frac{r}{R}\right)^{n}}$$

where A, B, m, and n are functions of bend angle, α. This simplification will not be processed any further.

7.3 Discussion

Throughout this chapter, various approximate formulae for unpressurised and pressurised piping elbows under an out-of-plane bending have been developed. All the formulae have been obtained by curve fitting. While errors are expected in this approximation, it will be seen that the error is essentially small.

Comparisons of results obtained from the present Chapter for out-of-plane bending will be made with respect to the results for in-plane closing and opening bending. Comparison with the current design piping code will also be made. The discussion will be divided into two main sections: unpressurised and pressurised condition.

7.3.1 Unpressurised Conditions

In developing the formulae for unpressurised piping elbows, the effect of radius ratio has been taken into account. The dependency of flexibility and stresses on radius ratio is represented by the term in the square bracket for the following equations:

$$k = \frac{1.65}{\lambda}[a + b\ln(\lambda)] \tag{7-13}$$

$$\gamma = \frac{1.89}{\lambda^{2/3}}[a + b\ln(\lambda)] \tag{7-32}$$

Equations (7-13) and (7-32) have been developed following the form of equation proposed by Fujimoto and Soh [92]. In the above equations, the term outside the square bracket is the asymptotic solution of Clark and Reissner [20] for in-plane bending. The second terms in the square bracket as a constant multiplied by the logarithm of pipe bend parameter, are different from the equation due to Fujimoto and Soh [92], where these terms were expressed in a power law as given in equation (2-63) and (2-64) for flexibility factor. The reason for this difference might be caused by the large deformation effects, the effects which were not considered in Fujimoto and Soh's analysis.

Figure 7.43 shows flexibility factor for short-radius piping elbows under out-of-plane bending (OPB) calculated using equations (7-13) in comparison with the flexibility factor for in-plane opening (IPO) and closing (IPC) bending. It can be seen that the out-of-plane flexibility is much smaller than the in-plane flexibility. It can be noticed that the flexibility factor for unpressurised piping elbows loaded by an out-of-plane bending is not directly proportional to the bend angle. With reference to the way the out-of-plane bending is applied, i.e., about an axis perpendicular to tangent of the bend at the free end of the loaded tangent, the amount of bending (and ovalisation) at the junction of the bends with the fixed tangent is different for every bend angle. For 90-deg elbows, this end is subjected to pure torsion and no ovalisation occurs. For 180-deg elbows, this end is subjected to pure bending. For other bend angles, this

end is subjected to bending and torsion. As can be seen from Fig.7.43, there is an increasing value of flexibility factor for increasing α = 30-deg to α = 45-deg, but it decreases for 90-deg pipe elbows and further decreases for 180-deg pipe elbows compared to the flexibility of 45-deg pipe elbows.

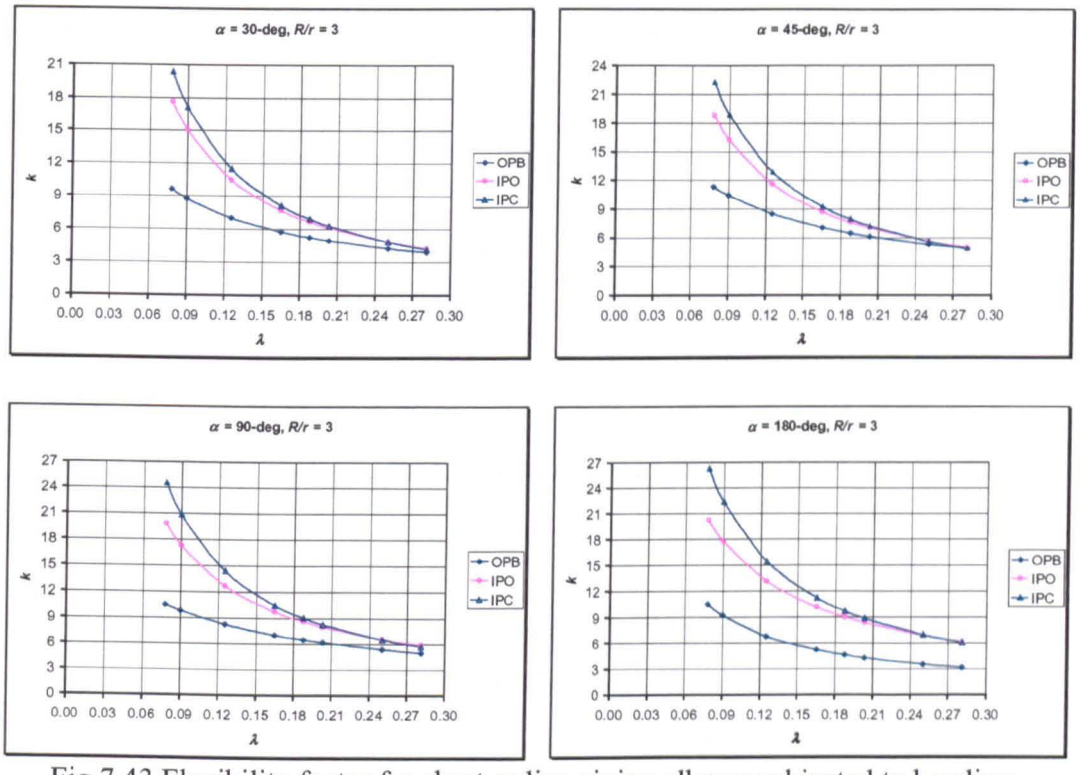

Fig.7.43 Flexibility factor for short-radius piping elbows subjected to bending

Figure 7.44 shows a comparison of flexibility factor for long-radius piping elbows under out-of-plane and in-plane bending. Figure 7.44 shows that for small angle piping elbows ($\alpha \leq$ 90-deg), the flexibility under out-of-plane bending is bigger than under in-plane bending for high pipe bend parameters, but smaller for low pipe bend parameters. For large angle bend (α = 180-deg), the out-of-plane flexibility is smaller than the in-plane flexibility for all pipe bend parameters as expected.

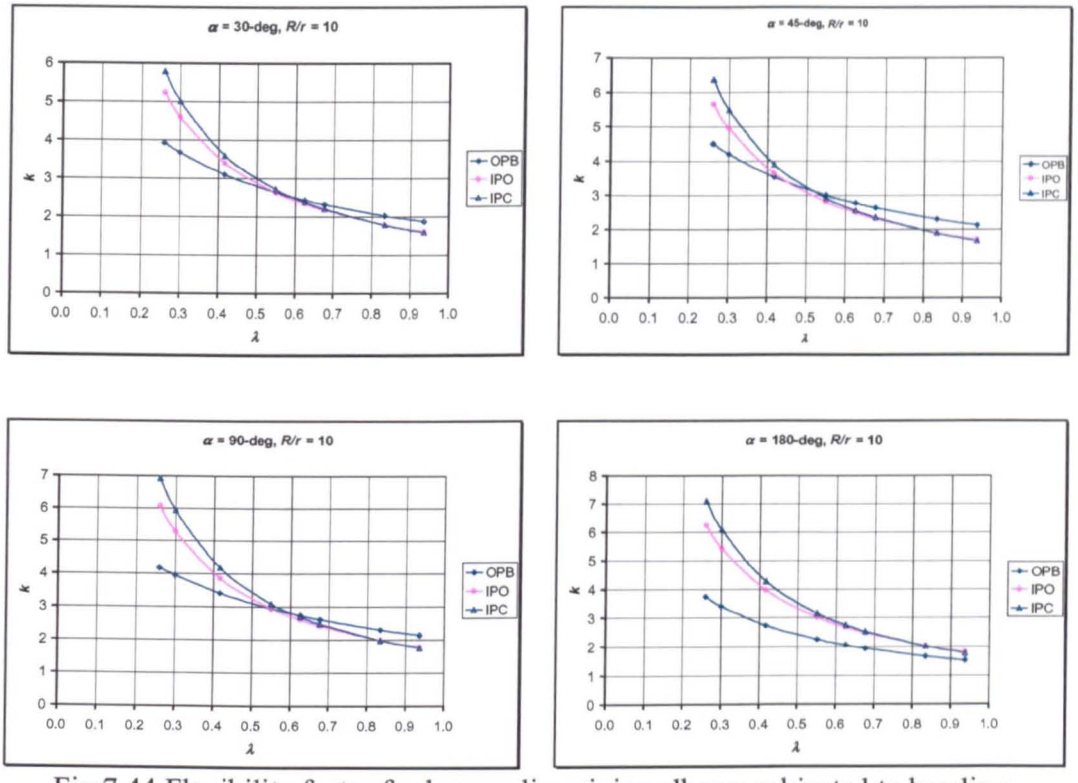

Fig.7.44 Flexibility factor for long-radius piping elbows subjected to bending

Figure 7.45 shows comparison of stress-intensification factor for short-radius piping elbows under in-plane and out-of-plane bending. The result calculated using the formula of Markl [23] as adopted in the ASME Process Piping Code [120] is also included in the graphs. It should be note that the ASME formula for stress-intensification factor produces values smaller than unity if it is applied to pipe bend of large λ, but it is usually as unity. It can be seen from Fig.7.45 that the out-of-plane stress-intensification is smaller than the in-plane stress-intensification as expected. The difference for stress-intensification between out-of-plane and in-plane becomes greater as the bend angle becomes larger. Overall, it can be seen that the formula used in the ASME B31.3 [120] produces a much lower stress-intensification factor compared to the results from the present analysis.

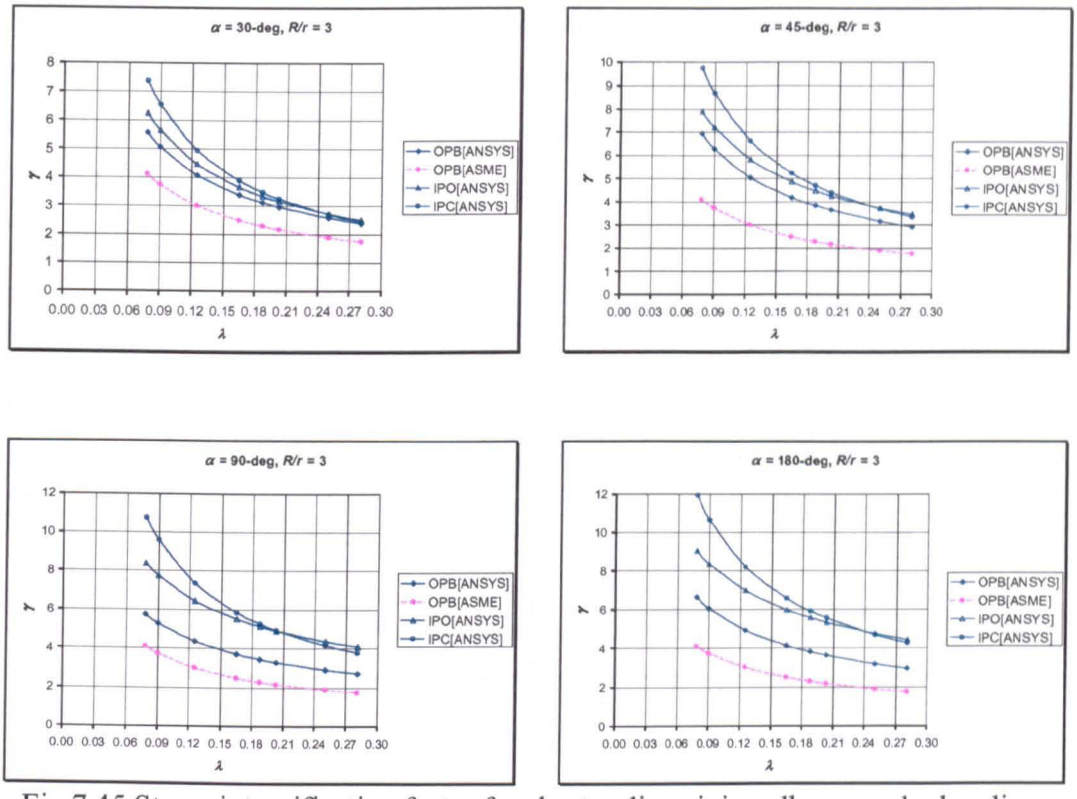

Fig.7.45 Stress-intensification factor for short-radius piping elbows under bending

Figure 7.46 shows comparison of stress-intensification factor for long-radius piping elbows under in-plane and out-of-plane bending. Again the result calculated using the formula in the ASME Process Piping Code [120] is also included in the graphs. It can be seen from Fig.7.46 that the out-of-plane stress-intensification is smaller than the in-plane stress-intensification, because elbows are stiffer under out-of-plane bending than under in-plane bending. The difference for stress-intensification between out-of-plane and in-plane becomes greater as the bend angle becomes larger. In addition, it can be seen that the formula used in the ASME B31.3 [120] produces a much lower stress-intensification factor compared to the results from the present analysis. Table 7.6 below summarises the comparison of the formula in ASME B31.3 and the results from the present analysis. The percentage in Table 7.6 are calculated as:

$$percentage = 1 - \frac{\text{OPB[ASME]}}{\text{OPB[ANSYS]}}$$

where OPB is the out-of-plane stress-intensification factor. For ASME B31.3, the OPB is adopted from the fatigue tests conducted by Markl [27] as given by equation (2-58). For the present analysis, OPB is calculated from equation (7-24) and Table 7.3 and 7.4.

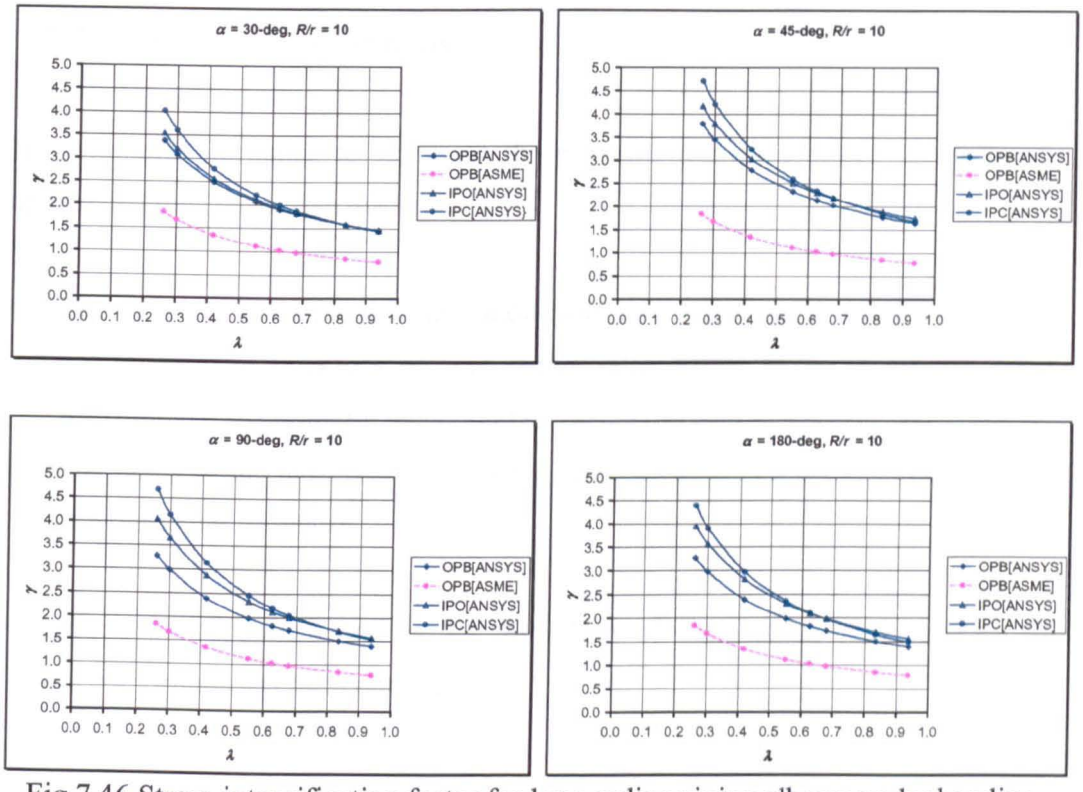

Fig.7.46 Stress-intensification factor for long-radius piping elbows under bending

Table 7.6 Comparison of stress-intensification factor between ASME B31.3 and the present FEA results

α	Short-radius (Fig.7.39)		Long-radius (Fig.7.40)	
	Low λ	High λ	Low λ	High λ
30-deg	26%	27%	45%	46%
45-deg	41%	40%	51%	52%
90-deg	28%	36%	44%	44%
180-deg	38%	41%	44%	44%

It can also be inferred from Table 7.6 that stress-intensification factor for 90-deg piping elbows is lower than 180-deg for short-radius piping elbows, but become level for long-radius piping elbows. Table 7.6 also shows that the stress-intensification factor under out-of-plane bending is not directly proportional to the bend angle.

7.3.2 Pressurised Conditions

In developing formulae to represent the pressure reduction effect, the following approximations have been made:

(1) The relation between pressure reduction and nondimensional pressure *p/E*, nondimensional thickness *r/t* and radius ratio *R/r* is linear in log-log graph. Accordingly, the pressure reduction has been expressed in a power law.
(2) The index of the term *p/E, r/t,* and *R/r* has been based on one-particular data of one-particular geometry.

Based on this approach and taking the effect of bend angle into account, the following formula has been obtained:

Flexibility factor:

$$k_p = \frac{k}{1 + A\left(\frac{p}{E}\right)\left(\frac{r}{t}\right)^{19/6}\left(\frac{R}{r}\right)^{m}} \qquad (7\text{-}43a)$$

$$k_p = \frac{k}{1 + B\left(\frac{pr^3}{3D}\right)\left(\frac{1}{\lambda}\right)^{1/6}\left(\frac{R}{r}\right)^{n}} \qquad (7\text{-}43b)$$

Stress-intensification factor:

$$\gamma_p = \frac{\gamma}{1 + A\left(\frac{p}{E}\right)\left(\frac{r}{t}\right)^{7/3}\left(\frac{R}{r}\right)^m} \qquad (7-44a)$$

$$\gamma_p = \frac{\gamma}{1 + B\left(\frac{pr^3}{3D}\right)\lambda^{2/3}\left(\frac{R}{r}\right)^n} \qquad (7-44b)$$

where A, B, m, and n are functions of bend angle, α, summarised in Table 7.7 and 7.8 for flexibility and stress-intensification factors respectively.

Table 7.7 Values of A, B, m, and n in equation (7-43) for flexibility factor

Bend angle	A	B	m	N
30-deg	0.385	0.106	0.033	0.199
45-deg	0.295	0.080	0.149	0.316
60-deg	0.225	0.062	0.244	0.411
90-deg	0.175	0.048	0.322	0.489
180-deg	0.300	0.057	0.231	0.554

Table 7.8 Values of A, B, m, and n in equation (7-44) for stress-intensification factor

Bend angle	A	B	m	n
30-deg	19.00	5.22	0.119	0.548
45-deg	12.30	3.40	0.289	0.378
60-deg	9.70	2.67	0.394	0.273
90-deg	9.25	2.53	0.426	0.241
180-deg	8.30	2.29	0.466	0.201

As before, the percentage error is defined as:

$$Err = \left|1 - \frac{fd}{fe}\right| x100\%$$

where *fd* represents either flexibility or stress-intensification factor obtained from the derived formula and *fe* is the data directly taken from finite element results.Using this definition, the maximum error in percent is given in table 7.9 and 7.10:

Table 7.9 Maximum error for flexibility, %

α	$R/r = 2$	$R/r = 3$	$R/r = 6$	$R/r = 10$
30-deg	8.5	8.5	7.7	6.3
45-deg	7.3	6.7	6.7	7.3
60-deg	7.0	6.2	6.8	6.5
90-deg	6.3	6.8	6.8	6.4
180-deg	9.1	7.7	8.9	7.1

Table 7.10 Maximum error for stress-intensification, %

α	$R/r = 2$	$R/r = 3$	$R/r = 6$	$R/r = 10$
30-deg	8.5	8.7	5.8	4.7
45-deg	4.1	4.5	4.8	4.3
60-deg	4.9	3.3	3.9	4.3
90-deg	5.7	5.7	4.7	4.5
180-deg	4.4	3.9	3.6	4.1

It can be seen from Table 7.9 that the maximum error for the approximate flexibility factor is less than 10%. It should be noted that the flexibility factor has been derived based on the concept of end rotation and end rotation has been derived from the displacement of crown nodes at the elbow-straight tangent junction. Based on this concept, it was assumed that the plane cross-section remains plane after bending and

there no warping occurs. However, the error in the approximate equation is acceptable from the practical point of view being less than 10%.

In the case of the stress-intensification factor, the error introduced compared to the direct finite element result is not significant from a practical point of view, except perhaps for elbows of small bend angle (30-deg and below) and short radius.

The are not many theoretical results concerning the pressure reduction effect on flexibility and stress-intensification factors. In the ASME B31.3 Process Piping code [120], the pressure reduction proposed by Rodabaugh and George [30] has been applied equally to pipe bends subjected to any direction of moment, and the flexibility and stress-intensification factors for unpressurised out-of-plane bending have been taken from the asymptotic solution of Clark and Reissner [20] for in-plane bending and the fatigue tests of Markl [20] for out-of-plane bending.

Figure 7.47 shows a comparison of out-of-plane flexibility factor for short-radius ($R/r = 3$), 90-deg pipe elbows obtained from the present analysis and the Rodabaugh and George [30] solution as adopted in the ASME B31.3 Process Piping code. The pressure reduction for in-plane flexibility factor is also shown in Fig.7.47. Recall the formula for the out-of-plane flexibility factor of 90-deg piping elbows:

$$\left.\begin{aligned} k_p &= \frac{k}{1+0.175\left(\frac{p}{E}\right)\left(\frac{r}{t}\right)^{19/6}\left(\frac{R}{r}\right)^{0.322}} \\ k &= \frac{1.65}{\lambda}[1.193+0.2727\ln(\lambda)] \end{aligned}\right\} \quad \text{present analysis}$$

$$\left.\begin{aligned} k_p &= \frac{k}{1+6\left(\frac{p}{E}\right)\left(\frac{r}{t}\right)^{7/3}\left(\frac{R}{r}\right)^{1/3}} \\ k &= \frac{1.65}{\lambda} \end{aligned}\right\} \quad \text{ASME B31.3 [120]}$$

where k is flexibility factors in the absence of internal pressure.

It can be seen from the above equations that the index of (r/t) is much bigger in the present analysis, but the index of (R/r) is more or less the same in magnitude. This is followed by the marked difference in coefficient (0.175 rather than 6) – much lower in the present analysis. It can be seen from Fig.7.47 that the pressure reduction effect is more pronounced for low pipe bend parameter (thin-walled elbows). Figure 7.48 extracted from Fig.7.47 shows that the magnitude of pressure reduction represented by equation (5-45) is smaller for out-of-plane bending and bigger for closing bending, while it level for opening bending and the ASME code.

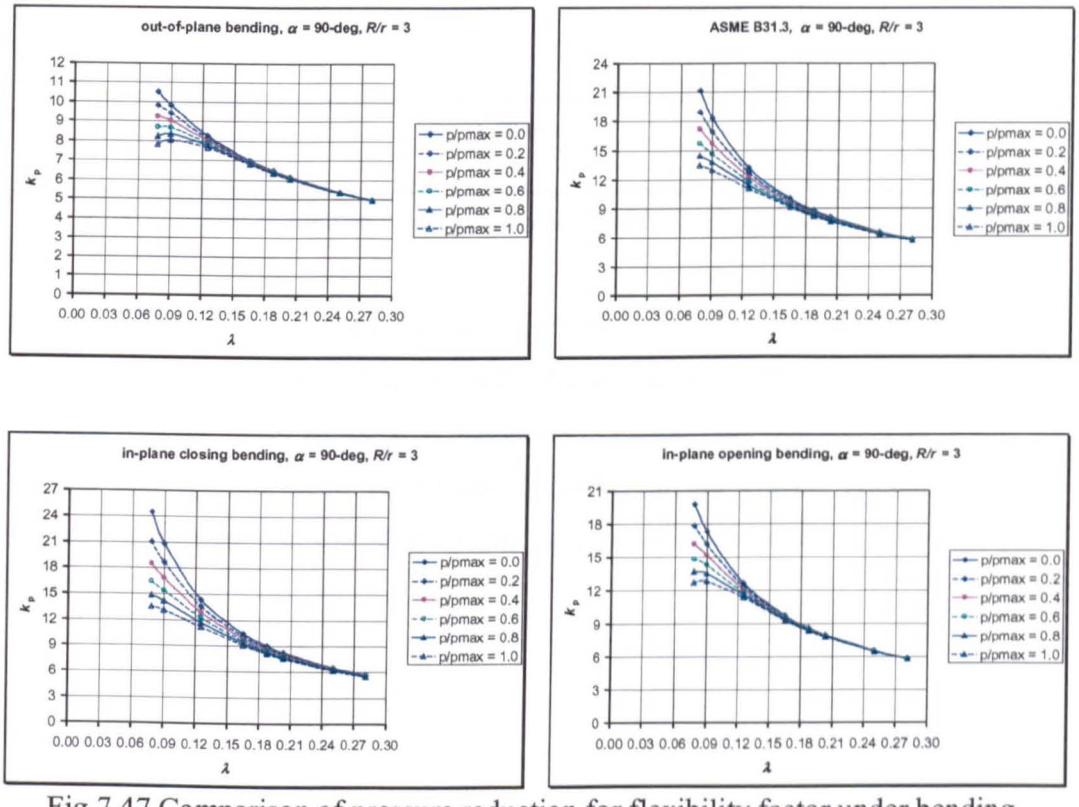

Fig.7.47 Comparison of pressure reduction for flexibility factor under bending

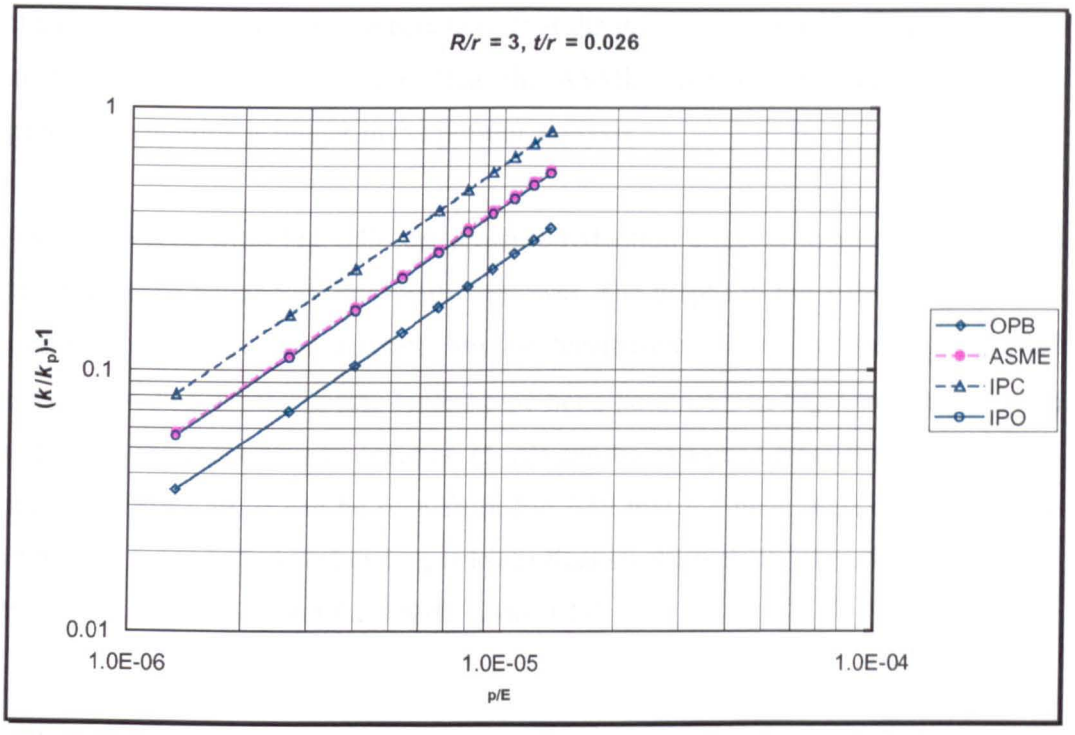

Fig.7.48 Pressure reduction on flexibility for a short-radius thin-walled pipe elbow

Figure 7.49 shows a comparison of stress-intensification factors of 90-deg pipe elbows under out-of-plane bending and internal pressure obtained from the present analysis and the result of the Rodabaugh and George [30] analysis. The results for closing and opening bending are also included in the graphs. Again, recall the formula for stress-intensification factors of pipe elbow loaded by an out-of-plane bending:

$$\left.\begin{aligned} \gamma_p &= \frac{\gamma}{1+9.25\left(\frac{p}{E}\right)\left(\frac{r}{t}\right)^{7/3}\left(\frac{R}{r}\right)^{0.426}} \\ \gamma &= \frac{1.89}{\lambda^{2/3}}\left[0.7818+0.0573\ln(\lambda)\right] \end{aligned}\right\} \quad \text{present analysis}$$

$$\left.\begin{aligned} \gamma_p &= \frac{\gamma}{1+3.25\left(\frac{p}{E}\right)\left(\frac{r}{t}\right)^{5/2}\left(\frac{R}{r}\right)^{2/3}} \\ \gamma &= \frac{0.75}{\lambda^{2/3}} \end{aligned}\right\} \quad \text{ASME B31.3[120]}$$

It can be seen from the above equations that the index of r/t and R/r from the present analysis is considerably smaller than the ASME code, but the coefficient of the pressure reduction is bigger in the present analysis.

As can be seen from Fig.7.49, the pressure reduction effect is more pronounced for low pipe bend parameter (thin-walled elbows). The graphs in Fig.7.49 are not easy to compare since they have different stress-intensification factor for the unpressurised conditions. For $\lambda = 0.078$ (the lowest pipe bend parameter in Fig.7.49), the pressure reduction corresponding to equation (5-70) can be extracted from Fig.7.49 and it is shown in Fig.7.50. It can be seen from Fig.7.50 that the magnitude of the pressure reduction for out-of-plane bending is lower than in-plane closing bending, but greater than opening bending and the ASME code [120].

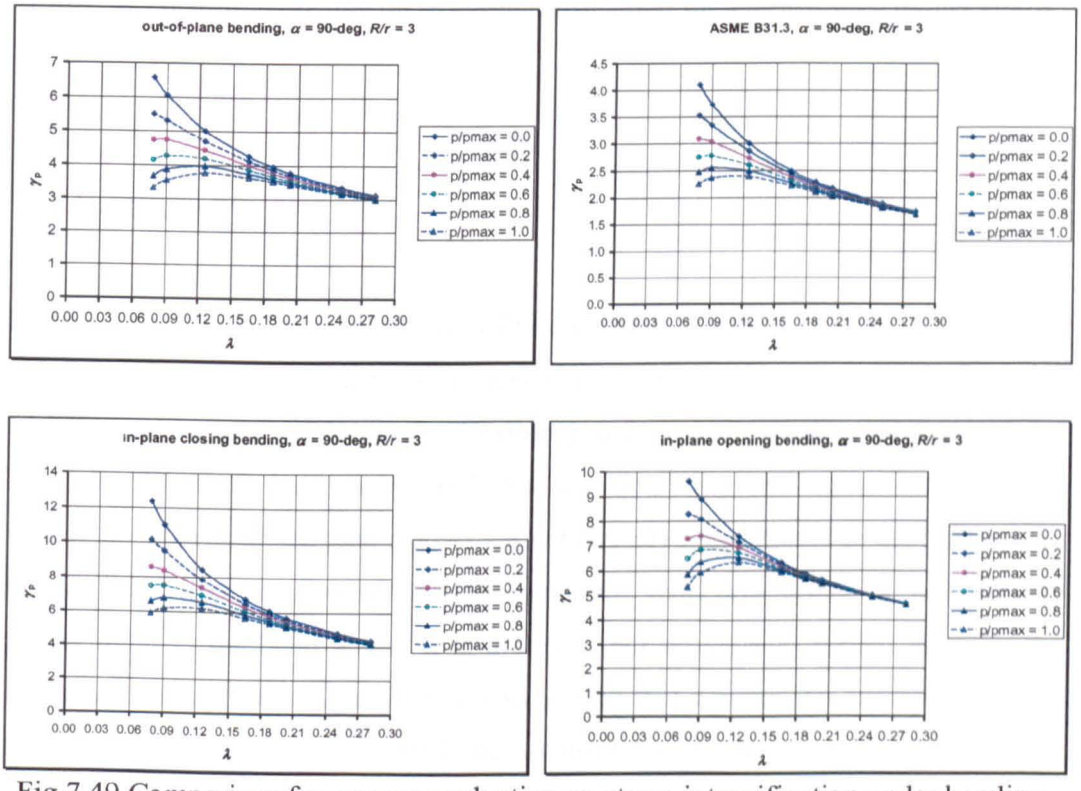

Fig.7.49 Comparison for pressure reduction on stress-intensification under bending

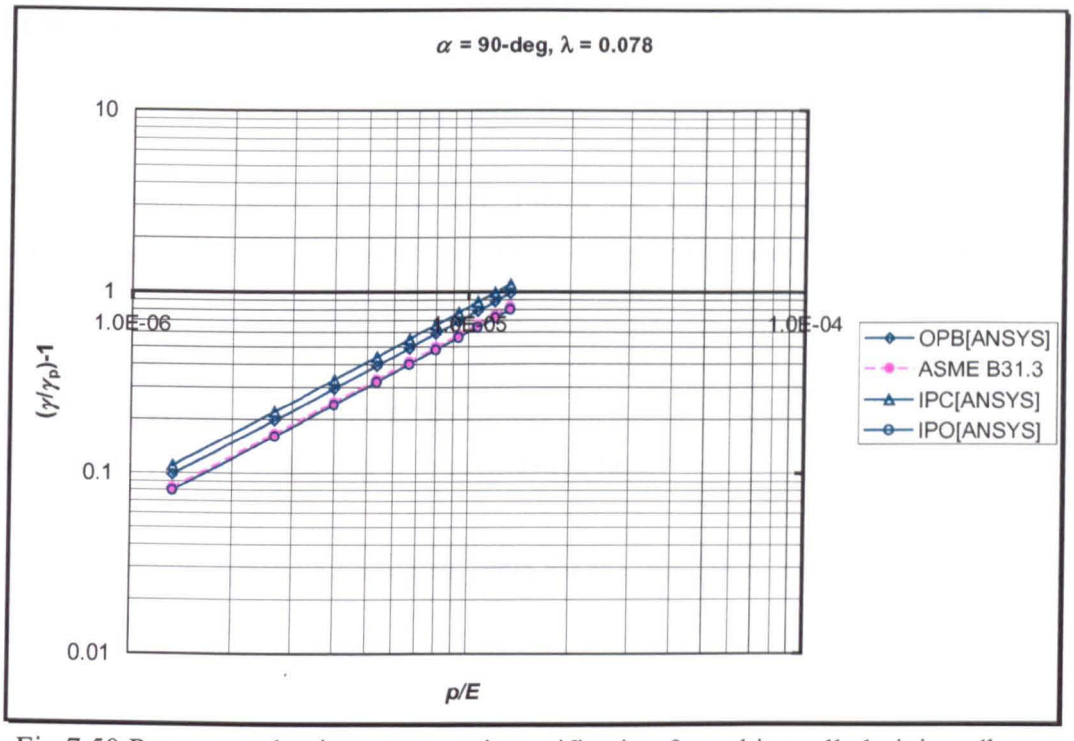

Fig.7.50 Pressure reduction on stress-intensification for a thin-walled piping elbow

7.4 Summary

Detailed non-linear large deformation finite element of piping elbows under out-of-plane bending and internal pressure has been carried out. Approximate formulae which could be used in design for flexibility and stress-intensification factors have been developed. It has been found that the flexibility and stress-intensification factors for unpressurised pipe elbows are not directly proportional to the bend angle. It has been also discovered that the pressure reduction effect is not directly proportional to the bend angle. It is therefore not possible to further simplify the formula for other bend angles, but it is suggested that a parameter survey be carried out if required. However, the bend angle considered in the present analysis covers practical bend angles. In general, it has been found that pipe elbows under out-of-plane bending are much stiffer than under in-plane bending. It follows that the stress-intensification factor is much smaller than those produced by in-plane bending load.

Appendix C7

This appendix present Figures and Tables for out-of-plane bending. All the approximate formulae presented in this Chapter have been derived from these Figures:

Fig.A7.1 – A7.5: for Flexibility factor

Fig.A8.6 – A8.10: for Stress-intensification factor

The end of this Appendix presented Table for the location of maximum stress under out-of-plane bending.

Continue to the next pages...→

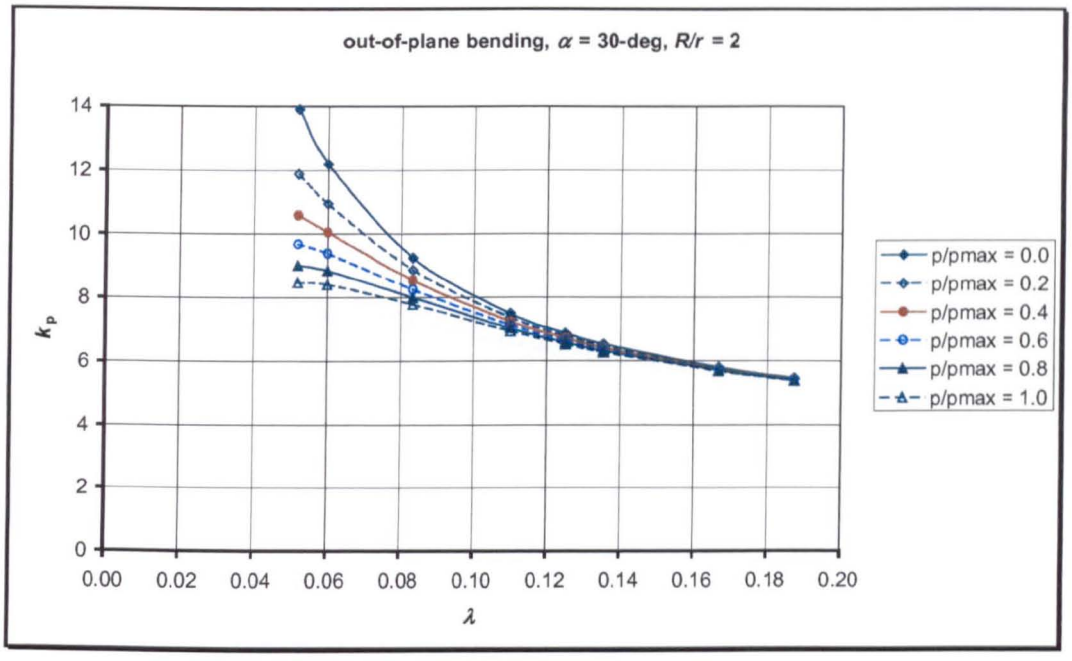

(a)

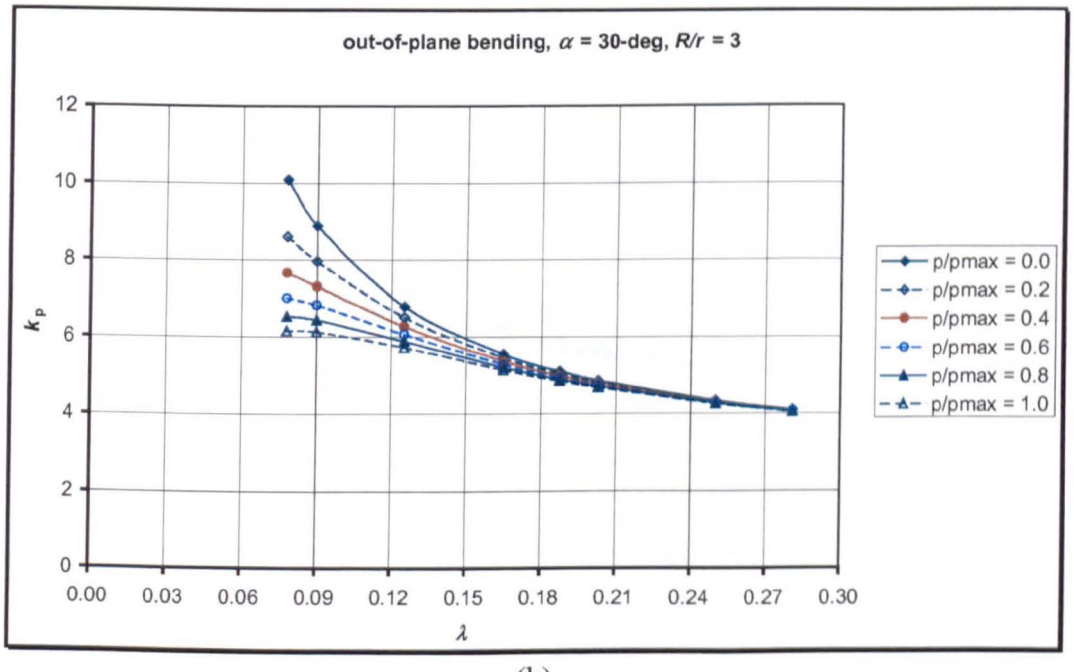

(b)

Fig.A7.1 Flexibility factor for 30-deg pipe elbows subjected to out-of-plane bending: (a) $R/r = 2$, (b) $R/r = 3$

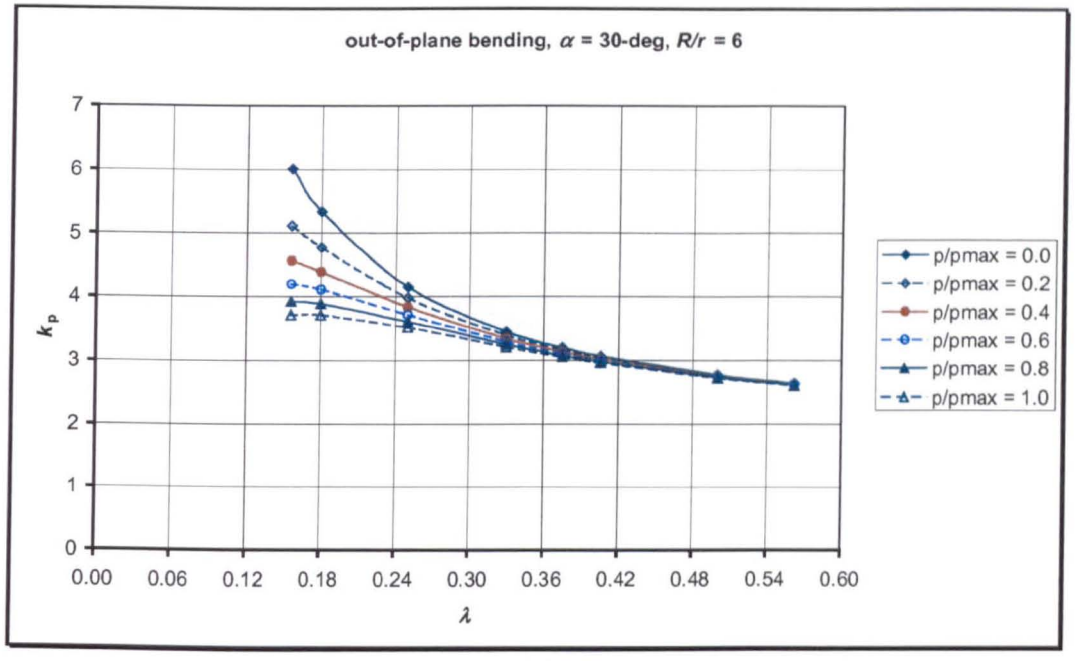

(c)

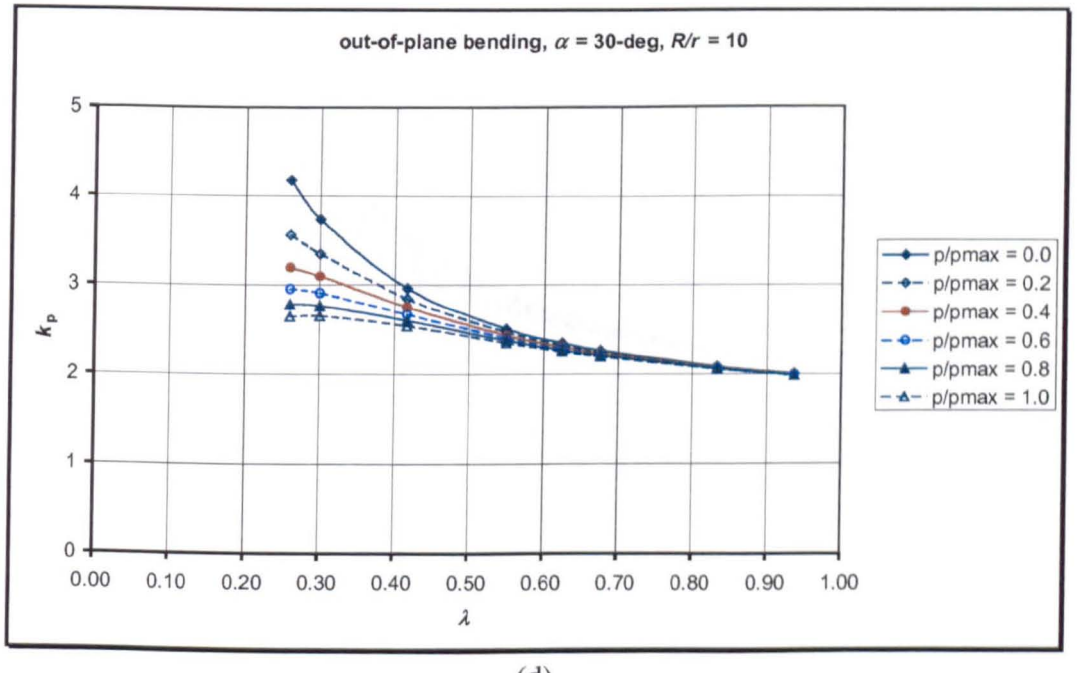

(d)

Fig.A7.1 Flexibility factor for 30-deg pipe elbows subjected to out-of-plane bending: (c) $R/r = 6$, (d) $R/r = 10$

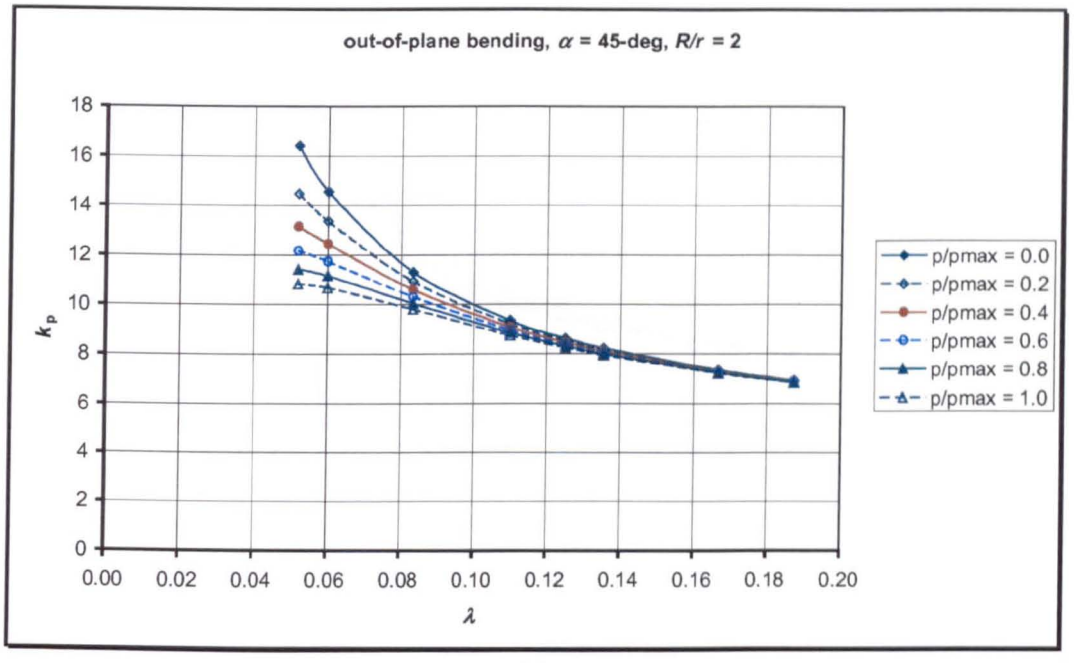

(a)

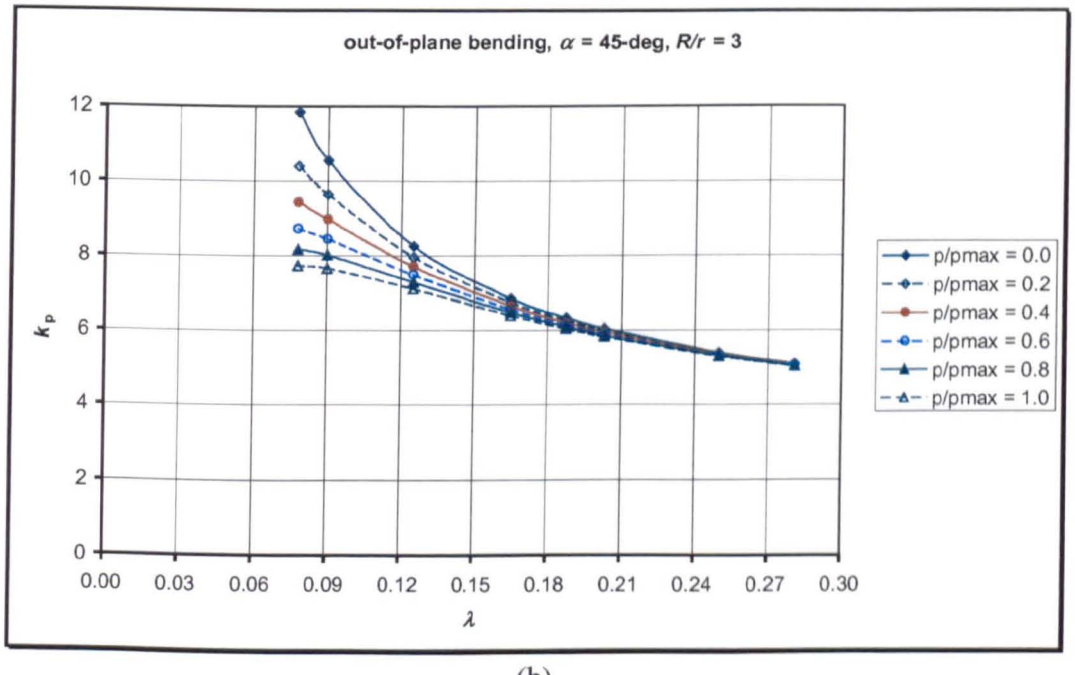

(b)

Fig.A7.2 Flexibility factor for 45-deg pipe elbows subjected to out-of-plane bending: (a) $R/r = 2$, (b) $R/r = 3$

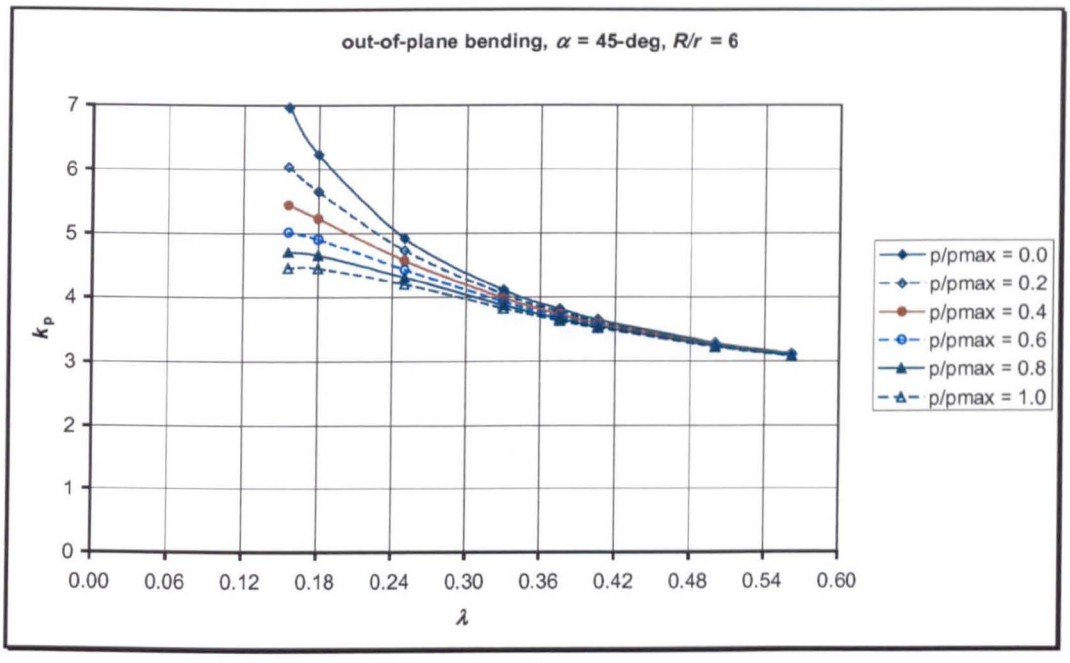

(c)

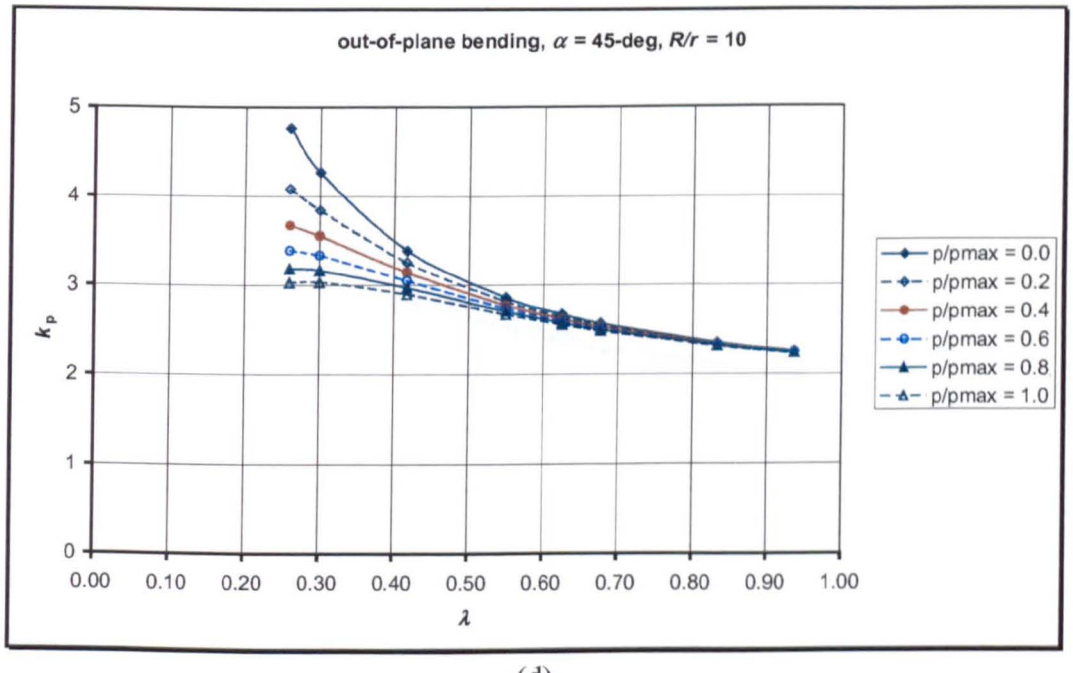

(d)

Fig.A7.2 Flexibility factor for 45-deg pipe elbows subjected to out-of-plane bending: (c) $R/r = 6$, (d) $R/r = 10$

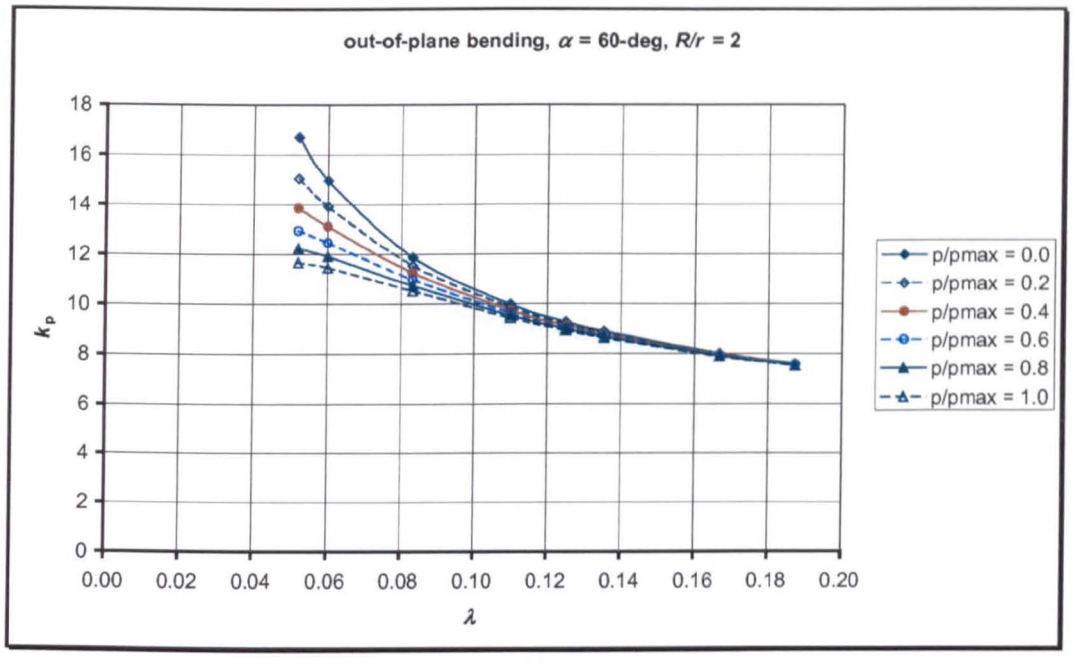

(a)

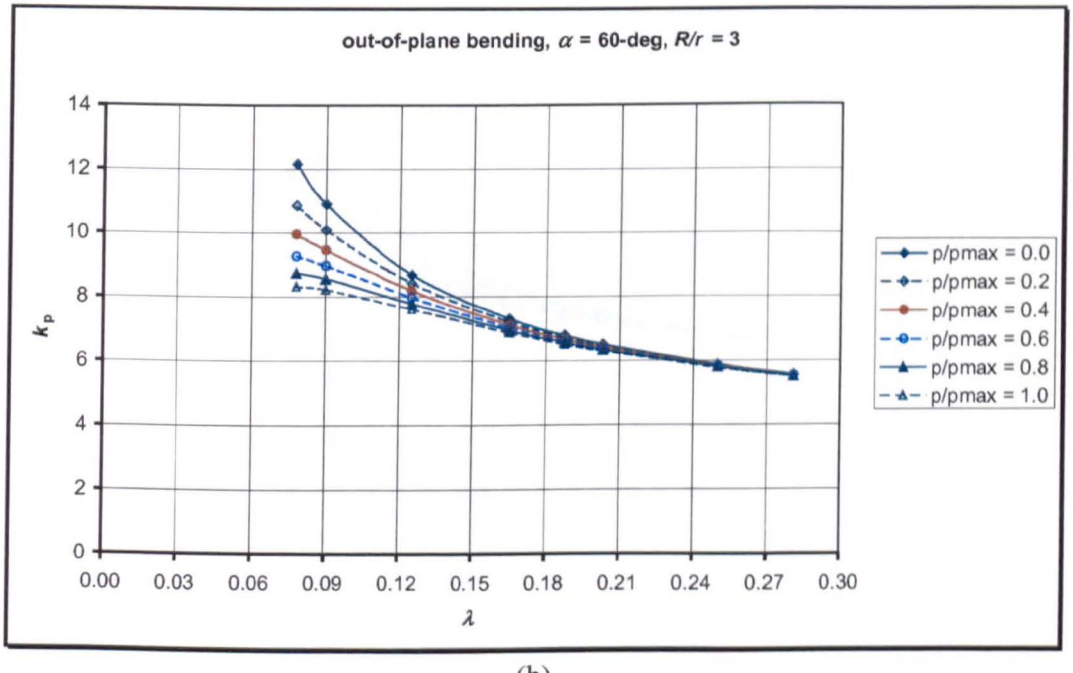

(b)

Fig.A7.3 Flexibility factor for 60-deg pipe elbows subjected to out-of-plane bending: (a) $R/r = 2$, (b) $R/r = 3$

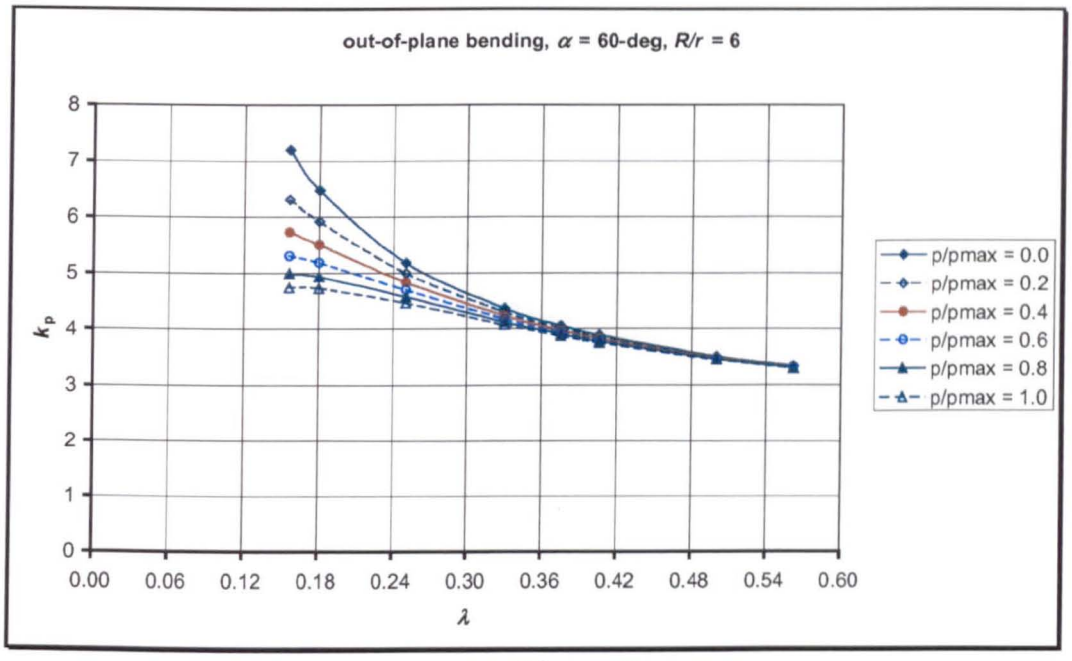

(c)

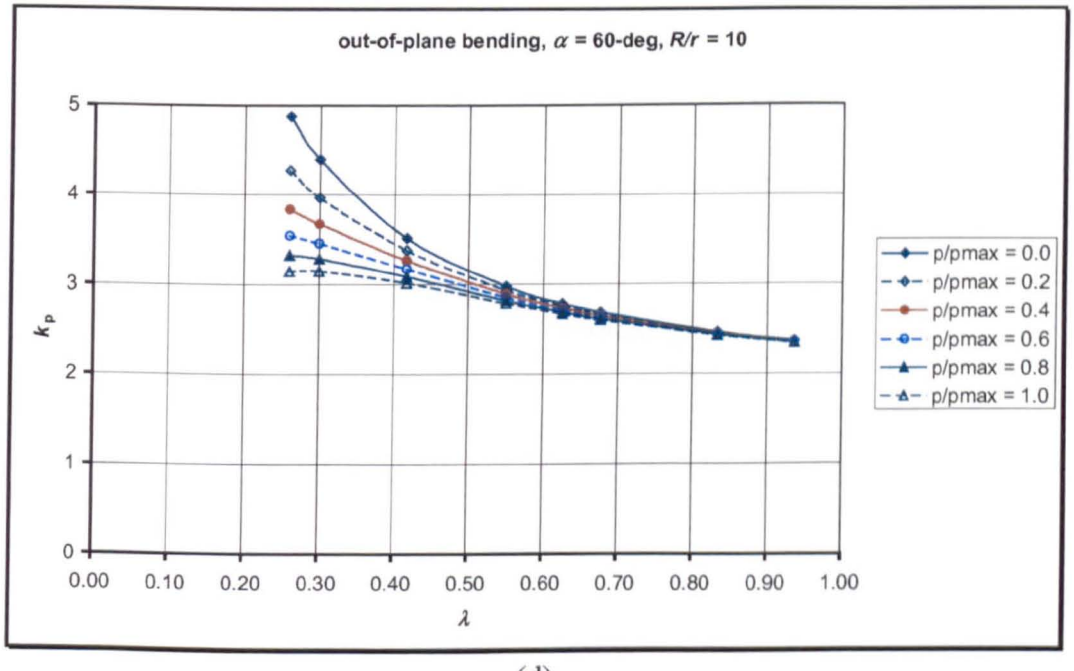

(d)

Fig.A7.3 Flexibility factor for 60-deg pipe elbows subjected to out-of-plane bending: (c) $R/r = 6$, (d) $R/r = 10$

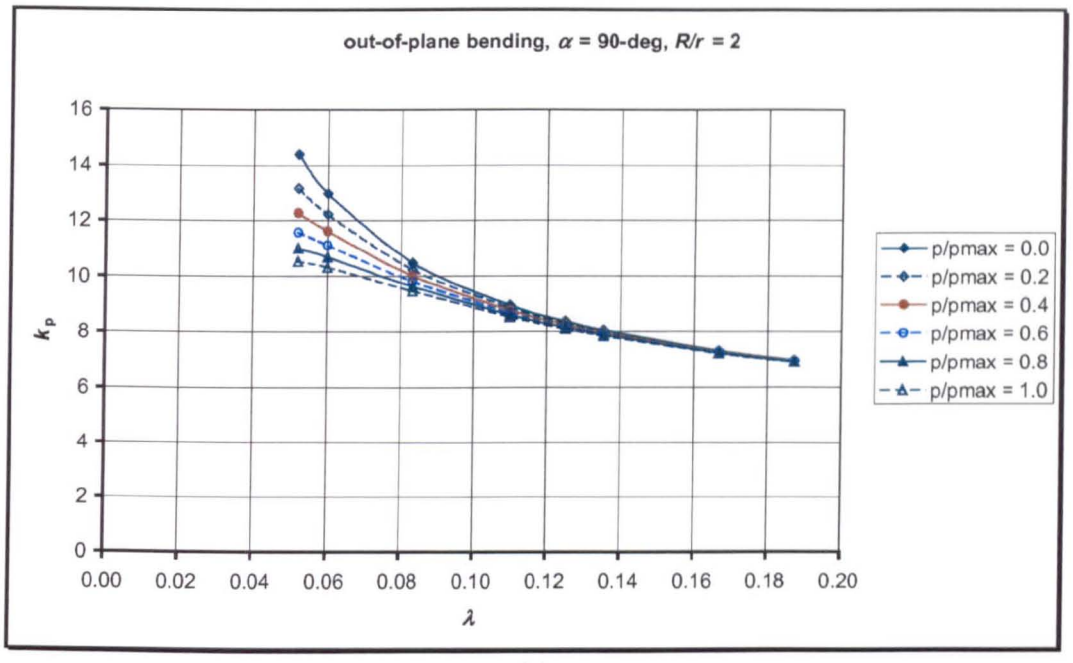

(a)

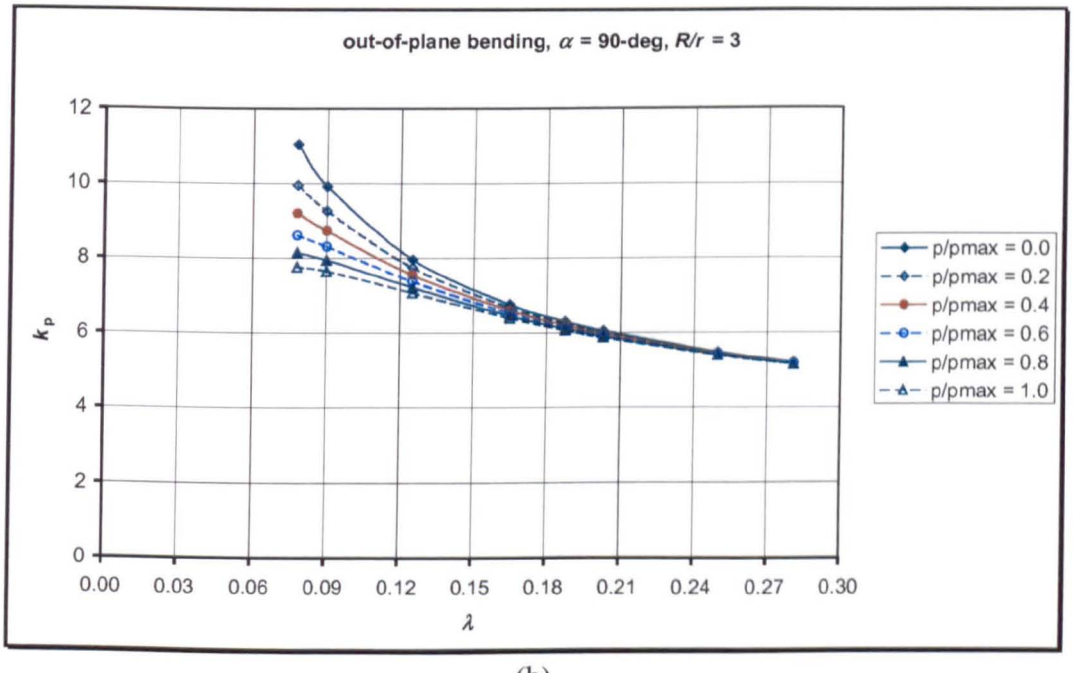

(b)

Fig.A7.4 Flexibility factor for 90-deg pipe elbows subjected to out-of-plane bending: (a) $R/r = 2$, (b) $R/r = 3$

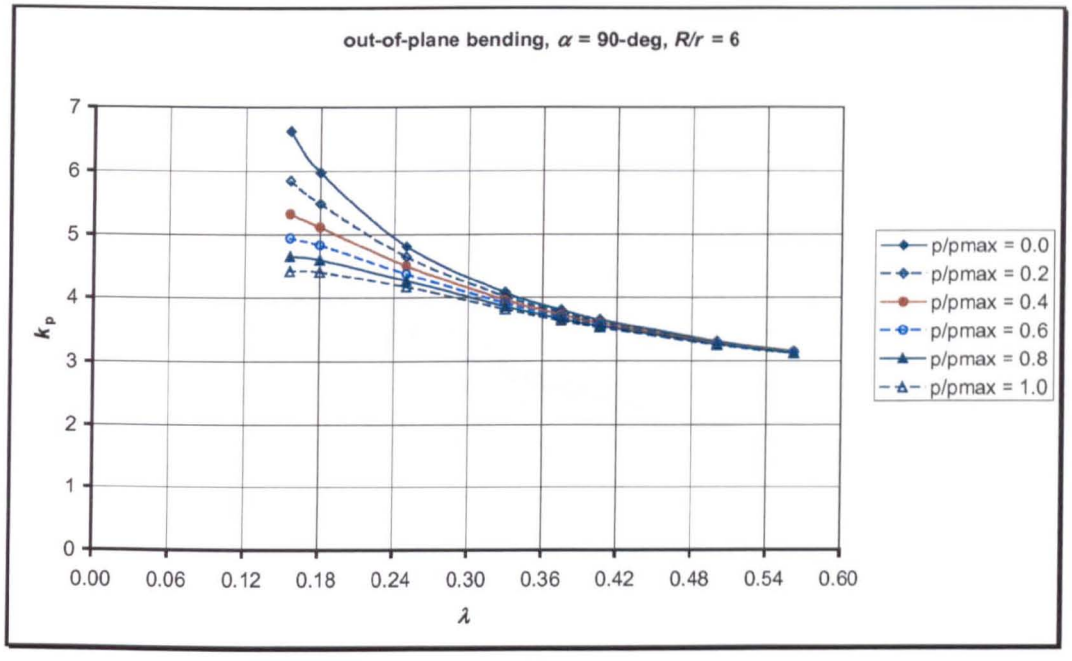

(c)

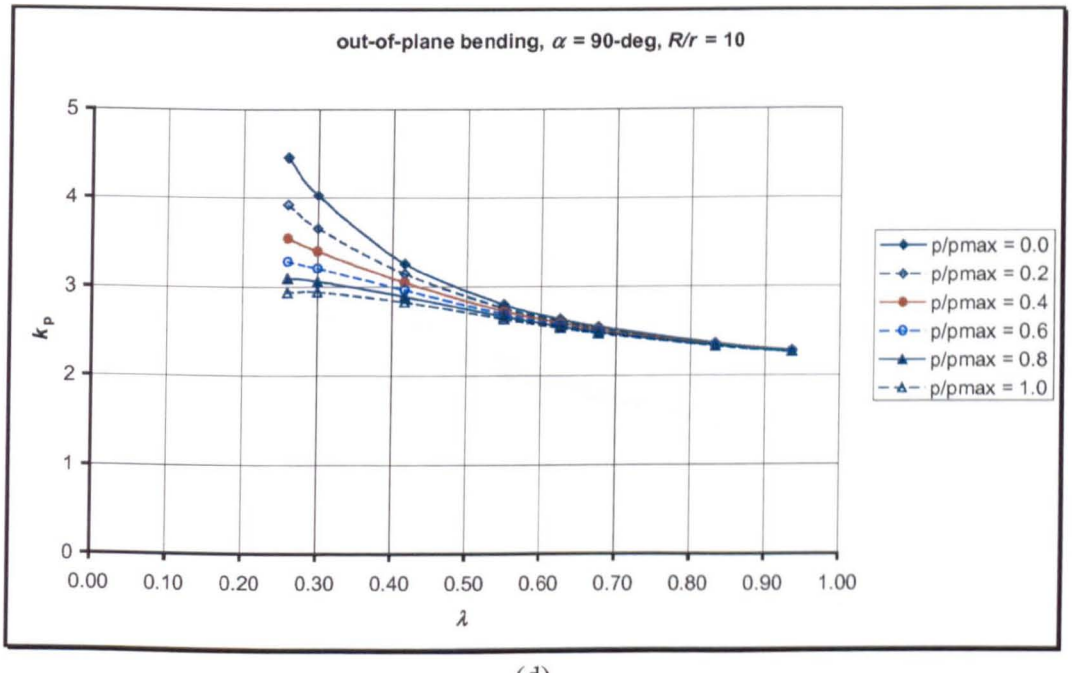

(d)

Fig.A7.4 Flexibility factor for 90-deg pipe elbows subjected to out-of-plane bending: (c) $R/r = 6$, (d) $R/r = 10$

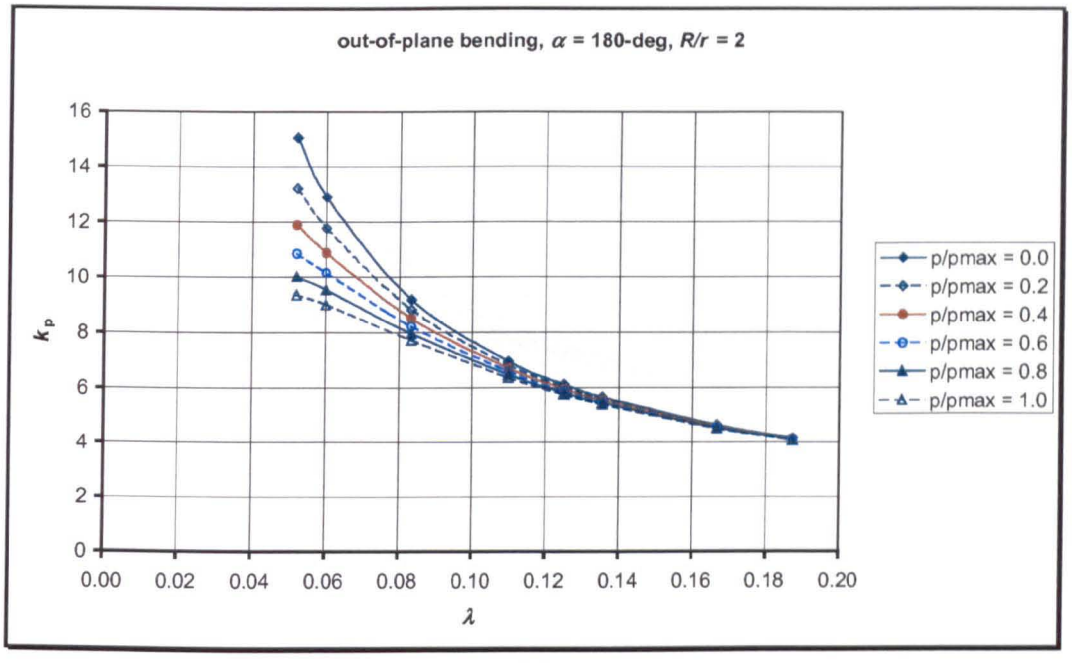

(a)

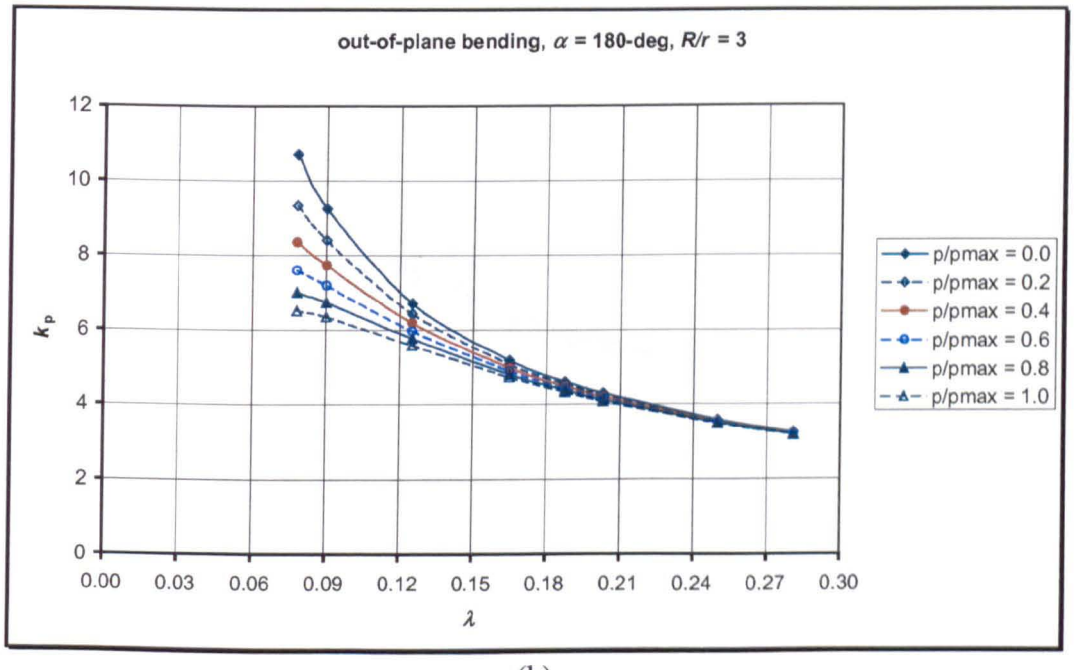

(b)

Fig.A7.5 Flexibility factor for 180-deg pipe elbows subjected to out-of-plane bending: (a) $R/r = 2$, (b) $R/r = 3$

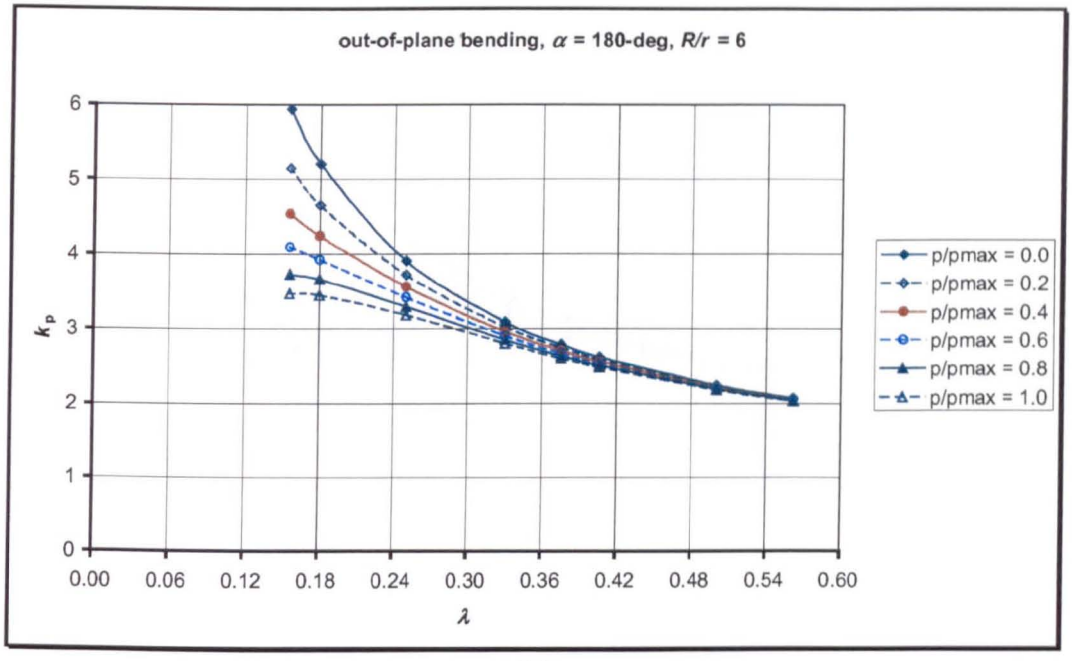

(c)

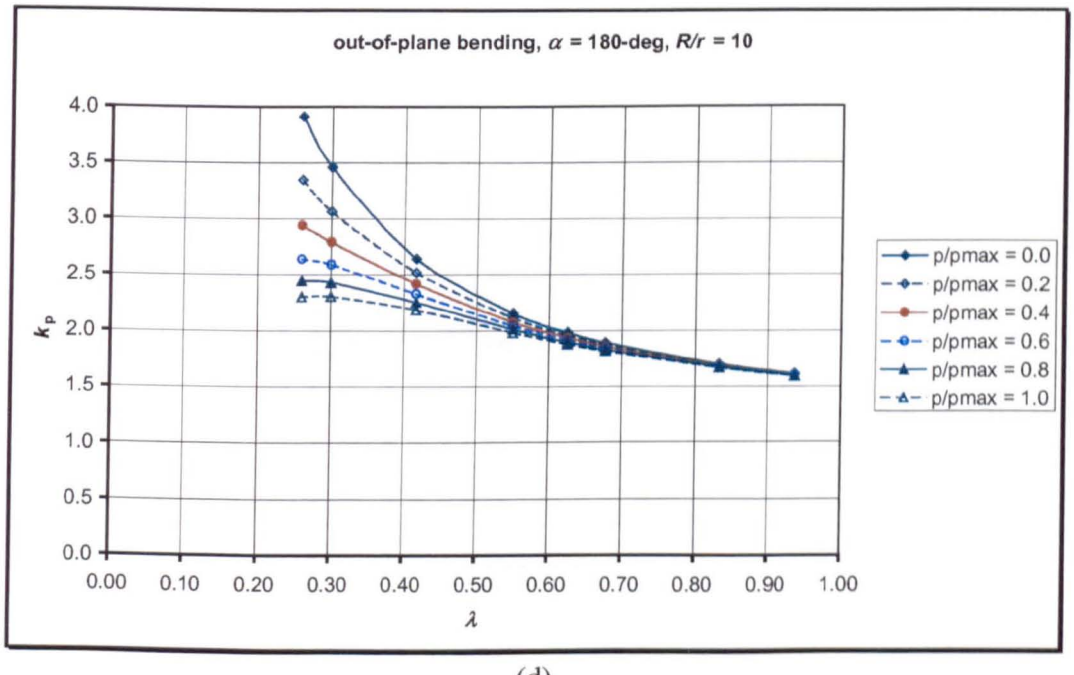

(d)

Fig.A7.5 Flexibility factor for 180-deg pipe elbows subjected to out-of-plane bending: (c) $R/r = 6$, (d) $R/r = 10$

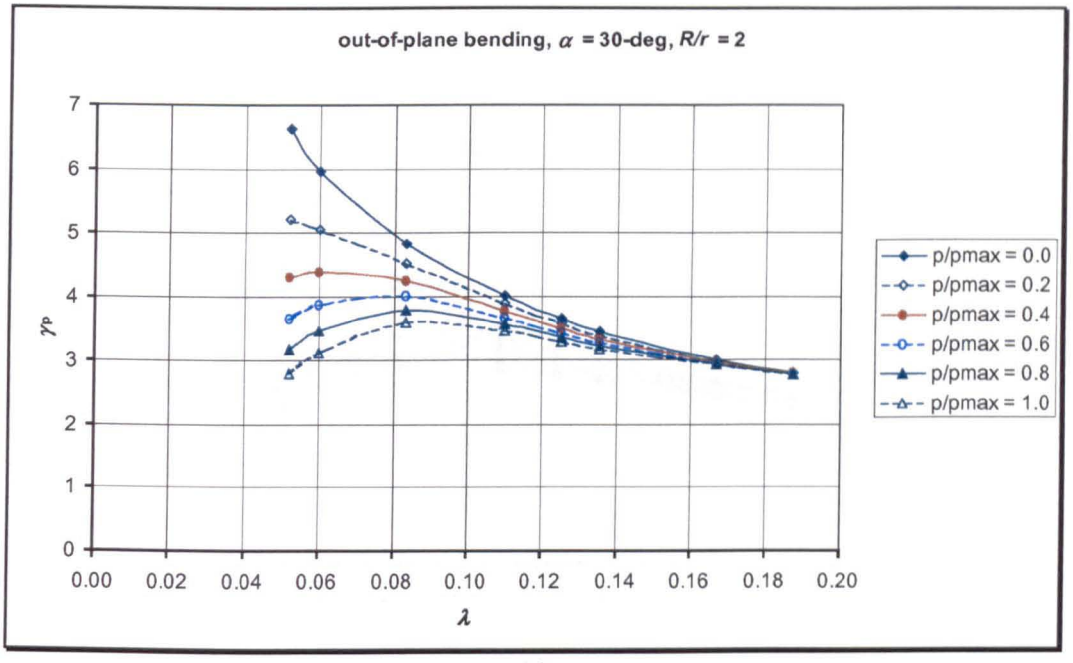

(a)

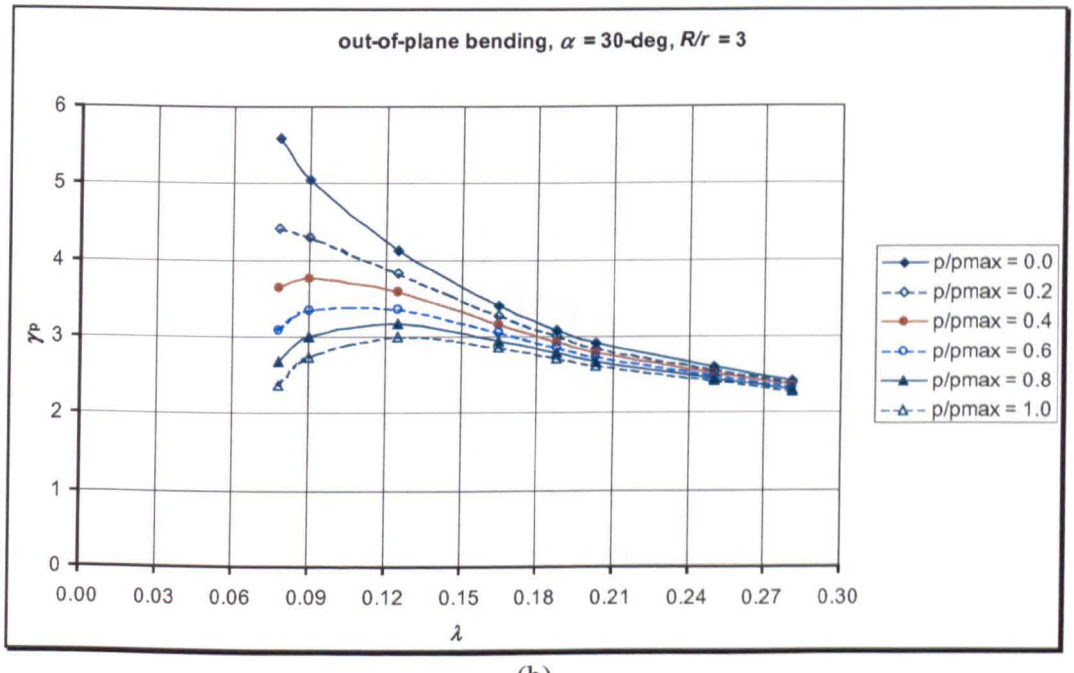

(b)

Fig.A7.6 Stress-intensification factor for 30-deg pipe elbows subjected to out-of-plane bending: (a) $R/r = 2$, (b) $R/r = 3$

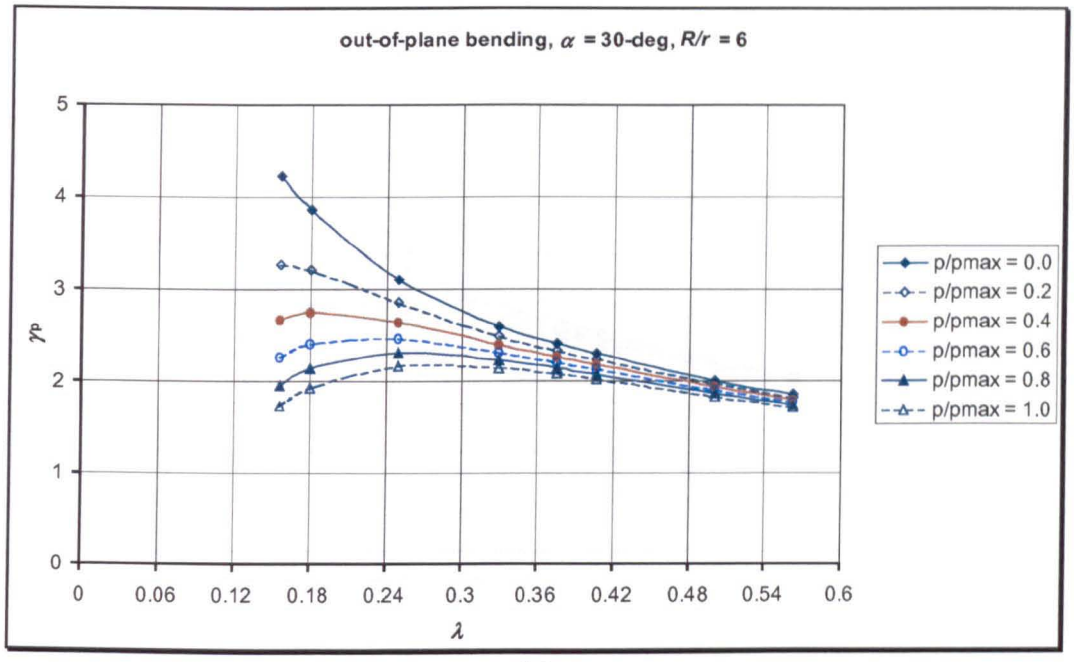

(c)

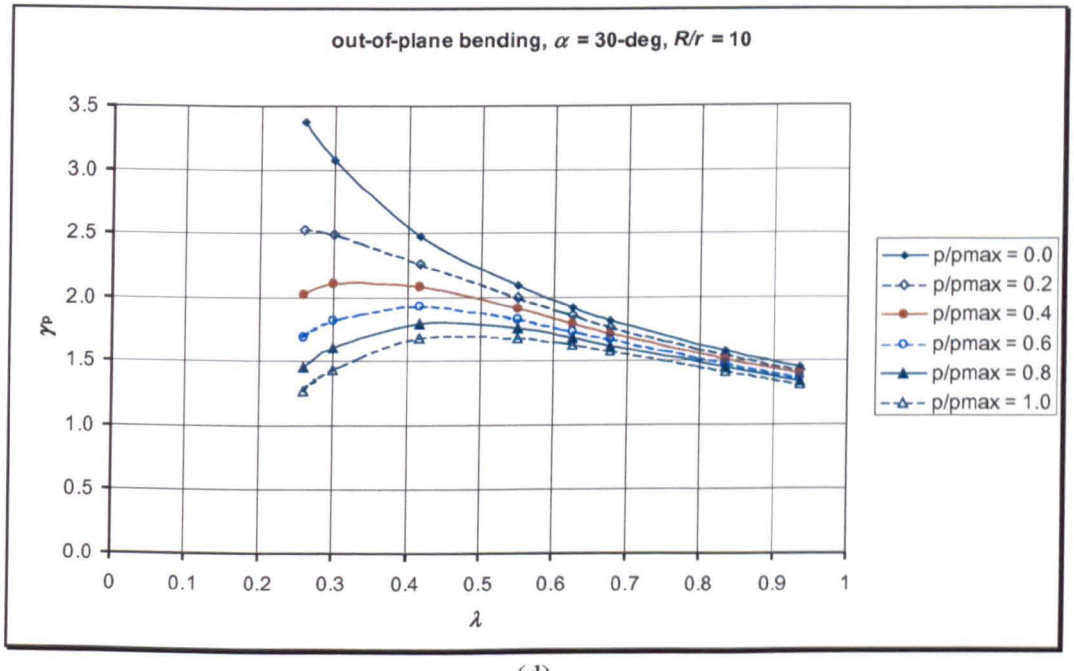

(d)

Fig.A7.6 Stress-intensification factor for 30-deg pipe elbows subjected to out-of-plane bending: (c) $R/r = 6$, (d) $R/r = 10$

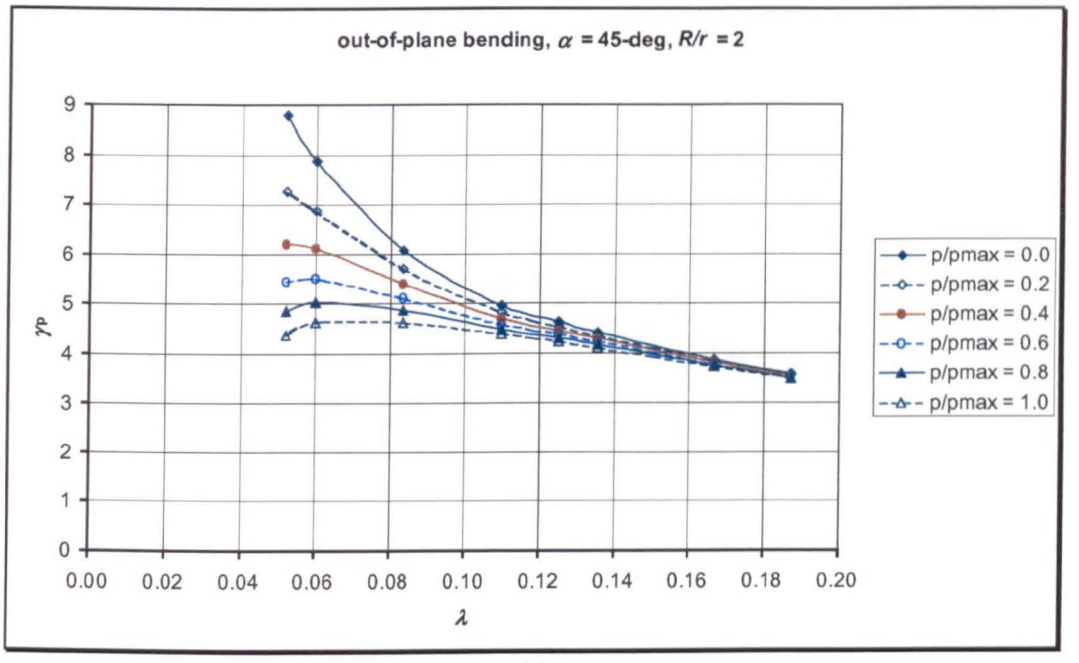

(a)

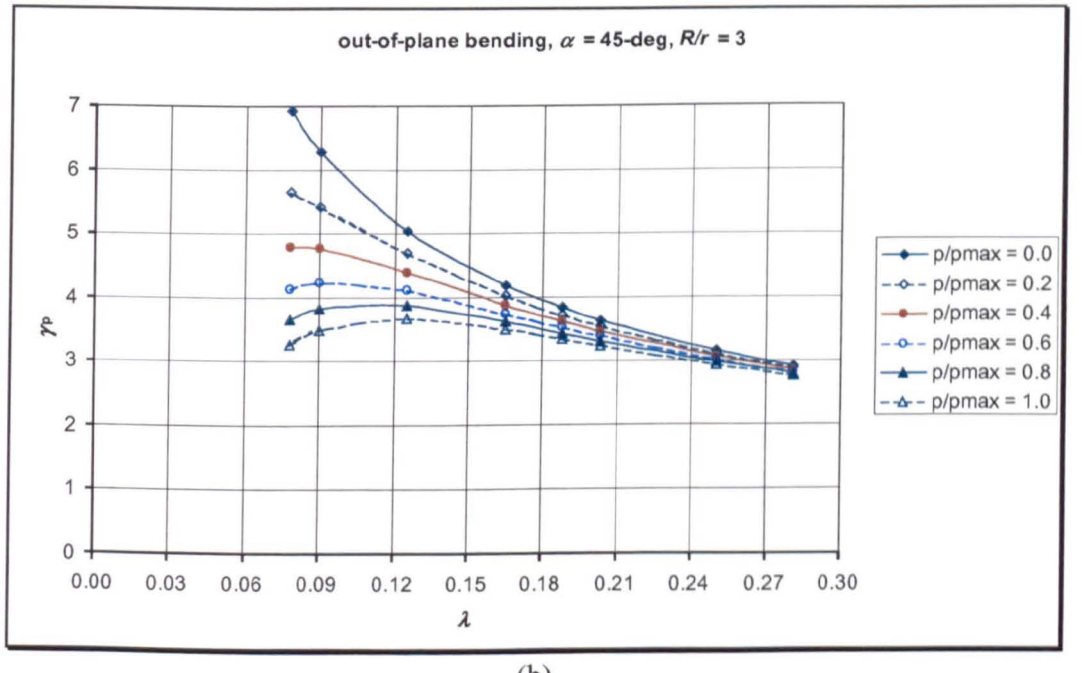

(b)

Fig.A7.7 Stress-intensification factor for 45-deg pipe elbows subjected to out-of-plane bending: (a) $R/r = 2$, (b) $R/r = 3$

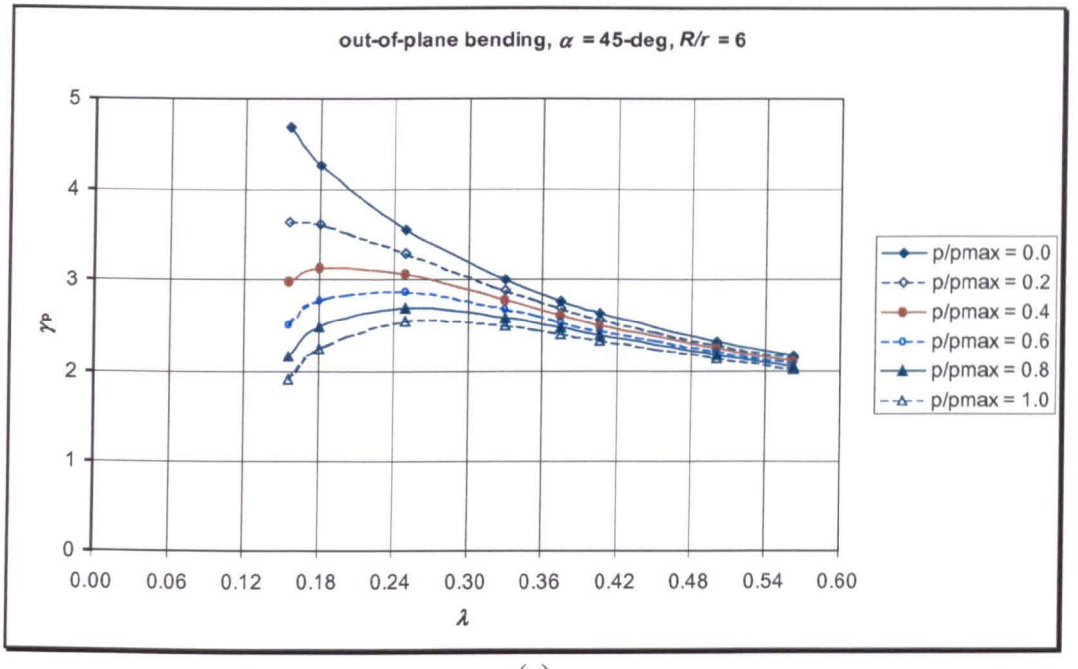

(c)

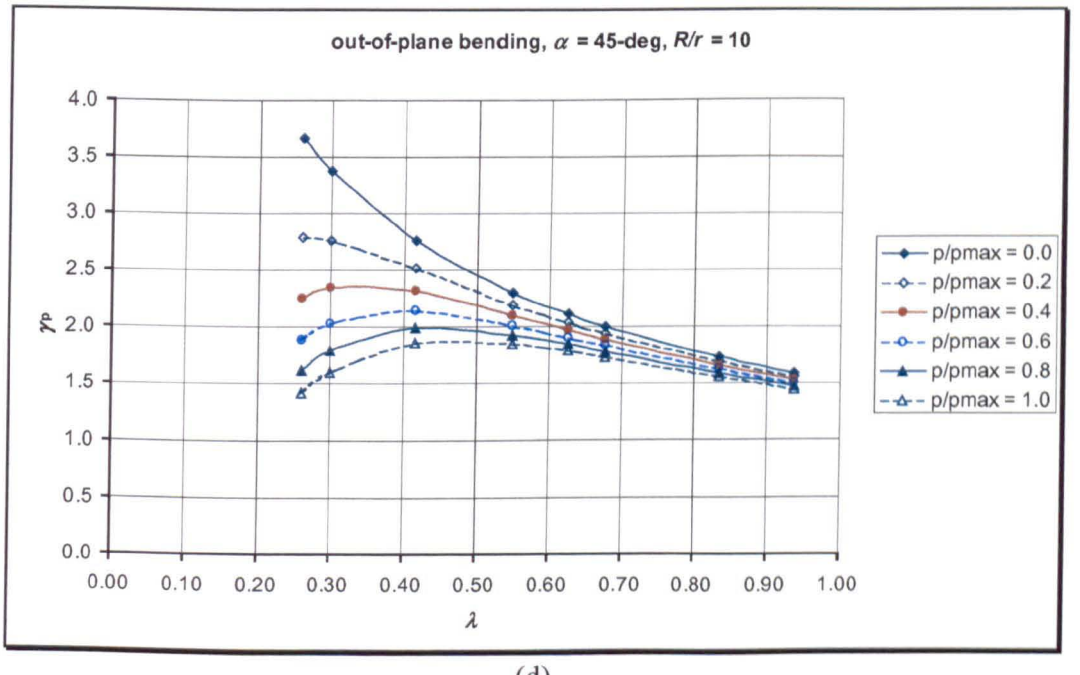

(d)

Fig.A7.7 Stress-intensification factor for 45-deg pipe elbows subjected to out-of-plane bending: (c) $R/r = 6$, (d) $R/r = 10$

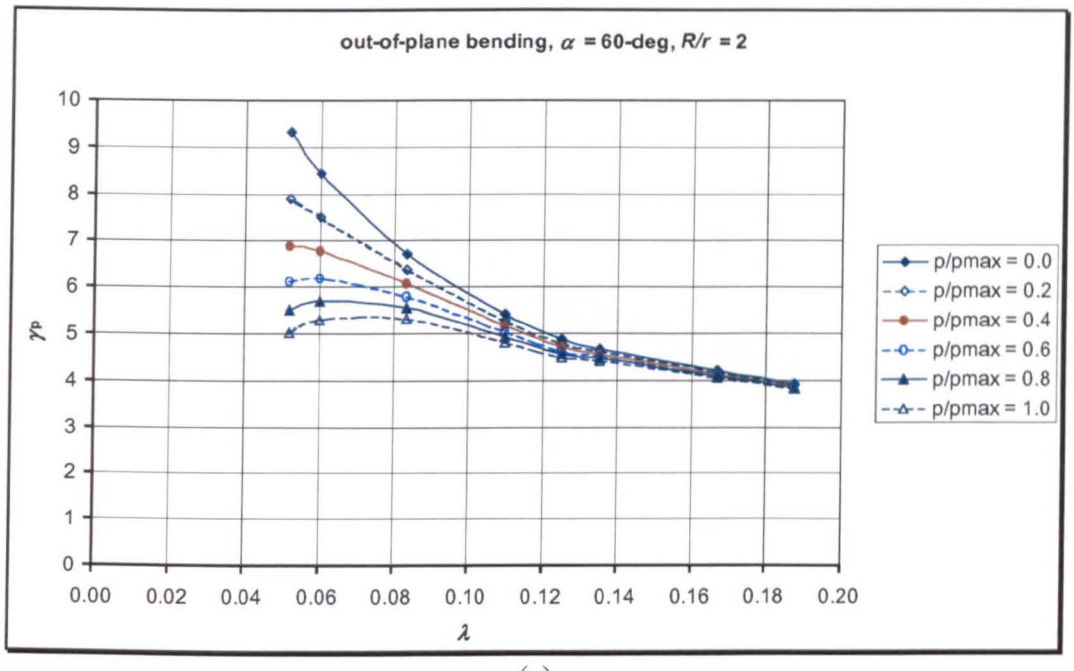

(a)

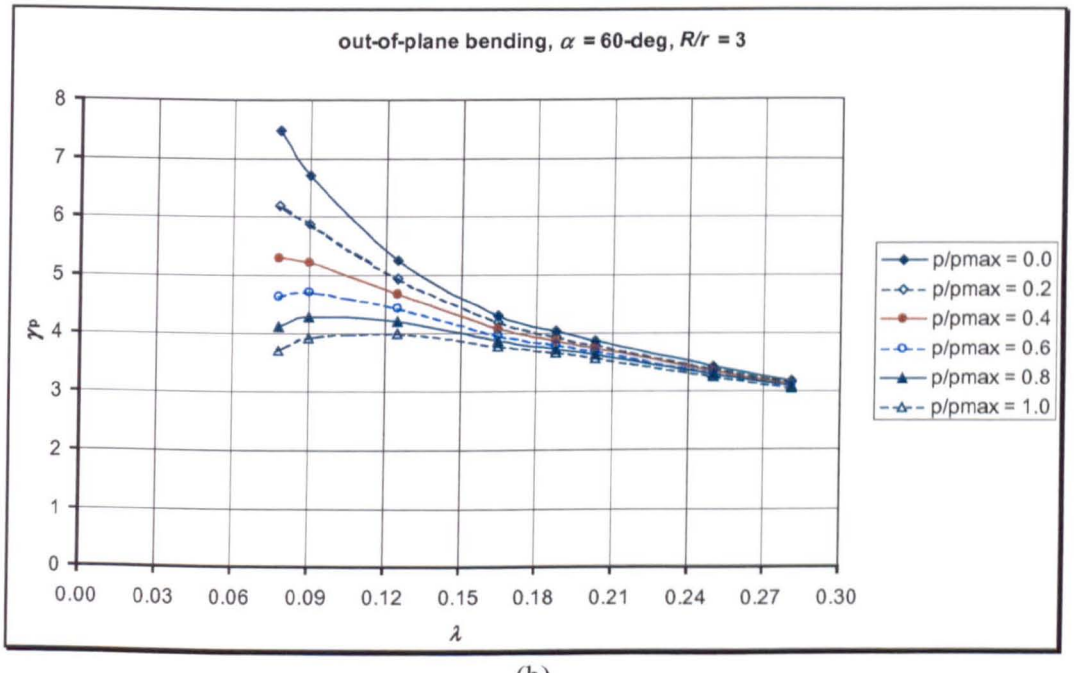

(b)

Fig.A7.8 Stress-intensification factor for 60-deg pipe elbows subjected to out-of-plane bending: (a) $R/r = 2$, (b) $R/r = 3$

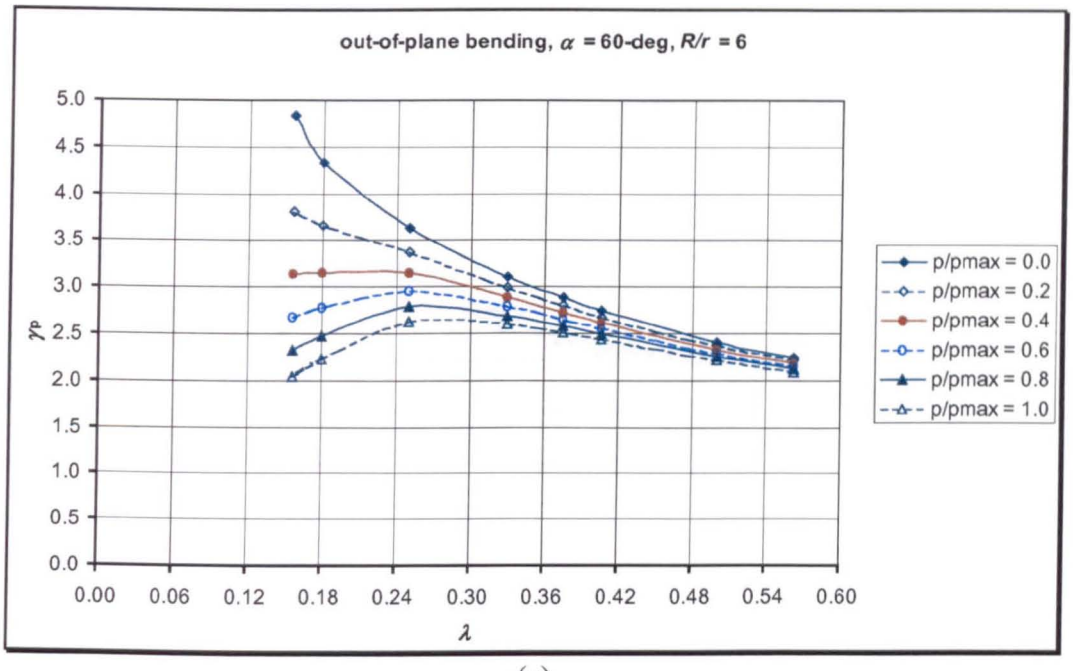

(c)

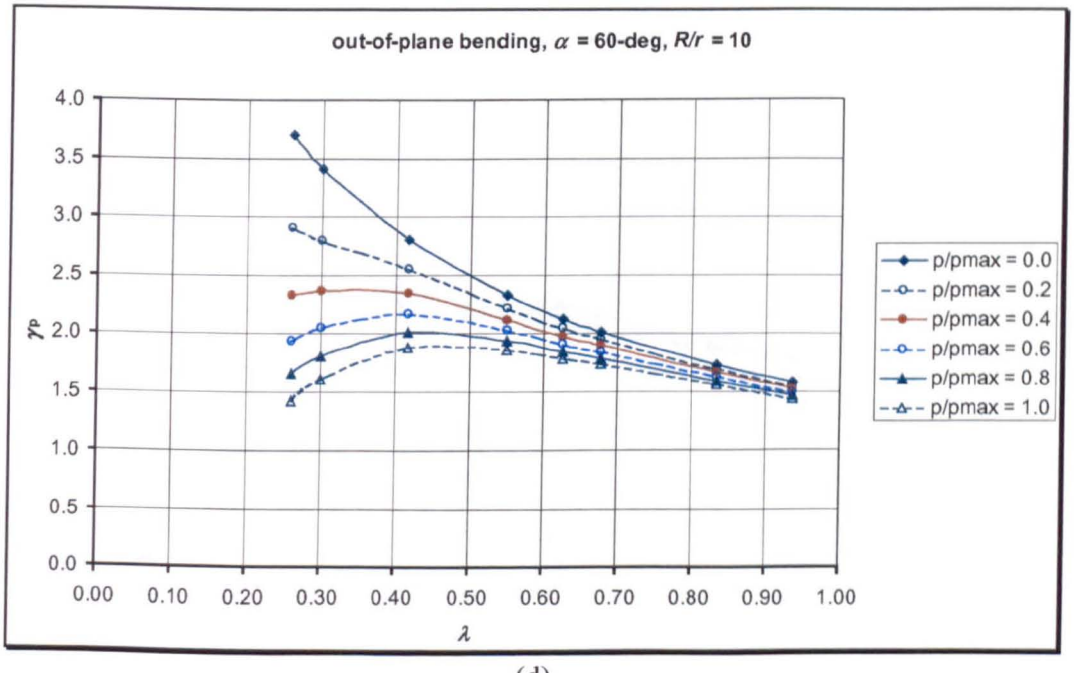

(d)

Fig.A7.8 Stress-intensification factor for 60-deg pipe elbows subjected to out-of-plane bending: (c) $R/r = 6$, (d) $R/r = 10$

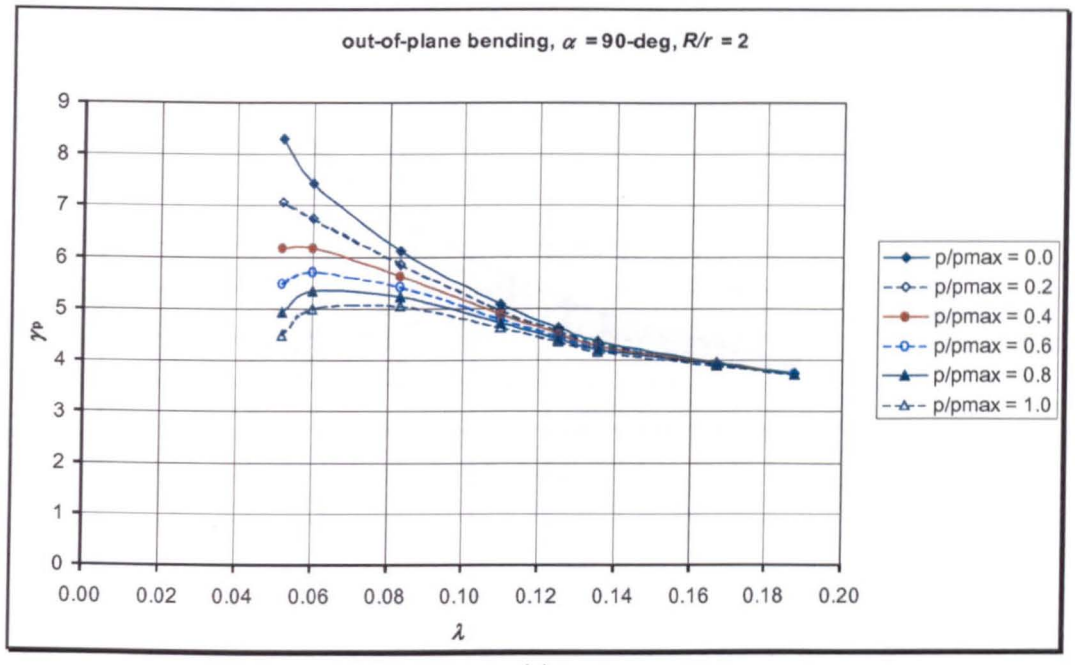

(a)

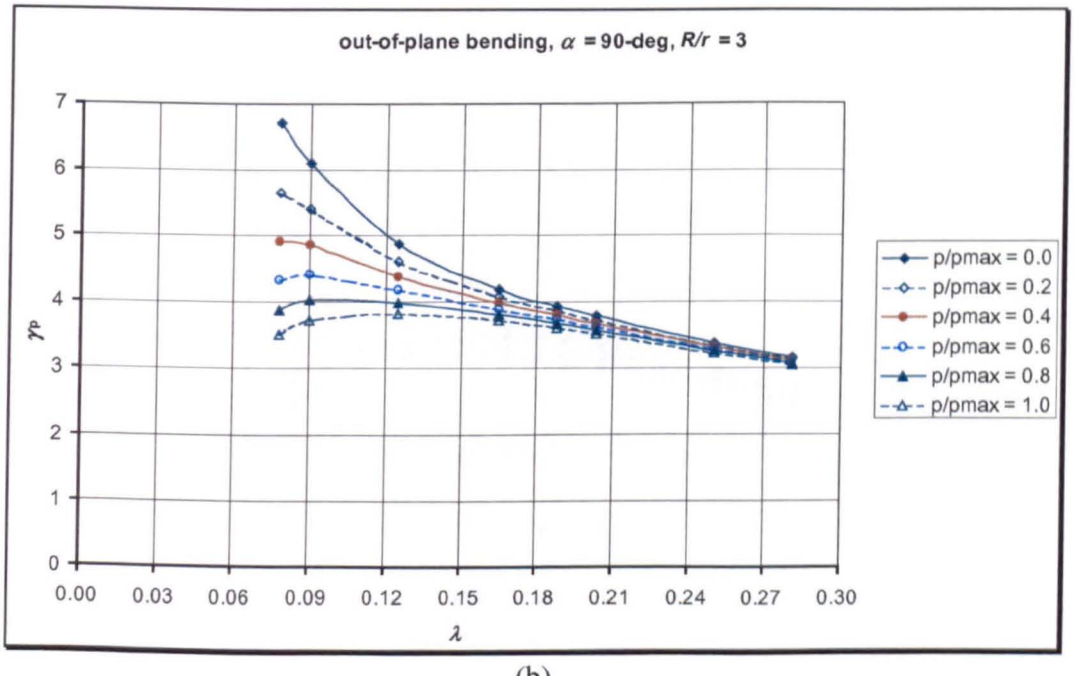

(b)

Fig.A7.9 Stress-intensification factor for 90-deg pipe elbows subjected to out-of-plane bending: (a) $R/r = 2$, (b) $R/r = 3$

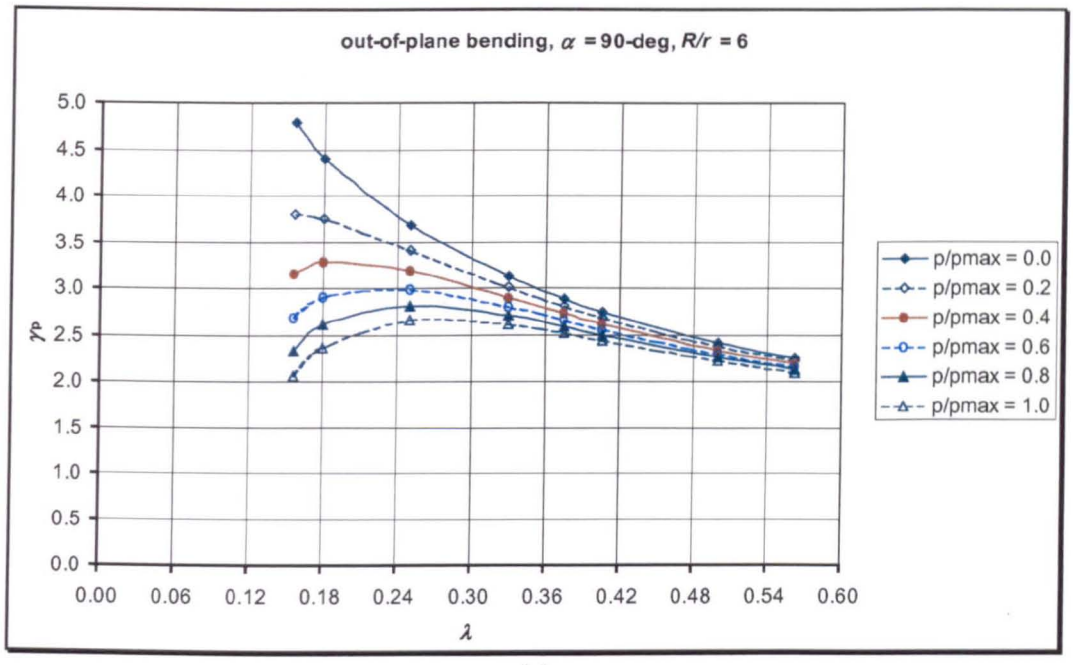

(c)

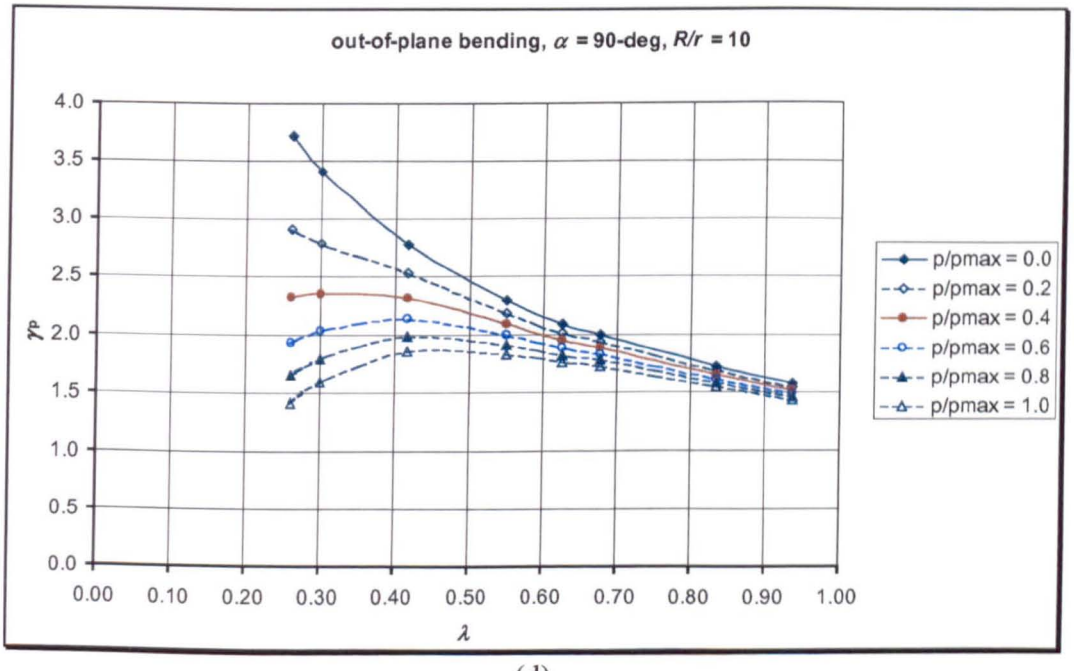

(d)

Fig.A7.9 Stress-intensification factor for 90-deg pipe elbows subjected to out-of-plane bending: (c) $R/r = 6$, (d) $R/r = 10$

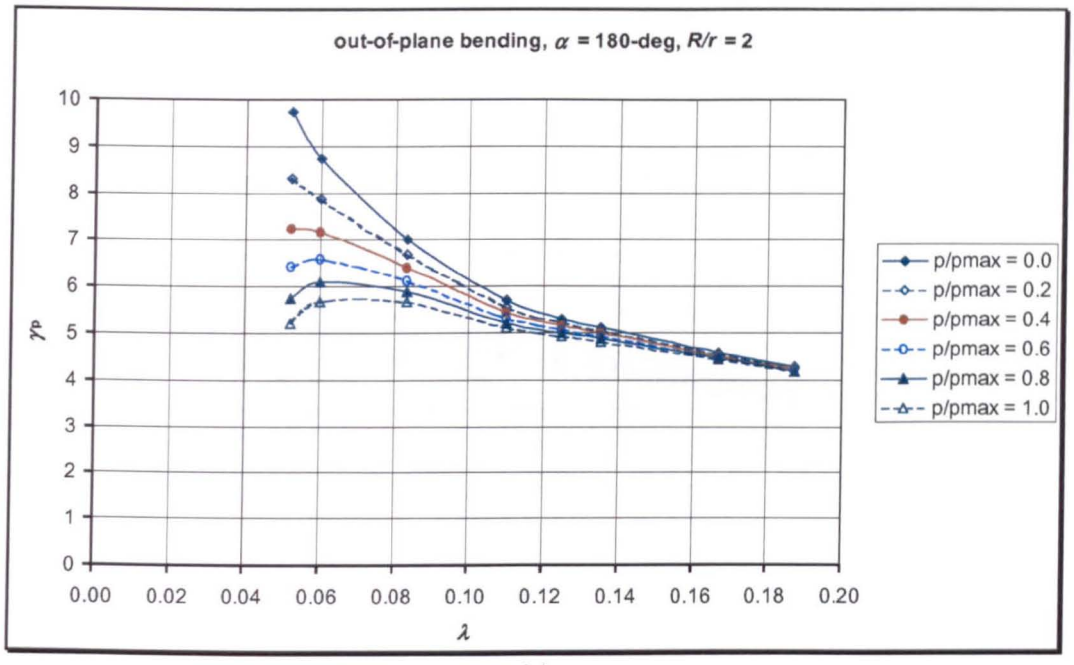

(a)

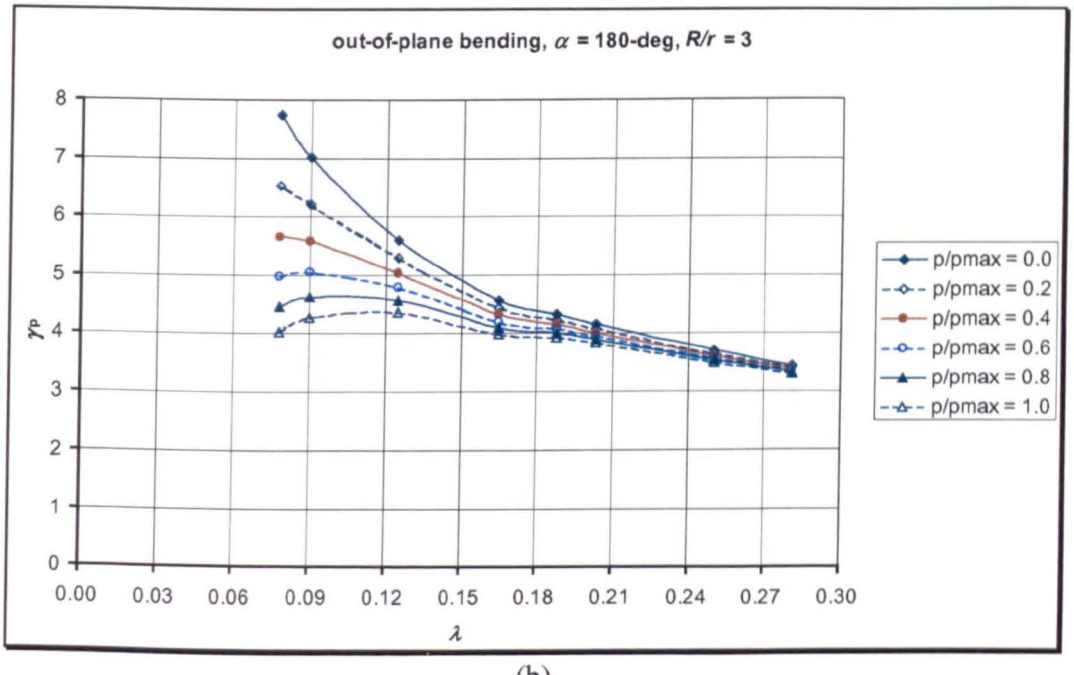

(b)

Fig.A7.10 Stress-intensification factor for 180-deg pipe elbows subjected to out-of-plane bending: (a) $R/r = 2$, (b) $R/r = 3$

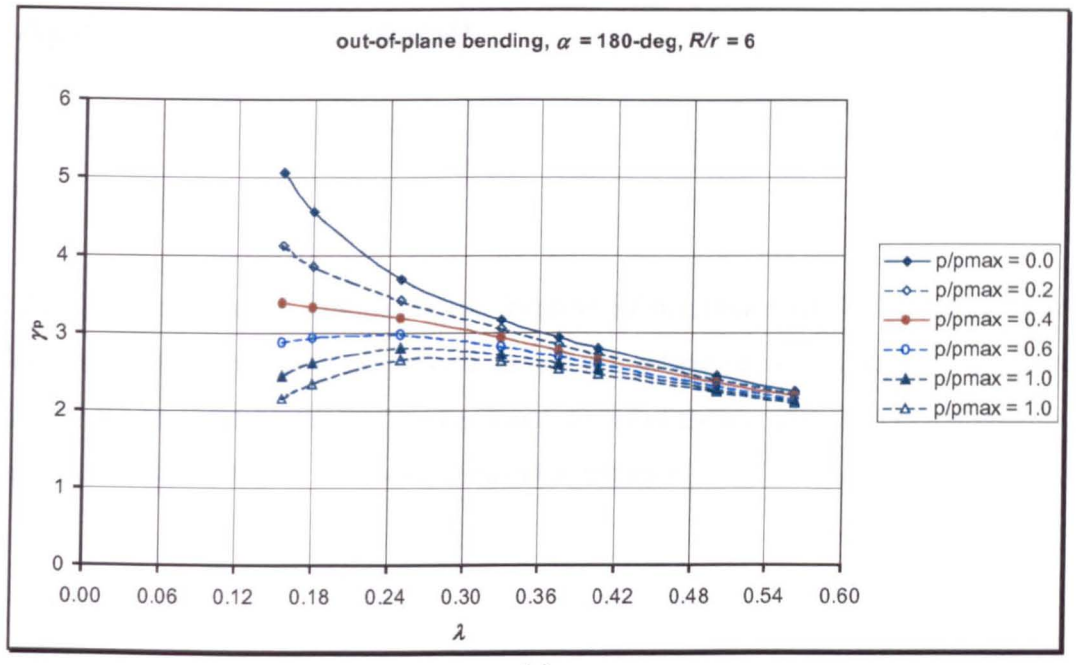

(c)

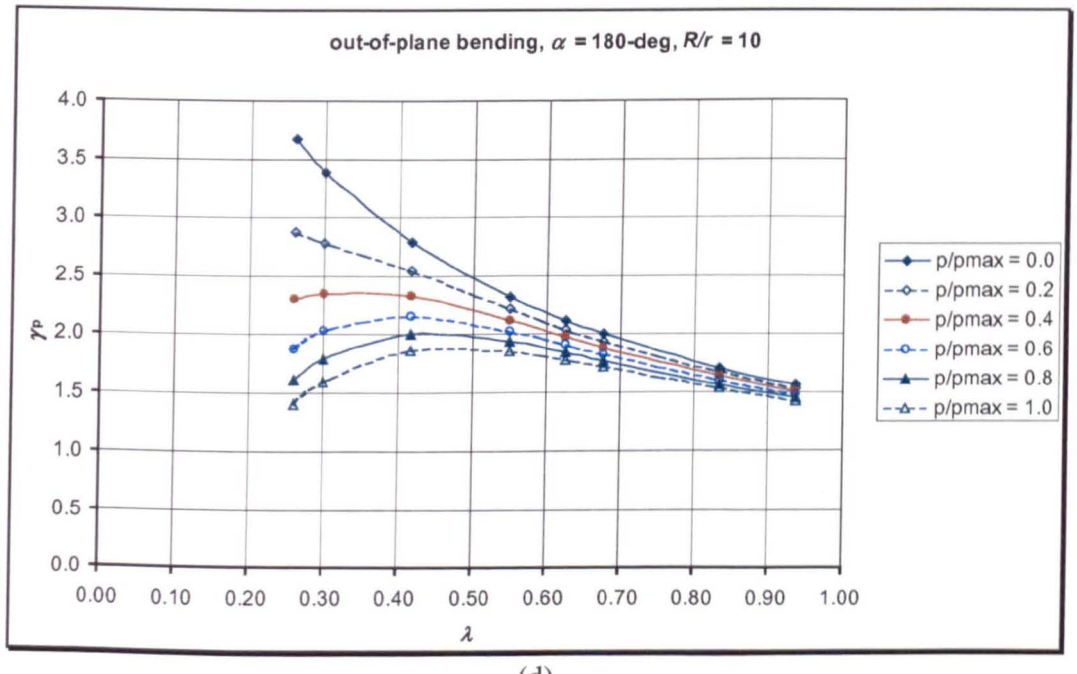

(d)

Fig.A7.10 Stress-intensification factor for 180-deg pipe elbows subjected to out-of-plane bending: (c) $R/r = 6$, (d) $R/r = 10$

Appendix C7 (Continued)

The following Tables summarise the location of maximum stress for out-of-plane bending. The location is expressed as (θ, ϕ), where θ is longitudinal position measured from the junction of the bend and the fixed tangent and ϕ is circumferential position measured from the crown toward the intrados.

Continue to the next pages...→

Table 7A-1 Location of maximum stress (θ, ϕ) for α = 30-deg

	$R/r = 2$	$R/r = 3$	$R/r = 6$	$R/r = 10$
$t/r = 0.0260$	(15, 30)	(15, 30)	(15, 45)	(15, 45)
$t/r = 0.0300$	(15, 30)	(15, 45)	(15, 45)	(15, 45)
$t/r = 0.0417$	(15, 45)	(15, 45)	(15, 45)	(15, 45)
$t/r = 0.0550$	(15, 45)	(15, 45)	(15, 45)	(15, 45)
$t/r = 0.0625$	(15, 45)	(15, 45)	(15, 45)	(15, 45)
$t/r = 0.0677$	(15, 45)	(15, 45)	(15, 45)	(15, 45)
$t/r = 0.0833$	(15, 45)	(15, 45)	(15, 45)	(15, 45)
$t/r = 0.0937$	(15, 45)	(15, 45)	(15, 45)	(15, 45)

Table 7A-2 Location of maximum stress (θ, ϕ) for α = 45-deg

	$R/r = 2$	$R/r = 3$	$R/r = 6$	$R/r = 10$
$t/r = 0.0260$	(24, 30)	(24, 30)	(24, 30)	(24, 45)
$t/r = 0.0300$	(24, 30)	(24, 30)	(24, 45)	(24, 45)
$t/r = 0.0417$	(24, 30)	(24, 30)	(24, 45)	(24, 45)
$t/r = 0.0550$	(24, 45)	(24, 45)	(24, 45)	(24, 45)
$t/r = 0.0625$	(24, 45)	(24, 45)	(24, 45)	(24, 45)
$t/r = 0.0677$	(24, 45)	(24, 45)	(24, 45)	(24, 45)
$t/r = 0.0833$	(24, 45)	(24, 45)	(24, 45)	(24, 45)
$t/r = 0.0937$	(24, 45)	(24, 45)	(24, 45)	(24, 45)

Table 7A-3 Location of maximum stress (θ, ϕ) for α = 60-deg

	$R/r = 2$	$R/r = 3$	$R/r = 6$	$R/r = 10$
$t/r = 0.0260$	(30, 30)	(30, 30)	(33, 30)	(39, 45)
$t/r = 0.0300$	(30, 30)	(30, 30)	(33, 30)	(39, 45)
$t/r = 0.0417$	(30, 30)	(30, 30)	(36, 45)	(39, 45)
$t/r = 0.0550$	(30, 30)	(33, 45)	(36, 45)	(39, 45)
$t/r = 0.0625$	(30, 30)	(33, 45)	(36, 45)	(39, 45)
$t/r = 0.0677$	(30, 45)	(33, 45)	(36, 45)	(39, 45)
$t/r = 0.0833$	(30, 45)	(33, 45)	(36, 45)	(39, 45)
$t/r = 0.0937$	(30, 45)	(33, 45)	(36, 45)	(39, 45)

Table 7A-4 Location of maximum stress (θ, ϕ) for α = 90-deg

	$R/r = 2$	$R/r = 3$	$R/r = 6$	$R/r = 10$
$t/r = 0.0260$	(45, 20)	(57, 30)	(63, 30)	(66, 45)
$t/r = 0.0300$	(45, 30)	(57, 30)	(66, 45)	(66, 45)
$t/r = 0.0417$	(48, 30)	(60, 30)	(66, 45)	(66, 45)
$t/r = 0.0550$	(48, 30)	(63, 45)	(66, 45)	(66, 45)
$t/r = 0.0625$	(48, 30)	(63, 45)	(66, 45)	(69, 45)
$t/r = 0.0677$	(51, 30)	(63, 45)	(66, 45)	(69, 45)
$t/r = 0.0833$	(57, 45)	(63, 45)	(66, 45)	(69, 45)
$t/r = 0.0937$	(57, 45)	(63, 45)	(66, 45)	(69, 45)

Table 7A-5 Location of maximum stress (θ, ϕ) for α = 180-deg

	$R/r = 2$	$R/r = 3$	$R/r = 6$	$R/r = 10$
$t/r = 0.0260$	(153, 10)	(153, 30)	(153, 30)	(159, 45)
$t/r = 0.0300$	(153, 30)	(153, 30)	(153, 30)	(159, 45)
$t/r = 0.0417$	(153, 30)	(153, 30)	(153, 45)	(159, 45)
$t/r = 0.0550$	(153, 30)	(153, 30)	(153, 45)	(159, 45)
$t/r = 0.0625$	(156, 45)	(153, 45)	(153, 45)	(159, 45)
$t/r = 0.0677$	(156, 45)	(153, 45)	(153, 45)	(159, 45)
$t/r = 0.0833$	(156, 45)	(153, 45)	(153, 45)	(159, 45)
$t/r = 0.0937$	(156, 45)	(153, 45)	(153, 45)	(159, 45)

CHAPTER 8

CONCLUSIONS AND RECOMMENDATIONS

Detailed non-linear elastic large deformation finite element analyses of the behaviour of pressurised piping elbows have been carried out. The main aim was to reassess the pressure reduction effect on flexibility and stress-intensification factors, but it was extended to obtain similar results for the ovalisation factor. The combined loading of internal pressure with separated in-plane closing moment, in-plane opening moment, and out-of-plane bending has been considered. Approximate formulae for ovalisation, flexibility and stress-intensification factors have been obtained. Prior to develop approximate formulae for the pressure reduction effect, formulae for bending load only was first established.

8.1 Conclusions

Detailed finite element study carried out in Chapter 4 shows that their structural behaviour is a conservative system (path-independent structure). Accordingly, the order of the bending and internal pressure is applied does not affect the final results for stresses and deformations.

The following concluding remarks apply for unpressurised conditions:

(1) The general behaviour of piping elbows depends on its geometry: bend angle α, thickness to cross-section radius ratio, t/r, radius ratio, R/r, and pipe bend parameter, λ.

(2) The behaviour of a pipe elbow under in-plane bending in term of ovalisation is different between closing and opening mode. Ovalisation factor for closing mode can be expressed in a power law, while ovalisation factor for opening mode can be expressed in an exponential law. Overall, the ovalisation factor under closing mode is bigger than under opening mode for low pipe bend parameters, but become level for high pipe bend parameter.

(3) For in-plane closing bending, the ovalisation factor is directly proportional to the bend angle for short-radius pipe elbows. For long radius pipe elbows, the ovalisation factor is directly proportional to the bend angle only for bend angle less than 90-deg.

(4) For in-plane opening bending, the ovalisation factor is directly proportional to the bend angle for short radius. For long radius pipe elbows, the ovalisation factor is directly proportional to the bend angle for 90-deg bend angle and smaller.

(5) Flexibility factors can be expressed as the asymptotic solution of Clark and Reissner [20] multiplied by a factor obtained from a linear equation in logarithm of pipe bend parameter, λ for each radius ratio, R/r.

(6) Flexibility factor for in-plane closing bending obtained from the present analysis is bigger than the ASME code [120] for bend angle of 45-deg and greater. It is expected that the difference result from the large deformation effects.

(7) Flexibility factor under in-plane bending is directly proportional to the bend angles regardless the magnitude of radius ratio. Flexibility factor for out-of-plane bending is not directly proportional to the bend angle. The reason for this is that the pure bending assumption can not be applied for this case. If the bending load is applied such that one end of the bend is subjected to pure bending, the other end of the bend is subjected to bending and torsion, in which the amount of bending and torsion at this end being strongly depends on the bend angle. For 90-deg pipe bend, this end is subjected to pure torsion, while for 180-deg bend, this end is subjected to pure bending. However, for bend angle less than 60-deg (probably less than 90-deg), the flexibility factor is directly proportional to bend angle. Overall, the flexibility factor under in-plane bending is bigger than under out-of-plane bending. For in-plane bending, flexibility factor under closing mode is bigger than under opening mode bending.

(8) The maximum stress at the outer and inner surfaces are opposite in sign, but different in magnitude. This fact violates the in-extensibility assumption adopted in many theoretical developments.

(9) For in-plane bending, the maximum stress was located at crown for 180 and 90-deg elbows and moves progressively toward the intrados as the bend angle becomes smaller

(10) For out-of-plane bending, the location of maximum stress in the longitudinal direction is at the mid-section for small bend angle and between the mid-section and the junction with the loaded tangent for large bend angle. The location of maximum stress in the circumferential direction is generally at 45-deg from the crown toward the intrados, except for short radius, thin-walled, large angle bend.

(11) Stress-intensification factor under in-plane bending is bigger than under out-of-plane bending. For in-plane bending, stress-intensification factor under closing mode is bigger than under opening mode.

Of course, the reader will now be all too aware that a simple piping elbow under straightforward loading exhibits very complex stress and deformation behaviour: the preceding represents only a summary of the main features.

Finally, the following concluding remarks apply for pressurised conditions:

(1) The effect of internal pressure on ovalisation is different for in-plane closing and opening bending perhaps as expected, but not quantified previously in the literature. For closing mode, there are limitations for value of r/t where the formulae developed can be applied. If the value of r/t below certain limit, the effect of internal pressure is no longer reduce the ovalisation, but increase the ovalisation. As a result, the corresponding formulae need to be modified.

(2) For in-plane bending, the effect of internal pressure on flexibility is the opposite of the preceding conclusion. Internal pressure reduces the flexibility for closing bending for all pipe bend parameters. For opening mode, internal pressure reduces the flexibility for thin-walled pipe but increases the flexibility for thick-walled pipe. Again, the formulae for the pressure reduction on flexibility factor

need to be modified for opening bending. For out-of-plane bending, internal pressure always reduces the flexibility factor.

(3) For both in-plane and out-of-plane bending, internal pressure always reduces the stress-intensification factor for thin and thick-walled pipe.

(4) The effect of internal pressure on flexibility and stress-intensification is more pronounced for smaller wall thickness

8.2 Recommendations for Design Formulae

The approximate formulae proposed for design purposes are summarised for convenience in Appendix A for unpressurised conditions and in Appendix B for pressurised conditions. It is clear that the structural behaviour of piping elbows is completely different for in-plane and out-of-plane bending. In addition, the behaviour of piping elbows under in-plane bending are different under closing and opening mode.

The formulae given in the Appendices are recommended for using in piping design as an alternative to the current piping code [120]. It can be seen from the Appendix for unpressurised conditions that the flexibility factor under in-plane closing bending for 90-deg bend and larger is very close to the current ASME Code for long-radius bends. This fact validated the assumption involved in most theoretical development that the radius of the bend is much bigger than the radius of pipe cross-section. Formulae for various bend angle and radius ratio developed in this study show that different formulae should be used for different bend angle, radius ratio, and direction of bending load.

Design formulae for pressurised conditions summarised in Appendix B are further recommended for design purposes. For the flexibility factor, the magnitude of the pressure reduction used in the ASME code [120] is significantly smaller than the proposed formula developed in this study. However, if the ASME formula is applied for in-plane opening bending and out-of-plane bending, the pressure reduction is

much bigger than the proposed formulae. It is clear that different formulae for pressure reduction on flexibility should also be used for different bend angle and direction of bending load.

The formula in the ASME code for pressure reduction on stress-intensification is considerably smaller than the present analysis for in-plane closing bending and out-of-plane bending. However, if the ASME code is applied to in-plane opening bending, it overestimates the pressure reduction obtained from the present analysis. It is again recommend that different formulae for pressure reduction on stress-intensification should be used for different bend angle and direction of bending load.

8.3 Recommendations for Further Study

The work and analysis conducted in this study has identified several areas where further research might be required:

(1) A further parameter survey for other large bend angle (120 and 150-deg) to refine the formulae obtained from the present analysis in order to further simplify the formula for the pressure reduction effect in term of bend angle.

(2) A study to obtain the end rotation for in-plane bending from the axial displacement of all nodes at the bend-straight pipe junction rather than from the axial displacement of only extrados and intrados node at that cross-section.

(3) A review of the concept of end rotation to define the flexibility of a pipe bend subjected to out-of-plane bending. The concept of end rotation is more suitable for in-plane bending where the pure bending assumption can be tolerated. For out-of-plane bending, the pure bending assumption is not truly applicable for out-of-plane bending. The concept of strain energy might be applied as alternative

REFERENCES

[1] **Bantlin, A.** – 1910: Formanderung und Beanspruchung Federnder Ausgleichrohren. *Zeitschrift des Vereines deutscher Ingenieure, Vol. 54, 43 – 49.*

[2] **Von Karman, Th.** – 1911: Ueber die Formanderung dunnwandiger Rohre, insbesondere federnder Ausgleichrohre. *Zeitschrift des Vereines deutscher Ingenieure, Vol. 55, Part 2, pp. 1889 – 95.*

[3] **Crocker, S.**, and **Sanford, S. S.** – 1922: The Elasticity of Pipe Bends. *Transactions of the ASME, Vol. 44, Paper No. 1860, pp. 547 – 98.*

[4] **Hovgaard, W.** – 1926/27: The Elastic Deformation of Pipe Bends. *Journal of Mathematics and Physics, Massachusetts Institute of Technology, Vol. 6(2), pp. 69 – 118.*

[5] **Hovgaard, W.** – 1927/28(a): Deformation of Plane Pipes. *Journal of Mathematics and Physics, Massachusetts Institute of Technology, Vol. 7(3), pp. 198 – 238.*

[6] **Hovgaard, W.** – 1927/28(b): Further Research on Pipe Bends. *Journal of Mathematics and Physics, Massachusetts Institute of Technology, Vol. 7(4), pp. 239 – 97.*

[7] **Wahl, A. M.** – 1927/28: Stresses and Reactions in Expansions Pipe Bends. *Transactions of the ASME, Vol. 49/50, paper FSP-50-49, pp. 241 – 62.*

[8] **Shipman, W. H.** – 1929: Design of Steam Piping to Care for Expansion. *Transactions of the ASME, Vol. 51, paper FSP-51-52, pp. 415 – 46.*

[9] **Cope, E. T.**, and **Wert, E. A.** – 1932: Load Deflection Relation for Large, Plain Corrugated, and Creased Pipe Bends. *Transactions of the ASME, Vol. 54, paper FSP-54-12, pp. 115 – 59.*

[10] **Hovgaard, W.** – 1935: Stresses in Three-Dimensional Pipe Bends. *Transactions of the ASME, Vol. 57, paper FSP-57-12, pp. 401 – 15.*

[11] **Haigh, B. P.** – 1936: An Estimate of the Stresses Induces in a Tube that is not Initially Quite Circular. *Proceeding of the Institution of Mechanical Engineers, Vol. 133, pp. 96 – 98.*

[12] **Dean, W. R.** – 1939: The Distortion of Curved Tube Due to Internal Pressure. *Philosophical Magazine, Vol.28, pp. 452 – 64.*

[13] **Vigness, I.** – 1943: Elastic Properties of Curved Tubes. *Transactions of the ASME, Vol.65, pp.105 – 20.*

[14] **Beskin, L.** – 1945: Bending of Curved Thin Tubes. *Transaction of the ASME, Vol. 67, pp. A1 – 7.*

[15] **Symonds, P. S.**, and **Vigness, I.** – 1946: Discussion to Beskin's Paper. *Transaction of the ASME, Vol. 68, pp. A66 – 67.*

[16] **Wolf, A.** – 1946: An Elementary Theory of the Bourdon Gage. *Transaction of the ASME, Vol. 68, pp. A207 – 10.*

[17] **Markl, A. R. C.** – 1947: Fatigue Test of Welding Elbows and Comparable Double-Mitre Bends. *Transactions of the ASME, Vol. 69, pp. 869 – 79.*

[18] **Huber, M. T.** – 1948: The Bending of Curved Tube of Elliptic Cross-Section. *Proceeding of the 7th International Congress for Applied Mechanics, Vol. 1, pp. 322 – 28.*

[19] **Reissner, E.** – 1949: On Bending of Curved Thin-Walled Tubes. *Proceeding of the National Academy of Science, USA, Vol. 35, pp. 204 – 08.*

[20] **Clark, R. A.**, and **Reissner, E.** – 1951: Bending of Curved Tubes. In *Advances in Applied Mechanics, Vol. II, pp. 93 – 122, edited by Richard von Mises and Theodore von Karman, Academic Press Inc.*

[21] **Pardue, T. E.**, and **Vigness, I.** – 1951: Properties of Thin-Walled Curved Tubes of Short-Bend Radius. *Transaction of the ASME, Vol. 73, pp. 77 – 87.*

[22] **Clark, R. A., Gilroy, T. I.**, and **Reissner, E.** – 1952: Stresses and Deformations of Toroidal Shells of Elliptical Cross-section. *Transaction of the ASME, Journal of Applied Mechanics, Vol. 19(1), pp. 37 – 48.*

[23] **Markl, A. R. C.** – 1952: Fatigue Tests of Piping Components. *Transaction of the ASME, Vol. 74, pp. 287 – 303.*

[24] **Gross, N.** – 1952/53: Experiments on Short-radius Pipe Bends. *Proceedings of the Institution of Mechanical Engineers, Vol. 1B, pp. 465 – 79.*

[25] **Gross, N.**, and **Ford, H.** – 1952/53: The Flexibility of Short-radius Pipe Bends. *Proceedings of the Institution of Mechanical Engineers, Vol. 1B, pp. 480 – 91.*

[26] **Vissat, P. L.**, and **Del Buono, A. J.** – 1955: In-Plane Bending Properties of Welding Elbows. *Transactions of the ASME, Vol. 77, pp. 161 – 75.*

[27] **Crandall, S. H.**, and **Dahl, N. C.** – 1956: The Influence of Pressure on the Bending of Curved Tubes. *Proceeding of the 9th International Congress for Applied Mechanics, Brussels, pp. 101 – 11, ASME.*

[28] **Jennings, F. B.** – 1956: Theories of Bourdon Tubes. *Transaction of the ASME, Vol. 78, pp. 55 – 64.*

[29] **Kafka, P. G.**, and **Dunn, M. B.** – 1956: Stiffness of Curved Circular Tubes with Internal Pressure. *Transactions of the ASME, Journal of Applied Mechanics, Vol. 23, pp. 247 – 54.*

[30] **Rodabaugh, E. C.**, and **George, H. H.** – 1957: Effect of Internal Pressure on Flexibility and Stress-Intensification Factors of Curved Pipes or Welding Elbows. *Transactions of the ASME, Vol. 79, pp. 939 – 48.*

[31] **Turner, C. E.**, and **Ford, H.** – 1957: Examination of the Theories for Calculating the Stresses in Pipe Bends Subjected to In-Plane Bending. *Proceedings of the Institution of mechanical Engineers, Vol. 171, pp. 513 – 25.*

[32] **Timoshenko, S. P.** – 1958: Strength of Materials. *Part I, Chapter XII, 3rd edition, D. van Nostrand Co.*

[33] **Reissner, E.** – 1959: On Finite Bending of Pressurized Tubes. *Transaction of the ASME, Vol. 81, pp. 386 – 92.*

[34] **Jordan, P. F.** – 1962: Stresses and Deformations of the Thin-Walled Pressurized Torus. *Journal of Aerospace Science, Vol. 29, pp. 213 – 25.*

[35] **Findlay, G. E.**, and **Spence, J.** – 1966: In-Plane Bending of a Large 90^0 Smooth Bend. *Journal of Strain Analysis, Vol. 1(4), pp. 290 – 300.*

[36] **Jones, N.** – 1967: In-Plane Bending of a Short-Radius Curved Pipe Bend. *Transaction of the ASME, Journal of Engineering for Industry, Vol. 89(B)(2), pp. 271 – 77.*

[37] **Smith, R. T.** – 1967: Theoretical Analysis of the Stresses in Pipe Bends Subjected to Out-of-Plane Bending. *Journal of Mechanical Engineering Science, Vol. 9(2), pp. 115 – 23.*

[38] **Smith, R. T.**, and **Ford, H.** – 1967: Experiments on Pipelines and Pipe Bends Subjected to Three-Dimensional Loading. *Journal of Mechanical Engineering Science, Vol. 9(2), pp. 124 – 37.*

[39] **British ESDU No. 68048** – 1968: Straight Pipe Under Internal Pressure: Effect of Initial Non-circularity on Maximum Stress.

[40] **Cheng, D. H.**, and **Thailer, H. J.** – 1968: In-Plane Bending of Curved Circular Tubes. *Transaction of the ASME, Journal of Engineering for Industry, Vol. 90(B)(4), pp. 666 – 70.*

[41] **Cheng, D. H.**, and **Thailer, H. J.** – 1970: On Bending of Curved Circular Tubes. *Transaction of the ASME, Journal of Engineering for Industry, Vol. 92(B)(1), pp. 62 – 66.*

[42] **Kitching, R.** – 1970: Smooth and Mitred Pipe Bends. In *The Stress Analysis of Pressure Vessels and Pressure Vessel Components, Chapter 7, edited by S. S. Gill, Pergamon Press Ltd.*

[43] **Spence, J.** – 1970: On the Bounding of Pipe Bend Flexibility Factors. *Nuclear Engineering and Design, Vol. 12, pp. 39 – 47, North-Holland Publishing Company, Amsterdam.*

[44] **Thailer, H. J.**, and **Cheng, D. H.** – 1970: In-Plane Bending of a U-Shaped Circular Tube with End Constraints. *Transaction of the ASME, Journal of Engineering for Industry, Vol. 92(B)(4), pp.792 – 96.*

[45] **Findlay, G. E.**, and **Spence, J.** – 1971: Bending of Pipe Bends with Elliptic Cross Section. *Welding Research Council Bulletin No. 164.*

[46] **Sutcliffe, W. J.** – 1971: Stress Analysis of Toroidal Shells of Elliptical Cross-Section. . *International Journal of Mechanical Science, Vol. 13(11), pp. 951 – 58.*

[47] **Blomfield, J. A.**, and **Turner, C. E.** – 1972: Theory of Thin Elastic Shells Applied to Pipe Bends Subjected to Bending and Internal Pressure. *Journal of Strain Analysis, Vol. 7(4), pp. 285 – 93.*

[48] **Dodge, W. G.**, and **Moore, S. E.** – 1972: Stress Indices and Flexibility Factors for Moment Loading on Elbows and Curved Pipe. *WRC Bulletin No. 179.*

[49] **Findlay, G. E.**, and **Spence, J.** – 1973: The Effects of Flange on Smooth Pipe Bends in Piping Systems. *Transaction of the 2nd International Conference on Structural Mechanics in Reactor Technology, Paper F3/5, Germany, 10 – 14 September.*

[50] **Flügge, W.** – 1973: Stresses in Shells. *Second Edition, Springer – Verlag, Berlin.*

[51] **Imamasa, J.**, and **Uragami, K.** – 1973: Experimental Study of Flexibility Factors and Stresses of Welding Elbows with End Effects. *Proceedings of the 2nd International Conference on Pressure Vessels technology, San Antonio, USA, Part I-30, pp. 417 – 26.*

[52] **British ESDU No. 74043** – 1974: Flexibilities of and Stresses in Unrestrained Pressurised Thin Pipe Bends Subjected to In-Plane Bending.

[53] **Mello, R. M.**, and **Griffin, D. S.** – 1974: Plastic Collapse Loads for Pipe Elbows Using Inelastic Analysis. *Transaction of the ASME, Journal of Pressure Vessels Technology, Vol., 96(3), pp. 177 – 83.*

[54] **British ESDU No. 75014** – 1975: Flexibilities of and Stresses in Thin Pipe Bends under In-Plane Bending: Influence of Bend Angle and Tangent Pipe Ends.

[55] **Natarajan, R.**, and **Blomfield J. A.** – 1975: Stress Analysis of Curved Pipe with End Restraints. *Computers & Structures, Vol. 5(2/3), pp. 187 – 96.*

[56] **Vrillon, B., Montfort, C.**, and **Befre, J.** – 1975: Experimental Analysis on Piping Components of Fast Breeder Reactors. *Transaction of the 3rd International Conference on Structural Mechanics in Reactor Technology, Paper F3/4, London, UK, 1 – 5 September.*

[57] **Boyle, J. T.**, and **Spence, J.** – 1977: The Non-linear Analysis of Pressurized Curved Pipes. *Proceeding of the 3rd International Conference on Pressure Vessel Technology, Tokyo, pp. 121 – 31.*

[58] **Kano, T., et al** – 1977: Stress Distribution in an Elbow with Straight Pipes. *Transaction of the 4th International Conference on Structural Mechanics in Reactor Technology, Paper F1/5, San Francisco, California, USA, 15 – 19 August.*

[59] **Ohtsubo, H.**, and **Watanabe, O.** – 1977: Flexibility and Stress Factors of Pipe Bends - An Analysis by the Finite Ring Method. *Transaction of the ASME, Journal of Pressure Vessels Technology, Vol. 99(2), pp. 281 – 90.*

[60] **Sobel, L. H.** – 1977: In-Plane Bending of Elbows. *Computer and Structures, Vol. 7, pp. 701 – 15.*

[61] **Ohtsubo, H.**, and **Watanabe, O.** – 1978: Stresses Analysis of Pipe Bends by Ring Elements. *Transaction of the ASME, Journal of Pressure Vessels Technology, Vol. 100(1), pp. 112 – 22.*

[62] **Brouard, D., Tremblais, A.**, and **Vrillon, B.** – 1979: In-Plane and Out-of-Plane Bending Tests on Carbon Steel Pipe Bends. *Transaction of the 5th International Conference on Structural Mechanics in Reactor Technology, Paper F3/1, Berlin, Germany.*

[63] **Findlay, G. E.**, and **Spence, J.** – 1979(a): Flexibility of Smooth Circular Curved Tubes with Flanged End Constraints. *International Journal of Pressure Vessel and Piping, Vol. 7(1), pp.13 – 29.*

[64] **Findlay, G. E.**, and **Spence, J.** – 1979(b): Stress Analysis of Smooth Curved Tubes with Flanged End Constraints. *International Journal of Pressure Vessel and Piping, Vol. 7(2), pp.83 – 103.*

[65] **Kano, T., et al** – 1979: Detailed Analysis of Three Elbows – Pipe Assemblies for Typical Load Case. *Transaction of the 5th International Conference on Structural Mechanics in Reactor Technology, Paper F3/7, Berlin, Germany.*

[66] **Whatham, J. F.**, and **Thomson, J. J.** – 1979: The Bending and Pressurising of Pipe Bends with Flanged Tangents. *Nuclear Engineering and Design, Vol. 54, pp. 17 – 28.*

[67] **Boyle, J. T.**, and **Spence, J.** – 1980: A Simple Analysis for Oval, Pressurised Pipe Bends under External Bending. *Proceeding of the 4th International Conference on Pressure Vessels Technology, Vol. II, pp. 201 – 07.*

[68] **Dhalla, A. K.** – 1980: Plastic Collapse of Piping Elbow: Effects of Finite Element Convergence and Residual Stresses. *Proceeding of the 4th International Conference on Pressure Vessels Technology, Vol. II, pp. 243 – 49.*

[69] **Kwee, H. K.** – 1980: Stress Distribution and Flexibility of the Suction Bend of the Primary Sodium Pump-LMFBR-SNR 300. *International Journal of Pressure vessel and Piping, Vol. 8, pp. 357 – 76.*

[70] **Sobel, L. H.**, and **Newman, S. Z.** – 1980: Comparison of Experimental and Simplified Analytical Results for the In-Plane Plastic Bending and Buckling of an Elbow. *Transaction of the ASME, Journal of Pressure Vessels Technology, Vol. 102(4), pp. 400 – 09.*

[71] **Spence, J.**, and **Findlay, G. E.** – 1980: The Effect of Thickness Variations on the Behaviour of Smooth Curved Pipes under External Bending. *Transaction of the ASME, Journal of Pressure Vessels Technology, Vol. 102(1), pp. 45 – 48.*

[72] **Thomas, K.** – 1980: The Effect of Geometric Irregularities on the Design Analysis of Thin-Walled Piping Elbows. *Transaction of the ASME, Journal of Pressure Vessels Technology, Vol. 102(4), pp. 410 – 18.*

[73] **Thomson, G.** – 1980: The Influence of Ends Constraints on Pipe Bends. *PhD Thesis, University of Strathclyde, Glasgow, Scotland, UK.*

[74] **British ESDU No. 81041** – 1981: Flexibility of and Stresses in Thin Unpressurized Pipe Bends with Flanged Ends Under In-Plane Bending: Influence of Bend Angle.

[75] **Natarajan, R.**, and **Mirza, S.** – 1981: Stress Analysis of Curved Pipe with End Restraints Subjected to Out-of-Plane Moment. *Transaction of the 6th International Conference on Structural Mechanics in Reactor Technology, Paper F2/8.*

[76] **Thomson, G.**, and **Spence, J.** – 1981: The Influence of End Constraints on Smooth Pipe Bend. *Transaction of the 6th International Conference on Structural Mechanics in Reactor Technology, Paper F2/7.*

[77] **Rodabaugh, E. C.**, and **Moore, S. E.** – 1982: End Effects on Elbows Subjected to Moment Loadings. In *"Design Method for Piping Elbows Considering End Effects", ASME PVP Special Publication H00213.*

[78] **Thomas, K.** – 1982: Stiffening Effects on Thin-Walled Piping Elbows of Adjacent Piping and Nozzle Constraints. *Transaction of the ASME, Journal of pressure Vessel Technology, Vol. 104(3), pp. 180 – 87.*

[79] **Whatham, J. F.** – 1982: Analysis of Circular Pipe Bends with Flanged Ends. *Nuclear Engineering and Design, Vol. 72, pp. 175 – 87, North-Holland Publishing Company.*

[80] **Natarajan, R.**, and **Mirza, S.** – 1983: Effect of Internal Pressure on the Flexibility and Stresses in Pipe Elbows with End Constraints. *Transaction of the 7th International Conference on Structural Mechanics in Reactor Technology, Chicago, Paper G/F5/8, pp. 397 – 404.*

[81] **Thomson, G.**, and **Spence, J.** – 1983(a): Combined Pressure and In-Plane Bending on Pipe Bends with Flanges. *Transaction of the 7th International Conference on Structural Mechanics in Reactor Technology, Chicago, Paper F2/9,pp. 405 – 12.*

[82] **Thomson, J.**, and **Spence, J.** – 1983(b): The Influence of Flanged End Constraints on Smooth Curved Tubes under In-Plane Bending. *International Journal of Pressure Vessels and Piping, Vol. 13(2), pp. 65 – 83, Applied Science Publishers Ltd.*

[83] **Thomson, J.**, and **Spence, J.** – 1983(c): Maximum Stresses and Flexibility Factors of Smooth Pipe Bends with Tangent Pipe Terminations under In-Plane Bending. *Transaction of the ASME, Journal of Pressure Vessel Technology, Vol. 105(4), pp. 329 – 36.*

[84] **Natarajan, R.**, and **Mirza, S.** – 1984: Effect of Thickness Variation on Stress Analysis of Piping Elbows under Internal Pressure. *Computers and Structures, Vol.18(5), pp. 767 – 78.*

[85] **Spence, J.**, and **Thomson, G.** – 1984: Flanged Pipe Bends under Combined Pressure and In-Plane Bending. *Proceedings of the 5th International Conference on Pressure Vessel Technology, San Francisco.*

[86] **Thomson, G.**, and **Spence, J.** – 1984: A Survey of End Constraints in Piping Elbows. *Proceeding of the 3rd Simposio Brasileiro Sobre Tubulacoes e Vasos de Pressao, Salvador, 29 – 31 October, pp. 33 – 55.*

[87] **Natarajan, R.**, and **Mirza, S.** – 1985: Effect of Internal Pressure on Flexibility Factors in Pipe Elbows with End Constraints. *Transaction of the ASME, Journal of Pressure Vessel Technology, Vol. 107(1), pp.60 – 63.*

[88] **Hubner, W.** – 1986: Curved Tubes with Flanges under Bending. *Applied Solid Mechanics-1, pp. 255 – 73, edited by A. S. Tooth and J. Spence, Elsevier Applied Science Publication, London.*

[89] **Sobel, L. H.**, and **Newman, S. Z.** – 1986: Simplified, Detailed, and Isochronous Analysis and Test Results for the In-Plane Elastic-Plastic and Creep Behaviour of an Elbow. *Transaction of the ASME, Journal of Pressure Vessel Technology, Vol. 108(3), pp. 297 – 304.*

[90] **Dhalla, A. K.** – 1987: Collapse Characteristic of a Thin-Walled Elbow: Validation of an Analytical Procedure. *Transaction of the ASME, Journal of Pressure Vessel Technology, Vol. 109(4), pp. 394 – 401.*

[91] **Calladine, C. R.** – 1988: Curved Tubes and Pipe Bends. In *Theory of Shell Structures, Chapter 13, Cambridge University press.*

[92] **Fujimoto, T.**, and **Soh, T.** – 1988: Flexibility Factors and Stress Indices for Piping Components with D/T ≥ 100 Subjected to In-Plane or Out-of-Plane Moment. *Transaction of the ASME, Journal of Pressure Vessel Technology, Vol. 110(4), pp. 374 – 86.*

[93] **Glickstein, A. B.**, and **Schmitz, L. M.** – 1989: A Study of Flexibility Factors Associated with Closely Spaced Thin-walled Elbows. In *"Design and Analysis of Piping Components", ASME PVP-Vol. 169, pp. 1 – 9.*

[94] **Suzuki, N.**, and **Nasu, M.** – 1989: Non-linear Analysis of Welded Elbows Subjected to In-Plane Bending. *Computers & Structures, Vol. 32(3/4), pp. 871 – 81, Maxwell Pergamon Macmillan plc.*

[95] **Natarajan, R.** – 1990: Analysis of Flexibility and Stress Intensification Factors in 90-deg Bends with End Restraints. *ASME-PVP-Vol.188: Design and Analysis of Piping and Components, edited by Q. N. Truong et al.*

[96] **Glickstein, A. B.**, and **Schmitz, L. M.** – 1991: Stress Factors Associated with Closely Spaced Thin-walled Elbows. In *"Piping Components Analysis", ASME PVP-Vol. 218, pp. 81 – 87.*

[97] **Kitching, R.**, and **Hose, D. R.** – 1992: The Influence of the Variation in Wall Thickness of Glass Fibre Reinforced Plastic Pipe Bends Subjected to In-Plane Bending. *Journal of Strain Analysis, Vol. 27(2), pp. 113 – 21, Institution of Mechanical Engineers.*

[98] **BS 806** – 1993: Specification for Design and Construction of Ferrous Piping Installations for and in Connection with Land Boilers.

[99] **Hose, D. R.**, and **Kitching, R.** – 1993: Behaviour of GRP Smooth Pipe Bends with Tangent Pipes under Flexure or Pressure Loads: A Comparison of Analyses by Conventional and Finite Element Techniques. *International Journal of Mechanical Science, Vol. 35(7), pp. 549 – 75.*

[100] **Cook, R. D.** – 1995: Finite Element Modelling for Stress Analysis. *John Wiley & Sons, Inc., New York.*

[101] **Weib, E., Lietzmann, A.,** and **Rudolph, J.** – 1996: Linear and Non-linear Finite Element Analysis of Pipe Bends. *International Journal of Pressure Vessel and Piping, Vol. 67(2), pp. 211 – 17, Elsevier.*

[102] **Orinyak, I. V.** – 1997: Calculation of the Ultimate Plastic State of Thick-Walled Pipe Bend in the Circumferential Direction. *International Journal of Pressure Vessel and Piping, Vol. 73(3), pp. 229 – 39.*

[103] **ASME BPV Code** – 1998: ASME Boiler and Pressure Vessel Code, Section III, Division 1.

[104] **Matzen, V. C.,** and **Yu, L.** – 1998: Elbow Stress Indices using Finite Element Analysis. *Nuclear Engineering and Design, Vol. 181, pp. 257 – 65, Elsevier.*

[105] **Shalaby, M. A.,** and **Younan, M. Y. A.** – 1998: Non-linear Analysis and Plastic Deformation of Pipe Elbows Subjected to In-Plane Bending. *International Journal of Pressure Vessel and Piping, Vol. 75(8), pp. 603 – 11, Elsevier.*

[106] **Shalaby, M. A.,** and **Younan, M. Y. A.** – 1998: Limit Loads for Pipe Elbows with Internal Pressure under In-Plane Closing Bending Moments. *Transaction of the ASME, Journal of Pressure Vessel Technology, Vol. 120(1), pp. 35 – 42.*

[107] **Liu, T., et al.** – 1999: Stress Indices for Feeder Pipe Bends Based on Finite Element Analysis. *ASME-PVP-Vol.388, Fracture, Design Analysis of Pressure Vessels, Heat Exchangers, Piping Components, and Fitness for Service.*

[108] **Shalaby, M. A.,** and **Younan, M. Y. A.** – 1999: Limit Loads for Pipe Elbows Subjected to In-Plane Opening Moment and Internal Pressure. *Transaction of the ASME, Journal of Pressure Vessel Technology, Vol. 121(1), pp. 17 – 23.*

[109] **Yu, L.,** and **Matzen, V. C.** – 1999: B_2 Stress Index for Elbow Analysis. *Nuclear Engineering and Design, Vol. 192, pp. 261 – 70, Elsevier.*

[110] **ANSYS 5.6** – 2000: *Swanson Analysis System.*

[111] **Chattopadhyai, J., et al.** – 2000: Closed-Form Collapse Moment Equations of Elbows Under Combined Internal Pressure and In-Plane Bending Moment. *Transaction of the ASME, Journal of Pressure Vessel Technology, Vol. 122(4), pp. 431 – 36.*

[112] **Ohtaki, S.** – 2000: FEM Analysis of Pipe Bends Subjected to Out-of-Plane Bending. *European Congress on Computational Methods in Applied Science and Engineering, Barcelona, 11 – 14 September.*

[113] **ANSYS 5.7** – 2001: *Swanson Analysis System.*

[114] **ASME B31.1** – 2001: Power Piping. *ASME Code for Pressure Piping.*

[115] **Boyle, J. T.** - 2001: Design and Analysis of Piping Systems. *A Short Course, University of Strathclyde, Glasgow.*

[116] **Cherniy, V. P.** – 2001: Effect of Curved Bar Properties on Bending of Curved Pipes. *Transaction of the ASME, Journal of Applied Mechanics, Vol. 68(4), pp.650 – 55.*

[117] **Kumar, R.**, and **Saleem, M. A.** – 2001: Bend Angle Effect on B_2 and C_2 Stress Indices for Piping Elbows. *Transaction of the ASME, Journal of Pressure Vessel Technology, Vol. 123(2), pp. 226 – 31.*

[118] **Mourad, H. M.**, and **Younan, M. Y. A.** – 2001: Non-linear Analysis of Pipe Bends Subjected to Out-of-Plane Moment Loading and Internal Pressure. *Transaction of the ASME, Journal of Pressure Vessel Technology, Vol. 123(2), pp. 253 – 58.*

[119] **ANSYS 6.1** – 2002: *Swanson Analysis System.*

[120] **ASME B31.3** – 2002: Process Piping. *ASME Code for Pressure Piping.*

[121] **Chattopadhyai, J. – 2002**: The Effect of Internal Pressure on In-Plane Collapse Moment of Elbows. *Nuclear Engineering and Design, Vol. 212(1-3), pp. 133 – 44.*

[122] **Kumar, R.**, and **Saleem, M. A.** – 2002: B_2 and C_2 Stress Indices for Large-Angle Bends. *Transaction of the ASME, Journal of Pressure Vessel Technology, Vol. 124(2), pp. 177 – 86.*

[123] **Mourad, H. M.**, and **Younan, M. Y. A.** – 2002: Limit Load Analysis of Pipe Bends under Out-of-Plane Moment Loading and Internal Pressure. *Transaction of the ASME, Journal of Pressure Vessel Technology, Vol. 124(1), pp. 32 – 37.*

[124] **Orynyak, I. V.** – 2002: First Approximation to Elastic Analysis of End-Effects in Pipe Bends. *International Journal of Pressure Vessels and Piping, Vol. 79(2), pp. 157 – 64.*

[125] **Tan, Y.**, and **Matzen, V.C.** – 2002: Correlation of In-Plane Bending Test and FEA Results for Thin-Walled Elbows. *Nuclear Engineering and Design, Vol. 217(1), pp. 21 – 39.*

[126] **Tan, Y.**, **Wilkins, K.**, and **Matzen, V.C.** – 2002: Correlation of Test and FEA Results for Elbows Subjected to Out-of-Plane Loading. *Nuclear Engineering and Design, Vol. 217(3), pp. 213 – 24.*

[127] **Cherniy, V. P.** – 2003: The Bending of Curved Pipes with Variable Wall Thickness. *Transaction of the ASME, Journal of Applied Mechanics, Vol. 70(2), pp. 253 – 59.*

APPENDIX G:

DESIGN FORMULAE FOR UNPRESSURISED CONDITIONS

This appendix summarises approximate formulae and Tables for ovalisation, flexibility, and stress-intensification factors for bending load. The approximate formulae for the pressure reduction effect are given in Appendix H.

Continue to the next pages...→

(1) Ovalisation factor for in-plane closing bending

$$\xi = \frac{0.565}{\lambda^{2/3}}[a + b\ln(\lambda)] \qquad \text{in - plane closing bending} \qquad \text{(G - 1)}$$

Table G1-a Value of coeffecient "*a*" in equation (G-1) for in-plane closing bending

R/r	Bend angle				
	30-deg	45-deg	60-deg	90-deg	180-deg
2	0.4434	0.6346	0.7722	0.9501	1.1437
3	0.5395	0.7603	0.9193	1.1179	1.2303
4	0.6006	0.8293	0.9936	1.1430	1.2145
5	0.6577	0.8922	1.0509	1.1651	1.1801
6	0.6897	0.9050	1.1024	1.1781	1.1247
7	0.7235	0.9279	1.1187	1.1907	1.0705
8	0.7528	0.9454	1.1096	1.1542	1.0362
9	0.7787	0.9593	1.0751	1.0915	1.0074
10	0.7968	0.9554	1.0115	0.9996	0.9669

Table G1-b Values of coefficient "*b*" in equation (G-1) for in-plane closing bending

R/r	Bend angle				
	30-deg	45-deg	60-deg	90-deg	180-deg
2	0.0543	0.0954	0.1266	0.1682	0.2156
3	0.0686	0.1219	0.1635	0.2177	0.2463
4	0.0756	0.1356	0.1802	0.2251	0.2352
5	0.0800	0.1414	0.1866	0.2161	0.2182
6	0.0816	0.1418	0.1812	0.1966	0.1806
7	0.0792	0.1326	0.1625	0.1705	0.1599
8	0.0732	0.1152	0.1310	0.1261	0.1196
9	0.0636	0.0896	0.0867	0.0673	0.0703
10	0.0526	0.0539	0.0324	0.0001	0.0151

(2) Ovalisation factor for in-plane opening bending

$$\xi = 1.656\exp(-1.175\lambda)(a - b\lambda) \qquad \text{in - plane openng bending} \qquad (G-2)$$

Table G2-a Value of coeffecient "*a*" in equation (G-2) for in-plane opening bending

R/r	Bend angle				
	30-deg	**45-deg**	**60-deg**	**90-deg**	**180-deg**
2	0.7216	0.8675	0.9507	1.0393	1.1102
3	0.7194	0.8624	0.9421	1.0254	1.0557
4	0.7172	0.8602	0.9406	1.0244	1.0280
5	0.7140	0.8580	0.9414	1.0242	1.0035
6	0.7108	0.8561	0.9425	1.0239	0.9882
7	0.7076	0.8547	0.9435	1.0147	0.9676
8	0.7044	0.8533	0.9445	1.0105	0.9538
9	0.7012	0.8522	0.9453	1.0062	0.9417
10	0.6954	0.8513	0.9469	1.0000	0.9291

Table G2-b Values of coefficient "*b*" in equation (G-2) for in-plane opening bending

R/r	Bend angle				
	30-deg	**45-deg**	**60-deg**	**90-deg**	**180-deg**
2	1.5307	1.4318	1.2443	0.9026	0.4071
3	0.8669	0.7529	0.5938	0.3452	0.1146
4	0.5185	0.4516	0.3747	0.1502	0.1075
5	0.3144	0.2582	0.2086	0.0535	0.0557
6	0.1998	0.1229	0.0644	0.0466	0.0553
7	0.0811	0.0372	0.0188	0.0068	-0.0034
8	0.0082	-0.0319	-0.0405	0.0024	-0.0219
9	-0.0485	-0.0856	-0.0866	0.0009	-0.0363
10	-0.1149	-0.1142	-0.1236	0.0002	-0.0431

(3) Flexibility factor for in-plane closing bending

$$k = \frac{1.65}{\lambda}[a - b\ln(\lambda)] \qquad \text{in - plane closing bending} \qquad \text{(G - 3)}$$

Table G3-a Value of coeffecient "*a*" in equation (G-3) for in-plane closing bending

R/r	Bend angle				
	30-deg	**45-deg**	**60-deg**	**90-deg**	**180-deg**
2	0.3340	0.5120	0.5237	0.6715	0.7090
3	0.4545	0.6110	0.6990	0.7800	0.8290
4	0.5659	0.6734	0.7659	0.8133	0.8692
5	0.6280	0.7380	0.8010	0.8551	0.8950
6	0.7097	0.7853	0.8453	0.8775	0.9090
7	0.7644	0.8325	0.8679	0.9183	0.9470
8	0.8118	0.8757	0.8850	0.9433	0.9607
9	0.8536	0.9157	0.8982	0.9654	0.9714
10	0.9028	0.9470	0.9130	0.9880	0.9990

Table G3-b Values of coefficient "*b*" in equation (G-3) for in-plane closing bending

R/r	Bend angle				
	30-deg	**45-deg**	**60-deg**	**90-deg**	**180-deg**
2	0.2142	0.1866	0.1911	0.1716	0.1812
3	0.2000	0.1744	0.1593	0.1485	0.1624
4	0.1707	0.1565	0.1520	0.1560	0.1499
5	0.1558	0.1486	0.1421	0.1450	0.1397
6	0.1177	0.1201	0.1240	0.1364	0.1278
7	0.0912	0.1019	0.1120	0.1230	0.1180
8	0.0647	0.0837	0.1012	0.1120	0.1089
9	0.0382	0.0655	0.0914	0.1010	0.1005
10	0.0074	0.0433	0.0820	0.0774	0.0901

(4) Flexibility factor for in-plane opening bending

$$k = \frac{1.65}{\lambda}[a - b\ln(\lambda)] \qquad \text{in - plane opening bending} \qquad \text{(G - 4)}$$

Table G4-a Value of coeffecient "*a*" in equation (G-4) for in-plane opening bending

R/r	Bend angle				
	30-deg	45-deg	60-deg	90-deg	180-deg
2	0.5483	0.8000	0.9438	1.0926	1.2190
3	0.6131	0.8140	0.9352	1.0580	1.1480
4	0.6797	0.8360	0.9268	1.0217	1.0931
5	0.7307	0.8566	0.9250	0.9980	1.0497
6	0.7690	0.8735	0.9280	0.9800	1.0215
7	0.8149	0.8993	0.9358	0.9770	1.0007
8	0.8509	0.9214	0.9484	0.9797	0.9951
9	0.8840	0.9440	0.9658	0.9912	1.0021
10	0.9220	0.9700	0.9900	1.0084	1.0266

Table G4-b Values of coefficient "*b*" in equation (G-4) for in-plane opening bending

R/r	Bend angle				
	30-deg	45-deg	60-deg	90-deg	180-deg
2	0.0961	0.0286	-0.0135	-0.0584	-0.0970
3	0.0865	0.0304	-0.0076	-0.0475	-0.0750
4	0.0613	0.0300	0.0009	-0.0261	-0.0466
5	0.0391	0.0247	0.0029	-0.0156	-0.0290
6	0.0305	0.0120	0.0020	-0.0077	-0.0144
7	-0.0053	0.0039	-0.0051	-0.0096	-0.0124
8	-0.0275	-0.0116	-0.0151	-0.0141	-0.0134
9	-0.0497	-0.0305	-0.0291	-0.0236	-0.0206
10	-0.0719	-0.0581	-0.0472	-0.0385	-0.0316

(5) Flexibility factor for out-of-plane bending

$$k = \frac{1.65}{\lambda}[a + b\ln(\lambda)] \qquad \text{out - of - plane bending} \qquad \text{(G - 5)}$$

Table G5-a Value of coeffecient "*a*" in equation (G-5) for out-of-plane bending

R/r	Bend angle				
	30-deg	**45-deg**	**60-deg**	**90-deg**	**180-deg**
2	0.8110	1.0880	1.2427	1.1760	0.4617
3	0.8650	1.1224	1.2618	1.1930	0.5860
4	0.9181	1.1440	1.2714	1.2039	0.6468
5	0.9570	1.1633	1.2772	1.2132	0.7037
6	0.9890	1.1850	1.2800	1.2180	0.7480
7	1.0187	1.1930	1.2840	1.2272	0.7894
8	1.0443	1.2050	1.2861	1.2328	0.8234
9	1.0674	1.2157	1.2877	1.2378	0.8535
10	1.0910	1.2322	1.2900	1.2440	0.8788

Table G5-b Values of coefficient "*b*" in equation (G-5) for out-of-plane bending

R/r	Bend angle				
	30-deg	**45-deg**	**60-deg**	**90-deg**	**180-deg**
2	0.1320	0.2001	0.2510	0.2520	0.0020
3	0.1603	0.2300	0.2800	0.2727	0.0346
4	0.1871	0.2404	0.2967	0.2904	0.0552
5	0.2143	0.2636	0.3179	0.3107	0.0818
6	0.2424	0.3000	0.3385	0.3341	0.1062
7	0.2687	0.3100	0.3603	0.3558	0.1350
8	0.2959	0.3332	0.3815	0.3807	0.1616
9	0.3231	0.3564	0.4027	0.4074	0.1882
10	0.3501	0.3880	0.4242	0.4348	0.2146

(6) Stress-intensification factor for in-plane closing bending

$$k = \frac{1.89}{\lambda^{2/3}}[a - b\ln(\lambda)] \qquad \text{in - plane closing bending} \qquad \text{(G - 6)}$$

Table G6-a Value of coeffecient "*a*" in equation (G-6) for in-plane closing bending

R/r	Bend angle				
	30-deg	**45-deg**	**60-deg**	**90-deg**	**180-deg**
2	0.2558	0.4175	0.5823	0.5617	0.7706
3	0.3932	0.5748	0.7312	0.7715	0.8953
4	0.4866	0.6576	0.7897	0.8617	0.9126
5	0.5476	0.7318	0.8287	0.9241	0.9087
6	0.6032	0.7620	0.8547	0.9342	0.8944
7	0.6414	0.7948	0.8733	0.9150	0.8826
8	0.6716	0.8203	0.8872	0.9019	0.8723
9	0.6961	0.8407	0.8980	0.9018	0.8633
10	0.7215	0.8410	0.9067	0.8785	0.8537

Table G6-b Values of coefficient "*b*" in equation (G-6) for in-plane closing bending

R/r	Bend angle				
	30-deg	**45-deg**	**60-deg**	**90-deg**	**180-deg**
2	0.1333	0.1637	0.1540	0.2092	0.2145
3	0.1256	0.1437	0.1276	0.1650	0.1674
4	0.1218	0.1298	0.1106	0.1550	0.1508
5	0.1180	0.1210	0.1010	0.1500	0.1427
6	0.1158	0.1128	0.0952	0.1390	0.1440
7	0.1137	0.1103	0.0977	0.1516	0.1501
8	0.1118	0.1118	0.1070	0.1656	0.1607
9	0.1102	0.1173	0.1231	0.1884	0.1636
10	0.1092	0.1311	0.1501	0.2054	0.1711

(7) Stress-intensification factor for in-plane opening bending

$$k = \frac{1.89}{\lambda^{2/3}}[a - b\ln(\lambda)] \qquad \text{in - plane opening bending} \qquad \text{(G - 7)}$$

Table G7-a Value of coeffecient "*a*" in equation (G-7) for in-plane opening bending

R/r	**Bend angle**				
	30-deg	**45-deg**	**60-deg**	**90-deg**	**180-deg**
2	0.4320	0.7277	0.9776	1.2553	1.4185
3	0.5314	0.7992	1.0033	1.1992	1.3031
4	0.6005	0.8266	1.0045	1.1541	1.1765
5	0.6422	0.8452	1.0017	1.1085	1.1033
6	0.6685	0.8692	0.9931	1.0606	1.0413
7	0.6934	0.8666	0.9861	1.0227	1.0014
8	0.7102	0.8733	0.9699	0.9823	0.9636
9	0.7236	0.8785	0.9481	0.9435	0.9314
10	0.7400	0.8826	0.9217	0.9078	0.9029

Table G7-b Values of coefficient "*b*" in equation (G-7) for in-plane opening bending

R/r	**Bend angle**				
	30-deg	**45-deg**	**60-deg**	**90-deg**	**180-deg**
2	0.0380	-0.0052	-0.0616	-0.1259	-0.1389
3	0.0283	-0.0140	-0.0638	-0.1062	-0.1182
4	0.0246	-0.0166	-0.0627	-0.0802	-0.0896
5	0.0220	-0.0181	-0.0573	-0.0555	-0.0651
6	0.0203	-0.0155	-0.0476	-0.0355	-0.0330
7	0.0191	-0.0139	-0.0345	-0.0061	-0.0161
8	0.0182	-0.0082	-0.0171	0.0186	0.0084
9	0.0175	-0.0001	0.0043	0.0433	0.0329
10	0.0169	0.0129	0.0309	0.0706	0.0539

(8) Stress-intensification factor for out-of-plane bending

$$k = \frac{1.89}{\lambda^{2/3}}[a + b\ln(\lambda)] \qquad \text{out - of - plane bending} \qquad \text{(G - 8)}$$

Table G8-a Value of coeffecient "*a*" in equation (G-8) for out-of-plane bending

R/r	**Bend angle**				
	30-deg	**45-deg**	**60-deg**	**90-deg**	**180-deg**
2	0.4749	0.5725	0.6331	0.6726	0.7468
3	0.5473	0.6564	0.7074	0.7818	0.7964
4	0.5965	0.7227	0.7707	0.8229	0.8159
5	0.6343	0.7578	0.8168	0.8297	0.8352
6	0.6793	0.8096	0.8494	0.8509	0.8461
7	0.6913	0.8100	0.8622	0.8276	0.8486
8	0.7140	0.8136	0.8615	0.8248	0.8427
9	0.7339	0.8244	0.8452	0.8219	0.8284
10	0.7424	0.8332	0.8167	0.8065	0.8081

Table G8-b Values of coefficient "*b*" in equation (G-8) for out-of-plane bending

R/r	**Bend angle**				
	30-deg	**45-deg**	**60-deg**	**90-deg**	**180-deg**
2	-0.0031	-0.0217	-0.0163	0.0236	0.0143
3	0.0038	-0.0049	0.0001	0.0573	0.0239
4	0.0103	0.0239	0.0335	0.0650	0.0353
5	0.0145	0.0390	0.0491	0.0648	0.0403
6	0.0176	0.0493	0.0620	0.0610	0.0404
7	0.0175	0.0494	0.0551	0.0554	0.0383
8	0.0163	0.0447	0.0455	0.0408	0.0313
9	0.0133	0.0334	0.0275	0.0196	0.0203
10	0.0099	0.0114	0.0041	-0.0029	0.0005

APPENDIX H:

DESIGN FORMULA FOR PRESSURISED CONDITIONS

This appendix tabulated approximate formulae for pressure reduction for ovalisation, flexibility, and stress-intensification factors.

Continue to the next pages...→

Table H1.1 Ovalisation factor

α, deg	In-plane closing bending	In-plane opening bending	Out-of-plane bending
30	$\xi_p = \frac{\xi}{1 \pm 0.405 \left(\frac{p}{E}\right)\left(\frac{r}{t}\right)^{10/3}\left(\frac{R}{r}\right)^{0.165}}$	$\xi_p = \frac{\xi}{1 + 175 \left(\frac{r}{t}\right)^{5/3}\left(\frac{R}{r}\right)^{0.206}}$	
45	$\xi_p = \frac{\xi}{1 \pm 0.305 \left(\frac{p}{E}\right)\left(\frac{r}{t}\right)^{10/3}\left(\frac{R}{r}\right)^{0.275}}$	$\xi_p = \frac{\xi}{1 + 126 \left(\frac{p}{E}\right)\left(\frac{r}{t}\right)^{5/3}\left(\frac{R}{r}\right)^{0.333}}$	
60	$\xi_p = \frac{\xi}{1 \pm 0.255 \left(\frac{p}{E}\right)\left(\frac{r}{t}\right)^{10/3}\left(\frac{R}{r}\right)^{0.355}}$	$\xi_p = \frac{\xi}{1 + 100 \left(\frac{p}{E}\right)\left(\frac{r}{t}\right)^{5/3}\left(\frac{R}{r}\right)^{0.43}}$	
90	$\xi_p = \frac{\xi}{1 \pm 0.205 \left(\frac{p}{E}\right)\left(\frac{r}{t}\right)^{10/3}\left(\frac{R}{r}\right)^{0.464}}$	$\xi_p = \frac{\xi}{1 + 76 \left(\frac{p}{E}\right)\left(\frac{r}{t}\right)^{5/3}\left(\frac{R}{r}\right)^{0.57}}$	
180	$\xi_p = \frac{\xi}{1 \pm 0.155 \left(\frac{p}{E}\right)\left(\frac{r}{t}\right)^{10/3}\left(\frac{R}{r}\right)^{0.590}}$	$\xi_p = \frac{\xi}{1 + 52 \left(\frac{p}{E}\right)\left(\frac{r}{t}\right)^{5/3}\left(\frac{R}{r}\right)^{0.725}}$	

Table H1.2 Ovalisation factor (Continuied)

α, deg	In-plane closing bending	In-plane opening bending	Out-of-plane bending
30	$\xi_p = \dfrac{\xi}{1 \pm 0.110 \left(\dfrac{pr^3}{3D}\right)\left(\dfrac{1}{\lambda}\right)^{1/3}\left(\dfrac{R}{r}\right)^{0.53}}$	$\xi_p = \dfrac{\xi}{1 + 48.0 \left(\dfrac{pr^3}{3D}\right)\lambda^{4/3}\left(\dfrac{r}{R}\right)^{1.125}}$	
45	$\xi_p = \dfrac{\xi}{1 \pm 0.085 \left(\dfrac{pr^3}{3D}\right)\left(\dfrac{1}{\lambda}\right)^{1/3}\left(\dfrac{R}{r}\right)^{0.67}}$	$\xi_p = \dfrac{\xi}{1 + 34.5 \left(\dfrac{pr^3}{3D}\right)\lambda^{4/3}\left(\dfrac{r}{R}\right)^{1.005}}$	
60	$\xi_p = \dfrac{\xi}{1 \pm 0.070 \left(\dfrac{pr^3}{3D}\right)\left(\dfrac{1}{\lambda}\right)^{1/3}\left(\dfrac{R}{r}\right)^{0.765}}$	$\xi_p = \dfrac{\xi}{1 + 27.5 \left(\dfrac{pr^3}{3D}\right)\lambda^{4/3}\left(\dfrac{r}{R}\right)^{0.905}}$	
90	$\xi_p = \dfrac{\xi}{1 \pm 0.055 \left(\dfrac{pr^3}{3D}\right)\left(\dfrac{1}{\lambda}\right)^{1/3}\left(\dfrac{R}{r}\right)^{0.86}}$	$\xi_p = \dfrac{\xi}{1 + 21.0 \left(\dfrac{pr^3}{3D}\right)\lambda^{4/3}\left(\dfrac{r}{R}\right)^{0.765}}$	
180	$\xi_p = \dfrac{\xi}{1 \pm 0.045 \left(\dfrac{pr^3}{3D}\right)\left(\dfrac{1}{\lambda}\right)^{1/3}\left(\dfrac{R}{r}\right)^{0.97}}$	$\xi_p = \dfrac{\xi}{1 + 14.5 \left(\dfrac{pr^3}{3D}\right)\lambda^{4/3}\left(\dfrac{r}{R}\right)^{0.61}}$	

Table H2.1 Flexibility factor

α, deg	In-plane closing bending	In-plane opening bending	Out-of-plane bending
30	$k_p = \frac{k}{1+18.5\left(\frac{p}{E}\right)\left(\frac{r}{t}\right)^{9/4}\left(\frac{R}{r}\right)^{0.096}}$	$k_p = \frac{k}{1\pm 0.300\left(\frac{p}{E}\right)\left(\frac{r}{t}\right)^{10/3}\left(\frac{R}{r}\right)^{0.037}}$	$k_p = \frac{k}{1+0.385\left(\frac{p}{E}\right)\left(\frac{r}{t}\right)^{19/6}\left(\frac{R}{r}\right)^{0.033}}$
45	$k_p = \frac{k}{1+15.65\left(\frac{p}{E}\right)\left(\frac{r}{t}\right)^{9/4}\left(\frac{R}{r}\right)^{0.177}}$	$k_p = \frac{k}{1\pm 0.225\left(\frac{p}{E}\right)\left(\frac{r}{t}\right)^{10/3}\left(\frac{R}{r}\right)^{0.174}}$	$k_p = \frac{k}{1+0.295\left(\frac{p}{E}\right)\left(\frac{r}{t}\right)^{19/6}\left(\frac{R}{r}\right)^{0.149}}$
60	$k_p = \frac{k}{1+13.5\left(\frac{p}{E}\right)\left(\frac{r}{t}\right)^{9/4}\left(\frac{R}{r}\right)^{0.247}}$	$k_p = \frac{k}{1\pm 0.185\left(\frac{p}{E}\right)\left(\frac{r}{t}\right)^{10/3}\left(\frac{R}{r}\right)^{0.266}}$	$k_p = \frac{k}{1+0.225\left(\frac{p}{E}\right)\left(\frac{r}{t}\right)^{19/6}\left(\frac{R}{r}\right)^{0.244}}$
90	$k_p = \frac{k}{1+11.75\left(\frac{p}{E}\right)\left(\frac{r}{t}\right)^{9/4}\left(\frac{R}{r}\right)^{0.31}}$	$k_p = \frac{k}{1\pm 0.145\left(\frac{p}{E}\right)\left(\frac{r}{t}\right)^{10/3}\left(\frac{R}{r}\right)^{0.376}}$	$k_p = \frac{k}{1+0.175\left(\frac{p}{E}\right)\left(\frac{r}{t}\right)^{19/6}\left(\frac{R}{r}\right)^{0.322}}$
180	$k_p = \frac{k}{1+9.25\left(\frac{p}{E}\right)\left(\frac{r}{t}\right)^{9/4}\left(\frac{R}{r}\right)^{0.412}}$	$k_p = \frac{k}{1\pm 0.115\left(\frac{p}{E}\right)\left(\frac{r}{t}\right)^{10/3}\left(\frac{R}{r}\right)^{0.481}}$	$k_p = \frac{k}{1+0.300\left(\frac{p}{E}\right)\left(\frac{r}{t}\right)^{19/6}\left(\frac{R}{r}\right)^{0.231}}$

Table H2.2 Flexibility factor (Continuied)

α, deg	In-plane closing bending	In-plane opening bending	Out-of-plane bending
30	$k_p = \dfrac{k}{1+5.10\left(\dfrac{pr^3}{3D}\right)\lambda^{3/4}\left(\dfrac{r}{R}\right)^{0.654}}$	$k_p = \dfrac{k}{1\pm 0.084\left(\dfrac{pr^3}{3D}\right)\left(\dfrac{1}{\lambda}\right)^{1/3}\left(\dfrac{R}{r}\right)^{0.37}}$	$k_p = \dfrac{k}{1+0.106\left(\dfrac{pr^3}{3D}\right)\left(\dfrac{1}{\lambda}\right)^{1/6}\left(\dfrac{R}{r}\right)^{0.199}}$
45	$k_p = \dfrac{k}{1+4.30\left(\dfrac{pr^3}{3D}\right)\lambda^{3/4}\left(\dfrac{r}{R}\right)^{0.573}}$	$k_p = \dfrac{k}{1\pm 0.062\left(\dfrac{pr^3}{3D}\right)\left(\dfrac{1}{\lambda}\right)^{1/3}\left(\dfrac{R}{r}\right)^{0.507}}$	$k_p = \dfrac{k}{1+0.080\left(\dfrac{pr^3}{3D}\right)\left(\dfrac{1}{\lambda}\right)^{1/6}\left(\dfrac{R}{r}\right)^{0.316}}$
60	$k_p = \dfrac{k}{1+3.70\left(\dfrac{pr^3}{3D}\right)\lambda^{3/4}\left(\dfrac{r}{R}\right)^{0.503}}$	$k_p = \dfrac{k}{1\pm 0.051\left(\dfrac{pr^3}{3D}\right)\left(\dfrac{1}{\lambda}\right)^{1/3}\left(\dfrac{R}{r}\right)^{0.599}}$	$k_p = \dfrac{k}{1+0.062\left(\dfrac{pr^3}{3D}\right)\left(\dfrac{1}{\lambda}\right)^{1/6}\left(\dfrac{R}{r}\right)^{0.411}}$
90	$k_p = \dfrac{k}{1+3.25\left(\dfrac{pr^3}{3D}\right)\lambda^{3/4}\left(\dfrac{r}{R}\right)^{0.44}}$	$k_p = \dfrac{k}{1\pm 0.040\left(\dfrac{pr^3}{3D}\right)\left(\dfrac{1}{\lambda}\right)^{1/3}\left(\dfrac{R}{r}\right)^{0.709}}$	$k_p = \dfrac{k}{1+0.048\left(\dfrac{pr^3}{3D}\right)\left(\dfrac{1}{\lambda}\right)^{1/6}\left(\dfrac{R}{r}\right)^{0.489}}$
180	$k_p = \dfrac{k}{1+2.55\left(\dfrac{pr^3}{3D}\right)\lambda^{3/4}\left(\dfrac{r}{R}\right)^{0.338}}$	$k_p = \dfrac{k}{1\pm 0.031\left(\dfrac{pr^3}{3D}\right)\left(\dfrac{1}{\lambda}\right)^{1/3}\left(\dfrac{R}{r}\right)^{0.814}}$	$k_p = \dfrac{k}{1+0.057\left(\dfrac{pr^3}{3D}\right)\left(\dfrac{1}{\lambda}\right)^{1/6}\left(\dfrac{R}{r}\right)^{0.553}}$

Table H3.1 Stress-intensification factor

α, deg	In-plane closing bending	In-plane opening bending	Out-of-plane bending
30	$\gamma_p = \dfrac{\gamma}{1+16.90\left(\frac{p}{E}\right)\left(\frac{r}{t}\right)^{7/3}\left(\frac{R}{r}\right)^{0.197}}$	$\gamma_p = \dfrac{\gamma}{1+0.330\left(\frac{p}{E}\right)\left(\frac{r}{t}\right)^{10/3}\left(\frac{R}{r}\right)^{0.245}}$	$\gamma_p = \dfrac{\gamma}{1+19.0\left(\frac{p}{E}\right)\left(\frac{r}{t}\right)^{7/3}\left(\frac{R}{r}\right)^{0.120}}$
45	$\gamma_p = \dfrac{\gamma}{1+12.50\left(\frac{p}{E}\right)\left(\frac{r}{t}\right)^{7/3}\left(\frac{R}{r}\right)^{0.318}}$	$\gamma_p = \dfrac{\gamma}{1+0.230\left(\frac{p}{E}\right)\left(\frac{r}{t}\right)^{10/3}\left(\frac{R}{r}\right)^{0.393}}$	$\gamma_p = \dfrac{\gamma}{1+12.3\left(\frac{p}{E}\right)\left(\frac{r}{t}\right)^{7/3}\left(\frac{R}{r}\right)^{0.290}}$
60	$\gamma_p = \dfrac{\gamma}{1+10.25\left(\frac{p}{E}\right)\left(\frac{r}{t}\right)^{7/3}\left(\frac{R}{r}\right)^{0.407}}$	$\gamma_p = \dfrac{\gamma}{1+0.183\left(\frac{p}{E}\right)\left(\frac{r}{t}\right)^{10/3}\left(\frac{R}{r}\right)^{0.502}}$	$\gamma_p = \dfrac{\gamma}{1+9.7\left(\frac{p}{E}\right)\left(\frac{r}{t}\right)^{7/3}\left(\frac{R}{r}\right)^{0.394}}$
90	$\gamma_p = \dfrac{\gamma}{1+10.25\left(\frac{p}{E}\right)\left(\frac{r}{t}\right)^{7/3}\left(\frac{R}{r}\right)^{0.435}}$	$\gamma_p = \dfrac{\gamma}{1+0.172\left(\frac{p}{E}\right)\left(\frac{r}{t}\right)^{10/3}\left(\frac{R}{r}\right)^{0.546}}$	$\gamma_p = \dfrac{\gamma}{1+9.25\left(\frac{p}{E}\right)\left(\frac{r}{t}\right)^{7/3}\left(\frac{R}{r}\right)^{0.426}}$
180	$\gamma_p = \dfrac{\gamma}{1+7.50\left(\frac{p}{E}\right)\left(\frac{r}{t}\right)^{7/3}\left(\frac{R}{r}\right)^{0.567}}$	$\gamma_p = \dfrac{\gamma}{1+0.124\left(\frac{p}{E}\right)\left(\frac{r}{t}\right)^{10/3}\left(\frac{R}{r}\right)^{0.685}}$	$\gamma_p = \dfrac{\gamma}{1+8.3\left(\frac{p}{E}\right)\left(\frac{r}{t}\right)^{7/3}\left(\frac{R}{r}\right)^{0.466}}$

Table H3.2 Stress-intensification factor (Continuied)

α, deg	In-plane closing bending	In-plane opening bending	Out-of-plane bending
30	$\gamma_p = \dfrac{\gamma}{1+4.65\left(\dfrac{pr^3}{3D}\right)\lambda^{2/3}\left(\dfrac{r}{R}\right)^{0.47}}$	$\gamma_p = \dfrac{\gamma}{1+0.091\left(\dfrac{pr^3}{3D}\right)\left(\dfrac{1}{\lambda}\right)^{1/3}\left(\dfrac{r}{R}\right)^{0.578}}$	$\gamma_p = \dfrac{\gamma}{1+5.22\left(\dfrac{pr^3}{3D}\right)\lambda^{2/3}\left(\dfrac{r}{R}\right)^{0.548}}$
45	$\gamma_p = \dfrac{\gamma}{1+3.45\left(\dfrac{pr^3}{3D}\right)\lambda^{2/3}\left(\dfrac{r}{R}\right)^{0.35}}$	$\gamma_p = \dfrac{\gamma}{1+0.063\left(\dfrac{pr^3}{3D}\right)\left(\dfrac{1}{\lambda}\right)^{1/3}\left(\dfrac{r}{R}\right)^{0.726}}$	$\gamma_p = \dfrac{\gamma}{1+3.40\left(\dfrac{pr^3}{3D}\right)\lambda^{2/3}\left(\dfrac{r}{R}\right)^{0.378}}$
60	$\gamma_p = \dfrac{\gamma}{1+2.82\left(\dfrac{pr^3}{3D}\right)\lambda^{2/3}\left(\dfrac{r}{R}\right)^{0.26}}$	$\gamma_p = \dfrac{\gamma}{1+0.050\left(\dfrac{pr^3}{3D}\right)\left(\dfrac{1}{\lambda}\right)^{1/3}\left(\dfrac{r}{R}\right)^{0.835}}$	$\gamma_p = \dfrac{\gamma}{1+2.67\left(\dfrac{pr^3}{3D}\right)\lambda^{2/3}\left(\dfrac{r}{R}\right)^{0.273}}$
90	$\gamma_p = \dfrac{\gamma}{1+2.80\left(\dfrac{pr^3}{3D}\right)\lambda^{2/3}\left(\dfrac{r}{R}\right)^{0.23}}$	$\gamma_p = \dfrac{\gamma}{1+0.047\left(\dfrac{pr^3}{3D}\right)\left(\dfrac{1}{\lambda}\right)^{1/3}\left(\dfrac{r}{R}\right)^{0.879}}$	$\gamma_p = \dfrac{\gamma}{1+2.53\left(\dfrac{pr^3}{3D}\right)\lambda^{2/3}\left(\dfrac{r}{R}\right)^{0.240}}$
180	$\gamma_p = \dfrac{\gamma}{1+2.05\left(\dfrac{pr^3}{3D}\right)\lambda^{2/3}\left(\dfrac{r}{R}\right)^{0.10}}$	$\gamma_p = \dfrac{\gamma}{1+0.034\left(\dfrac{pr^3}{3D}\right)\left(\dfrac{1}{\lambda}\right)^{1/3}\left(\dfrac{r}{R}\right)^{1.019}}$	$\gamma_p = \dfrac{\gamma}{1+2.29\left(\dfrac{pr^3}{3D}\right)\lambda^{2/3}\left(\dfrac{r}{R}\right)^{0.201}}$